ABSTRACT

Title of Dissertation:	PROBING THE NATURE OF COMPACT OBJECTS: SCATTERING, TIDES AND QUASINORMAL MODES
	Venkata Sai Saketh Muddu Doctor of Philosophy, 2025
Dissertation Directed by:	Professor Alessandra Buonanno Department of Physics

The LIGO-VIRGO-KAGRA (LVK) collaboration has detected 90 confirmed gravitational-wave (GW) events and nearly 200 confident triggers across four observational runs. Coalescing black-hole (BH) and neutron-star (NS) binaries are primary GW sources, offering the unique possibility to probe the nature of compact objects and gravitational dynamics. This dissertation investigates how the intrinsic properties of compact objects affect their dynamics and GW emission, using worldline effective field theories (WEFTs) and BH perturbation theory (BHPT), with emphasis on selected scattering processes in General Relativity (GR).

Scattering of two BHs in the post-Minkowskian (PM) regime has proven valuable for extracting binary dynamics from gauge-invariant scattering observables. As a simpler analog, we study electromagnetic (EM) scattering of two charged particles in the post-Lorentzian (PL) expansion. We compute scattering observables to 3PL order and map them to their bound-orbit counterparts, deriving new boundary-to-bound (B2B) relations. We verified these mappings for gravity at first post-Newtonian (PN) order.

Another key setup involves GWs scattering off compact objects i.e., gravitational Compton/Raman scattering. We compute the classical Compton amplitude at linear order in the mass of the scattering body, and to third order in spin, for generic parity-invariant compact objects, using a WEFT with spin-induced multipole couplings, finding agreement with expectations from amplitude-based methods in the Kerr BH case, while presenting new results for generic objects.

We extract the low-frequency tidal response of Kerr BHs by matching the tidal contribution to the Raman amplitude computed in BHPT to its WEFT counterpart, thereby constraining key tidal coefficients such as Love numbers and dissipation numbers. We then use the dissipation numbers to compute horizon-flux-induced mass and angular-momentum loss in Kerr-BH binaries, resolving longstanding discrepancies with the test-body limit and obtaining waveform corrections up to 4PN order. Additionally, we recover the vanishing of BH Love numbers and identify a nonlinear mixing of tidal and non-tidal effects, resulting in a scale-dependent tidal response via classical renormalization group flow.

We also extend this approach to NSs, and extract electric, quadrupolar, Love and dissipation numbers from the Raman amplitude as a function of the boundary conditions for the metric perturbations at the stellar surface, that are determined by numerically solving the metric- and matter-perturbation equations inside the NS. This allows us to roughly quantify the impact of tidal heating on the GW phase during the inspiral across different equations of state.

Finally, we study the interplay between quasinormal modes (QNMs) and reflectivity for generic compact objects modeled in the membrane paradigm—a phenomenological framework that encodes interior structure via a fictitious surface fluid. We extend the phenomenological framework to linear order in spin, we analyze how membrane parameters influence the QNM spectrum and reflectivity.

PROBING THE NATURE OF COMPACT OBJECTS: SCATTERING, TIDES, AND QUASINORMAL MODES

by

VENKATA SAI SAKETH MUDDU

Dissertation submitted to the Faculty of the Graduate School of the
University of Maryland, College Park in partial fulfillment
of the requirements for the degree of
Doctor of Philosophy
2025

Dissertation Committee:
Professor Alessandra Buonanno (Advisor, Committee co-Chair)
Professor Theodore A. Jacobson (Committee Chair)
Professor Bei-Lok Bernard Hu
Professor Michael Coleman Miller (Dean's Representative)
Professor Anson Hook

Acknowledgments

I am deeply grateful to my advisor, Prof. Alessandra Buonanno, for her unwavering support, guidance, and the opportunity to collaborate with leading experts in the field. She fostered my independence in exploring various research topics while providing invaluable advice on sound research practices. Her mentorship taught me how to write effective papers and encouraged me to present my work. I greatly admire her ability to engage with a diverse range of subfields within gravitational-wave astronomy while maintaining a clear vision of the broader scientific landscape—an approach I aspire to emulate in the future.

I am also immensely grateful to Dr. Justin Vines and Dr. Jan Steinhoff at MPI for Gravitational Physics, Potsdam, for their continuous support and guidance. Their willingness to engage with me and help me navigate various aspects of gravitational dynamics was invaluable. They inspired me to strive for competence while fostering a culture of kindness and support. It is safe to say that I aspire to emulate their approach when I have the opportunity to guide and support others in the future.

I sincerely thank all my collaborators : Alessandra Buonanno, Debarati Chatterjee, Suprovo Ghosh, Mikhail Ivanov, Elisa Maggio, Jan Steinhoff, Justin Vines, and Zihan Zhou. They have greatly helped me expand my knowledge beyond my primary domain, and also inspired me to perform better through their contributions to the research in this dissertation.

I also thank my dissertation committee members —Prof. Bei-Lok Hu, Prof. Anson Hook, Prof. Ted Jacobson and Prof. Cole Miller —for their interest in my work and their time.

I thank Josiland Chambers at UMD, Brit Holand and Darya Niakhaichyk at AEI for helping me out regarding formalities associated with my stay at UMD and AEI. I also sincerely thank members at ISSS of UMD for guiding me through the various steps.

In addition, I thank my friends, especially Mohammed Khalil for helping me navigate various formal requirements regarding visa and PhD. I also thank Cheng, Elise, Hector, Jung-Wook, Lorenzo, Lorenzo Speri, Marcus, Nihar, Niko, Peter, Raj, Ricardo, Trevor, Zihan, and others, for making my PhD experience more enjoyable.

Finally, I thank my wife — Meghana, my dear parents — Uma and Swamy, and my brother — Sudhir, for their unwavering support and encouragement towards my career.

Table of Contents

List of Tables

List of Figures

List of Abbreviations

ADM	Arnowitt-Deser-Misner
BBH	binary black hole
BH	black hole
BHPT	black hole perturbation theory
EFT	effective field theory
EMRI	extreme-mass-ratio inspiral
EOB	effective one body
GR	general relativity
GW	gravitational wave
GSF	gravitational self-force
ISCO	innermost stable circular orbit
KAGRA	KAmioka GRAVitational detector
LIGO	Laser Interferometer Gravitational-Wave Observatory
LISA	Laser Interferometer Space Antenna
LO	leading order
MPD	Mathisson-Papapetrou-Dixon
MS	minimal subtraction
MST	Mano-Sasaki-Takasugi
NLO	next-to-leading order
NNLO	next-to-NLO
NR	numerical relativity
NS	neutron star
PN	post-Newtonian
PM	post-Minkowskian
PL	post-Lorentzian

QFT	quantum field theory
QNM	quasi-normal mode
RR	radiation reaction
SPA	stationary phase approximation
SPT	Stellar perturbation theory
SSC	spin-supplementary condition
WEFT	Worldline effective field theory

Summary of Research Contributions

The research I present in this dissertation has been conducted in collaboration with my advisor and several coauthors, and was published in Refs. [1–6]. I had substantial contributions to these papers, and thus included them as chapters 2 – 7. In Sec. 1.5, I summarize the topics covered in these chapters, while here, I describe my contributions to each chapter.

Chapter 1 provides an introduction and overview of the research presented in the rest of the dissertation. I was the sole author of this chapter.

Chapter 2, published as Ref. [1], presents our derivation of observables such as impulse, radiated energy, and angular momentum for electromagnetic scattering of two massive charged particles up to 3rd post-Lorentzian order. We also introduced new boundary-to-bound (B2B) maps relating radiated energy and angular momentum between unbound and bound systems. I carried out all computations using *Mathematica* under the guidance of J. Steinhoff, J. Vines, and A. Buonanno, and I derived the B2B maps. I contributed the majority of the writing, which was cross-checked and refined by J. Vines and J. Steinhoff, with feedback from A. Buonanno. The idea to study the electromagnetic case as a simplified classical scattering setup and explore mappings between unbound and bound systems arose from discussions among all authors.

Chapter 3, published as Ref. [2], presents our computation of the tree-level gravitational Compton amplitude to third order in spin for generic parity-preserving compact objects. I performed the entire calculation in *Mathematica*, with J. Vines advising and optimizing portions of the code. I also contributed the majority of the writing. The idea for this study was originally conceived by J. Vines.

Chapter 4, published as Ref. [3], derives the changes in mass and angular momentum due to horizon fluxes in quasi-circular Kerr black hole binaries. This was achieved by extracting the dissipative tidal response of Kerr black holes from the scattering phase of gravitational waves off Kerr black holes. The scattering problem was solved analytically using Mano-Sasaki-Takasugi (MST) techniques in black hole perturbation theory. The idea emerged from discussions between J. Steinhoff and me. I carried out all calculations with guidance from J. Steinhoff and J. Vines. I also wrote most of the manuscript, with inputs from J. Steinhoff, J. Vines, and A. Buonanno. The suggestion to use horizon fluxes to compute waveform corrections at 4PN came from A. Buonanno, who also provided guidance on that part of the paper.

Chapter 5, published as Ref. [4], constrains both conservative and dissipative tidal responses of Kerr black holes, as defined in effective worldline theory, to next-to-next-to-leading order in frequency. We demonstrated the vanishing of the static conservative tidal response (Love numbers) and showed that the next-to-leading order conservative response, as well as the next-to-next-to-leading order dissipative response, exhibit classical renormalization group flow. We also identified the origins of this running behavior, linking a portion of it to tail effects—i.e., the scattering of gravitational waves off the background metric before/after inducing tidal moments. The idea was developed in discussions between Z. Zhou, M. Ivanov and me. The calculations were done by Z. Zhou and me, with frequent discussions where M. Ivanov provided valuable guidance. The writing was a joint effort among the three co-authors.

Chapter 6, published as Ref. [5], rigorously extracts the relativistic tidal response of non-spinning viscous neutron stars from the gravitational Raman amplitude. Unlike black holes, where metric perturbations suffice, neutron star perturbations involve coupled matter and metric equations. We expanded and solved the interior perturbation equations to linear order in frequency, numerically solving them up to the stellar surface. These solutions then served as boundary conditions for the exterior metric perturbation equations, allowing us to analytically determine the scattering amplitude and extract the Love number and leading dissipation number. We showed that the dissipation number is sensitive to shear viscosity under certain conditions and computed its effect on the gravitational waveform for symmetric binary neutron-star systems. The idea to extend our methods to non-black-hole objects arose from discussions between Z. Zhou and me. These ideas were further refined with input from S. Ghosh and D. Chatterjee, who also provided neutron star equation-of-state profiles. J. Steinhoff guided us in discussions. The calculations were primarily done by Z.Zhou and me. The writing was primarily done by Z. Zhou, S. Ghosh, and me, with additional input from J. Steinhoff and D. Chatterjee.

Chapter 7, published as Ref. [6], extends the membrane paradigm to linear order in spin and explores its implications for quasi-normal modes, reflectivity, and membrane parameters. The membrane paradigm provides a generic framework for parametrizing the interior of compact objects via an effective fluid at the object's surface. The idea emerged from discussions with E. Maggio regarding her earlier work on non-spinning horizonless compact objects. I performed most of the calculations, including deriving boundary conditions for spinning membranes, computing reflectivity properties, and determining quasi-normal mode frequencies using *Mathematica*. E. Maggio provided reference codes from her non-spinning analysis. The writing was a joint effort between both authors.

Chapter 8 summarizes the findings of the previous chapters and discusses potential directions for future work. I am the sole author of this chapter.

Throughout the rest of this dissertation, I use the pronoun ‘‘we’’ instead of ‘‘I’’ while referring to myself.

Chapter 1: Introduction and Overview

1.1 GWs as probes of compact objects

The universe teems with a variety of gravitationally bound configurations, including stars, planets, solar systems, and galaxies. Of particular interest among these are highly compact objects, such as black-holes (BHs) [7, 8] and neutron-stars (NSs) [9], which exist at the very extremes of relativistic gravity and matter. The study of these objects serves as a powerful probe into both gravitational physics and the properties of dense matter. Furthermore, as modern theoretical physics seeks to understand the quantum nature of gravity, investigating these compact configurations provides a unique window into potential quantum-gravitational effects [10, 11] and the fundamental nature of gravity itself.

Until recently, these objects were studied entirely through electromagnetic observations. NSs were primarily detected as pulsars [12], while supermassive BHs were inferred from the energetic emissions of accretion disks [13] at galactic centers [14]. However, since September 14, 2015 [15], a new observational window into these objects — specifically, the binaries they inhabit — has emerged: gravitational waves (GWs).

GWs are the gravitational analog of electromagnetic waves, generated by accelerating masses such as those in compact binaries [16–18]. They can be detected by terrestrial observatories — Laser Interferometer Gravitational-Wave Observatory (LIGO), VIRGO and KAmioka GRAvitational detector (KAGRA) [19–22] — carry crucial information about binary dynamics and the nature of their compact components [15, 23–25]. As a result, GW observations offer a novel and direct means of studying these objects. The overarching goal of the work in this dissertation is the identification and investigation of compact objects via GWs. To this end, we begin with a brief discussion of GWs, their detection, and the analytical tools required to interpret the observed signals.

1.1.1 GWs

Over a century ago, Albert Einstein introduced the theory of general relativity (GR), fundamentally transforming our understanding of gravitation [16]. In this framework, gravitation is described as the curvature of spacetime, mathematically represented by a pseudo-Riemannian manifold. The metric tensor $g_{\mu\nu}$ serves as the dynamical field, determining the distances between nearby points on this manifold.

The Einstein equation articulates the relationship between spacetime curvature, which is encoded in the Riemann curvature tensor $R^{\alpha}{}_{\beta\gamma\delta}$, and the energy-momentum content:

$$R_{\mu\nu} - \frac{1}{2} g_{\mu\nu} R + \Lambda g_{\mu\nu} = \kappa T_{\mu\nu}, \tag{1.1}$$

$$\text{where} \quad R_{\mu\nu} = g^{\alpha\beta} R_{\alpha\mu\beta\nu},\ R = g^{\mu\nu} R_{\mu\nu},\ \kappa = \frac{8\pi G}{c^4}. \tag{1.2}$$

The energy-momentum tensor $T_{\mu\nu}$ satisfies the local covariant conservation law $\nabla_{\mu} T^{\mu\nu} = 0$.

GR has yielded several profound predictions, such as perihelion precession, gravitational time dilation, gravitational lensing, cosmic expansion, etc [26]. Among these, the existence of GWs stands out as a remarkable consequence. These are wave-like solutions to Einstein equation, representing propagating disturbances in the curvature of spacetime. Typically, GWs are treated as a linear metric perturbation over a fixed background metric [27]. In this approximation, GWs behave analogously to massless particles in the limit of geometric optics, propagating at the speed of light.

When perturbing over flat spacetime, the metric tensor can be expressed as:

$$g_{\mu\nu} = \eta_{\mu\nu} + h_{\mu\nu}, \quad h = \eta^{\mu\nu} h_{\mu\nu}, \quad \bar{h}_{\mu\nu} = h_{\mu\nu} - \frac{1}{2}\eta_{\mu\nu} h. \tag{1.3}$$

where $\eta_{\mu\nu}$ is the Minkowski metric, and $h_{\mu\nu}$ represents a linear perturbation. We define $\bar{h}_{\mu\nu}$ for later convenience.

Since the dynamical field is the metric of the spacetime manifold, GR enjoys a natural gauge invariance under coordinate transformations. A convenient gauge for the purpose of this discussion is the Lorenz gauge defined as $\partial^{\nu}\bar{h}_{\mu\nu} = 0$. In this gauge, the Einstein equation for the perturbation is given by

$$\Box \bar{h}_{\mu\nu} = -16\pi T_{\mu\nu} + O(h^2), \tag{1.4}$$

where $\Box = \eta^{\mu\nu}\nabla_{\mu}\nabla_{\nu}$ is the D'Alembertian operator in flat spacetime. Going forward, we adopt natural units with $G = c = 1$ and use the mostly positive metric signature $(-, +, +, +)$ in this chapter. Note, however, that the individual chapters that follow are based on research papers published at different times and in collaboration with different coauthors, and may therefore adopt different conventions suited to their respective contexts.

1.1.1.1 GWs in vacuum

Note that when $T_{\mu\nu} = 0$, $\bar{h}_{\mu\nu}$ satisfies the usual wave equation as is typical of massless waves. We can easily study polarizations of propagating GWs in this case. To that end, it is convenient to further specialize to the traceless transverse (TT) gauge.

The TT gauge is characterized by a timelike vector v^μ, and the metric perturbation obeys

$$\bar{h}^{\mu\nu} v_\nu = 0, \quad h^\mu{}_\mu = 0. \tag{1.5}$$

Aligning the timelike basis vector of our coordinate system with v^μ, the constraints, along with the Lorenz gauge condition are simply

$$h^{0\mu} = 0, \quad h^i{}_i = 0, \quad \partial^j h_{ij} = 0. \tag{1.6}$$

In the Fourier domain $h_{ij}(x) = \int d^4x \exp(ik\cdot x)\mathcal{H}_{ij}(k)$, the constraints are algebraic and we have just two independent components $(10-4-1-3 = 2)$ per mode corresponding to two polarizations.

1.1.1.2 Plane GWs and effect on test masses

Restricting to a single harmonic, we can write a plane-wave solution to Eq. (1.4) in TT gauge as

$$h^{\mathrm{TT}}_{ij}(t,z) = \mathcal{H}_+ \begin{pmatrix} 1 & 0 & 0 \\ 0 & -1 & 0 \\ 0 & 0 & 0 \end{pmatrix} \cos(\omega(t-z)) + \mathcal{H}_\times \begin{pmatrix} 0 & 1 & 0 \\ 1 & 0 & 0 \\ 0 & 0 & 0 \end{pmatrix} \cos(\omega(t-z)), \tag{1.7}$$

where we choose the wave to be traveling along the spatial z axis for convenience.

Now, consider a pair of test masses at $x^\mu_{A=1,2}$ on the x-y plane, subject to this plane GW radiation. They will follow geodesic motion in the spacetime defined by the metric $g_{\mu\nu} = \eta_{\mu\nu} + h^{TT}_{\mu\nu}(t,z)$.

$$\frac{d^2x^\mu_A}{d\tau^2} + \Gamma^\mu_{\nu\rho}(x)\frac{dx^\nu_A}{d\tau}\frac{dx^\rho_A}{d\tau} = 0. \tag{1.8}$$

Letting $dx^\mu/d\tau = \{1,0,0,0\}$ at $t = 0$, the spatial coordinates at $t = 0$, obey the equation $d^2x^i_A/d\tau^2 = -\Gamma^i_{00}$ at $\tau = 0$, and since $\Gamma^i_{00} = 0$ to linear order in metric perturbation in the TT gauge, the particles remain at rest throughout, i.e., $x^i_A = 0$ for all $\tau \geq 0$.

However, this motion is peculiar to the given coordinate system and not easily related to an observable. Instead, we can consider the variation of proper length between the two worldlines at a given time t. Let $x^i_1(t = 0) = \{0,0,0\}$ and $x^i_2(t = 0) = \{L,0,0\}$. Then, since we know the coordinates remain unchanged in this gauge, the proper length between them is given by $l_p^2 = g_{xx}L^2$, meaning $l_p = L[1 + 2\mathcal{H}_+ \cos(\omega(t - z))]$. Thus, the proper distance oscillates as the GW passes through.

Alternatively, we can consider the motion of one test mass in the frame of another. This can be accomplished using the geodesic deviation equation. Defining the displacement vector relating two closely separated[1] worldlines as $x^\mu_2 = x^\mu_1 + \xi^\mu$, ξ^μ obeys the covariant equation

$$\frac{D^2\xi^\mu}{D\tau^2} = -R^\mu{}_{\nu\rho\sigma}\xi^\rho \frac{dx^\nu}{d\tau}\frac{dx^\sigma}{d\tau}. \tag{1.9}$$

This can be understood as the tidal force due to the GWs pulling (or pushing) the two objects apart (or towards each other). In a locally inertial, comoving frame for one particle, the coordinates can be locally chosen to correspond to proper lengths, and the proper time as coordinate time. We can then write

$$\frac{d^2\xi^{\hat{i}}}{dt^2} = -R^{\hat{i}}{}_{\hat{0}\hat{j}\hat{0}}\xi^{\hat{j}}. \tag{1.10}$$

where the hatted indices refer to the new coordinates. In these coordinates, the curvature tensor

[1] The separation should be small compared to the curvature length scale, which is set by the wavelength of the GW.

can be written as $R^{\hat{i}}{}_{\hat{0}\hat{j}\hat{0}} = -\ddot{h}^{\mathrm{TT}}_{ij}/2$, yielding

$$\ddot{\xi}_{\hat{i}} = \omega^2 h^{\mathrm{TT}}_{ij} \xi^{\hat{j}}_{t=0}, \tag{1.11}$$

where we have replaced the deviation vector with its constant initial value to restrict the analysis to leading order. This again shows that the deviation vector, in the locally inertial rest frame, oscillates at the same frequency as the GW.

While we have demonstrated the influence of linearized GWs in a simple manner, the existence of GWs and their ability to carry energy was a subject of some confusion in the early development of GR. This was primarily due to confusion arising from coordinate ambiguities concerning the physical reality of GWs, as well as the absence of a gauge-invariant definition of GW energy density. The skepticism was further reinforced by Einstein's own uncertainty regarding their physical existence [28, 29]. F. A. E. Pirani addressed the gauge-invariance issue by formulating the effect of GWs in terms of the curvature tensor, demonstrating that the proper separation of neighbouring geodesics changes according to Eq.(1.9) [30, 31]. Richard P. Feynman extended this argument at the Chapel Hill conference, famously proposing a thought experiment involving two beads constrained to slide along a rigid stick with friction. The oscillations in proper separation induced by the GW would result in the beads rubbing against the stick, leading to dissipation and providing a clear physical demonstration that GWs transport energy [32]. Some residual skepticism remained regarding the use of the linearized approximation in deriving these results. However, such concerns were largely dismissed by physicists like Feynman, who argued that linear perturbation theory had been thoroughly validated in other field theories, including in EM. Ultimately, any remaining skepticism was irrelevant after the discovery of the Hulse–Taylor binary pulsar system, whose observed orbital decay precisely matched the predictions from GW energy loss in GR [33–35]. Today, we have come much farther since, directly detecting GWs from coalescences of compact binaries.

1.1.1.3 GW detection

The current state-of-the-art GW detector is the (advanced) Laser Interferometer Gravitational-wave Observatory (LIGO/aLiGO) [19, 36]. It consists of two perpendicular 4 km arms. Mirrors at the ends of the arms serve as test masses, with laser beams passing through a beam splitter into Fabry-Perot optical cavities. Multiple reflections between the mirrors effectively extend the arm length. GWs induce tiny changes in arm length, detected via optical interference. Signal recycling mirrors enhance laser power for sharper interference patterns. A detailed understanding of interferometric GW detectors can be found in Ref. [37], and LIGO in particular in Ref. [38].

LIGO (LIGO-Hanford and LIGO-Livingston) in the USA, together with Virgo in Italy [39] and KAGRA in Japan [40, 41], forms the current global network of ground-based GW detectors. Advanced LIGO operates in the 10 Hz–1 kHz range, with peak strain sensitivity around 10^{-22} near 100 Hz. The first GW event, GW150914 [15], was observed in the frequency range of 35–250 Hz, producing a peak strain amplitude of about 10^{-21} near 150 Hz. This corresponds to differential arm length changes of order 4×10^{-18} m for LIGO's 4km arms. However, not all GW events induce strain amplitudes comparable to the strain sensitivity, which is limited by various sources of noise [42]. This necessitates the use of advanced data-analysis techniques.

The primary method for detecting GWs is matched filtering, where the detector output $d(t) = n(t) + h(t)$ — a combination of noise and a possible signal — is correlated with a set of theoretical waveform templates (a template bank). This technique maximizes the signal-to-noise ratio by optimally extracting weak signals buried in noise, typically assuming that the noise is approximately stationary and Gaussian [42]. Since the parameters of a GW signal are unknown in advance, the data must be compared against a template bank [43], a dense collection of representative waveforms spanning the expected parameter space. More accurate templates improve detection confidence, reduce the risk of missing weak signals, enable precise parameter estimation, and allow tests of GR [44]. Building such waveforms relies on detailed analytical and numerical modeling of the dynamics of compact binaries, such as BHs and NSs.

This dissertation primarily aims to investigate how the intrinsic properties of compact objects — such as tidal response and reflectivity — influence their dynamics in binaries and imprint characteristic signatures on the GW signal. To set the stage for this study, we briefly review the various stages of binary coalescence.

1.1.2 Inspiral, merger and ringdown — binary coalescence

The primary sources of detectable GW radiation are coalescences of compact binaries. A binary coalescence can be roughly divided into three parts — inspiral, merger and ringdown, as shown in Fig. 1.1.

1.1.2.1 Inspiral

The inspiral phase of binary coalescence is particularly amenable to analytical investigation and serves as the primary focus of this dissertation. During this stage, the binary components are initially well separated and may be approximated as point masses. As they emit gravitational radiation and draw closer, finite-size effects become significant. These effects, arising from prop-

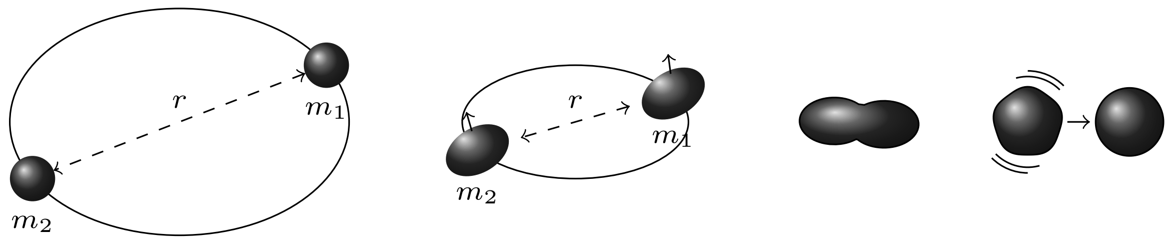

Figure 1.1: A merger-event can be roughly divided into three phases. The first phase is the inspiral, when the compact objects are far apart and are spiralling inwards due to the loss of orbital energy in the form of gravitational radiation. Early inspiral can be approximated as due to a binary of point particles. As inspiral progresses, the finite-size of the objects and associated physics becomes relevant, such as due to spin, spin-induced and tidal deformation. Eventually, they plunge and merge in a highly non-linear process, the details of which can vary significantly based on the nature of compact objects involved. Finally, the remnant settles to a stable configuration through the emission of GWs at characteristic quasinormal mode (QNM) frequencies.

erties such as spin, spin-induced deformation, and tidal deformation, are crucial can help identify the nature of the compact objects involved [45] during the inspiral.

The analysis of binary dynamics during the inspiral phase is effectively carried out in the post-Newtonian (PN) expansion [46–49]. This method systematically incorporates general relativistic corrections to the motion of compact objects by exploiting the non-relativistic speeds ($v \ll 1$) and the large separation ($\sim r$) between the objects compared to their sizes ($\sim \mathcal{R}$), i.e., we have $r \gg \mathcal{R}$. The virial theorem[2] relates these conditions through $v^2 \sim M/r$, where M is the typical mass of a compact object in the binary, establishing v or M/r as the expansion parameter in the PN series.

Finite-size effects, such as spin, and spin-induced and tidal deformations, are relevant at

[2]The virial theorem relates the kinetic energy ($K \sim v^2$) and the potential energy ($V \sim -M/r$) to the dynamics of the moment of inertia (I) of the binary as $4K + 2V = (d^2/dt^2)I$ in Newtonian gravity, where the right hand side vanishes for circular orbit binaries, leading to $2K = -V$ or $v^2 \sim M/r$. This does not hold for eccentric inspirals except in the long-time average. However, eccentricity is rapidly lost during inspiral and orbits are generally approximately circular when they enter the detection band.

higher PN orders [45, 50, 51] due to their dependence on the ratio $\mathcal{R}/r \ll 1$. Spin becomes relevant starting from 1.5PN order, with spin-induced quadrupolar deformation influencing dynamics from the 2PN order [50, 52–54]. Tidal deformations, resulting from mutual gravitational interactions, are characterized by tidal-response coefficients and enter the dynamics formally at the 5PN order [55–57]. However, dissipative tidal effects enter at 2.5PN (4PN) into the waveform for spinning (nonspinning) bodies [58–65]. Finite-size effects depend on the rich internal physics of compact objects, and characterize the deviation of the system from that of a binary of point particles. Their effects on the dynamics of compact objects in binaries during the inspiral are best captured using worldline effective field theories (WEFTs) [47, 48, 51] in which the compact object is systematically treated as a worldline-entity (point-like particle). We discuss this in some depth later in Sec. 1.3.

The PN approximation method has a rich history, originating with Einstein's application at the first PN (1PN) order to account for Mercury's perihelion precession [66]. This approach gained significant attention following the observation of GW-induced orbital decay in the Hulse–Taylor binary pulsar [33–35]. Subsequent decades have witnessed substantial advancements in deriving higher-order PN corrections, enhancing our understanding of gravitational dynamics. Some detailed reviews of PN efforts and state-of-the-art can be found in Ref. [46–49].

In addition to the PN scheme, another analytical approach is the gravitational self-force (GSF) formalism suitable for analyzing the inspiral phase of extreme mass-ratio systems, such as a stellar-mass BH orbiting a supermassive BH [67**?** –70]. In these scenarios, the smaller object (of mass m) induces perturbations in the spacetime geometry of the larger BH (with mass M), and the GSF formalism systematically accounts for the back-reaction of these perturbations on the smaller body's motion [71, 72]. The expansion parameter is then the mass ratio $q = m/M \ll 1$, while the relativistic effects are included non-perturbatively. This method is particularly advantageous for describing the long inspiral of the smaller body deep into the strong-field regime above the innermost stable circular orbit (ISCO) of the supermassive BH. The GSF approach has been instrumental in modeling such extreme mass-ratio inspirals (EMRIs), which are anticipated to be significant sources of GWs detectable by observatories such as the Laser Interferometer Space Antenna (LISA) [73, 74]. Some detailed reviews are Refs. [70, 73].

In recent times, the study of scattering processes in GR has also proven very useful in developing analytical tools to describe binary dynamics during the inspiral. This includes, for instance, the study of two-body scattering, where two BHs (say) scatter off each other due to mutual gravitational interaction. This setup is typically studied in the post-Minkowskian (PM) expansion. Another important scattering setup is that of GWs scattering off an isolated compact object, a process referred to as gravitational Compton/Raman scattering. This is typically studied in a low-frequency (of the GW) expansion. The study of such scattering processes is central to this dissertation, and we describe them in greater detail in Sec. 1.2, and also in Chapters 2, 3, 4, 5, 6 [1–5].

1.1.2.2 The end of inspiral, plunge and merger

Following the inspiral, the binary transitions towards a plunge phase. For EMRI systems, this is marked by a sharp boundary located at $r = 6M$ for a test particle around a Schwarzschild BH. However, for comparable-mass binaries, the system appears to smoothly transition from the inspiral to the plunge. During the plunge, the two bodies accelerate toward each other along dynamical trajectories, culminating in a highly nonlinear merger. This phase necessitates numerical-relativity (NR) simulations [75] for full resolution, though extreme mass-ratio systems [76] and effective frameworks [77, 78] provide alternative avenues for its study.

NR simulations offer the most accurate waveforms across all stages of coalescence, where available. In it, spacetime is discretized into a sequence of spacelike hypersurfaces, each representing a snapshot in time. These hypersurfaces are evolved numerically using the Einstein equation, typically formulated in a 3+1 decomposition such as the Arnowitt-Deser-Misner (ADM) formalism [79]. In practice, modern NR approaches employ more stable formulations, such as the Baumgarte–Shapiro–Shibata–Nakamura formalism [80, 81] or the generalized harmonic gauge [82], as implemented, for example, in the SpEC code [83]. While NR provides the most exact treatment of binary evolution, its high computational cost and runtime impose practical limitations. Given the vast parameter space of binary systems, NR simulations alone cannot densely sample all configurations, necessitating complementary analytical approaches. Moreover, analytical methods offer deeper physical insight into various dynamical features of binary coalescence.

However, purely analytical methods struggle to accurately model the late inspiral, plunge, and merger due to the increasingly nonlinear nature of the dynamics. A highly successful strategy to bridge this gap is the effective-one-body (EOB) formalism [77], which synthesizes multiple analytical approximations while incorporating calibration from NR [84, 85].

In the EOB framework, the two-body Hamiltonian and radiation-reaction effects — derived from the PN and, more recently, PM expansions — are mapped onto an equivalent description of a single test mass moving in a deformed Schwarzschild or Kerr background, with the deformation parameter being the symmetric mass ratio. This mapping is advantageous because it captures non-perturbative features absent in the standard PN expansion. Notably, the EOB formalism naturally encodes the exact strong-field solution in the test-mass/spin limit. The deformation of the background metric accounts for deviations from the exact test-body limit, effectively incorporating strong-field effects. Furthermore, NR simulations refine the EOB Hamiltonian and waveforms through calibration beyond the currently available PN/PM order, resulting in a framework capable of describing both the inspiral and plunge up to the merger, and the ringdown.

1.1.2.3 Ringdown

Following the merger, the system then settles into a stable remnant through the emission of GWs [86]. This phase also starts out highly nonlinear, but after a suitable amount of time, can be represented using BH perturbation theory (BHPT).

In this linear regime, the system emits GWs at characteristic QNM frequencies [87, 88], which are unique to a compact object and thus aid in identifying the merger remnant. The waveform is a superposition of damped sinusoids at these characteristic frequencies.

The QNM frequencies are obtained by imposing certain boundary conditions upon the metric perturbations, namely outgoing boundary conditions at infinity and suitable boundary conditions at the surface of the compact object. For a BH, this corresponds to ingoing boundary conditions at the horizon, whereas reflective boundary conditions are relevant for horizonless objects such as NSs [89].

The boundary condition at the surface is thus closely related to the properties of the system, such as the presence/absence of a horizon or other modes of dissipation. This is of great interest when it comes to probing deviations from the BH paradigm [89, 90]. While the BH paradigm has been highly successful, it comes with certain conceptual hurdles such as violation of unitarity due to Hawking radiation, which has led to proposals of several exotic compact objects (ECOs) [89, 91–93]. We can seek such objects during inspiral from their modified finite-size effects such as spin or tidal effects. Alternatively, during ringdown, we can seek their presence by studying their QNM frequencies and comparing against observations and the BH scenario. The subfield which studies the QNMs of various models of compact objects and seeks to quantify them from available data is known as BH spectroscopy [87, 94].

In Chapter 7 [6], we study the fundamental QNM of slowly spinning compact objects with arbitrary reflectivity using the membrane paradigm [90, 95–97].

1.2 Gravitational scattering setups

Although the primary scenario of astrophysical interest during the inspiral is a binary of compact objects, it is conceptually intriguing and practically relevant to explore alternative scenarios involving compact objects and GWs. Notably, scattering processes offer insightful perspectives. Two important scenarios are:

1. **Two-body scattering**: This involves the deflection of two compact objects as they pass near each other, influenced by their mutual gravitational attraction. These systems can be analytically studied without compromising on special-relativistic aspects when the deflection is weak.

2. **Gravitational Raman/Compton scattering**: The process of weak GWs scattering off a compact object can be referred to as gravitational Compton or Raman scattering, with the latter term used when the object has excitable internal degrees of freedom. The associated amplitude encodes the coupling of the compact object with an external gravitational field. The Compton/Raman amplitude can be analytically computed, for instance, in BHPT for small frequencies.

Scattering scenarios are not only theoretically compelling but also of practical relevance. They often admit more tractable analytical treatments than bound systems and, through various means, can inform our understanding of bound dynamics. The study of scattering setups, especially Raman scattering, is central to this dissertation, and thus we briefly digress upon them here.

1.2.1 Two-body scattering

The study of gravitational deflection of two particles is analytically tractable within the PM expansion. Here, at leading order (0PM), we just have two unperturbed, straight, worldlines (representing uniform motion) in flat spacetime. At next-to-leading order (NLO), i.e., at 1PM, we consider the leading deflection to the trajectories, due to the leading perturbation to the flat Minkowskian metric. The expansion parameters are $m_A/|b|$ for $A = 1, 2$, where m_1 and m_2 are the two masses, and $|b| = \sqrt{b^\mu b_\mu}$, is the impact parameter marking the minimum separation between the unperturbed zeroth order worldlines. Since the particles are free in the distant past and future, observables pertaining to the objects in the asymptotic past and future are sufficient to describe the process, for example, the initial and final momenta of particles.

Typically, the change in observables due to the scattering process — for example, the impulse of one of the masses as $\Delta p_A^\mu = p_{\mathrm{f},A}^\mu - p_{\mathrm{i},A}^\mu$ — is presented perturbatively as a PM expansion. Unlike the PN expansion, the speeds of the bodies are not assumed to be small compared to the speed of light, making the PM framework well suited for capturing special-relativistic effects in two-body encounters.

The study of two-body scattering in the weak-field, arbitrary-speed regime has a long history, dating back to the 1950s [98, 99]. Major early developments included work by K. Westpfahl and collaborators, who extended the analysis to 2PM order [100–105], alongside important contributions from L. Bel, T. Damour, N. Deruelle, and G. Schäfer [106–108]. More recently, its relevance to bound binaries was recognized [109, 110], sparking renewed interest in the PM framework. Over the past decade, high-energy theorists have contributed significantly [111–125], leveraging quantum field theory (QFT) techniques to tackle the classical two-body problem, particularly in the context of BH scattering. Significant progress has also been made in incorporating spin [126–141] and dissipative effects [1, 142–155]. The current state of the art extends to 4PM [119, 120, 141, 155, 156], with partial results at 5PM [157]. Moreover, substantial effort has been devoted to mapping scattering results onto bound dynamics, particularly via PM-informed effective-one-body (EOB) models [109, 158, 159].

We briefly demonstrate the PM scheme at the first nontrivial order (1PM) below.

1.2.1.1 1PM scattering

In the distant past, we have two spherically symmetric objects with momenta $p_A^{(0),\mu} = m_A u_A^\mu$. The worldlines of the particles at 0PM are straight and non-intersecting, and are separated by a spacelike vector — b^μ — the impact parameter. It satisfies $b_\mu u_A^\mu = b \cdot u = 0$, and $|b| = \sqrt{b^\mu b_\mu}$ is the minimum distance between the 0PM worldlines. The two worldlines at 0PM can be written as

$$z_1^{(0),\mu} = u_1^\mu \tau_1, \quad z_2^{(0),\mu} = u_2^\mu \tau_2 + b^\mu, \tag{1.12}$$

where τ_A are the proper times of the particles. We want to compute the leading-order interaction between them, which perturbs their motion. The setup is demonstrated in Fig. 1.2 below. At 0PM, the spacetime is also flat and so $g_{\mu\nu} = \eta_{\mu\nu}$. To compute the 1PM deflection, we need to compute the leading metric perturbation. Writing $g_{\mu\nu}(x) = \eta_{\mu\nu} + h^{(1)}_{\mu\nu}(x)$, we can use Eq. (1.4) to

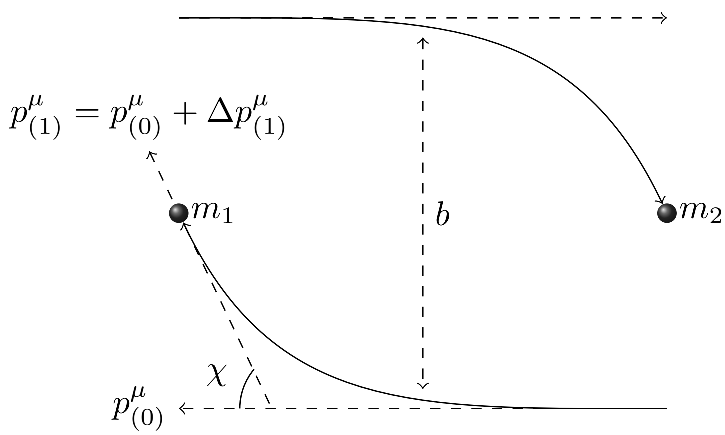

Figure 1.2: Two bodies weakly scatter off each other due to their mutual gravitational interaction. At 0PM, their worldlines represent uniform motion. Gravitational interaction causes them to deflect, gaining an impulse $\Delta p^{(\mu)}$, and with a scattering angle χ. At 1PM, no radiation is emitted, and thus the impulse is equal and opposite for each particle. The scattering angle is proportional to the component of the impulse $\Delta p^{\mu}_{(1)}$ along the impact parameter b^{μ}. The arrows show the spatial direction of the 4-vectors in the center-of-momentum frame.

write

$$\Box \bar{h}^{(1)}_{\mu\nu} = -16\pi \sum_{A=1,2} T^{(0),A}_{\mu\nu}. \tag{1.13}$$

Since the PM expansion is valid when the worldlines are well separated compared to their Schwarzschild radii, we can treat the compact objects as point particles[3] . The stress energy tensor for spherically symmetric, point-like particles is given by

$$T^{(0),A}_{\mu\nu}(x) = \int \mathrm{d}\tau_A \, m_A u^A_\mu u^A_\mu \frac{\delta^4(x - z^{(0)}_A)}{\sqrt{-g}} \,. \tag{1.14}$$

Plugging this into Eq. (1.13) and solving for the retarded metric perturbation yields

$$\bar{h}^{(1)}_{\mu\nu}(x) = 4 \sum_{A=1,2} m_A u^A_\mu u^A_\nu \frac{1}{r_A}, \tag{1.15}$$

[3]The notion of treating compact objects as point particles can be refined in WEFT, see Sec. 1.3.

where $r_A = \{(x - z_A)^2 + [u_A \cdot (x - z_A)]^2\}^{1/2}$ is the spatial distance of the coordinate point x^μ from $z_A^{(0),\mu}(\tau)$ in each particle's rest frame. Here τ is the proper time at which x lies on the future light cone of $z^\mu(\tau)$.

We can now substitute Eq. (1.15) into the geodesic equation written in the form

$$\frac{\mathrm{d}p_{\mathrm{A}\mu}}{\mathrm{d}\tau_{\mathrm{A}}} = -\frac{1}{2}\partial_\mu g^{\alpha\beta}(x_{\mathrm{A}})p_{\mathrm{A}\alpha}p_{\mathrm{A}\beta}, \tag{1.16}$$

and then integrate from $-\infty$ to $+\infty$ to obtain the impulse. This yields

$$\Delta p_{A\mu}^{(1)} = -\frac{1}{2}\int_{-\infty}^{+\infty} \mathrm{d}\tau_{\mathrm{A}}\, \partial_\mu g^{\alpha\beta}(x_{\mathrm{A}})p_{A\alpha}^{(0)}p_{A\beta}^{(0)}, \tag{1.17}$$

which evaluates to

$$\Delta p_1^{(1),\mu} = -\Delta p_2^{(1),\mu} = -\frac{2m_1m_2}{\sqrt{\gamma^2 - 1}}(2\gamma^2 - 1)\frac{b^\mu}{|b|^2}, \tag{1.18}$$

where $\gamma = -u_1 \cdot u_2$. We can subsequently use the impulse to evaluate observables such as the scattering angle in the center-of-momentum (COM) frame (frame of reference in which the spatial components of total momentum is zero). In particular, the key quantity needed is the norm of the spatial components of the initial momentum, i.e., $|p_1|_3$ in the COM frame, which can be evaluated at zeroth order. Using relativistic kinematics, it can be shown that [1]

$$|p_1|_3 = \frac{m_1m_2\gamma v}{E}, \tag{1.19}$$

where $E = \sqrt{m_1^2 + m_2^2 + 2m_1m_2\gamma}$ is the total energy in the COM frame, and $v = \sqrt{1 - \gamma^{-2}}$ is the relative velocity.

The scattering angle χ can then be obtained by noting that it is related to the component of the impulse $\Delta p_1^{(1)}$ along the impact parameter b^μ, while the initial momentum has a vanishing component along b^μ (see Fig. 1.2). For $\chi \ll 1$, $\sin(\chi) \approx \chi$, and we have

$$\chi = \frac{\Delta p_1^{(1)} \cdot b}{|p_1|_3|b|}. \tag{1.20}$$

Substituting the expressions for the impulse and the spatial momentum, we obtain

$$\chi = \frac{E\Delta p_1^{(1)} \cdot b}{m_1 m_2 \gamma v |b|} = -\frac{2E(2\gamma^2 - 1)}{\gamma^2 v^2 |b|}. \tag{1.21}$$

Thus, we conclude the scattering problem at 1PM. Note that there is no radiation emitted at this order, and thus the final state consists only of two bodies asymptotically far away.

In Chapter 2, we perform a similar computation as above to third order for EM, where the post-Lorentzian (PL) expansion is employed to iteratively solve the problem in the weak-deflection regime. The PL expansion is analogous to the PM expansion used in GR, except that electromagnetic interaction between the two bodies is perturbatively included in the regime of weak deflection. We also derive relations mapping scattering observables, such as the radiated energy and angular momentum to those in the bound inspiral scenario and demonstrate their validity for both EM and GR.

1.2.2 Gravitational Raman/Compton scattering

The use of scattering events to probe molecular structures and particle interactions has been fundamental in shaping our understanding of the universe. Raman scattering [160] involves the inelastic scattering of light off molecules with vibrational or rotational modes, providing insights into the molecular structure. Compton scattering [161], on the other hand, refers to the interaction of high-energy photons with electrons, whether free or bound, to study relativistic kinematics and their surrounding environment.

In this dissertation, the terms gravitational Compton scattering and gravitational Raman scattering are used to refer to the scattering of (linearized) GWs off compact objects such as BHs and NSs. Raman scattering is used in contexts where internal excitations of the compact object, such as the induction of tidal multipoles, also become relevant. Thus, Raman scattering is treated as the more general term, encompassing also Compton scattering. The aim is to gain insight into how these objects couple to external gravitational fields by analyzing their response to GW perturbations in a scattering framework. For brevity, the prefix gravitational may be omitted in what follows when no confusion arises.

The simplicity of the setup in gravitational Raman scattering, consisting of a single compact object perturbed by weak radiation, makes it analytically tractable through various approaches in a low-frequency expansion, where the wavelength of the radiation is much larger than the size of the body ($\lambda_{\rm GW} \gg \mathcal{R}$). The fact that this regime is amenable to a wide range of analytical and numerical methods makes it an excellent tool for calibrating different techniques used to model compact objects, as well as for gaining deeper insights into the physical interactions involved.

A natural classical approach to solving this scattering problem is via BHPT, which is introduced in Sec. 1.4. The study of GWs scattering off compact objects has a long history, beginning around 1970 with C. V. Vishveshwara's numerical investigation [162] of axial GW perturbations scattering off Schwarzschild BHs. This was followed by analytical calculations by P. C. Peters [163] and by M. P. Ryan and R. A. Matzner [164], in the low-frequency limit for Schwarzschild BHs, and later extended to higher orders in frequency and to linear order in spin by Sam Dolan [165, 166]. More recently, this problem has gained renewed attention, as it has been shown that the Compton/Raman amplitude can also provide valuable insights into the dynamics of binary systems [3–5, 111, 115, 167–173]. This has led to further extensions of the computation to higher orders in spin [174], higher orders in frequency [4], and even to non-BH compact objects [5, 175]. Additionally, scattering processes involving scalar or electromagnetic fields off compact objects with strong gravitational fields have been studied as simpler toy models [135, 176].

Another way of approaching this problem in a classical framework is through WEFTs, which are discussed in Sec. 1.3. In this approach, compact objects are treated as point-particle worldlines, similar to the 1PM computation shown earlier in Sec. 1.2.1.1. This method is particularly useful when the wavelength of the perturbation is much larger than the object's size, allowing for an effective point-particle description. In WEFT, the compact object is replaced by a skeletonized stress-energy tensor in a weakly perturbed spacetime. However, unlike in BHPT, the worldline description of compact objects is not uniquely fixed a priori. As a result, the scattering amplitudes computed in this framework may contain free coefficients that must be determined by matching with full-theory results, often obtained via BHPT [3–5, 176]. In some cases, when these coefficients have already been constrained through simpler methods, WEFT can serve as a simpler and more efficient way to study the scattering process [2].

Here, as a pedagogical demonstration, we study the scattering of plane GWs at linear order in their frequency (more precisely, at $O(M\omega)$). In this limit, the spin of the BH, or other intrinsic properties, are irrelevant, and the computation is straightforward.

1.2.2.1 Low-frequency gravitational Compton scattering

Let us consider a plane GW in vacuum on flat Minkowskian background, moving along the z-axis in the rest-frame of the scattering body. We can write it nicely as $\bar{h}_{\mu\nu} = -\mathfrak{a}\,\varepsilon^{\mu}_{\pm}\varepsilon^{\nu}_{\pm}\exp[i\omega(z-t)]$. Here $\mathfrak{a}$ is the amplitude of the incident wave and we restrict to linear order in it. Let us further choose for it to be in the TT gauge. The vectors $\varepsilon^{\mu}_{\pm}$ are the helicity vectors, with $\varepsilon^{\mu}_{\pm} \equiv (1/\sqrt{2})\{0, 1, \pm i, 0\}$ corresponding to ± 2 helicities respectively. Note that this satisfies the Lorenz

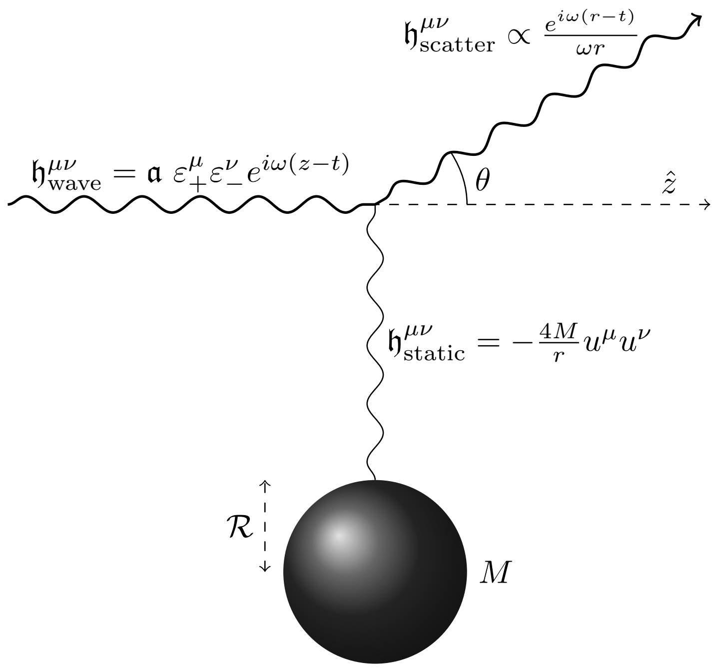

Figure 1.3: An incoming linearized plane GW scatters off a spinless body and its gravitational field, as viewed in the rest frame of the body. Here $\mathfrak{h}^{\mu\nu} = \sqrt{-g}g^{\mu\nu} - \eta^{\mu\nu} \approx -\bar{h}^{\mu\nu} + O(h^2)$, characterizes the metric perturbation over Minkowskian spacetime. We use harmonic coordinates (DeDonder gauge), and describe the waves in the TT gauge. The incoming plane wave is moving along the z-axis and has positive helicity, as characterized by the polarization vector $\varepsilon^{\mu} \equiv \{0, 1, i, 0\}$. It is monoharmonic with frequency $\omega \sim \lambda^{-1}_{\text{GW}}$, where $\mathcal{R}\omega \ll 1$, with $\mathcal{R}$ being the size of the scattering body. In this limit (and in this gauge), scattering is dominated by the nonlinear interaction between the static gravitational field of the body and the incoming plane wave. The resultant scattered wave takes the form of an outgoing, spherical, wave far away from the body. The accompanying tensor encodes the scattering amplitudes.

gauge condition. We assume the positive helicity for brevity in what follows.

We want to study how the plane wave interacts with a spinless object and its gravitational field at leading order in frequency. We then want to extract out the radiative outgoing part of the scattered wave that is generated from this interaction. The process is demonstrated in Fig. 1.3 below.

To that end, it is useful to rewrite the Einstein equation suggestively in the Landau-Lifshitz form as [46]

$$\eta^{\rho\sigma}\partial_\rho\partial_\sigma\mathfrak{h}^{\alpha\beta} = 16\pi\tau^{\alpha\beta}, \tag{1.22a}$$

$$\tau^{\alpha\beta} = |g|T^{\alpha\beta} + \frac{1}{16\pi}\Lambda^{\alpha\beta}, \tag{1.22b}$$

$$\begin{aligned}\Lambda^{\alpha\beta} = &-\mathfrak{h}^{\mu\nu}\partial^2_{\mu\nu}\mathfrak{h}^{\alpha\beta} + \partial_\mu\mathfrak{h}^{\alpha\nu}\partial_\nu\mathfrak{h}^{\beta\mu}\\ &+ \frac{1}{2}g^{\alpha\beta}g_{\mu\nu}\partial_\lambda\mathfrak{h}^{\mu\tau}\partial_\tau\mathfrak{h}^{\nu\lambda} - g^{\alpha\mu}g_{\nu\tau}\partial_\lambda\mathfrak{h}^{\beta\tau}\partial_\mu\mathfrak{h}^{\nu\lambda}\\ &- g^{\beta\mu}g_{\nu\tau}\partial_\lambda\mathfrak{h}^{\alpha\tau}\partial_\mu\mathfrak{h}^{\nu\lambda} + g_{\mu\nu}g^{\lambda\tau}\partial_\lambda\mathfrak{h}^{\alpha\mu}\partial_\tau\mathfrak{h}^{\beta\nu}\\ &+ \frac{1}{8}(2g^{\alpha\mu}g^{\beta\nu} - g^{\alpha\beta}g^{\mu\nu})(2g_{\lambda\tau}g_{\epsilon\pi} - g_{\tau\epsilon}g_{\lambda\pi})\\ &\times\partial_\mu\mathfrak{h}^{\lambda\pi}\partial_\nu\mathfrak{h}^{\tau\epsilon},\end{aligned} \tag{1.22c}$$

$$\mathfrak{h}^{\mu\nu} = \sqrt{-g}g^{\mu\nu} - \eta^{\mu\nu}, \qquad \partial_\mu\mathfrak{h}^{\mu\nu} = 0 \tag{1.22d}$$

Here, $T^{\mu\nu}$ is the matter energy-momentum tensor. Note that for linear perturbations about flat spacetime, we can drop $\Lambda^{\alpha\beta}$, and substitute $|g| = 1$ in RHS. Additionally, we have $\mathfrak{h}^{\mu\nu} = -\bar{h}^{\mu\nu}$ at leading order, and the equation is then identical to Eq. (1.4). However, we are interested here in the case where the metric perturbation of the wave is subject to the background metric sourced by the body.

We now substitute into Eq. (1.22):

$$\mathfrak{h}^{\mu\nu} = -\bar{h}^{\mu\nu}_{\text{static}} + \mathfrak{a}\ \varepsilon^\mu\varepsilon^\nu\ \exp[i\omega(z-t)] + \mathfrak{a}\mathfrak{h}^{\mu\nu}_{\text{scatter}}, \tag{1.23}$$

where[4] $\bar{h}^{\mu\nu}_{\text{static}} = u^\mu u^\mu(4M/r) \equiv \delta^\mu_0\delta^\nu_0(4M/r)$ is the static metric perturbation of a spinless body in harmonic gauge at linear order in M (see Eq. (1.15)), and $\mathfrak{h}^{\mu\nu}_{\text{scatter}}$ is the waveform for the scattered wave to be solved for. Since we only want to work out the leading-order scattering computation, we collect terms of the order $O(M\mathfrak{a})$ in Eq. (1.23).

[4] $\bar{h}^{\mu\nu}$ was defined in Eq. (1.3).

We can infer from Eq. (1.22), that terms with the scaling $M\mathfrak{a}$ can arise on the RHS from products of $\bar{h}^{\mu\nu}_{\text{static}}$ (and derivatives) with $\mathfrak{a}\ \varepsilon^{\mu}\varepsilon^{\nu}\ \exp[i\omega(z-t)]$ (and derivatives). Additionally, they could arise from perturbations to $T^{\alpha\beta}$ of the body due to the plane wave. However, for a spinless body that can be approximated as a point particle — i.e., when the GW wavelength is much larger than the size of the object — the perturbations to its energy-momentum tensor $T^{\alpha\beta}$ can be neglected. As shown in Sec. 1.1.1.2, a GW in TT gauge does not displace a freely falling particle initially at rest. Since the expression for $T^{\alpha\beta}$ in Eq. (1.14) depends on the particle's position and velocity, which remain unchanged, it is not affected by the wave. Additionally, while $T^{\alpha\beta}$ also depends on the determinant g of the metric, this too remains unaltered at leading order, as the metric perturbation due to the incident wave is traceless and does not contribute to g at linear order in $\mathfrak{a}$. Consequently, in this limit, the scattering is governed solely by the nonlinear interaction between the incoming wave and the static gravitational field. Finally, we are only interested in the radiative (or on-shell) part of $\mathfrak{h}^{\mu\nu}_{\text{scatter}}$, and thus focus only on solving for its TT projection. The transversality w.r.t outgoing momentum will be imposed later, for now we just ignore the 0μ components of both sides in Eq. (1.22a) .

We then get the equation for the relevant part of the scattered wave as

$$(-\partial_t^2+\nabla^2)\mathfrak{h}^{ij}_{\text{rad,scatter}} = -\omega^2\frac{M}{r}\varepsilon^i\varepsilon^j\ \exp(i\omega(z-t)), \tag{1.24}$$

which can be solved for retarded boundary conditions as

$$\mathfrak{h}^{ij}_{\text{rad,scatter}}(t,\mathbf{x}) = \frac{\omega^2 M\varepsilon^i\varepsilon^j}{4\pi}\int \frac{e^{i\omega(z'-t+|\mathbf{x}-\mathbf{x}'|)}}{|\mathbf{x}-\mathbf{x}'|\,|\mathbf{x}'|}\,d^3\mathbf{x}', \tag{1.25}$$

which in the far-field limit, $|\vec{x}|=r\to\infty$, becomes

$$\mathfrak{h}^{ij}_{\text{rad,scatter}}(t,\mathbf{x}) \to \frac{M\omega\varepsilon^i\varepsilon^j}{8\pi\sin^2(\theta/2)}\frac{\exp(i\omega(t-r))}{\omega r}, \tag{1.26}$$

where θ is the angle between the direction of $\vec{x}$ and the incoming wave $\vec{k}$. This has the expected form of an outgoing spherical wave. Sufficiently far from the scattering body, the position vector $\vec{x}$ defines the direction of propagation, with the outgoing wavevector given by $\vec{l} = \omega\hat{x}$, where $\hat{x} = \vec{x}/r$. Thus, we want to project out the scattered wave orthogonal to it (so that it is transverse to the outgoing wave vector). We then get

$$\mathfrak{h}^{ij,\text{asymp}}_{\text{TT,scatter}}(x^\mu) = \frac{\exp(i\omega(t-r))}{\omega r}\frac{M\omega}{8\pi\sin^2(\theta/2)}[\cos^4(\theta/2)\zeta_+(\hat{x})^i\zeta_+(\hat{x})^j + \sin^4(\theta/2)\zeta_-(\hat{x})^i\zeta_-(\hat{x})^j]. \tag{1.27}$$

Here $\zeta_\pm(\hat{x}) \equiv (0, \cos\theta, \pm i, -\sin\theta)$ are the polarization vectors for outgoing radiation, satisfying the transversality condition $\zeta(\hat{x}) \cdot \vec{l} = 0$, and they are null vectors (thus the metric perturbation is traceless). The prefactors before them are proportional to the scattering amplitudes, with $\mathcal{M}_{++} \sim \cos^4(\theta/2)/\sin^2(\theta/2)$ and $\mathcal{M}_{+-} \sim \sin^2(\theta/2)$, being the amplitudes for same-helicity vs opposite-helicity scattering. This can be seen more precisely in momentum space, as shown in Chapter 3 [2]. Note that time-reversal and parity invariance together fix the $\mathcal{M}_{-\pm}$ amplitudes as well, and thus we do not lose any generality by assuming a positive helicity incoming wave.

This concludes the solution to the scattering problem at leading order. The total differential scattering cross section (summing the modulus square of the amplitudes over final states) can then be computed to be

$$\left|\frac{d\sigma}{d\Omega}\right| = M^2\frac{\sin^8(\theta/2) + \cos^8(\theta/2)}{\sin^4(\theta/2)}. \tag{1.28}$$

which is consistent with earlier results [135, 164].

Going beyond the low-frequency/large-wavelength limit requires methods to perturbatively incorporate the features of the compact object and higher-order corrections to its static field. Additionally, the dynamics of the compact object, in response to the incident wave, also need to be taken into account. This can be done systematically in either BHPT or WEFT frameworks. In Chapter 3 [2], we compute the gravitational Compton amplitude for parity-invariant spinning bodies up to third order in spin and at leading order in the mass M, incorporating spin-induced quadrupole and octupole moments in a WEFT framework. In Chapters 4, 5, 6, [3–5] we match solutions to the Raman scattering problem obtained through BHPT and WEFT, in order to constrain tidal effects in BHs and NSs.

Given the central role of Compton/Raman scattering process in this dissertation and the focus on solving it using both WEFT and BHPT, it is important to discuss these two approaches in greater detail, which we do in the following sections.

1.3 EFT approach to modeling compact objects

A variety of compact objects may inhabit gravitating binaries. While BHs [177] and NSs [178, 179] are the most likely and astrophysically justified candidates, a variety of other compact object models have been proposed to resolve conceptual issues associated with BHs, or GR, and also to probe the possibility of new fields in the universe or modified theories of gravity [89, 180]. Even within GR, BHs and NSs can exhibit significant variation due to properties like spin and, in the case of NSs, the underlying EOS [181]. Modeling this richness in full microscopic detail is very challenging, owing to the rich and incompletely understood microscopic physics and/or due to the calculational complexity arising from the nonlinearity of GR. However, within the inspiral regime, it is possible to treat the compact objects in an approximate manner in a WEFT framework [47, 48, 51, 182]. We briefly outline this below, partially following the discussions in Ref. [182] and other comprehensive reviews [47, 48].

In the WEFT approach, we exploit the separation of scales present in the binary-inspiral problem. The relevant scales for the same are a) the size of the compact object(s) $\sim \mathcal{R}$, b) the separation between the objects $\sim r$, c) the wavelength of emitted radiation $\sim \lambda_{\rm GW} \sim \omega_{\rm GW}^{-1} \sim \sqrt{r^3/M_{\rm T}}$. During the inspiral, we can write $\mathcal{R} \ll r \ll \lambda_{\rm GW}$. Accordingly, the dynamics of compact objects can be treated using worldlines when we are interested in studying orbital dynamics, and the binary itself may be treated as a worldline when we are interested in studying GW radiation by the system as a whole. This is illustrated in Fig. 1.3. In this dissertation however, we will mostly be interested in the former, i.e., the treatment of compact objects as worldlines when modeling the binary dynamics.

A WEFT description for a single body can be constructed by identifying the relevant infrared (IR) degrees of freedom required to describe its dynamics. While the object itself may carry essentially infinite degrees of freedom, it should still appear point-like when viewed from 'afar' and primarily described by a worldline $z^\mu(s)$. The precise notion of 'afar' can be understood if we think of perturbing the particle via say a gravitational field with a characteristic wavelength $\lambda \sim \omega^{-1}$. As long as $\lambda \gg \mathcal{R}$, or alternatively $\mathcal{R}\omega \ll 1$, the interaction of the field and object can be viewed as that between a field and a worldline. This also brings with it an additional relevant IR degree of freedom $g_{\mu\nu}(x)$, the metric field.

We briefly demonstrate the construction of WEFTs, and the inclusion of finite-size effects in the following subsections.

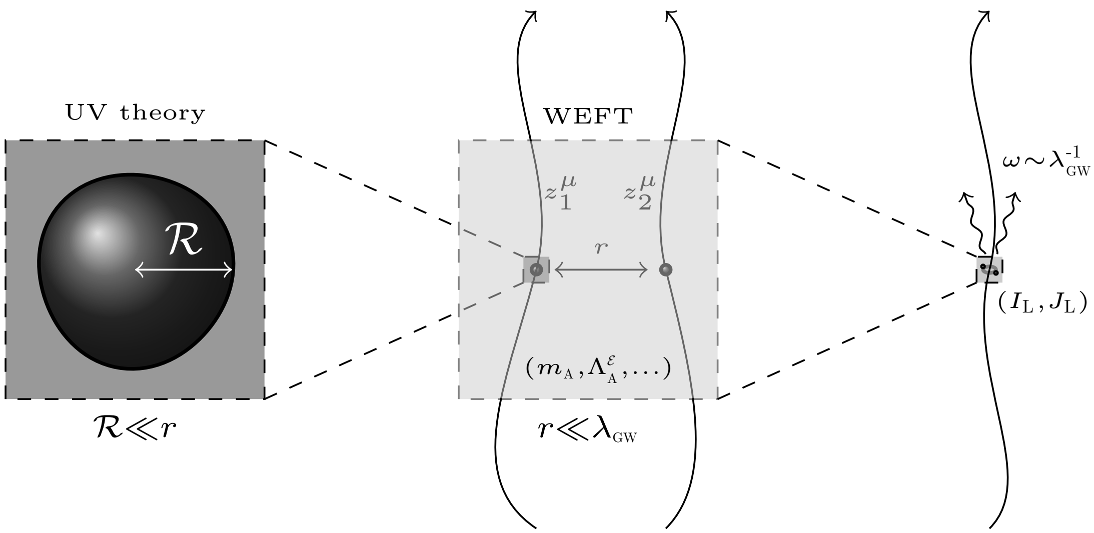

Figure 1.4: During the inspiral, the characteristic size of compact objects is much smaller than their separation, $\mathcal{R} \ll r$. This separation of scales enables an EFT approach, where the system is described in terms of the infrared degrees of freedom — namely, the worldlines of the objects and the gravitational field mediating their interaction. The complex ultraviolet dynamics of the compact objects can be systematically incorporated through operators in a worldline action, each accompanied by Wilson coefficients $(m_A, \Lambda_A^{\mathcal{E}} \ldots)$ that encode the object's specific properties. To maintain locality, while capturing effects such as spin and tidal dissipation, additional degrees of freedom may be introduced (see Sec. 1.3.2 and Sec. 1.3.3.2). Similarly, the binary as a whole can be described as an EFT when we are interested in the radiation emitted by the system, in which case the binary may be described by several radiative multipoles (I_L, J_L), which evolve due to the dynamics of the binary components and radiation reaction due to emitted GWs.

1.3.1 The point-particle limit

It is reasonable to assume that in the limit $\mathcal{R}\omega \to 0$, the dynamics are entirely described by an action with the worldline $z^\mu(s)$, and the metric $g_{\mu\nu}$ as the degrees of freedom. We need to write down the most general action in terms of them. We should also demand general covariance, and reparametrization invariance (i.e., invariance under $s \to s'$) from the action. We can then write :

$$S = S_{\rm pp}[g_{\mu\nu}, x^\mu(s)] + S_{\rm EH}[g_{\mu\nu}], \tag{1.29}$$

where $S_{\rm EH}[g_{\mu\nu}]$ is the Einstein-Hilbert action governing the metric field.

We can further expand $S_{\rm pp}$ as a series based on number of spacetime derivatives acting on the metric field. This is correct since the WEFT description is valid when the field varies slowly over the size of the body. We can then write $S_{\rm pp} = S_{\rm pp}^{(0)} + S_{\rm pp}^{(1)} + \dots$. The leading term, $S_{\rm pp}^{(0)}$ is then uniquely fixed by reparametrization invariance and general covariance as

$$S_{\rm pp}^{(0)} = -m \int \sqrt{-g_{\mu\nu}\frac{dz^\mu}{ds}\frac{dz^\nu}{ds}} ds = -m \int d\tau, \tag{1.30}$$

which is simply the action for a test particle. Here τ is the proper time. For the compact object, we can interpret τ as the time measured by an observer sufficiently far away but comoving with the object. Varying this w.r.t the worldline simply yields the geodesic equation.

Note however that the free parameter m cannot be constrained based on symmetries or invariances. Such free parameters in an EFT are called Wilson coefficients. They can be fixed by matching with a known result. To that end, we can instead vary the action $S_{\rm EH}[g_{\mu\nu}] + S_{\rm pp}^{(0)}$ w.r.t the metric field to get the Einstein equation:

$$G^{\mu\nu} = 8\pi T^{\mu\nu}|_{\rm pp} = 8\pi\, m \int d\tau \frac{\delta^{(4)}(x^\alpha - z^\alpha(\tau))}{\sqrt{-g}} \frac{dz^\mu}{d\tau}\frac{dz^\nu}{d\tau}. \tag{1.31}$$

Now, treating the metric perturbatively over flat spacetime, we can evaluate this integral in Minkowskian coordinates in the rest frame where $\frac{dz^\mu}{d\tau} = \{1, 0, 0, 0\}$, yielding

$$T^{\mu\nu}|_{\text{pp,flat}} = m\delta^{(3)}(\vec{x})\delta^\mu_0\delta^\nu_0. \tag{1.32}$$

Similarly, we can evaluate the Einstein tensor to linear order in the metric perturbation $h_{\mu\nu}$. In the harmonic gauge where $\partial_\nu h^{\mu\nu} = \frac{1}{2}\delta^\mu h$ with $h = h^\mu{}_\mu$. we get:

$$\Box\bar{h}^{\mu\nu} = -16\pi m\delta^{(3)}(\vec{x})\delta^\mu_0\delta^\nu_0, \tag{1.33}$$

with the solution $\bar{h}_{\mu\nu} = (4m/r)u_\mu u_\nu$, and $h_{\mu\nu} = (2m/r)(2u_\mu u_\nu + \eta_{\mu\nu})$. In the rest frame of the body, $u^\mu \equiv (1, 0, 0, 0)$, we can then write

$$ds^2 = -\left(1 - \frac{2m}{r}\right)dt^2 + \left(1 + \frac{2m}{r}\right)\delta_{ij}dx^i dx^j. \tag{1.34}$$

Now, we can compare this with the Schwarzschild metric after transforming to identical coordinates at large distances from the origin, where it may be viewed as a weak perturbation over flat spacetime (equivalently, at linear order in mass of the body). The metric of a spherically symmetric object in the deDonder gauge at large distances from the object is

$$ds^2 = -\left(1 - \frac{2M_{\text{ADM}}}{r}\right)dt^2 + \left(1 + \frac{2M_{\text{ADM}}}{r}\right)\delta_{ij}dx^i dx^j + O\left(\frac{1}{r^2}\right), \tag{1.35}$$

Matching Eqs. (1.34) and (1.35), we find that M_{ADM} can be identified with the parameter m in the WEFT. This is a simple, pedagogical example of a matching computation.

1.3.2 Incorporating spin effects

As $\mathcal{R}\omega$ increases — equivalently, as the binary contracts during the inspiral and $\mathcal{R}/r$ grows — finite-size effects become increasingly significant, and the point-particle approximation no longer suffices. The principles for inclusion of additional effects are quite straightforward in a WEFT, merely requiring additional degrees of freedom and coupling terms to be incorporated into the action [51]. An important such finite-size effect is the spin of a compact object, which can be incorporated by including an orthonormal tetrad of vectors $e_A{}^\mu(s)$, satisfying $e_A{}^\mu e_{B\mu} = \eta_{AB}$, $e_A{}^\mu e^{A\nu} = g^{\mu\nu}$ [183], as additional degrees of freedom. The tetrad can be imagined as rigidly fixed to the body, and corotating with it. The angular velocity of the body in the local frame can be identified with $\Omega_{AB} = e_A{}^\mu De_{B\mu}/Ds = -\Omega_{AB}$. Here D/Ds is used to denote the covariant derivative along the worldline.

Now, we can once again construct a general worldline action, except that we now additionally demand the action to be invariant under boosts and rotations of the local frame indices $A, B, \ldots$. This means that the new degrees of freedom, the tetrad vectors, can only appear through the combination $\Omega_{\mu\nu} = \Omega_{AB}e^A{}_\mu e^B_\nu$ in the action. We provide here a brief and particularly simple treatment of a spinning particle following the implicit action approach in [184].

As an illustration, let us consider a simple action of the form

$$S = \int dsL(\dot{z}^\mu = \frac{dz^\mu}{ds}, \Omega_{\mu\nu}, g_{\mu\nu}) \tag{1.36}$$

It is convenient to leave it implicit for now. We can define the linear momentum and spin as

$$p_\mu = \frac{\partial L}{\partial \dot{z}^\mu}, \quad S_{\mu\nu} = 2\frac{\partial L}{\partial \Omega^{\mu\nu}}. \tag{1.37}$$

Now, the equation for the spin can be obtained by varying the action w.r.t e^μ_A under the constraints restricting an orthonormal tetrad. A simple way to implement that is by writing the variation $\delta e^\mu_A = \theta_{AB}e^{B\mu}$, where $\theta_{AB} = -\theta_{BA}$. This trivially satisfies the orthonormality constraints, and variation yields the relation

$$\frac{DS^{\mu\nu}}{D\tau} = 2\Omega^{[\mu}{}_\rho S^{\nu]\rho}, \tag{1.38}$$

where [...] is the antisymmetrized sum over the contained indices. Now, consider an infinitesimal, local Lorentz transformation of the form $\delta V^\mu = \Lambda^\mu{}_\nu V^\nu$, where $\Lambda^{\mu\nu} = -\Lambda^{\nu\mu}$. The metric tensor $g_{\mu\nu}(z)$ is unaffected, whereas $\delta\dot{z}^\mu = \Lambda^\mu{}_\nu \dot{z}^\nu$, and $\delta\Omega^{\mu\nu} = \Lambda^\mu{}_\alpha \Omega^{\alpha\nu} + \Lambda^\nu{}_\alpha \Omega^{\mu\alpha}$. The invariance of the Lagrangian under an arbitrary transformation then yields $p^{[\mu}\dot{z}^{\nu]} + S^{[\mu}{}_\rho \Omega^{\nu]\rho} = 0$. Thus, we have

$$\frac{DS^{\mu\nu}}{D\tau} = 2p^{[\mu}u^{\nu]}, \quad u^\nu = \frac{\dot{z}^\nu}{\sqrt{-g_{\alpha\beta}\dot{z}^\alpha \dot{z}^\beta}}, \; u^2 = -1. \tag{1.39}$$

We can similarly get the momentum equation by varying the action w.r.t worldline, yielding

$$\frac{Dp_\mu}{D\tau} = -\frac{1}{2} R_{\mu\nu\rho\sigma} u^\nu S^{\rho\sigma}. \tag{1.40}$$

Eqs. (1.39) and (1.40) are known as the Mathison-Papapetrou-Dixon (MPD) equations [185–188]. Specifically, they are the MPD equations to linear order in spin, where spin-induced deformation can be neglected. Note however that we still do not know the relationship between p^μ and u^μ. An implicit Lagrangian is insufficient for that. Without that knowledge, the MPD equations are insufficient for time evolution. To eliminate u^μ, we need three extra conditions. This is done by imposing a spin supplementarity condition (SSC) [189], which accounts for the fact that there is ambiguity in choosing a particular worldline as representing a given compact object due to its finite-size [190]. The SSC also reduces the antisymmetric spin tensor $S^{\mu\nu}$ from six to three physical degrees of freedom, as expected for spin in a spacetime with three spatial dimensions. Various SSCs appear in the literature, all of which correspond to choosing a time-like vector v^μ and imposing $S^{\mu\nu}v_\nu = 0$. While v^μ may be a dynamical vector that evolves along the worldline, not all choices lead to consistent dynamics. In particular, the Pirani condition $v^\mu = u^\mu$ [30] is known to produce pathological motion and is inconsistent at higher orders in spin [191]. A well-motivated and widely used choice is to take $v^\mu = p^\mu$, known as the Tulczyjew–Dixon condition [187, 189, 191], which selects a unique representative worldline and yields a consistent relation between p^μ and u^μ. In the Newtonian limit, this corresponds to identifying the worldline with the center of mass.

Then, we can obtain the relationship between u^μ and p^μ by writing $D(S^{\mu\nu}p_\nu)/Ds = 0$ and using Eqs. (1.39), (1.40) along with the constraint $p^2 = -m^2$ to obtain

$$p^\mu = mu^\mu + \mathcal{O}(S^2), \tag{1.41}$$

completing the system of equations.

An explicit action consistent with the linear-in-spin MPD equations and relationship (1.41) is given by

$$S = \int d\sigma \left[-\left(m - \frac{J^2}{4\mathcal{I}}\right)\upsilon + \frac{\mathcal{I}}{4\upsilon}\Omega^{\mu\nu}\Omega_{\mu\nu} \right], \;\; \upsilon = \sqrt{-\dot{z}^\mu \dot{z}^\nu g_{\mu\nu}} \tag{1.42}$$

where $J = \sqrt{S_{\mu\nu}S^{\mu\nu}}$ is the conserved intrinsic angular momentum (magnitude of spin) and $\mathcal{I}$ is the moment of inertia. From this action, we can obtain

$$S_{\mu\nu} = \mathcal{I}\Omega_{\mu\nu}, \quad p_\mu = mu_\mu. \tag{1.43}$$

Since the explicit action has the same form as the implicit one used earlier, it reproduces the MPD equations at linear order in spin as well. Note that we use the constraint on the spin magnitude only at the level of the equations of motion in order to set $p^2 = -m^2$, and this is justified as it is a conserved quantity.

1.3.2.1 Spin-induced deformation

An important effect of spin in compact objects is to deform them, causing them to develop multipole moments, which in turn affects their motion in curved spacetime [192]. Spin-induced deformation can be systematically incorporated by including terms containing the curvature tensor $R_{\mu\nu\rho\sigma}$ in the action [183]. For instance, the spin-induced quadrupole moment may be incorporated by including a term linear in $R^{\mu\nu\rho\sigma}$ into the Lagrangian and defining

$$J_{\mathrm{Q}}^{\mu\nu\rho\sigma} = -6\frac{\partial L}{\partial R_{\mu\nu\rho\sigma}}, \text{ alternatively, we add, } \Delta S_{\mathrm{quad}} = \int d\tau \frac{-1}{6} J_{\mathrm{Q}}^{\mu\nu\rho\sigma} R_{\mu\nu\rho\sigma}. \tag{1.44}$$

where $J_{\mathrm{Q}}^{\mu\nu\rho\sigma}$ is built out of $S_{\mu\nu}$ and u^μ. We can then write the MPD equations to second order as [192]

$$\frac{DS^{\mu\nu}}{D\tau} = 2p^{[\mu}u^{\nu]} + \frac{4}{3}R^{[\mu}{}_{\lambda\rho\sigma}J_{\mathrm{Q}}^{\nu]\lambda\rho\sigma}, \tag{1.45}$$

$$\frac{Dp_\mu}{D\tau} = -\frac{1}{2}R_{\mu\nu\rho\sigma}u^\nu S^{\rho\sigma} - \frac{1}{6}J_{\mathrm{Q}}^{\lambda\nu\rho\sigma}\nabla_\mu R_{\lambda\nu\rho\sigma}. \tag{1.46}$$

Then, we can obtain the relationship between u^μ and p^μ in covariant SSC to be

$$p^\mu = mu^\mu - \frac{1}{2m}S^{\mu\nu}R_{\mu\lambda\rho\sigma}u^\lambda S^{\rho\sigma} + \frac{4}{3}R^{[\mu}{}_{\lambda\rho\sigma}J_{\mathrm{Q}}^{\nu]\lambda\rho\sigma}u_\nu, \tag{1.47}$$

completing the system of equations.

In Chapter 3 [2], we use this approach with covariant SSC to third order in spin, including spin-induced quadrupole and octupole moments for generic parity-preserving spinning compact objects to study the process of gravitational Compton scattering and compute the relevant scattering amplitudes.

1.3.3 Incorporating tidal deformation

In addition to spin and spin-induced deformation, an important class of finite-size effects are tidal effects, which arise due to the deformation of a body in response to an external tidal field. Similar to spin-induced multipole moments, tidal deformation leads to the development of quadrupole and higher-order multipole moments. An everyday example of this is the Earth's oceanic bulge due to the Moon's tidal field [193, 194].

In the Newtonian limit, tidal deformation can be understood as the fluid displacement (bulge) in an appropriate coordinate system. For an initially spherically symmetric body, the induced tidal quadrupole moment can be written as proportional to the external tidal field due to a mass m_{ext} in a binary system:

$$Q_{ij} \propto \mathcal{E}_{ij} \sim \partial_i \partial_j U \sim \frac{m_{\text{ext}}}{r^5} r_i r_j . \tag{1.48}$$

The tidally deformed body, having lost its spherical symmetry, also modifies the gravitational potential it sources. The Newtonian potential of a body with a quadrupole moment is given by [195]:

$$U = -\frac{m_{\text{body}}}{r} - \frac{1}{2} Q_{ij} \frac{x^i x^j}{r^5} . \tag{1.49}$$

The companion mass m_{ext} experiences this deformed potential, altering the dynamics of the binary. In GR, tidal interactions are more complex due to the additional degrees of freedom in the gravitational field encoded in the metric tensor $g_{\mu\nu}$. Moreover, coordinate invariance makes the definition of tidal deformation more subtle. Nevertheless, the WEFT formalism provides a systematic approach to incorporating tidal effects into the binary dynamics [51].

In fact, tidal deformation can be conveniently incorporated in a manner similar to spin-induced deformation, except that the multipole tensors $J_{\mathrm{Q}}^{\mu\nu\rho\sigma}, \ldots$ now also depend on the external field in the object's environment.

1.3.3.1 Conservative tides

Conservative tides can be included in WEFT by including terms which are quadratic in the Riemann curvature tensor into the action. In vacuum, the Riemann tensor reduces to the Weyl tensor $C_{\mu\nu\rho\sigma}$. The 10 independent components of the Weyl tensor can be decomposed into two symmetric trace-free rank-2 tensors using a normalized timelike vector v^μ — typically chosen as the normalized four-momentum p^μ/m, of the body being tidally deformed:

$$\mathcal{E}_{\mu\nu} = C_{\mu\rho\nu\sigma} v^\rho v^\sigma , \quad \mathcal{B}_{\mu\nu} = \tilde{C}_{\mu\rho\nu\sigma} v^\rho v^\sigma , \tag{1.50}$$

where $\tilde{C}_{\mu\nu\rho\sigma} = \frac{1}{2}\epsilon_{\mu\nu\alpha\beta} C^{\alpha\beta}{}_{\rho\sigma}$. The electric and magnetic parts of the Weyl tensor, $\mathcal{E}_{\mu\nu}$ and $\mathcal{B}_{\mu\nu}$, are symmetric, trace-free, and orthogonal to v^μ. In the frame defined by v^μ, it can be shown that $\mathcal{E}_{\mu\nu}$ reduces, in the Newtonian limit, to the familiar quadrupolar tidal field, scaling as $\sim \partial_i \partial_j U$. In this work, we refer to $\mathcal{E}^{\mu\nu}$, $\mathcal{B}^{\mu\nu}$, and their covariant derivatives — after symmetrization, and trace removal — as the tidal fields.

Leading, static, conservative tidal effects in a spherically symmetric compact body can then be captured through terms in the worldline action at fourth order in derivatives as

$$\begin{aligned} S^{(4)}_{\text{pp}} = S_{\text{finite-size}} = c_{\mathcal{E}} m \mathcal{R}^4 \int d\tau \, \mathcal{E}_{\mu\nu}\mathcal{E}^{\mu\nu} + c_{\mathcal{B}} m \mathcal{R}^4 \int d\tau \, \mathcal{B}_{\mu\nu}\mathcal{B}^{\mu\nu} \\ + \tilde{c}_{\mathcal{E}\mathcal{B}} m \mathcal{R}^4 \int d\tau \, \mathcal{B}_{\mu\nu}\mathcal{E}^{\mu\nu} , \end{aligned} \tag{1.51}$$

where the third term violates parity invariance and is generally disregarded. The coupling coefficients $c_{\mathcal{E}}$ and $c_{\mathcal{B}}$ correspond to the electric and magnetic Love numbers, respectively [56, 57, 193].

For spinning bodies, additional terms arise where indices contract with tensors built from the spin tensor, increasing the number of Wilson coefficients. Spin can also couple tidal tensors of different ranks. In Chapter 4 [3], we write the most general expression for the relevant coupling terms in the action for parity-preserving spinning bodies.

1.3.3.2 Dynamical and dissipative tides

More generally, tidal effects can be dynamical, meaning that a changing tidal environment alters the response of a body, modifying its dynamics. Leading, dynamical, conservative tidal effects can be captured by adding terms quadratic in the proper-time derivative of the tidal fields, for instance:

$$\Delta S_{\text{dyn.tides}} \sim \int d\tau\, \dot{\mathcal{E}}^{\alpha\beta}\dot{\mathcal{E}}_{\alpha\beta}, \tag{1.52}$$

where $\dot{\mathcal{E}}_{\alpha\beta} = D\mathcal{E}_{\alpha\beta}/D\tau$. However, dynamical tides can sometimes be associated with tidal resonances [196] which cannot be perturbatively captured using a finite number of terms with time derivatives. This necessitates introducing nonlocal terms in the action [51], such as:

$$\Delta S_{\text{dyn.tides}} \sim -\int d\tau d\tau' \mathcal{E}(\tau')\lambda(\tau' - \tau)\mathcal{E}(\tau). \tag{1.53}$$

To avoid the complications of nonlocal actions, an alternative approach is preferred.

Additionally, tidal effects can be dissipative, leading to energy exchange between the orbit and the compact objects [3, 5, 60, 64, 197–199]. For instance, in the Earth-moon system, the Earth loses rotational energy and angular momentum to the orbital motion due to oceanic -fluid viscosity. In BHs, the event horizon, and in NSs, fluid viscosity, can lead to similar effects. Such dissipative effects violate time-reversal invariance and therefore cannot be included directly via quadratic-in-curvature terms in the usual worldline action. For example, adding a term of the form

$$\int d\tau \dot{\mathcal{E}}^{\mu\nu}\mathcal{E}_{\mu\nu} \tag{1.54}$$

would be fruitless, as it is a total time derivative.

Instead, dynamical tides — including dissipative effects — can be incorporated analogously to spin-induced multipoles. For instance, quadrupolar tidal effects can be captured by adding a term to the action of the form $J_{\mathrm{Q}}^{\mu\nu\rho\sigma}R_{\mu\nu\rho\sigma}$. However, unlike in the spin case where $J_{\mathrm{Q}}^{\mu\nu\rho\sigma}$ is constructed purely from intrinsic quantities such as the spin tensor and four-velocity, here it is treated as a time dependent dynamical multipole moment. It is convenient to express $J_{\mathrm{Q}}^{\mu\nu\rho\sigma}$ as [3]

$$J_{\mathrm{Q}}^{\mu\nu\rho\sigma} = 3v^{[\mu}Q_{\mathcal{E}}^{\nu][\rho}v^{\sigma]} - \frac{3}{2}Q_{\mathcal{B}}^{\alpha\langle\rho}\epsilon_{\beta\alpha}{}^{\mu\nu}v^{|\beta|}v^{\sigma\rangle_{\mathrm{R}}}, \tag{1.55}$$

where $[..]$ represents anti-symmetrization of indices, and $\langle...\rangle_{\mathrm{R}}$ means symmetrization of the contained indices (except $|\beta|$) according to the symmetries of the Riemann tensor $R^{\mu\nu\rho\sigma}$. This allows us to rewrite the term in the action as

$$\Delta L_{\mathrm{quad}} = -\frac{1}{6}J_{\mathrm{Q}}^{\mu\nu\rho\sigma}R_{\mu\nu\rho\sigma} = -\frac{1}{2}Q_{\mathcal{E}}^{\mu\nu}\mathcal{E}_{\mu\nu} - \frac{1}{2}Q_{\mathcal{B}}^{\mu\nu}\mathcal{B}_{\mu\nu}. \tag{1.56}$$

This brings the action into a more intuitive form, where the tidal deformation is described by an electric and a magnetic quadrupole moment tensor, both of which are symmetric, trace-free, and orthogonal to v^μ (typically the normalized four-momentum p^μ/m), and couple to the tidal fields $\mathcal{E}_{\mu\nu}$ and $\mathcal{B}_{\mu\nu}$. It can be shown that the quadrupole moment defined in this manner corresponds to the physical quadrupole in the Newtonian limit.

We then promote $Q_{\mathcal{E}}$ and $Q_{\mathcal{B}}$ to dynamical degrees of freedom living on the worldline [197], and accordingly modify the action to include terms describing their time evolution:

$$S = S_{\mathrm{pp}} - \int d\tau \frac{1}{2}Q_{\mathcal{E}}^{\mu\nu}\mathcal{E}_{\mu\nu} - \int d\tau \frac{1}{2}Q_{\mathcal{B}}^{\mu\nu}\mathcal{B}_{\mu\nu} + S[Q_{\mathcal{E}}, Q_{\mathcal{B}}, X, \dots], \tag{1.57}$$

where X accounts for additional degrees of freedom that the object may possess. These additional degrees of freedom can couple to the multipole moments, enabling a wide range of tidal interactions. In particular, if X contains a sufficiently large number of internal degrees of freedom coupled to $Q_{\mathcal{E}}$ and $Q_{\mathcal{B}}$, it can give rise to tidal dissipation, as the tidal energy stored in the multipole moments may be irreversibly transferred to these internal modes [61, 197]. Restricting to conservative tides, the action for the tidal quadrupole can be written in analogy with that of a harmonic oscillator, which is a good approximation for compact objects such as NSs. [200].

More generally, inclusion of dissipative effects explicitly in the action is a challenge in the WEFT formalism as presented here. This is relevant not only for including the dissipative tidal response of a compact object, but also for the radiation-reaction forces experienced by a binary due to GW radiation. This ultimately follows from the fact that the action formalism presented here is the ''in-out" formalism, which corresponds to assuming vacuum boundary conditions in the distant past and future [201]. This necessitates the inclusion of dissipation at the level of equations of motion (see below Sec. 1.3.3.3). An alternative approach involves using the ''in-in'' formalism, where dissipation is manifestly taken into account with the help of doubled degrees of freedom, and the boundary conditions correspond to the physical boundary conditions corresponding to a vacuum state in the distant past, but no constraints are enforced on the distant future. We do not employ this formalism in this work, but the ''in-in'' formalism is very useful to work consistently within an action formalism [69, 202, 203]

1.3.3.3 Tidal response

Writing an explicit action describing the dynamics of the tidal multipoles along with any additional degrees of freedom X, is in general very difficult, especially for BHs. It is far more convenient instead to take inspiration from linear-response theory. Linear-response theory is valid when both tidal field amplitudes and the induced response remain small. This holds during the early and mid-inspiral phases of a binary, but breaks down near resonances, tidal disruptions, or strong-field regimes. Nonetheless, linear theory is commonly applied throughout the inspiral, even in resonance-involving scenarios such as for systems containing NSs [200]. Rigorous studies are needed to quantify its regime of validity and to incorporate nonlinear tidal effects. While some progress has been made on static nonlinear tides within the WEFT framework [204], a complete dynamical nonlinear treatment remains open. In this work, we assume the validity of linear response theory throughout the inspiral.

The multipole moments should be induced by the tidal fields. For spherically symmetric, parity-invariant bodies, $Q_{\mathcal{E}}^{\mu\nu}$ ($Q_{\mathcal{B}}^{\mu\nu}$) can only be induced by $\mathcal{E}_{\mu\nu}$ ($\mathcal{B}_{\mu\nu}$). Further, for weak external tidal fields, we can restrict to a linear response and write

$$Q_{\mathcal{E}}^{\mu\nu} = -\frac{1}{2}\int_{-\infty}^{\tau} d\tau' g(\tau - \tau')\mathcal{E}^{\mu\nu}(\tau'), \tag{1.58}$$

and similarly for $\mathcal{E} \leftrightarrow \mathcal{B}$. The induction is nonlocal but in the limit of slowly changing fields (such as during early inspiral), we can rewrite this as a local expression of the form

$$Q_{\mathcal{E}}^{\mu\nu}(\tau) = -M^5[\Lambda^{\mathcal{E}} - MH_{\omega}^{\mathcal{E}}\frac{D}{D\tau} + \ldots]\mathcal{E}_{\mu\nu}, \tag{1.59}$$

and similarly for the magnetic sector. Note that this further restricts our analysis to quasi-stationary scenarios, where the external tidal field varies slowly. It can be shown that contributions from terms containing more time derivatives enter at higher PN orders. Nevertheless, regardless of PN order, the terms containing more time derivatives are important when nonperturbative effects, such as tidal resonances, become relevant. In this work, we do not consider tidal resonances, and restrict to the regime where tidal effects are slowly varying. The unknown coefficients entering it — $\Lambda_{\mathcal{E}}, H_{\omega}^{\mathcal{E}}$, are the Love and dissipation numbers, respectively. More generally, we refer to the coefficients relating the tidal fields to the tidal multipoles as tidal-response coefficients in this dissertation.

Equipped with the action and the linear tidal response, both conservative and dissipative tidal effects can be studied systematically in the worldline framework. As mentioned earlier, it is also possible to work only with a worldline action, without accepting the tidal response as a separate input, within the ''in-in'' formalism.

Once again, spin introduces several complexities regarding which tidal multipoles can be induced by which tidal fields, and also in the form of the response. In Chapter 4 [3] and 5 [4], we show the most general expression for the tidal response of a parity-invariant spinning body. We also classify the coefficients as conservative and dissipative based on the time-reversibility of the terms they accompany.

However, the picture remains incomplete without a method to fix the coefficients entering the tidal response. Without this final step, the WEFT can represent a wide class of compact objects. In contrast to the mass parameter m, which can be identified with M_{ADM} by examining the static metric sourced by the object, the tidal-response coefficients do not appear in the metric of an unperturbed body. Instead, one must appeal to observables involving perturbations. In this dissertation, we generally rely on the gravitational Raman amplitude — corresponding to the scattering of GWs off a compact object (e.g., a BH) — to fix the tidal-response coefficients in WEFT. This approach is particularly convenient because the Raman scattering problem can be solved relatively easily for isolated objects within BHPT. We therefore briefly review aspects of BHPT relevant to this approach in the next section.

1.4 Black hole perturbation theory

A stationary BH is described by a metric that depends only on its mass, charge and angular momentum [205, 206]. In astrophysical scenarios, charged BHs are unlikely and the most important BH solution is thus described by the well known Kerr metric, first obtained by Roy Kerr [207]. The Kerr metric encodes all the spin-induced multipoles ($J_{\mathrm{Q}}^{\mu\nu\rho\sigma}, \ldots$), aside from the mass M (monopole moment) and angular momentum J (dipole moment), of an unperturbed spinning BH [208].

In the Boyer-Lindquist (BL) coordinates, it is given by

$$\begin{aligned} ds^2 = &-\left(1 - \frac{2Mr}{\Sigma}\right) dt^2 - \frac{4Mar\sin^2\theta}{\Sigma} dt d\phi + \frac{\Sigma}{\Delta} dr^2 + \Sigma d\theta^2 \\ &+ \left(r^2 + a^2 + \frac{2Ma^2 r\sin^2\theta}{\Sigma}\right) \sin^2\theta d\phi^2, \end{aligned} \tag{1.60}$$

where $\Sigma = r^2 + a^2\cos^2\theta$, and $\Delta = r^2 - 2Mr + a^2$, and $a = J/M$. The roots of Δ are the radial coordinates of the outer and inner horizon (r_+ and r_-). In the spinless limit, $r_+ \to 2M$ and $r_- \to 0$.

However, in a binary, a BH is perturbed by the companion, and it thus becomes relevant to also study the dynamics of the perturbed Kerr solution. During the inspiral, as the two BHs are separated by a large distance compared to their sizes $r \gg \mathcal{R} \sim M$, we can treat the perturbation as small, and restrict to linear perturbation theory. This significantly simplifies the problem, making it analytically tractable. This is also true when a BH is perturbed by a weak GW, such as in the Raman-scattering scenario.

Intuitively, one might approach this problem by perturbing the metric in Eq. (1.60), and then deriving the Einstein equation to linear order in the perturbations. This program has been successful in the Schwarzschild case, where the metric perturbation equations can be reduced to a single scalar equation — the Regge Wheeler (RW) [209] equation or the Zerilli equation [210]. This is not so in the case of Kerr BHs.

However, another approach based on the Newmann-Penrose null-tetrad formalism [211], where one studies the equations governing the components of the Weyl tensor, projected onto the null tetrad, has been much more successful. In this case, a single master equation — the Teukolsky equation — can be obtained, which captures the dynamics of the linearly perturbed Kerr spacetime, and is separable [212, 213].

1.4.1 Teukolsky equation

Let us define four null vectors $n^\mu, l^\mu, m^\mu, \bar{m}^\mu$ satisfying $l \cdot n = 1, m \cdot \bar{m} = -1, l \cdot m = l \cdot \bar{m} = n \cdot m = n \cdot \bar{m} = 0$ (where $\bar{m}^\mu$ is the complex conjugate of m^μ) as

$$n^\mu = (r^2 + a^2, -\Delta, 0, a)/(2\Sigma), \tag{1.61}$$

$$l^\mu = \left(\frac{r^2 + a^2}{\Delta}, 1, 0, \frac{a}{\Delta}\right), \tag{1.62}$$

$$m^\mu = (ia\sin\theta, 0, 1, i/\sin\theta)/(\sqrt{2}(r + ia\cos\theta)). \tag{1.63}$$

The Weyl scalar [211] is defined as $\psi_4 = -C_{\alpha\beta\gamma\delta} n^\alpha \bar{m}^\beta n^\gamma m^\delta$. For the purpose of this dissertation, we restrict to source-free perturbations, i.e., vacuum perturbations. In this case, the rescaled quantity, $\phi = \rho^{-4}\psi_4$, where $\rho = (r - ia\cos\theta)^{-1}$, obeys the following equation.

$${}_{s=-2}O\phi = 0, \tag{1.64}$$

where ${}_{s=-2}O$ is a second order differential operator. Importantly, the equation admits separability [214] in '-2' spin-weighted spheroidal harmonic basis, and we can substitute

$$\phi = \sum_{\ell m} \int d\omega e^{-i\omega t + im\phi} {}_{-2}S_{\ell m}(\theta, a\omega) R_{\ell m\omega}(r). \tag{1.65}$$

Here, the spin-weighted (with spin weight $s = -2$) spheroidal harmonic ${}_{-2}S_{\ell m}(\theta, a\omega)$ satisfies the angular Teukolsky equation [215]:

$$\Big[\frac{1}{\sin\theta}\frac{d}{d\theta}\Big\{\sin\theta\frac{d}{d\theta}\Big\} - a^2\omega^2\sin^2\theta - \frac{(m+s\cos\theta)^2}{\sin^2\theta}+$$
$$2as\omega\cos\theta + s + 2ma\omega + \lambda\Big]{}_sS_{\ell m} = 0, \quad s = -2. \tag{1.66}$$

The radial Teukolsky equation governing $R_{\ell m\omega}(r)$ is then simply

$$\Delta^{-s}\frac{d}{dr}\left(\Delta^{s+1}\frac{R_{\ell m\omega}}{r}\right) - V(r)R_{\ell m\omega} = 0, \tag{1.67}$$

where $V(r) = -\frac{K^2-2is(r-M)K}{\Delta} - 4si\omega r + \lambda$, $K = (r^2+a^2)\omega - ma$, $s = -2$ and $\lambda = \ell(\ell+1)-2+O(a\omega)$ is the eigenvalue of ${}_{-2}S_{\ell m}(\theta, a\omega)$.

The solution to the radial Teukolsky equation can be understood as a combination of incoming/outgoing waves close to the horizon and at infinity. The asymptotic solutions outside a Kerr BH are

$$R^{\text{in}}_{\ell m\omega} \to \begin{cases} B^{\text{trans}}_{\ell m\omega}\Delta^2 e^{-ikr^*}, & \text{for } r \to r_+, \\ \\ r^3 B^{\text{ref}}_{\ell m\omega}e^{i\omega r^*} + r^{-1}B^{\text{inc}}_{\ell m\omega}e^{-i\omega r^*}, & \text{for } r \to \infty, \end{cases} \tag{1.68}$$

where we assume vanishing data on the past horizon. Viewing this as a time-independent scattering setup, the scattering phase is encoded in the ratio of amplitudes of outgoing and incoming waves at $r \to \infty$, i.e., $B^{\text{ref}}_{\ell m\omega}/B^{\text{inc}}_{\ell m\omega}$. The task is to relate $B^{\text{trans}}_{\ell m\omega}$ with the reflection and incidence coefficients at infinity. For this, we need to know the solution more generally, and not just in the asymptotic limits.

There are various methods in the literature to solve the radial Teukolsky equation. The most important method for the purposes of this dissertation is the Mano-Suzuki-Takasugi (MST) [216] formalism named after the authors who developed it. In this, one expands the scalar into infinte sums of hypergeometric functions in different regions of the spacetime, and then constrains them according to appropriate boundary conditions. We briefly review the MST approach below focusing on solving the Raman scattering problem in BHPT, while a detailed review of BHPT, including the MST formalism and applications to the binary problem can be found in Ref. [217].

1.4.2 Analytical solutions using the MST approach

In the MST approach, the Teukolsky equation is solved using series expansions with $\epsilon = 2M\omega$ as the expansion parameter. The equation is first analyzed in two asymptotic regions: (a) the near zone, defined by $r - r_+ \ll \lambda \sim \omega^{-1}$, and (b) the far zone, where $r \gg r_+$. Here r_+ is the outer horizon of the Kerr BH. We consider $\omega > 0$ without loss of generality. The near and far zones overlap for $\lambda \gg r \gg r_+$. From each zone, a series solution is developed whose radius of convergence extends well beyond the strict asymptotic regime, overlapping with the solution from the other zone.

The near-zone series solution is regular at the horizon and convergent everywhere except at infinity. More precisely, for any $\infty > r \geq r_+$, the frequency may be adjusted so that the series is convergent [216, 217]. In the limit $r \gg r_+$, the convergence is limited by $\omega r < 1/2$. In practice, since we truncate the series solution at a finite order, the solution works best in asymptotic near zone, defined by $r - r_+ \ll \lambda$. Conversely, the far-zone solution is regular at infinity and convergent for all r except at the outer horizon, i.e., $\infty \geq r > r_+$, regardless of frequency [216, 217]. Once again, due to truncation, the solution works best in the asymptotic far-zone regime, where $r \gg r_+$.

Both solutions are valid for the common region of convergence, $\infty > r > r_+$, where they can be analytically matched from their respective series solutions. Crucially, the near-zone solutions, which are constrained by the boundary conditions at the horizon, inform and constrain the far-zone solutions through the matching procedure. For BHs in GR, a near-zone solution is obtained by enforcing ingoing boundary conditions at the horizon. When computing oscillation modes, or QNMs, outgoing conditions at infinity and ingoing conditions at the horizon are imposed. The requirement of consistency between these boundary conditions leads to a discrete set of complex frequencies: the QNM spectrum.

In this dissertation, we primarily employ the MST approach to study the Raman scattering problem. For Kerr BHs, we impose ingoing boundary conditions at the horizon and match the resulting near-zone solution to the far-zone solution at real frequencies. Taking the asymptotic limit $r \gg \lambda \gg r_+ \sim M$ of the exact far-zone solution allows us to extract the wave-like behavior of the scattered radiation. From this, we obtain the scattering phase and other relevant observables. This is relevant for Chapters 4 [3], and 5 [4].

We also address Raman scattering for NSs in Chapter 6 [5], using MST solutions to the Regge–Wheeler (RW) equation [218, 219]. In this case, boundary conditions at the stellar surface are determined by numerically solving the metric- and matter-perturbation equations in the interior. The near-zone solution is then fixed to be consistent with these boundary conditions and matched to the far-zone solution.

The MST treatments of the Teukolsky and RW equations closely parallel one another [219]. Additionally, the RW equation can be mapped to the spinless limit of the Teukolsky equation: the Bardeen-Press equation [220, 221]. Therefore, we focus our current discussion on the MST approach for the Teukolsky equation.

1.4.2.1 Near-zone solution

The near-zone solution satisfying ingoing boundary conditions can be written as

$$R^{\rm in} = e^{i\epsilon\kappa x}(-x)^{-s-i(\epsilon+\tau)/2}(1-x)^{i(\epsilon-\tau)/2}p_{\rm in}(x), \tag{1.69}$$

where we have suppressed the ℓ, m labels for brevity, and $\epsilon = 2M\omega$, $x = (z_+ - z)/(\epsilon\kappa)$, $z = \omega r$, $\kappa = \sqrt{1-\chi^2}$, $\chi = a/M$, $\tau = (\epsilon - m\chi)/\kappa$, $\epsilon_\pm = (\epsilon \pm \tau)/2$. Here, $p_{in}(x)$ is finite for $x = 0$, where $r = r_+$ (i.e., at the horizon). The prefactor ensures ingoing behaviour at the horizon. More generally, the function $p_{\rm in}(x)$ is expanded as a sum of hypergeometric functions as

$$p_{in}(x) = \sum_{n=-\infty}^{n=\infty} a_n p_{n+\nu}(x), \tag{1.70}$$

$$p_{n+\nu}(x) = F(n+\nu+1-i\tau, -n-\nu-i\tau; 1-s-i\epsilon-i\tau, x) \tag{1.71}$$

Here, the coefficients a_n obey a three-term recurrence relation of the form

$$\alpha_n^\nu a_{n+1} + \beta_n^\nu a_n + \gamma_n^\nu a_{n-1} = 0, \tag{1.72}$$

where the coefficients are given by

$$\alpha_n^\nu = \frac{i\epsilon\kappa(n+\nu+1+s+i\epsilon)(n+\nu+1+s-i\epsilon)(n+\nu+1+i\tau)}{(n+\nu+1)(2n+2\nu+3)}, \tag{1.73}$$

$$\begin{aligned}\beta_n^\nu &= -\lambda - s(s+1) + (n+\nu)(n+\nu+1) + \epsilon^2 + \epsilon(\epsilon - mq) \\ &\quad + \frac{\epsilon(\epsilon-mq)(s^2+\epsilon^2)}{(n+\nu)(n+\nu+1)},\end{aligned} \tag{1.74}$$

$$\gamma_n^\nu = -\frac{i\epsilon\kappa(n+\nu-s+i\epsilon)(n+\nu-s-i\epsilon)(n+\nu-i\tau)}{(n+\nu)(2n+2\nu-1)}, \tag{1.75}$$

where the parameter $\nu = \ell + O(\epsilon) + \ldots$, known as the renormalized angular momentum, can be chosen such that the solution to the recurrence relation is finite and convergent for $n \to \pm\infty$.

Physically, the renormalized angular momentum captures the impact of tail effects in the Raman scattering process, i.e., the modification of scattering amplitudes due to nonlinear interactions between an external perturbation and the body's gravitational field [222].

For later convenience when matching the near- and far-zone solutions, it is convenient to split the ingoing solution as

$$R_{\rm in} = R_0^{\nu} + R_0^{-\nu-1}, \tag{1.76}$$

$$\begin{aligned} R_0^{\nu} = e^{i\epsilon\kappa x}(-x)^{-s-\frac{i}{2}(\epsilon+\tau)}(1-x)^{\frac{i}{2}(\epsilon+\tau)+\nu} \sum_{n=-\infty}^{\infty} a_n \frac{\Gamma(1-s-i\epsilon-i\tau)\Gamma(2n+2\nu+1)}{\Gamma(n+\nu+1-i\tau)\Gamma(n+\nu+1-s-i\epsilon)} \\ \times (1-x)^n F(-n-\nu-i\tau, -n-\nu-s-i\epsilon; -2n-2\nu; 1/(1-x)). \end{aligned} \tag{1.77}$$

Note that the near-zone solution in Eq. (1.69) is convergent everywhere for $0 \leq |x| < \infty$, i.e., for all $r_+ < r < \infty$.

1.4.2.2 Far-zone solutions

Unlike in the near zone, where the purely ingoing nature of the horizon specified a unique solution, the far zone a priori has two independent solutions (i.e., solution space is spanned by two basis solutions) which can be chosen to be analogous to the two pieces in Eq. (1.76). Their precise combination needs to be fixed by matching with the near-zone solution in the overlap region.

We can write two independent solutions as R_C^{ν} and $R_C^{-\nu-1}$, where

$$R_C^{\nu} = \hat{z}^{-1-s}\left(1 - \frac{\epsilon\kappa}{\hat{z}}\right)^{-s-i(\epsilon+\tau)/2} f(\hat{z}), \tag{1.78}$$

where[5] $\hat{z} = \omega(r - r_-) = \epsilon\kappa(1 - x)$.

$$f_\nu = \sum_{n=-\infty}^{n} (-i)^n \frac{(\nu + 1 + s - i\epsilon)_n}{(\nu + 1 - s + i\epsilon)_n} a_n F_{n+\nu}(-is - \epsilon, \hat{z}), \tag{1.79}$$

where $F_L(\eta, \hat{z}) = e^{-i\hat{z}} 2^L \hat{z}^{L+1} \frac{\Gamma(L+1-i\eta)}{\Gamma(2L+2)} {}_1F_1(L + 1 - i\eta, 2L + 2; 2iz)$. Note that the same parameter ν, and the same coefficients a_n also appear here.

The far-zone solutions converge everywhere but at $r = r_+$, the horizon.

1.4.2.3 Matching

R_C^ν and $R_C^{-\nu-1}$, and similarly R^ν and $R^{-\nu-1}$, exhibit the same leading nonanalytic prefactor when expressed in identical coordinates. Thus, they can be consistently matched in the overlap region at any point.

Expanding both solutions in powers of $\hat{z}$ within the region $\epsilon\kappa < \hat{z} < \infty$, we find

$$R_0^\nu = K^\nu R_C^\nu, \tag{1.80}$$

$$\begin{aligned} K^\nu = {} & e^{i\epsilon\kappa}(2\epsilon\kappa)^{s-\nu-r} 2^{-\nu} i^r \Gamma(1 - s - 2i\epsilon_+) \frac{\Gamma(r + 2\nu + 2)}{\Gamma(r + \nu + 1 - s + i\epsilon)\Gamma(r + \nu + 1 + i\tau)\Gamma(r + \nu + 1 + s + i\epsilon)} \\ & \times \sum_{n=r}^{\infty} (-1)^n \frac{\Gamma(n + r + 2\nu + 1)}{(n - r)!} \frac{\Gamma(n + \nu + 1 + s + i\epsilon)}{\Gamma(n + \nu + 1 - s - i\epsilon)} \frac{\Gamma(n + \nu + 1 + i\tau)}{\Gamma(n + \nu + 1 - i\tau)} a_n \\ & \times \left[\sum_{n=-\infty}^{r} \frac{(-1)^n}{(r - n)!(r + 2\nu + 2)_n} \frac{(\nu + 1 + s - i\epsilon)_n}{(\nu + 1 - s + i\epsilon)_n} a_n \right]^{-1}, \end{aligned} \tag{1.81}$$

where r can be chosen freely and it does not affect the result upon evaluating the expression, and is conveniently set to 0. A crucial point to note here is that while the matching procedure is exact for any frequency and radial coordinate, we are limited by the order in ϵ to which we evaluate the

[5] $r_- < r_+$ is the radial coordinate of the inner horizon.

various coefficients a_n, and ν, in a perturbative analysis. Thus, the validity of our results is also constrained by the requirement $\epsilon \ll 1$, or $M \ll \lambda$.

Thus, the linear combination of far-zone solutions can now be uniquely fixed using Eq. (1.76), as

$$R^{\text{in}} = K_\nu R_C^\nu + K_{-\nu-1} R_C^{-\nu-1}. \tag{1.82}$$

We can now extract on-shell properties of the solution, (i.e., the wave-like behaviour at $r \gg \lambda$), from which useful observables such as the scattering phase can be extracted.

Note that more generally, the solution at the surface of the body may not be purely ingoing. This can happen for non BH compact objects, or BH endowed with reflectivity. In such cases, the coefficients K_ν and $K_{-\nu-1}$ can be modified. These coefficients thus encode the boundary conditions at the surface of the body, which in turn depends on its properties. For instance, this is shown in the case of a nonspinning NS in Chapter 6 [5].

1.4.3 Scattering phase

To study the scattering behavior of the wave-like solutions in the asymptotic regime, it is convenient to switch to another basis of solutions in the far zone, which correspond to incoming and outgoing radiation at the asymptotic infinity.

To that end, the solutions R_C can be expanded as

$$R_C^\nu = R_+^\nu + R_-^\nu, \tag{1.83}$$

$$R_C^{-\nu-1} = -i\exp(-i\pi\nu)\frac{\sin(\pi(\nu - s + i\epsilon))}{\sin(\pi(\nu - s - i\epsilon))}R_+^\nu + i\exp(i\pi\nu)R_-^\nu$$

$$R_+^\nu = 2^\nu e^{-\pi\epsilon} e^{i\pi(\nu+1-s)} \frac{\Gamma(\nu+1-s+i\epsilon)}{\Gamma(\nu+1+s-i\epsilon)} e^{-i\hat{z}} \hat{z}^{\nu+i\epsilon_+} (\hat{z}-\epsilon\kappa)^{-s-i\epsilon_+}$$

$$\times \sum_{n=-\infty}^{\infty} i^n a_n (2\hat{z})^n \Psi(n+\nu+1-s+i\epsilon, 2n+2\nu+2; 2i\hat{z}), \tag{1.84}$$

$$R_-^\nu = 2^\nu e^{-\pi\epsilon} e^{-i\pi(\nu+1+s)} e^{i\hat{z}} \hat{z}^{\nu+i\epsilon_+} (\hat{z}-\epsilon\kappa)^{-s-i\epsilon_+}$$

$$\times \sum_{n=-\infty}^{\infty} i^n \frac{(\nu+1+s-i\epsilon)_n}{(\nu+1-s+i\epsilon)_n} a_n (2\hat{z})^n \Psi(n+\nu+1+s-i\epsilon, 2n+2\nu+2; -2i\hat{z}), \tag{1.85}$$

where $\psi(a,b,z)$ is the irregular confluent hypergeometric function.

The new basis of solutions, $R_\pm^\nu$ can be interpreted as outgoing/ingoing solutions at the asymptotic infinity. This can be seen by considering their asymptotic behavior in the limit $\hat{z} \to \infty$ by using $\psi(a,b,\hat{z}) \to z^{-a}$ as $z \to \infty$. We find

$$R_+ \sim A_+ z^{-1} e^{-i(z+\epsilon \ln z)}, \tag{1.86}$$

$$R_- \sim A_- z^{-1-2s} e^{i(z+\epsilon \ln z)}, \tag{1.87}$$

$$A_+ = e^{-\frac{\pi}{2}\epsilon} e^{\frac{\pi}{2}i(\nu+1-s)} 2^{-1+s-i\epsilon} \frac{\Gamma(\nu+1-s+i\epsilon)}{\Gamma(\nu+1+s-i\epsilon)} \sum_{n=-\infty}^{\infty} a_n, \tag{1.88}$$

$$A_- = 2^{-1-s+i\epsilon} e^{-\frac{\pi}{2}i(\nu+1+s)} e^{-\frac{\pi}{2}\epsilon} \sum_{n=-\infty}^{\infty} (-1)^n \frac{(\nu+1+s-i\epsilon)_n}{(\nu+1-s+i\epsilon)_n} a_n. \tag{1.89}$$

The outgoing and incoming wave-like nature of R_- and R_+, respectively, is evident from their form. The time dependence of the perturbations, factored out as $e^{-i\omega t}$, when combined with the asymptotic behavior $z \sim \omega r$ and $z \gg \ln z$, reveals that the solutions scale as $e^{i\omega(t\mp r)}$ at large r, characteristic of outgoing and incoming waves.

The precise combination of incoming and outgoing solution consistent with the ingoing nature of the horizon can be obtained by substituting Eqs. (1.83) into Eqs. (1.82), yielding

$$R^{in} = \left[K_\nu - i\exp(-i\pi\nu)\frac{\sin(\pi(\nu - s + i\epsilon))}{\sin(\pi(\nu - s - i\epsilon))}K_{-\nu-1}\right]R_+^\nu + \left[K_\nu + i\exp(i\pi\nu)K_{-\nu-1}\right]R_-^\nu. \tag{1.90}$$

From this, it can be shown that the ratio of reflection and incidence amplitudes, as defined in Eq. (1.68), is given by

$$\frac{B^{\rm ref}_{\ell m\omega}}{B^{\rm inc}_{\ell m\omega}} = \omega^{-2s}e^{2i\epsilon[\log\epsilon-(1-\kappa)]}\frac{A_-}{A_+} \times \frac{\left[K_\nu + i\exp(i\pi\nu)K_{-\nu-1}\right]}{\left[K_\nu - i\exp(-i\pi\nu)\frac{\sin(\pi(\nu-s+i\epsilon))}{\sin(\pi(\nu-s-i\epsilon))}K_{-\nu-1}\right]}. \tag{1.91}$$

The ratio of reflection and incidence amplitudes is further related to the scattering phase and degree of absorption for each parity mode $\mathrm{P} = \pm 1$ for a given choice of ℓ, m as [166]

$$\eta^{\rm P}_{\ell m}e^{2i\delta^{\rm P}_{\ell m}} = (-1)^{\ell+1}\frac{\mathrm{Re}(C) + 12iM\omega\,\mathrm{P}}{16\omega^4} \times \frac{B^{(\rm refl)}_{\ell m\omega}}{B^{(\rm inc)}_{\ell m\omega}}, \tag{1.92}$$

where

$$\begin{aligned}[\mathrm{Re}(C)]^2 = &\left((\lambda+2)^2 + 4am\omega - 4a^2\omega^2\right)\left[\lambda^2 + 36am\omega - 36a^2\omega^2\right] \\ &+ (2\lambda+3)(96a^2\omega^2 - 48a\omega m) - 144\omega^2a^2.\end{aligned} \tag{1.93}$$

Here, $\delta^{\rm P}_{\ell m}$ is real, and $\eta^{\rm P}_{\ell m}$ is the degree of absorption/amplification that the scattered waves experience relative to the incident wave. Absorption, indicated by $\eta^{\rm P}_{lm} < 1$, is physically understood as a portion of the incident radiation energy falling into the horizon. Amplification, indicated by $\eta^{\rm P}_{lm} > 1$, is understood as superradiant scattering and is only permitted when the spin is nonzero. The scattering phase can be further related to the scattering amplitude as well, which can be computed, for instance, in WEFT.

In Chapter 4 [3], we evaluate the expression for $\eta^{\rm P}_{\ell m}$ in a Taylor series of frequency to NLO in BHPT (using Eq. (1.92)) and in WEFT (by solving the equations of motion for worldline and multipole moments in a GW background). We then compare them to fix the dissipative tidal-response coefficients for a Kerr BH to NLO, and to compute horizon fluxes in a quasicircular Kerr binary to next-to-next-to-leading order (NNLO) in a PN expansion (4PN).

In Chapter 5 [4], we relate the complete scattering phase (i.e., not just degree of absorption) with its EFT counter part. In this way, we constrain static conservative Love numbers, and show that dynamical Love numbers at NLO, and dissipation numbers at NNLO exhibit classical renormalization group flow in the EFT w.r.t frequency.

In Chapter 6 [5], we study a perturbed spinless NS. There, in addition to the metric perturbations, the matter perturbations for the stellar fluid is also important. We numerically solve the metric and matter perturbations inside the star to inform the boundary conditions for the solution to the metric perturbations in the vacuum outside. The latter is described using the RW equation solved via the MST method.

Aside from the Raman scattering problem, BHPT finds extensive applications across several subfields central to GW astronomy. Notably, BHPT forms the backbone of the GSF approach for modeling EMRIs [72, 223]. It is also instrumental in the computation of QNMs of BHs and other compact objects, which encode the characteristic ringdown signal in GW observations [88]. In Chapter 7 [6], we investigate the behaviour of metric perturbations outside a generic, slowly spinning compact object to examine how the fundamental QNM frequency depends sensitively on the object's properties.

1.5 Research Overview

This section summarizes the research presented in the rest of the dissertation, and it is structured as follows:

- § 1.5.1 summarizes Chapter 2, which was published as Ref. [1].

  We first study the problem of classical electromagnetic scattering of two charged particles to third order in the PL expansion (weak coupling, large impact parameter). We include both conservative and dissipative effects to calculate the impulse (change in momentum of each particle), the scattering angle, and radiated energy and angular momentum. We use the Abraham-Lorentz-Dirac (ALD) force to include the radiation-reaction force on each particle. We then study some techniques used to compute quantities relevant to bound two-body systems from solutions to the corresponding scattering problem. In particular, we derive two maps based on analytical continuation, relating radiated energy and angular momentum of the scattering problem with the bound problem. We verify their validity for the EM case, and also in the gravitational case to first PN order. We also comment on the practical utility of these maps to obtain new results for the physically relevant system of a compact binary of BHs/ NSs.

- § 1.5.2 summarizes Chapter 3, which was published as Ref. [2]. We study the process of GWs scattering off a spinning body with arbitrary spin-induced quadrupole and octupole moments. We model the body in WEFT, where the dynamics is described by a worldline with a vectorial degree of freedom to capture spin. We solve the classical equations of motion at linear order in the mass of the scattering body, but to third order in its spin, and derive the scattering amplitude (gravitational Compton amplitude). When the spin-induced multipole moments are chosen to be that of a Kerr BH, the resultant amplitude is consistent with the results obtained via BHPT in the appropriate limit.

- § 1.5.3 summarizes Chapters 4, which was published as Ref. [3]. We study horizon fluxes in Kerr BHs in binaries which change their mass and angular momentum during the inspiral. We model the dynamics of Kerr BHs in WEFT, where horizon fluxes can be modeled as tidal heating (dissipation associated with tidal deformation). Tides are incorporated in the worldline action by including multipolar degrees of freedom attached to the worldline, coupled to gravitational tidal fields. The induction is assumed to be linear, and we write down an ansatz for it in a low-frequency (slowly varying tidal fields) expansion. This ansatz can be constrained to an extent using symmetries, but not entirely. The remaining freedom, parameterized as free coefficients is fixed by matching with results that we compute in BHPT.

  Thus, we study the process of gravitational Raman scattering for a Kerr BH, and compute the degree of absorption analytically in BHPT using MST solutions. The same problem is also solved in WEFT theory to obtain the degree of absorption as a function of the unknown tidal-response coefficients. Comparing the two results then fixes the dissipative tidal-response coefficients in the worldline theory.

  Once the coefficients are fixed in this (relatively) simpler one-body problem, we can study the dynamics of Kerr BHs in various systems. Specifically, we then consider a binary of Kerr BHs, and compute the consequences of tidal heating i.e., horizon fluxes and their effect on the mass and angular momentum of the BHs. We also compute the associated effect on the gravitational waveform to 4PN (NNLO) [6] . The resultant formulae are consistent with known results from the test-body limit, solving an inconsistency that lasted for a decade from results obtained earlier via a different approach [60].

- § 1.5.4 summarizes Chapter 5, which was published as Ref. [4]. We study conservative and dissipative tidal response in Kerr BHs to NNLO in frequency.

  In the previous Chapter 4 [3], we restricted to dissipative tidal coefficients up to NLO in frequency. We also do not rigorously include tail effects and their effect on the gravitational Raman amplitude.

  In Chapter 5 [4], we rigorously compute the tidal part of the gravitational Raman amplitude using the machinery of Feynman diagrams in a WEFT. The tidal-response coefficients are defined as before, as parameters entering the ansatz of the inducible multipole moments. We match the WEFT amplitudes with the complete scattering phase in Eq. (1.92), obtained in BHPT using the analytical MST solutions.

  Through the matching, we recover the vanishing of the static Love number, as well as recover the dissipative tidal-response coefficients at leading order and NLO. Additionally, we show that the dynamical Love numbers at NLO and NNLO, and the dynamical dissipation numbers at NNLO, exhibit classical renormalization flow. This arises from two types of divergences in the EFT, both due to the nonlinear nature of GR. One class stems from the distortion of the GW by the background Kerr metric in addition to the induction of tidal multipole moments. The other class originates purely from nonlinear interaction between the GW and the Kerr background and is insensitive to the tidal response.

[6] horizon fluxes enter the waveform at 2.5PN for spinning bodies. NLO is 3.5PN and NNLO is at 4PN. For nonspinning bodies, horizon fluxes (and more generally tidal dissipation) enter at 4PN.

- § 1.5.5 summarizes Chapter 6, which was published as Ref. [5]. We study leading order (4PN) tidal dissipation in spherical NSs for various EOSs. We obtain metric and matter perturbation equations in a spherical relativistic star including fluid viscosity at linear order in frequency, and solve them numerically up to the stellar surface. At the stellar surface, we match this with analytical MST solutions of the RW equation which governs the behaviour of metric perturbations outside the NS. We then choose steady-state, single-frequency, scattering solutions corresponding to GWs scattering off the NS, and extract the scattering phase as a function of the boundary conditions at the stellar surface.

  From the scattering phase, using and extending methods developed in previous works, we extract expressions for the static Love number, and leading dissipation number. The former, which characterizes leading conservative tidal deformability, is seen to be consistent with previous results [55], and the latter, which characterizes tidal heating is obtained for the first time. We show that the leading dissipation number is independent of bulk viscosity in the regime where the low-frequency expansion is well-defined. Thus, the shear-viscosity, which is primarily due to electron-electron scattering, controls tidal heating. We compute its effect on the number of GW cycles, and find that it is comparable to other conservative 4PN contributions for very cold and less compact stars.

- § 1.5.6 summarizes Chapter 7, which was published as Ref. [6]. We study the QNMs of a slowly spinning compact object in the membrane paradigm. The membrane paradigm is a way to phenomenologically study generic compact objects, by replacing them with a fluid membrane [95–97, 224]. We impose Israel-Damour junction conditions at the membrane surface, yielding the boundary conditions for the outside metric. This has been used before in Ref. [90] to study nonspinning compact objects. We extend this work to linear order in spin, where the metric outside the membrane is the linearized Kerr metric when unperturbed. We derive boundary conditions for linearized metric perturbations to first order in spin, and then study the system under suitable boundary conditions. Specifically, we impose purely outgoing solutions at infinity, and the derived boundary conditions at the membrane surface. Such solutions are valid only at specific frequencies — QNM frequencies — which serve as a fingerprint for a given model of compact object. We study how the fundamental mode varies as a function of the fluid membrane parameters, including spin. We show that the fundamental mode becomes longer lived as spin is increased when the fluid parameters are chosen such that the body is highly reflective, tending towards instability.

1.5.1 Classical relativistic scattering and the relation to bound systems

In Chapter 2, we study the scattering of two charged particles in EM in the PL expansion (the electromagnetic analog of PM expansion discussed in Sec. 1.2.1).

We solve the scattering problem to 3PL order, consistently including all conservative and dissipative effects in Ref. [1], while treating the objects as spinless, charged, particles in a worldline framework. We also derive new maps based on analytical continuation of radiated energy and angular momentum between unbound and bound systems of classical particles.

We briefly summarize results for select scattering observables up to 3PL and then present the new boundary-to-bound (B2B) maps for radiative observables. Although the work focuses on electromagnetic scattering, it is instructive to compare with analogous results in GR from other studies where available. We therefore also include the corresponding GR expressions below.

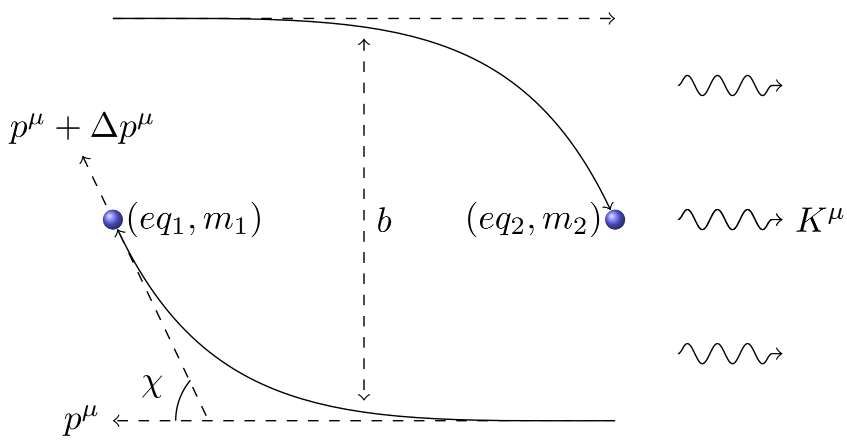

Figure 1.5: Classical scattering of two charged particles in the COM frame. We denote with eq_1 and eq_2 the electric charges, where we introduce the factor e to keep track of the order of calculation since we solve the scattering problem in a weak-field/coupling expansion. We denote with m_1, m_2 the masses, p^μ is the initial spatial momentum in the COM frame, and $\sqrt{b^2} = |b|$ is the impact parameter. Finally, χ is the scattering angle and K^μ is the radiated momentum.

1.5.1.1 Electromagnetic scattering to 3PL

For both the EM and GR cases, the net results of a two-body scattering encounter can be expressed as functions of the asymptotic incoming state at past infinity, where interactions are perturbatively negligible, with the two bodies moving uniformly on straight-line trajectories in (asymptotically) Minkowski spacetime. We identify the initial state as the zeroth-order state in our perturbative expansion. It is specified by the initial momenta $p_1^\mu = m_1 u_1^\mu$ and $p_2^\mu = m_2 u_2^\mu$, where m_A are the rest masses and u_A^μ are the 4-velocities with $u_A^2 = -1$, and by the initial impact parameter vector b^μ (pointing 2→1) orthogonally separating the two initial uniform-motion worldlines. The initial relative velocity v, the corresponding Lorentz factor γ, and the initial total energy E in the COM frame are defined by

$$\gamma = \frac{1}{\sqrt{1-v^2}} = -\frac{p_1 \cdot p_2}{m_1 m_2},$$
$$E^2 = -(p_1 + p_2)^2 = m_1^2 + m_2^2 + 2m_1 m_2 \gamma. \tag{1.94}$$

The COM frame has velocity $(p_1^\mu + p_2^\mu)/E$. The ''relative momentum'' $p^\mu = p_1^\mu - p_2^\mu$, is equal to the spatial momentum of body 1 (which is equal and opposite to that of body 2) in the COM frame, and its magnitude $|p|$ are given by

$$p^\mu = \frac{m_1 m_2}{E^2}[(m_2 + m_1\gamma)u_1^\mu - (m_1 + m_2\gamma)u_2^\mu],$$
$$|p| = \frac{m_1 m_2 \gamma v}{E}. \tag{1.95}$$

The magnitude of the initial COM-frame total angular momentum is $J = |p||b|$.

The perturbations of the worldlines due to EM or GR interactions can be computed by iteratively solving the relevant field equations and equations of motion, while working perturbatively in the masses[7] m_A ($A = 1, 2$), in GR, or in e^2 in EM, where e is an order-counting parameter such that the two charges are eq_1 and eq_2. We work in Gaussian units in the EM case. While we use m_A and e^2 as formal expansion parameters, the true dimensionless quantities, which we assume to be small, are essentially the leading terms in the scattering angles in Eqs. (1.97) and (1.98) below; our fundamental assumption is that the scattering particles' trajectories are small perturbations of straight-line inertial motion. All quantities of interest (impulse, radiated energy, and angular momentum) are obtained from the perturbed worldlines computed to the relevant order. This follows the same scheme outlined earlier in Sec. 1.2.1.1, now iterated three times to reach the desired order. A further subtlety at higher orders is the radiation of energy and angular momentum.

The impulses up to second order for both the EM and GR cases were first computed by

[7] It is more convenient to use G for tracking the order of expansion, but we use the masses to be consistent with the conventions in the rest of this chapter.

Westpfahl in Ref. [104]. Through this order, no net 4-momentum is radiated away, so the impulses on the two bodies are equal and opposite, $\Delta p_2^\mu = -\Delta p_1^\mu$. They are given in terms of the COM-frame scattering angle χ by[8]

$$\Delta p_1^\mu = |p| \sin\chi \frac{b^\mu}{|b|} + (\cos\chi - 1) p^\mu + O(e^6, m_A^4), \tag{1.96}$$

The second-order scattering angles for EM and GR respectively are

$$\chi_{\text{EM}} = \frac{2e^2 q_1 q_2 E}{m_1 m_2 \gamma v^2 |b|} - \frac{\pi e^4 q_1^2 q_2^2 M_{\text{T}} E}{2 m_1^2 m_2^2 \gamma^2 v^2 |b|^2} + O(e^6), \tag{1.97}$$

$$\chi_{\text{GR}} = -\frac{2E(2\gamma^2 - 1)}{\gamma^2 v^2 |b|} - \frac{3\pi M_{\text{T}} E(5\gamma^2 - 1)}{4\gamma^2 v^2 |b|^2} + O(m_A^3). \tag{1.98}$$

Here, $M_{\text{T}} = m_1 + m_2$ is the sum of the rest masses.

While there is no radiation of linear momentum up to the second order, the dynamics is not purely conservative at these orders, as there is a loss of angular momentum which is encoded in the second-order trajectories. We compute this directly from the trajectories for the EM case, finding the radiated angular momentum (which is equal and opposite to the change in the particles' orbital angular momentum) in the COM frame to be

$$J_{\text{rad,EM}} = 2\frac{e^4 q_1^2 q_2^2}{E|b|} I_{\text{EM}}(v) + O(e^6), \tag{1.99}$$

$$I_{\text{EM}}(v) = -\frac{2}{3}\gamma \left(\frac{q_1/m_1}{q_2/m_2} + \frac{q_2/m_2}{q_1/m_1} \right) + \frac{2}{v^2} - \frac{2 \operatorname{arctanh} v}{\gamma^2 v^3}, \tag{1.100}$$

The analogous result for GR,

$$J_{\text{rad,GR}} = 2\frac{m_1^2 m_2^2 (2\gamma^2 - 1)}{E|b|} I_{\text{GR}}(v) + O(m_A^4), \tag{1.101}$$

$$I_{\text{GR}}(v) = -\frac{16}{3} + \frac{2}{v^2} + \frac{2(3v^2 - 1)}{v^3} \operatorname{arctanh} v, \tag{1.102}$$

[8]We use the notation $O(m_A^n)$ to denote all terms with mass order n.

was derived in Ref. [142] by directly computing the total angular momentum radiated away in the gravitational field. Note that both results feature a factor of the rapidity, $\operatorname{arctanh} v = \operatorname{arccosh}\gamma = 2\operatorname{arcsinh}\sqrt{(\gamma-1)/2}$. Also note that $J_{\text{rad,GR}}$ is always positive, so that the orbital angular momentum always decreases in magnitude, while $J_{\text{rad,EM}}$ is positive for opposite-sign charges (attraction) but can be negative for same-sign charges (repulsion), so that the orbital angular momentum can increase in magnitude in the latter case.

At the 3rd order, in both the EM and GR cases, linear momentum is radiated away as well. The impulse on body 1 (with results for body 2 obtained by exchanging identities, $1 \leftrightarrow 2$, and flipping the signs of b^μ and p^μ) can be written in both cases as follows,

$$\Delta p_1^\mu = \Delta p^\mu_{1,\text{cons}} + \Delta p^\mu_{1,\text{rad}}, \tag{1.103}$$

$$\Delta p^\mu_{1,\text{cons}} = |p|\sin\chi_{\text{cons}}\frac{b^\mu}{|b|} + (\cos\chi_{\text{cons}} - 1)p^\mu, \tag{1.104}$$

$$\Delta p^\mu_{1,\text{rad}} = -\frac{K\cdot u_2}{(\gamma v)^2}(u_2^\mu - \gamma u_1^\mu) + |p|\chi_{\text{rad}}\frac{b^\mu}{|b|}, \tag{1.105}$$

where χ_{cons} is the conservative part of the scattering angle, χ_{rad} is the radiative part of the scattering angle, and K^μ is the radiated momentum. We argue for this structure based on general grounds, and also confirm it explicitly by directly computing the full impulse from the 3rd order force in the EM case.

For the conservative scattering angles, we have $\chi_{\text{cons}} = \chi^{(1)} + \chi^{(2)} + \chi^{(3)}_{\text{cons}} + \mathcal{O}(m_A^4, e^8)$, where the first- and second-order parts are given in Eq. (1.97). At the 3rd order in the EM case, we obtain

$$\chi^{(3)}_{\text{cons,EM}} = \frac{e^6 q_1^3 q_2^3 E\left[(m_1^2+m_2^2)(4\gamma^2-6) - 4m_1m_2\gamma(\gamma^2-3v^2)\right]}{3m_1^3m_2^3\gamma^5v^6|b|^3}. \tag{1.106}$$

This matches the result later derived from potential-region integration of the two-loop amplitude in Ref. [225]. The analogous result for GR,

$$\chi^{(3)}_{\text{cons,GR}} = -\frac{E^3}{|b|^3}\bigg[2\frac{64\gamma^6 - 120\gamma^4 + 60\gamma^2 - 5}{3(\gamma v)^6} \\ - \frac{8m_1 m_2}{E^2}\bigg(\frac{14\gamma^2+25}{3\gamma v^2} + \frac{4\gamma^4 - 12\gamma^2 - 3}{(\gamma v)^3}\text{arctanh}\, v\bigg)\bigg], \tag{1.107}$$

was first derived in Ref. [116], also from potential-region integration of the two-loop amplitude. The GR result has a logarithmic divergence in the high-energy limit due to the arctanh v term, a feature which is not present in the EM result (1.106). This divergence is removed by adding the radiative contribution to the scattering angle χ_{rad}, which was first computed in Ref. [142] by using the relation derived in Ref. [226],

$$\chi_{\text{rad}} = -\frac{1}{2}\frac{\partial \chi_{\text{cons}}}{\partial J} J_{\text{rad}} + O(m_A^4, e^8), \tag{1.108}$$

where J_{rad} is the radiated angular momentum given in Eqs. (1.99), and Eqs. (1.101), (and with $\partial/\partial J = (1/|p|)(\partial/\partial|b|)$). Using the expressions for radiated angular momentum, we obtain

$$\chi_{\text{rad,EM}} = \frac{2e^6 q_1^3 q_2^3 E}{m_1^2 m_2^2 \gamma^2 v^3 |b|^3} I_{\text{EM}}(v) + O(e^8), \tag{1.109}$$

$$\chi_{\text{rad,GR}} = -\frac{2m_1 m_2 E}{|b|^3}\frac{(2\gamma^2-1)^2}{\gamma^3 v^3} I_{\text{GR}}(v) + O(m_A^4), \tag{1.110}$$

where the I functions are given in Eqs. (1.99) and (1.101). We confirm that this result for $\chi_{\text{rad,EM}}$, that is derived from the relation (1.108) using $J_{\text{rad,EM}}$ (computed from the second-order trajectories), matches the result we obtain directly from the 3PL impulse. The result of Ref. [142] for $\chi_{\text{rad,GR}}$ from $J_{\text{rad,GR}}$ via (1.108) has also been independently confirmed by the direct calculation of the third-order impulse in Ref. [150].

The final ingredients in the expression for radiative impulse in Eq. (1.105) is the radiated momentum K^μ. We compute K^μ_{EM} in Chapter 2 [1] from the full third-order impulses, using

$K^\mu = -\Delta p_1^\mu - \Delta p_2^\mu$, obtaining

$$K^\mu_{\rm EM} = \frac{\pi e^6 q_1^2 q_2^2}{4|b|^3}\left\{\left(\frac{q_1^2}{m_1^2}u_1^\mu + \frac{q_2^2}{m_2^2}u_2^\mu\right)\frac{3\gamma^2+1}{3\gamma v} - \frac{q_1 q_2}{m_1 m_2}\frac{u_1^\mu + u_2^\mu}{\gamma+1}\mathcal{F}(v)\right\} + O(e^8), \tag{1.111}$$

$$\mathcal{F}(v) = \frac{1}{(\gamma v)^3}\left\{(3\gamma^2+1)\left(\gamma - \frac{\operatorname{arctanh} v}{\gamma v}\right) - 4(\gamma-1)^2\right\}. \tag{1.112}$$

By performing the momentum-space integral given in Eq. (6.32) of Ref. [113], we also find that Eq. (1.111) precisely matches the direct calculation of the momentum radiated to infinity by the EM field. The radiated momentum for the GR case was first computed in Ref. [149] using the Kosower-Maybee-O'Connell (KMOC) formalism [113], with the result

$$K^\mu_{\rm GR} = \frac{m_1^2 m_2^2}{|b|^3}\frac{u_1^\mu + u_2^\mu}{\gamma+1}\mathcal{E}(v) + O(m_A^5), \tag{1.113}$$

$$\frac{\mathcal{E}(v)}{\pi} = f_1 + f_2 \log\frac{\gamma+1}{2} + f_3\frac{\operatorname{arctanh} v}{2v}, \tag{1.114}$$

where the f_n are polynomials in γ divided by powers of γv given in Eq. (9) of Ref. [149]. This, along with the full (third-order) impulse structure in Eqs. (1.104) (1.105) and all of the GR results above, has also been confirmed by the calculation in Ref. [150] of the complete $\Delta p^\mu_{1,\rm GR}$ using the KMOC formalism [113] applied to the two-loop amplitude.

1.5.1.2 Unbound-to-bound mapping

An important reason for analyzing scattering problems is to learn more about bound systems. One way to achieve this is by mapping corresponding observables from unbound to bound orbits, as shown in Refs. [131, 227], by relating the scattering angle χ for unbound orbits to the periastron advance $\Delta\phi$ for bound orbits,

$$\Delta\phi(E, J) = \chi(E, J) + \chi(E, -J). \tag{1.115}$$

Such maps are referred to as B2B maps in the literature. Note that the above relation arises from analytic continuation, not a physical transformation. In particular, $\chi(E, -J)$ on the right-hand side does not represent the scattering angle for a system with physically reversed angular momentum. Rather, it denotes the analytic continuation of the function $\chi(E, J)$ under $J \to -J$. This continuation requires a careful choice of contour, as discussed in Refs. [131, 227]. Similarly, recall that bound systems satisfy $E < M_{\mathrm{T}}$, while scattering systems have $E > M_{\mathrm{T}}$. Hence, the relation also involves analytic continuation in energy.

We obtain similar B2B maps relating energy and angular momentum losses between unbound and bound orbits. The relation for the energy loss reads

$$E_{\mathrm{rad}}^{\mathrm{bound}}(E, J) = E_{\mathrm{rad}}^{\mathrm{unbound}}(E, J) - E_{\mathrm{rad}}^{\mathrm{unbound}}(E, -J), \tag{1.116}$$

as also noted previously in Refs. [228]. Here we additionally find an analogous relation for the angular momentum loss,

$$J_{\mathrm{rad}}^{\mathrm{bound}}(E, J) = J_{\mathrm{rad}}^{\mathrm{unbound}}(E, J) + J_{\mathrm{rad}}^{\mathrm{unbound}}(E, -J). \tag{1.117}$$

We verify these maps for the EM case and the GR case at 1PN, and using the maps, discover an error in the 1PN expression for angular momentum radiated away by a binary in a radial period as given in Ref. [229].

In principle, these maps can be used to recover resummed (in v) relativistic expressions for radiative losses in bound orbits. However, since the PM/weak field expansion is also an expansion in $1/J$ (see expressions of scattering angles in Eq. (1.110) for relevant dimensionless quantities, the initial angular momentum is related to impact parameter as $J = |p||b|$), we only recover the leading order $1/J^3$ $(1/J)$ part of the energy (angular momentum) losses, respectively, from the leading order radiative losses. For gravity, the 0PN energy loss for generic bound orbits also contains terms that scale as $1/J^5$ and $1/J^7$, and the coefficient of these terms cannot be recovered directly through the map. The situation is worse for angular-momentum loss where the 0PN angular-momentum loss only contains even powers of $1/J$ (as would be expected from Eq. (1.117)) and thus leading 2PM angular momentum loss does not provide any contribution.

Naively, this would lead to the discouraging conclusion that one needs to solve till 7PM for gravity to recover even the 0PN energy loss. However, we can circumvent this by using an alternate method of fixing radiative losses for generic orbits in the PN expansion. We do it by constructing an ansätz for radiative losses in generic orbits, parametrized by a finite number of unknown coefficients which are then fixed by evaluating the energy losses in the weak field expansion where it should match with the PM results. Further constraints on the coefficients can be obtained by using the relation between energy and angular-momentum losses for circular orbits and some coefficients can be discarded by adding Schott/total time derivative terms [230] to the radiative losses. We reason that this method allows us to fix the 0PN energy losses from just 4PM results.

1.5.2 Tree-level scattering of GWs off spinning objects

We discussed the importance of studying the scattering of GWs off compact objects in Sec. 1.2.2. The associated scattering amplitude encodes the coupling of an object to the gravitational field. Several methods have been developed to relate the gravitational Compton/Raman amplitude of a single body to the dynamics of two gravitationally interacting bodies [4, 5, 111, 115, 167–173]. Such methods require computing the Compton/Raman amplitude for various models of compact objects as input. An ansatz for the Compton amplitude of a Kerr BH at linear order in M (tree level) but up to fifth order in spin S^5, was provided earlier [231]. However, it was not established by a corresponding classical calculation, and instead inferred by demanding a well-behaved high energy/frequency limit on a more general ansatz.

To rectify this, in Chapter 3, which was published as Ref. [2], we compute the tree-level gravitational Compton amplitude to third order in spin, for a generic parity-invariant spinning compact object with spin-induced quadrupole and octupole moments in a WEFT framework. In the special case where the spinning multipole moments are chosen to be that of a Kerr BH, it reduces to the earlier proposal in Ref. [231].

1.5.2.1 Setup

We discussed the worldline action describing the dynamics of a spinning body with spin-induced quadrupole moment in Eq. (1.44) of Sec. 1.3.2. The octupolar multipole moment can be similarly included via a term linear in the covariant derivative of the curvature tensor, i.e., $-(1/12)J_{\rm O}^{\lambda\mu\nu\rho\sigma}\nabla_\lambda R_{\mu\nu\rho\sigma}$. The multipole moment tensors $J_{\rm Q}^{\mu\nu\rho\sigma}$ and $J_{\rm O}^{\lambda\mu\nu\rho\sigma}$ depend on the spin tensor and the four-velocity. Imposing parity invariance constrains the forms of these tensors, leaving a single degree of freedom for each, proportional to two constants, which are labeled as C_2 and C_3, respectively [184]. Consequently, the action describes a parity-invariant spinning object with arbitrary spin-induced quadrupole ($\propto C_2$) and octupole ($\propto C_3$) moments[9].

Let this body initially be at rest in flat spacetime. It is characterized by its mass M, spin

[9] C_1 would tune the spin-induced dipole moment, which is the spin itself. Thus, we can redefine the spin parameter to set $C_1 = 1$.

S, and two coefficients C_2, C_3. The direction and magnitude of the spin can be described by the spin tensor $S^{\mu\nu}$, with $S^{\mu\nu}p_\nu = 0$ and $S^2 = (1/2)S^{\mu\nu}S_{\mu\nu}$, or the Pauli-Lubanski spin vector $s^\mu = -(1/(2M))\epsilon^\mu{}_{\nu\rho\sigma}p^\nu S^{\rho\sigma}$, where p^μ is the momentum of the particle. C_2 and C_3 control the magnitude of its spin-induced quadrupole and octupole moments. In flat spacetime, the particle sources a stationary metric perturbation $-\bar{h}^{\mu\nu} \approx \mathfrak{h}^{\mu\nu} = \sqrt{-g}g^{\mu\nu} - \eta^{\mu\nu}$, given at linear order in M as [128]

$$\begin{aligned}\bar{h}^{\mu\nu} &= -u^\mu u^\nu [1 - \frac{C_2}{2}(a\cdot\partial)^2]\frac{M}{r} \\ &\quad - u^{(\mu}\epsilon^{\nu)}{}_{\rho\alpha\beta}u^\rho a^\alpha \partial^\beta [1 - \frac{C_3}{3!}(a\cdot\partial)^2]\frac{4M}{r},\end{aligned} \tag{1.118}$$

where $u^\mu = (1/M)p^\mu$ is the 4-velocity of the particle in flat-spacetime and $a^\mu = (1/M)s^\mu$, with $a \cdot u = 0$. The actual non-linear metric sourced by the body approaches this form asymptotically. In the rest frame of the particle, this can be rewritten as

$$\begin{aligned}\bar{h}^{00} &= [1 - \frac{C_2}{2}(\vec{a}\cdot\vec{\partial})^2]\left(-\frac{4M}{r}\right), \quad h^{ij} = 0, \\ \bar{h}^{0i} &= \epsilon^i{}_{jk}a^j\partial^k [1 - \frac{C_3}{3!}(\vec{a}\cdot\vec{\partial})^2]\frac{2M}{r},\end{aligned} \tag{1.119}$$

where $\vec{a}$ can be identified as the spin vector. Comparison of the above expression with the most general asymptotic past-stationary spacetime given in Eq.(36) of Ref. [46] shows that the metric perturbation in Eq. (3.2) can be recovered by imposing stationarity (all multipole moments being constant in time) and identifying the mass-type multipole moments as $I = M$, $I_i = 0$, $I_{ij} = -C_2 M a_{\langle i}a_{j\rangle}$, $I_{ijk} = 0$ and current-type multipole moments as $J_i = Ma_i$, $J_{ij} = 0$, $J_{ijk} = -(2/3)C_3 M a_{\langle i}a_j a_{k\rangle}$ and require that all other multipole moments either vanish or are higher orders in spin.

If the particle respects parity and only has spin-induced multipole moments, the vanishing or irrelevance of all other multipole moments follows trivially from parity invariance. Thus, M, S, C_2 and C_3 parametrize the most general axisymmetric, parity-preserving, stationary linearized metric perturbation. Also note, that adding trace terms to the multipole moments (e.g., $\delta_{ij}|a|^2$ to I_{ij}) only modifies it by terms proportional to $\partial^2(1/r) \propto \delta^{(3)}(x)$ thus modifying the field only at the location of the particle. Such corrections are expected to be irrelevant since the field at the location of the particle is ill-defined.

We now subject this parity-preserving, stationary, axisymmetric body to an external linearized GW incident upon it, which is characterized as [10]

$$
\begin{aligned}
&\mathfrak{h}^{\mu\nu}_{\text{wave}} = \mathfrak{a}\ \varepsilon^{\mu}_{\pm}\varepsilon^{\nu}_{\pm} \exp[ik \cdot x], \\
&k^{\mu} \equiv \omega(1,0,0,1),\ \varepsilon^{\mu}_{\pm} \equiv \frac{1}{\sqrt{2}}(0,1,\pm i,0),
\end{aligned}
\tag{1.120}
$$

where $\mathfrak{a}$ is the amplitude of the incoming wave, k^{μ} is the wave-vector, fixing the direction of propagation, ω its frequency and ε^{μ} is a complex null vector which that the helicity of the incoming wave. The metric perturbation due to the incident wave affects the momentum, spin and subsequently the spin-induced multipole moments, according to the MPD equations. We presented the MPD equations for a spinning particle with spin-induced quadrupole moment in Eq. (1.45). Including octupolar coupling, the MPD equations are modified as

$$
\begin{aligned}
\frac{DS^{\mu\nu}}{D\tau} - 2p^{[\mu}u^{\nu]} = N^{\mu\nu} = \frac{4}{3}R^{[\mu}{}_{\lambda\rho\sigma}J_{\mathrm{Q}}^{\nu]\lambda\rho\sigma} \\
+ \frac{2}{3}\nabla^{\lambda}R^{[\mu}{}_{\tau\rho\sigma}J_{O\lambda}{}^{\nu]\tau\rho\sigma} + \frac{1}{6}\nabla^{[\mu}R_{\lambda\tau\rho\sigma}J_{\mathrm{O}}^{\nu]\lambda\tau\rho\sigma},
\end{aligned}
\tag{1.121a}
$$

$$
\begin{aligned}
\frac{Dp_{\mu}}{D\tau} + \frac{1}{2}R_{\mu\nu\rho\sigma}u^{\nu}S^{\rho\sigma} = F^{\mu} = -\frac{1}{6}J_{\mathrm{Q}}^{\lambda\nu\rho\sigma}\nabla_{\mu}R_{\lambda\nu\rho\sigma} \\
- \frac{1}{12}J_{\mathrm{O}}^{\tau\lambda\nu\rho\sigma}\nabla_{\mu}\nabla_{\tau}R_{\lambda\nu\rho\sigma}.
\end{aligned}
\tag{1.121b}
$$

[10]Here, we use the notation $a^{\mu} \equiv \{a^{\hat{0}}, a^{\hat{1}}, a^{\hat{2}}, a^{\hat{3}}\}$ to mean the components in the rest frame of the body. Thus $k^{\mu} \equiv \omega(1,0,0,1)$ means the 4-vector k is pointing along the z-axis and has frequency ω in the rest frame.

We also impose the covariant SSC condition $S_{\mu\nu}p^{\nu} = 0$. The MPD equations along with the SSC constraint can be used to solve for perturbations to spin and momentum due to the external GW.

These three perturbed quantities — momentum, spin, spin-induced multipole moments — in turn perturb the stress energy tensor of the object, leading to a radiated scattered wave through the Einstein equation. Additionally owing to the nonlinear nature of GR, the incident wave also scatters off the static metric perturbation sourced by the particle. Together, these two contributions lead to a scattered wave. As previously explained in Sec. 1.2.2.1, the form of the scattered wave, encodes the scattering amplitude. In the particle's rest frame, the scattered wave takes the asymptotic form (i.e., at large distances from the particle) [2]

$$\begin{aligned}\mathfrak{h}^{\mu\nu}_{\text{scatter}}(r,\hat{n}) \equiv\ & [\mathcal{M}_{\pm+}(\hat{n})\zeta^{\mu}_{+2}(\hat{n})\zeta^{\nu}_{+2}(\hat{n}) \\ & + \mathcal{M}_{\pm-}(\hat{n})(\hat{n})\zeta^{\mu}_{-2}(\hat{n})\zeta^{\nu}_{-2}(\hat{n})]\frac{\exp[i\omega(r-t)]}{\omega r},\end{aligned} \tag{1.122}$$

where $\mathcal{M}_{\pm\pm}(\hat{n})$ are the scattering amplitudes for a given pair of incoming and outgoing helicities. $\hat{n}$ is the spatial unit vector in a given direction in the rest frame of the particle, $\zeta^{\mu}_{\pm}(\hat{n})$ are the complex null polarization vectors for a wave vector given by $l^{\mu} \equiv \omega(1,\hat{n})$. Thus, $\mathcal{M}_{\pm\pm}(\hat{n})$ is the amplitude for an incident wave with wave vector $k^{\mu} \equiv \omega(1,0,0,1)$, helicity ± 2, scattering into another wave vector $l^{\mu} \equiv \omega(1,\hat{n}) \equiv \omega(1,\sin\theta,\cos\theta,0)$ with helicity ± 2.

1.5.2.2 Gravitational Compton amplitude

At zeroth order in spin (or for spinless case), we obtain the amplitudes [2]

$$\mathcal{M}_{ab} = \frac{4M\omega^3(\varepsilon_a\cdot\zeta_b)^2}{(l-k)^2}, \tag{1.123}$$

$$\mathcal{M}_{++} = \mathcal{M}_{--} = M\omega\frac{\cos^4\left(\frac{\theta}{2}\right)}{\sin^2\left(\frac{\theta}{2}\right)}, \tag{1.124}$$

$$\mathcal{M}_{+-} = \mathcal{M}_{-+} = M\omega \sin^2\left(\frac{\theta}{2}\right), \tag{1.125}$$

where θ is the angle between the incoming and outgoing wave vectors (k^μ and l^μ with $2\omega^2 \sin^2\left(\frac{\theta}{2}\right) = -k \cdot l$). Note that there is mixing of helicities (nonzero $\mathcal{M}_{+-}$ and $\mathcal{M}_{-+}$) even at zeroth order in spin. This is not true for electromagnetic waves scattering off BHs. The above amplitudes are consistent with those obtained in Ref. [232] for spinless BHs, and our discussion in Sec. 1.2.2.1. Next, to first order in spin (or for a spinning rigid particle with no spin-induced deformation). We obtain the amplitudes [2]

$$\begin{aligned}
\mathcal{M}_{++} =& M\omega \frac{\cos^4\left(\frac{\theta}{2}\right)}{\sin^2\left(\frac{\theta}{2}\right)}\Bigg[1 - \tan^2\left(\frac{\theta}{2}\right)\frac{s^\mu}{M}(k_\mu + l_\mu) \\
&- i\frac{S_{\mu\nu}k^\mu l^\nu}{M\omega\cos^2\left(\frac{\theta}{2}\right)}\Bigg], && (1.126)\\
\mathcal{M}_{+-} =& M\omega \sin^2\left(\frac{\theta}{2}\right)\left[1 + \frac{s^\mu(k_\mu - l_\mu)}{M}\right], && (1.127)\\
\mathcal{M}_{--} =& \bar{\mathcal{M}}_{++}(S^{\mu\nu} \to -S^{\mu\nu},\ s^\mu \to -s^\mu), && (1.128)\\
\mathcal{M}_{-+} =& \bar{\mathcal{M}}_{+-}(S^{\mu\nu} \to -S^{\mu\nu},\ s^\mu \to -s^\mu), && (1.129)
\end{aligned}$$

where the spin tensor $S^{\mu\nu}$, $S^{\mu\nu}p_\nu = 0$, and the Pauli-Lubanski spin vector s^μ, appear for the first time. A bar denotes complex conjugation. Note that the spin tensor/vector appearing in the amplitude is that of the initial unperturbed particle, prior to the wave like perturbation. We find that the amplitudes are related to their helicity-flipped versions, via a spin-flip and complex conjugation. This is because the helicities of the incoming and outgoing GW can be flipped via a combination of parity-flip and time-reversal operation on the whole system, which flips the spin (s^μ, $S^{\mu\nu}$), complex conjugates the amplitudes ($\mathcal{M} \to \bar{\mathcal{M}}$) but leaves the momenta (k^μ, l^μ) unchanged. The differential cross-section resulting from these amplitudes agrees with Eq. (3) of [166], where it was derived using BHPT.

The coefficients C_2 and C_3 associated with the spin-induced quadrupole ($\propto S^2$) and octupole ($\propto S^3$) moments finally show themselves at second and third order in spin respectively. For the case of a BH, $C_2 = C_3 = 1$, the scattering amplitudes to third order are found to be simply the exponentiated versions of the first order in spin amplitudes in Eqs. (1.126), (1.127), (1.128), (1.129). We get (to third order in spin)

$$\mathcal{M}_{++} = M\omega \frac{\cos^4\left(\frac{\theta}{2}\right)}{\sin^2\left(\frac{\theta}{2}\right)} \exp\left[-\frac{s^\mu}{M}(k_\mu + l_\mu)\tan^2\left(\frac{\theta}{2}\right) - \frac{i}{M\omega\cos^2(\frac{\theta}{2})}S^{\mu\nu}k_\mu l_\nu\right], \tag{1.130}$$

$$\mathcal{M}_{+-} = M\omega \sin^2\left(\frac{\theta}{2}\right) \exp\left[\frac{s^\mu}{M}(k_\mu - l_\mu)\right], \tag{1.131}$$

$$\mathcal{M}_{--} = \bar{\mathcal{M}}_{++}(S^{\mu\nu} \to -S^{\mu\nu},\ s^\mu \to -s^\mu), \tag{1.132}$$

$$\mathcal{M}_{-+} = \bar{\mathcal{M}}_{+-}(S^{\mu\nu} \to -S^{\mu\nu},\ s^\mu \to -s^\mu), \tag{1.133}$$

which matches the amplitude given in spinor helicity formalism in Ref. [233], obtained from Ref. [111] using QFT-based methods. It is also consistent with the amplitudes obtained via BHPT in Ref. [174].

The amplitudes do not exponentiate when C_2 and C_3 are generic. Thus, they correct the amplitudes in Eqs. (1.130), (1.131), (1.132), (1.133) by adding terms proportional to $(C_{2/3} - 1)^n$. The general expressions for the amplitudes with generic C_2 and C_3 for generic polarization vectors are given in the Appendix B of Chapter 3 [2]. The expressions for the helicity-conserving amplitudes ($\mathcal{M}_{++}$ and $\mathcal{M}_{--}$) for generic C_2 and C_3 after substitution of polarization vectors can be simplified considerably by introducing the vector

$$w_{\mathrm{S}}^\mu = \frac{1}{2\omega\cos^2\left(\frac{\theta}{2}\right)}[\omega(k^\mu + l^\mu) - i\epsilon^\mu{}_{\alpha\beta\gamma}k^\alpha l^\beta u^\gamma], \tag{1.134}$$

which coincides with half the complex conjugate of the vector w^μ from Ref. [233]. We also define $a^\mu = s^\mu/m$. Then, in terms of w_S^μ, k^μ, l^μ, and a^μ, the helicity-conserving amplitudes for the BH case $C_2 = C_3 = 1$ can be rewritten as

$$\mathcal{M}_{++} = M\frac{\cos^4\left(\frac{\theta}{2}\right)}{\sin^2\left(\frac{\theta}{2}\right)}\ \exp[a\cdot(k+l-2w_\mathrm{S})], \tag{1.135}$$

$$\mathcal{M}_{--} = \bar{\mathcal{M}}_{++}(a^\mu \to -a^\mu). \tag{1.136}$$

The helicity-conserving scattering amplitudes for a spinning particle, with spin-induced quadrupole moments with generic C_2 and C_3 to third order in spin, is given by

$$\begin{aligned}\mathcal{M}_{++} = {} & M\omega\frac{\cos^4(\theta/2)}{\sin^2(\theta/2)}\Bigg(\exp[a\cdot(k+l-2w_\mathrm{S})] \\ & + \frac{C_2-1}{2}\{[(k-w_\mathrm{S})\cdot a]^2 + [(l-w_\mathrm{S})\cdot a]^2\} \\ & + \frac{C_2-1}{2}[(k-w_\mathrm{S})\cdot a][(l-w_\mathrm{S})\cdot a][(k+l-2w_\mathrm{S})\cdot a] \\ & - (C_2-1)^2[(k-w_\mathrm{S})\cdot a][(l-w_\mathrm{S})\cdot a](w_\mathrm{S}\cdot a) \\ & + \frac{C_3-1}{6}\{[(k-w_\mathrm{S})\cdot a]^3 + [(l-w_\mathrm{S})\cdot a]^3\}\Bigg).\end{aligned} \tag{1.137}$$

$$\mathcal{M}_{--} = \bar{\mathcal{M}}_{++}(a^\mu \to -a^\mu). \tag{1.138}$$

The expressions and the corresponding basis for simplification of helicity-reversing amplitudes are complicated and are given in the relevant Chapter 3 [2].

1.5.3 Horizon fluxes for Kerr BHs

The defining feature of a BH is the presence of an event horizon, a one-way membrane that permits only infalling matter and radiation to cross it in finite proper time. For perturbations, including linearized metric fluctuations, ingoing boundary conditions must be imposed at the horizon [213]. Crucially, the horizon enables dissipation and irreversible behavior [234].

In the context of binaries, the horizon permits an irreversible transfer of energy and angular momentum between the orbit and the BH(s). This transfer is captured by horizon fluxes [235], which measure the rate at which energy and angular momentum cross into the BH. For Kerr BHs, horizon fluxes can also tap into the hole's rotational energy, leading to a decrease in both mass and spin, in a process akin to the Penrose mechanism [236, 237] driven by scattering in the ergoregion. The accumulated transfer of energy and angular momentum ultimately affects the gravitational waveform, modifying the rate of inspiral much like the fluxes radiated to infinity.

Compared to the energy and angular-momentum fluxes of GWs radiated to infinity, the horizon fluxes enter at 2.5PN order for Kerr BHs and 4PN for Schwarzschild BHs [58–65]. They begin affecting the waveform at the same respective orders. The lower-order onset for spinning BHs arises from the fact that horizon fluxes are sourced by time-dependent perturbations, and a spinning BH perceives even a static external field as time-dependent in its corotating frame [61].

In the test-body limit, the horizon fluxes can be computed via BHPT by solving the Teukolsky equation [58], but generalizing to arbitrary mass ratios is challenging. This was achieved at leading 2.5PN order for aligned-spin circular orbits [59] and later extended to 4PN (NNLO) via BHPT and near-zone matching [60, 198]. However, the 4PN result for spinning BHs contradicted the test-body limit findings [58], leaving an unresolved discrepancy.

Another approach to the computation of horizon fluxes is through WEFT. As explained in Sec. 1.3.3, in a WEFT, finite-size effects are captured through intrinsic and induced multipole moments. Since horizon fluxes arise only in a perturbed BH, they fall into the latter category and may be incorporated as dissipative tidal effects. However, a WEFT must be calibrated to the specific compact object of interest through a matching computation. In Ref. [61] (see also [197, 238–241]), a WEFT was formulated to capture the leading-order (2.5PN) horizon fluxes, with the Wilson coefficients entering the tidal-response ansatz fixed by comparing to perturbative calculations of the absorption cross section of plane GWs by BHs [242]. A key advantage of this approach is that a gauge-invariant quantity (the absorption cross section) is used to fix the freedom in the WEFT in an unambiguous way, and subsequently to compute the change in mass and angular momentum in a quasicircular binary at leading order. However, the NLO (3.5PN) and NNLO (4PN) order results are unavailable in the WEFT approach, and thus the discrepancy regarding horizon fluxes at 4PN remains unaddressed.

In Chapter 4, which was originally published as Ref. [3], we resolve this long-standing discrepancy by correctly computing horizon fluxes to 4PN order using a WEFT approach to model dissipative tidal effects, addressing both conceptual and computational challenges along the way. Additionally, to enable calibrating our WEFT beyond leading order, i.e., fixing the tidal-response coefficients at higher orders, we use the MST method to analytically compute the degree of absorption in BHPT for GWs scattering off a Kerr BH, to NLO in their frequency. We then match the degree of absorption in this scattering setup between WEFT and BHPT to fix the tidal response to the desired order (NLO), enabling the computation of horizon fluxes up to NNLO for spinning bodies. We find that our results are consistent with the test-body limit.

In the following subsections, we briefly describe the methodology and results for computing the rate of change of mass and angular momentum due to horizon fluxes using WEFT and BHPT.

1.5.3.1 Equations of motion for a spinning body with tidal moments

Following the discussion in Sec. 1.3.3.2, the action for a spinning particle with inducible quadrupolar and octupolar tidal moments can be written in an implicit form as

$$S = \int d\tau L(u^\mu, \Omega^{\mu\nu}, g_{\mu\nu}, Q_{\mathcal{E}}^{\mu\nu}, \dot{Q}_{\mathcal{E}}^{\mu\nu}, Q_{\mathcal{B}}^{\mu\nu}, \dot{Q}_{\mathcal{B}}^{\mu\nu}, O_{\mathcal{E}}^{\mu\nu\rho}, \dot{O}_{\mathcal{E}}^{\mu\nu\rho}, O_{\mathcal{B}}^{\mu\nu\rho}, \dot{O}_{\mathcal{B}}^{\mu\nu\rho}, R_{\mu\nu\rho\sigma}, \nabla_\lambda R_{\mu\nu\rho\sigma}). \tag{1.139}$$

This leads to equations of motion identical to the MPD equations presented in Eq. (1.121), except that the multipole tensors are given by

$$J_{\mathrm{Q}}^{\mu\nu\rho\sigma} = -6\frac{\partial L}{\partial R_{\mu\nu\rho\sigma}} = -3u^{[\mu}Q_{\mathcal{E}}^{\nu][\rho}u^{\sigma]} + \frac{3}{2}Q_{\mathcal{B}}^{\alpha\langle\rho}\epsilon_{\beta\alpha}{}^{\mu\nu}u^{|\beta|}u^{\sigma\rangle_R} \tag{1.140}$$

$$J_{\mathrm{O}}^{\lambda\mu\nu\rho\sigma} = -12\frac{\partial L}{\partial \nabla_\lambda R_{\mu\nu\rho\sigma}} = -6u^{\langle\mu}O_{\mathcal{E}}^{\nu\rho\lambda}u^{\sigma\rangle_{\nabla R}} + 3O_{\mathcal{B}}^{\alpha\langle\rho\lambda}\epsilon_{\beta\alpha}{}^{\mu\nu}u^{|\beta|}u^{\sigma\rangle_{\nabla R}}, \tag{1.141}$$

where $\langle\ldots\rangle_{\nabla R}$ implies imposing the symmetries of the derivative of the Riemann curvature tensor ($\nabla_\lambda R_{\mu\nu\rho\sigma}$) on the contained indices except β. Additionally, the spin tensor $S^{\mu\nu}$ here is the sum of intrinsic and tidal spin , i.e.,

$$S^{\mu\nu} = S_{\mathrm{rot}}^{\mu\nu} + S_{\mathrm{tidal}}^{\mu\nu}, \quad S_{\mathrm{rot}}^{\mu\nu} = \frac{\partial L}{\partial \Omega_{\mu\nu}}, \tag{1.142}$$

$$S_{\mathrm{tidal}}^{\mu\nu} = -2[P_{\mathcal{E}}^{[\mu}{}_{\nu}Q_{\mathcal{E}}^{\nu]\mu} + (\mathcal{E} \leftrightarrow \mathcal{B})] - 3[P_{\mathcal{E}}^{[\mu}{}_{\nu\rho}O_{\mathcal{E}}^{\nu]\mu\rho} + (\mathcal{E} \leftrightarrow \mathcal{B})],$$

$$P_{\mu\nu}^{\mathcal{E}(\mathcal{B})} = \frac{\partial L}{\partial \dot{Q}_{\mathcal{E}(\mathcal{B})}^{\mu\nu}}, \quad P_{\mu\nu\rho}^{\mathcal{E}(\mathcal{B})} = \frac{\partial L}{\partial \dot{O}_{\mathcal{E}(\mathcal{B})}^{\mu\nu\rho}}.$$

These equations follow naturally from our discussion in Sec. 1.3.3, and the derivation is outlined in Chapter 4 [3]. We showed in Sec. 1.3.3.2 that substituting Eq. (1.55) (or Eq. (1.140)), splits the interaction term $\sim J_{\mathrm{Q}}^{\mu\nu\rho\sigma}R_{\mu\nu\rho\sigma}$ as $\sim -Q_{\mathcal{E}}^{\mu\nu}\mathcal{E}_{\mu\nu} - Q_{\mathcal{B}}^{\mu\nu}\mathcal{B}_{\mu\nu}$. Similarly, substituting Eq. (1.141) splits the octupolar interaction term $\sim J_{\mathrm{O}}^{\lambda\mu\nu\rho\sigma}\nabla_\lambda R_{\mu\nu\rho\sigma}$ as $\sim -O_{\mathcal{B}}^{\mu\nu\rho}\mathcal{B}_{\mu\nu\rho} - O_{\mathcal{E}}^{\mu\nu\rho}\mathcal{E}_{\mu\nu\rho}$. This shows the octupolar tidal multipoles, coupled to the octupolar tidal fields given by

$$\mathcal{E}_{\mu\nu\rho} = \nabla_{\langle\rho}\mathcal{E}_{\mu\nu\rangle}, \quad \mathcal{B}_{\mu\nu\rho} = \nabla_{\langle\rho}\mathcal{B}_{\mu\nu\rangle}, \tag{1.143}$$

where $\langle ... \rangle$ means symmetrization and trace removal of contained indices. The parity of the electric and magnetic tidal fields is given by $(-1)^{\ell}$ and $(-1)^{\ell+1}$ respectively, where ℓ is the number of indices (rank of the corresponding field tensor). So, for quadrupolar (octupolar) fields, $\mathcal{E}_{\mu\nu}$ ($\mathcal{B}_{\mu\nu\rho}$) is even whereas $\mathcal{B}_{\mu\nu}$ ($\mathcal{E}_{\mu\nu\rho}$) is odd under parity flip. This has implications for the tidal response as shown in the next subsubsection.

The rate of change of mass, and angular momentum due to horizon fluxes/tidal heating is then obtained by defining mass/spin as the magnitude of $p^{\mu}, S_{\mu\nu}$ respectively as $M^2 = -p^{\mu}p_{\mu}$, $J^2 = (1/2)S^{\mu\nu}S_{\mu\nu}$, and differentiating w.r.t time. We then use the MPD equations in Eq. (1.121), along with Eqs. (1.140), (1.141), to obtain the formulae

$$\frac{dM}{d\tau} = \frac{1}{2}Q_{\mathcal{E}}^{\rho\sigma}\dot{\mathcal{E}}_{\rho\sigma} + \frac{1}{2}O_{\mathcal{E}}^{\rho\sigma\lambda}\dot{\mathcal{E}}_{\rho\sigma\lambda} + (\mathcal{E} \leftrightarrow \mathcal{B}), \tag{1.144}$$

$$\frac{dJ}{d\tau} = \frac{1}{J}Q_{\mathcal{E}}^{\mu\nu}\mathcal{E}_{\mu}{}^{\rho}S_{\rho\nu} + \frac{3}{2J}O_{\mathcal{E}}^{\mu\nu\lambda}\mathcal{E}_{\mu\lambda}{}^{\rho}S_{\rho\nu} + (\mathcal{E} \leftrightarrow \mathcal{B}), \tag{1.145}$$

as a function of the induced tidal moments. The remaining task is to compute the time evolution of these moments.

1.5.3.2 Tidal response

We assume a linear tidal response as explained in Sec. 1.3.3.3. For Kerr BHs (and spinning bodies in general), the same logic applies, but now the relationship need not be directly proportional, but through a tidal-response tensor that could depend on the spin tensor. Additionally, quadrupolar moments may be induced by octupolar fields and vice-versa in a manner consistent with parity invariance. This is due to breaking of spherical symmetry in the presence of spin. For our purposes, it is sufficient to write the tidal response to NLO in time derivatives (more precisely, sixth order in M) as

$$
\begin{aligned}
Q^{\mu\nu}_{\mathcal{E}} &= M^5 \lambda^{\mu\nu}_{\mathcal{E},0\rho\sigma}\mathcal{E}^{\rho\sigma} + M^6 \lambda^{\mu\nu}_{\mathcal{E},1\rho\sigma}\frac{D}{D\tau}\mathcal{E}^{\rho\sigma} \\
&\quad + M^6 \nu^{\mu\nu}_{\mathcal{B},0\langle\rho\sigma}\hat{s}_{\gamma\rangle}\mathcal{B}^{\rho\sigma\gamma}, \\
O^{\mu\nu\rho}_{\mathcal{B}} &= M^6 \hat{s}^{\langle\rho}\xi^{\mu\nu\rangle}_{\mathcal{E},0\,\alpha\beta}\mathcal{E}^{\alpha\beta},
\end{aligned}
\tag{1.146}
$$

and similarly for $(\mathcal{E} \leftrightarrow \mathcal{B})$. Here

$$
\begin{aligned}
\lambda^{\mu\nu}_{\mathcal{E},a\rho\sigma} &= f^0_{\mathcal{E},a}\mathcal{P}^{\langle\mu}_{\langle\rho}\mathcal{P}^{\nu\rangle}_{\sigma\rangle} + f^1_{\mathcal{E},a}\hat{S}^{\langle\mu}{}_{\langle\rho}\mathcal{P}^{\nu\rangle}_{\sigma\rangle} + f^2_{\mathcal{E},a}\hat{s}^{\langle\mu}\hat{s}_{\langle\rho}\delta^{\nu\rangle}_{\sigma\rangle} + f^3_{\mathcal{E},a}\hat{s}^{\langle\mu}\hat{s}_{\langle\rho}\hat{S}^{\nu\rangle}{}_{\sigma\rangle} \\
&\quad + f^4_{\mathcal{E},a}\hat{s}^{\langle\mu}\hat{s}_{\langle\rho}\hat{s}^{\nu\rangle}\hat{s}_{\sigma\rangle} \text{ for } a = 0,\ 1,
\end{aligned}
\tag{1.147a}
$$

$$
\begin{aligned}
\nu^{\mu\nu}_{\mathcal{B},0\rho\sigma} &= g^0_{\mathcal{B},0}\mathcal{P}^{\langle\mu}_{\langle\rho}\mathcal{P}^{\nu\rangle}_{\sigma\rangle} + g^1_{\mathcal{B},0}\hat{S}^{\langle\mu}{}_{\langle\rho}\mathcal{P}^{\nu\rangle}_{\sigma\rangle} + g^2_{\mathcal{B},0}\hat{s}^{\langle\mu}\hat{s}_{\langle\rho}\delta^{\nu\rangle}_{\sigma\rangle} + g^3_{\mathcal{B},0}\hat{s}^{\langle\mu}\hat{s}_{\langle\rho}\hat{S}^{\nu\rangle}{}_{\sigma\rangle} \\
&\quad + g^4_{\mathcal{B},0}\hat{s}^{\langle\mu}\hat{s}_{\langle\rho}\hat{s}^{\nu\rangle}\hat{s}_{\sigma\rangle}
\end{aligned}
\tag{1.147b}
$$

$$
\begin{aligned}
\xi^{\mu\nu}_{\mathcal{E},0\rho\sigma} &= h^0_{\mathcal{E},0}\mathcal{P}^{\langle\mu}_{\langle\rho}\mathcal{P}^{\nu\rangle}_{\sigma\rangle} + h^1_{\mathcal{E},0}\hat{S}^{\langle\mu}{}_{\langle\rho}\mathcal{P}^{\nu\rangle}_{\sigma\rangle} + h^2_{\mathcal{E},0}\hat{s}^{\langle\mu}\hat{s}_{\langle\rho}\delta^{\nu\rangle}_{\sigma\rangle} + h^3_{\mathcal{E},0}\hat{s}^{\langle\mu}\hat{s}_{\langle\rho}\hat{S}^{\nu\rangle}{}_{\sigma\rangle} \\
&\quad + h^4_{\mathcal{E},0}\hat{s}^{\langle\mu}\hat{s}_{\langle\rho}\hat{s}^{\nu\rangle}\hat{s}_{\sigma\rangle}
\end{aligned}
\tag{1.147c}
$$

and similarly for $(\mathcal{E} \leftrightarrow \mathcal{B})$.

Here, $\hat{S}^{\mu\nu}$ and $\hat{s}^{\mu}$ are the normalized versions of the spin-tensor ($\hat{S}^{\mu\nu}\hat{S}_{\mu\nu} = 2$) and spin-vector ($s^{\mu} \approx -(1/2)\epsilon^{\mu}{}_{\nu\rho\sigma}u^{\nu}\hat{S}^{\rho\sigma}$, $\hat{s}^{\mu}\hat{s}_{\mu} = 1$), and so they are dimensionless and independent of any parameter. $\mathcal{P}^{\mu}_{\nu} = \delta^{\mu}_{\nu} + u^{\mu}u_{\nu}$, is a projection tensor used to project the tensors orthogonal to the four-velocity u^{μ}. $\langle\ldots\rangle$ denotes symmetrization and trace removal for the contained indices. Using the identities governing the spin-tensor and spin-vector, we show that this is the most general form for the tidal-response tensor of a parity-preserving, spinning, compact object [3, 4] to NLO. Note that the electric, quadrupole moment may be induced by the magnetic, octupolar tidal field, and vice-versa, consistent with parity invariance.

The forty coefficients ($40 = (5\times2+5+5)\times2$) appearing in Eq. (1.147) are the tidal-response coefficients. They encode both conservative and dissipative tidal effects. Among the coefficients entering $\lambda^{\mu\nu}_{\mathcal{E},0\rho\sigma}$, $f^i_{\mathcal{E},0}$ for $i = 0, 2, 4$ are conservative, whereas $f^j_{\mathcal{E},0}$ for $j = 1, 3$ are dissipative. This classification follows directly from the time-reversal properties of the accompanying tensors. The electric tidal field $\mathcal{E}^{\mu\nu}$ is even under time reversal, while the spin tensor and spin vector are odd. Consequently, terms involving an even (odd) number of spin tensors or vectors are time-reversal even (odd) respectively, and hence correspond to conservative (dissipative) tidal induction. The same is true for the magnetic sector.

However, the covariant derivative operator $D/D\tau$ is odd under time reversal, which reverses this assignment at NLO: $f^i_{\mathcal{E}/\mathcal{B},1}$ with $i = 0, 2, 4$ are dissipative, whereas $f^j_{\mathcal{E}/\mathcal{B},1}$ with $j = 1, 3$ are conservative.

Similar reasoning classifies the tidal-response coefficients associated with cross-induction between the quadrupolar and octupolar sectors, namely $g^i_{\mathcal{B}(\mathcal{E}),0}$ and $h^i_{\mathcal{E}(\mathcal{B}),0}$ for $i = 0, 1, 2, 3, 4$, though care must be taken since the magnetic tidal field and the octupole moment are odd under time reversal. They exhibit a similar splitting as $f^i_{\mathcal{E}(\mathcal{B}),0}$.

Overall, there are a total of 18 dissipative tidal-response coefficients. Note that for nonspinning bodies, only four coefficients — $f^0_{\mathcal{E}/\mathcal{B},0}$ and $f^1_{\mathcal{E}/\mathcal{B},0}$ — are present, and we can identify the former two with the Love numbers and the latter two as dissipation numbers. Also, we can recover Eq. (1.59) by identifying $f^0_{\mathcal{E},0} = -\Lambda^{\mathcal{E}}$, and $f^1_{\mathcal{E},0} = H^{\mathcal{E}}_{\omega}$.

The six conservative coefficients $f^i_{\mathcal{E}/\mathcal{B},0}$ for $i = 0, 2, 4$, which characterize the leading-order, quadrupolar, static tidal response of the body, are known as the Love numbers [193]. These vanish for Kerr BHs [243]. The four dissipative coefficients $f^i_{\mathcal{E}/\mathcal{B},0}$ for $i = 1, 3$ are known to be nonzero for Kerr BHs and once caused confusion regarding the vanishing of Love numbers [244]. A crucial point is that such dissipative coefficients are not allowed in the static tidal response of Schwarzschild BHs, since there is no spin tensor or vector to break time-reversal invariance in the absence of time-derivative operators. From the EFT perspective, this is precisely why dissipative effects such as horizon fluxes are expected to appear at a lower PN order in the presence of spin.

1.5.3.3 Raman scattering amplitudes in BHPT and matching with WEFT amplitudes

We fix the 18 dissipative tidal-response coefficients by studying the absorption of GWs scattering off a Kerr BH in BHPT, and in the WEFT, where it depends on the tidal-response coefficients. We explained previously in Sec. 1.4.3 that the degree of absorption $\eta^{\mathrm{P}}_{\ell m}$, for a given spheroidal mode can be obtained from the MST solution to the Teukolsky equation via Eq. (1.92). For our purposes, it is sufficient to compute up to sixth power in ϵ, where $\epsilon = 2M\omega$, and restrict to[11] $\ell = 2, 3$ and we obtain

$$
\begin{aligned}
1 - |\eta^{\mathrm{P}=\pm}_{2m}| =& -\left(\frac{\epsilon}{2}\right)^5 m\left[\frac{2\mathcal{A}^1_0}{5} - (m^2-4)\frac{2}{15}\mathcal{A}^3_0\right](1+\epsilon\pi) \\
&+\left(\frac{\epsilon}{2}\right)^6\left\{\frac{4\mathcal{A}^0_1}{5} - (m^2-4)\left[\frac{2\mathcal{A}^2_1}{15} + \frac{2\mathcal{A}^4_1}{15}(m^2-1)\right]\right\} + \mathcal{O}(\epsilon^7),
\end{aligned} \tag{1.148}
$$

$$
1 - |\eta^{\mathrm{P}=\pm}_{3m}| = \mathcal{O}(\epsilon^7), \tag{1.149}
$$

where

$$
\mathcal{A}^1_0 = \frac{16\chi}{45}(1+3\chi^2),\ \mathcal{A}^3_0 = -\frac{4\chi^3}{3}, \tag{1.150a}
$$

[11] Quadrupolar (octupolar) tidal deformation primarily affects $\eta^{P}_{\ell m}$, at $\ell = 2$ ($\ell = 3$). For Schwarzschild BH, this identification is exact. For Kerr BHs, recall that ℓm are labels of spheroidal harmonics and not spherical harmonics. Thus, ℓ does not neatly map to the rank of the tidal multipole tensor.

$$\mathcal{A}_1^0 = \frac{16}{405}(9 + 9\kappa + 97\chi^2 + 117\kappa\chi^2 - 6\chi^4 + 54\sigma\chi^4 + 36\chi B_2 + 108\chi^3 B_2), \tag{1.150b}$$

$$\mathcal{A}_1^2 = -\frac{8}{135}(115\chi^2 + 135\kappa\chi^2 + 5\chi^4 + 90\kappa\chi^4 - 24\chi B_1 + 18\chi^3 B_1 + 48\chi B_2 + 144\chi^3 B_2), \tag{1.150c}$$

$$\mathcal{A}_1^4 = \frac{8}{135}(20\chi^4 + 45\kappa\chi^4 - 24\chi B_1 + 18\chi^3 B_1 + 12\chi B_2 + 36\chi^3 B_2), \tag{1.150d}$$

where $B_m = \text{Im}[\text{PolyGamma}(0, 3 + im\chi/\kappa)]$, and $\kappa = \sqrt{1-\chi^2}$ and $\chi = J/M^2$.

We also compute this in WEFT, where the scattering problem can be studied using the MPD equations, Einstein equation and the tidal response to solve for the degree of absorption as a function of the unknown, dissipative, tidal-response coefficients. A crucial point to remember is that we solve the WEFT problem entirely in flat spacetime, considering only the contribution of the tidal multipoles to the scattering problem, We carry out this computation in the spherical basis, which can be related perturbatively in $M\omega$ to the spheroidal basis. We then match with the BHPT results in Eqs.(1.148) and (1.150) to fix the dissipative coefficients in Eqs. (1.147), as well as demand that WEFT respect spheroidal invariance, i.e., different spheroidal modes should not mix with each other. This yields the following constraints:

$$f^1_{\mathcal{E}/\mathcal{B},0} = \frac{16\chi}{45}(1 + 3\chi^2), \quad f^3_{\mathcal{E}/\mathcal{B},0} = -\frac{4\chi^3}{3}, \tag{1.151}$$

$$f^0_{\mathcal{E}/\mathcal{B},1} = \frac{16}{405}(9 + 9\kappa + 97\chi^2 + 117\kappa\chi^2 - 6\chi^4 + 54\kappa\chi^4 + 36\chi B_2 + 108\chi^3 B_2),$$

$$f^2_{\mathcal{E}/\mathcal{B},1} = -\frac{8}{135}(115\chi^2 + 135\kappa\chi^2 + 5\chi^4 + 90\kappa\chi^4 - 24\chi B_1 + 18\chi^3 B_1 + 48\chi B_2 + 144\chi^3 B_2), \tag{1.152}$$

$$f^4_{\mathcal{E}/\mathcal{B},1} = \frac{8}{135}(20\chi^4 + 45\kappa\chi^4 - 24\chi B_1 + 18\chi^3 B_1 + 12\chi B_2 + 36\chi^3 B_2), \tag{1.153}$$

$$g^i_{\mathcal{B},0} = h^i_{\mathcal{E},0} = \frac{2}{3}\chi f^i_{\mathcal{E},0}, \quad (i = 1,\ 3), \tag{1.154}$$

$$g^i_{\mathcal{E},0} = h^i_{\mathcal{B},0} = -\frac{2}{3}\chi f^i_{\mathcal{B},0}, \quad (i = 1,\ 3). \tag{1.155}$$

The remaining 22 unfixed coefficients in Eqs. (1.147), as explained earlier, characterize the conservative tidal response and do not contribute to the degree of absorption or other dissipative effects such as horizon fluxes.

1.5.3.4 Horizon fluxes in quasicircular binary BH systems

With the dissipative tidal-response coefficients fixed, we can now use Eqs. (1.144) and (1.145) to obtain the effect of horizon fluxes upon the mass and angular momentum. We apply them for the physically interesting case of a binary of Kerr BHs, albeit restricted to the case of circular orbits.

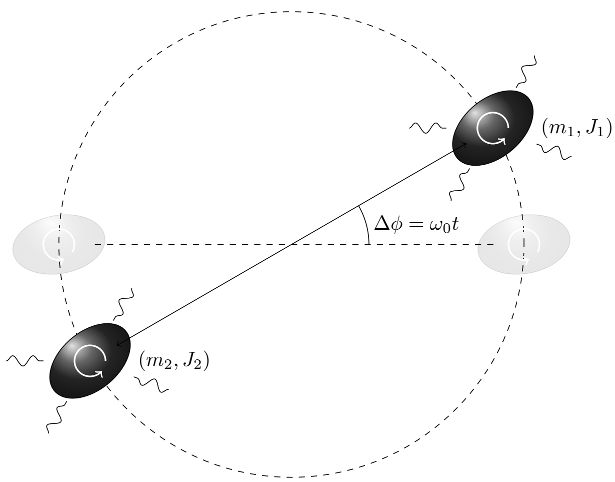

Figure 1.6: Two Kerr BHs with masses m_A and angular momenta $J_A = m_A^2\chi_A$ (with A = 1, 2) are in a quasi-circular binary. Their mutual gravitational interaction induces tidal deformations, enabling dissipative transfer of energy between the orbit and the individual BHs. The orbital angular velocity in the COM frame is ω_0. Energy transfer can occur in both directions: the horizon allows the BHs to accrete mass by acting as a one-way membrane, while rotational energy may be extracted, leading to a decrease in mass and angular momentum. In either case, the area of each BH increases in accordance with the second law of BH thermodynamics.

In this case the horizon fluxes are independent of time, and can be trivially averaged over an orbit. To 4PN (relative to the GW energy flux carried away to infinity), we obtain

$$\left\langle \frac{dm_1}{dt} \right\rangle = \Omega(\Omega_{\rm H} - \Omega) C_x, \tag{1.156}$$

$$\left\langle \frac{dJ_1}{dt} \right\rangle = (\Omega_{\rm H} - \Omega) C_x, \tag{1.157}$$

$$\left\langle \frac{dA}{dt} \right\rangle = \frac{(dm_1 - \Omega_{\rm H} dJ_1)}{dt} \frac{8\pi}{\kappa} = \frac{-8\pi}{\kappa} (\Omega_H - \Omega)^2 C_x, \tag{1.158}$$

where

$$\begin{aligned} C_x = & -\frac{16}{5} m_1^2 X_1^2 \eta^2 (1+\kappa_1) x^{12} \Bigg(1 + 3\chi_1^2 + \frac{1}{4}\left[3(2+\chi_1^2) + 2X_1(1+3\chi_1^2)(2+3X_1)\right] x^2 \\ & + x^3 \Bigg\{ \frac{1}{2}(-4+3\chi_1^2)\chi_2 - 2X_1(1+3\chi_1^2)\left[X_1(\chi_1+\chi_2) + 4B_2(\chi_1)\right] \\ & + X_1 \Bigg[-\frac{2}{3}(23+30\kappa_1)\chi_1 + (7-12\kappa_1)\chi_1^3 + 4\chi_2 + \frac{9\chi_1^2\chi_2}{2} \Bigg] \Bigg\} \Bigg). \end{aligned} \tag{1.159}$$

Here, $M_{\rm T} = m_1 + m_2$ is the total mass, $x = (M_{\rm T}\omega_0)^{1/3} \sim v$, where ω_0 is the orbital angular velocity in the center-of-mass frame. Ω is the orbital angular velocity in the frame of body 1. $\chi_A = J_A/m_A^2$ is the spin parameter of body A. Ω_H is the horizon angular velocity of body 1, with $\Omega_H \propto \chi_1$ in the small-spin limit. $X_A = m_A/M_{\rm T}$ are the mass fractions. $\eta = X_1 X_2$ is the symmetric mass ratio. Finally $\kappa_A = \sqrt{1-\chi_A^2}$ with $A = 1, 2$.

Eq. (1.159) has the correct test-body limit [58] unlike previous work [60]. We also use it to compute the correction to the waveform up to 4PN due to horizon fluxes for quasi-circular Kerr BHs. The estimates of their effect on the number of GW cycles for different choices of mass ratios within the LIGO band can be found in Chapter 4 [3].

1.5.4 Dynamical tidal response of Kerr BHs

As shown in Chapter 4 [3] and summarized in Sec.1.5.3, the dissipative tidal-response coefficients up to NLO in $M\omega$ are extracted by comparing the degree of absorption in the Raman scattering problem between BHPT and WEFT. However, this approach leaves the conservative coefficients entering the tidal response undetermined. These encode conservative tidal effects, such as the static deformation of the object characterized by the Love numbers, and influence the binary dynamics and waveform beginning at 5PN [12]. It is thus natural to ask whether matching the full scattering phase, given in Eq. (1.92), rather than just its absorptive part, can also constrain these coefficients. This is the main question we address in the next chapter.

Another issue that arises in this context — relevant to both conservative and dissipative coefficients — is the omission of tail effects in the WEFT formulation of Raman scattering in Chapter 4 [3]. In this setup, GWs propagate in flat spacetime and interact with a worldline carrying inducible multipoles. This neglects the distortion of the incoming and outgoing waves due to the Kerr background, which modifies the degree of absorption at NLO and complicates matching with BHPT, where such effects are naturally included. In Chapter 4 [3], this discrepancy is handled by introducing a frequency-dependent correction into the WEFT amplitude by hand, without rigorous justification — except in the scalar case, as detailed in the Appendix C of the same chapter [3]. In Chapter 5 [4], we systematically incorporate NLO and NNLO tail effects consistently within our amplitude-based framework.

[12] Static conservative tidal effects scale as $(\mathcal{R}/r)^4 \times (M/r) = C^{-4}(M/r)^5$, where $C = M/\mathcal{R}$. Since M/r is the PN-expansion parameter, this makes tidal effects formally start at 5PN. However, note that this is linear in M, and is really a Newtonian effect.

1.5.4.1 Systematic computation of the Raman amplitude in WEFT

In WEFT, the scattering problem can be systematically organized as a series of Feynman diagrams. Focusing first on the tidal contributions to the amplitude, we obtain diagrams that represent the physical process wherein an external GW induces a multipole moment — such as a quadrupole — which subsequently radiates a scattered wave. In the rest frame of the BH, and at leading order in $M\omega$, this process is captured by the tree-level diagram[13]

$$Q^{\mathcal{E}}_{ij} \qquad Q^{\mathcal{E}}_{kl} \quad , \tag{1.160}$$

and similarly for ($\mathcal{E} \leftrightarrow \mathcal{B}$). Going forward, we restrict our discussion to the electric sector in this subsubsection for brevity. Analogous results hold for the magnetic sector as well. Here, the vertices arise from the interaction term $\frac{1}{2}Q^{\mathcal{E}}_{ij}\mathcal{E}^{ij}$ in the worldline action. The propagator is related to the retarded Green's function of the quadrupole as

$$Q^{\mathcal{E}}_{ij}$$  $$Q^{\mathcal{E}}_{kl} \,, \equiv i\langle[Q^{\mathcal{E}}_{ij}(\tau)Q^{\mathcal{E}}_{kl}(0)]\rangle\theta(\tau) \,, \tag{1.161}$$

and it encodes the time evolution of the quadrupole moment and thus contains the ansatz for the tidal response, including all of the coefficients in Eq. (1.147). In classical language, this corresponds to a GW in flat spacetime interacting with a compact object that possesses an inducible electric quadrupole moment. In the above diagram, the worldline is treated as static apart from the induced multipole moment. This is justified because tidal effects enter at linear order in the perturbing wave's amplitude; incorporating worldline dynamics (e.g., changes in spin, momentum, or velocity) would yield corrections at second and higher orders. Such contributions are relevant

[13]Latin indices suffice for the multipole moments as we carry out the computation in the initial rest frame of the body. Since the tidal multipoles are induced linearly in the strength of external GW perturbation, any correction due to the body gaining an impulse can be safely neglected as a nonlinear (in perturbation) effect.

for nonlinear tidal effects, which lie beyond the scope of this dissertation. This diagram begins at $(M\omega)^5$, as is also evident from the expressions for the degree of absorption in Eq. (1.148). More generally, the leading order diagram, also known as the tree-level diagram, for the multipole moment with order ℓ (i.e., the corresponding tensor has rank ℓ, for instance Q_{ij} has rank 2) has its leading frequency dependence as $(M\omega)^{2\ell+1}$ [245].

Through the optical theorem, the imaginary part of this diagram is proportional to the absorption cross section, which is related to the degree of absorption, in Eq. (1.92), which is essentially the quantity of interest in the previous chapter.

However, going beyond the leading order, new contributions arise such as

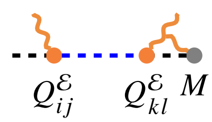

$$+\ldots . \tag{1.162}$$

These diagrams capture the modification of the incoming and outgoing GWs due to nonlinear interactions with the background metric, in addition to scattering off the induced quadrupole. Such contributions are known as tail effects. In the diagram shown, beyond the vertex involving the quadrupole moment, one must also include nonlinear interactions from the Einstein-Hilbert action, as well as the vertex associated with the leading $1/r$ potential, i.e., $-\int d\tau\, M \approx -\int dt M(1+\frac{1}{2}g_{00})+\mathcal{O}(v^2)$. Diagrams such as this contain integrals over the momenta of intermediate graviton states and thus also known as loop diagrams.

Collectively, all these diagrams that depend on inducible multipole moments are classified as near-zone diagrams. They are sensitive to the tidal response of the body, and hence to the microscopic physics characterizing the compact object.

Additionally, there are diagrams that are not directly sensitive to the microscopic physics, and arise solely from the nonlinear interaction between the GW and the background metric of the unperturbed body. The simplest such diagram is

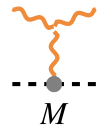

(1.163)

This is precisely the diagram whose contribution we derived (albeit without using the diagrammatic language) in Sec. 1.2.2 while introducing the setup of gravitational Raman scattering. These diagrams arise already at linear order in $M\omega$, as evident from Eq. (1.2.2). Beyond linear order, we encounter more complicated loop diagrams, as with the near-zone diagrams. This includes diagrams such as

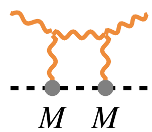

$$+\dots \tag{1.164}$$

These diagrams, which are insensitive to tidal multipole moments, are referred to as the far-zone diagrams. They should be identical for different bodies with the same metric outside, such as for all spherically symmetric bodies in GR. In addition to diagrams describing scattering off the background metric, the far-zone diagrammatic expansion also includes diagrams where the incident GWs perturb the worldline dynamics. In Chapter 3 [2], the Compton amplitude for GW scattering off a spinning compact object incorporates such worldline effects, though not in diagrammatic form. These contributions are known to be captured by far zone diagrams [174].

Since the far-zone diagrams begin at $O(M\omega)$, whereas the near-zone diagrams begin at $O(M\omega^{2\ell+1})$, one has to compute the far-zone diagrams to several higher loop orders than the near-zone diagrams in order to achieve a consistent matching with BHPT. This significantly complicates the extraction of tidal-response coefficients from the full BHPT amplitude. In Chapter 4 [3], this difficulty is avoided by focusing exclusively on dissipative effects, which do not receive any contributions from the far zone. However, far-zone diagrams do contribute to the scattering phase, and therefore must be carefully accounted for when attempting to isolate conservative tidal effects. Additionally, even among the near-zone diagrams, there are loop-level contributions — arising from tail effects — that must also be incorporated in a consistent treatment of the scattering amplitude.

1.5.4.2 BHPT phase shift and near-zone — far-zone separation

In BHPT, the scattering phase automatically includes all relevant contributions to the problem, as it provides a complete description of linear perturbations in a Kerr background. This complicates comparison with WEFT, where computing higher-order, multi-loop, far-zone diagrams is currently infeasible using state-of-the-art EFT methods. As a result, it is desirable to identify a procedure that isolates the tidal contribution to the scattering phase directly within BHPT.

A scheme for isolating the tidal contribution was proposed in Ref. [246], which we now restate. It is based on recognizing specific structural features of the scattering phase derived via the MST formalism in BHPT. As shown in Eq. (1.92), the scattering phase is directly related to the ratio of amplitudes of outgoing and incoming wave-like solutions to the Teukolsky equation. This ratio, given in Eq. (1.91), and reproduced below, naturally factorizes into two components. In Ref. [246], it was proposed that each of these can be identified with contributions from the near-zone or the far-zone diagrams, respectively, as indicated:

$$\frac{B^{\rm ref}_{\ell m\omega}}{B^{\rm inc}_{\ell m\omega}} \propto \underbrace{\frac{\left[K_\nu + i\exp(i\pi\nu)K_{-\nu-1}\right]}{\left[K_\nu - i\exp(-i\pi\nu)\frac{\sin(\pi(\nu-s+i\epsilon))}{\sin(\pi(\nu-s-i\epsilon))}K_{-\nu-1}\right]}}_{\text{Near zone}} \times \underbrace{e^{2i\epsilon[\log\epsilon-(1-\kappa)]}\frac{A_-}{A_+}}_{\text{Far zone}}, \tag{1.165}$$

In principle, this identification implies that all near-zone diagrams in WEFT are encoded in the first factor of Eq. (1.165), and all far-zone diagrams in the second[14]. In practice, however, it is not

[14]Note that this is different from the near-zone — far-zone terminology used to classify regions and MST solutions

currently feasible to systematically exploit this factorization beyond the first few orders.

Before proceeding, it is important to emphasize that this near-far separation remains a working hypothesis motivated by several observations, but not yet rigorously established. The main supporting evidence comes from the scaling behavior with respect to $M\omega$, and from the matching of specific features of the BHPT phase to expectations from WEFT. We summarize some of these motivations below:

- When evaluating the near-zone and far-zone factors in the MST formalism for generic (non-integer) values of ℓ, i.e., under analytic continuation in ℓ, one finds that the far-zone contribution scales as $M\omega$, with corrections at integer powers: $M\omega(1 + \alpha_1 M\omega + \dots)$. The near-zone contribution, on the other hand, scales as $(M\omega)^{2\nu+1}(1 + \beta_1 M\omega + \dots)$, where ν is the renormalized angular momentum introduced earlier, and approximates ℓ in the low-frequency limit. This behavior is consistent with the scaling of the corresponding diagrams in WEFT, where near-zone diagrams involving induced multipoles scale as $(M\omega)^{2\ell+1}$, and far-zone diagrams begin at $O(M\omega)$ [245].

- Perturbatively, the contribution of the far-zone factor at low orders matches the scattering of GWs off the background field of the compact object, captured by the far-zone diagrams [174].

- It can be shown that the far-zone factor in Eq. (1.165) has unit modulus, while the near-zone part controls the absorption coefficient $\eta^{\mathrm{P}}_{\ell m}$, in Eq. (1.92). This aligns with the expectation that only tidal degrees of freedom can induce absorption or superradiance in the EFT. This is

in Sec. 1.4. However, there is a relation. The far-zone factor arises purely from the far-zone series solutions, whereas the near-zone factor contains terms that arise from matching the near-zone and far-zone solutions, and is thus sensitive to the boundary conditions at the horizon.

also consistent with our findings in Ref. [3], presented in Chapter 4, on the topic of horizon fluxes in BH, and in Ref, [5], presented in Chapter 6, on the topic of tidal dissipation in NSs.

- Modifying the boundary conditions of the radial Teukolsky equation at the horizon (or at the surface of a compact object) affects only the near-zone factor [175], as shown for NSs in Chapter 6 [5], further consistent with the expectation that the near-zone diagrams capture the tidal response while the far-zone diagrams remain universal.

Finally, we note that there are ongoing efforts to either rigorously establish the near-far separation or to bypass the need for it by directly extending loop computations to higher orders. Promising progress has been made in the scalar case [247, 248].

In Chapter 5 [4], assuming the validity of the proposal in Ref. [245], we were able to match the near-zone factor in BHPT to the near-zone diagrams derived in WEFT, thereby fixing the free coefficients in the tidal response to an extent. In doing so, we recovered the vanishing of the static Love numbers for BHs, as well as the leading order and NLO dissipation numbers also obtained earlier in Chapter 4 [3].

Furthermore, by analyzing divergences in WEFT diagrams for both near and far-zone processes, we identified a classical RG running in the NLO Love numbers and NNLO dissipation numbers. This reflects the requirement that observables in BHPT — a UV-complete theory — must remain finite. We briefly discuss these aspects in Sec. 1.5.4.3.

While the direct matching of Love numbers and dissipation coefficients by comparing the scattering problem in WEFT and BHPT is novel, the vanishing of the static Love numbers of Kerr BHs has been established in earlier works [243, 246], and the dissipation coefficients are matched in Chapter 4 [3], and previously presented in Section 1.5.3. Therefore, we focus here on briefly presenting the results on the divergences in WEFT diagrams, and RG flow observed in the tidal response of Kerr BHs — both in the conservative and dissipative sectors — as developed in Chapter 5 [4].

1.5.4.3 Divergent diagrams and RG flow in the tidal response

Loop diagrams introduce an additional layer of complexity in the inclusion of tidal effects within WEFT. They give rise to divergences that must be carefully interpreted and, in some cases, regulated. This is not unexpected in an EFT, and is related to the fact that it is an incomplete description of the underlying UV physics. Such divergences signal sensitivity to short-distance (high-frequency) behavior that is not resolved within the EFT itself. As is standard in EFTs, some of these divergences can be absorbed into a redefinition of the coefficients multiplying allowed operators in the action and the tidal response, leading to a renormalization-group flow that captures how the effective description evolves with scale.

One divergent diagram is, in fact, the very first diagram in Eq. (1.162). This diagram is known to produce a divergence upon integrating over the momentum of the intermediate graviton. In dimensional regularization — where the number of spacetime dimensions is analytically continued to regulate divergences — the result takes the form [249]

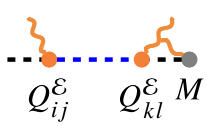

$=$
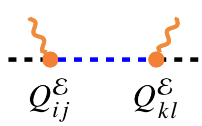

$$\times \left[\epsilon\pi + i\epsilon \left(\frac{2}{(d-4)_{\mathrm{IR}}} + \log \frac{\omega^2}{\pi\mu^2} + \gamma_E - \frac{11}{6} \right) \right] , \quad (1.166)$$

Here, μ is the arbitrary frequency scale introduced to maintain dimensional consistency as d, the total number of spacetime dimensions, is analytically continued away from 4. In the physical limit $d \to 4$, the diagram develops a divergence. However, this divergence is unphysical in the sense that it does not affect any observable such as the cross-section. This follows from the fact that it exponentiates and thus drops out of the squared amplitude as shown in Ref. [249]. Such divergences are classified as IR divergences [250], and they do not require any renormalization of the tidal response.

That said, the diagram is not without consequence, as the accompanying factor also contains a finite real piece that modifies physical observables and does not exponentiate as a phase, such as the degree of absorption, starting at NLO. In fact, this diagram accounts for the factor of $(1+\epsilon\pi)$ that appears in Eq. (1.148). This contribution is absent in the WEFT expression for the degree of absorption in Chapter 4 [3], as the computation is carried out in flat spacetime. As a result, the $(1+\epsilon\pi)$ factor is inserted manually in order to match with the BHPT result, albeit justified for the scalar case in the Appendix C of the chapter. In Chapter 5 [4], we show that including this diagram explicitly allows for a direct and consistent matching with BHPT, thereby eliminating the need for such an ad-hoc correction.

There are however, other diagrams, whose divergences do contribute to physical observables such as the scattering cross section. Such divergences, known as UV divergences, cannot be disregarded. Among the near-zone diagrams, they enter at 2-loops or NNLO through diagrams such as

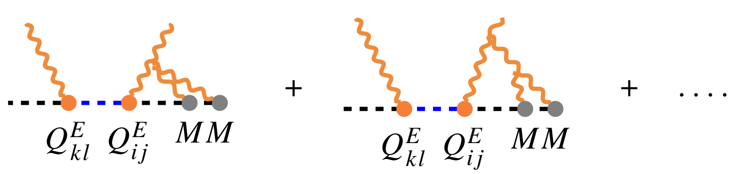

(1.167)

The explicit expressions for the relevant divergences are presented in Chapter 5 [4]. These divergences take a form analogous to that of Eq. (1.166), i.e., they are proportional to the tree-level diagram in Eq. (1.160), multiplied by a divergent prefactor. Unlike the IR divergence discussed earlier, these do not cancel in physical observables and must be removed through renormalization. This necessitates the introduction of counter terms in the WEFT. Since the divergence is proportional to the tree-level structure, the required counter term has the same operator form and corresponds to the contribution of the NNLO tidal-response coefficients.

To make this explicit, let us recall the ansatz for the quadrupole moment from Eq. (1.146), now extended to include the NNLO term. For simplicity, we ignore coupling to other multipolar sectors:

$$Q^{\mu\nu}_{\mathcal{E}} = M^5 \lambda^{\mu\nu}_{\mathcal{E},0\rho\sigma} \mathcal{E}^{\rho\sigma} + M^6 \lambda^{\mu\nu}_{\mathcal{E},1\rho\sigma} \frac{D}{D\tau} \mathcal{E}^{\rho\sigma} + M^7 \lambda^{\mu\nu}_{\mathcal{E},2\rho\sigma} \frac{D^2}{D\tau^2} \mathcal{E}^{\rho\sigma}. \tag{1.168}$$

The leading divergence arising from two-loop diagrams, such as those in Eq. (1.167), is proportional to the static tidal-response tensor $\lambda^{\mu\nu}_{\mathcal{E},0\rho\sigma}$. Each loop contributes a factor of $M\omega$, so the overall amplitude scales as $(M\omega)^2$ relative to the tree-level result. Thus, its tensorial structure matches that of the NNLO term involving $\lambda^{\mu\nu}_{\mathcal{E},2\rho\sigma}$, as each time derivative produces a factor of $-i\omega$. This suggests that the divergence can be absorbed by letting the NNLO tidal-response coefficient act as a counterterm. Specifically, in Chapter 5 [4], we show that imposing

$$\lambda^{\mu\nu,\text{bare}}_{\mathcal{E},2\rho\sigma} = -\frac{214}{105} \times \left[\frac{1}{(d-4)_{\text{UV}}} + \gamma_{\mathcal{E}} - \log(4\pi) \right] \lambda^{\mu\nu}_{\mathcal{E},0\rho\sigma} + \text{ finite part}, \tag{1.169}$$

regulates the 2-loop divergences. We can then define a renormalized, NNLO, tidal-response tensor, $\lambda^{\mu\nu}_{\mathcal{E},2\rho\sigma}(\mu)$, as

$$\lambda^{\mu\nu,\text{bare}}_{\mathcal{E},2\rho\sigma} = \mu^{2(d-4)} \left(\lambda^{\mu\nu}_{\mathcal{E},2\rho\sigma}(\mu) - \frac{214}{105} \left[\frac{1}{(d-4)_{\text{UV}}} + \gamma_{\mathcal{E}} - \log(4\pi) \right] \lambda^{\mu\nu}_{\mathcal{E},0\rho\sigma} \right). \tag{1.170}$$

Then, using the fact that the LHS is independent of μ, we obtain the RG flow equation as

$$\mu \frac{d\lambda^{\mu\nu}_{\mathcal{E},2\rho\sigma}}{d\mu} = \frac{428}{105} \lambda^{\mu\nu}_{\mathcal{E},0\rho\sigma}. \tag{1.171}$$

This can be solved to yield:

$$\lambda^{\mu\nu}_{\mathcal{E},2\rho\sigma}(\mu) = \lambda^{\mu\nu,\text{fixed}}_{\mathcal{E},2\rho\sigma} + \frac{428}{105}\lambda^{\mu\nu}_{\mathcal{E},0\rho\sigma}\log(GM\mu). \tag{1.172}$$

This running behavior has since been confirmed in other works as well [156, 251]. Physically, this running leads to contributions in the equations of motion that resemble tidal forces and torques, but with coefficients that depend logarithmically on the dynamical scale of the system, as in (1.172), with μ replaced by the relevant frequency scale, such as the orbital frequency in a binary inspiral. This scale dependence arises from the cancellation of the μ-dependence in the renormalized tidal response coefficients with that from the loop integrals. For example, as shown in Ref. [251], computing the two-body Hamiltonian for a binary with dynamical tides by integrating out the gravitational field reveals tidal terms that exhibit such running. This running behaviour enters at relative 3PN order to leading-order tidal effects (conservative or dissipative), which could become important when tidal deformation is strong, such as in the event of a tidal resonance for binaries containing NSs.

Finally, UV-divergent diagrams also arise from high-loop far-zone processes that are independent of the lower-order tidal response or any internal structure beyond the static background metric. These divergences, while unrelated to tidal dynamics, still require regularization and are absorbed by introducing higher-order tidal-response counterterms, as in the near-zone case. Although difficult to compute directly due to their complex loop structure, their presence is inferred from BHPT via $\log(M\omega)$ terms in the scattering cross-section that lack corresponding divergent near-zone contributions. Their far-zone origin is confirmed by the fact that the associated running is independent of horizon boundary conditions. Some examples have been computed analytically in the scalar case [247]. In Chapter 5 [4], we identify such terms in the BHPT scattering phase and extract the resulting RG flow for various dynamical tidal-response tensors in Kerr BHs. It is important to note that the RG flow in the tidal response can, in principle, be derived entirely within the WEFT, without input from BHPT. Renormalization is a structural feature of the EFT, while BHPT provides a complete, UV-finite description. For instance, the two-loop divergence and the running of the NNLO tidal response can be obtained directly within WEFT, as shown in Ref. [249], which derives the running of the quadrupole moment in generic GW emission. However, it remains crucial to verify that BHPT exhibits the expected signatures — such as $\sim \log(M\omega)$ terms — consistent with the renormalization in the EFT. This agreement ensures that the tidal model is physically correct, and that the observed running is not an artifact of using a bad EFT. Additionally, since some far-zone diagrams are difficult to compute directly, BHPT results provide indirect evidence for the existence of divergent diagrams requiring renormalization.

Overall, the emergence of renormalization in the tidal response is a distinctive feature of GR, arising from its inherent nonlinearity. It means that the effective tidal-response coefficients evolve with frequency during the inspiral, as determined by their RG flow. This running challenges the notion of fixed, intrinsic tidal parameters and highlights that tidal and non-tidal contributions to scattering become intertwined beyond leading order. Consequently, while EFT provides a powerful organizing framework, it also makes clear that a clean separation between near-zone and far-zone physics — and thus between tidal and background contributions — is currently untenable at higher orders.

1.5.5 Tidal Heating in NSs

Tidal effects depend on the internal structure and compactness of an object. For BHs in GR, the size is set by the Schwarzschild radius M, and their static tidal response vanishes [4, 56, 243]. In contrast, NSs have lower compactness $C = M/\mathcal{R}$, typically around 0.1–0.2, and support a rich spectrum of tidal deformations governed by their EOS. This leads to a nonzero Love number, and generally stronger tidal effects.

While the static Love number for NSs has been treated in full generality [55, 57, 252], dynamical tides and viscous dissipation are often analyzed only within the Newtonian approximation [196, 253]. In Chapter 6 [5], we address this gap by rigorously modeling leading-order tidal heating driven by fluid viscosity in NSs by extending the framework we developed previously for BHs. To that end, we study Raman scattering in nonspinning NSs using both WEFT and stellar perturbation theory (SPT) [254–256], working to NLO in frequency. This allows us to derive general expressions for the static Love number and leading dissipation numbers in terms of boundary conditions for metric perturbations at the stellar surface. We then solve for these boundary conditions for various EOSs across a range of compactnesses, compute the corresponding tidal coefficients, and estimate their effect on the number of GW cycles accumulated in the LIGO band.

1.5.5.1 WEFT treatment

The WEFT treatment of nonspinning NSs for near-adiabatic tides parallels that of Schwarzschild BHs, involving a similar number of free coefficients in the tidal response. The discussion in Sec. 1.3.3.3 suffices, and we aim to determine the coefficients entering the linear response for the electric quadrupole moment, whose ansatz to NLO in time derivative was presented in Eq. (1.59). We restate it here as

$$Q_{\mathcal{E}}^{\mu\nu}(\tau) = -M^5[\Lambda^{\mathcal{E}} - MH_{\omega}^{\mathcal{E}}\frac{D}{D\tau} + \ldots]\mathcal{E}_{\mu\nu}, \tag{1.173}$$

or in Fourier domain as

$$\tilde{Q}_{\mathcal{E}}^{\mu\nu} = -\frac{1}{2}F(\omega)\tilde{\mathcal{E}}_{\mu\nu},\ F(\omega) = 2M^5[\Lambda^{\mathcal{E}} + i(M\omega)H_{\omega}^{\mathcal{E}} + \ldots] \tag{1.174}$$

A similar relationship can be written for the magnetic quadrupole; however, the dominant tidal contribution for NSs (and more generally for all stars) is the electric part, and we restrict our attention to this sector. We also neglect octupole and higher multipole moments, which may also be tidally induced, as they are relevant at higher PN orders.

As before, we compare the solution to the scattering problem between effective and complete descriptions, aiming to fix the coefficients $\Lambda^{\mathcal{E}}$ and $H_{\omega}^{\mathcal{E}}$. The coefficient $\Lambda^{\mathcal{E}}$ is known as the static Love number, and its computation is well known and studied for NSs [55]. However, the dissipation number $H_{\omega}^{\mathcal{E}}$ has not been rigorously computed in a relativistic framework. We constrain both of these quantities by studying the Raman scattering process.

In the WEFT, the tree-level scattering due to the electric quadrupole is captured by the diagram given earlier in Eq. (1.160). We rewrite it below as

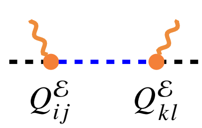

$$= 4i\ (M\omega)^5 G^{\text{ret}}_{ij,kl}(\omega)\varepsilon_h^{ij}\left(\vec{k}_{\text{in}}\right)\varepsilon_{h'}^{*kl}\left(\vec{k}_{\text{out}}\right), \tag{1.175}$$

where $G^{\text{ret}}_{ij,kl} = F(\omega)\,\delta^{ik}\delta^{jl}$, and $\varepsilon_h^{ij}(\vec{k}_{\text{in}})$ and $\varepsilon_h^{\prime kl}(\vec{k}_{\text{out}})$ are the graviton polarization tensors for the incoming and outgoing plane GWs, respectively. Physically, an incoming monochromatic plane wave induces a quadrupole moment via the tidal-response ansatz, which then radiates according to the Einstein equation, resulting in a scattered wave.

Since we are interested in working to NLO in frequency, we also need to include the first diagram in Eq. (1.162). However, as explained in Sec. 1.5.4.3, its only physical contribution of this diagram is to multiply the tree-level result by a factor $(1 + \epsilon\pi)$, as also seen in Eq. (1.148), and it is therefore trivially taken into account.

The scattering problem in SPT is more naturally formulated in a spherical basis with fixed parities due to the spherical symmetry and parity invariance of the background. Accordingly, we transform from the plane-wave basis with fixed helicities to spherical basis with fixed parities, as also done in Chapter 5 [4]. The relevant methods and expressions for this transformation are detailed in Appendix D of Chapter 5 [4]. We now briefly describe the scattering problem in the context of SPT.

1.5.5.2 Raman scattering in SPT

We describe the NS as comprised of a stellar fluid with the following energy-momentum tensor:

$$T_{\mu\nu} = \rho u_\mu u_\nu + (p - \zeta \nabla_\alpha u^\alpha) P_{\mu\nu} - 2\eta P^\alpha_\mu P^\beta_\nu \sigma_{\alpha\beta} \tag{1.176}$$

where ζ and η are the bulk and shear viscosity, ρ is the energy density and p is the pressure.

When the star is unperturbed, it is spherically symmetric and the metric everywhere in spacetime can be decribed using the ansatz

$$ds^2_{(0)} = g^{(0)}_{\mu\nu} dx^\mu dx^\nu = -e^{\nu(r)} dt^2 + e^{\lambda(r)} dr^2 + r^2 d\Omega^2, \tag{1.177}$$

where the functions $\nu(r)$ and $\lambda(r)$, along with the pressure and density profiles $(p(r), \rho(r))$ obey the Tolman–Oppenheimer–Volkoff [9, 257] equations, which can be solved for a given EOS. The unperturbed star is assumed to be in chemical equilibrium.

When the star is perturbed, both the metric tensor and the stress energy tensor change. The metric perturbations for the electric (polar) sector can be written as [254][15]

$$\begin{aligned}\delta g_{\mu\nu}dx^{\mu}dx^{\nu} = -e^{-i\omega t}\bar{r}^{\ell}Y_{\ell m}[&H_0(r)e^{\nu}dt^2 \\ &- 2i\omega H_1(r)dtdr + e^{\lambda}H_2(r)dr^2 + K(r)r^2d\Omega^2],\end{aligned} \tag{1.178}$$

where $\bar{r} = r/\mathcal{R}$ inside the star ($r < \mathcal{R}$), $\mathcal{R}$ being the radial coordinate of the unperturbed stellar surface and $\bar{r} = 1$ outside, and $d\Omega^2 = d\theta^2 + \sin^2\theta d\phi^2$.

The matter perturbations include a) the perturbation to pressure Δp, b) the perturbation to density $\Delta\rho$, and c) the fluid displacement vector ξ^{μ} (i.e., the displacement of a fluid packet at x^{μ} to $x^{\mu} + \xi^{\mu}$).

The displacement vector can be parametrized in terms of the functions

$$\begin{aligned}\xi^t = 0,\ \xi^r &= e^{-i\omega t}\frac{\bar{r}^{\ell}}{r}e^{-\frac{\lambda}{2}}W\,Y_{\ell m}, \\ \{\xi^{\theta},\xi^{\phi}\} &= -e^{-i\omega t}\frac{\bar{r}^{\ell}}{r^2}V\{\partial_{\theta}Y_{\ell m},\frac{\partial_{\phi}Y_{\ell m}}{\sin^2\theta}\}\ .\end{aligned} \tag{1.179}$$

Here, W characterizes the radial displacement of fluid elements, whereas V characterizes the azimuthal and polar displacement.

$\Delta\rho$ follows trivially from the first-law of thermodynamics. Assuming isentropic perturbations about a background in chemical equilibrium, we have

$$\Delta\rho = -(p+\rho)(\Delta v/v),$$

[15] There are some conventional differences here w.r.t. Ref. [254].

where $\Delta v/v$ is the fractional change in volume given by

$$\frac{\Delta v}{v} = -Y_{\ell m}\frac{\bar{r}^{\ell}e^{-i\omega t}}{2}\left(H_2 + 2K - \frac{2\ell(\ell+1)V}{r^2} - \frac{2e^{-\frac{\lambda}{2}}[(\ell+1)W + rW']}{r^2}\right).$$

It is convenient to define an additional function X at this stage as

$$X(r)Y_{\ell m}e^{-i\omega t} \equiv \frac{\Delta v}{v}\bar{r}^{-\ell}(e^{\nu/2}p\gamma - i\omega\zeta)\ . \tag{1.180}$$

Unlike $\Delta\rho$, Δp depends sensitively on whether the chemical reactions in the NS are able to maintain equilibrium when perturbed. We show that the low-frequency expansion, in the manner performed in Chapter 6, is well defined only when the reaction rates are too slow to maintain equilibrium. In that case, we can assume the particle fractions x_i are fixed and write

$$\Delta p = \frac{\gamma p}{p+\rho}\Delta\rho, \tag{1.181}$$

where $\gamma = \frac{\partial p}{\partial \rho}\Big|_{x_i} \times (p+\rho)/p$.

With the expressions for the perturbations of various quantities in hand, and working to linear order in perturbations of the Einstein equation, we show that, to first order in frequency (i.e., $\mathcal{R}\omega$), the full system reduces to two coupled first-order equations for the metric perturbation variables H_0 and K. These are given in Eqs. (1.182), and (1.183). At linear order in frequency, only shear viscosity η contributes to these equations. This arises from a form of adiabatic incompressibility seen in Newtonian limits [258, 259], where perturbed fluid elements preserve volume. Also note that while the equations do contain additional functions V, W, and X along with their derivatives, they can be perturbatively eliminated in terms of H_0 and K and their first derivatives using relations valid in the static limit (i.e., for $\omega = 0$).

$$-\frac{2K}{r} + H_0' + \frac{H_0\left(\kappa r^2 p e^{\lambda} + e^{\lambda} + 1\right)}{r} - K' - \frac{2i\kappa\omega\eta e^{-\frac{\nu}{2}}\left(\kappa r^2 p e^{\lambda}V + rV' + e^{\lambda}V + V - e^{\frac{\lambda}{2}}W\right)}{r}$$

$$= O(\omega^2) \tag{1.182}$$

$$\begin{aligned}
&H_0' + \frac{H_0 e^{\lambda}\left(\kappa r^2(p-\rho)+8\right)}{2r} + \frac{1}{2}K'\left(e^{\lambda(r)}\left(\kappa r^2 p+1\right)-3\right) + \frac{K\left(e^{\lambda}\left(\kappa r^2 p-1\right)-3\right)}{r} \\
&- \frac{i\kappa\omega\eta e^{-\frac{\nu}{2}}}{2r}[8\left(4e^{\lambda}+1\right)V + V'\left(\kappa r^3 e^{\lambda}\rho - r e^{\lambda} + r\right) - 2r^2 V'' + 4e^{\frac{\lambda}{2}}W + r^2 e^{\lambda}(H_0 - 4K)] \\
&- \frac{i\kappa r\omega\eta e^{\lambda-\nu}}{3p\gamma}X - ie^{-\frac{\nu}{2}}\kappa\omega\eta'(r)\left(e^{\frac{\lambda}{2}}W - rV'\right) = O(\omega^2)\ .
\end{aligned} \tag{1.183}$$

It is important to emphasize that this analysis and the resultant master equations are valid only when the orbital frequency ω is much smaller than the characteristic frequency of convective oscillations in the star, known as the Brunt–Väisälä frequency $N_{\rm ch}$ (typically in the range 150–700 Hz, depending on mass and EOS). This condition is also derived by analyzing the perturbation equations of a Newtonian star in Appendix E of Chapter 6 [5]. It is expected to hold during the early to mid inspiral. In contrast, the results of Ref. [260] likely probe the opposite regime ($\omega \gg N_{\rm ch}$), highlighting the need for further work to understand the transition between these regimes. Physically, $N_{\rm ch}$ sets the scale for gravity-modes — a set of normal modes of a convectively stable NS [256]. Since oscillation modes of a body correspond to poles in the tidal response (at least in the Newtonian approximation), a Taylor expansion in ω is expected to break down as ω approaches $N_{\rm ch}$, rendering the low-frequency expansion invalid in that regime.

The master equations can be numerically solved up to the stellar surface. Outside the NS, matter perturbations vanish and the system of metric perturbation equations reduces to a single RW equation,

$$\frac{d^2\phi(r)}{dr_*^2} + \left[\omega^2 - f(r)V(r)\right]\phi(r) = 0, \tag{1.184}$$

$$V(r) = \left(\frac{\ell(\ell+1)}{r^2} - \frac{6M}{r^3}\right),\ r_* = r + 2M\log(r-2M).$$

The scattering problem can be conveniently solved from the RW equation. Using the interior master equations, we first numerically obtain the RW variable ϕ and its radial derivative at the stellar surface. The stellar interior information is fully encoded in

$$T \equiv \frac{r}{\phi}\frac{d\phi}{dr_*}\bigg|_{r=\mathcal{R}} = T_0 - i\mathcal{R}\omega T_1 + O(\omega^2), \tag{1.185}$$

where T_0 and T_1 capture conservative and dissipative tidal responses at leading order, respectively, and r_* is the tortoise coordinate for a Schwarzschild BH. Sufficiently far from the NS, the RW equation admits simple wave-like solutions as

$$\phi(r)|_{r\to\infty} = A^{\text{in}}_{\ell,\omega}e^{-i\omega r_*} + A^{\text{out}}_{\ell,\omega}e^{+i\omega r_*}, \tag{1.186}$$

We use the MST method for the RW equation [219][16], to analytically compute the ratio $A^{\text{out}}_{\ell,\omega}/A^{\text{in}}_{\ell,\omega}$ to the relevant order as function of T_0 and T_1. This ratio is the scattering phase, and should be matched with the scattering amplitude obtained in WEFT in Eq. (1.175).

1.5.5.3 Love number and dissipation number for arbitrary compactness

Similar to our discussion in Sec.1.5.4.1 for Kerr BHs, matching the scattering phase computed from SPT with the WEFT amplitudes is complicated by the fact that Eq. (1.175) contains only the near-zone diagram. This does not affect the extraction of the dissipation number $H^{\mathcal{E}}_{\omega}$, for the same reasons as in Chapter 4 [3] where we study horizon fluxes in BHs: far-zone diagrams do not contribute to dissipation. However, the absence of far-zone contributions does complicate matching the Love number.

Although the Love number of a NS is well established in the literature, it is nevertheless interesting to ask whether it can be extracted directly from the Raman scattering problem. In

[16]The MST method for RW equation closely parallels that for the Teukolsky equation described earlier in Sec. 1.4.2.

Chapter 6 [5], we explore multiple approaches to isolating the Love number from the scattering phase.

One method is to use the near-zone — far-zone factorization proposed in Ref. [246] and discussed in Sec. 1.5.4.2. A technical subtlety arises because the proposed factorization appears to hold only when the angular momentum number ℓ is analytically continued, rather than fixed at $\ell = 2$ as appropriate for quadrupolar perturbations. However, in contrast to the BH case, the NS perturbation equations must be solved numerically in the interior. Nevertheless, we find that the factorization remains valid at leading order if ℓ is analytically continued in the solution of the RW equation outside, while $\ell = 2$ is held fixed in the numerical integration of the perturbation equations inside the NS. With this approach, we recover the known expression for the static Love number from Ref. [55].

Another method relies on the universality of the far-zone diagrams. As discussed in Sec.1.5.4.1, these diagrams depend only on the external background metric of the undisturbed object. Since a nonspinning NS shares the same exterior geometry as a Schwarzschild BH, the far-zone contributions to the scattering phase are identical. Therefore, by subtracting the scattering amplitude for the BH from that of the NS, we isolate the tidal contribution. Because the BH has zero Love number, the leading-order difference must encode the NS Love number. This difference should match the WEFT amplitude in Eq. (1.175), and hence corresponds to the difference in the exponential of the scattering phases: $e^{2i\delta_{\ell=2}^{\mathrm{P,NS}}} - e^{2i\delta_{\ell=2}^{\mathrm{P,BH}}}$. We show that this procedure works as well, and again recover the correct expression for the NS Love number [55].

Having established both approaches, we obtain explicit expressions for the Love number and dissipation number in terms of the boundary conditions at the stellar surface for the RW equation.

Defining the rescaled Love number and dissipation number as

$$k_2^{\mathcal{E}} = \frac{3}{2}\Lambda^{\mathcal{E}} C^5 \,, \qquad \nu_2^{\mathcal{E}} = \frac{3}{2} H_\omega^{\mathcal{E}} C^6 \,, \tag{1.187}$$

where $C = M/\mathcal{R}$ is the compactness, we find:

$$\begin{aligned}
k_2^{\mathcal{E}} &= -\frac{8C^5\left(6C-3+T_0\right)}{\mathcal{D}}\,, \quad \nu_2^{\mathcal{E}} = \frac{3840C^{10}T_1}{\mathcal{D}^2}\,, \\
\mathcal{D} &= 5(-2C\left(C\left(6C^2+4C+3\right)+3\right)T_0 + 6(C-1)C\left(4C^3+2C^2-3\right) \\
&\quad -3\left(6C-3+T_0\right)\log(1-2C).
\end{aligned} \tag{1.188}$$

The expressions above are consistent with the BH limit, where $T_0 = 0$, $T_1 = 1$ and $\mathcal{R} \to 2M$, $C \to 1/2$. The expression for the Love number is consistent with Ref. [55].

For a quantitative study, we use Eq. (1.188) to compute $k_2^{\mathcal{E}}$ and $\nu_2^{\mathcal{E}}$ for various EOS and compactness values (Table 1.1). As bulk viscosity does not contribute, dissipation is entirely due to shear viscosity, dominated by e-e scattering [196, 261]. Since this viscosity scales as T^{-2}, we multiply by $(T_K/10^5)^2$ to factor out this dependence, providing the dissipation number at $T = 10^5 K$. Notably, $H_\omega^{\mathcal{E}}$ falls steeply with compactness ($\sim C^{-6}$) and temperature ($\sim T^{-2}$).

1.5.5.4 Effect on number of GW cycles

We estimate the effect of tidal heating on the gravitational waveform at leading 4PN order using the stationary phase approximation [3, 262–264]. The change in the number of GW cycles for a binary NS system, assuming the GW frequency is twice the orbital frequency, is given by:

$$\begin{aligned}
\delta\mathcal{N}_{\rm GW} &= \frac{\delta\phi[(M_{\rm T}\pi\omega_f)^{1/3}] - \delta\phi[(M_{\rm T}\omega_i\pi)^{1/3}]}{\pi}, \\
&= \sum_{A=1,2} \frac{25\mathcal{R}_A^6 \nu_2^{E,A}}{512 m_A^3 (M_{\rm T}-m_A) M_{\rm T}^2} \times M_{\rm T}(\omega_i - \omega_f).
\end{aligned} \tag{1.189}$$

Here, m_A are the NS masses, $M_{\rm T} = m_1 + m_2$, $\mathcal{R}_A$ are their radii, and ν_2^A are the rescaled dissipation numbers, $A = 1, 2$. We take the initial frequency (where the signal enters the LVK band) as $\omega_i = 30$ Hz, and the final frequency (marking the transition to plunge or the upper limit of the LVK band) as $\omega_f = \min\left(1000\ \text{Hz},\ \omega_{\rm ISCO} = 1/(6^{3/2} M_{\rm T})\ \text{Hz}\right)$. Note that for binaries with generic mass ratio, there is no sharp ISCO, and we use the ISCO frequency of a test body in circular orbit around a mass $M_{\rm T}$ as an approximation for the plunge-onset frequency.

Since bulk viscosity does not contribute at this order, the dominant effect comes from shear viscosity due to electron-electron scattering, which scales as T^{-2}. To remove this dependence, we multiply by $(T_K/10^5)^2$, setting the dissipation number at $T = 10^5$ K.

We evaluate Eq. (1.189) for symmetric NS binaries across different EOS and compactness values within the LIGO band and compare with other 4PN conservative contributions [265]. Results in Table 1.2 show that cold, low-compactness NSs have the strongest tidal heating imprint. Notably, for sufficiently cold and less-compact NSs, viscous dissipation can be comparable to other conservative 4PN effects.

1.5.6 QNMs of slowly spinning horizonless compact objects

The previous chapters have focused on building and constraining effective worldline theories for generic compact objects. Constraining was accomplished through comparisons with known models of compact objects such as BHs and NSs. However, there remains the remote possibility of the existence of compact objects in binaries relevant for GWs that are not BHs or NSs. Several such models of exotic compact objects (ECOs) have been proposed, and it is desirable to have an effective scheme that can incorporate them in a single, parameterized, phenomenological

EOS	M (in $M_\odot$)	R (in km)	M/R	k_2	$H_\omega^{\mathcal{E}} \times (T_\mathrm{K}/10^5)^2$	$(H_\omega^{\mathcal{E}})_\mathrm{NS}/(H_\omega^{\mathcal{E}})_\mathrm{BH} \times (T_\mathrm{K}/10^5)^2$	$\nu_2^E \times (T_\mathrm{K}/10^5)^2$
FSU2 [266]	1.01	14.00	0.107	0.133	22037.9	30990.9	0.0486
	1.34	13.95	0.141	0.121	3456.3	4860.4	0.0412
	1.71	13.95	0.180	0.099	617.0	867.7	0.0318
	2.34	13.8	0.25	0.056	47.8	67.3	0.0175
GM1 [267]	1.01	12.85	0.115	0.140	17966.3	25265.2	0.0640
	1.34	12.85	0.154	0.118	2462.4	3462.8	0.0502
	1.71	12.7	0.199	0.089	395.1	555.6	0.0367
	2.3	11.55	0.294	0.027	13.9	19.6	0.0135
HZTCS [268]	1.01	12.45	0.120	0.140	15916.7	22382.6	0.0701
	1.34	12.65	0.156	0.122	2511.6	3531.9	0.0547
	1.71	12.66	0.200	0.100	440.3	619.2	0.0417
	2.34	12.60	0.274	0.044	28.4	39.9	0.0180

Table 1.1: Tidal-response characteristics for various EOS and compactness for non-spinning NSs at $T = 10^5 K$.

EOS	M (in $M_\odot$)	R (in km)	M/R	$H^E_\omega \times (T_{\rm K}/10^5)^2$	$\nu^E_2 \times (T_{\rm K}/10^5)^2$	$\delta\mathcal{N}_{\rm GW} \times (T_{\rm K}/10^5)^2$	$\mathcal{N}^{\rm 0PN}_{\rm GW}$	$\mathcal{N}^{\rm 4PN}_{\rm GW}$
FSU2	1.01	14.00	0.107	22037.9	0.0486	-7.775	4428.93	-0.099
	1.34	13.95	0.141	3456.3	0.0412	-1.618	2764.77	-0.106
	1.71	13.95	0.180	617.0	0.0318	-0.369	1841.51	-0.108
	2.34	13.8	0.25	47.8	0.0175	-0.037	1091.46	-0.101
GM1	1.01	12.86	0.115	17966.3	0.0640	-6.339	4428.93	-0.099
	1.34	12.85	0.154	2462.4	0.0502	-1.153	2764.77	-0.106
	1.71	12.70	0.199	395.1	0.0367	-0.237	1823.70	-0.108
	2.30	11.55	0.294	13.9	0.0135	-0.011	1123.38	-0.102
HZTCS	1.01	12.45	0.120	15916.7	0.0701	-5.620	4428.93	-0.099
	1.34	12.65	0.156	2511.6	0.0547	-1.176	2764.77	-0.106
	1.71	12.65	0.200	440.3	0.0417	-0.265	1841.51	-0.108
	2.34	12.60	0.274	28.4	0.0180	-0.022	1091.46	-0.101

Table 1.2: Correction to GW cycles due to tidal heating ($\delta\mathcal{N}_{\rm GW}$) in symmetric spinless NS-NS binaries at $T = 10^5$ K.

framework.

In Chapter 7, which was originally published as Ref. [6], we model generic slowly spinning compact objects in GR using the membrane paradigm. The membrane paradigm was originally envisioned to describe horizons of BHs in a more intuitive way, as a stretched membrane just above the horizon, with physical properties such as viscosity, conductivity, etc., chosen such that the behaviour of the membrane is identical to that of physical BHs with horizons [95–97, 224]. In Ref. [90], this method was applied to generic nonspinning compact objects, to study how the behaviour of the object changes as the membrane parameters are moved away from the BH values. In a sense, this is similar to letting the free parameters entering the worldline action (or equations of motion) to be different than that of (say) a BH or NS, but unlike in WEFTs, the membrane paradigm allows us to fully explore the strong gravitational fields close to the surface of the body, and to understand how features close to the surface affect its behaviour when seen from far far away. In Ref. [6], we develop this idea further by incorporating spin effects at linear order. This helps us understand how the reflectivity characteristics and QNM frequencies are modified for slowly spinning reflective ECOs.

1.5.6.1 Boundary conditions at membrane surface

In the membrane paradigm, we replace the compact object with a fluid membrane. We impose the Israel-Damour junction condition [269, 270] at the membrane, while setting the extrinsic curvature inside the membrane to zero (i.e., using $a, b = 0, 1, 2$ indices to denote coordinates spanning the 3-dimensional membrane surface),

$$(K_{ab} - Kh_{ab})^{+} - (K_{ab} - Kh_{ab})^{-} = -8\pi T_{ab}\,, \qquad h^{+}_{ab} - h^{-}_{ab} = 0\,, \quad K^{-}_{ab} = 0, \tag{1.190}$$

Where h_{ab} is the induced metric, K_{ab} the extrinsic curvature, $K = K_{ab}h^{ab}$, and T_{ab} the membrane's fluid stress-energy tensor, given by

$$T_{ab} = \rho u_a u_b + (p - \zeta\Theta)\gamma_{ab} - 2\eta\sigma_{ab} \,. \tag{1.191}$$

Here, ρ is the surface density, p is the surface pressure, ζ is the bulk viscosity, η is the shear viscosity, and $\Theta = \nabla_a u^a$ is the divergence of the fluid velocity. $\gamma_{ab} = h_{ab} + u_a u_b$ is the projector tensor, $\sigma_{ab} = \frac{1}{2}\left(u_{a;c}\gamma^c_b + u_{b;c}\gamma^c_a - \Theta\gamma_{ab}\right)$ is the shear tensor, and the semicolon is a covariant derivative with the induced metric.

We assume the validity of GR everywhere outside the membrane. Then, to linear order in spin, the metric for an uncharged membrane, which is axially symmetric, is uniquely fixed to be [271]

$$ds^2 = -f(r)dt^2 + \frac{1}{f(r)}dr^2 + r^2 d\Sigma^2 - 4\frac{J}{r}\sin^2\theta dt d\phi + O(J^2) \,, \tag{1.192}$$

where $d\Sigma^2 = d\theta^2 + \sin^2\theta\, d\phi^2$, $f(r) = 1 - 2M/r$, M is the mass, and J is the angular momentum. Any deviation from the linear-in-spin Kerr form would require the presence of additional spin-induced multipole moments, which only appear at second order in spin. Nevertheless, if a compact object possesses large spin-induced multipole moments, the linear-in-spin approximation would have a limited regime of validity. Furthermore, compact objects in alternative theories of gravity may have a different metric even at linear order in spin. We neglect these subtleties in this work, and instead assume that the metric coincides with the linearized-in-spin Kerr metric everywhere outside the membrane.

Using the junction conditions in Eq. (1.190), the unperturbed values for the membrane parameters are found to be:

$$\rho_0 = -\frac{\sqrt{f(r_0)}}{4\pi r_0},\ p_0 = \frac{1 + f(r_0)}{16\pi r_0\sqrt{f(r_0)}},\ u^a_0 = \left(\frac{1}{\sqrt{f(r_0)}}, 0, \frac{2J}{r_0^3\,(1 - 3f(r_0))\,\sqrt{f(r_0)}}\right),$$

where r_0 is the radius of the membrane surface. The subscript 0 is to denote that these are the parameters of the unperturbed membrane. Note that the shear and bulk viscosity are not fixed by simply imposing the junction condition for the background metric. They instead determine the response of the membrane to external perturbations.

When the metric is linearly perturbed, the junction conditions are satisfied only when the membrane parameters are also appropriately perturbed. The metric perturbations outside the star can be decomposed into several spherical modes (ℓ, m), and within each, into two parity modes — axial and polar. The different (ℓ, m) modes couple with each other due to the spin angular momentum, but this coupling may be neglected to linear order in frequency of perturbation ω as far as the computation of QNMs is concerned [85].

Outside the membrane, the Einstein equation governing the metric perturbations can be reduced to two Schrödinger-like equations, namely the RW-like and Zerilli-like equations describing axial and polar perturbations to linear order in spin respectively [209, 210]. They are of the form:

$$\frac{d^2\psi(r)}{dr_*^2} + \left[\omega^2 - \frac{4mJ\omega}{r^3} - V(r)\right]\psi(r) = 0\,, \tag{1.193}$$

where the RW effective potential at linear order in the spin is [272, 273]

$$V_{\rm RW} = f(r)\left[\frac{\ell(\ell+1)}{r^2} - \frac{6M}{r^3} + \frac{24Jm(3r-7M)}{\ell(\ell+1)\omega r^6}\right]\,, \tag{1.194}$$

The Zerilli potential is more complicated and thus we do not explicitly write it here. The tortoise coordinate r_* is defined as $dr_*/dr = 1/f(r)$.

We find the boundary condition at the membrane-surface for axial perturbations to be

$$\frac{1}{\psi_{\rm RW}(r)}\frac{d\psi_{\rm RW}(r)}{dr_*}\bigg|_{r=r_0} = -\frac{i\omega}{\nu} + \frac{My^2V_{\rm RW}(r_0)}{2w(3w-y)} +$$
$$\frac{m\chi}{2\ell(\ell+1)My^5(y-3w)^2\nu}\Big\{w^3\Big[36w^2y\Big(i\left(\ell^2+\ell+9\right)y+$$

$$16\nu + \nu y^2\Big)+6wy^2\Big(\Big(\ell^2+\ell-7\Big)\nu y^2 - 2iy\Big(2\ell^2+2\ell+13\Big)$$
$$-42\nu\Big)+y^3\Big(-3\Big(\ell^2+\ell-4\Big)\nu y^2+4i\Big(\ell^2+\ell+6\Big)y+$$
$$36\nu\Big)-216iw^3\left(y-2i\nu\right)\Big]-3w^3(2w-y)\left(6w-\ell(\ell+1)y\right)$$
$$\Big[\Big(4w-2y+y^3\Big)\nu-2iy(3w-y)\Big]\Big\}, \tag{1.195}$$

where $\nu = 16\pi\eta$, $y = \omega r_0$, and $w = M\omega$. The polar boundary condition turns out to be

$$\frac{1}{\psi_{\rm Z}(r)}\frac{d\psi_{\rm Z}(r)}{dr_*}\Big|_{r=r_0} = -16\pi\eta i\omega + G(r_0,\omega,\eta,\zeta) + m\chi H(r_0,\omega,\eta,\zeta)\,, \tag{1.196}$$

where $G(r_0,\omega,\eta,\zeta)$ is given in Ref. [90], and the supplemental Mathematica notebook in [274] contains the complete expression for the polar boundary condition including H.

Defining a parameter for tuning compactness as[17] $\epsilon = (r_0 - 2M)/2M$, the BH boundary condition is recovered in the $\epsilon \to 0$ limit, for which $V(r_0) = 0$ and $y = 2w$, and by setting the membrane shear and bulk viscosity to BH values as as $-\zeta = \eta = 1/(16\pi)$. In this limit, the axial and polar boundary conditions in Eqs. (1.195) and (1.196) reduce to

$$\frac{d\psi_{\rm RW}(r)/dr_*}{\psi_{\rm RW}(r)}\Big|_{r=r_+} = \frac{d\psi_{\rm Z}(r)/dr_*}{\psi_{\rm Z}(r)}\Big|_{r=r_+} = -i\tilde{\omega}\,, \tag{1.197}$$

where $\tilde{\omega} = \omega - m\Omega_H$ and $\Omega_H = J/(4M^3)$ is the horizon angular velocity. This is consistent with the expected BH boundary condition of a purely ingoing perturbation near the horizon, i.e.,

$$\psi_{\rm RW}(r) \sim \psi_{\rm Z}(r) \sim e^{-i\tilde{\omega}r_*}\,, \quad \text{as } r_* \to -\infty\,. \tag{1.198}$$

[17]The ϵ here should not be confused with $\epsilon = 2M\omega$ defined in Sec. 1.4.

1.5.6.2 The fundamental QNM for spinning horizonless ECOs

We analyze the shift in the fundamental mode frequency of an ultracompact object by imposing outgoing boundary conditions at the asymptotic infinity and impose the boundary conditions in Eqs. (1.195) and (1.196) at the membrane surface, as we vary the parameters away from that of a BH. The reflectivity is governed by the shear viscosity parameter η in the limit $r_0 \to 2M$, where $\eta = (16\pi)^{-1}$ corresponds to pure absorption (BH case), while $\eta \to 0$ and $\eta \to \infty$ lead to total reflection.

Fig. 1.7 shows the variation of the real and imaginary parts of the fundamental $\ell = m = 2$, QNM with η for different spin values. As reflectivity increases, the fundamental mode deviates sharply from the BH case, with the imaginary part increasing for higher spin values, indicating faster decay. For $\eta \to 0, \infty$, the object becomes perfectly reflective. Interestingly, in the fully reflective limit, the $m = -2$ (counter-rotating) mode's imaginary part crosses zero above a critical spin, signaling an instability. Fig. 1.8 confirms that for $\eta \to 0, \infty$, this instability emerges at $\chi \sim 0.11, 0.15$, aligning with earlier ergoregion instability results [275].However, since there is no ergoregion at linear order in spin, it is unclear whether anything more can be inferred beyond the observation that the counter-rotating modes tend to become longer lived. The existence of an actual instability may only be confirmed by extending the analysis to higher orders in spin. The behavior of polar QNMs under viscosity variations follows a similar trend to the axial case.

We also examine QNM variations with compactness by varying the parameter $\epsilon = r_0/(2M) - 1$ at fixed shear viscosity ($\eta = \eta_{\rm BH}$). Fig. 1.9 illustrates that for $\epsilon \to 0$, we recover the Kerr BH fundamental QNM, while increasing ϵ leads to deviations from the BH spectrum. Axial and polar modes lose isospectrality, with the latter also depending on the bulk viscosity ζ, of the membrane.

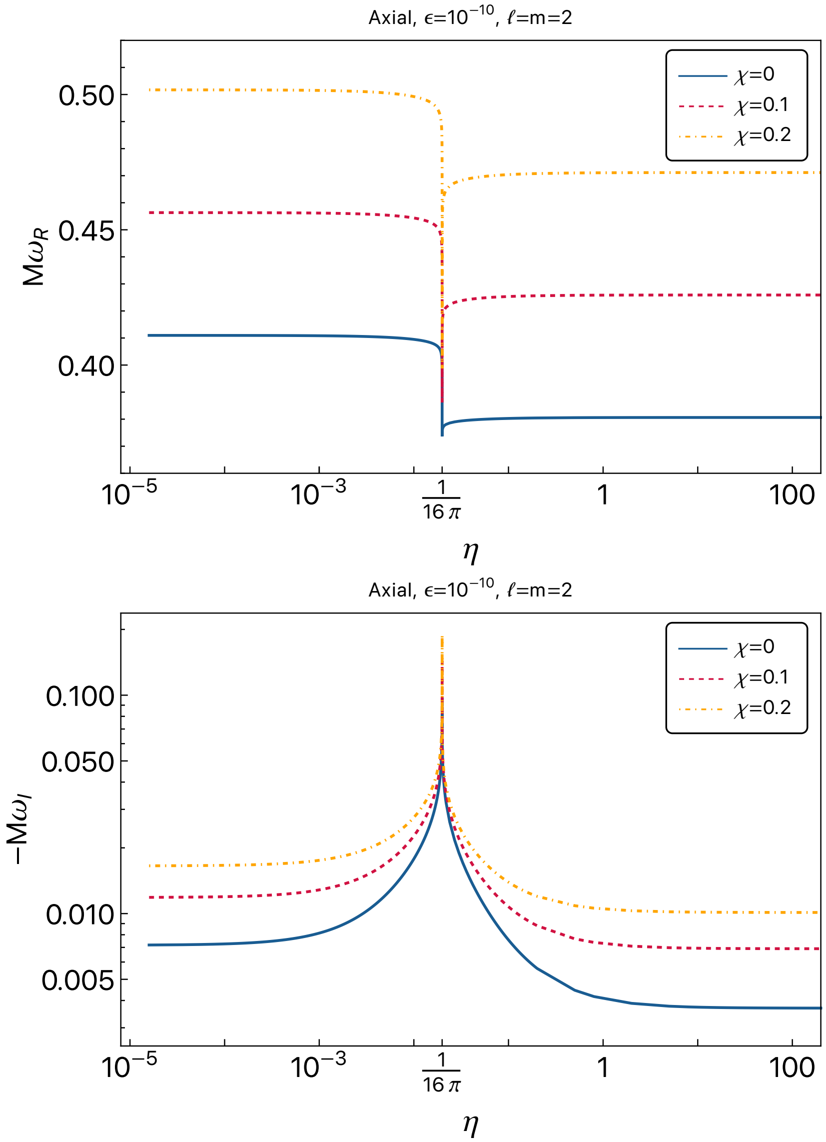

Figure 1.7: Real (top panel) and imaginary (bottom panel) part of the fundamental $\ell = m = 2$ QNM of an ultracompact object as a function of the viscosity parameter η for different values of the spin. For $\eta = 1/(16\pi)$, the compact object is totally absorbing; whereas for $\eta \to 0$ and $\eta \to \infty$, the compact object is perfectly reflecting.

By comparing Fig. 1.9 with the analogous plots in Ref. [90], we find that the variation of the real part of the fundamental mode as a function of ϵ is suppressed by the spin. However, the variation of the imaginary part of the fundamental mode is enhanced by the spin and it crosses

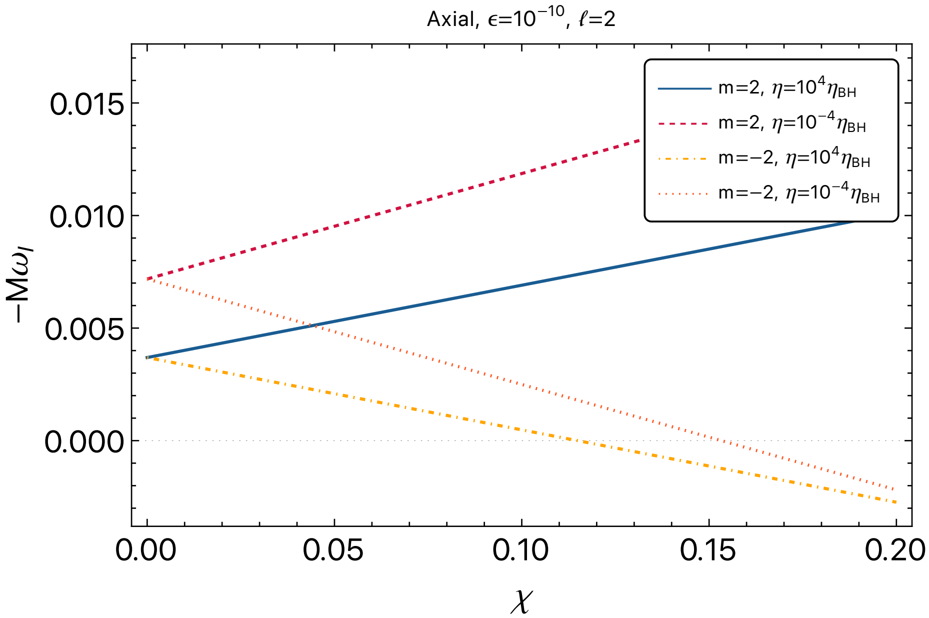

Figure 1.8: Imaginary part of the $\ell = 2$, $m = \pm 2$ QNMs of an ultracompact object as a function of the spin for a perfectly reflecting compact object with viscosity $\eta \gg \eta_{\rm BH}$ and $\eta \ll \eta_{\rm BH}$. Note that the imaginary part for $m = -2$ changes sign above a critical value of the spin rendering the mode unstable.

the shaded band for smaller values of ϵ than in the nonspinning case. Fig. 1.9 shows that spinning ($\chi = 0.2$) horizonless compact objects with $\epsilon \lesssim 0.05$ are compatible with measurement accuracy of the fundamental QNM in GW150914. This suggests that spinning horizonless compact objects may be more easily differentiated than nonspinning ones in the prompt ringdown. Moreover, the breaking of isospectrality between axial and polar modes may be more readily seen when increasing the values of the compactness in the presence of spin.

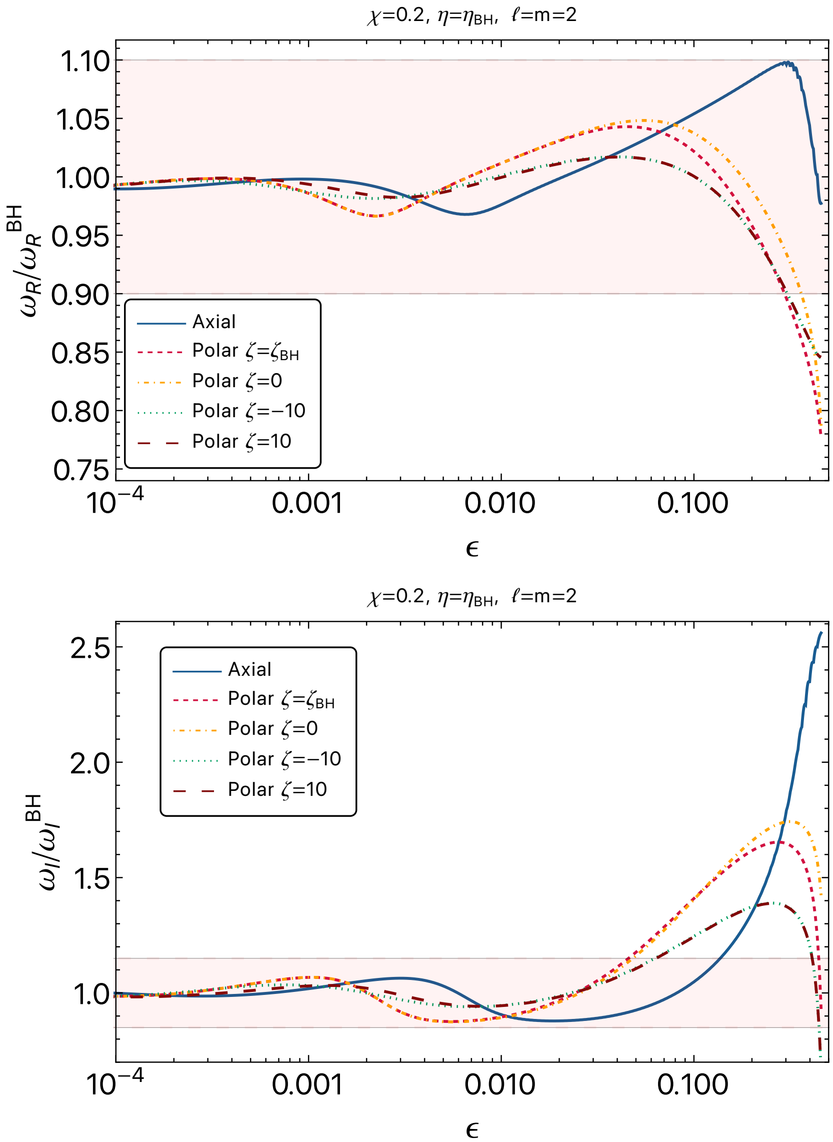

Figure 1.9: Real (top panel) and imaginary (bottom panel) part of the fundamental $\ell = m = 2$ QNM of a compact object with effective shear viscosity $\eta = \eta_{\rm BH}$, with respect to their corresponding value for the BH case. The QNMs are functions of the parameter ϵ, which is related to the compactness of the object. For $\epsilon \to 0$, we recover the fundamental BH QNM and axial and polar modes are isospectral. The shaded band correspond to the error bars (10% and 15%, respectively) for the real and the imaginary part of the fundamental QNM for the merger event GW150914 [276].

Chapter 2: Conservative and radiative dynamics in classical relativistic scattering and bound systems

Authors[1]: *M. V. S. Saketh, Justin Vines, Jan Steinhoff, Alessandra Buonanno*

Abstract: As recent work continues to demonstrate, the study of relativistic scattering processes leads to valuable insights and computational tools applicable to the relativistic bound-orbit two-body problem. This is particularly relevant in the post-Minkowskian approach to the gravitational two-body problem, where the field has only recently reached a full description of certain physical observables for scattering orbits, including radiative effects, at the third post-Minkowskian (3PM) order. As an historically instructive simpler example, we consider here the analogous problem in electromagnetism in flat spacetime. We compute for the first time the changes in linear momentum of each particle and the total radiated linear momentum, in the relativistic classical scattering of two point-charges, at sixth order in the charges (analogous to 3PM order in gravity). We accomplish this here via direct iteration of the classical equations of motion, while making comparisons where possible to results from quantum scattering amplitudes, with the aim of contributing to the elucidation of conceptual issues and scalability on both sides. We also discuss further extensions to radiative quantities of recently established relations which analytically continue certain observables from the scattering regime to the regime of bound orbits,

[1]Originally published as Phys. Rev. Res. **4**, no.1, 013127 (2022)

applicable for both the electromagnetic and gravitational cases.

2.1 Introduction

The dawn of gravitational-wave astronomy [23, 177, 277–279] and the promise of more sensitive future detectors [280–282] have renewed interest in varied approaches to solving the two-body problem in general relativity (GR). In particular, much recent work has focused on importing advanced tools from quantum field theory to treat classical scattering of massive bodies in the post-Minkowskian (PM) regime, with large impact parameters, but unconstrained speeds. Knowledge gained in this regime may also be used to develop a better understanding of inspiraling bound systems, with the aim of constructing more precise waveform models for detection and analysis of gravitational waves from compact binaries.

Alongside gravitational scattering, there is significant interest in (and overlap with) analogous but simpler problems in Yang-Mills theories, including the Abelian case, electromagnetism, in flat spacetime. In spite of the lesser nonlinearity, making calculations more easily tractable, scattering problems in gauge theories still share many of the same technical difficulties encountered in gravity, and thus can serve as instructive toy models. A further reason for this interest stems from the study of double-copy relations between gauge and gravity theories [283–286] and their uses in accomplishing gravity calculations with simpler gauge-theory building blocks.

A significant milestone in the gravitational case has been the recent completion of the calculation of the relativistic impulse (net change in momentum) of each body, in the scattering of two spinless massive bodies, at the third post-Minkowskian (3PM) order. Following important works such as Refs. [110, 112, 114], which established connections between scattering amplitudes and classical dynamics at the 2PM level, the study of the 3PM level began in Refs. [116, 287], which determined the conservative sector of the 3PM dynamics by matching to amplitudes computed via modern on-shell techniques, such as generalized unitarity [288–290] and the double copy [284–286], employing the effective-field-theory matching procedure set up in Ref. [114]. These results have been confirmed using various complementary methods [145, 146, 291, 292], including calculations based on classical worldlines instead of quantum fields [292]. The resultant 3PM conservative contribution to the scattering angle function presented a puzzle [293] in that it did not have a well-behaved high-energy limit, and did not smoothly connect to previous results for scattering of massless particles first derived in Ref. [294] and more recently confirmed in Refs. [295–297].

The resolution of this tension was first suggested in Ref. [297], which demonstrated, in the case of $\mathcal{N} = 8$ supergravity at two-loop order, the importance of including radiative effects in order to obtain a well-behaved ultrarelativistic limit. Subsequently, in the case of GR, Ref. [142] showed that a smooth high-energy limit (and a match to the massless results from Ref. [294] in that limit) is restored by including the radiative contribution to the scattering angle in addition to the conservative one, with the former being determined (via a relation derived in [226]) by the total radiated angular momentum at 2PM order. As we will detail below, the complete (conservative plus radiative) 3PM impulses are determined by the complete 3PM scattering angle along with the total linear (energy-)momentum radiated away in gravitational waves, first appearing at 3PM order. This last missing piece, the radiated momentum, was calculated in Ref. [149], by employing the formalism of Ref. [113] (KMOC) for computing classical observables from on-shell amplitudes. Finally, Ref. [150] also used the KMOC formalism to directly compute the impulses through 3PM order, thereby confirming and combining all the results mentioned above. In further confirmation, the radiative contributions to the 3PM impulse have been reproduced by a classical variation of constants method in Ref. [143], and the full 3PM scattering angle has been reproduced by a complementary quantum double-copy method in Ref. [147]. Meanwhile, the analysis of the 4PM level has been initiated in Refs. [119, 298].

Another strategy to solve the scattering problem in a way that includes both conservative and radiative dynamics is direct iteration of the classical equations of motion, in the situation where one lets two particles (representing compact bodies) perform a fly-by with a large impact parameter. One then constructs the particles' worldlines as expansions in the coupling strength, in the weak field (large impact parameter, small deflection) regime, with the zeroth-order worldlines given by uniform (straight-line) motion. The field equations and the equations of motion are then solved iteratively, informing each other to the required order. Any radiative/dissipative effects are included at each order by employing retarded boundary conditions (for fields) and using a regularization technique to evaluate the effect of each particle's field on itself. Historically, this route was followed in Ref. [104] where the impulse was calculated for both electromagnetism (EM) and GR up to 2^{nd} order.

Here we push this method to the 3^{rd} order in the EM case. In addition to including radiative effects, another advantage of the classical method is that it is relatively simple to automate the iteration to go to higher orders with the only potential challenge being computation of one-dimensional integrals. This may be useful for efficiently computing scattering observables, which can then be used for subsequently understanding bound orbits. It would also be highly interesting to connect this efficient classical iteration to perturbative scattering-amplitude calculations, for instance by expressing amplitudes using the so-called worldline quantum field theory [124, 125]. Furthermore, the classical method is also perhaps the simplest to justify, being most closely related to the actual situation of classical scattering of compact objects, and it gives detailed information about the time-dependent worldlines at each order as another benefit.

Having in hand results for the scattering problem, we investigate the possibility of mapping observables from unbound to bound orbits via analytic continuation, following Refs. [131, 227], where the basis of the mapping procedure was explained and used to relate the scattering angle for unbound orbits to the periastron advance angle for bound orbits. An analogous map between energy losses was presented in Ref. [228], and was subsequently verified from the results of Ref. [149] for the radiated linear momentum in the GR case. Here we provide a general relation between observables (satisfying certain criteria) for bound and unbound orbits following the method given in Ref. [227], and we explicitly relate angular momentum losses between bound and unbound orbits. We verify the map between energy losses using the expression for leading order radiated momentum in EM derived earlier, and we use the map between angular momentum losses to uncover an error in the expression for angular momentum losses for 1 post-Newtonian (PN) unbound orbits in GR given in Ref. [229]. We also comment on the scope of using these relations in computing resummed expressions for observables in the bound case.

2.1.1 Outline

The chapter is organized as follows. In Sec. 2.2, we explain in detail the process of solving for the worldline corrections iteratively via the classical method to 3$^{\text{rd}}$ order. In Sec. 2.3.1, we write down the impulse up to 3$^{\text{rd}}$ order and express it in terms of the conservative and radiative parts of the scattering angle and radiated momentum. In Sec. 2.3.2, we derive the leading order angular momentum loss and show that it is correctly related to the leading order radiative correction to the scattering angle. We then investigate the high-energy and nonrelativistic limit of relevant observables in Sec. 2.3.3 and Sec. 2.3.4, respectively. In Sec. 2.4, we show how the method of analytic continuation shown in Refs. [131, 227] can be extended to other observables if certain conditions are satisfied, and explicitly show how these mappings can be used to extract partial results for bound orbits, and their scope. We then conclude in Sec. 2.5 with a short summary. In Appendix. A.1, we explain in detail how we compute the 2nd order correction worldlines and explicitly write down the 2nd order worldline correction for particle 1. In Appendix A.2, we translate the 3rd order force correction diagrams to expressions and give brief comments regarding the source of each diagram.

2.2 Relativistic scattering of two point charges

We consider here the motion of two charged point particles in classical relativistic electromagnetism in flat spacetime. The particles have charges eq_1 and eq_2, masses m_1 and m_2, and proper-time–parametrized worldlines $x^\mu = z_1^\mu(\tau_1)$ and $x^\mu = z_2^\mu(\tau_2)$. The Lorenz-gauge field equation for the gauge field $eA_\mu(x)$, with $\partial_\mu A^\mu = 0$, is

$$\partial^2(eA^\mu) = 4\pi J^\mu. \tag{2.1}$$

We take out a factor of the order-counting parameter e from the gauge field (and the field strength below) for later convenience. The current density is

$$J^\mu(x) = e\sum_a q_a \int d\tau_a\, \dot{z}_a^\mu \delta^4(x - z_a), \tag{2.2}$$

with $a = 1, 2$. The equation of motion for each worldline can be taken as the Lorentz-Dirac equation,

$$m_a \ddot{z}_a^\mu = e^2 q_a F^\mu{}_\nu(z_a)\dot{z}_a^\nu + \frac{2e^2 q_a^2}{3}(\dddot{z}_a^\mu + \dot{z}_a^\mu \ddot{z}_a^2), \tag{2.3}$$

where $eF_{\mu\nu} = 2e\partial_{[\mu}A_{\nu]}$ is the *external* field strength (due to the field of the other particle), while the second term accounts for the action of the self field [299]. Our task is to construct an iterative solution to these equations working perturbatively in the coupling strength, measured by e^2.

At zeroth order in e^2, the particles follow inertial trajectories, and their worldlines can be written as

$$z_1^{(0)\mu} = b^\mu + u_1^\mu \tau_1, \quad z_2^{(0)\mu} = u_2^\mu \tau_2, \tag{2.4}$$

where u_1^μ and u_2^μ are the zeroth-order 4-velocities, with $u_1 \cdot u_2 \equiv \gamma$, and b^μ is the impact parameter vector with $b \cdot u_1 = 0 = b \cdot u_2$, so that the minimum separation between the zeroth-order trajectories is given by $|b|$.

The field sourced by particle a, on a general trajectory $x^\mu = z_a^\mu(\tau_a)$, obeys

$$\partial^2(A_a^\mu) = 4\pi q_a \int d\tau_a \, \dot{z}_a^\mu \, \delta^4(x - z_a(\tau_a)), \tag{2.5}$$

which has multiple solutions, corresponding to different boundary conditions. Choosing the retarded (no-incoming radiation) boundary conditions, the solution is

$$A_a^\mu(x) = \frac{q_a \dot{z}_{a,\mathrm{ret}}^\mu}{\dot{z}_{a,\mathrm{ret}} \cdot (x - z_{a,\mathrm{ret}})}, \tag{2.6}$$

where we use the shorthand $f_{\mathrm{ret}} = f(\tau_{\mathrm{ret}})$. The retarded proper time $\tau_{a,\mathrm{ret}}$ is the proper time at which the trajectory of the source particle a intersects the past light cone of the field point x. It is obtained by solving $|x - z_a(\tau_a)|^2 = 0$, and choosing the solution that makes $x - z_a(\tau_a)$ a future-directed null vector. Then, the field strength sourced by particle a is given by

$$\begin{aligned} F_a^{\mu\nu}(x) &= 2\partial^{[\mu} A_a^{\nu]} \\ &= \frac{2q}{r_a^3} \rho_a^{[\mu} \Big(r \ddot{z}_{a,\mathrm{ret}}^{\nu]} - \dot{z}_{a,\mathrm{ret}}^{\nu]} (\ddot{z}_{a,\mathrm{ret}} \cdot \rho_a - 1) \Big), \end{aligned} \tag{2.7}$$

where we have defined $\rho_a^\mu = (x - z_{a,\mathrm{ret}})^\mu$, $r_a = \dot{z}_{a,\mathrm{ret}} \cdot \rho_a$ and used $\partial^\mu \tau_{a,\mathrm{ret}} = \rho_a^\mu / r_a$.

Taking the field-sourcing particle above to be particle $a = 2$, the equation of motion for the other particle, 1, reads

$$m_1 \ddot{z}_1^\mu = e^2 q_1 F_2^{\mu\nu}(z_1) \dot{z}_{1,\nu} + \frac{2e^2 q_1^2}{3} \left(\dddot{z}_1^\mu + \ddot{z}_1^2 \dot{z}_1^\mu \right). \tag{2.8}$$

The first term in the RHS of Eq. (2.8) is the well known Lorentz force, giving the influence of the field sourced by particle 2 on particle 1. The second term is the Abraham-Lorentz-Dirac (ALD) self-force which accounts for the particle's influence on itself, which can be derived from the traditional Lorentz force law in various ways. The simplest method for our purposes is to use a regularization procedure to deal with the divergence when evaluating particle's field on its own worldline, as was done in Ref. [104]. In the case of EM, this can be done once, and the divergence-free expression in Eq. (2.8) can be used at all orders in the perturbative expansion in e^2 (see however the following paragraph). In contrast, in the GR case, one must repeat the regularization procedure at each order to compute the self-influence due to non-linearities in the theory.

Dissipative effects are included in the time-asymmetric part of the force which come from the choice of retarded propagator as well as from the ALD term (which is odd in $\tau_1 \to -\tau_1$). The validity of the self-force expression in EM is a nontrivial issue, associated with runaway solutions and pre-acceleration. In general, one expects the ALD force to be valid as long as the particle is not too large or too small. In Ref. [299], this was defined more precisely by requiring that the particle be small enough to enable fast communication between portions of its body ($l \ll t_c$, where l is the size of the particle and t_c is the time scale of changes in any external force field) but not so compact that the electromagnetic self-energy is larger than the mass (i.e., the positive bare mass condition $0 \leq m_0 \equiv m - e^2q^2/l$, or $e^2q^2/l \leq m$). The latter of these constraints in particular turns out to be important for making sense of divergences in the high-energy limit for some radiative quantities, as will be shown later in Sec. 2.3.3.

To iteratively solve Eq. (2.8), we expand the worldlines in powers of e^2, with the zeroth orders given by Eq. (2.4),

$$z_1^\mu(\tau_1) = b^\mu + u_1^\mu \tau_1 + e^2 z_1^{(1),\mu}(\tau_1) + e^4 z_1^{(2),\mu}(\tau_1) + \dots, \tag{2.9}$$

$$z_2^\mu(\tau_2) = u_2^\mu \tau_2 + e^2 z_2^{(1),\mu}(\tau_2) + e^4 z_2^{(2),\mu}(\tau_2) + \dots. \tag{2.10}$$

We use $|z_1(\tau_1) - z_2(\tau_{2,\mathrm{ret}})|^2 = 0$ to solve for the retarded time $\tau_{2,\mathrm{ret}}$ in terms of the worldline corrections ($z^{(n),\mu}$).

$$\tau_{2,\mathrm{ret}} = \tau_{2,\mathrm{ret}}^{(0)} + e^2 \tau_{2,\mathrm{ret}}^{(1)} + e^4 \tau_{2,\mathrm{ret}}^{(2)} + \dots, \tag{2.11}$$

which we then substitute into Eq. (2.8) to get a similar expansion for the force,

$$\begin{aligned} &e^2 m_1 \ddot{z}_1^{(1)} + e^4 m_1 \ddot{z}_1^{(2)} + e^6 m_1 \ddot{z}_1^{(3)} + \dots \\ &= e^2 f^{(1)} + e^4 f^{(2)} + e^6 f^{(3)} + \dots. \end{aligned} \tag{2.12}$$

Now collecting terms by powers of e^2, we get the correction to the force ($e^{2n} f^{(n)}$) at each order as a function of lower-order worldline corrections. These 2$^{\text{nd}}$ order differential equations can be then iteratively solved starting from the lowest order to acquire the worldline corrections at each order.

It is sufficient to solve for the worldline corrections of particle 1 since the analogous quantities for the second particle can be then obtained by simply swapping $1 \leftrightarrow 2$ and $b^\mu \to -b^\mu$.

2.2.0.1 Diagrams and rules

The correction to the force at each order $f^{(n)}$ [see the RHS of Eq. (2.12)] depends on the corrections to worldlines and retarded time at lower orders (along with zeroth-order quantities). For instance, $f^{(1)}$ only depends on the zeroth-order quantities ($z_1^{(0)}$, $z_2^{(0)}$, $\tau_{2,\text{ret}}^{(0)}$), whereas $f^{(2)}$ depends on $z_{a=1,2}^{(1)}$ and $\tau_{2,\text{ret}}^{(1)}$, as well. Put simply, $f^{(n)}$ is the n^{th} term in the Taylor expansion of the Lorentz and ALD forces w.r.t. the variables z_1, z_2, and $\tau_{2,\text{ret}}$. Thus, it is a linear combination of derivatives of the Lorentz (and ALD) force multipled by the corrections to these quantities. At higher orders, we find it convenient to split the force correction $f^{(n)}$ into various diagrams, as a way to illustrate the method of calculation and its increasing complexity with each order. It is important to note that these will *not* be Feynman or Feynman-like diagrams. We illustrate the rules for understanding the diagrams with an example below.

Diagrams with two worldlines represent terms in the Taylor expansion of the Lorentz force term i.e., $e^2 q_1 \dot{z}_{1,\nu} F_2^{\mu\nu}[z_1, z_2(\tau_{2,\text{ret}}), \dot{z}_2(\tau_{2,\text{ret}}), \ddot{z}_2(\tau_{2,\text{ret}})]$, via corrections from z_1, z_2 (and derivatives), and $\tau_{2,\text{ret}}$, for example:

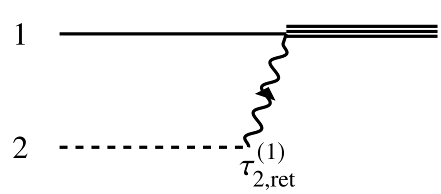

(2.13)

The directed photon (wavy) line conveys that the field is sourced by 2 to affect 1's worldline.

1. The part of the diagram to the **right** of the photon line tells the order at which this diagram contributes, according to the conventions:

1st order correction

2nd order corrections

and so on.

2. The part of the diagram to the **left** of the photon line tells us which derivatives to act on $eq_1 F_2^{\mu\nu} \dot{z}_{1,\nu}$ and which corrections to multiply. The derivatives are to be evaluated at zeroth order.

   a. Dashed lines represent contributions solely from unperturbed zeroth-order worldlines. They merely contribute a factor of 1 to the diagram.

   no derivative (zeroth order)

   b. Linear corrections (of any order) are represented using single/closely-spaced lines,

   $e^2 \sum_{n=0}^{3} d_{\tau_i}^n z_i^{(1)} \frac{\partial}{\partial d_{\tau_i}^n z_i}$ (1st order)

   $e^4 \sum_{n=0}^{3} d_{\tau_i}^n z_i^{(2)} \frac{\partial}{\partial d_{\tau_i}^n z_i}$ (2nd order)

   and so on. Here we are using the shorthand notation $d_{\tau_i}^n z_i = (d/d\tau_i)^n z_i(\tau_i)$

   c. Quadratic corrections are represented using wedges as follows,

   $\frac{e^4}{2} \sum_{m,n=0}^{m,n=3} (d_{\tau_1}^m z_i^{(1)})(d_{\tau_1}^n z_i^{(1)}) \frac{\partial^2}{\partial d_{\tau_1}^m z_i \partial d_{\tau_1}^n z_i}$

   $\frac{e^6}{2} \sum_{m,n=0}^{m,n=3} (d_{\tau_i}^m z_i^{(1)})(d_{\tau_i}^n z_i^{(2)}) \frac{\partial^2}{\partial d_{\tau_i}^m z_i \partial d_{\tau_i}^n z_i}$

and so on. All the derivatives are to be evaluated at zeroth-order retarded time ($\tau_2 = \tau_{2,\text{ret}}^{(0)}$).

4. The label at the intersection of particle 2's worldline with the photon (wavy line) $(\tau_{2,\text{ret}}^{(m)})^n$ contributes

   $$e^{2nm}(\tau_{2,\text{ret}}^{(m)})^n \times (1/n!)(d/d\tau_{2,\text{ret}})^n,$$

   where $\tau_{2,\text{ret}}^{(m)}$ is the m^{th} order correction to retarded time. Once again, the derivatives are evaluated at zeroth-order retarded time $\tau_{2,\text{ret}}^{(0)}$. Note that we are separating the dependence on retarded time purely for convenience, since $\tau_{2,\text{ret}}^{(n)}$ can be written in terms of worldline corrections $z_a^{(m)}$ via the relation $|z_1(\tau_1) - z_2(\tau_{2,\text{ret}})|^2 = 0$.

Thus, based on these rules, the above diagram (2.13) gives a 3rd order contribution and is equal to

$$e^6 \sum_{n=0}^{3} (d_{\tau_1}^n z_1^{(1)}) \frac{\partial}{\partial(d_{\tau_1}^n z_1)} (\tau_{2,\text{ret}}^{(1)})(d/d\tau_{2,\text{ret}})(q_1 F_2^{\mu\nu} \dot{z}_{1,\nu})|_{(0)}.$$

Contributions from the ALD (self-)force are constructed using the same rules, but only have one particle's worldline. Also, the derivatives act on the ALD force term i.e., $e^2(2q_1^2/3)(\dddot{z}_1 + \ddot{z}_1^2 \dot{z}_1^\mu)$, and there is no contribution to ALD force from $z_2^{(m)}$ (particle 2's worldline corrections) or retarded time corrections $\tau_{2,\text{ret}}^{(n)}$. For instance,

(2.14)

is a 2nd self force (ALD) contribution which gives

$$e^2 \sum_{n=0}^{3} (d_{\tau_1}^n z_1^{(1)}) \frac{2e^2 q_1^2 \partial}{3\partial(d_{\tau_1}^n z_1)} (\dddot{z}_1 + \ddot{z}_1^2 \dot{z}_1^\mu) = e^4(2q_1^2/3)(\dddot{z}_1^{(1)}).$$

Note that there are no photon lines in diagram (2.14) since ALD force is not due to the interaction between two particles. We thus simply have a second order worldline correction (the double line on the right) produced by first order worldline correction (single line on the left) through the ALD force term.

2.2.1 1st order

At leading order, we can substitute the zeroth-order worldlines (2.4) into the formula for retarded field tensor (2.7), the self-force can be neglected. The only relevant diagram is given here.

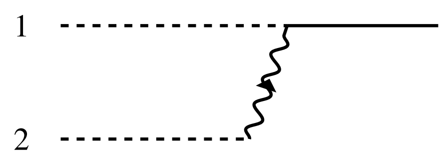

(2.15)

The corresponding equations are

$$e^2 m_1 \frac{d^2 z_1^{(1)\mu}}{d\tau^2} = e^2 q_1 u_{1,\nu} F_2^{\mu\nu}(z_1^{(0)})[z_2^{(0)}(\tau_{2,\mathrm{ret}}^{(0)})], \tag{2.16}$$

$$F_2^{(0)\mu\nu} = \frac{2q_2 \rho_2^{(0)[\mu} u_2^{\nu]}}{(r_2^{(0)})^3}, \quad r_2^{(0)} = u_2 \cdot \rho_2^{(0)}, \tag{2.17}$$

$$\rho_2^{(0)\mu} = [z_1^{(0)}(\tau_1) - z_2^{(0)}(\tau_{2,\mathrm{ret}}^{(0)})]^\mu. \tag{2.18}$$

The retarded proper-time at zeroth order $\tau_{2,\mathrm{ret}}^{(0)}$ is obtained by solving

$$|\rho^{(0)}|^2 = (|b|^2 + \tau_1^2 + \tau_{2,\mathrm{ret}}^{(0),2} - 2\tau_1 \tau_{2,\mathrm{ret}}^{(0)} \gamma) = 0,$$

$$\Rightarrow \tau_{2,\mathrm{ret}}^{(0)} = \gamma\tau_1 - \sqrt{|b|^2 + (\gamma v)^2 \tau_1^2}. \tag{2.19}$$

Defining

$$r_{21} = r_2^{(0)} = \sqrt{|b|^2 + (\gamma v)^2 \tau_1^2}, \tag{2.20}$$

we can now write the field tensor explicitly as

$$F_2^{\mu\nu} = \frac{2q_2}{r_{21}^3}(b^{[\mu}u_2^{\nu]} + \tau_1 u_1^{[\mu}u_2^{\nu]}), \tag{2.21}$$

which we substitute into Eq. (2.17) to get the 4-acceleration $a_a^\mu = \ddot{z}^\mu(\tau_a)$ for particle 1,

$$a_1^{(1)\mu} = \frac{q_1 q_2[\gamma b^\mu + \tau_1(\gamma u_1 - u_2)^\mu]}{m_1 r_{21}^3}. \tag{2.22}$$

This can be integrated twice w.r.t. τ_1 to get

$$v_1^{(1)\mu} = \frac{q_1 q_2[\gamma^2 v s_1 b^\mu + |b|^2(-\gamma u_1^\mu + u_2^\mu)]}{\gamma v^2 m_1 |b|^2 r_{21}}, \tag{2.23}$$

$$z_1^{(1)\mu} = \frac{q_1 q_2[\gamma v s_1 b^\mu + |b|^2 \log(\gamma v s_1)(-\gamma u_1^\mu + u_2^\mu)]}{m_1 |b|^2 (\gamma v)^3}, \tag{2.24}$$

as the 1st order velocity [$v_a^\mu = \dot{z}_a^\mu(\tau_a)$] and worldline corrections, where

$$s_1 = \gamma v \tau_1 + r_{21}(\tau_1) = \gamma v \tau_1 + \sqrt{|b|^2 + (\gamma v)^2 \tau_1^2}. \tag{2.25}$$

The constants of integration have been chosen such that initial velocity and impact parameter remain unchanged, i.e. $v_1^{(1)\mu} \to 0$ and $z_1^{(1)} \cdot b = 0$ for $\tau_1 \to -\infty$. The corrections for particle 2 can be obtained by sending $(1 \leftrightarrow 2)$ and $b^\mu \to -b^\mu$ to get

$$z_2^{(1),\mu} = \frac{q_1 q_2[-\gamma v s_2 b^\mu + |b|^2 \log(\gamma v s_2)(-\gamma u_2^\mu + u_1^\mu)]}{4 m_2 |b|^2 \pi (\gamma v)^3},$$

$$s_2 = \gamma v \tau_2 + r_{12}, \quad r_{12}(\tau_2) = \sqrt{|b|^2 + (\gamma v \tau_2)^2}. \tag{2.26}$$

We will find that the complexity of expressions (for force correction) greatly increases at 2nd order and beyond. These expressions can be rather simplified by the use of certain substitutions and variables. Thus, at 2nd and 3rd order, we use the variables $s_1 = \gamma v \tau_1 + r_{21}$ as the worldline variable (in place of τ_1) to express all integrands. This helps get rid of all square roots involving expressions of τ_1 while also making the integrals analytically tractable. In some places, we also use the rapidity parameter $\cosh(\phi) = \gamma$ which simplifies terms involving $\text{arcsinh}(\gamma v) = \text{arcosh}(\gamma)$, etc.

2.2.2 2nd order

We can now use the 1st order worldline corrections ($z_1^{(1)}$ and $z_2^{(1)}$) to compute the worldlines at 2nd order. We need to evaluate the 2nd order force correction, $f^{(2)} = m_1 \ddot{z}_1^{(2)}$, that is

$$m_1 \ddot{z}_1^{(2),\mu} = [e^4] \left[e^2 q_1 F_2^{\mu\nu} \dot{z}_{1,\nu} + \frac{2e^2 q_1^2}{3} \left(\dddot{z}_1^{\mu} + \ddot{z}_1^2 \dot{z}_1^{\mu} \right) \right], \tag{2.27}$$

$$z_1 \longrightarrow z_1^{(0)}(\tau_1) + e^2 z_1^{(1)}(\tau_1), \quad z_{2,\text{ret}} \longrightarrow z_{2,\text{ret}}^{(0)} + e^2 z_{2,\text{ret}}^{(1)},$$
$$\tau_{2,\text{ret}} = \gamma\tau_1 - r_{21} + e^2 \tau_{2,\text{ret}}^{(1)}. \tag{2.28}$$

Here $[x^n] f(x)$ is the coefficient of x^n in $f(x)$. To evaluate this, we split the contributions from corrections to z_1, z_2, and $\tau_{2,\text{ret}}$ as mentioned before. The 1st order worldline corrections $z_1^{(1)}$ and $z_2^{(1)}$, were derived in the last subsection (see Eq. (2.24) and Eq.(2.26)), the 1st order retarded time correction $\tau_{2,\text{ret}}^{(1)}$, in terms of $z_a^{(1)}$ is given in Eq. (A.16). The relevant diagrams are shown and labeled here,

I II

$e^4 f^{(2)} =$ 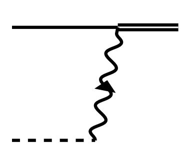 $+$ 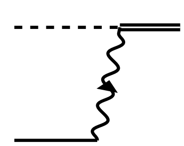

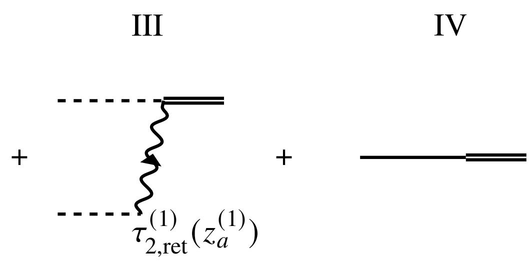

(2.29)

The diagrams in Fig. (2.29) can be used to compute the second-order correction to the force ($f^{(2)} = m_1\ddot{z}_1^{(2)}$) using the rules given in Sec. (2.2.0.1). This has been done explicitly in Appendix. A.1. One needs to then integrate each term twice w.r.t τ_1 to get the 2[nd] order worldline corrections, $z_1^{(2)}(\tau_1)$. We impose the same boundary conditions as in first order worldline corrections (see the paragraph below Eq. (2.23)). We briefly discuss the integration process below.

Diagrams I, II, and III are due to corrections to the Lorentz force term ($eq_1F_2^{\mu\nu}\dot{z}_{1,\nu}$) from 1[st] order worldline corrections. Their contribution to second-order force correction consists of various terms such as

$$\frac{s_1}{r_{21}^4}, \frac{s_1^3}{r_{21}^3 r_{12}^3}, \frac{s_1^2}{r_{21}^4}, \frac{\log(s_1)}{r_{21}^3}, \frac{s_1\log(s_1)}{r_{21}^4}\dots \tag{2.30}$$

where τ_2 and all quantities that depend on it

$$r_{12} = \sqrt{|b|^2 + \gamma^2 v^2 \tau_2^2}, \quad s_2 = \gamma v \tau_2 + r_{12}, \tag{2.31}$$

are to be evaluated at zeroth order retarded time

$$\tau_{2,\text{ret}}^{(0)} = \gamma\tau_1 - \sqrt{|b|^2 + \gamma^2 v^2 \tau_1^2}. \tag{2.32}$$

Thus, there are many square roots and nested square roots in the expression, which makes analytical integration complicated. The square roots can be eliminated by rewriting them as functions of $s_1 = \gamma v \tau_1 + r_{21}$ along with the relations given in Eq. (A.21). With these simplifications, we get expressions in terms of s_1 that only contain rational functions and logarithms as the ingredients, i.e. terms of the form

$$\frac{s_1^3 \text{Poly}(s_1)\log(s_1)}{(m_1 \text{ or } m_2)(1+s_1^2)^5}, \quad \frac{s_1^3 \text{Poly}(s_1)}{(m_1 \text{ or } m_2)(1+s_1^2)^5}, \\ \frac{s_1^3 \text{Poly}(s_1)}{m_2(1+s_1^2)^4(e^{2\phi}+s_1^2)^3}, \tag{2.33}$$

where $\text{Poly}(s_1)$ stands for polynomial function of s_1. Such terms can be easily integrated twice w.r.t. τ_1 via the relation $d\tau_1 = (d\tau_1/ds_1)ds_1 = \{r_{21}/(s_1 \sinh(\phi))\}ds_1$ to obtain their contribution to the 2$^{\text{nd}}$ order worldline correction ($z_1^{(2)}$). The reader is reffered to Appendix. A.1 for a detailed discussion of the contributions from various diagrams and the process of integration.

Diagram IV comes from the ALD force term $[(2e^2q_1^2/3)\left(\dddot{z}_1 + \ddot{z}_1^2\dot{z}_1^\mu\right)]$ and only its first term contributes at 2$^{\text{nd}}$ order, which is proportional to the 1$^{\text{st}}$ order jerk $\dddot{z}_1^{(1)}$. Thus, its contribution to 2nd order worldline correction is simply

$$\begin{aligned} z_1^{(2)}|_{\text{IV}} &= \frac{2e^4q_1^2}{3m_1}\dot{z}_1^{(1),\mu} \\ &= \frac{2e^4q_1^3q_2[\gamma^2 v s_1 b^\mu + |b|^2(-\gamma u_1^\mu + u_2^\mu)]}{3\gamma v^2 m_1^2 |b|^2 r_{21}}. \end{aligned} \tag{2.34}$$

After integration, collecting the contribution of all diagrams gives us the the complete 2nd order worldline correction $z_1^{(2)}(\tau_1)$. The explicit expression for $z_1^{(2)}(\tau_1)$ is given in Eq. (A.25). We can now use this to evaluate the force correction and subsequently impulse at 3$^{\text{rd}}$ order where dissipative effects appear for the first time.

2.2.3 3rd order

At 3rd the force correction given by $m_1\ddot{z}_1^{(3)} = f^{(3)}$, gains contributions from both 1st and 2nd order worldline corrections. The 1st order corrections contribute quadratically as $e^4(z_a^{(1)})^2$, whereas the 2nd order corrections contribute linearly via $e^4 z_a^{(2)}$. Further, their contributions are independent, in the sense that there are no cross terms since $e^2 z_a^{(1)} \times e^4 z_b^{(2)} \sim e^6$. It is thus possible to separate their contributions. As before, there are also corrections to retarded time $\tau_{2,\text{ret}}$ to take into account. Since the retarded time is obtained by solving a quadratic relation $|z_1 - z_2|^2 = 0$, the 2nd order retarded time correction $\tau_{2,\text{ret}}^{(2)}$ gains contribution from both 1st and 2nd order worldline corrections, once again quadratic in $e^2 z_a^{(1)}$ and linear in $e^4 z_a^{(2)}$. Since there are no cross contributions $(z_a^{(1)} \times z_b^{(2)})$, we can also separate the 2nd order retarded time correction $\tau_{2,\text{ret}} = \tau_{2,\text{ret}}^{(1)}(z_a^{(1)}) + \tau_{2,\text{ret}}^{(1)}(z_a^{(2)})$.

Thus, we can divide the contributions into quadratic (in $z^{(1)}$) and linear (in $z^{(2)}$) types. The various diagrams corresponding to these contributions are given in Fig. (2.35) and Fig. (2.36) respectively, where we have accordingly separated the force correction, $f^{(3)} = f^{(3)}(z_a^{(1)}) + f^{(3)}(z_b^{(2)})$

.

$$e^6 f^{(3)}(z_a^{(1)}) =$$

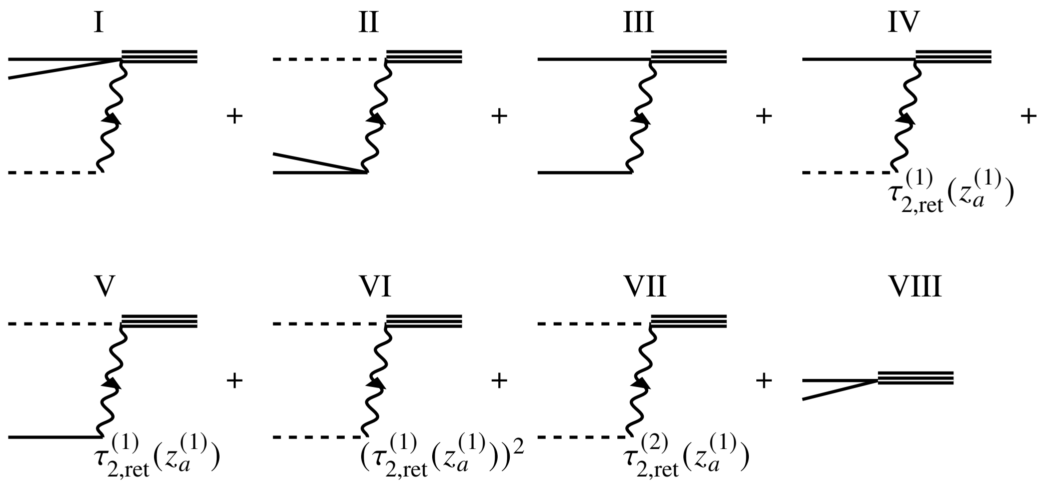

(2.35)

$$e^6 f^{(3)}(z_a^{(2)}) =$$

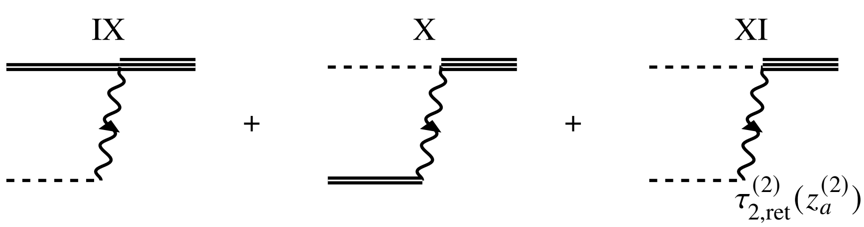

(2.36)

Quadratic contributions from $z_a^{(1)}$ and derivatives: Diagrams in Fig. (2.35) are contributions to 3rd force corrections ($f^{(3)}$) that are quadratic in 1st order worldline corrections (and derivatives).

Among these, diagrams I through VII are corrections to the Lorentz force term ($e^2 q F_2^{\mu\nu} \dot{z}_{1,\nu}$) term and give expressions composed of similar terms. Explicit calculation gives a linear combination with terms having $\log(bs_1)$, $\log(bs_1)^2$, and polynomial functions of (s_1) (written as Poly(s_1) from now on) as numerators, and $(1+s_1^2)^n \times (e^{2\phi}+s_1^2)^m$ as denominators. This is in accordance with what we expect from the form of 1st order worldline corrections, see Eqs. (2.23) and (2.26), and the expression for the field tensor Eq. (2.7), after writing everything in terms of s_1 and using the relations in Eq. (A.21). To evaluate their contribution to the impulse, we multiply by the

Jacobian factor and integrate over the entire worldline $\tau_1 \in (-\infty, \infty)$, or $s_1 \in (0, \infty)$ using the relation $d\tau_1 = (d\tau_1/ds_1) \times ds_1 = \{r_{21}/[s_1 \sinh(\phi)]\} ds_1$. The integrals to be evaluated are a linear combination of the following types of terms,

$$\begin{aligned}
&\frac{\mathrm{Poly}(s_1)}{(1+s_1^2)^4(e^{2\phi}+s_1^2)^3}, \quad \frac{\log(s_1)\mathrm{Poly}(s_1)}{(1+s_1^2)^4(e^{2\phi}+s_1^2)^3}, \\
&\frac{\log(s_1)^2}{(1+s_1^2)^4}.
\end{aligned} \tag{2.37}$$

`Mathematica` is once again able to evaluate them in a relatively short time once they have been separated into these types. Although we only require the definite integral, it is convenient for some terms to evaluate the indefinite integrals and then take the limits.

Diagram VIII comes from the second term in the ALD force $[(2e^2 q_1^2/3)\left(\dddot{z}_1 + \ddot{z}_1^2 \dot{z}_1^\mu\right)]$ (the first term does not contribute to the impulse). It's contribution at 3rd order is given by $(2/3)\, e^6 q_1^2 (\ddot{z}_1^{(1)})^2 u_1^\mu$ and it contributes to the radiative part of the impulse. It is worth noting here that this term is proportional to the initial momentum $p_1 = m_1 u_1$ and thus it cannot be the sole contribution to the radiative part of the impulse, even in the test-body limit, since that would change the rest mass. Additional contributions to the radiative part of the impulse come from corrections to the Lorentz-force term $(e^2 q_1 F_2^{\mu\nu} \dot{z}_{1\nu})$ (included in other diagrams). Together, they lead to a radiative contribution to the impulse that conserves the rest mass. Specifically in the test-body limit, the only other contribution to radiative impulse comes from the contribution of $z^{(2)}|_{\mathrm{IV}}$, see Eq. (2.34) to the Lorentz force term $(e^2 q_1 F_2^{\mu\nu} \dot{z}_{1\nu})$. This additional contribution was ignored in Ref. [113] in their calculation of net impulse in the test-body limit, leading to an incorrect result for the net radiative impulse in the test-body case that was proportional to p_1 .

Linear contributions from $z^{(2)}$: Diagrams in Fig. (2.36) are contributions to 3rd force corrections ($f^{(3)}$) that are linear in 2nd order worldline corrections (and derivatives).

All three diagrams are due to corrections to the Lorentz-force term ($e^2 q_1 F_2^{\mu\nu} \dot{z}_{1,\nu}$). Only the first term in the ALD force $[(2e^2 q_1^2/3)\left(\dddot{z}_1 + \ddot{z}_1^2 \dot{z}_1^\mu\right)]$ contributes linearly in 2nd order worldline corrections ($z^{(2)}$) at 3rd order and we have not included it's contribution since it is a total time derivative of a quantity that vanishes at infinite past/future (acceleration), and we are only interested in the net impulse.

Thus, all three diagrams give expressions composed of similar terms. We get a linear combination of terms with $\arctan(\gamma v s_1/|b|)$, $\arctan(s_1)$, $\log(|b|\gamma v s_1)$, $\arctan(r_{21}/|b|)$, and $\text{Poly}(s_1)$ in numerators, and $(1+s_1^2)^m \times (e^{2\phi}+s_1^2)^n$ in denominators. This is in accordance with the expression for 2nd order worldline correction given in Eq. (A.25) and the expression for the field tensor Eq. (2.7), after expressing everything in terms of s_1 using the relations in Eq. (A.21).

Once again, to get the impulse, we multiply with the Jacobian factor and integrate over the whole worldline $s_1 \in (0, \infty)$, where `Mathematica` has no trouble evaluating the integrals. Indefinite integrals sometimes give non-elementary polylogarithms, but they do not pose a challenge as far as computing the impulse is concerned. This however indicates that one might have to deal with non-elementary functions starting from 4th order (i.e. e^8).

Finally, performing the integration and adding the quadratic and linear contributions to the impulse, we obtain the complete expression for the 3rd correction to the impulse Δp_1 ($\Delta p_1^{(3)}$). The explicit expression for the same is given below in Eq. (2.40).

Now, we will use the key results of this section (i.e. 1st and 2nd order worldline corrections), and the 3rd order correction to the impulse $\Delta p_1^{(3)}$, to compute observables associated with the scattering process (e.g., the impulses).

2.3 Observables in the scattering process

2.3.1 Net impulses

The net impulse (defined as change in momentum) of particle 1 to 3rd order can be written as

$$\Delta p_1 = e^2 \Delta p_1^{(1)} + e^4 \Delta p_1^{(2)} + e^6 \Delta p_1^{(3)}. \tag{2.38}$$

We can derive $\Delta p_1^{(1)}$ and $\Delta p_1^{(2)}$ from the time-dependent worldlines upto 2nd order given in Eq. (2.24) and Eq. (A.25). With $z_1(\tau_1) = z_1^{(0)} + e^2 z_1^{(1)} + e^4 z_1^{(2)}$, we have

$$\begin{aligned} e^2 \Delta p_1^{(1)} + e^4 \Delta p_2^{(2)} &= \lim_{\tau_1 \to \infty} m_1 \dot{z}_1(\tau_1) - \lim_{\tau_1 \to -\infty} m_1 \dot{z}_1(\tau_1), \\ &= \frac{2e^2 q_1 q_2}{v|b|^2} b^\mu - \frac{e^4 q_1^2 q_2^2 E(v^2 |p| M \pi b^\mu + 4E|b| p^\mu)}{2 m_1^2 m_2^2 \gamma^2 v^4 |b|^3}. \end{aligned} \tag{2.39}$$

We can now add to Eq. (2.39) the 3rd order correction to the impulse. We described the process of computing $\Delta p_1^{(3)}$ in Sec. 2.2.3, and the result is

$$\begin{aligned} \Delta p_1^{(3)} =& -\frac{2q_1^3 q_2^3 [\gamma m_1^2 + \gamma m_2^2 + 2m_1 m_2 (1 + \gamma^4 v^2)]}{m_1^2 m_2^2 |b|^4 \gamma^5 v^5} b^\mu + \frac{\pi M E^2 q_1^3 q_2^3}{m_1^3 m_2^3 |b|^3 \gamma^3 v^4} p^\mu \\ &+ \frac{4 q_1^2 q_2^2}{3 m_1^2 m_2^2 |b|^4 \gamma^2 v^4} b^\mu \left[(m_2^2 q_1^2 + m_1^2 q_2^2) \gamma^2 v^2 - 3 m_1 m_2 q_1 q_2 \left(\gamma - \frac{\operatorname{arctanh} v}{\gamma v} \right) \right] \\ &+ \frac{\pi q_1^2 q_2^2}{4 \gamma^2 v^2 |b|^3} \left[\left(\frac{q_1^2}{m_1^2} \gamma + \frac{q_2^2}{m_2^2} \right) \frac{3\gamma^2 + 1}{3 \gamma v} - \frac{q_1 q_2}{m_1 m_2} \mathcal{F}(\gamma) \right] (u_2^\mu - \gamma u_1^\mu), \end{aligned} \tag{2.40}$$

where

$$\mathcal{F}(\gamma) = \frac{1}{(\gamma v)^3} \left[(3\gamma^2 + 1) \left(\gamma - \frac{\operatorname{arctanh} v}{\gamma v} \right) - 4(\gamma - 1)^2 \right]. \tag{2.41}$$

We can simplify this somewhat bulky expression by splitting the result into conservative and radiative parts and writing these in terms of the scattering angles and the total radiated momentum. To do so, we first evaluate the total scattering angle as

$$\sin\chi = \frac{-\Delta p_1 \cdot b}{|p||b|} + O(e^8), \tag{2.42}$$

which yields

$$\chi = \chi_{\text{cons}} + \chi_{\text{rad}}, \tag{2.43}$$

$$\begin{aligned}\chi_{\text{cons}} &= \frac{2e^2 E q_1 q_2}{m_1 m_2 \gamma |b| v^2} - \frac{\pi e^4 M E q_1^2 q_2^2}{2 m_1^2 m_2^2 \gamma^2 |b|^2 v^2} \\ &+ \frac{e^6 q_1^3 q_2^3 E [(m_1^2 + m_2^2)(4\gamma^2 - 6) - 4 m_1 m_2 \gamma(\gamma^2 - 3v^2)]}{3 m_1^3 m_2^3 |b|^3 \gamma^5 v^6},\end{aligned} \tag{2.44}$$

$$\begin{aligned}\chi_{\text{rad}} &= -\frac{4e^6 q_1^2 q_2^2 E}{3 m_1^3 m_2^3 |b|^3 \gamma^3 v^5}\Big[(\gamma v)^2 (m_2^2 q_1^2 + m_1^2 q_2^2) \\ &- 3 m_1 m_2 q_1 q_2 \Big(\gamma - \frac{\operatorname{arctanh} v}{\gamma v}\Big)\Big].\end{aligned} \tag{2.45}$$

where the conservative (radiative) scattering angle has been defined to be the part that is even (odd) under $v \to -v$. We can now define the conservative part of the impulse as the result of a simple rotation in the scattering plane by the angle χ_{cons}, and define the radiative part of the impulse to be the remainder,

$$\Delta p^\mu_{1,\text{cons}} = |p| \sin\chi_{\text{cons}} \frac{b^\mu}{|b|} + (\cos\chi_{\text{cons}} - 1) p^\mu, \tag{2.46}$$

$$\Delta p_{1,\text{rad}} = \Delta p_1 - \Delta p_{1,\text{cons}} \tag{2.47}$$

As we will see below, $\Delta p_{1,\text{rad}}$ is fully determined by the radiative contribution to the scattering angle χ_{rad} together with the total radiated momentum K^μ. The latter is found from summing the impulse (2.40) on particle 1 and its $(1 \leftrightarrow 2)$ version, yielding

$$\begin{aligned} K^\mu &= -\Delta p_1^\mu - \Delta p_2^\mu = -\Delta p_{1,\mathrm{rad}}^\mu - \Delta p_{2,\mathrm{rad}}^\mu \\ &= \frac{\pi e^6 q_1^2 q_2^2}{4|b|^3}\left[\left(\frac{q_1^2}{m_1^2}u_1^\mu + \frac{q_2^2}{m_2^2}u_2^\mu\right)\frac{3\gamma^2+1}{3\gamma v}\right. \\ &\quad \left. - \frac{q_1 q_2}{m_1 m_2}\frac{u_1^\mu + u_2^\mu}{\gamma+1}\mathcal{F}(\gamma)\right], \end{aligned} \tag{2.48}$$

where $\mathcal{F}(\gamma)$ was defined in Eq. (2.41). Now, the conservative part of the impulse of each particle separately conserves the particle's rest mass (i.e. $(p_{1,i}+\Delta p_{1,\mathrm{cons}})^2 = m_1^2$). Thus, the leading-order radiative effect must satisfy $\Delta p_{1,\mathrm{rad}} \cdot u_1 = 0$, so that the total impulse conserves the rest mass to 3rd order. Furthermore, $\Delta p_{1,\mathrm{rad}}$ is solely responsible for both radiated momentum and radiative part of the scattering angle. Thus, we obtain the following expression for $\Delta p_{1,\mathrm{rad}}$

$$\Delta p_{1,\mathrm{rad}}^\mu = \frac{K \cdot u_2}{(\gamma v)^2}(u_2^\mu - \gamma u_1^\mu) + |p|\chi_{\mathrm{rad}}\frac{b^\mu}{|b|}, \tag{2.49}$$

as anticipated in Eq. (1.105).

2.3.2 Radiation of angular momentum

The emitted radiation also carries away angular momentum. Unlike radiated momentum, angular momentum loss can be seen already at 2nd order. Radiated angular momentum can be evaluated using the relations

$$J_{\mathrm{rad}}^\mu = -J_{\mathrm{f}}^\mu + J_{\mathrm{i}}^\mu, \tag{2.50}$$

$$J_{\mathrm{f/i}}^\mu = \lim_{\tau_1,\tau_2\to\pm\infty} -\epsilon^\mu{}_{\nu\rho\sigma}\frac{p_1^\nu p_2^\sigma}{E}(z_1 - z_2)^\sigma, \tag{2.51}$$

$$p_a^\mu = m_a \dot{z}_a^\mu. \tag{2.52}$$

Note that the evaluation of this quantity requires the complete time-dependent worldlines and thus we cannot evaluate it to 3rd order. However, we can evaluate the radiated angular momentum at 2nd order by substituting $z_a^\mu = z_a^{(0)\mu} + e^2 z_a^{(1)\mu} + e^4 z_a^{(2)\mu}$ to get

$$J^\mu_{\text{rad}} = -2\frac{e^4 q_1^2 q_2^2}{E|b|^2\gamma v} I(v)\epsilon^\mu{}_{\nu\rho\sigma} b^\nu u_1^\rho u_2^\sigma + O(e^6), \tag{2.53}$$

$$I(v) = -\frac{2}{3}\gamma(\frac{q_1/m_1}{q_2/m_2} + \frac{q_2/m_2}{q_1/m_1}) + \frac{2}{v^2} - \frac{2\,\text{arctanh}\, v}{\gamma^2 v^3}. \tag{2.54}$$

This leading (2nd) order change in angular momentum determines the leading (3rd) order radiative contribution to the scattering angle (2.45), via the relation (1.108) above, as derived in Ref. [226].

2.3.3 High-energy limits of observables

We define the high-energy (HE) limit by requiring that the system of particles have energies much higher than their total rest mass in the COM reference frame. The energy of the system in this frame is given by $E = \sqrt{m_1^2 + m_2^2 + 2m_1 m_2\gamma}$ and we choose it to be much larger than $m_1 + m_2$ by setting $\gamma \gg 1$, which is the high-energy limit. Note that we are not sending m_1, m_2 to 0, which is the massless limit. The high-energy/ultra-relativistic limit is not equivalent to the massless limit in EM. We will see the need for this distinction soon. We further require that $q_1 \sim q_2$ and $m_1 \sim m_2$ and they will be treated as fixed when taking the high-energy limit.

The conservative scattering angle to 3rd order for EM in the HE limit is given by

$$\chi_{\text{cons,EM}|\text{HE}} \to \frac{4e^2 q_1 q_2}{|b|E} - \frac{16e^6 q_1^3 q_2^3}{3|b|^3 E^3}. \tag{2.55}$$

It is finite and well behaved unlike GR where the conservative part of the scattering angle exhibits a logarithmic divergence $\propto \log(\gamma)$ at 3rd order that cancels against contributions from the radiative part. The radiative part of the scattering angle in the HE limit is given by

$$\chi_{\text{rad}|\text{HE}} \rightarrow -\frac{8e^6 q_1 q_2}{3E|b|}\left(\frac{q_1^3 q_2}{m_1^2|b|^2} + \frac{q_2^3 q_1}{m_2^2|b|^2} - \overbrace{\frac{6q_1^2 q_2^2}{E^2|b|^2}}^{\text{finite}}\right). \tag{2.56}$$

Here, we see the importance of distinguishing between the HE limit and the massless limit. The above expression is linearly divergent in γ in the massless limit ($m_1, m_2 \rightarrow 0, \gamma \rightarrow \infty$ while fixing E, the overbrace highlights the part that is finite in this limit). We encounter a similar situation for the radiated angular momentum, as well, which is given by

$$\frac{|J_{\text{rad,EM}}|}{J}|_{\text{HE}} \rightarrow -\frac{4e^4}{3}\left(\frac{q_1^3 q_2}{m_1^2|b|^2} + \frac{q_2^3 q_1}{m_2^2|b|^2} - \overbrace{\frac{6q_1^2 q_2^2}{E^2|b|^2}}^{\text{finite}}\right). \tag{2.57}$$

This kind of divergent behaviour for radiative scattering angle and radiated angular momentum is absent for gravity. This can be understood by noting that the divergence in these quantities comes from the ALD force, which is asymmetric in charges $\sim q_1^3 q_2$, $\sim q_1 q_2^3$. The expression for classical ALD (self-)force should be regarded as valid only when $e^2 q_a^2/l \leq m_a$ (i.e. the bare mass is positive, $m \sim m_0 + e^2 q_a^2/l$) as argued in Ref. [299], where l is the size of the charged particle. In our setup, the size of the charged particles must be much smaller than the impact parameter $|b|$, and thus we must have $e^2 q_a^2/m_a \ll |b|$. It is easy to see that the above expressions diverge precisely when this condition is violated.

However, the fraction of energy radiated in the COM frame per mass-energy, $K \cdot u_{\text{com}}/E$, seems to diverge in the HE limit regardless of masses. In the HE limit, it is given by

$$\frac{K \cdot u_{\text{com}}}{E}|_{\text{HE}} \rightarrow \gamma \frac{\pi e^6 q_1 q_2}{2|b|^3}\left[\left(\frac{q_1^3 q_2}{m_1^3} + \frac{q_2^3 q_1}{m_2^3}\right)\right.$$

$$- \frac{3q_1^2 q_2^2}{E^3}\Bigg]. \tag{2.58}$$

This diverges for $E \gg M$ ($\gamma \gg 1$), once again due to the self-force (asymmetric in charges) terms. It is important to note however that the divergence in fraction of energy radiated is also present in gravity for which the analogous result was recently obtained in Ref. [149]. Either way, this signals that the e^2- or G-expansion is not uniformly valid at arbitrarily high energies.

2.3.4 Nonrelativistic limit

We now consider both particles be moving at nonrelativistic (NR) speeds in the COM frame. This is achieved by simply sending $\gamma \to 1$, and we recover (to leading order) the Newtonian result $E = m_1 + m_2$ (where E is the total energy in the COM frame). The radiated energy (in the COM frame) is then given by

$$K_{\text{EM}} \cdot u_{\text{com}}|_{\text{NR}} \to \frac{\pi e^6 q_1^2 q_2^2}{3|b|^3 v}\left(\frac{q_1}{m_1} - \frac{q_2}{m_2}\right)^2. \tag{2.59}$$

The dependence on $(q_1/m_1 - q_2/m_2)^2$ is consistent with the expectation that the dipole approximation should suffice for computing the radiated energy in the NR limit via the term $2\ddot{p}^2/3$. We can see this explicitly by considering a hyperbolic orbit (an exact trajectory in the NR limit) and evaluating the dipolar energy loss along it. We work in the centre-of-mass frame (equivalent to the centre-of-momentum frame in the NR limit) where the expression for the dipolar energy loss is given by

$$P = -\frac{dE}{dt}|_{\text{NR}} = \frac{2|\ddot{\boldsymbol{p}}|^2}{3}, \quad \boldsymbol{p} = \left(\frac{q_1}{m_1} - \frac{q_2}{m_2}\right)\mu \boldsymbol{r}. \tag{2.60}$$

We denote the NR energy per reduced mass and angular momentum with the symbols $\mathcal{E} = (E - M)/\mu$ and J respectively. The orbit is then given in the NR limit as

$$
\begin{aligned}
&\mu \ddot{\boldsymbol{r}} = \frac{e^2 q_1 q_2 \boldsymbol{r}}{r^3}, \quad r = \frac{R}{1 + e\cos\phi}, \quad R = \frac{J^2}{e^2 q_1 q_2 \mu} \\
&e^2 = 1 + \frac{2\mathcal{E}J^2}{e^4 q_1^2 q_2^2} > 1, \quad J = \mu r^2 \frac{d\phi}{dt}.
\end{aligned} \tag{2.61}
$$

We can now integrate P over the entire trajectory, $\phi \in (-\arccos(-1/e), \arccos(-1/e))$ and obtain the total radiated energy

$$
-\mu\Delta\mathcal{E} = \int d\phi \frac{2e^4 q_1^2 q_2^2}{3R^4}\left(\frac{q_1}{m_1} - \frac{q_2}{m_2}\right)^2 (1 + e\cos\phi)^4. \tag{2.62}
$$

To make contact with Eq. (2.59), we take the limit of high angular momentum (low $e^2 q^2/J$, weak-field limit) where a perturbative analysis of the orbit is valid and get

$$
-\mu\Delta\mathcal{E}_{|HE} = \frac{2\pi e^6 q_1^2 q_2^2 \mu^3 \mathcal{E}}{3J^3}\left(\frac{q_1}{m_1} - \frac{q_2}{m_2}\right)^2. \tag{2.63}
$$

This is equal to Eq. (2.59) in the NR limit once we identify $\mathcal{E} = v^2/2 + O(v^4)$ and $J = \mu v|b|(1 + O(v^2))$ thus confirming our expectations.

2.4 From scattering to bound orbits

We now consider the case of generic classical scattering of point-charges to study general relations between bound and unbound motion [131, 227]. This is of particular interest for gravitational interactions and gravitational-wave physics. Indeed, mergers of bound compact binaries are much more likely to be observed than scattering encounters through gravitational-wave radiation. We are then motivated to investigate the methods by which knowledge of bound orbits can be obtained by looking at scattering events. One such method is via the maps for certain observables between bound and unbound orbits based on analytic continuation, as shown in Ref. [131], which related the unbound scattering angle to the bound periastron-advance angle. These maps can be extended or motivated for some other observables as well, as shown below.

Let us briefly explain the basis of the mapping procedure given in Refs. [131, 227] before extending it to other observables. Consider a system of two nonspinning relativistic compact bodies whose interaction can be effectively described by conservative local dynamics. We can write down an effective Hamiltonian for the system in the COM frame (in an isotropic gauge [114, 116, 129, 131, 227, 287]) as

$$H(\boldsymbol{p}, r) = \sqrt{\boldsymbol{p}^2 + m_1^2} + \sqrt{\boldsymbol{p}^2 + m_2^2} + V(r, \boldsymbol{p}^2), \tag{2.64}$$

where $\boldsymbol{p}^2(E, J, r) = p_r^2(E, J, r) + J^2/r^2$. The position coordinates are $q = (r, \phi)$, in polar coordinates in the plane of the motion. The Hamiltonian has no explicit dependence on t, ϕ, and thus we have conserved quantities $E = H(\boldsymbol{p}, r)$ (energy) and $J = p_\phi$ (angular momentum). We interpret $\pm\boldsymbol{p}$ to be the physical spatial momentum of either particle when they are far apart (which happens when $r \to \infty$, $V(r, \boldsymbol{p}^2) \to 0$).

When the system is bound ($E < M = m_1 + m_2$), there are two turning points r_{min} and r_{max} where $\dot{r} = 0$. Since $\dot{r} = \partial_{p_r} H \propto p_r$, the turning points occur at $p_r(E, J, r) = 0$. When the system is unbound ($E > M$), one of the turning points r_{max} becomes negative, and thus non-physical. However, the roots can be generally related to each other via the relation $r_{\text{min}}(\mathcal{E}, -J) = r_{\text{max}}(\mathcal{E}, J)$ (where $\mathcal{E} = (E - M)/\mu$) for both bound and unbound orbits. Since r_{max} tends to $\pm\infty$ as $-\mathcal{E} \to \pm 0$, we work instead with the variable $u = 1/r$. We define $u_+ = 1/r_{\text{min}}$ and $u_- = 1/r_{\text{max}}$ which are continuous if we vary $\mathcal{E}$ for fixed J with $u_{\text{max}} \to 0$ if $\mathcal{E} \to 0$. The relation between the roots is the same as before, $u_-(\mathcal{E}, J) = u_+(\mathcal{E}, -J)$.

This relation between the roots was used to relate the scattering angle for unbound orbits to periastron advance for bound orbits in Ref. [131] as follows. The scattering angle for an unbound system is given by

$$\chi(\mathcal{E}, J) = -\pi + \Delta_{\text{tot}}\phi = -\pi + \int_{\text{tot}} \frac{d\phi/dt}{du/dt} du, \tag{2.65}$$

$$= -\pi - 2\int_{u_+(\mathcal{E},J)}^{0} \frac{J}{p_r(u, \mathcal{E}, J)} du, \tag{2.66}$$

where we use $\dot{\phi}/\dot{r} = J/(r^2 p_r)$ and the fact that the contribution to $\Delta_{\text{tot}}\phi$ from $r = \infty$ to r_{min} (or $u = 0$ to u_+) is the same as that from the subsequent journey from r_{min} to $r = \infty$, hence the factor of 2.

Now, consider the quantity

$$\chi(\mathcal{E}, J) + \chi(\mathcal{E}, -J) = -2\pi - 2\int_{u_+}^{0} \frac{J}{p_r} du - 2\int_{u_-}^{0} \frac{-J}{p_r} du,$$

$$= -2\pi + 2\int_{u_-(\mathcal{E},J)}^{u_+(\mathcal{E},J)} \frac{J}{p_r(\mathcal{E}, J)} du, \tag{2.67}$$

where we use $u_+(\mathcal{E}, J) = u_-(\mathcal{E}, -J)$. It is not difficult to recognize the second term in Eq. (2.67) as the expression for the total angle subtended by a bound binary in one radial orbit (analytically continued to $\mathcal{E} > 0$). Thus, we have for Eq. (2.67)

$$-2\pi + 2\pi(K + 1) = 2\pi K(\mathcal{E} > 0, J), \tag{2.68}$$

where $2\pi K$ is the angle of periastron advance. This gives us the relation

$$\chi(\mathcal{E}, J) + \chi(\mathcal{E}, -J) = 2\pi K(\mathcal{E}, J), \tag{2.69}$$

as obtained in Ref [131]. Note that the LHS of the relation is only valid for $\mathcal{E} > 0$ and vice-versa for the RHS; this relation is thus based on analytical continuation of the expressions for scattering angle and periastron advance.

2.4.1 Analytic continuation of general observables

Assume that an observable $\mathrm{O}_{\mathrm{bound}}(\mathcal{E}, J)$ associated with a nonspinning bound system can be expressed as an integral over one radial period (of the conservative dynamics) as

$$2\int_{u_-}^{u_+} f(u, \mathcal{E}, J) du = \mathrm{O}_{\mathrm{bound}}(\mathcal{E}, J), \tag{2.70}$$

Here, we are assuming that the function f only depends on u, not on ϕ (reflecting rotational invariance). Now, the corresponding observable for an unbound orbit $\mathrm{O}_{\mathrm{unbound}}(\mathcal{E}, J)$ can be written as

$$2\int_{0}^{u_-} f(u, \mathcal{E}, J) du = \mathrm{O}_{\mathrm{unbound}}(\mathcal{E}, J). \tag{2.71}$$

Again, with this integral evaluated along the conservative dynamics, we have the mapping given in Ref. [227], $u_-(\mathcal{E}, -J) = u_+(\mathcal{E}, J)$.

Further assuming that $f(u, \mathcal{E}, J)$ is either odd or even in J (reflecting a certain behavior under time reversal), we have

$$\mathrm{O}_{\mathrm{bound}}(\mathcal{E}, J) = \mathrm{O}_{\mathrm{unbound}}(\mathcal{E}, J) + \theta(f)\mathrm{O}_{\mathrm{unbound}}(\mathcal{E}, -J), \tag{2.72}$$

with $\theta(f) = \pm 1$ if f is odd/even, respectively. Note that the LHS is not really an observable for bound orbits unless $\mathcal{E} < 0$. This is a formal relation between the functions based on analytical continuation of the expressions.

2.4.2 Radiated energy

It is reasonable to assume that the rate of energy loss (power) for generic orbits can be expressed as $dE/dt = P(u = 1/r, \mathcal{E}, J^2)$ (i.e. as an even function of J) — for example see Sec. 2.4.4

for a motivation of this property in the PN context. Thus, we can write the energy radiated per radial orbit in the bound case as

$$E_{\rm rad}^{\rm bound} = \oint P(u, \mathcal{E}, J^2) dt = 2\int_{u_-}^{u_+} P(u, \mathcal{E}, J^2) \frac{-1}{u^2 p_r} du, \tag{2.73}$$

and for the unbound case

$$E^{\rm rad}_{\rm unbound} = 2\int_{0}^{u_-} P(u, \mathcal{E}, J^2) \frac{-1}{u^2 p_r} du, \tag{2.74}$$

where we have defined $E^{\rm rad}_{\rm bound}$ as the energy loss per orbit for bound systems and $E^{\rm rad}_{\rm unbound}$ as the total energy loss for an unbound trajectory. Then, using the general relation derived in Eq. (2.72), we get the relation between unbound and bound energy losses as

$$E_{\rm rad}^{\rm bound}(\mathcal{E}, J) = E_{\rm rad}^{\rm unbound}(\mathcal{E}, J) - E_{\rm rad}^{\rm unbound}(\mathcal{E}, -J), \tag{2.75}$$

which was given earlier in Ref. [228]. We now use this relation to compute partial results for bound orbits in EM and verify it with explicit calculations in the NR limit.

To compute the RHS of Eq. (2.75), we use the expression for the energy radiated in the COM frame in a scattering event in the NR limit given in Eq. (2.59). We write it in terms of $\mathcal{E}$ and J using the relations $\mathcal{E} = v^2/2$, and $J = \mu v|b|$, obtaining

$$E_{\rm rad}^{\rm unbound}(\mathcal{E}, J) = \frac{2\pi e^6 q_1^2 q_2^2 \mu^3 \mathcal{E}}{3J^3}\left(\frac{q_1}{m_1} - \frac{q_2}{m_2}\right)^2, \tag{2.76}$$

which is odd in J. Thus, in this case the RHS in Eq. (2.75) is

$$\text{RHS of (2.75)} = \frac{4\pi e^6 q_1^2 q_2^2 \mathcal{E} \mu^3}{3J^3}\left(\frac{q_1}{m_1} - \frac{q_2}{m_2}\right)^2. \tag{2.77}$$

We should acquire the same result to the highest power in $1/J$ if we compute the radiated energy per orbit for bound orbits in the NR limit. We use the fact that, in this limit, the orbits are conic sections and the power can be obtained from the dipole approximations. We computed the dipole-power loss for unbound orbits in Eq. (2.62), we now do the same for bound orbits.

Thus, once again using the dipole formula for the power $P = 2\ddot{\boldsymbol{p}}^2/3$, with $\boldsymbol{p} = \Big(q_1/m_1 - q_2/m_2\Big)\mu\boldsymbol{r}$, where $\boldsymbol{r}$ is the separation vector from particle 2 to particle 1, $|\boldsymbol{r}| = r = R/(1+e\cos\phi)$, $\mu r^2 d\phi/dt = J$, with $R = J^2/(e^2 q_1 q_2 \mu)$, $e^2 = 1 + 2\mathcal{E}J^2/(e^4 q_1^2 q_2^2)$, we integrate over one period and obtain

$$E_{\rm rad}^{\rm bound} = \frac{2\pi\mu^3 e^6 q_1^2 q_2^2 (3e^4 q_1^2 q_2^2 + 2\mathcal{E}J^2)}{3J^5}\Big(\frac{q_1}{m_1} - \frac{q_2}{m_2}\Big)^2. \tag{2.78}$$

We then take the limit $J \to \infty$ and get

$$E_{\rm rad}^{\rm bound} \to \frac{4\pi e^6 q_1^2 q_2^2 \mathcal{E}\mu^3}{J^3}\Big(\frac{q_1}{m_1} - \frac{q_2}{m_2}\Big)^2, \tag{2.79}$$

which is identical to Eq. (2.77) as expected.

2.4.3 Radiated angular momentum

The angular momentum is a vector, and symmetry requires that the rate of angular-momentum loss be in the same direction as the angular momentum. Thus, we expect a relation of the form

$$\frac{d\boldsymbol{J}}{dt} = \boldsymbol{J}\, P_J(u, \mathcal{E}, J^2), \tag{2.80}$$

which gives the following rate of change for the magnitude of the angular-momentum loss

$$\frac{dJ}{dt} = J\, P_J(u, \mathcal{E}, J^2), \tag{2.81}$$

which is odd in J. Now, defining $J^{\rm rad}_{\rm unbound}$ as the total angular-momentum loss for an unbound trajectory and $J^{\rm rad}_{\rm bound}$ as the angular-momentum loss per orbit for bound systems, we derive the relation

$$J_{\rm rad}^{\rm bound}(\mathcal{E},J)=J_{\rm rad}^{\rm unbound}(\mathcal{E},J)+J_{\rm rad}^{\rm unbound}(\mathcal{E},-J), \tag{2.82}$$

which has the opposite sign in the RHS compared to Eq. (2.75).

The above relation, unfortunately, cannot be used to obtain partial result for the angular-momentum loss for bound orbits using only the leading-order result we have derived in this chapter, since the angular-momentum loss at leading order is odd in J, as seen in Eqs. (1.99) and (1.101). We need to evaluate it to at least 3rd order in the weak-field expansion. Nevertheless, as an illustration, we verify this relation at 1PN order in gravity. We compute the 1PN angular momentum loss for unbound orbits following the method in Ref. [229] to obtain

$$\begin{aligned}\Delta J_{\rm rad}^{\rm unbound}=\frac{-8Gm_1m_2\nu}{5c^5h^4}\Bigg\{&\arccos\left(\frac{-1}{h\sqrt{1/h^2+2\mathcal{E}}}\right)(15+14\mathcal{E}h^2)+\sqrt{2\mathcal{E}}h(15+4\mathcal{E}h^2)\\&+\frac{1}{1008h^2c^2}\Bigg[\arccos\left(\frac{-1}{h\sqrt{1/h^2+2\mathcal{E}}}\right)\big(105(1077-940\nu)\\&+252(535-748\nu)\mathcal{E}h^2+12(4283-3976\nu)\mathcal{E}^2h^4\big)\\&+\frac{\sqrt{2\mathcal{E}h^2}}{1+2\mathcal{E}h^2}\big(105(1077-940\nu)+224(1275-1429\nu)\mathcal{E}h^2\\&+4(42711-61600\nu)\mathcal{E}^2h^4+288(109-35\nu)\mathcal{E}^2h^6\big)\Bigg]\Bigg\}.\end{aligned} \tag{2.83}$$

Substituting this into the RHS of Eq. (2.82) and using $\arccos(-x)=\pi-\arccos(x)$, we obtain:

$$\begin{aligned}\Delta J_{\rm rad}^{\rm bound}=\frac{-8\pi Gm_1m_2\nu}{5c^5h^4}\Bigg[&(15+14\mathcal{E}h^2)+\frac{105(1077-940\nu)+252(535-748\nu)\mathcal{E}h^2}{1008h^2c^2}\\&+\frac{12(4283-3976\nu)\mathcal{E}^2h^4}{1008h^2c^2}\Bigg].\end{aligned} \tag{2.84}$$

where $h=J/(GM\mu)$ and thus we recover the correct expression for the angular-momentum radiated per bound orbit at 1PN order, obtained by multiplying Eq. (30) in Ref. [229] for the average angular momentum flux by the orbital period $P = 2\pi/n$, with n given in Eq. (26) of Ref. [229]. We also verified this expression by doing the explicit calculation for angular momentum loss in case of bound orbits (at 1PN). Note that the expression for angular momentum losses in unbound orbit in Eq. (1.99) does not completely match that given in Ref. [229], there is a minor computational error in their result.

2.4.4 Total radiative losses from instantaneous fluxes

Given the maps provided in the last two subsections, one can find resummed relativistic expressions for the energy and angular momentum losses for bound orbits via the following simple algorithm: (i) solve the scattering problem in the weak-field expansion to compute energy- and angular-momentum losses, and (ii) use the maps provided earlier to find partial expressions for the energy- and angular-momentum losses of bound orbits.

However, this method is limited by the order to which the scattering problem can be solved in the weak-field regime. Since this is an expansion in large impact parameters $|b|$, the observables are obtained in powers of $1/|b|$ — for example see Eq. (1.101) and Eq. (1.113). Using the relation between $|b|$ and initial angular momentum, $J = (\mu M/E)\gamma v|b|$, we see that this is also an expansion in $1/J$.

In particular, the leading-order energy loss in the scattering case goes as $1/J^3$ [see Eq. (1.113)]. Thus, the map only gives us the $1/J^3$ part of the energy loss for bound orbits. However, the expression for 0PN energy loss per orbit for bound systems is given (from Einstein's quadrupole formula) by

$$\Delta E_{\rm GR} =$$
$$\frac{2\pi\mu^2}{Mc^5}\left(\frac{148}{15}\mathcal{E}^2\frac{G^3M^3}{J^3}+\frac{244}{5}\mathcal{E}\frac{G^5M^5}{J^5}+\frac{85}{3}\frac{G^7M^7}{J^7}\right) \tag{2.85}$$

$+O(1/c^7)$, and we do not recover the $1/J^5$ and $1/J^7$ terms. Each higher order in the PM expansion adds a power of $1/J$, and thus naively, one needs to solve to 7^{th} order (7PM, G^7) to recover the complete expressions for even the 0PN energy loss via the maps. This leads to a discouraging conclusion regarding the possibility of recovering expressions for bound-orbit radiative losses via results for the scattering encounter.

However, an alternative way of recovering bound-orbit observables is to fix the form of (gauge-dependent) instantaneous fluxes of energy and angular momentum that are directly applicable to both bound and unbound orbits (at least for local-in-time contributions). Following the known forms of PN expansions of these fluxes, one can write down general ansätze parametrized by unknown coefficients, which can then be fixed by computing the energy and angular momentum losses along near-straight-line (small-deflection-regime) trajectories, which should equal the results obtained from the weak-field expansion.

For example, in the gravitational case, the expressions for energy and angular momentum fluxes through 1PN order [229, 300] suggest that suitable ansätze can be written as

$$\begin{aligned}\Phi_E &= \frac{G^3M^2\mu^2}{c^5r^4}\left(\sum_{i=1}^{3}\alpha_i\mathcal{X}_i+\frac{1}{c^2}\sum_{i,j=1}^{3}\alpha_{ij}\mathcal{X}_i\mathcal{X}_j+\dots\right),\\ \Phi_J &= \frac{G^2M\mu J}{r^3c^5}\left(\sum_{i=1}^{3}\beta_i\mathcal{X}_i+\frac{1}{c^2}\sum_{i,j=1}^{3}\beta_{ij}\mathcal{X}_i\mathcal{X}_j+\dots\right),\end{aligned} \tag{2.86}$$

$$(2.87)$$

$$\mathcal{X}_i = \left\{ \boldsymbol{v}^2, \left(\frac{\boldsymbol{v}\cdot\boldsymbol{r}}{r}\right)^2, \frac{GM}{r} \right\}, \quad \mu = \frac{m_1 m_2}{m_1 + m_2}, \tag{2.88}$$

where $\boldsymbol{v}$ is the velocity and $\boldsymbol{r}$ is the relative position, in the PN context. For the purpose of demonstration, consider the leading-PN-order (0PN) fluxes,

$$\Phi_E = \frac{G^3 M^2 \mu^2}{c^5 r^4}\left[\alpha_1 \boldsymbol{v}^2 + \alpha_2 \left(\frac{\boldsymbol{v}\cdot\boldsymbol{r}}{r}\right)^2 + \alpha_3 \frac{GM}{r}\right], \tag{2.89}$$

$$\Phi_J = \frac{G^2 M \mu J}{r^3 c^5}\left[\beta_1 \boldsymbol{v}^2 + \beta_2 \left(\frac{\boldsymbol{v}\cdot\boldsymbol{r}}{r}\right)^2 + \beta_3 \frac{GM}{r}\right]. \tag{2.90}$$

The above expressions are subject to a gauge freedom in that we can add terms that are total time derivatives, the so-called Schott terms $\dot{E}_{\text{Schott}}$ and $\dot{J}_{\text{Schott}}$, which are functions of $\boldsymbol{r}$ and $\boldsymbol{v}$ (under the Newtonian equations of motion $\dot{\boldsymbol{r}} = \boldsymbol{v}$ and $\dot{\boldsymbol{v}} = -GM\boldsymbol{r}/r^3$) and vanish at infinity. This does not change the total energy and angular momentum losses, obtained by integrating over one radial period for the bound case or the entire orbit for the unbound case. The relevant Schott terms at 0PN order are

$$E_{\text{Schott}} = a\frac{G^3 M^2 \mu^2}{c^5 r^4}(\boldsymbol{v}\cdot\boldsymbol{r}), \tag{2.91}$$

$$J_{\text{Schott}} = b\frac{G^2 M \mu J}{c^5 r^3}(\boldsymbol{v}\cdot\boldsymbol{r}). \tag{2.92}$$

We find that we can choose $a = \alpha_2/4$ and $b = \beta_2/3$ and set the coefficients of the $(\boldsymbol{v}\cdot\boldsymbol{r})^2$ terms in Eqs. (2.89) and (2.90) to zero. This leaves us with an isotropic gauge for the fluxes, in which they depend only on $\boldsymbol{v}^2$ and r; we can then also express the fluxes as functions only of r and $\mathcal{E} = \boldsymbol{v}^2/2 - GM/r + O(1/c^2)$. With $\tilde{\Phi}_E = \Phi_E + \dot{E}_{\text{Schott}}$ and similarly for J, we are left with

$$\tilde{\Phi}_E = \frac{G^3 M^2 \mu^2}{c^5 r^4}\left(\tilde{\alpha}_1 \mathcal{E} + \tilde{\alpha}_2 \frac{GM}{r}\right) + O\left(\frac{1}{c^7}\right), \tag{2.93}$$

$$\tilde{\Phi}_J = \frac{G^2 M\mu J}{r^3 c^5}\left(\tilde{\beta}_1 \mathcal{E} + \tilde{\beta}_2 \frac{GM}{r}\right) + O\left(\frac{1}{c^7}\right), \tag{2.94}$$

with $\tilde{\alpha}_1 = 2\alpha_1 + \alpha_2/2$, $\tilde{\alpha}_2 = 2\alpha_1 + \alpha_2/4 + \alpha_3$, $\tilde{\beta}_1 = 2\beta_1 + 2\beta_2/3$ and $\tilde{\beta}_2 = 2\beta_1 + \beta_2/3 + \beta_3$. There is now a direct correspondence (via integration over the Newtonian orbit) between these coefficients $\tilde{\alpha}_{1,2}$ and $\tilde{\beta}_{1,2}$ and the coefficients in the PN-PM expansion of the total radiative losses for a scattering orbit; the former can be determined from the latter. We see that the orders in the weak-field-scattering expansion needed to recover the Newtonian fluxes (and thus also the bound-orbit losses) are considerably less than those needed in the direct use of the analytic-continuation maps. For example, to determine the (effective) 0PN energy flux $\tilde{\Phi}_E$, instead of 7PM, we need $\Delta E_{\text{rad}}^{\text{unbound}}$ only to 4PM order, to $O(G^4)$. Still we cannot recover the complete 0PN fluxes from the leading orders in the weak-field expansions of $\Delta E_{\text{rad}}^{\text{unbound}}$ (leading G^3) and $\Delta J_{\text{rad}}^{\text{unbound}}$ (leading G^2). [2]

2.5 Summary

We have considered the relativistic scattering of two charged point particles in classical electrodynamics and have calculated, via direct iteration of the classical equations of motion, the impulse on each particle through 3rd order in the weak-field expansion (through 6th order in the charges). This is the order at which radiative effects first appear in the impulse, and we have consistently included them by using retarded boundary conditions and by accounting for each particle's influence on itself by using the ALD force (see Sec. 2.2). We have related the impulse

[2] Note however that at least one further constraint on the four coefficients in Eq. (2.93) is provided by the condition $\tilde{\Phi}_E - \omega\tilde{\Phi}_J = 0$ for circular orbits, where $\omega = \dot{\phi}$ is the orbital frequency; this ensures that adiabatic radiation reaction takes circular orbits to circular orbits (adiabatically).

It is interesting to note in this context that Ref. [298] has derived a relativistic expression for the instantaneous flux at 3PM order for the gravity case, noting its relation to the coefficient of the dimensional-regularization pole in the effective action at 4PM order.

up to 3$^{\text{rd}}$ order to the conservative scattering angle, the radiated momentum and the radiative correction to the scattering angle (see Sec. 2.3.1). We have completely or partially verified the latter quantities by comparisons with other results and consistency tests in the literature. In particular, we have verified the general relationship derived in Ref. [226] between the radiated angular momentum (see Eq. (2.53)) at 2$^{\text{nd}}$ order and the radiative contribution to the scattering angle (see Eq. (2.45)) at 3$^{\text{rd}}$ order, by separately computing these quantities within our setup. We have also verified that the conservative scattering angle matches the result of Ref. [116], and that the total radiated momentum matches the result of an integral given in Ref. [113]. We have considered both the nonrelativistic ($v \ll c$) and high-energy ($v \to c$) limits of observables such as the scattering angle and the radiated energy (see Sec. 2.3.3 and Sec. 2.3.4). We found consistency with known (well-behaved) results in the nonrelativistic limit, but encountered certain divergences in the high-energy limit (See Eq. (2.56), Eq. (2.57) and Eq. (2.58)). Whilst some of these divergences seem to arise from limitations of the validity of ALD self-force (or more generally of the zero-size point-particle idealization), the divergence in the fraction of energy radiated signals a breakdown of weak-field perturbation theory for arbitrarily high energies, a feature in common with the gravitational case, as discussed in Ref. [149]. It would be highly instructive to see if our results for the complete 3$^{\text{rd}}$ order impulse match those which would be produced by applying the KMOC formalism [113] to the relevant amplitudes up to 2-loop order in (scalar) quantum electrodynamics, and to explore how the methodologies compare.

We have also investigated the scope of relating observables via analytic continuation between unbound and bound orbits, following Ref. [227] (see Sec. 2.4). We have derived a general map between generic unbound and bound observables that satisfy certain reasonable requirements (see Sec. 2.4.1). We have shown that the different maps known so far are special cases of this general map (see Eq. (2.72)), and we have also derived a new map between loss of angular momentum (see Eq. (2.82)). We have explicitly verified this new map for the gravitational case through the next-to-leading order in the PN expansion, and we have uncovered an error in the expression for the loss of angular momentum in hyperbolic encounters obtained in Ref. [300] (See Eq. (1.99) for corrected expression). The previously known map between energy losses was further verified for the electromagnetic case by comparing to the leading order in the nonrelativistic limit (see Sec. 2.4.2). We have found that directly using the analytic-continuation maps, to obtain complete expressions for bound-orbit radiative observables in the nonrelativistic limit, requires going to quite high orders in the weak-field expansion in the scattering regime. Conversely, we saw that lower orders for scattering are required to fix the coefficients in general ansätze for (gauge-dependent) instantaneous fluxes (see Eq. (2.89) and Eq. (2.90)), from which one can derive the total radiated energy and angular momentum for both unbound and bound orbits (for local-in-time contributions) (see Sec. 2.4.4). These investigations are valuable for understanding and modeling the relativistic binary problem in EM and GR (its dynamics and radiation) over the full range of eccentricities.

Chapter 3: Scattering of gravitational waves off spinning compact objects with an effective worldline theory

Authors[1]: *M. V. S. Saketh and Justin Vines*

Abstract: We study the process, within classical general relativity, in which an incident gravitational plane wave, of weak amplitude and long wavelength, scatters off a massive spinning compact object, such as a black hole or neutron star. The amplitude of the asymptotic scattered wave, considered here at linear order in Newton's constant G while at higher orders in the object's multipole expansion, is a valuable characterization of the response of the object to external gravitational fields. This amplitude coincides with a classical ($\hbar \to 0$) limit of a quantum 4-point (object and graviton in, object and graviton out) gravitational Compton amplitude, at the tree (linear-in-G) level. Such tree-level Compton amplitudes are key building blocks in generalized-unitary-based approaches to the post-Minkowskian dynamics of binaries of spinning compact objects. In this chapter, we compute the classical amplitude using an effective worldline theory to describe the compact object, determined by an action functional for translational and rotational degrees of freedom, including couplings of spin-induced higher multipole moments to spacetime curvature. We work here up to the levels of quadratic-in-spin quadrupole and cubic-in-spin octupole couplings, respectively involving Wilson coefficients C_2 and C_3. For the special case

[1]Originally published as Phys. Rev. Lett. **106**, no.12, 124026 (2022)

$C_2 = C_3 = 1$ corresponding to a black hole, we find agreement through cubic-in-spin order between our classical amplitude and previous conjectures arising from considerations of quantum scattering amplitudes. We also present new results for general C_2 and C_3, anticipating instructive comparisons with results from effective quantum theories.

3.1 Introduction

Since Einstein's proposal of general relativity as the correct description of gravity in 1915 [16, 301], a significant body of research has been developed in understanding and testing its consequences. Even today, more than a century later, there is still work to be done in this regard. In the age of gravitational-wave (GW) astronomy [177, 277**?** –279], progress depends on deepening our understanding of the general relativistic two-body problem, as the primary sources of GWs are binary systems of compact objects such as black holes and neutron stars. Identifying and characterizing such GW signals requires efficiently generated and highly accurate waveform templates, constructed both from interpolations of large-scale numerical simulations of binary spacetimes and from semi-analytic approximations to binary dynamics. The demand in accuracy has been further enhanced in recent years, with the promise of upcoming more sensitive detectors [280–282], with the exciting possibility of identifying finite size effects such as spin, spin-induced deformations and tidal effects in the future. In this work, we will primarily focus on the inclusion of spin and spin-induced multipole moments into the dynamics of compact bodies in the context of the two-body problem.

Black holes and compact bodies are extended objects, and their surfaces probe very strong gravitational fields. Nevertheless, it can be convenient to treat them as point particles moving along worldlines when describing their dynamics. As long as one is viewing them from afar, a representative worldline can be chosen describing the bulk motion, and the strong gravitation and (possibly complicated) internal structure can be taken into account by letting the ‘‘particle’’ couple non-minimally to the external gravitational field. Frameworks which treat the dynamics of extended bodies in this way may be collectively referred to as ‘‘effective worldline theories.’’ This framework is especially useful for dealing with spinning bodies, which are necessarily extended. Rotation also tends to deform the body, endowing it with a tower of multipole moments, with the 2^l-pole moment scaling as ma^l, where $S = ma$ is the spin (intrinsic) angular momentum and m is the mass of the body (with $c = 1$). The problem of including spin and spin-induced multipole moments into the gravitational dynamics of the body has been tackled in various ways historically. Focussing on effective worldline approaches, some of the earliest works are Refs. [185, 186], in which the equations of motion for a spinning particle were established at linear order in spin.

Beyond linear order in spin, one also needs to include the effects of spin-induced multipole moments on the dynamics, starting with a quadrupole moment scaling as ma^2. One approach is to construct an ansatz for an effective worldline stress-energy tensor for the particle, including spin and higher multipoles, and then appropriate equations of motion follow from the conservation law $\nabla_\mu T^{\mu\nu} = 0$; see e.g. Ref. [302–305]. Alternatively, one can construct an ansatz for a worldline action with rotational degrees of freedom and higher multipole couplings. This was approached for a spinning point particle in flat spacetime in Ref. [306], and generalized for curved space and arbitrary multipolar structure in Ref. [307].

In the context of the post-Newtonian (PN) approximation of the two-body problem, the action approach was developed in an effective field theory (EFT) treatment in Ref. [183], which computed the leading order (LO) spin-orbit contributions (at 1.5PN order) and the LO spin^2-

quadrupole contributions (at 2PN order) to the effective Hamiltonian. The effect of the spin-induced quadrupole moment was included in this work by adding a quadratic-in-spin coupling term, linear in the Riemann curvature tensor, to the action, along with an undetermined coefficient to be fixed by a further matching calculation. The leading contribution of a generic spin-induced quadrupole moment to binary dynamics and gravitational wave form was also computed earlier in Ref. [308]. A significant amount of work has been since done in the inclusion of spin into binary dynamics, as reviewed e.g. in Refs. [46–48], pushing the state-of-the-art for spinning particles to the N^{3}LO spin-orbit [309, 310], N^{3}LO quadratic-in-spin [311–313], NLO cubic-in-spin [314], and NLO quartic-in-spin [315]. Spinning binary dynamics may also be treated in a post-Minkowskian expansion, where one works to all orders in speeds but perturbatively in the strength of the fields, regulated by powers of the gravitational constant G, as in the post-Minkowskian worldline approaches in Refs. [124, 125, 138, 139, 292, 316–320]. Although the post-Minkowskian expansion is more suitable for dealing with scattering encounters, one can extract the dynamics of bound binaries as well from the observables associated with scattering encounters. This can be done either via boundary-to-bound maps between scattering and bound observables (see Refs. [1, 131, 153, 227]) or by constructing a Hamiltonian (see Refs. [109, 110, 129]).

Apart from worldline based approaches, a significant body of recent research has been dedicated to quantum field theory (QFT) based or amplitude-based methods. In these approaches, the key quantity of interest is usually the 2-to-2 scattering amplitude: two particles (representing massive compact objects) in, and two particles out. Given this amplitude, the relevant scattering observables (see e.g. Ref. [112, 113]) or a classical Hamiltonian (see e.g. Ref. [114]) can be derived from its classical limit. Similar to the worldline approaches, there are multiple sub-classes among the QFT-based methods for tackling the classical two-body problem as well.

One line of approaches employ an explicit quantum field, with an action that couples it to gravitation. The quanta of this field, in a classical limit, are used as avatars for black holes or other compact bodies. The 2-to-2 scattering amplitude (for two such quanta in, exchanging gravitons, and two quanta out) can be used to derive binary conservative dynamics. For spinless black holes, an effective conservative Hamiltonian describing binary dynamics was derived at 2PM order ($O(G^2)$) in Ref. [114], at 3PM in Ref. [116] and at 4PM in Refs. [119, 120], where a massive scalar field minimally coupled to gravity was employed. An important early work in the inclusion of spin in these approaches was done in Ref. [321], where the scattering amplitude for the scattering of a scalar quantum (ϕ) and a quantum of a spinning field (ψ), $\phi\psi \to \phi\psi$, was computed and subsequently used to derive a classical Hamiltonain describing their interaction at the leading PN orders. It was seen that the Hamiltonian matched that of a two-body system with one spinning and one spinless black hole up to fourth order in spin when the spinning member was a quantum of a spin-2 field minimally coupled to gravity. The scattering amplitude for the case where both particles were spinning, and subsequently a Hamiltonian describing their dynamics was derived in Ref. [132] at linear order in the spin of each particle at 2PM order (or at order G^2S), and to all orders in spin at 1PM order (at GS^∞). This was extended in Ref. [136] to G^2S^2, and then to G^2S^5 in [322]. These works used an arbitrary-spin-s quantum field, coupled to gravity via all symmetry-permitted non-mimimal coupling terms, parametrized by unknown coefficients. These unknown coefficients were fixed for the case of a black hole in Ref. [322] by requiring a best-behaved high-energy limit and a certain ‘‘shift symmetry’’ conjecture (in addition to matching with known tree-level results).

An important point regarding these approaches (and others discussed below), which is relevant here, is that the 2-to-2 scattering amplitude is constructed from simpler building block amplitudes, namely the (gravitational) Compton amplitude and the 3-point amplitude, via generalized unitarity. The Compton amplitude (here) is the scattering amplitude for a graviton scattering off a massive spinning quantum, and the 3-point amplitude is the vertex for two massive spinning particles joining a graviton and is related directly to the classical particle's linearized gravitational field. These serve as building blocks for the 2-to-2 scattering amplitude, which brings us to another class of amplitude-based methods.

Another series of works has sought to directly fix or constrain the two-body scattering amplitudes or their building blocks (Compton and 3-point), without going through an explicit QFT action functional, primarily focusing on the black hole case. In Ref. [111], a particular 3-point amplitude (dubbed ''minimal coupling'') for an arbitrary-spin-s particle was singled out by its uniquely well-behaved high-energy limit; a certain (remarkably simple) Compton amplitude consistent with this 3-point was also singled out, though exhibiting spurious poles for spins $s > 2$ (eventually corresponding to beyond fourth order in classical spin). These 3-point and Compton amplitudes were conjectured to correspond to black holes and used to compute the 2-to-2 scattering amplitudes to G^1S^∞ and G^2S^4 orders in Ref. [167]. The 2-to-2 amplitudes were later used to compute a classical aligned-spin scattering angle function in Ref. [168], and contributions to binary effective potentials in Ref. [169], and finally a complete binary Hamiltonian for generic spin orientations in Ref. [170], all through the same G^1S^∞ and G^2S^4 orders. The same Compton amplitude for spins $s \leq 2$ from Ref. [111] was re-derived from BCFW recursion applied to the 3-point in Ref. [233] employing a heavy-particle EFT formalism; its double-copy properties and its further applications were studied in Refs. [115, 323], and in Ref. [324] which first produced the Compton for both helicity configurations from a double copy prescription.

Pushing beyond fourth order in spin, Ref. [325] gave a parametrization of a spurious-pole-free Compton amplitude, using the heavy-particle EFT formalism, while enforcing consistency with general principles and with the ''minimal-coupling'' (black-hole) 3-point ampitudes, *and* while conjecturally imposing a certain ''black-hole spin structure'' observed at lower orders (which for 2-to-2 amplitudes is equivalent to the ''shift symmetry'' posited in Ref. [322]). Constructing the 2-to-2 amplitude from their parametrized Compton, they found that all freedom therein was fixed by additionally requiring a best-behaved high-energy limit (also just as in Ref. [322]), producing results at fifth order in spin in complete agreement with those from the simultaneous Ref. [322], as well as results at higher orders in spin. [2] It was argued that these considerations in fact fix the 2-to-2 amplitude at $O(G^2)$ to all orders in spin (while leaving freedom in the Compton to which the 2-to-2 is insensitive), at least for the case of the 2-to-2 amplitude for a spinless particle meeting a spinning black hole, at order G^2S^∞, as explicitly constructed in Ref. [140].

These works represent impressive progress in constraining effective black-hole–graviton amplitudes at higher orders in spin, but it is important to stress their conjectural nature. While the 3-point amplitudes have been very concretely matched (in many of the above references) with the linearized Kerr metric and the corresponding linearized effective worldline action [54, 128, 328, 329], constraints on the black-hole Compton amplitude at higher orders in spin (beyond consistency with the 3-point) have thus far been based on good-amplitude considerations without a direct connection to black hole physics. [3] As suggested in Ref. [135], a promising approach is

[2]The quintic-in-spin Compton as constrained by requiring the best-behaved high-energy limit in Ref. [325] was shown there to be at odds with a Compton derived in Ref. [326] from a Lagrangian for a massive spin-5/2 particle which is uniquely determined by its 3-point satisfying ''the current constraint'' (known from higher-spin theory and necessary for the existence of an underlying unitary theory) and requiring a minimal number of derivatives in the coupling. An interesting question is whether such tension may be alleviated with the generalization of such higher-spin Lagrangians to the large-spin limit.

It is also of note that the extrapolated ''shift symmetry'' [322] used (at the level of the 2-to-2 amplitude) to constrain higher-spin tree-level Compton amplitudes has been observed not to hold in general (directly) in the 1-loop-order Compton amplitude as computed recently in Ref. [327].

[3]A first confrontation of the black-hole Compton amplitude conjectures with actual black hole physics was carried out in Ref. [330], which compared the (2-to-2) aligned-spin scattering angle through G^2S^4 order from Ref. [168] with

to identify the classical limit of the quantum Compton amplitude with the amplitude for classical scattering of a gravitational plane wave off a Kerr background, determined by solutions of the Teukolsky equation describing linear gravitational perturbations of a spinning black hole. Such calculations have a long history [164, 165], but have so far produced explicitly results of the necessary kind only through linear order in spin [166]. (The toy model of a massless scalar field scattering off Kerr was studied at higher orders in spin in Ref. [135], leaving the gravitational-wave case for future work.) In the present work, we show that the same (tree-level) ‘‘classical Compton amplitude’’ can be usefully computed from an effective worldline action description, not only for black holes, but also for bodies with general spin-induced mutlipole moments.

The universally accessible nature of Compton amplitudes (specifically its classical limit) suggests that it can be a valuable tool in comparison and calibration of different effective approaches (worldline or QFT) and also with the real system of a (say) a Kerr black hole. For instance, both the worldline and the QFT-based methods are essentially effective approaches to model the dynamics of spinning compact bodies, and both approaches have free coefficients that need to be fixed through matching to produce the dynamics of the desired compact body. As described earlier, in the worldline based approaches, this freedom shows up as unspecified multipole moments, or in the worldline stress energy tensor, or as undetermined couplings in the action. In the amplitude-(or QFT-)based methods, this shows up in the freedom to choose the quantum-field and/or in its coupling to gravitation, or in the parametrization of the building block Compton or 3-point amplitudes. However, the relation between the freedom in these two (worldline vs. amplitude) classes of approaches is not easy to relate. It is known (since Ref. [322]) for example

‘‘self-force’’ calculations of the linearized perturbations of a Kerr black hole produced by a small orbiting body. This provided partial verification of the conjectures but left open freedom which may be best fixed by direct comparison of (classical) Compton amplitudes.

that there seem to be more free parameters in the action in QFT based approaches compared to worldline-based approaches to the same order in spin. It is thus of great interest to compare common quantities in these two approaches with each other for understanding the effect and physical meaning of these parameters. This is typically done by computation of the scattering angle, or the Hamiltonain, or other quantities relevant to the two-body system. These are however complicated quantities associated with the interaction between two bodies, when the undetermined coefficients themselves parametrize the interaction of just one body with the external gravitational field. Thus, a convenient quantity requiring just one body, and well-defined for both effective approaches and also easily calculable from the full theory of general relativity is desired. The Compton amplitude satisfies all of these requirements.

Finally, the universal accessibility of the Compton amplitude also means that it may be computed via non QFT-based methods and then employed in a QFT-based framework for the computation of (the classical limit of) the two particle scattering amplitude and subsequently dynamics thus enabling the different ways of studying compact bodies to complement and support each other. This is particularly useful if it is sometimes simpler to compute the Compton amplitude in certain approaches over others. Additionally, it serves as a crucial point of comparison to verify the conjectures that are employed in QFT/amplitude-based methods in constructing the Compton amplitude, which is necessary to trust that the resultant dynamics indeed describe the desired compact body.

In this work, with these motivations in mind, we derive the Compton amplitude for gravitational waves scattering off a stationary-axisymmetric, parity-preserving spinning compact body to S^3 for generic values for the undetermined coefficients ($C_2,\ C_3$ up to S^3, see Sec. 3.1.1) in an effective worldline approach. We do this with a multitude of objectives in mind. Primarily, having the Compton amplitude for generic spinning bodies may be subsequently used for deriving the dynamics of generic bodies in the future. Furthermore, this can be quite useful for comparison with the Compton amplitude derived from effective quantum approaches and understanding the relation between the free coefficients in either approach such as understanding the reason behind having more free parameters in the QFT-based approach in Ref. [322]. Additionally, when the coefficients C_2 and C_3 are fixed for the case of a black hole, we obtain a Compton amplitude consistent with that derived in Refs. [111, 233] thus corroborating (up to S^3) the conjecture relied upon in Refs. [167–170] that this Compton amplitude properly describes a black hole (in the classical limit). Finally, we aim to propose the Compton amplitude as a valuable tool for comparison and calibration of the diverse approaches currently being used for studying the motion of compact bodies under gravitational interaction.

Worldline EFT approach to Compton amplitude: For the purpose of deriving the classical Compton amplitudes in this work, we treat the compact body as a point particle equipped with spin-induced quadrupole ($\propto S^2$) and octupole ($\propto S^3$) moments in a worldline formalism as laid out in Ref. [184]. We subject this particle to an external linearized gravitational plane wave perturbation with a large wavelength i.e., $\lambda \gg r_{\text{CB}}$, where r_{CB} is of the order of the size of the compact body. The incident plane wave perturbs the particle's momentum, spin and subsequently the spin-induced multipole moments which in turn perturb the stress-energy tensor of the particle. When the perturbed stress energy tensor is plugged into the Einstein equation, one finds that it generates an additional wave like perturbation in the metric, which forms a part of the scattering of the incident wave. Additionally, owing to the non-linear nature of gravity, the incident wave also scatters of the static gravitational field of the particle which adds another contribution to the scattered wave also through the Einstein equation. Comparing the total scattered wave to the incident wave gives us the scattering amplitude at linear order in G and up to third order in spin. We find that this is consistent with the Compton amplitude derived in Ref. [111] for the case of black holes. The following section 3.1.1 succinctly summarizes the our results.

3.1.1 Summary of framework and results

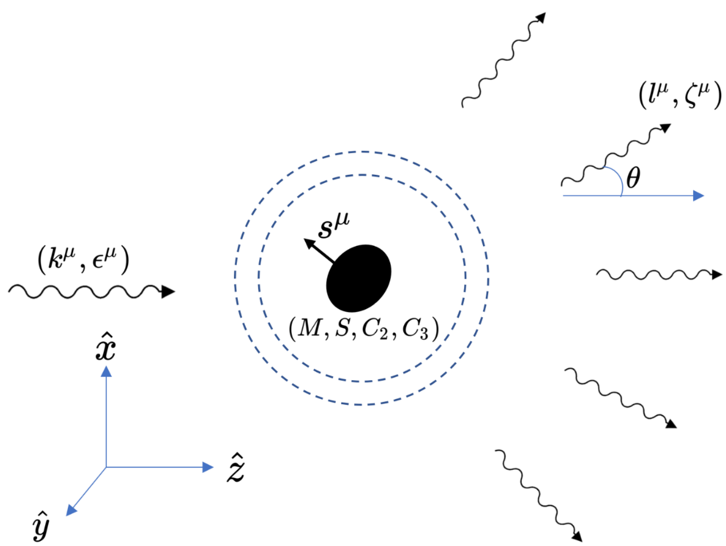

Figure 3.1: The spinning body is characterized by its mass M, spin S and spin-induced quadrupole and octupole moments whose magnitudes are controlled by two dimensionless coefficients C_2 and C_3. An incident wave moving along the $+z$-direction, with wave vector k^μ and complex polarization vector ϵ^μ, scatters off the particle producing a scattered wave. Far away from the particle, the scattered wave is a superposition of plane waves with wave vector l^μ and polarization vector ζ^μ. We fix the outgoing wave vector to be in the x-z-plane for convenience. θ is the angle between the outgoing and incident wave vectors in the rest frame of the particle.

A spinning classical particle with spin-induced quadrupole and octupole moments rests in flat spacetime. It is characterized by its mass M, spin S, and two coefficients C_2, C_3. The direction and magnitude of the spin is usually written together in the spin tensor $S^{\mu\nu}$, with $S^{\mu\nu} p_\nu = 0$ and $S^2 = (1/2) S^{\mu\nu} S_{\mu\nu}$, or the Pauli-Lubanski spin vector $s^\mu = -(1/2m) \epsilon^\mu{}_{\nu\rho\sigma} p^\nu S^{\rho\sigma}$, where p^μ is the momentum of the particle. C_2 and C_3 control the magnitude of its spin induced quadrupole and octupole moments. In flat space-time, the particle sources a stationary metric perturbation $h^{\mu\nu} = \sqrt{-g}g^{\mu\nu} - \eta^{\mu\nu}$, given in the linearized limit by

$$\begin{aligned} h^{\mu\nu} &= -u^\mu u^\nu [1 - \frac{C_2}{2}(a\cdot\partial)^2]\frac{4GM}{r} \\ &\quad - u^{(\mu}\epsilon^{\nu)}{}_{\rho\alpha\beta}u^\rho a^\alpha \partial^\beta [1 - \frac{C_3}{3!}(a\cdot\partial)^2]\frac{4GM}{r}, \end{aligned} \tag{3.1}$$

where $u^\mu = (1/m)p^\mu$ is the 4-velocity of the particle in flat-space-time and $a^\mu = (1/m)s^\mu$, with $a\cdot u = 0$. The actual non-linear metric sourced by the body approaches this form asymptotically. In the rest frame of the particle, this can be rewritten as

$$\begin{aligned} h^{00} &= [1 - \frac{C_2}{2}(\vec{a}\cdot\vec{\partial})^2]\left(-\frac{4GM}{r}\right),\ h^{ij} = 0, \\ h^{0i} &= \epsilon^i{}_{jk}a^j\partial^k[1 - \frac{C_3}{3!}(\vec{a}\cdot\vec{\partial})^2]\frac{2GM}{r}, \end{aligned} \tag{3.2}$$

where $\vec{a}$ can be identified as the spin vector. Comparison of the above expression with the most general asymptotic past-stationary spacetime given in Eq.(36) of Ref. [46] shows that the metric perturbation in Eq. (3.2) can be recovered by imposing stationarity (all multipole moments being constant in time) and identifying the mass-type multipole moments as $I = M$, $I_i = 0$, $I_{ij} = -C_2 M a_{\langle i}a_{j\rangle}$, $I_{ijk} = 0$ and current-type multipole moments as $J_i = Ma_i$, $J_{ij} = 0$, $J_{ijk} = -(2/3)C_3 M a_{\langle i}a_j a_{k\rangle}$ and require that all other multipole moments either vanish or are higher orders in spin.

If the particle respects parity and only has spin induced multipole moments, the vanishing or irrelevance of all other multipole moments follows trivially from parity invariance. Thus, M, S, C_2 and C_3 parametrize the most general axisymmetric parity-preserving stationary linearized metric perturbation. Also note, that adding trace-terms to the multipole moments (e.g., $\delta_{ij}|a|^2$ to

I_{ij}) only modifies it by terms proportional to $\partial^2(1/r) \propto \delta^{(3)}(x)$ thus modifying the field only at the location of the particle. Such corrections are expected to be irrelevant since the field at the location of the particle is ill-defined anyway.

We now subject this parity-preserving stationary axisymmetric body to an external linearized gravitational wave perturbation is incident upon it, which is characterized as[4]

$$h^{\mu\nu}_{\text{wave}} = \sqrt{-g}g^{\mu\nu} - \eta^{\mu\nu} = \epsilon\, \varepsilon^{\mu}\varepsilon^{\nu} \exp[ik \cdot x],$$
$$k^{\mu} \equiv \omega(1,0,0,1),\ \varepsilon^{\mu} \equiv \frac{1}{\sqrt{2}}(0,1,\pm i,0), \tag{3.3}$$

where ϵ is the amplitude of the incoming wave, k^{μ} is the wave-vector, fixing the direction of propagation, ω its frequency and ε^{μ} is a complex null vector which fixes the helicity of the incoming wave. The metric perturbation due to the incident wave affects the momentum, spin and subsequently the spin-induced multipole moments. These three quantities in turn perturb the stress energy tensor of the particle, leading to a radiated scattered wave through the Einstein equation. Additionally owing to the non-linear nature of gravity, the incident wave also scatters off the static metric perturbation sourced by the particle. Together, these two contributions lead to a scattered wave. The form of the scattered wave, encodes the scattering amplitude. In the particle's rest frame, the scattered wave takes the form (at large distances from the particle)

$$G\,\epsilon\, h^{\mu\nu}_{\text{scatter}}(r,\hat{n}) \equiv \epsilon[\mathcal{M}_{\pm+}(\hat{n})\zeta^{\mu}_{+2}(\hat{n})\zeta^{\nu}_{+2}(\hat{n}) \tag{3.4}$$
$$+ \mathcal{M}_{\pm-}(\hat{n})(\hat{n})\zeta^{\mu}_{-2}(\hat{n})\zeta^{\nu}_{-2}(\hat{n})]\frac{\exp[i\omega(r-t)]}{\omega r},$$

where $\mathcal{M}_{\pm\pm}(\hat{n})$ are the scattering amplitudes for a given pair of incoming and outgoing helicities. $\hat{n}$ is the spatial unit vector in a given direction in the rest frame of the particle, $\zeta^{\mu}_{\pm}(\hat{n})$ are the

[4] Starting below, we use the notation $\equiv$ to mean the form of the tensor object in the zero-momentum frame in the coordinate system shown in Fig. 3.1.1. Thus $k^{\mu} \equiv \omega(1,0,0,1)$ means the 4-vector k is pointing along the positive 'z' direction in this coordinate system.

complex null polarization vectors for a wave vector given by $l^\mu \equiv \omega(1,\hat{n})$. Thus. $\mathcal{M}_{\pm\pm}(\hat{n})$ is the amplitude for an incident wave with wave vector $k^\mu \equiv \omega(1,0,0,1)$, helicity ± 2, scattering into another wave vector $l^\mu \equiv \omega(1,\hat{n}) \equiv \omega(1,\sin(\theta),\cos(\theta),0)$ with helicity ± 2.

At zeroth order in spin (or for spinless case), We obtain the amplitudes

$$\mathcal{M}_{ab} = \frac{4GM\omega^3(\varepsilon_a\cdot\zeta_b)^2}{(l-k)^2}, \tag{3.5}$$

$$\mathcal{M}_{++} = \mathcal{M}_{--} = GM\omega\frac{\cos^4\left(\frac{\theta}{2}\right)}{\sin^2\left(\frac{\theta}{2}\right)}, \tag{3.6}$$

$$\mathcal{M}_{+-} = \mathcal{M}_{-+} = GM\omega\sin^2\left(\frac{\theta}{2}\right), \tag{3.7}$$

where θ is the angle between the incoming and outgoing wave vectors (k^μ and l^μ with $2\omega^2\sin^2\left(\frac{\theta}{2}\right) = -k\cdot l$). Note that there is mixing of helicities (non zero $\mathcal{M}_{+-}$ and $\mathcal{M}_{-+}$) even at zeroth order in spin. This is not true for electromagnetic waves scattering off black holes. The above amplitudes are consistent with those obtained in Ref. [232] for spinless black holes. Next, to first order in spin (or for a spinning rigid particle with no spin-induced deformation). We obtain the amplitudes

$$\begin{aligned}\mathcal{M}_{++} =& GM\omega\frac{\cos^4\left(\frac{\theta}{2}\right)}{\sin^2\left(\frac{\theta}{2}\right)}\Bigg[1-\tan^2\left(\frac{\theta}{2}\right)\frac{s^\mu}{M}(k_\mu+l_\mu)\\ &-i\frac{S_{\mu\nu}k^\mu l^\nu}{M\omega\cos^2\left(\frac{\theta}{2}\right)}\Bigg],\end{aligned} \tag{3.8}$$

$$\mathcal{M}_{+-} = GM\omega\sin^2\left(\frac{\theta}{2}\right)\left[1+\frac{s^\mu(k_\mu-l_\mu)}{M}\right], \tag{3.9}$$

$$\mathcal{M}_{--} = \bar{\mathcal{M}}_{++}(S^{\mu\nu}\to -S^{\mu\nu},\ s^\mu\to -s^\mu), \tag{3.10}$$

$$\mathcal{M}_{-+} = \bar{\mathcal{M}}_{+-}(S^{\mu\nu}\to -S^{\mu\nu},\ s^\mu\to -s^\mu), \tag{3.11}$$

where the spin tensor $S^{\mu\nu}$, $S^{\mu\nu}p_\nu = 0$, and the Pauli-Lubanski spin vector s^μ, appear for the first time. A bar denotes complex conjugation. Note that the spin tensor/vector appearing in the amplitude is that of the initial undisturbed particle, prior to the wave like perturbation. We find that the amplitudes are related to their helicity-flipped versions, via a spin-flip and complex conjugation. This is because the helicities of the incoming and outgoing gravitational wave can be flipped via a combination of parity and time-reversal operation on the whole system, which flips the spin (s^μ, $S^{\mu\nu}$), complex conjugates the amplitudes ($\mathcal{M} \to \bar{\mathcal{M}}$) but leaves the momenta (k^μ, l^μ) unchanged. The differential cross section resulting from these amplitudes agrees with Eq. (3) of [166], derived there from black hole perturbation theory.

The coefficients C_2 and C_3 associated with the spin-induced quadrupole ($\propto S^2$) and octupole ($\propto S^3$) moments finally show themselves at second and third order in spin respectively. For the case of a black hole, $C_2 = C_3 = 1$, the scattering amplitudes to third order are found to be simply the exponentiated version of the first order in spin amplitudes (in Eqs. (3.8-3.11)). We get (to third order in spin)

$$\begin{aligned}\mathcal{M}_{++} = GM\omega\frac{\cos^4\left(\frac{\theta}{2}\right)}{\sin^2\left(\frac{\theta}{2}\right)}\ \exp\Bigg[&-\frac{s^\mu}{M}(k_\mu + l_\mu)\tan^2\left(\frac{\theta}{2}\right)\\ &-\frac{i}{M\omega\cos^2(\frac{\theta}{2})}S^{\mu\nu}k_\mu l_\nu\Bigg],\end{aligned} \tag{3.12}$$

$$\mathcal{M}_{+-} = GM\omega\sin^2\left(\frac{\theta}{2}\right)\ \exp\left[\frac{s^\mu}{M}(k_\mu - l_\mu)\right], \tag{3.13}$$

$$\mathcal{M}_{--} = \bar{\mathcal{M}}_{++}(S^{\mu\nu} \to -S^{\mu\nu},\ s^\mu \to -s^\mu), \tag{3.14}$$

$$\mathcal{M}_{-+} = \bar{\mathcal{M}}_{+-}(S^{\mu\nu} \to -S^{\mu\nu},\ s^\mu \to -s^\mu), \tag{3.15}$$

which matches the amplitude given in spinor helicity formalism in Ref. [233], obtained from Ref. [111] using QFT-based methods.

The amplitudes do not exponentiate when C_2 and C_3 are generic. Thus, they correct the amplitudes in Eqs. (3.12), (3.13), (3.14), (3.15) by adding terms proportional to $(C_{2,3} - 1)^n$. The general expressions for the amplitudes with generic C_2 and C_3 for generic polarization vectors are given in the Appendix. The expressions for the helicity-conserving amplitudes ($\mathcal{M}_{++}$ and $\mathcal{M}_{--}$) for generic C_2 and C_3 after substitution of polarization vectors can be simplified considerably with help of the vector

$$w_{\mathrm{S}}^{\mu} = \frac{1}{2\omega\cos^2\left(\frac{\theta}{2}\right)}[\omega(k^{\mu}+l^{\mu}) - i\epsilon^{\mu}{}_{\alpha\beta\gamma}k^{\alpha}l^{\beta}u^{\gamma}], \tag{3.16}$$

which coincides with half the complex conjugate the vector w^{μ} from Ref. [233]. We also define $a^{\mu} = s^{\mu}/m$. Then, in terms of w_{S}^{μ}, k^{μ}, l^{μ}, and a^{μ}, the helicity-conserving amplitudes for the BH case $C_2 = C_3 = 1$ can be rewritten as

$$\mathcal{M}_{++} = GM\frac{\cos^4\left(\frac{\theta}{2}\right)}{\sin^2\left(\frac{\theta}{2}\right)}\ \exp[a\cdot(k+l-2w_{\mathrm{S}})], \tag{3.17}$$

$$\mathcal{M}_{--} = \bar{\mathcal{M}}_{++}(a^{\mu}\to -a^{\mu}). \tag{3.18}$$

The helicity-conserving scattering amplitudes for a spinning particle, with spin-induced quadrupole moments with generic C_2 and C_3 to third order in spin, is given by

$$\begin{aligned}\mathcal{M}_{++} = {}& GM\omega\frac{\cos^4(\theta/2)}{\sin^2(\theta/2)}\Bigg(\exp[a\cdot(k+l-2w_{\mathrm{S}})]\\
&+\frac{C_2-1}{2}\{[(k-w_{\mathrm{S}})\cdot a]^2+[(l-w_{\mathrm{S}})\cdot a]^2\}\\
&+\frac{C_2-1}{2}[(k-w_{\mathrm{S}})\cdot a][(l-w_{\mathrm{S}})\cdot a][(k+l-2w_{\mathrm{S}})\cdot a]\\
&-(C_2-1)^2[(k-w_{\mathrm{S}})\cdot a][(l-w_{\mathrm{S}})\cdot a](w_{\mathrm{S}}\cdot a)\\
&+\frac{C_3-1}{6}\{[(k-w_{\mathrm{S}})\cdot a]^3+[(l-w_{\mathrm{S}})\cdot a]^3\}\Bigg).\end{aligned} \tag{3.19}$$

$$\mathcal{M}_{--} = \bar{\mathcal{M}}_{++}(a^{\mu}\to -a^{\mu}). \tag{3.20}$$

The expressions and the corresponding basis for simplification of helicity-reversing amplitudes is given later in Sec. 3.5 in Eq. (3.99). Having compactly summarized the key results, we now proceed to the main part of the text.

In Sec. 3.2.1, the framework describing the dynamics of spinning black holes in a worldline EFT framework is presented, along with the Mathison-Papapetrou-Dixon (MPD) equations of motion at cubic order in spin and the expressions for the spin-induced quadrupole and octupole moments. In Sec. 3.2.2, The expression for the skeletonized stress energy tensor of the black hole is presented and the static metric sourced by the unperturbed spinning black hole is derived. Further, it is explained how the comparison of static metric with the linearized Kerr metric (up to a gauge transformation) can be used to fix the unknown coefficients in the spin-induced multipole moments. In Sec. 3.2.3, the properties and representation of the incident plane wave and its amplitude, polarization and frequency are presented. In Sec. 3.3, The computation of the perturbation to black hole's spin, velocity, momentum, spin-induced multipole moments and stress-energy tensor due to the incident plane wave is explained. In Sec. 3.4, the methodology for solving for the scattered wave is presented, as well as the relation between the scattered wave and the scattering amplitudes. In Sec. 3.5, the expressions for the scattering amplitudes are presented. Finally, we conclude in Sec. 3.6.

3.2 Setup

3.2.1 The worldline action for the particle

Let $z^\mu(\tau)$ denote the worldline of the particle, and $dz^\mu(\tau)/d\tau = u^\mu$ denote the the 4-velocity. Here τ is the parameter used to characterize the worldline and not constrained to be the proper time in the action. At the level of equations of motion (eom), one can fix τ to be the proper time by imposing $u^{\mu}u_{\mu} = -1$. To describe the rotation and subsequently the spin of the particle, we attach to the particle a body-fixed tetrad $\epsilon_A{}^{\mu}$ satisfying

$$\epsilon^{A\mu}(\tau)\epsilon^{B}{}_{\mu}(\tau) = \eta^{AB},\ \epsilon^{A}{}_{\mu}(\tau)\epsilon_{A\nu}(\tau) = g_{\mu\nu}(z(\tau)), \tag{3.21}$$

i.e. orthonormality and completeness respectively. The body fixed tetrad spins along with the particle and thus the variation of the tetrad $\epsilon_A{}^{\mu}$ with τ encodes the particle's rotational motion. To see this more clearly, one can also define a global background tetrad $e_a{}^{\mu}(x)$ also satisfying orthonormality ($e^{a\mu}e^{b}{}_{\mu} = \eta^{ab}$) and completeness [$e^{a}{}_{\mu}(x)e_{a\nu}(x) = g_{\mu\nu}(x)$] and relate it to the body-fixed tetrad via a Lorentz transformation,

$$\epsilon_A{}^{\mu} = \Lambda_A{}^{a}e_a{}^{\mu}, \tag{3.22}$$

$$\Lambda_{Aa}\Lambda_B{}^{a} = \eta_{AB}, \quad \Lambda_{Aa}\Lambda^{A}{}_{b} = \eta_{ab}.$$

The Lorentz matrices $\Lambda^{a}{}_{A}$ contain six degrees of freedom, corresponding to 3 boost and 3 rotational degrees of freedom. However, since we want to use the body fixed tetrad to deal with the rotation of the body, we want to eliminate the boost degrees of freedom. In the non relativistic case, this is trivially accomplished by choosing the boost degrees of freedom such that Λ maps the background time vector $e_0{}^{\mu}$ to the 4-velocity of the centre-of-mass of the body. However, there is no unique notion of centre of mass in relativistic case and thus there is an ambiguity in choosing a worldline $z^{\mu}(\tau)$ to represent the motion of the compact body. This can only be resolved by imposing a spin-supplementary condition (SSC), which removes three degrees of freedom. We will do that later, at the level of equations of motion.

For now, we proceed with describing the degrees of freedom that can enter our action. We define the covariant angular velocity as

$$\Omega^{\mu\nu} = \epsilon_A{}^{\mu} \frac{D\epsilon^{A\nu}}{D\tau}. \tag{3.23}$$

In the non relativistic case, in the rest frame of the centre-of-mass of the body, this is equal to the 3-D dual of the angular velocity. ($\Omega^{ij} \sim \epsilon^{ijk} w_k, i, j = 1, 2, 3$). The dynamics of the particle should be independent of the choice of orientation of the body fixed frame tetrad vectors ($\epsilon_A{}^{\mu}$), thus the body fixed tetrad enters the worldline action only through the angular velocity $\Omega^{\mu\nu}$. For a structureless spinning particle (i.e., one without spin-induced multipole moments), the position $z^{\mu}(\tau)$ only enters the action through the metric $g_{\mu\nu}$. We implement the presence of finite-size effects in the action by allowing further dependence on the curvature tensor and its covariant derivativies. Thus, our ansatz for the action is

$$S[z^{\mu}(\tau), \epsilon_A{}^{\mu}(\tau)] = \int d\tau L[u^{\mu}, \Omega^{\mu\nu}, g_{\mu\nu}, R_{\mu\nu\rho\sigma}, \nabla_{\lambda} R_{\mu\nu\rho\sigma}]. \tag{3.24}$$

This ansatz is sufficient to derive the equations of motion (see Ref. [184]). Here, we simply write them down. We first define the quantities

$$\begin{aligned} p_{\mu} &= \frac{\partial L}{\partial u^{\mu}}, \quad S_{\mu\nu} = 2\frac{\partial L}{\partial \Omega^{\mu\nu}}, \quad J_{\mathrm{Q}}^{\mu\nu\rho\sigma} = -6\frac{\partial L}{\partial R^{\mu\nu\rho\sigma}}, \\ J_{\mathrm{O}}^{\lambda\mu\nu\rho\sigma} &= -12\frac{\partial L}{\partial \nabla_{\lambda} R_{\mu\nu\rho\sigma}}. \end{aligned} \tag{3.25}$$

where p_{μ} and $S_{\mu\nu}$ are identified with the physical 4-momentum and spin tensor of the black hole respectively, related to the black hole's angular momentum as $S^{\mu\nu}S_{\mu\nu} = 2J^2$, where J is the magnitude of the intrinsic angular momentum of the spinning black hole. $J_{\mathrm{Q}}^{\mu\nu\rho\sigma}$ and $J_{\mathrm{O}}^{\lambda\mu\nu\rho\sigma}$

are the quadrupole and octupole [5] moments respectively. In this manner, as mentioned before, allowing the action to depend on $R^{\mu\nu\lambda\rho}$ and its covariant derivatives implement finite size effects. We will neglect all higher multipole moments in this work. The equations of motion are then given by

$$\frac{DS^{\mu\nu}}{D\tau} - 2p^{[\mu}u^{\nu]} = N^{\mu\nu} = \frac{4}{3}R^{[\mu}{}_{\lambda\rho\sigma}J_{\rm Q}^{\nu]\lambda\rho\sigma} + \frac{2}{3}\nabla^{\lambda}R^{[\mu}{}_{\tau\rho\sigma}J_{O\lambda}{}^{\nu]\tau\rho\sigma} + \frac{1}{6}\nabla^{[\mu}R_{\lambda\tau\rho\sigma}J_{\rm O}^{\nu]\lambda\tau\rho\sigma}, \tag{3.26}$$

$$\frac{Dp_{\mu}}{D\tau} + \frac{1}{2}R_{\mu\nu\rho\sigma}u^{\nu}S^{\rho\sigma} = F^{\mu} = -\frac{1}{6}J_{\rm Q}^{\lambda\nu\rho\sigma}\nabla_{\mu}R_{\lambda\nu\rho\sigma} - \frac{1}{12}J_{\rm O}^{\tau\lambda\nu\rho\sigma}\nabla_{\mu}\nabla_{\tau}R_{\lambda\nu\rho\sigma}. \tag{3.27}$$

Solving these equations in the presence of an incident wave will reveal the perturbation to the spin and motion of the black hole. However note that these equations are not sufficient to solve for p^{μ} $S^{\mu\nu}$ and u^{μ}. We have 10 equations of motion, but 14 quantities. Thus we need four constraints. One constraint is obtained from the normalization condition $u^{\mu}u_{\mu} = -1$. Three more constraints are obtained from the spin-supplementary condition (SSC), which eliminates the boost degrees of freedom in the Lorentz matrices as mentioned before. In this work, we choose the covariant SSC defined by $S^{\mu\nu}p_{\nu} = 0$. This is equivalent to the requirement that the mass-dipole moment of the body vanish in the zero-momentum frame of the body. The SSC helps fix the relation between p^{μ} and u^{μ} thus completing the set of equations. More generally, one can work with an action that has an additional Gauge invariance associated with changing the SSC and a corresponding shift in the choice of the worldline (see Ref. [190]). However, it is much more convenient to work directly with Covariant SSC at the level of equations of motion (equivalently via a Lagrange multiplier in

[5] Strictly speaking, the quadrupole moment can also couple with the covariant derivative of the Riemann curvature tensor, and thus the octupole moment $J_{\rm O}^{\lambda\mu\nu\rho\sigma}$ as defined in Eq. (3.25) may not be a pure octupole moment. We will however continue to refer to $J_{\rm Q}^{\mu\nu\rho\sigma}$ and $J_{\rm O}^{\lambda\mu\nu\rho\sigma}$ as quadrupolar and octupolar moments respectively.

the action). The two approaches are physically equivalent (see Ref. [331]).

In this work, we only work with spin-induced moments as opposed to tidally-induced moments. Thus, the multipole moments cannot depend on the external curvature or it's derivatives, but only upon the spin of the black hole and the momentum (or 4-velocity). Since we are only interested to third order in spin in this chapter, since the multipole moments start at S^2, we can conveniently switch p^μ with mu^μ in the expression for multipole moments since the p is aligned with u until S^2. The indices of the multipole moments obey the same symmetries as that of the Riemann tensor and its derivatives by definition (see Eq. (3.25)). Finally, the traces of the quadrupole moment are irrelevant, since all dependence in the action on $R^{\mu\nu}$, R (traces of the Riemann tensor) can be removed as their dependence can be absorbed into a redefinition of variables (see Refs. [51, 332]). The same reasoning (along with the Bianchi identity) implies that the traces of octupole moment should be irrelevant as well. Thus, we can modify both $J^{\mu\nu\rho\sigma}$ and $J^{\lambda\mu\nu\rho\sigma}$ upto trace terms to make them simpler.

These considerations along with the covariant SSC constraint ($S^{\mu\nu}p_\nu \approx mS^{\mu\nu}u_\nu + O(S^3) = 0$) were used to fix their form in Ref. [184] as given below,

$$J_{\rm Q}^{\mu\nu\rho\sigma} = \frac{3C_2}{m} u^{[\mu}S^{\nu]\lambda}S_\lambda{}^{[\rho}u^{\sigma]}, \tag{3.28}$$

$$\begin{aligned} J_{\rm O}^{\lambda\mu\nu\rho\sigma} = \frac{C_3}{4m^2}[&\Theta^{\lambda[\mu}u^{\nu]}S^{\rho\sigma} + \Theta^{\lambda[\rho}u^{\sigma]}S^{\mu\nu} - \Theta^{\lambda[\mu}S^{\nu]\rho}u^\sigma \\ &- \Theta^{\lambda[\rho}S^{\sigma][\mu}u^{\nu]} - S^{\lambda[\mu}\Theta^{\nu][\rho}u^{\sigma]} - S^{\lambda[\rho}\Theta^{\sigma][\mu}u^{\nu]}], \end{aligned} \tag{3.29}$$

where $\Theta^{\mu\nu} = S^{\mu\lambda}S^\nu{}_\lambda$, $m = \sqrt{-p^2}$ and the prefactors have been chosen such that $C_2 = C_3 = 1$ for Kerr black holes (see subsection. 3.2.2).

As an explicit check that any additions to the above expressions for multipole moment tensors that are either trace terms or terms that violate the SSC are irrelevant for the final result, we added some additional terms to the multipole tensors with arbitrary coefficients and ensured that the results were in line with expectations. For example, we used the following modified expression for the quadrupole moment tensor,

$$\begin{aligned} J_Q^{\mu\nu\rho\sigma} &= \frac{3C_2}{m} u^{[\mu} S^{\nu]\lambda} S_\lambda{}^{[\rho} u^{\sigma]} + \alpha S^{\alpha\beta} S_{\alpha\beta} g^{\mu\rho} u^\nu u^\sigma \\ &+ \beta S^{\mu\alpha} S^\rho{}_\alpha g^{\nu\sigma} + \sigma S^{\alpha\beta} S_{\alpha\beta} g^{\mu\rho} g^{\nu\sigma} + \frac{3H_2}{4m} S^{\mu\rho} S^{\nu\sigma}, \end{aligned} \tag{3.30}$$

where $\alpha,\ \beta,\ \gamma$ are coefficients next to various non-vanishing traces of the original C_2 term. H_2 is next to a term that is identical to the original C_2 term up to trace-terms and terms violating the covariant SSC constraint. Thus, the final Compton amplitude should be independent of $\alpha,\ \beta,\ \sigma$ and should only depend on the combination $C_2 + H_2$. This is indeed what we found. We added similarly parametrized corrections to the octupolar moment tensor and observed that the final Compton amplitude was appropriately in line with the expectation that we can neglect trace terms and consistently work with the covariant SSC constraint.

3.2.2 Stress energy tensor and the static gravitational field

The particle has a stress energy tensor arising from its mass, spin and the spin-induced multipole moments. The expression for the stress energy tensor can obtained from the action. We first rewrite the action as

$$S[z^\mu(\tau), \epsilon_A{}^\mu(\tau)] = \int d^4x \int d\tau\ L\ \delta^{(4)}(x - z(\tau)), \tag{3.31}$$

and then the stress energy tensor is given simply by

$$T^{\mu\nu} = \frac{1}{\sqrt{-g}}\frac{\delta S}{\delta g_{\mu\nu}}, \tag{3.32}$$

where all dependency (implicit and explicit) of the action on $g_{\mu\nu}$ needs to be taken into account during the variation. This variation was performed in Ref. [184] to obtain Eqs. (3.33).

$$T^{\mu\nu} = T^{\mu\nu}_{\text{pole-dipole}} + T^{\mu\nu}_{\text{quadrupole}} + T^{\mu\nu}_{\text{octupole}}, \tag{3.33a}$$

$$T^{\mu\nu}_{\text{pole-dipole}} = \int d\tau p^{(\mu}u^{\nu)}\frac{\delta^{(4)}(x-z)}{\sqrt{-g}} - \nabla_\rho \int d\tau S^{\rho(\mu}u^{\nu)}\frac{\delta^{(4)}(x-z)}{\sqrt{-g}}, \tag{3.33b}$$

$$T^{\mu\nu}_{\text{quadrupole}} = \int d\tau \frac{1}{3}R^{(\mu}{}_{\lambda\rho\sigma}J_{\text{Q}}^{\nu)\lambda\rho\sigma}\frac{\delta^{(4)}(x-z)}{\sqrt{-g}} - \nabla_\rho\nabla_\sigma \int d\tau \frac{2}{3}J_{\text{Q}}^{\rho(\mu\nu)\sigma}\frac{\delta^{(4)}(x-z)}{\sqrt{-g}}, \tag{3.33c}$$

$$\begin{aligned} T^{\mu\nu}_{\text{octupole}} = &\int d\tau \left[\frac{1}{6}\nabla^\lambda R^{(\mu}{}_{\xi\rho\sigma}J_{\text{O}\lambda}{}^{\nu)\xi\rho\sigma} + \frac{1}{12}\nabla^{(\mu}R_{\xi\tau\rho\sigma}J_{\text{O}}^{\nu)\xi\tau\rho\sigma}\right]\frac{\delta^{(4)}(x-z)}{\sqrt{-g}} \\ &+ \nabla_\rho \int d\tau \left[-\frac{1}{6}R^{(\mu}{}_{\xi\lambda\sigma}J_{\text{O}}^{|\rho|\nu)\xi\lambda\sigma} - \frac{1}{3}R^{(\mu}{}_{\xi\lambda\sigma}J_{\text{O}}^{\nu)\rho\xi\lambda\sigma} + \frac{1}{3}R^{\rho}{}_{\xi\lambda\sigma}J_{\text{O}}^{(\mu\nu)\xi\lambda\sigma}\right]\frac{\delta^{(4)}(x-z)}{\sqrt{-g}} \\ &+ \nabla_\lambda\nabla_\rho\nabla_\sigma \int d\tau \frac{1}{3}J_{\text{O}}^{\sigma\rho(\mu\nu)\lambda}\frac{\delta^{(4)}(x-z)}{\sqrt{-g}}. \end{aligned} \tag{3.33d}$$

Eqs. (3.33) contains the stress energy tensor for a spinning particle with spin-induced quadrupole and octupole moments at all times. We want to compute the static metric in harmonic Gauge ($\partial_\mu h^{\mu\nu} = 0$) sourced by the black hole in flat background space-time. Thus, we disregard the curvature dependent terms in the stress energy tensor and substitute it in the Einstein equation.

$$G^{\mu\nu} = -\frac{8\pi G}{c^4}T^{\mu\nu}|_{\text{in flat space-time}}, \tag{3.34}$$

$$\begin{aligned} T^{\mu\nu} = &\int d\tau [m u^\mu u^\nu - \partial_\rho S^{\rho(\mu}u^{\nu)} \\ &- \partial_\rho\partial_\sigma \frac{2}{3}J_{\text{Q}}^{\rho(\mu\nu)\sigma} + \partial_\lambda\partial_\rho\partial_\sigma\frac{1}{3}J_{\text{O}}^{\sigma\rho(\mu\nu)\lambda}]\delta^{(4)}(x-u\tau), \end{aligned} \tag{3.35}$$

where we have used $z^\mu = u^\mu\tau$ which holds as the motion is uniform and $p^\mu = mu^\mu$, which holds true in flat space even for spinning particles in the covariant SSC. We will only work at linear order in G and thus linearize the Einstein equation by substituting $Gh^{\alpha\beta} = \sqrt{-g}g^{\alpha\beta} - \eta^{\alpha\beta}$ and discarding all $O(G^2)$ terms. This yields the linearized Einstein equation

$$\Box h^{\alpha\beta}_{\text{static}} = \frac{16\pi}{c^2} T^{\alpha\beta}, \tag{3.36}$$

where $\Box = \eta^{\mu\nu}\partial_\mu\partial_\nu$. It is easiest to solve in the rest frame of the unperturbed (by external curvature) black hole since the metric is then static i.e. it does not vary with background time. In this frame, we have $\dot{z}^\mu = u^\mu \equiv (1,0,0,0)$, $S^{0\nu} \equiv 0$ [6] and the equation takes the form

$$\begin{aligned}\delta^{ij}\partial_i\partial_j h^{\mu\nu}_{\text{static}} = \frac{16\pi}{c^2}[m u^\mu u^\nu - S^{j(\mu}u^{\nu)}\partial_j \\ - \frac{2}{3}J_{\text{Q}}^{k(\mu\nu)l}\partial_k\partial_l + \frac{1}{3}J_{\text{O}}^{kj(\mu\nu)i}\partial_i\partial_j\partial_k]\delta^{(3)}(x),\end{aligned} \tag{3.37}$$

where the indices $i, \ j$ run over $1,2,3$ whereas $\mu, \ \nu$ run over $0,1,2,3$. In 3-D Fourier space, the solution to this is simply

$$\begin{aligned}\tilde{h}^{\mu\nu}_{\text{static}} = \frac{-16\pi}{c^2\vec{q}^2}[m u^\mu u^\nu + i q_j S^{j(\mu}u^{\nu)} \\ + q_k q_l \frac{2}{3}J_{\text{Q}}^{k(\mu\nu)l} + i q_i q_j q_k \frac{1}{3}J_{\text{O}}^{kj(\mu\nu)i}],\end{aligned} \tag{3.38}$$

where, $\tilde{h}^{\mu\nu}_{\text{static}} \equiv \int d^3\vec{x}\exp[-i\vec{q}\cdot\vec{x}]h^{\mu\nu}(\vec{x})$ and $i = \sqrt{-1}$. We can Fourier invert Eq. (3.38) to find the expression in position space which gives

$$\begin{aligned}h^{\mu\nu}_{\text{static}} = -\frac{4}{c^2}[m u^\mu u^\nu\left(\frac{1}{r}\right) - S^{j(\mu}u^{\nu)}\partial_j\left(\frac{1}{r}\right) \\ - \frac{2}{3}J_{\text{Q}}^{k(\mu\nu)l}\partial_k\partial_l\left(\frac{1}{r}\right) + \frac{1}{3}J_{\text{O}}^{kj(\mu\nu)i}\partial_i\partial_j\partial_k\left(\frac{1}{r}\right)].\end{aligned} \tag{3.39}$$

Substituting the expressions for the multipole moments, and switching to the use of the mass-normalized Pauli-Lubanski spin vector $a^\mu = -(1/2m)\epsilon^\mu{}_{\nu\rho\sigma}u^\nu S^{\rho\sigma}$ we get

$$h^{\mu\nu}_{\text{st.}} = -u^\mu u^\nu[1 - \frac{C_2}{2}(a\cdot\partial)^2]\frac{4GM}{r}$$

[6] We are using $\equiv$ symbol to denote the expressions in the black hole's rest frame, as defined by its 4-velocity prior to any external disturbance.

$$- u^{(\mu}\epsilon^{\nu)}{}_{\rho\alpha\beta}u^{\rho}a^{\alpha}\partial^{\beta}[1 - \frac{C_3}{3!}(a\cdot\partial)^2]\frac{4GM}{r}$$
$$+ \text{terms containing } (\partial^2(1/r) = \delta^{(3)}(x)), \tag{3.40}$$

where we can neglect the delta function corrections since they only affect the metric at the location of the particle, where the field is anyway ill-defined. These terms essentially come from the non-zero traces of the quadrupole and octupole tensors in Eqs. (3.28, 3.29). As mentioned below Eqs. (3.28, 3.29), they do not contribute to the final result.

Comparing the above metric perturbation (after dropping the delta function terms) to the linearized Kerr metric (see Ref. [128]), we can fix the coefficients to $C_2 = C_3 = 1$ for the case of a black hole. However, we will continue to work with generic C_2 and C_3 for the rest of this work as it may be useful to have Compton amplitudes for generic compact bodies (satisfying parity-symmetry, stationarity and axisymmetry).

3.2.3 Incident wave

To compute the gravitational Compton amplitude, corresponding to the process of gravitational waves scattering off a black hole, we subject the black hole to an incoming gravitational wave. Although a realistic setup would involve a localized wave packet that eventually reaches the black hole and scatters off (and partially absorbed), we treat this situation in the manner of time-independent perturbation theory, and instead consider a monochromatic plane wave that had always been present. The monochromatic plane wave adds an additional metric perturbation ($h^{\mu\nu} = \sqrt{-g}g^{\mu\nu} - \eta^{\mu\nu}$) which we characterize as[7]

$$h_{\mathrm{w}}^{\mu\nu} = \epsilon\, \varepsilon^{\mu}\varepsilon^{\nu}\exp[ik\cdot x],\ \varepsilon^{\mu}\varepsilon_{\mu} = 0,$$

[7]Note that the metric perturbation should be real, and not a complex function but it is fine to work with $\exp[-ik\cdot x]$ as long as we truncate at linear order in ϵ.

$$\varepsilon^{\mu} u_{\mu}^{(0)} = 0, \quad \varepsilon^{\mu} k_{\mu} = 0, \quad k^{\mu} u_{\mu} = -\omega \tag{3.41}$$

where ϵ is the field strength and ε^{μ} is a complex null vector. The conditions ensure that $h^{\mu\nu}_{\text{wave}}$ is spatial, transverse and traceless, in the rest frame of the unperturbed particle and propagates at the speed of light. In this way, only the relevant radiative degrees of freedom are included. There are only two linearly independent vectors we can choose for ε^{μ}, which fixes the helicity/polarization of the incoming gravitational wave. In the initial rest frame of the particle, choosing $\varepsilon^{\mu}_{+2} \equiv (1/\sqrt{2})(0, 1, \pm i, 0)$ fixes the wave in ± 2 helicity respectively. In the rest frame of the particle, we also choose the wave to be propagating along the +ve 'z' direction, $k^{\mu} \equiv \omega(1, 0, 0, 1)$.

Subject to this incident plane linearized gravitational wave, the black hole experiences the following metric tensor.

$$\begin{aligned} g^{\mu\nu} &= \eta^{\mu\nu} + h^{\mu\nu}_{\text{w}}, \quad g_{\mu\nu} = \eta_{\mu\nu} - h_{\text{w},\mu\nu}, \\ \sqrt{-g} &= 1 + O(\epsilon^2). \end{aligned} \tag{3.42}$$

The leading order Christoffel connection and the curvature due to the wave are given by

$$\begin{aligned} \Gamma^{\rho}_{\mu\nu} &= \frac{-i\epsilon}{2}(\varepsilon^{\rho}\varepsilon_{\nu}k_{\mu} + \varepsilon^{\rho}\varepsilon_{\mu}k_{\nu} - k^{\rho}\varepsilon_{\nu}\varepsilon_{\mu}) \exp[ik \cdot x] \\ &= \epsilon \exp[ik \cdot x]\ \Delta\Gamma^{\rho}_{\mu\nu}, \end{aligned} \tag{3.43}$$

$$R^{\mu}{}_{\nu\alpha\beta} = \partial_{\alpha}\Gamma^{\mu}_{\nu\beta} - \partial_{\beta}\Gamma^{\mu}_{\nu\alpha} = \epsilon \exp[ik \cdot x]\ \Delta R^{\mu}{}_{\nu\alpha\beta}, \tag{3.44}$$

where we have defined $\Delta\Gamma^{\rho}_{\mu\nu}$ and $\Delta R^{\mu}{}_{\nu\alpha\beta}$ as the leading order in ϵ corrections to Christoffel connection after removing the factor $\epsilon \exp[ik \cdot x]$ for later convenience. The particle's dynamics (momentum, spin, etc.) are affected by the incident wave, subsequently perturbing stress energy tensor given in Eq. (3.33) in an oscillatory fashion. We study the dynamics of the particle subject to this weak perturbation in the next section.

3.3 Gravitational wave perturbation to the black hole's motion, spin and stress energy tensor

3.3.1 Solving for momentum, spin and 4-velocity

As mentioned earlier in Sec. 3.2.1, the equations of motion in Eqs. (3.26, 3.27) are incomplete. They are completed by the spin supplementary condition (SSC) $S^{\mu\nu}p_\nu = 0$ and the normalization condition $u^\mu u_\mu = -1$. Further, the 4-velocity u^μ appears in the spin equation of motion (see Eq. (3.26)), and thus they cannot be solved independently. We need to identify the relation between p^μ and u^μ to solve for the spin. For that, we act upon the SSC with a $(D/D\tau)$ and get

$$\begin{aligned}
\frac{DS^{\mu\nu}}{D\tau}p_\nu + S^{\mu\nu}\frac{Dp_\nu}{D\tau} = 0 &= 2p^{[\mu}u^{\nu]}p_\nu + N^{\mu\nu}p_\nu \\
&+ S^{\mu\nu}F_\nu - \frac{1}{2}R_{\nu\alpha\rho\sigma}u^\alpha S^{\rho\sigma}S^{\mu\nu}, \qquad (3.45)\\
&= p^\mu(u\cdot p) + m^2u^\mu + N^{\mu\nu}p_\nu + S^{\mu\nu}F_\nu \\
&- \frac{1}{2}R_{\nu\alpha\rho\sigma}u^\alpha S^{\rho\sigma}S^{\mu\nu}, \qquad (3.46)\\
-u^\mu &= p^\mu\frac{u\cdot p}{m^2} + \frac{1}{m^2}(N^{\mu\nu}p_\nu + S^{\mu\nu}F_\nu) \\
&- \frac{1}{2m^2}R_{\nu\alpha\rho\sigma}u^\alpha S^{\rho\sigma}S^{\mu\nu}, \qquad (3.47)
\end{aligned}$$

where F^μ and $N^{\mu\nu}$ were defined earlier in Eqs. (3.26, 3.27). Now, contracting with u_μ on both sides and using $p^\mu = mu^\mu + O(R)$ (i.e., momentum and 4-velocity are parallel in absence of external curvature) and $u^\mu u_\mu = -1$, we get

$$1 = \frac{(u.p)^2}{m^2} + O(R^2). \tag{3.48}$$

Note that the m that appears here is not a fixed parameter, but a time-dependent mass function defined as $p^2 = -m^2$. We can compute the mass function as follows,

$$\begin{aligned}
& -2p \cdot \frac{Dp}{d\tau} = -\frac{Dp^2}{d\tau} = \frac{dm^2}{d\tau} \\
& \approx m \frac{D}{D\tau}\left(\frac{1}{3} J_{\mathrm{Q}}^{\lambda\nu\rho\sigma} R_{\lambda\nu\rho\sigma} + \frac{1}{6} J_{\mathrm{O}}^{\tau\lambda\nu\rho\sigma} \nabla_\tau R_{\lambda\nu\rho\sigma}\right), \\
& \implies m = M + \frac{1}{6} J_{\mathrm{Q}}^{\lambda\nu\rho\sigma} R_{\lambda\nu\rho\sigma} + \frac{1}{12} J_{\mathrm{O}}^{\tau\lambda\nu\rho\sigma} \nabla_\tau R_{\lambda\nu\rho\sigma},
\end{aligned} \tag{3.49}$$

where M is the constant of integration to be interpreted as the constant mass in absence of spin-induced multipole moments and curvature. We also note that m can be treated as a constant up to S^2. In the absence of curvature, or upto second order in spin, we can also write $p^\mu = M u^\mu$.

Now, substituting the expression for force F^μ, and torque $N^{\mu\nu}$, from Eqs. (3.26, 3.27), in Eq. (3.47) and simplifying, we get

$$u^\mu = \frac{p^\mu}{m} + \frac{1}{m^2}(N^{\mu\nu} p_\nu + S^{\mu\nu} F_\nu) \tag{3.50}$$

$$- \frac{1}{2m^2} R_{\nu\alpha\rho\sigma} u^\alpha S^{\rho\sigma} S^{\mu\nu}. \tag{3.51}$$

The commutator $p^{[\mu} u^{\mu]}$ that enters the expression for $DS^{\mu\nu}/D\tau$ (see Eq. (3.26)) can now be computed. Thus, we have now assembled all the expressions needed to solve for the perturbations to the 4-velocity, momentum and spin of the particle due to the incident gravitational wave perturbation.

3.3.2 Correction to momentum, spin and spin-induced multipole moments

The gravitational perturbation is an incident plane wave, that goes as $\exp[ik\cdot x] \approx \exp[-i\omega\tau]$ at the particle's location. Thus, we anticipate that at linear order in wave strength ϵ, the dynamical variables are going to be affected in an oscillatory fashion, and expand them as

$$p^\mu = p^{(0)\mu} + \epsilon \exp[-i\omega\tau]\, \Delta p^\mu, \tag{3.52}$$

$$u^\mu = u^{(0)\mu} + \epsilon \exp[-i\omega\tau]\, \Delta u^\mu, \tag{3.53}$$

$$S^{\mu\nu} = S^{(0)\mu\nu} + \epsilon \exp[-i\omega\tau]\, \Delta S^{\mu\nu}, \tag{3.54}$$

where ϵ is the strength of the wave, and $u^{(0)\mu} \equiv (1,0,0,0)$, $p^{(0)\mu} = mu^{(0)\mu}$, and $S^{(0)\mu\nu}$ are the undisturbed original constant values in the absence of the external perturbation. The correction to the momentum can be easily solved by substituting the expansions in Eqs. (3.52, 3.43, 3.44) into Eq. (3.27) which gives

$$\begin{aligned} -i\omega\Delta p_\mu &= +M\Delta\Gamma^\nu_{\mu\gamma} u^{(0)\gamma} u^{(0)}_\nu - \frac{1}{2} u^\nu S^{\rho\sigma} \Delta R_{\mu\nu\rho\sigma} \\ &- \frac{i}{6} J_{\mathrm{Q}}^{(0)\lambda\nu\rho\sigma} k_\mu \Delta R_{\lambda\nu\rho\sigma} + \frac{1}{12} J_{\mathrm{O}}^{(0)\tau\lambda\nu\rho\sigma} k_\mu k_\tau \Delta R_{\lambda\nu\rho\sigma}, \end{aligned} \tag{3.55}$$

where $\Delta R_{\lambda\nu\rho\sigma}$ is proportional to the curvature perturbation due to the incident wave defined earlier in Eq. (3.44). The connection term arises from expanding the covariant derivative. The correction to the 4-velocity can be easily obtained by taking the variation of either Eq. (3.47) or Eq. (3.50) (here we use the former expression), which gives

$$\begin{aligned} \Delta u^\mu &= \Delta(p^\mu/m) - \frac{1}{i\omega M^2}(M N^{\mu\nu} p^{(0)}_\nu + S^{(0)\mu\nu} F_\nu) \\ &- \frac{1}{2M^2} \Delta R_{\nu\alpha\rho\sigma} u^{(0)\alpha} S^{(0)\rho\sigma} S^{(0)\mu\nu}. \end{aligned} \tag{3.56}$$

Finally, we can solve for the spin by taking the variation on both sides of Eq. (3.26) to get

$$
\begin{aligned}
-i\omega\Delta S^{\mu\nu} = &-2u^{(0)\lambda}S^{(0)\delta[\nu}\Delta\Gamma^{\mu]}_{\lambda\delta} - 2i\omega\Delta(p^{[\mu}u^{\nu]}) \\
&+ \frac{4}{3}\Delta R^{[\mu}{}_{\lambda\rho\sigma}J_{Q}^{(0)\nu]\lambda\rho\sigma} + \frac{2}{3}ik^{\lambda}\Delta R^{[\mu}{}_{\tau\rho\sigma}J_{\mathrm{O}\lambda}^{(0)\nu]\tau\rho\sigma} \\
&+ \frac{ik^{[\mu}}{6}\Delta R_{\lambda\tau\rho\sigma}J_{\mathrm{O}}^{(0)\nu]\lambda\tau\rho\sigma},
\end{aligned}
\tag{3.57}
$$

where $\nabla\Gamma^{\mu}_{\nu\delta}$ is proportional to the Christoffel connection defined in Eq. (3.43). The correction to the worldline can be obtained from the correction to the 4-velocity as

$$
z^{\mu}(\tau) = \int d\tau u^{\mu}(\tau) = \int d\tau[u^{(0)} + \epsilon\exp[-i\omega\tau]\Delta u^{\mu}] \tag{3.58}
$$

$$
= u^{(0)}\tau - \frac{1}{i\omega}\epsilon\exp[-i\omega\tau]\Delta u^{\mu}. \tag{3.59}
$$

The correction to the spin-induced multipole moments can be obtained by substituting into their expressions into Eqs. (3.28, 3.29), the expansions in Eqs. (3.52, 3.53, 3.54) (for p, u, and S) and Eq. (3.42) (as the metric enters the expressions for multipole moments through contractions). The explicit expressions are not very illuminating but it is useful to separate the two ways in which the multipole moments are perturbed. We first rewrite the expressions for the multipole moments in Eqs. (3.28, 3.29) as

$$
J_{\mathrm{Q}}^{\mu\nu\rho\sigma} = \frac{3C_2}{m}u^{[\mu}S^{\nu]\lambda}g_{\lambda\alpha}S^{\alpha[\rho}u^{\sigma]}, \tag{3.60}
$$

$$
\begin{aligned}
J_{\mathrm{O}}^{\lambda\mu\nu\rho\sigma} = &\frac{C_3}{4m^2}[\Theta^{\lambda[\mu}u^{\nu]}S^{\rho\sigma} + \Theta^{\lambda[\rho}u^{\sigma]}S^{\mu\nu} - \Theta^{\lambda[\mu}S^{\nu]\rho}u^{\sigma} \\
&- \Theta^{\lambda[\rho}S^{\sigma][\mu}u^{\nu]} - S^{\lambda[\mu}\Theta^{\nu][\rho}u^{\sigma]} - S^{\lambda[\rho}\Theta^{\sigma][\mu}u^{\nu]}],
\end{aligned}
$$

$$
\Theta^{\mu\nu} = S^{\mu\lambda}S^{\nu\alpha}g_{\lambda\alpha}, \tag{3.61}
$$

and define

$$
\Delta J_{Q,\mathrm{contact}}^{\mu\nu\rho\sigma} = -\frac{\partial J_{Q}^{\mu\nu\rho\sigma}}{\partial g_{\alpha\beta}}\varepsilon_{\alpha}\varepsilon_{\beta}, \tag{3.62}
$$

$$\Delta J^{\mu\nu\rho\sigma}_{Q,\text{matter}} = \frac{\partial J^{\mu\nu\rho\sigma}_Q}{\partial S^{\alpha\beta}}\Delta S^{\alpha\beta} + \frac{\partial J^{\mu\nu\rho\sigma}_Q}{\partial u^\alpha}\Delta u^\alpha, \tag{3.63}$$

$$\Delta J^{\lambda\mu\nu\rho\sigma}_{O,\text{contact}} = -\frac{\partial J^{\lambda\mu\nu\rho\sigma}_O}{\partial g_{\alpha\beta}}\varepsilon_\alpha\varepsilon_\beta, \tag{3.64}$$

$$\Delta J^{\lambda\mu\nu\rho\sigma}_{O,\text{matter}} = \frac{\partial J^{\lambda\mu\nu\rho\sigma}_O}{\partial S^{\alpha\beta}}\Delta S^{\alpha\beta} + \frac{\partial J^{\lambda\mu\nu\rho\sigma}_O}{\partial u^\alpha}\Delta u^\alpha. \tag{3.65}$$

The quantities with subscript ''contact'' are corrections to the multipole moments through the explicit dependence on metric tensor (after removing the factor $\epsilon\exp[-i\omega\tau]$). The quantities with subscript ''matter'' are corrections acquired through the corrections to 4-velocity and spin tensor (variables describing the dynamics of matter). This separation is gauge dependent and purely for our convenience. With these conventions, the expressions for the perturbed spin-induced multipole moments are given by

$$J^{\mu\nu\rho\sigma}_Q = J^{(0)\mu\nu\rho\sigma}_Q + \epsilon\exp[-i\omega\tau](\Delta J^{\mu\nu\rho\sigma}_{Q,\text{contact}} + \Delta J^{\mu\nu\rho\sigma}_{Q,\text{matter}}) \tag{3.66}$$

$$J^{\mu\nu\rho\sigma}_O = J^{(0)\mu\nu\rho\sigma}_O + \epsilon\exp[-i\omega\tau](\Delta J^{\mu\nu\rho\sigma}_{O,\text{contact}} + \Delta J^{\mu\nu\rho\sigma}_{O,\text{matter}}) \tag{3.67}$$

3.3.3 Correction to the stress energy tensor

Finally, equipped with the perturbations to momentum, spin, 4-velocity and the worldline (Eqs. (3.55, 3.56, 3.57, 3.58)), and the spin-induced multipole moments (Eqs. (3.62, 3.65)), we can compute the perturbation to the stress energy tensor of the particle. This is accomplished by simply substituting the expansions in Eqs. (3.53, 3.52, 3.54, 3.66, 3.67) and expressions for curvature tensor and connection coefficients given in Eqs. (3.44, 3.43) into the expression for the stress energy tensor given in Eq. (3.33) and then truncating at leading order in ϵ. We also discard any $O(S^4)$ contributions.

The explicit expressions for the corrections to the stress energy tensor are quite complicated and thus will not be written here, but we find it convenient to separate them into pieces in a manner similar to how we separated the corrections to the multipole moments (see Eqs. (3.62, 3.65)). The stress energy tensor too gains corrections from two sources: (i) from the correction to the dynamical variables describing the particle (matter content, p, u, S, z) and (ii) from the explicit dependence on the curvature tensor (and derivatives), Christoffel connection terms (from the covariant derivatives), and on the metric tensor (that enters the multipole moments) in Eq. (3.33). The latter contributes even if the particle's motion and dynamics are unaffected. Thus, after expanding out the covariant derivatives in the stress energy tensor in Eq. (3.33), we define

$$
\begin{aligned}
\Delta T^{\mu\nu}_{\text{contact}}(x) = {} & \frac{\partial T^{\mu\nu}}{\partial R^{\alpha\beta\gamma\delta}} \Delta R^{\alpha\beta\gamma\delta} \exp[ik\cdot x] + \frac{\partial T^{\mu\nu}}{\partial(\partial_\lambda R^{\alpha\beta\gamma\delta})} \Delta R^{\alpha\beta\gamma\delta} i k_\lambda \exp[ik\cdot x] \\
& - \frac{\partial T^{\mu\nu}}{\partial(\partial_\lambda \partial_\rho R^{\alpha\beta\gamma\delta})} \Delta R^{\alpha\beta\gamma\delta} k_\lambda k_\rho \exp[ik\cdot x] + \frac{\partial T^{\mu\nu}}{\partial \Gamma^{\alpha}_{\beta\gamma}} \Delta\Gamma^{\alpha}_{\beta\gamma} \exp[ik\cdot x] \\
& + \frac{\partial T^{\mu\nu}}{\partial J^{\alpha\beta\gamma\delta}_{Q,\text{contact}}} \Delta J^{\alpha\beta\gamma\delta}_{Q,\text{contact}} \exp[-i\omega\tau] + \frac{\partial T^{\mu\nu}}{\partial J^{\tau\alpha\beta\gamma\delta}_{O,\text{contact}}} \Delta J^{\tau\alpha\beta\gamma\delta}_{O,\text{contact}} \exp[-i\omega\tau]
\end{aligned} \tag{3.68}
$$

$$
\Delta T^{\mu\nu}_{\text{matter}}(x) = \frac{\partial T^{\mu\nu}}{\partial p^\alpha} \Delta p^\alpha \exp[-i\omega\tau] + \frac{\partial T^{\mu\nu}}{\partial S_{\alpha\beta}} \Delta S_{\alpha\beta} \exp[-i\omega\tau] + \frac{\partial T^{\mu\nu}}{\partial u^\alpha} \Delta u^\alpha \exp[-i\omega\tau] \tag{3.69}
$$

$$
+ \frac{\partial T^{\mu\nu}}{\partial z^\alpha} \Delta z^\alpha \exp[-i\omega\tau] + \frac{\partial T^{\mu\nu}}{\partial J^{\alpha\beta\gamma\delta}_{Q,\text{matter}}} \Delta J^{\alpha\beta\gamma\delta}_{Q,\text{matter}} \exp[-i\omega\tau] \tag{3.70}
$$

$$
+ \frac{\partial T^{\mu\nu}}{\partial J^{\tau\alpha\beta\gamma\delta}_{O,\text{matter}}} \Delta J^{\tau\alpha\beta\gamma\delta}_{O,\text{matter}} \exp[-i\omega\tau]
$$

Once again, the idea is to separate the perturbation due to matter/dynamical variables (p, S, u, z) and that due to explicit corrections to metric, connection and Christoffel coefficients. Note that there is no difference between $\epsilon \exp[ik \cdot x]$ and $\epsilon \exp[-i\omega\tau]$ as all terms in the stress energy tensor contain $\delta^{(4)}(x - z(\tau))$ or its derivatives. Thus, as $z^\mu(\tau) = u^\mu \tau + O(\epsilon)$, $\epsilon \exp[ik \cdot x] = \epsilon \exp[-i\omega\tau] + O(\epsilon^2)$.

With these conventions, the perturbed stress energy tensor is thus given by

$$\begin{aligned} T^{\mu\nu}(x) &= T^{(0)\mu\nu} + \epsilon \Delta T^{\mu\nu} \\ &= T^{(0)\mu\nu}(x) + \epsilon \Delta T^{\mu\nu}_{\text{matter}}(x) + \epsilon \Delta T^{\mu\nu}_{\text{contact}}(x), \end{aligned} \tag{3.71}$$

where $T^{(0)\mu\nu}(x)$ is the unperturbed stress energy tensor of the free particle given in Eq. (3.35). The correction terms to the stress energy tensor consist of terms of the form

$$\begin{aligned} \Delta T^{\mu\nu}_{m/c} = \sum \int d\tau A^{\mu\nu KL}_{m/c}[e^\alpha, S^{(0)\alpha\beta}, u^{(0)\alpha}, m] \\ \times \partial_K [\exp[ik \cdot x] \partial_L \delta^{(4)}(x - u^{(0)\mu}\tau)], \end{aligned} \tag{3.72}$$

where we are using the multi-index notation $L = \mu_1\mu_2 ... \mu_l$, to denote a chain of indices. The $\sum$ shows that the net result is a linear combination of such terms (with different l, k and $A^{\mu\nu}$). m/c refers to ‘‘matter/contact’’, both types of corrections have the same form. We now proceed to compute the scattering amplitude by solving the Einstein equation for the scattered wave.

3.4 Computation of the scattering amplitude

3.4.1 Differential equation for the scattered wave

To derive a differential equation governing the scattered wave, we first rewrite the Einstein equation in Landau-Lifshitz form (see Ref. [46]), i.e.,

$$\eta^{\rho\sigma}\partial_\rho\partial_\sigma h^{\alpha\beta} = 16\pi G\tau^{\alpha\beta}, \tag{3.73a}$$

$$\tau^{\alpha\beta} = |g|T^{\alpha\beta} + \frac{1}{16\pi G}\Lambda^{\alpha\beta}, \tag{3.73b}$$

$$\begin{aligned}\Lambda^{\alpha\beta} = {}& -h^{\mu\nu}\partial^2_{\mu\nu}h^{\alpha\beta} + \partial_\mu h^{\alpha\nu}\partial_\nu h^{\beta\mu} \\ & + \frac{1}{2}g^{\alpha\beta}g_{\mu\nu}\partial_\lambda h^{\mu\tau}\partial_\tau h^{\nu\lambda} - g^{\alpha\mu}g_{\nu\tau}\partial_\lambda h^{\beta\tau}\partial_\mu h^{\nu\lambda} \\ & - g^{\beta\mu}g_{\nu\tau}\partial_\lambda h^{\alpha\tau}\partial_\mu h^{\nu\lambda} + g_{\mu\nu}g^{\lambda\tau}\partial_\lambda h^{\alpha\mu}\partial_\tau h^{\beta\nu} \\ & + \frac{1}{8}(2g^{\alpha\mu}g^{\beta\nu} - g^{\alpha\beta}g^{\mu\nu})(2g_{\lambda\tau}g_{\epsilon\pi} - g_{\tau\epsilon}g_{\lambda\pi}) \\ & \times \partial_\mu h^{\lambda\pi}\partial_\nu h^{\tau\epsilon},\end{aligned} \tag{3.73c}$$

$$h^{\mu\nu} = \sqrt{-g}g^{\mu\nu} - \eta^{\mu\nu}. \tag{3.73d}$$

We then substitute

$$\begin{aligned}\sqrt{-g}g^{\mu\nu} - \eta^{\mu\nu} = h^{\mu\nu} = {}& Gh^{\mu\nu}_{\text{static}} + \epsilon\, \varepsilon^\mu\varepsilon^\nu\ \exp[ik\cdot x] \\ & + G\epsilon h^{\mu\nu}_{\text{scatter}},\end{aligned} \tag{3.74}$$

anticipating the scaling of the various metric perturbations. Here, $h^{\mu\nu}_{\text{static}}$ is the static metric correction given in Eq. (3.39), sourced by the compact body and $\propto G$. The second term is the incident wave given earlier in Eq. (3.41) and $\propto \epsilon$. Finally, the last term is the scattered wave which starts at leading order in $G\epsilon$. To isolate the leading order (in G) scattered wave, we take the coefficient of $G\epsilon$ in both sides of Eq. (3.73) after substitution. This gives us

$$\eta^{\rho\sigma}\partial_\rho\partial_\sigma h^{\mu\nu}_{\text{scatter}}(x) = 16\pi\Delta T^{\mu\nu}_{\text{matter}}(x) + 16\pi\Delta T^{\mu\nu}_{\text{contact}}(x) + \Lambda^{(1,1),\mu\nu}(x), \tag{3.75}$$

where $\Delta T^{\mu\nu}_{\text{matter,contact}}$ are the leading order (in ϵ) perturbations to the stress energy tensor of the particle due to the incident plane wave defined in Eqs. (3.68, 3.69). $\Lambda^{(1,1),\mu\nu}$ is the term proportional to $G\epsilon$ when we substitute $\sqrt{-g}g^{\mu\nu} - \eta^{\mu\nu} = Gh^{\mu\nu}_{\text{static}} + \epsilon\, \varepsilon^\mu\varepsilon^\nu \exp(ik\cdot x)$ in $\Lambda^{\mu\nu}$ [8] . This is the contribution from non linear interactions in gravity, between the incident wave and the static curvature. Thus the scattered wave obeys a wave equation with a source term derived from three contributions,a ''matter'' part from $\Delta T^{\mu\nu}_{\text{matter}}$ which comes from the perturbing the dynamics (p^μ, $S^{\mu\nu}$) and kinematics (u^μ, z^μ) of the particle, a ''contact'' part from $\Delta T^{\mu\nu}_{\text{contact}}$ which is due to the explicit dependence of the stress energy tensor on the metric and its derivatives. This also includes the corrections to stress energy tensor arising from the explicit metric dependence in the expression for multipole moments. The last part comes from $\Lambda^{(1,1)\mu\nu}$ is due to the non linear interactions in gravity, wherein the incident wave scatters off the static linearized gravitational field sourced by the particle. We refer to the last contribution as the ''graviton'' part. This separation is primarily for convenience and is gauge dependent, i.e., they mix with each other under coordinate transformations.

3.4.2 Solving for the scattered wave

It is more convenient to solve the differential equation. (3.75) for the scattered wave in Fourier space. Furthermore, we are only interested in the radiative on-shell modes whose mode-

[8]Thus, we are not interested in the non linear interactions proportional to G^2 or ϵ^2 in this work. They do not contribute to the leading order scattered wave which goes as $G\epsilon$.

vectors l^μ satisfy the null condition ($l^2 = 0$). In Fourier space, Eq. (3.75) becomes

$$-l^2 \tilde{h}^{\mu\nu}_{\text{scatter}}(l) = \mathcal{F}[16\pi \Delta T^{\mu\nu}_{\text{matter}}(x) + 16\pi \Delta T^{\mu\nu}_{\text{contact}}(x) + \Lambda^{(1,1),\mu\nu}(x)](l), \tag{3.76}$$

where $\mathcal{F}$ is the Fourier transform operator defined as $\mathcal{F}(f(x)) = \int d^4x \exp[-il\cdot x] f(x)$.

The form of Fourier transform of $\Delta T^{\mu\nu}_{\text{matter/contact}}(x)$ can be evaluated using the fact that both of these corrections consist of terms of the form given in Eq. (3.72) as shown below.

$$\begin{aligned}
\mathcal{F}(\Delta T^{\mu\nu}_{\text{m/c}})(l) &= \int d\tau d^4x \exp[-il\cdot x] \Delta T^{\mu\nu}_{\text{m/c}}(x) \\
&= \sum A^{\mu\nu KL}_{m/c} \int \exp[-il\cdot x] \prod_{i=1}^{k} \partial_{\mu_i} \exp[ik\cdot x] \\
&\quad \times \prod_{j=1}^{l} \partial_{\mu_j} \delta^{(4)}(x - u^{(0)\mu}\tau), && \text{(3.77a)} \\
&= \sum A^{\mu\nu KL}_{m/c} (i)^l \int d\tau d^4x \prod_{i=1}^{k} l_{\mu_i} \exp[-i(l-k)\cdot x] \\
&\quad \times \prod_{j=1}^{l} \partial_{\mu_j} \delta^{(4)}(x - u^{(0)\mu}\tau), && \text{(3.77b)} \\
&= \sum (i)^n A^{\mu\nu KL}_{m/c} \int d\tau d^4x \prod_{i=1}^{k} l_{\mu_i} \prod_{j=1}^{l} (l-k)_{\mu_j} && \text{(3.77c)} \\
&\quad \times \exp[i(l-k)\cdot x] \delta^{(4)}(x - u^{(0)\mu}\tau), \\
&= \sum (i)^n 2\pi A^{\mu\nu KL}_{m/c} l_K (l-k)_L \delta(l\cdot u^{(0)} - k\cdot u^{(0)}) \\
&= \sum (i)^n 2\pi A^{\mu\nu KL}_{m/c} l_K (l-k)_L \delta(l\cdot u^{(0)} + \omega), && \text{(3.77d)}
\end{aligned}$$

where we see that the frequency preserving delta function $\delta(l\cdot u^{(0)} + \omega)$ ensures that the outgoing wave has the same frequency as the incoming wave. We have included the $\sum$ operator to indicate that the net result is a sum of multiple such terms.

The form of the Fourier transform of the ''graviton'' part from $\Lambda^{(1,1)}$ can be evaluated using the fact that it consists of sum of products of the static metric perturbation sourced by the particle given in Eq. (3.38) and the incident wave described in Eq. (3.41). Thus, $\Lambda^{(1,1)}$ is a sum of terms of the form $A_\lambda^{\mu\nu K}\exp[ik\cdot x]\times\partial_K\left(\frac{1}{r}\right)$, in the rest frame of the particle, and we have once again used the multi-index notation $K=\mu_1\mu_2...\mu_k$. We have

$$
\begin{aligned}
\mathcal{F}(\Lambda^{(1,1)}(x)) &\sim \sum\int d^4x A_\lambda^{\mu\nu K}\exp[-il\cdot x][\exp[ik\cdot x] \\
&\times \quad \prod_{i=1}^{k}\partial_{\mu_i}\left(\frac{1}{r}\right)] \qquad (3.78a)\\
&= \sum\int A_\lambda^{\mu\nu K} d^4x\exp[-i(l-k)\cdot x]\prod_{i=1}^{k}\partial_{\mu_i}\left(\frac{1}{r}\right),\\
&= \sum(i)^n\int d^4x A_\lambda^{\mu\nu K}[(l-k)_L]\exp[i(l-k)\cdot x]\left(\frac{1}{r}\right)\\
&= \sum A_\lambda^{\mu\nu K}(-1)^n(l-k)_K\frac{4\pi\delta(l^0-k^0)}{(\vec{l}-\vec{k})^2}, \qquad (3.78b)
\end{aligned}
$$

in the rest frame of the particle, we can make this covariant by writing $l^0=l\cdot u^{(0)\mu}$ (similarly for k) and using $(\vec{l}-\vec{k})^2=(l-k)^2+O(G,\epsilon)$. Thus, we get

$$
\mathcal{F}(\Lambda^{(1,1)}(x))=\sum A_\lambda^{\mu\nu K}(l-k)_K\frac{4\pi\delta(l\cdot u^{(0)}+\omega)}{(l-k)^2}, \tag{3.79}
$$

where once again we find the frequency preserving delta function.

Substituting the Fourier transforms of the matter, contact and graviton parts from Eqs. (3.77, 3.79) into Eq. (3.76), we get the scattered wave in the Fourier domain with the form

$$
\begin{aligned}
\tilde{h}^{\mu\nu}_{\text{scatter}}(l^\mu) &= \frac{-1}{4\pi}\sum\Bigg\{[A_m^{\mu\nu KL}+A_c^{\mu\nu KL}](i)^n l_K(l-k)_L\\
&\quad -2A_\lambda^{\mu\nu K}\frac{(l-k)_K}{(l-k)^2}\Bigg\}\frac{8\pi^2\delta(\omega+l\cdot u^{(0)})}{\omega l^2} \qquad (3.80)\\
&= A^{\mu\nu}((l-k)^\alpha,k^\alpha,\varepsilon^\alpha,S^{(0)\alpha\beta},u^{(0)\alpha},m)\\
&\quad\times\frac{8\pi^2\delta(\omega+l\cdot u^{(0)})}{\omega l^2}, \qquad (3.81)
\end{aligned}
$$

where the amplitude tensor $A^{\mu\nu}$ contains the scattering amplitudes for on-shell modes ($l^2 \to 0$). Finally, we define the amplitudes as

$$\mathcal{M}_{\pm+} = GA^{\mu\nu}\zeta_{-2\nu}\zeta_{-2\nu}, \mathcal{M}_{\pm-} = GA^{\mu\nu}\zeta_{+2\nu}\zeta_{+2\nu}, \tag{3.82}$$

where the first sign is fixed by the polarization of the incoming wave. The form of the wave in Fourier domain in Eq. (3.81) may seem a bit odd. It is much simpler to understand the form of the scattered wave in position space, where it is just a spherical wave with an angle dependent amplitude (in the rest frame of the particle). To see that, we will evaluate the Fourier transform of the scattered wave. We follow the procedure given in Ref. [113]. We first rewrite the differential equation in position space given in Eq. (3.75) as

$$\Box h^{\mu\nu}_{\text{scatter}}(x) = J^{\mu\nu}(x), \tag{3.83}$$

and write the solution as

$$h^{\mu\nu}(x) = \int d^4x'\, G(x-x')J^{\mu\nu}(x'), \tag{3.84}$$

$$G(x) = \frac{1}{2\pi}\theta(x^{(0)})\delta(x^2), \tag{3.85}$$

We now fourier transform only w.r.t. time in rest frame of BH (defined by u^μ) to get,

$$h^{\mu\nu}(\omega,\vec{x}) = \int dt \exp[i\omega t]h^{\mu\nu}(t,\vec{x}) \tag{3.86}$$

$$= \int dt' d^3\vec{x}' \frac{\exp[i\omega(t' + |\vec{x}-\vec{x}'|)]}{4\pi|\vec{x}-\vec{x}'|}J^{\mu\nu}(t',\vec{x}'), \tag{3.87}$$

$$= \frac{1}{4\pi}\int d^3x' \frac{\exp(i\omega|\vec{x}-\vec{x}'|)}{|\vec{x}-\vec{x}'|}J^{\mu\nu}(\omega,\vec{x}'), \tag{3.88}$$

Far away from the black hole, we can approximate $|\vec{x}'| \ll |\vec{x}|$, and thus write $|\vec{x}-\vec{x}'| \approx |\vec{x}| - i\omega\hat{x}\cdot\vec{x}'$

and ignore the correction to $|\vec{x}-\vec{x}'|$ in the denominator to get

$$\begin{aligned} h^{\mu\nu}(\omega,\vec{x}) &\approx \frac{\exp[i\omega|\vec{x}|]}{4\pi|\vec{x}|}\int d^3\vec{x}' \exp[-i\omega\hat{x}\cdot\vec{x}']J^{\mu\nu}(\omega,\vec{x}') \\ &= \frac{\exp[i\omega|\vec{x}|]}{4\pi|\vec{x}|}\tilde{J}^{\mu\nu}(\bar{k}), \end{aligned} \tag{3.89}$$

where $\tilde{J}^{\mu\nu}(\bar{k})$ is the 4-D Fourier transform of $J^{\mu\nu}(x)$ evaluated at $\bar{k}=(\omega,\omega\hat{x})$. Now, substituting the expression for $\tilde{J}^{\mu\nu}(\bar{k})$ from Eq. (3.81), we get

$$h^{\mu\nu}(\omega,\vec{x}) = \frac{2\pi\exp[i\omega|\vec{x}|]}{\omega\vec{\vec{x}}}\delta(\omega+l\cdot u^{(0)})A^{\mu\nu}, \tag{3.90}$$

and finally inverting the fourier transform along time, we get the result

$$h^{\mu\nu}(t,\vec{x}) = \frac{\exp[i\omega(r-t)]}{\omega r}A^{\mu\nu},\ r=|\vec{x}|. \tag{3.91}$$

We find that the $A^{\mu\nu}$ defined in Eq. (3.81) is simply the amplitude of a spherical wave $(\exp[i\omega(r-t)]/(\omega r))$ in position space, centred at the particle. Further, using the definition of the scattering amplitudes as given in Eq. (3.82), we can rewrite the relevant part of the scattered wave (the part that contributes to the amplitudes, $\mathcal{M}_{\pm\pm}$, as)

$$\begin{aligned} h^{\mu\nu}(t,\vec{x})|_{\text{relevant}} = \frac{\exp[i\omega(r-t)]}{G\omega r}(&\mathcal{M}_{\pm+}\zeta^{\mu}_{+2}\zeta^{\nu}_{+2} \\ &+\mathcal{M}_{\pm-}\zeta^{\mu}_{-2}\zeta^{\nu}_{-2}), \end{aligned} \tag{3.92}$$

where the first sign of the amplitudes is fixed by the polarization of the incoming wave.

3.5 Compton amplitudes

Finally, in this section, we project out the amplitude function $A^{\mu\nu}$ onto an appropriate set of polarization vectors and write down the scattering amplitudes to third order in spin, for generic C_2,

C_3. To do that, we first fix the incident wave at a given helicity (± 2), by choosing the polarization vectors appropriately ($\varepsilon^\mu \equiv (1/\sqrt{2})(0,1,\pm i,0)$). Then, the scattering amplitude for measuring an outgoing wave with wave vector l^μ, with +2 (-2) helicity is given by $\mathcal{M}_{\pm+} = GA^{\mu\nu}\zeta_{-2,\mu}\zeta_{-2,\nu}$ [$\mathcal{M}_{\pm-} = GA^{\mu\nu}\zeta_{+2,\mu}\zeta_{+2,\nu}$] respectively, where we are using the notation $\mathcal{M}_{\pm\pm}$ for the scattering amplitudes from a given incoming helicity to a given outgoing helicity. Here, $\zeta^\mu_{\pm 2}$ are the complex null polarization vectors orthogonal to the outgoing wavevector l^μ (just as ε^μ are the complex null polarization vectors for the incoming wave with wavevector k^μ), and they satisfy $\zeta_a \cdot \zeta_b = (1-\delta_{ab})$, $\zeta_a \cdot l = 0$.

With this formula, we obtain the following expressions for the amplitudes for the BH case, i.e., $C_2 = C_3 = 1$.

$$\begin{aligned}\mathcal{M}_{++} &= GM\omega \frac{\cos^4\left(\frac{\theta}{2}\right)}{\sin^2\left(\frac{\theta}{2}\right)} \exp\left[-\frac{s^\mu}{M}(k_\mu + l_\mu)\tan^2\left(\frac{\theta}{2}\right)\right. \\ &\quad \left. - \frac{i}{M\omega\cos^2(\frac{\theta}{2})} S^{\mu\nu}k_\mu l_\nu\right] + O(S^4), \qquad (3.93)\\ \mathcal{M}_{+-} &= GM\omega \sin^2\left(\frac{\theta}{2}\right) \exp\left[\frac{s^\mu}{M}(k_\mu - l_\mu)\right] + O(S^4),\end{aligned}$$

(3.94)

$$\mathcal{M}_{--} = \bar{\mathcal{M}}_{++}(S^{\mu\nu} \to -S^{\mu\nu},\ s^\mu \to -s^\mu), \qquad (3.95)$$

$$\mathcal{M}_{-+} = \bar{\mathcal{M}}_{+-}(S^{\mu\nu} \to -S^{\mu\nu},\ s^\mu \to -s^\mu), \qquad (3.96)$$

where $k^\mu \equiv \omega(1,0,0,1)$ is the incoming wave vector and $l^\mu \equiv \omega(1,\hat{n})$ is the outgoing wave vector, with $\hat{n}$ showing the spatial direction and we are using the notation $\bar{f}$ to denote the complex conjugate of f. θ is the angle between incident wave-vector and outgoing wave-vector and related to the wave-vectors via $-k \cdot l = \omega^2 - \omega^2\cos(\theta) = 2\omega^2\sin^2(\frac{\theta}{2})$. $s^\mu = -(1/2)\epsilon^\mu{}_{\nu\rho\sigma}u^\nu S^{\rho\sigma}$ is the Pauli-Lubanksi spin vector. The spin $S^{\mu\nu} = S^{(0)\mu\nu}$ and 4-velocity $u^\mu = u^{(0)\nu}$ appearing here are the unperturbed zeroth order spin and 4-velocity of the black hole. The above amplitudes, although written as an exponential are only verified by this method to third order in spin, as shown by the $+O(S^4)$ in the above expressions.

It is worth noting that there is mixing of polarization (i.e., non zero $\mathcal{M}_{+-}$ and $\mathcal{M}_{-+}$) even in absence of spin ($S^{\mu\nu} \to 0$). This is a known result and does not happen for electromagnetic wave scattering off black holes (see Ref. [333]). The above amplitudes are also consistent with the scattering cross sections in the spinless case given in Ref. [232]. They are also consistent with Eq. (22) in Ref. [334], valid at first order in spin. Most importantly, these amplitudes are identical to the exponentials in Eqs. (5.14) and and (5.17) in Ref. [233] in which the amplitudes of Ref. [111] were rewritten as an expansion in spin multipoles in spinor-helicity formalism[9] .

The expressions for amplitudes prior to substituting the incoming and outgoing polarization vectors and for generic $C_2,\ C_3$ are given in the appendix. However, after substitution of the polarization vectors, the expressions for the helicity-conserving (-reversing) amplitudes, $\mathcal{M}_{++}$, $\mathcal{M}_{--}$ ($\mathcal{M}_{+-}$, $\mathcal{M}_{-+}$) for generic C_2 and C_3 upto S^3 can be separately simplified by choosing the appropriate basis of vectors for writing them. For helicity-conserving amplitudes ($\mathcal{M}_{++},\ \mathcal{M}_{--}$), we choose the vectors

$$
\begin{aligned}
k^\mu,\ l^\mu,\ w_{\mathrm{S}}^\mu &= \frac{1}{2\omega\cos^2\left(\frac{\theta}{2}\right)}[\omega(k^\mu + l^\mu) - i\epsilon^\mu{}_{\alpha\beta\gamma}k^\alpha l^\beta u^\gamma], \\
a^\mu &= s^\mu/M.
\end{aligned} \tag{3.97}
$$

[9] Note that the conventions regarding helicity states are slightly different in Refs. [111, 233]. They have chosen the momenta of both gravitons to be incoming. In our case, this means $l^\mu \to -l^\mu$ and the helicity of the outgoing wave/graviton is flipped. As a result, their ‘‘same-helicity’’ (++) amplitude is our helicity-reversing (+−) amplitude, and their ‘‘opposite helicity’’ (+−) amplitude is our helicity-conserving (++) amplitude. Also, they have written the results in a spinor helicity formalism.

For helicity-reversing amplitudes ($\mathcal{M}_{+-},\ \mathcal{M}_{-+}$), we choose the vectors

$$
\begin{aligned}
k^\mu,\ l^\mu,\ w_{\mathrm{O}}^\mu &= \frac{-1}{2\omega\sin^2\left(\frac{\theta}{2}\right)}\left[\omega(k^\mu - l^\mu) + i\epsilon^\mu{}_{\alpha\beta\gamma}k^\alpha l^\beta u^\gamma\right],\\
a^\mu &= s^\mu/M.
\end{aligned}
\tag{3.98}
$$

In terms of these vector bases, the amplitudes for generic axisymmetric, parity-preserving, stationary compact bodies to third order in spin can be written as

$$
\begin{aligned}
\mathcal{M}_{++} = GM\omega\frac{\cos^4(\theta/2)}{\sin^2(\theta/2)}\Bigg(&\exp[a\cdot(k+l-2w_{\mathrm{S}})] + \frac{C_2-1}{2}\big[(k-w_{\mathrm{S}})\cdot a\big]^2 + \big[(l-w_{\mathrm{S}})\cdot a\big]^2\\
&+ \frac{C_2-1}{2}\big[(k-w_{\mathrm{S}})\cdot a\big]\big[(l-w_{\mathrm{S}})\cdot a\big]\big[(k+l-2w_{\mathrm{S}})\cdot a\big]\\
&- (C_2-1)^2\big[(k-w_{\mathrm{S}})\cdot a\big]\big[(l-w_{\mathrm{S}})\cdot a\big](w_{\mathrm{S}}\cdot a)\\
&+ \frac{C_3-1}{6}\Big\{\big[(k-w_{\mathrm{S}})\cdot a\big]^3 + \big[(l-w_{\mathrm{S}})\cdot a\big]^3\Big\}\Bigg),
\end{aligned}
\tag{3.99}
$$

$$
\mathcal{M}_{--} = \bar{\mathcal{M}}_{++}(a^\mu \to -a^\mu).
\tag{3.100}
$$

$$
\begin{aligned}
\mathcal{M}_{+-} = GM\omega\sin^2\left(\frac{\theta}{2}\right)\Bigg(&\exp[a\cdot(k-l)] + \frac{(C_2-1)}{2\cos^2(\theta/2)}\Big\{[(k-l)\cdot a]^2\\
&- \sin^2(\theta/2)\Big([(k-w_{\mathrm{O}})\cdot a]^2 + [(l+w_{\mathrm{O}})\cdot a]^2 - 4(w_{\mathrm{O}}\cdot a)^2\Big)\Big\}\\
&+ \frac{(C_2-1)}{2}\tan^2(\theta/2)\big[(k-l-6w_{\mathrm{O}})\cdot a\big]\big[(l-w_{\mathrm{O}})\cdot a\big]\big[(k+w_{\mathrm{O}})\cdot a\big]\\
&+ (C_2-1)^2\tan^2(\theta/2)\big[(w_{\mathrm{O}}+k)\cdot a\big]\big[(w_{\mathrm{O}}-l)\cdot a\big](w_{\mathrm{O}}\cdot a)\\
&+ \frac{(C_3-1)}{6\cos^2(\theta/2)}\Big([(k-l)\cdot a]^3 - \sin^2(\theta/2)\Big\{[(k-w_{\mathrm{O}})\cdot a]^3\\
&- [(l+w_{\mathrm{O}})\cdot a]^3 + 8(w_{\mathrm{O}}\cdot a)^3\Big\}\Big)\Bigg),
\end{aligned}
\tag{3.101}
$$

$$
\mathcal{M}_{-+} = \bar{\mathcal{M}}_{+-}(a^\mu \to -a^\mu).
\tag{3.102}
$$

This remarkable simplification of the Compton amplitudes in the appropriate vector basis can be helpful in the subsequent derivation of two-body dynamics. Unfortunately, the simplification for helicity-reversing amplitudes is not as nice as that of helicity-conserving amplitudes, but thus far we have not been able to find a better basis for simplification of helicity-reversing amplitudes.

Finally, it is also worth noting that the helicity flip ($+ \leftrightarrow -$) at the level of amplitudes can be carried out by reversing the direction of spin and a complex conjugation even in the most general case ($C_2,\ C_3 \neq 1$). This can be understood as a combination of time-reversal and parity transformation, which flips the helicities and the spin but leaves the (incoming and outgoing) momenta invariant. Thus, we have

$$\mathcal{M}(\epsilon_+, \zeta_+, k^\mu, l^\mu, a^\mu) \xrightarrow[\text{Time reversal}]{\text{Parity flip}} \bar{\mathcal{M}}(\epsilon_-, \zeta_-, k^\mu, l^\mu, -a^\mu), \tag{3.103}$$

$$\mathcal{M}(\epsilon_+, \zeta_-, k^\mu, l^\mu, a^\mu) \xrightarrow[\text{Time reversal}]{\text{Parity flip}} \bar{\mathcal{M}}(\epsilon_-, \zeta_+, k^\mu, l^\mu, -a^\mu), \tag{3.104}$$

yielding the previously seen relations $\mathcal{M}_{--} = \bar{\mathcal{M}}_{++}(a^\mu \to -a^\mu)$ and $\mathcal{M}_{+-} = \bar{\mathcal{M}}_{-+}(a^\mu \to -a^\mu)$.

3.6 Conclusion

In this work, we solved for the dynamics of a spinning compact body with spin-induced multipole moments subject to an external linearized gravitational plane wave, and solved for the scattered wave produced in response, to third order in spin of the body, at linear order in G. The compact body was described with an effective worldline formalism, where it was treated as a spinning point particle with non-minimal couplings of higher multipole moments to spacetime curvature. The spin-induced (electric) quadrupole and (magnetic) octupole moments of the particle could be controlled by varying two parameters C_2 and C_3, respectively, normalized so that $C_2 = C_3 = 1$ corresponds to the black hole case. We extracted the scattering amplitude for the scattering of gravitational waves off compact spinning bodies for generic C_2 and C_3, again up to order GS^3.

For the special case $C_2 = C_3 = 1$ corresponding to a black hole, we verified that our classical scattering amplitude matches the classical limit of the Compton amplitude originating from Ref. [111], in particular using its form in terms of the heavy-particle EFT variables from Ref. [233]. Assuming that the effective worldline theory is sufficiently general, and given that its only free parameters (contributing through order GS^3), C_2 and C_3, are fixed by matching to the linearized Kerr solution, this provides further evidence that the Compton amplitude from Refs. [111, 233] is indeed suitable for describing the dynamics of a black hole, at least to third order in spin. We note that a BCFW construction of Compton amplitudes for generic C_2 and C_3 (and so forth) has been given in Appendix B of Ref. [170]; the result for the helicity conserving (‘‘opposite helicity’’) amplitude notably differs from our result (3.99) by the absence of terms quadratic in C_2 (‘‘C_{S^2}’’) at third order in spin. We have verified that our Compton amplitudes for generic C_2 and C_3 (for both helicity configurations) are in agreement with the classical limits of the Compton amplitudes derived by the authors of Ref. [322] for use in their computation of the 2-to-2 scattering amplitudes, for a certain choice of their extra free parameter (specifically when their parameter H_2 equals 1).

An important direction for future work is to extend our results to fourth and fifth orders in spin, where the worldline theory will encounter additional Wilson coefficients multiplying couplings quadratic in the curvature. Input from the worldline theory may help to clarify issues such as the counting and interpretation of additional free parameters at higher orders in spin, in the comparison with effective quantum theories, and may facilitate the comparison of both of those approaches with results from black hole perturbation theory. Beyond the (fundamentally conservative) spin-induced multipole couplings of the type considered here, it will also be necessary, at sufficiently high orders in the long-wavelength scattering expansion, to include absorptive effects (e.g., absorption of mass-energy and angular momentum down a black hole horizon), as have been treated in an effective worldline theory (e.g.) in Ref. [61] and using black hole perturbation theory (e.g.) in Ref. [60].

acknowledgements

We thank Rafael Aoude, Fabian Bautista, Zvi Bern, Alessandra Buonanno, Donal O'Connell, Alfredo Guevara, Kays Haddad, Andreas Helset, Yu-tin Haung, Ted Jacobson, Gustav Jakobsen, Henrik Johansson, Chris Kavanagh, Jung-Wook Kim, Dimitrios Kosmopoulos, Andrés Luna, Gustav Mogull, Paolo Pichini, Jan Plefka, Radu Roiban, Jan Steinhoff and Fei Teng for helpful discussions regarding this work and/or comments on earlier versions of the paper in which this chapter has been published. We thank Gustav Mogull for computing and sharing with us the classical Compton amplitude computed via worldline QFT methods up to second order in spin for comparison with our results. We thank Fei Teng for simplifying and sharing the Compton amplitudes used in Ref. [322] for comparison with our results. We are grateful to the Kavli Institute for Theoretical Physics for their hospitality at the High-Precision Gravitational Waves Program where much of this work was completed. This research was supported in part by the National Science Foundation under Grant No. NSF PHY-1748958.

Chapter 4: Modeling horizon absorption in spinning binary black holes using effective worldline theory

Authors[1]: *M. V. S. Saketh, Jan Steinhoff, Justin Vines, Alessandra Buonanno*

Abstract: The study of scattering encounters continues to provide new insights into the general relativistic two-body problem. The local-in-time conservative dynamics of an aligned-spin binary, for both unbound and bound orbits, is fully encoded in the gauge-invariant scattering-angle function, which is most naturally expressed in a post-Minkowskian (PM) expansion, and which exhibits a remarkably simple dependence on the masses of the two bodies (in terms of appropriate geometric variables). This dependence links the PM and small-mass-ratio approximations, allowing gravitational self-force results to determine new post-Newtonian (PN) information to all orders in the mass ratio. In this chapter, we exploit this interplay between relativistic scattering and self-force theory to obtain the third-subleading (4.5PN) spin-orbit dynamics for generic spins, and the third-subleading (5PN) spin$_1$-spin$_2$ dynamics for aligned spins. We further implement these novel PN results in an effective-one-body framework, and demonstrate the improvement in accuracy by comparing against numerical-relativity simulations.

[1]Originally published as Phys. Rev. D **109**, 064058 (2024)

4.1 Introduction and summary

With ninety gravitational-wave (GW) events [335] from compact-binary coalescences observed by the LIGO-Virgo detectors [19, 39], GW astronomy has become an important instrument to explore our universe. While the worldwide network of detectors has recently included the KAGRA detector [21], and will continue to improve in sensitivity in the future [282, 336–339], the accuracy of waveform models needs to keep in step with the increasing sensitivity in order to avoid systematic errors in parameter estimation [340]. Predictions for GWs from the late stage of a binary inspiral and merger require full numerical solutions of the strong-field dynamics. Here we focus instead on the early inspiral, applying the post-Newtonian (PN, weak-field and slow motion) approximation, and calculate horizon-absorption effects on the GW phase from black hole (BH) binaries up to 4PN order.

The presence of the horizon leads to some interesting effects in BH binaries. In particular, GW energy can fall into (or out of, in the case of superradiance) the horizon, leading to a change in mass and magnitude of spin angular momentum[2] of the BHs in a binary. The change in these parameters is consistent with the second law of BH dynamics and always leads to an increase (or no change) in the area of the horizon [341]. A change in mass and spin can also happen for other compact bodies like neutron stars through tidal heating (see, e.g., Refs. [196, 342]). Future GW detectors may be sensitive to these dissipative effects, which can then provide a probe for the nature of BHs (e.g., the presence of a horizon) [343–346]. Horizon-absorption effects have been included in some effective-one-body (EOB) waveform models [347–349], but not yet in the state-of-the-art models used for LIGO-Virgo-KAGRA (LVK) data analysis.

[2] We will refer to the magnitude of spin angular momentum simply as ‘‘spin” in the rest of this work.

For spinning BHs, the leading-order flux into the horizon starts at 2.5PN with respect to the leading quadrupolar flux (of the binary) to infinity [58, 60–65]. Through the flux-phase relation, this means that the GW phase is also affected at 2.5PN order (see, e.g., Ref. [350, 351]). For nonspinning BHs, the same effect starts at 4PN [58, 62]. In the test-body limit, when there is a tiny BH orbiting a much larger spinning BH, one can solve for the horizon energy flux of the large BH via BH perturbation-theory (BHPT), which consists in this case of solving the Teukolsky equation with incoming boundary conditions at the horizon, and outgoing boundary conditions at infinity, as was done, e.g., in Ref. [58]. However, it is nontrivial to extend this calculation to generic mass ratios. This was accomplished at leading 2.5PN order in Ref. [59], for the case of aligned-spin circular orbits via arguments relating the spin-aligned–quasi-circular inspiral to the case when two spinning BHs are held at rest with respect to each other. The result was extended further to 1.5PN orders (to absolute 4PN order) in Refs. [60, 198] where BHPT was used along with a matching between the near zone and the orbital zone for BHs in a binary to derive the energy and angular-momentum fluxes across their horizons for generic mass ratios. However, for spinning BHs, the result was inconsistent with that obtained in the test-body limit in Ref. [58]. This discrepancy is yet to be settled in the literature and thus the correct expression for mass and angular-momentum evolution for generic mass ratios at 4PN is yet to be clarified. Settling this discrepancy is crucial to derive the correct horizon-flux contribution to the waveform phase at 4PN order, and it is one of the goals of this chapter.

The problem of computing the horizon fluxes for spinning BHs was tackled recently in an effective field theory (EFT) framework in Ref. [61] (see also, e.g., Refs. [197, 238–241, 352] for previous work in that direction and Refs. [51, 54, 183, 249, 353, 354] for the EFT formalism including spin and tidal effects), where the BH was treated as a point particle with tidally induced quadrupole moments. Then in an ‘‘in-in” formalism, a parametrized expression for the absorption cross section for a graviton being absorbed by the effective particle was computed, whose parameters were fixed by a matching calculation against the classical absorption cross section for gravitational plane waves by a spinning BH(from Ref. [242]). This in turn fixes the correlation function for the quadrupole moment, which was subsequently used to derive the dissipative part of the Green's function relating the tidal fields to the quadrupole moments. Once the tidal response was fixed in this way, the EFT was applied to compute the evolution equation for mass and spin by suitably defining them in the worldline theory from the effective action. This calculation was carried out at leading (2.5PN) order and the result was consistent with earlier works in Refs. [62–65].

In this work, we similarly develop an effective worldline framework to model the dissipative dynamics of spinning BHs, but extend it by 1.5PN orders. We follow Ref. [61] in treating the spinning BH as a point particle with tidally induced moments, but work in a purely classical framework. We identify and fix the dissipative part of the tidal response by comparing results from the scattering of GWs off the particle/BH between the effective and real theories (see also, e.g., Refs. [2, 135, 176, 245] for other works involving comparison of such a scattering process between real and effective theories). We then derive expressions for the evolution of mass and spin up to 1.5PN order (relative to the leading order). We find that the resulting expressions are consistent with earlier results obtained in the test-body limit in Ref. [58], thus weighing in on one side of the discrepancy discussed above. We then derive the 4PN contribution to the waveform phase due to the horizon fluxes, while consistently including the effects due to the changing parameters (mass and spin) of the members of the binary (extending an earlier 3.5PN result [351]).

To accomplish this, we write down in Sec. 4.2 an effective worldline action for a spinning particle with (gravito-electric and -magnetic) quadrupole and octupole moments, coupled accordingly to quadrupolar and octupolar (gravito-electric and -magnetic) tidal fields in the action. We then motivate ansätze relating the tidal fields linearly to the multipole moments. In the absence of spin, spherical symmetry and parity symmetry imply that a given tidal field only induces the corresponding multipole moment (e.g., the electric-type quadrupole $Q_{\mathcal{E}}^{\mu\nu}$ is induced only by the electric-type tidal field $\mathcal{E}^{\mu\nu}$). However, in the presence of spin, it is possible for octupolar tidal fields to induce quadrupolar tidal fields and vice-versa, while still preserving parity. This is an important property of the ansätze and turns out to be crucial for correctly modelling the dissipative dynamics of spinning BHs. In particular, the Teukolsky equation which governs the curvature perturbations in a Kerr background is separable in spheroidal harmonics with spin weight -2. This feature can be modelled in the effective theory only by including the interaction between quadrupole (octupole) fields and octupole (quadrupole) moments.

Once we motivate general ansätze for the multipole moments, we further specialize them by using the fact that the response tensors (relating the tidal fields to the multipole moments) can only have a nontrivial tensor structure due to the spin of the particle, which allows us to decompose them into a set of basis tensors with undetermined coefficients to be fixed. For this purpose, in Sec. 4.3, we place the effective particle at the origin and scatter GWs off of it, and then use the Einstein equation and the ansätze to solve for the scattered wave and then subsequently to compute the degree of absorption for the spheroidal $l = 2,\ 3$ modes of the wave to $\mathcal{O}(\epsilon^7)$, where $\epsilon = GM\omega$ with M being the BH mass and ω the GW angular frequency. Comparing the degree of absorption obtained by solving the scattering problem in the effective theory with that obtained by solving the same problem in the actual setup of GWs scattering off a spinning BH, using BHPT as governed by the Teukolsky equation [212], finally fixes the response coefficients that contribute to dissipation.

The response coefficients are notably nonpolynomial in the BH spin.

Once the (dissipative part of the) tidal response is fixed, we proceed to compute expressions for the evolution of mass and spin in the effective theory in Sec. 4.4. We first derive general evolution equations for mass m, and spin J, in terms of the tidal fields and multipole moments from the equations of motion obtained from the action, and then derive the explicit expressions for the special case parallel-spin–quasi-circular[3] binaries to relative 1.5PN order. We show its consistency (or lack thereof) with earlier results and then proceed to compute the effect on the waveform phase up to 4PN with respect to the leading-order quadrupolar flux of the system to infinity in Sec. 4.5. With that, we conclude our work in this chapter in Sec. 4.6.

We work with the (-,+,+,+) metric signature convention. We use greek symbols μ, ν, ..., for space-time indices ranging over $\{0, 1, 2, 3\}$ with 0 being used for the time-component, and latin symbols i, j, ..., for spatial indices ranging over $\{1, 2, 3\}$. We use $\epsilon_{0123} = \epsilon_{123} = 1$ as the convention for Levi-Civita tensor(s). We also use the multi-index notation where $\mu_L = \mu_1\mu_2 \dots \mu_l$ for conveniently representing a string of indices where useful and use the notation $\langle\mu_1\mu_2 ...\rangle$ to represent symmetrization and trace removal of a tensor over the contained indices. We set the speed of light $c = 1$ in the work. However, we keep the dependence on the Newton constant G explicit for most of the work, and mention explicitly when setting $G = 1$ as well to facilitate comparison with earlier works.

[3]In this work, by parallel-spin–quasi-circular binaries, we always mean BHs in a binary with their spin vectors parallel to each other and to the orbital angular momentum.

4.2 Setup in effective worldline theory

In this section, we discuss the effective worldline theory for the point particle used to model the spinning compact object. We first briefly outline the particle's multipole structure and how it can be used to model absorption. We then proceed to set up an effective action for the particle including the multipole moments, and then write down general ansätze with undetermined coefficients for the multipole moments as a linear function of the tidal fields consistent with axisymmetry and parity symmetry.

We model the horizon flux of the spinning BH in effective worldline theory as tidal heating of a composite paricle with several tidally induced multipole moments, whose degrees of freedom are contained in symmetric trace-free (STF) tensors $Q^{\mu_L}_{\mathcal{E},n}$, $Q^{\mu_L}_{\mathcal{B},n}$, $l \geq 2, n \geq 0$, satisfying $Q^{\mu_L} u_{\mu_i} = 0,\ 1 \leq i \leq l$. In the effective action, we choose the multipole moments to couple with the tidal fields

$$\begin{aligned}
\mathcal{E}_{\mu_L} &= \nabla_{\langle \mu_{L-2}} R_{\mu_{l-1}|\alpha|\mu_l\rangle\beta} u^\alpha u^\beta, \\
\mathcal{B}_{\mu_L} &= \frac{1}{2}\nabla_{\langle \mu_{L-2}} \epsilon_{|\gamma|\mu_{l-1}}{}^{\alpha\beta} R_{|\alpha\beta|\mu_l\rangle\delta} u^\gamma u^\delta,\ l \geq 2,
\end{aligned} \tag{4.1}$$

where u^μ is the four-velocity and we are using the notation $\langle \mu_L \rangle$ to denote symmetrization and trace-removal. In the effective action, we choose the electric '$\mathcal{E}$' (magnetic '$\mathcal{B}$') multipole moments to couple with electric (magnetic) tidal fields in accordance with the number of indices and parity as $S_{\text{tidal}} = (1/2)\sum_{l=2}^{\infty}\sum_n [Q^{\mu_L}_{\mathcal{E},n}\mathcal{E}_{\mu_L} + (\mathcal{E} \leftrightarrow \mathcal{B})]]$. We will only need to consider their coupling and induction by quadrupolar ($l = 2$) and octupolar ($l = 3$) tidal fields to the PN order relevant in this work. In addition, the various multipole moments are dynamical and are coupled to each other via an internal action S_{int} such that the energy tidally pumped into these modes may progressively escape into higher order/smaller length-scale multipoles effectively leading to dissipation. If there is a sufficiently large number of degrees of freedom, and if they are appropriately coupled, the recurrence time becomes essentially infinite and the system becomes effectively irreversible. We will not however explicitly model the process of dissipation and only use that as a justification to write down ansätze for the multipole moments in terms of the tidal fields that allows for dissipation. Note that at the end of the day, we only intend to mimic the BH's horizon absorption (as tidal heating) and acquire an effective model that may be used to study the associated dynamics. Whether there is any physical relation to the real microscopic degrees of freedom of a BH and this model is unknown and not directly relevant to this work. Our approach of incorporating tidal moments in the action is slightly different at a superficial level from the prescription used in Ref. [61] where instead a single quadrupole moment was used but allowed to be a function of several unknown microscopic degrees of freedom denoted by X. Practically however, there is not much of a difference.

In the absence of spin, an unperturbed BH is spherically symmetric, and the linear tides can only be induced by the fields to which they directly couple to in the action, e.g., as[4] ,

$$\sum_{n=0}^{\infty} Q^{\mu_L}_{\mathcal{E},n} = M \sum_{m=0}^{\infty} \lambda^{l}_{\mathcal{E},m} (GM)^{2+l+m} \frac{D^m}{D\tau^m} \mathcal{E}^{\mu_L},$$
$$\text{and similarly for } (\mathcal{E} \leftrightarrow \mathcal{B}) \tag{4.2}$$

where parity symmetry[5] prevents the magnetic (electric) tidal field for the same l from inducing the electric (magnetic) multipole moment, and spherical symmetry means there is no special tensor

[4]We will only ever need an ansatz for the sum of all multipole moments for a given l and parity ($\mathcal{E}/\mathcal{B}$) for computing the evolution equations for physical quantities such as total spin angular momentum or total linear momentum. We however allow for the presence of multiple multipole moments with the same l and parity labels $\mathcal{E}/\mathcal{B}$ for generality.

[5]In general, $\mathcal{E}_{\mu_L}$ (or $\mathcal{B}_{\mu_L}$) transforms under parity as $(-1)^l$ or $[(-1)^{(l+1)}]$. The multipole moments with which they explicitly couple in the action cannot be induced by tidal fields with a different transformation under parity if the particle is to be parity-preserving.

with which to contract the higher multipolar order tidal fields (or multiply the lower multipolar order ones) to contribute to the ansatz for $\sum_n Q^{\mu_L}_{\mathcal{E}(\mathcal{B}),n}$. Spherical symmetry is also the reason there is no mixing of indices in the response tensor. We can also identify from Eq. (4.2) which response coefficients are conservative and which are dissipative simply by looking at the transformation under time-reversal. The coefficients next to odd powers of time derivatives are dissipative and the ones next to even powers are conservative. This is less trivial for a spinning particle which allows for mixing of multipolar orders with the help of the spin tensor and Pauli-Lubanski spin vector.

However, a spinning BH can have induction between different multipolar orders, since the spin-tensor $S^{\mu\nu}$ defined in Eq. (4.6), or Pauli-Lubanski spin vector $s^\mu = -[1/(2m)]\epsilon^\mu{}_{\nu\rho\sigma}p^\nu S^{\rho\sigma}$, can appear in above relations (4.2). We still need to keep parity considerations in mind as spinning BHs obey parity symmetry. Crucially, for our purposes, we need to include the induction of octupole moments by quadrupolar fields and vice-versa to capture the tidal heating of the spinning BHs at relative 1.5PN order. We will write down a general ansatz for multipole moments in the spinning case in Subsec. 4.2.2. But first, we will write down in Subsec. 4.2.1 an effective action for a particle with spin and aforementioned multipole moments and derive the equations of motion for spin and four-momentum, and the effective stress-energy tensor, following closely the prescription in Ref. [184] but with suitable modifications to allow for the presence of tidally induced moments. We will then write down general parametrized ansätze for the multipole moments in terms of the tidal fields constrained by the symmetries of the particle (axisymmetry and parity invariance), which is somewhat similar to the approach used in Ref. [61] to fix the form of the correlation function of the quadrupole moments.

4.2.1 Action and equations of motion for momentum and spin angular momentum

To get the equations of motion, we will follow a direct extension of the simple procedure given in Ref. [184] for deriving the equations of motion from an implicit action, while including the aforementioned tidal moments. We include the spinning degrees of freedom by attaching to the particle a body-fixed tetrad ${\epsilon_A}^\mu$ satisfying orthonormality and completeness. The angular velocity of the particle is then measured with the quantity $\Omega^{\mu\nu} = {\epsilon_A}^\mu \frac{D\epsilon^{A\nu}}{D\tau}$. It is sufficient in this work just to include the spin at leading order and ignore spin-induced multipole moments. The worldline of the particle is denoted by $z^\mu(\tau)$, where τ is the proper time. We can then write down the action implicitly as

$$S = \int d\tau L(u^\mu, \Omega^{\mu\nu}, g_{\mu\nu}, Q^{\mu_L}_{\mathcal{E},n}, Q^{\mu_L}_{\mathcal{B},n}, \dot{Q}^{\mu_L}_{\mathcal{E},n}, \dot{Q}^{\mu_L}_{\mathcal{B},n},$$
$$R_{\mu\nu\rho\sigma}, \nabla_\lambda R_{\mu\nu\rho\sigma}), \tag{4.3}$$

where $u^\mu = dz^\mu/d\tau$ and we are using the notation $\dot{a} = Da/D\tau$. Additionally, we have assumed that only the first time derivative of each individual multipole moment needs to be included in the action. We have also restricted ourselves to including just the quadrupolar ($l = 2$) and octupolar ($l = 3$) tidal fields in the action explicitly as mentioned before. The coupling of tidal fields with higher order multipole moments is irrelevant to the PN order of interest in this work as we will see later. We do however keep all the higher multipolar order moments since tidal heating requires the presence of several additional degrees of freedom into which the system may pump energy. Additionally, as mentioned before, we choose the multipole moments to couple directly with the corresponding tidal fields (in accordance with number of indices and parity label) by imposing

$$\frac{\partial L}{\partial \mathcal{E}_{\mu_L}} = \frac{1}{2}\sum_n Q^{\mu_L}_{\mathcal{E},n}, \ \frac{\partial L}{\partial \mathcal{B}_{\mu_L}} = \frac{1}{2}\sum_n Q^{\mu_L}_{\mathcal{B},n}, \quad l = 2, \ 3 \tag{4.4}$$

which is equivalent to having in the action a linear combination of the form

$$S_{\text{tidal}} = \sum_{l=2}^{3}\sum_n \int d\tau \frac{1}{2}\mathcal{E}_{\mu_L} Q^{\mu_L}_{\mathcal{E},n} + (\mathcal{E} \leftrightarrow \mathcal{B}),$$

in the total action. We can derive the equations of motion for momentum and spin angular momentum directly from this implicit action. First, we consider a general variation

$$\begin{aligned}\delta L =& p_\mu \delta u^\mu + \frac{1}{2}S^{\text{rot}}_{\mu\nu}\delta\Omega^{\mu\nu} + \frac{\partial L}{\partial g_{\mu\nu}}\delta g_{\mu\nu} - \frac{1}{6}J^{\mu\nu\rho\sigma}\delta R_{\mu\nu\rho\sigma} - \frac{1}{12}J^{\lambda\mu\nu\rho\sigma}\delta\nabla_\lambda R_{\mu\nu\rho\sigma} \\ &+ \sum_{l=2}^{\infty}\sum_{n=0}^{\infty}\left(\frac{\partial L}{\partial Q^{\mu_L}_{\mathcal{E},n}}\delta Q^{\mu_L}_{\mathcal{E},n} + \frac{\partial L}{\partial \dot{Q}^{\mu_L}_{\mathcal{E},n}}\delta \dot{Q}^{\mu_L}_{\mathcal{E},n} + \frac{\partial L}{\partial Q^{\mu_L}_{\mathcal{B},n}}\delta Q^{\mu_L}_{\mathcal{B},n} + \frac{\partial L}{\partial \dot{Q}^{\mu_L}_{\mathcal{B},n}}\delta \dot{Q}^{\mu_L}_{\mathcal{B},n}\right),\end{aligned} \tag{4.5}$$

where we have defined

$$p_\mu = (\partial L/\partial u^\mu)|_{\Omega^{\mu\nu}}, \ S^{\text{rot}}_{\mu\nu} = \frac{1}{2}(\partial L/\partial\Omega^{\mu\nu}), \tag{4.6}$$

$$J^{\mu\nu\rho\sigma} = -6\frac{\partial L}{\partial R_{\mu\nu\rho\sigma}} = -3\sum_{n=0}^{\infty} u^{[\mu}Q^{\nu][\rho}_{\mathcal{E},n}u^{\sigma]} + \frac{3}{2}\sum_{n=0}^{\infty} Q^{\alpha\langle\rho}_{\mathcal{B},n}\epsilon_{\beta\alpha}{}^{\mu\nu}u^{|\beta|}u^{\sigma\rangle_R}, \tag{4.7}$$

$$J^{\lambda\mu\nu\rho\sigma} = -12\frac{\partial L}{\partial \nabla_\lambda R_{\mu\nu\rho\sigma}} = -6\sum_{n=0}^{\infty} u^{\langle\mu}Q^{\nu\rho\lambda}_{\mathcal{E},n}u^{\sigma\rangle_{\nabla R}} + 3\sum_{n=0}^{\infty} Q^{\alpha\langle\rho\lambda}_{\mathcal{B},n}\epsilon_{\beta\alpha}{}^{\mu\nu}u^{|\beta|}u^{\sigma\rangle_{\nabla R}}, \tag{4.8}$$

where the expressions for the J's follow trivially from Eq. (4.4) and we are using $\langle abcd\rangle_R$ ($\langle abcd\rangle_{\nabla R}$) to represent the symmetrization of indices according to the symmetries of the Riemann tensor (covariant derivative of the Riemann tensor) respectively. Now, if we consider a variation of the form $x^\mu \to x^\mu + \xi^\mu$ corresponding to an infinitesimal change of coordinates, we obtain the constraint

$$\begin{aligned}2\frac{\partial L}{\partial g_{\mu\nu}} =& p^\mu u^\nu + S^{\mu\rho}_{\text{rot}}\Omega^\nu{}_\rho + \frac{2}{3}R^\mu{}_{\lambda\rho\sigma}J^{\nu\lambda\rho\sigma} + \frac{1}{3}J^{\lambda\nu\tau\rho\sigma}\nabla_\lambda R^\mu{}_{\tau\rho\sigma} + \frac{1}{12}J^{\nu\lambda\tau\rho\sigma}\nabla^\mu R_{\lambda\tau\rho\sigma} \\ &+ \sum_{l=2}^{\infty}\frac{l}{2}\sum_{n=0}^{\infty}[\mathcal{M}^{\mu\ \mu_{L-1}}_{\mathcal{E},n}Q^{\mathcal{E},n\ \ \nu}_{\mu_{L-1}} + P^{\mu\ \mu_{L-1}}_{\mathcal{E},n}\dot{Q}^{\mathcal{E},n\ \ \nu}_{\mu_{L-1}} + (\mathcal{E}\leftrightarrow\mathcal{B})],\end{aligned} \tag{4.9}$$

where we have defined $\mathcal{M}^{\mu_L}_{\mathcal{E}(\mathcal{B}),n} = (\partial L/\partial Q^{\mathcal{E}(\mathcal{B}),n}_{\mu_L})$, and $P^{\mu_L}_{\mathcal{E}(\mathcal{B}),n} = (\partial L/\partial \dot{Q}^{\mathcal{E}(\mathcal{B}),n}_{\mu_L})$. Note that the equations of motion for the multipole moments obtained upon variation of the action with respect to them $(\partial L/\partial Q^{\mu_L}_{\mathcal{E}(\mathcal{B}),n}) - (D/D\tau)(\partial L/\partial \dot{Q}^{\mu_L}_{\mathcal{E}(\mathcal{B}),n}) = 0$, imply that $\mathcal{M}^{\mu_L}_{\mathcal{E}(\mathcal{B}),n} = \dot{P}^{\mu_L}_{\mathcal{E}(\mathcal{B}),n}$ on the actual worldline. Eq. (4.9) is a useful identity to eliminate the partial derivative with respect to the metric later in the equations of motion for momentum and spin angular momentum. First, we obtain the equation for spin angular momentum easily by variation of the action with respect to the tetrad variables $\epsilon_A{}^{\mu}$. We get the simple equation

$$\delta S = \int d\tau \frac{\partial L}{\partial \Omega^{\mu\nu}} \delta\Omega^{\mu\nu} = 0 \implies \frac{DS^{\mu\nu}_{\text{rot}}}{D\tau} = 2\Omega^{[\mu}{}_{\rho} S^{\nu]\rho}_{\text{rot}}, \tag{4.10}$$

and we can eliminate the RHS using Eq. (4.9) by taking its antisymmetric part [which leads to $(\partial L/\partial g_{\mu\nu})$ vanishing] and we get

$$\begin{aligned}\frac{DS^{\mu\nu}_{\text{rot}}}{D\tau} &= 2p^{[\mu}u^{\nu]} + \frac{4}{3}R^{[\mu}{}_{\lambda\rho\sigma}J_{\lambda}{}^{\nu]\tau\rho\sigma} + \frac{2}{3}\nabla^{\lambda}R^{[\mu}{}_{\tau\rho\sigma}J_{\lambda}{}^{\nu]\tau\rho\sigma} + \frac{1}{6}\nabla^{[\mu}R_{\lambda\tau\rho\sigma}J^{\nu]\lambda\tau\rho\sigma} \\ &+ \sum_{l=2}^{\infty}\sum_{n=0}^{\infty} l \frac{D}{D\tau}[P^{[\mu}_{\mathcal{E},n\mu_{L-1}} Q^{\nu]\mu_{L-1}}_{\mathcal{E},n} + (\mathcal{E} \leftrightarrow \mathcal{B})],\end{aligned} \tag{4.11}$$

where we have used $\mathcal{M}^{\mu_L}_{\mathcal{E}(\mathcal{B}),n} = \dot{P}^{\mu_L}_{\mathcal{E}(\mathcal{B}),n}$, valid on the worldline. We can now redefine the spin angular momentum as $S^{\mu\nu} = S^{\mu\nu}_{\text{rot}} - \sum_{l=2}^{\infty}\sum_{n=0}^{\infty} l[P^{[\mu}_{\mathcal{E},n\mu_{L-1}} Q^{\nu]\mu_{L-1}}_{\mathcal{E},n} + (\mathcal{E} \leftrightarrow \mathcal{B})]$, to get

$$\begin{aligned}\frac{DS^{\mu\nu}}{D\tau} &= 2p^{[\mu}u^{\nu]} + \frac{4}{3}R^{[\mu}{}_{\lambda\rho\sigma}J_{\lambda}{}^{\nu]\tau\rho\sigma} \\ &+ \frac{2}{3}\nabla^{\lambda}R^{[\mu}{}_{\tau\rho\sigma}J_{\lambda}{}^{\nu]\tau\rho\sigma} + \frac{1}{6}\nabla^{[\mu}R_{\lambda\tau\rho\sigma}J^{\nu]\lambda\tau\rho\sigma}.\end{aligned} \tag{4.12}$$

This is the appropriate definition of total spin angular momentum of the body as reinforced by the fact that this also shows up in the stress energy tensor (see Eq. 4.14) in the expected manner. To solve the equations of motion, we also need to impose a ‘‘spin supplementary condition’’ (SSC) to ensure that it is a spatial tensor with the right number of degrees of freedom. Here, we impose the ‘‘covariant’’ or Tulczyjew-Dixon SSC at the level of the equations of motion upon the total physical spin angular momentum as $S^{\mu\nu}p_\mu = 0$.

The equation of motion for momentum can be obtained by variation of the action with respect to the worldline $z^\mu(\tau)$, which can be done following the covariant approach as shown in Ref. [184] to get

$$\begin{aligned}\frac{Dp_\mu}{D\tau} = &-\frac{1}{2}R_{\mu\nu\rho\sigma}u^\nu S^{\rho\sigma} - \frac{1}{6}J^{\lambda\nu\rho\sigma}\nabla_\mu R_{\lambda\nu\rho\sigma}\\ &-\frac{1}{12}J^{\tau\lambda\nu\rho\sigma}\nabla_\mu\nabla_\tau R_{\lambda\nu\rho\sigma}.\end{aligned} \tag{4.13}$$

Note that only the sum of multipole moments $\sum_n Q^{\mu_l}_{\mathcal{E},n}$, appear in the expressions for the time derivatives of momentum and spin angular momentum.

Finally, the stress energy tensor of the particle can be derived by varying the effective action with respect to the metric $g_{\mu\nu}$ as $T^{\mu\nu} = \frac{1}{\sqrt{-g}}\frac{\delta S}{\delta g_{\mu\nu}}$, where all dependency of the action on $g_{\mu\nu}$ needs to be taken into account during the variation. This variation was performed in Ref. [184] to obtain

$$T^{\mu\nu} = T^{\mu\nu}_{\text{pole-dipole}} + T^{\mu\nu}_{\text{quadrupole}} + T^{\mu\nu}_{\text{octupole}}, \tag{4.14}$$

$$T^{\mu\nu}_{pole-dipole} = \int d\tau p^{(\mu}u^{\nu)}\frac{\delta^{(4)}(x-z)}{\sqrt{-g}} - \nabla_\rho\int d\tau S^{\rho(\mu}u^{\nu)}\frac{\delta^{(4)}(x-z)}{\sqrt{-g}}, \tag{4.15}$$

$$T^{\mu\nu}_{\text{quadrupole}} = \int d\tau\frac{1}{3}R^{(\mu}{}_{\lambda\rho\sigma}J^{\nu)\lambda\rho\sigma}\frac{\delta^{(4)}(x-z)}{\sqrt{-g}} - \nabla_\rho\nabla_\sigma\int d\tau\frac{2}{3}J^{\rho(\mu\nu)\sigma}\frac{\delta^{(4)}(x-z)}{\sqrt{-g}}, \tag{4.16}$$

$$\begin{aligned}T^{\mu\nu}_{\text{octupole}} = &\int d\tau\left[\frac{1}{6}\nabla^\lambda R^{(\mu}{}_{\xi\rho\sigma}J_\lambda{}^{\nu)\xi\rho\sigma} + \frac{1}{12}\nabla^{(\mu}R_{\xi\tau\rho\sigma}J^{\nu)\xi\tau\rho\sigma}\right]\frac{\delta^{(4)}(x-z)}{\sqrt{-g}}\\ &+\nabla_\rho\int d\tau\left[-\frac{1}{6}R^{(\mu}{}_{\xi\lambda\sigma}J^{|\rho|\nu)\xi\lambda\sigma} - \frac{1}{3}R^{(\mu}{}_{\xi\lambda\sigma}J^{\nu)\rho\xi\lambda\sigma} + \frac{1}{3}R^\rho{}_{\xi\lambda\sigma}J^{(\mu\nu)\xi\lambda\sigma}\right]\frac{\delta^{(4)}(x-z)}{\sqrt{-g}}\\ &+\nabla_\lambda\nabla_\rho\nabla_\sigma\int d\tau\frac{1}{3}J^{\sigma\rho(\mu\nu)\lambda}\frac{\delta^{(4)}(x-z)}{\sqrt{-g}},\end{aligned} \tag{4.17}$$

which holds true even in the presence of inducible multipole moments when the contribution of the multipole moments is included in the definitions of the momentum and spin angular momentum. Since we are only interested in linear tides, we can drop all nonlinear (in curvature or metric perturbation) contributions in the quadrupolar and octupolar stress energy tensor to get a simpler truncated stress energy tensor as

$$T^{\mu\nu} = \int d\tau p^{(\mu}u^{\nu)}\delta^{(4)}(x-z) - \nabla_\rho \int d\tau S^{\rho(\mu}u^{\nu)}\delta^{(4)}(x-z) - \nabla_\rho\nabla_\sigma \int d\tau \frac{2}{3} J^{\rho(\mu\nu)\sigma}\delta^{(4)}(x-z)$$
$$+ \nabla_\lambda\nabla_\rho\nabla_\sigma \int d\tau \frac{1}{3} J^{\sigma\rho(\mu\nu)\lambda}\delta^{(4)}(x-z). \tag{4.18}$$

This truncated stress energy tensor will be important later to solve the problem of GWs scattering off the effective particle.

To proceed further, we need to relate the tidal fields to the multipole moments. We will now motivate and write down general ansätze for the multipole moments.

4.2.2 Ansätze for multipole moments

Going forward, we define the sum of all multipole moments for a given l and parity (electric or magnetic) as individual moments for convenience as $Q_{\mathcal{E}}^{\mu_L} = \sum_n Q_{\mathcal{E},n}^{\mu_L}$. Now, as mentioned earlier, when the particle obeys spherical symmetry, only the tidal fields to which the multipole moment explicitly couples to in the action can affect it and we have Eq. (4.2). However, in the presence of spin, it is possible to have more fields in the formula for multipole moments. Since we intend to model the spinning BH, which breaks spherical symmetry but still respects parity, we can only have tidal fields with the same transformation under parity as the moment in the right hand side. The transformation under reflection is $(-1)^l$ for $\mathcal{E}$ fields and $(-1)^{l+1}$ for $\mathcal{B}$ fields.

Furthermore, we restrict our attention to quadrupolar and octupolar tidal fields as the higher multipolar order tidal fields are not relevant to the order of interest in this work. Thus, we can write a general ansatz as

$$
\begin{aligned}
Q_{\mathcal{E}}^{\mu\nu} &= M\sum_{m}^{\infty}(GM)^{4+m}\lambda^{\mu\nu}_{\mathcal{E},m\rho\sigma}\frac{D^m}{D\tau^m}\mathcal{E}^{\rho\sigma} + M\sum_{m}^{\infty}(GM)^{5+m}\zeta^{\mu\nu}_{\mathcal{B},m\rho\sigma\gamma}\frac{D^m}{D\tau^m}\mathcal{B}^{\rho\sigma\gamma}, \quad (\mathcal{E}\leftrightarrow\mathcal{B}),\\
Q_{\mathcal{B}}^{\mu\nu\rho} &= M\sum_{m}^{\infty}(GM)^{5+m}\eta^{\mu\nu\rho}_{\mathcal{E},m\sigma\gamma}\frac{D^m}{D\tau^m}\mathcal{E}^{\sigma\gamma} + M\sum_{m}^{\infty}(GM)^{6+m}\Lambda^{\mu\nu\rho}_{\mathcal{B},m\alpha\sigma\delta}\frac{D^m}{D\tau^m}\mathcal{B}^{\alpha\sigma\delta}, \quad (\mathcal{E}\leftrightarrow\mathcal{B}),
\end{aligned}
\tag{4.19}
$$

where we have rendered the response tensors dimensionless by removing factors of GM. The response tensors can only have a nontrivial structure due to the spin of the particle. Additionally, they must be orthogonal to u^μ and be traceless in the upper and lower set of indices separately. One can thus generally decompose the response tensors as linear combination of building-block tensors made up of the spin tensor $S^{\mu\nu}$, Pauli-Lubanski spin vector $s^\mu \approx -(1/2)\epsilon^{\mu}{}_{\nu\rho\sigma}u^\nu S^{\rho\sigma}$,[6] and the orthogonal (to four-velocity u^μ) projection operator $\mathcal{P}^\mu_\nu = \delta^\mu_\nu + u^\mu u_\nu$. While infinitely many such combinations may be written, only a handful of them are linearly independent and we can generally decompose the response tensors $\lambda,\ \zeta,\ \eta$, as (see, e.g., Ref. [61] where the correlation function for the quadrupole moment was fixed)

$$
\begin{aligned}
\lambda^{\mu\nu}_{\mathcal{E},n\rho\sigma} = {}& f^0_{\mathcal{E},n}\mathcal{P}^{\langle\mu}_{\langle\rho}\mathcal{P}^{\nu\rangle}_{\sigma\rangle} + f^1_{\mathcal{E},n}\hat{S}^{\langle\mu}{}_{\langle\rho}\mathcal{P}^{\nu\rangle}_{\sigma\rangle} + f^2_{\mathcal{E},n}\hat{s}^{\langle\mu}\hat{s}_{\langle\rho}\delta^{\nu\rangle}_{\sigma\rangle} + f^3_{\mathcal{E},n}\hat{s}^{\langle\mu}\hat{s}_{\langle\rho}\hat{S}^{\nu\rangle}{}_{\sigma\rangle}\\
&+ f^4_{\mathcal{E},n}\hat{s}^{\langle\mu}\hat{s}_{\langle\rho}\hat{s}^{\nu\rangle}\hat{s}_{\sigma\rangle},\ (\mathcal{E}\leftrightarrow\mathcal{B})\\
\zeta^{\mu\nu}_{\mathcal{B},n\rho\sigma\gamma} = {}& \lambda^{\mu\nu}_{\mathcal{E},n\langle\rho\sigma}\hat{s}_{\gamma\rangle}(f_{\mathcal{E},n}\to g_{\mathcal{B},n}),\ \eta^{\mu\nu\rho}_{\mathcal{E},n\ \rho\sigma} = \hat{s}^{\langle\rho}\lambda^{\mu\nu\rangle}_{\mathcal{E},n\rho\sigma}(f_{\mathcal{E},n}\to h_{\mathcal{E},n}), \quad (\mathcal{E}\leftrightarrow\mathcal{B})
\end{aligned}
\tag{4.20}
$$

[6] The Pauli Lubanski spin vector is actually defined as $s^\mu = -[1/(2m)]\epsilon^{\mu}{}_{\nu\rho\sigma}p^\nu S^{\rho\sigma}$. However, as $p^\mu = mu^\mu + O(R)$, we can neglect the curvature-dependent corrections when substituting in the linear tidal-response.

where the sets of coefficients f, g, h can now only depend on the spin parameter $\chi = J/(GM^2)$, where $J = \sqrt{(1/2)S^{\mu\nu}S_{\mu\nu}}$ is the magnitude of spin angular momentum. Also, we have defined $\hat{S}^{\mu\nu}$ and $\hat{s}^{\mu}$ as the normalized versions of the spin-tensor ($\hat{S}^{\mu\nu}\hat{S}_{\mu\nu} = 2$) and spin-vector ($\hat{s}^{\mu}\hat{s}_{\mu} = 1$) so they are dimensionless and independent of any parameter. Adding any other tensor made up of the same ingredients will be linearly dependent on the remaining pieces, which follows simply from the relations $\hat{S}^{\mu\nu}\hat{s}_{\nu} = 0$, and $\hat{S}^{\mu}{}_{\rho}\hat{S}^{\nu}{}_{\sigma} = -\mathcal{P}^{\mu}{}_{\sigma}\mathcal{P}^{\nu}{}_{\rho} + \mathcal{P}^{\mu\nu}\mathcal{P}_{\rho\sigma} - \mathcal{P}_{\rho\sigma}\hat{s}^{\mu}\hat{s}^{\nu} + \mathcal{P}^{\mu}{}_{\sigma}\hat{s}^{\nu}\hat{s}_{\rho} + \mathcal{P}^{\nu}{}_{\rho}\hat{s}^{\mu}\hat{s}_{\sigma} - \mathcal{P}^{\mu\nu}\hat{s}_{\rho}\hat{s}_{\sigma}$, and thus no more free coefficients can be introduced. We have transferred all freedom in choosing the response to the associated sets of χ-dependent parameters f, g, and h. We can similarly decompose the tensor $\Lambda^{\mu\nu\rho}_{\alpha\sigma\delta}$ but it turns out to be irrelevant to the order of interest in this work, so we just drop its contribution from now on. We can drop most of the time-derivatives of the tidal fields in the ansätze for the same reason and work with simplified truncated ansätze by including terms only up to $(GM)^5$,

$$\begin{aligned}
Q^{\mu\nu}_{\mathcal{E}} &= (GM)^4\lambda^{\mu\nu}_{\mathcal{E},0\rho\sigma}\mathcal{E}^{\rho\sigma} + (GM)^5\lambda^{\mu\nu}_{\mathcal{E},1\rho\sigma}\frac{D}{D\tau}\mathcal{E}^{\rho\sigma} \\
&\quad + (GM)^5\nu^{\mu\nu}_{\mathcal{B},0\langle\rho\sigma}\hat{s}_{\gamma\rangle}\mathcal{B}^{\rho\sigma\gamma}, \ (\mathcal{E}\leftrightarrow\mathcal{B}), \\
Q^{\mu\nu\rho}_{\mathcal{B}} &= (GM)^5\hat{s}^{\langle\rho}\xi^{\mu\nu\rangle}_{\mathcal{E},0\,\alpha\beta}\mathcal{E}^{\alpha\beta}, \ (\mathcal{E}\leftrightarrow\mathcal{B}),
\end{aligned} \tag{4.21}$$

where we have defined $\nu^{\mu\nu}_{\mathcal{B},0\rho\sigma} = \lambda^{\mu\nu}_{\mathcal{B}(\mathcal{E}),0\rho\sigma}(f_{\mathcal{E}(\mathcal{B}),0} \to g_{\mathcal{B}(\mathcal{E}),0})$, and $\xi^{\mu\nu}_{\mathcal{E},0\rho\sigma} = \lambda^{\mu\nu}_{\mathcal{E},0\rho\sigma}(f_{\mathcal{E}(\mathcal{B}),0} \to h_{\mathcal{E},0})$. The 40 coefficients, $f^{i}_{\mathcal{E}(\mathcal{B}),0}$, $f^{i}_{\mathcal{E}(\mathcal{B}),1}$, $g^{i}_{\mathcal{B}(\mathcal{E}),0}$, $h_{\mathcal{E}(\mathcal{B}),0}$ characterize the tidal response of the particle. Some contribute to dissipative effects whereas others contribute only to conservative effects. Unlike for the spinless case, it is not obvious here which ones contribute to dissipation and which ones do not, due to coupling between different multipolar orders. At leading order, focussing only on the quadrupolar tidal field inducing the quadrupolar multipole moment, it can be shown (see Ref. [61]) that the part of the tensor $\lambda^{\mu\nu\rho\sigma}_{\mathcal{E},0}$ that is antisymmetric under $\mu\nu \leftrightarrow$

$\rho\sigma$ contributes to dissipation. This criteria is flipped for $\lambda^{\mu\nu}_{\mathcal{E},1\rho\sigma}$ as it is next to an odd power of a time-derivative. This includes the coefficients $f^1_{\mathcal{E}(\mathcal{B}),0}$, $f^3_{\mathcal{E}(\mathcal{B}),0}$, $f^0_{\mathcal{E}(\mathcal{B}),1}$, $f^2_{\mathcal{E}(\mathcal{B}),1}$, $f^4_{\mathcal{E}(\mathcal{B}),1}$. It is less trivial for the coefficients entering tensors that mix the different multipolar orders. We will see in Sec. 4.3.4 which coefficients are conservative and which are dissipative among these. We accomplish this by scattering GWs off the effective particle and computing the degree of absorption for the $l = 2$ spheroidal modes and comparing with the analogous result obtained by solving the Teukolsky equation. This comparison, along with demanding that the different spheroidal modes of the Newman-Penrose scalar ψ_4 scatter independently in the effective theory will help identify which coefficients lead to dissipation and which only to conservative effects. Additionally, we will also be able to fix the coefficients that contribute to dissipative effects through comparison with results from BHPT.

4.3 Fixing the unknown parameters in ansätze for the multipole moments

To fix the dissipative part of the response, we now scatter GWs off the effective particle with mass M and compute a suitable quantity indicating the degree of absorption. We can then fix the free parameters by comparison with the analogous quantity for actual spinning BHs, obtained by solving the Teukolsky equation. We will only consider the effect of the linearly induced tidal moments in the scattering of the wave in what follows, since the other contributions to the scattered wave are expected to be purely conservative or irrelevant (up to the order of interest). However, in this way we also neglect the leading-order effect of nonlinearities due to the wave scattering off the stationary gravitational background, leading to certain subtleties when matching with the result from the Teukolsky equation which we will have to address.

4.3.1 The GW environment

Let the unperturbed particle be at the origin at rest, $u^\mu = (1,0,0,0)$ and $z^\mu = (\tau = t, 0,0,0)$, where τ is the proper time of the particle which is identical to the background time t when undisturbed. We add to the particle's background a general GW perturbation $h^{\mu\nu} = \sqrt{-g}g^{\mu\nu} - \eta^{\mu\nu}$. We choose the perturbation to be in the harmonic and transverse-traceless (TT) gauge, satisfying $\partial_\mu h^{\mu\nu} = 0$, $h^{\mu\nu}u_\nu = 0$, $h^{\mu\nu}\eta_{\mu\nu} = 0$. At zeroth order (in G), when the interactions of the metric perturbation with the stationary gravitational field of the particle are neglected, it just satisfies the flat space-time wave equation $\eta^{\mu\nu}\partial_\mu\partial_\nu h^{\alpha\beta} = 0$ (except at origin where the particle is present). Then, we can write the general tensor wave solution in the rest frame of the particle (defined by u^μ) at leading order as

$$h_{ij} = \sum_{l=2}^{\infty} \frac{1}{\omega^{l-2}} \left(C^{K_l}_{\mathcal{E},\mathrm{in}} \Pi^{k_{l-1}k_l}_{ij} \hat{\partial}_{K_{l-2}} + \frac{1}{\omega} C^{K_l}_{\mathcal{B},\mathrm{in}} \Pi^{k_l m}_{ij} \epsilon_{k_{l-1}mn} \hat{\partial}_{K_{l-2}n} \right) \psi_{\mathrm{in}} + (\mathrm{in} \to \mathrm{out}), \tag{4.22}$$

where ω is the frequency of the wave in the rest frame of the particle and $\Pi^{ij}_{kl} = (1/2)(P^i{}_k P^j{}_l + P^j{}_k P^i{}_l - P^{ij}P_{kl})$, with $P^{ij} = \delta^{ij} + \partial^i\partial^j/\omega^2$, is a differential projection operator which ensures that the harmonic and TT gauge conditions are satisfied. $\psi_{\mathrm{in}} = \exp[-i\omega(t+r)]/(\omega r)$ and $\psi_{\mathrm{out}} = \exp[-i\omega(t-r)]/(\omega r)$ are the incoming and outgoing wave solutions for the $l = 0$ mode of a scalar wave respectively. $C^{K_l}_{\mathcal{E}/\mathcal{B},\mathrm{in/out}}$ are dimensionless symmetric trace-free (STF) tensors characterizing the amplitudes of each l mode. $\mathcal{E}$, $\mathcal{B}$ label the coefficients tuning the electric and magnetic polarizations respectively.[7] The different l modes and polarizations ($\mathcal{E}$, $\mathcal{B}$) do not

[7] In general, there are two distinct solutions for each ω, l, and m for a massless tensor wave (except for scalars). We split them according to parity in this work, with $\mathcal{E}$ modes transforming as $(-1)^l$ and $\mathcal{B}$ modes transforming as $(-1)^{l+1}$ under reflection. The labels are also related to the manner in which different coefficients contribute to the tidal fields (see Eq. (4.26)).

mix under rotations. However, that does not mean we can tune them separately in the presence of the particle, as the particle's inducible multipole moments combined with its spin can couple different modes with each other. The general solution in Eq. (4.22) can be understood by noting that a basis of solutions to the homogeneous wave equation in flat space-time (albeit allowing for irregular behaviour at the origin) can be obtained by acting arbitrary number of spatial derivatives upon the spherically symmetric solutions, i.e., $\psi_{\rm in}$, $\psi_{\rm out}$ and any linear combination of them. We can then generally write the solution for h_{ij} as a linear combination of the basis solutions with undetermined tensors contracting them to get the appropriate tensor structure. One can then decompose them into rotationally independent pieces by splitting the undetermined tensors into STF tensors and then separating them according to parity ($\mathcal{E}$ and $\mathcal{B}$). Finally, one uses the projection operator Π^{ij}_{kl} to ensure h^{ij} is traceless and satisfies the harmonic gauge condition.

Now, we want to split the total general solution in Eq. (4.22) into two parts, one that can be regarded as the ''input'' part of the wave which corresponds to the part that induces the tidal moments and an ''output'' part which is sourced from the induced tidal moments. Naively, one might think that the input part can be obtained by simply setting the outgoing mode coefficients $C^{K_l}_{\mathcal{E}/\mathcal{B},\rm out} = 0$, but that is incorrect as there will be an outgoing wave in general even in the absence of a particle due to the the fact that an incoming wave packet in the distant past becomes an outgoing wave packet in the distant future (after crossing the origin). Also, the incoming part of the wave by itself is irregular at the origin and thus cannot be sustained without the presence of a particle. In fact, the correct splitting is given by the regular (input) and irregular (output) parts of the wave respectively, as follows

$$h_{ij} = \sum_{l=2}^{\infty} \frac{1}{\omega^{l-2}} \left(C^{K_l}_{\mathcal{E},\mathrm{reg}} \Pi_{ij}^{k_{l-1}k_l} \hat{\partial}_{K_{l-2}} + \frac{1}{\omega} C^{K_l}_{\mathcal{B},\mathrm{reg}} \Pi_{ij}^{k_l m} \epsilon_{k_{l-1}mn} \hat{\partial}_{K_{l-2}n} \right) \psi_{\mathrm{reg}} \tag{4.23}$$

$$+ (\mathrm{reg} \to \mathrm{irr}),$$

$$\psi_{\mathrm{reg}} = \frac{1}{2i}(\psi_{\mathrm{out}} - \psi_{\mathrm{in}}) = \frac{\exp(-i\omega t)\sin(\omega r)}{\omega r}, \quad \psi_{\mathrm{irr}} = (\psi_{\mathrm{out}} + \psi_{\mathrm{in}}) = \frac{\exp(-i\omega t)\cos(\omega r)}{\omega r},$$

$$C_{\mathrm{reg}} = (C_{\mathrm{out}} - C_{\mathrm{in}})i, \quad C_{\mathrm{irr}} = C_{\mathrm{out}} + C_{\mathrm{in}}, \tag{4.24}$$

where ψ_{reg} is regular at the origin and obeys the wave equation everywhere whereas ψ_{irr} is irregular at the origin and requires support from a source, such as the stress energy tensor of the effective particle. More specifically, $\eta^{\mu\nu}\partial_\mu\partial_\nu\psi_{\mathrm{reg}} = 0$, and $\eta^{\mu\nu}\partial_\mu\partial_\nu\psi_{\mathrm{irr}} = (4\pi/\omega)\delta^{(3)}(\vec{r})\exp(-i\omega t)$. Thus, we will use the regular part of h_{ij}, which has finite values at the origin to compute the tidal fields that will induce the multipole moments and the irregular part of the fields will be related to the stress energy tensor of the particle's induced tidal moments through the relation

$$\begin{aligned}
\eta^{\mu\nu}\partial_\mu\partial_\nu h^{\mathrm{irr}}_{ij} &= \sum_{l=2}^{\infty} \frac{\exp(-i\omega t)}{\omega^{l-1}} \left(C^{K_l}_{\mathcal{E},\mathrm{irr}} \Pi_{ij}^{k_{l-1}k_l} \hat{\partial}_{K_{l-2}} \right. \\
&\quad \left. + \frac{1}{\omega} C^{K_l}_{\mathcal{B},\mathrm{irr}} \Pi_{ij}^{k_l m} \epsilon_{k_{l-1}mn} \hat{\partial}_{K_{l-2}n} \right) 4\pi\delta^{(3)}(\vec{r}) \\
&= 16\pi G|g|\Pi_{ij}^{kl} T_{kl}(\vec{r}),
\end{aligned} \tag{4.25}$$

where we have projected out the stress energy tensor appropriately since we are focusing on the radiative part of the field and using h^{irr}_{ij} to label the irregular part of the metric perturbation (i.e., the part generated from acting spatial derivatives on ψ_{irr}) . We will have to solve this relation with the stress energy tensor corresponding to that due to the induced quadrupolar and octupolar multipole moments given to leading order in the curvature tensor in Eq. (4.18).

4.3.2 Induced multipole moments

As mentioned earlier, the regular part of the wave, which can exist without support and satisfies the homogeneous wave equation, should be seen as the input part of the wave. We will use this part of the metric perturbation to compute the tidal fields which will induce the multipole moments. With the definitions given earlier in Eqs. (4.1), and the formula for the regular part of the wave given in Eq. (4.23), we find that the value of the tidal fields at the origin is given by

$$\mathcal{E}^{ij}_{\text{origin}} = -\frac{1}{5}\omega^2 C^{ij}_{\mathcal{E},\text{reg}}, \tag{4.26a}$$

$$\mathcal{B}^{ij}_{\text{origin}} = \frac{i}{5}\omega^2 C^{ij}_{\mathcal{B},\text{reg}}, \tag{4.26b}$$

$$\mathcal{E}^{ijk}_{\text{origin}} = \frac{1}{21}\omega^3 C^{ijk}_{\mathcal{E},\text{reg}}, \tag{4.26c}$$

$$\mathcal{B}^{ijk}_{\text{origin}} = \frac{-i}{21}\omega^3 C^{ijk}_{\mathcal{B},\text{reg}}. \tag{4.26d}$$

The multipole moments can now be computed by substituting these fields in Eqs. (4.21). However, we see that the nontrivial (due to spin) response tensors mix the various components together. While this is inconvenient, a simple way to rewrite these expressions in a basis that does not mix components is to orient the coordinate system so that the Pauli-Lubanski spin vector is along the z-axis and expand in spin-weighted spherical harmonics. For later convenience, we choose spherical harmonics with spin weight '-2'. The simplest way to transform to this basis from the Cartesian basis is to define

$$\vec{m} = \frac{1}{\sqrt{2}}(\hat{\theta} + i\hat{\phi}),$$

$$\hat{\theta} = \cos(\theta)\cos(\phi)\hat{x} + \cos(\theta)\sin(\phi)\hat{y} - \sin(\theta)\hat{z},$$

$$\hat{\phi} = -\sin(\phi)\hat{x} + \cos(\phi)\hat{y},$$

$$\hat{r} = \sin(\theta)\cos(\phi)\hat{x} + \sin(\theta)\sin(\phi)\hat{y} + \cos(\theta)\hat{z}, \tag{4.27}$$

and then expand $Q^{ij}\bar{m}_i\bar{m}_j$ and $O^{ijk}\bar{m}_i\bar{m}_j\hat{r}_k$ in spin weight -2, spherical harmonics by projection as

$$\begin{aligned}
Q^{l=2,m}_{\mathcal{E}/\mathcal{B}} &= \int d\Omega\, Q^{ij}_{\mathcal{E}/\mathcal{B}}\bar{m}_i\bar{m}_j\bar{Y}^{l=2,m}_{-2}(\theta,\phi),\\
O^{l=3,m}_{\mathcal{E}/\mathcal{B}} &= \int d\Omega\, Q^{ijk}_{\mathcal{E}/\mathcal{B}}\bar{m}_i\bar{m}_j\hat{r}_k\bar{Y}^{l=3,m}_{-2}(\theta,\phi),
\end{aligned} \tag{4.28}$$

where we are using $Y^{lm}_{s=-2}(\theta,\phi)$ to denote spherical harmonics with spin weight -2. They are normalized to 1 [i.e., $\int d\Omega\, Y^{lm}_{-2}(\theta,\phi)\bar{Y}^{lm}_{-2}(\theta,\phi) = 1$]. We similarly define the incoming and outgoing mode coefficients in this basis as

$$\begin{aligned}
C^{l=2,m}_{\mathcal{E}/\mathcal{B}} &= \int d\Omega\, C^{ij}_{\mathcal{E}/\mathcal{B}}\bar{m}_i\bar{m}_j\bar{Y}^{2m}_{-2}(\theta,\phi)\\
C^{l=3,m}_{\mathcal{E}/\mathcal{B}} &= \int d\Omega\, C^{ijk}_{\mathcal{E}/\mathcal{B}}\bar{m}_i\bar{m}_j\hat{r}_k\bar{Y}^{3m}_{-2}(\theta,\phi),
\end{aligned} \tag{4.29}$$

where we have suppressed the 'in' ('out') subscript for brevity. The definitions are identical for both incoming and outgoing mode coefficients. Note that we are using the symbol O for octupole tensor in spherical harmonic (with spin weight -2) basis. Then, we can write down the expressions for the multipole moments obtained by substituting Eq. (4.26) into the ansätze in Eq. (4.21) simply as

$$\begin{aligned}
Q^{2m}_{\mathcal{E}} &= -e^{-i\omega t}M\omega^2\frac{(GM)^4}{30}\Big\{6\mathcal{F}^{0,\mathrm{reg}}_{\mathcal{E}} + 3i\mathcal{F}^{1,\mathrm{reg}}_{\mathcal{E}}\,m\\
&\quad + (m^2-4)\big[-\mathcal{F}^{2,\mathrm{reg}}_{\mathcal{E}} - i\mathcal{F}^{3,\mathrm{reg}}_{\mathcal{E}}\,m + \mathcal{F}^{4,\mathrm{reg}}_{\mathcal{E}}\,(m^2-1)\big]\Big\},\\
O^{3m}_{\mathcal{B}} &= -e^{-i\omega t}M\omega^2\frac{\sqrt{9-m^2}(GM)^5}{90\sqrt{7}}\Big\{6h^0_{\mathcal{E}} + 3ih^1_{\mathcal{E}}\,m\\
&\quad + (m^2-4)\big[-h^2_{\mathcal{E}} - ih^3_{\mathcal{E}}\,m + h^4_{\mathcal{E}}\,(m^2-1)\big]\Big\}C^{2m}_{\mathcal{E},\mathrm{reg}},
\end{aligned}$$

$$Q^{2m}_{\mathcal{B}} = ie^{-i\omega t}M\omega^2\frac{(GM)^4}{30}\Big\{6\mathcal{F}^{0,\text{reg}}_{\mathcal{B}} + 3i\mathcal{F}^{1,\text{reg}}_{\mathcal{B}}\, m$$
$$+ (m^2-4)\big[-\mathcal{F}^{2,\text{reg}}_{\mathcal{B}} - i\mathcal{F}^{3,\text{reg}}_{\mathcal{B}}\, m + \mathcal{F}^{4,\text{reg}}_{\mathcal{B}}\,(m^2-1)\big]\Big\},$$
$$O^{3m}_{\mathcal{E}} = ie^{-i\omega t}M\omega^2\frac{\sqrt{9-m^2}(GM)^5}{90\sqrt{7}}\Big\{6h^0_{\mathcal{B}} + 3ih^1_{\mathcal{B}}\, m$$
$$+ (m^2-4)\big[-h^2_{\mathcal{B}} - ih^3_{\mathcal{B}}\, m + h^4_{\mathcal{B}}\,(m^2-1)\big]\Big\}C^{2m}_{\mathcal{B},\text{reg}}, \tag{4.30}$$

where $\mathcal{F}^{i,\text{reg}}_{\mathcal{E}(\mathcal{B})} = (f^i_{\mathcal{E}(\mathcal{B}),0} - iGM\omega f^i_{\mathcal{E}(\mathcal{B}),1})C^{2m}_{\mathcal{E}(\mathcal{B}),\text{reg}} + [(i\sqrt{9-m^2})/(3\sqrt{7})]GM\omega g^i_{\mathcal{B}(\mathcal{E}),0}C^{3m}_{\mathcal{B}(\mathcal{E}),\text{reg}}$, and we see that there is no longer any mixing of different m modes. This is simply because we oriented the coordinate system so that the z-axis is along the spin, and thus it has 0 azimuthal quantum number to add or remove from that of the STF tensors characterizing the field. However, there is still mixing between different l modes due to the tidal response mixing the quadrupolar and octupolar sectors. This complicates the process of defining a degree of absorption or a scattering phase, and we will tackle this problem later in Sec. 4.3.4, by switching to a basis where there is no mixing of modes.

4.3.3 Solving for the outgoing wave

Now, we can use the wave equation with the appropriate source in Eq. (4.25) to relate the multipole moments to the irregular part of the wave. The relevant (projected) part of the stress energy tensor in the chosen coordinate system is given by

$$T^{kl}\Pi^{ij}_{kl} = \Pi^{ij}_{kl}\Big(\frac{1}{2}\ddot{Q}^{kl}_{\mathcal{E}} + \frac{1}{2}\epsilon^{\langle k}{}_{mn}\dot{Q}^{l\rangle n}_{\mathcal{B}}\partial^m - \frac{1}{2}\ddot{Q}^{kl}_{\mathcal{E}\,m}\partial^m$$
$$- \frac{1}{2}\epsilon^{\langle k}{}_{mn}\dot{Q}^{l\rangle no}_{\mathcal{B}}\partial^m\partial_o\Big)\delta^{(3)}(\vec{x}), \tag{4.31}$$

which is obtained by substituting the expressions for $J^{\mu\nu\rho\sigma}$ and $J^{\lambda\mu\nu\rho\sigma}$ in terms of the multipole moments given in Eqs. (4.7), (4.8) into the stress energy tensor Eq. (4.18) and discarding terms with components along u^μ (as they will be eliminated upon projection). Now, substituting Eq. (4.31) into the RHS of Eq. (4.25) and comparing, we get the relations

$$
\begin{aligned}
&e^{-i\omega t} C^{ij}_{\mathcal{E},irr} = 2G\omega^3 Q^{ij}_{\mathcal{E}},\ e^{-i\omega t} C^{ij}_{\mathcal{B},irr} = 2iG\omega^3 Q^{ij}_{\mathcal{B}},\\
&e^{-i\omega t} C^{ijk}_{\mathcal{E},irr} = -2G\omega^4 Q^{ijk}_{\mathcal{E}},\ e^{-i\omega t} C^{ijk}_{\mathcal{B},irr} = -2iG\omega^4 Q^{ijk}_{\mathcal{B}},
\end{aligned}
\tag{4.32}
$$

which are simple proportionality relations and thus can be trivially transformed to the l, m basis.

Substiting Eq. (4.32) in Eq. (4.30), we get the relations

$$
\begin{aligned}
C^{2m}_{\mathcal{E}/\mathcal{B},\mathrm{irr}} &= -\frac{\epsilon^5}{15}\{6\mathcal{F}^{0,\mathrm{reg}}_{\mathcal{E}/\mathcal{B}} + 3i\mathcal{F}^{1,\mathrm{reg}}_{\mathcal{E}/\mathcal{B}}\, m + (m^2-4)[-\mathcal{F}^{2,\mathrm{reg}}_{\mathcal{E}/\mathcal{B}} - i\mathcal{F}^{3,\mathrm{reg}}_{\mathcal{E}/\mathcal{B}}\, m + \mathcal{F}^{4,\mathrm{reg}}_{\mathcal{E}/\mathcal{B}}\, (m^2-1)]\},\\
C^{3m}_{\mathcal{B},\mathrm{irr}} &= i\frac{\sqrt{9-m^2}\epsilon^6}{45\sqrt{7}}\{6h^0_{\mathcal{E}} + 3ih^1_{\mathcal{E}}\, m + (m^2-4)[-h^2_{\mathcal{E}} - ih^3_{\mathcal{E}}\, m + h^4_{\mathcal{E}}\, (m^2-1)]\}C^{2m}_{\mathcal{E},\mathrm{reg}},\\
C^{3m}_{\mathcal{E},\mathrm{irr}} &= -i\frac{\sqrt{9-m^2}\epsilon^6}{45\sqrt{7}}\{6h^0_{\mathcal{B}} + 3ih^1_{\mathcal{B}}\, m + (m^2-4)[-h^2_{\mathcal{B}} - ih^3_{\mathcal{B}}\, m + h^4_{\mathcal{B}}\, (m^2-1)]\}C^{2m}_{\mathcal{B},\mathrm{reg}},
\end{aligned}
\tag{4.33}
$$

where we have defined $\epsilon = GM\omega$. Now, we can use the relations in Eqs. (4.24) to solve the the outgoing coefficients. Since we are only interested in linear tides, and the leading-order tidal effects already start at a very high order in ϵ, we can approximate in the RHS as $C^{lm}_{\mathcal{E}/\mathcal{B},\mathrm{reg}} \approx -2iC^{lm}_{\mathcal{E}/\mathcal{B},\mathrm{in}} + O(\epsilon^5)$. Then we get the expressions for $C^{lm}_{\mathcal{E}/\mathcal{B},\mathrm{out}}$ as

$$
\begin{aligned}
C^{2m}_{\mathcal{E}(\mathcal{B}),\mathrm{out}} &= -C^{2m}_{\mathcal{E}(\mathcal{B}),\mathrm{in}} + \frac{2i\epsilon^5}{15}\Big\{6\mathcal{F}^{0,\mathrm{in}}_{\mathcal{E}(\mathcal{B})} + 3i\mathcal{F}^{1,\mathrm{in}}_{\mathcal{E}(\mathcal{B})}\, m\\
&\qquad + (m^2-4)\big[-\mathcal{F}^{2,\mathrm{in}}_{\mathcal{E}(\mathcal{B})} - i\mathcal{F}^{3,\mathrm{in}}_{\mathcal{E}(\mathcal{B})}\, m + \mathcal{F}^{4,\mathrm{in}}_{\mathcal{E}(\mathcal{B})}\, (m^2-1)\big]\Big\},
\end{aligned}
\tag{4.34}
$$

$$
C^{3m}_{\mathcal{B},\mathrm{out}} = -C^{3m}_{\mathcal{B},\mathrm{in}} + \frac{2\sqrt{9-m^2}\epsilon^6}{45\sqrt{7}}\Big\{6h^0_{\mathcal{E}} + 3ih^1_{\mathcal{E}}\, m
$$

$$+ (m^2-4)\big[-h^2_{\mathcal{E}} - ih^3_{\mathcal{E}}\, m + h^4_{\mathcal{E}}\, (m^2-1)\big]\Big\} C^{2m}_{\mathcal{B},\mathrm{in}},$$

$$C^{3m}_{\mathcal{E},\mathrm{out}} = -C^{3m}_{\mathcal{E},\mathrm{in}} - \frac{2\sqrt{9-m^2}\epsilon^6}{45\sqrt{7}}\Big\{6h^0_{\mathcal{B}} + 3ih^1_{\mathcal{B}}\, m$$

$$+ (m^2-4)\big[-h^2_{\mathcal{B}} - ih^3_{\mathcal{B}}\, m + h^4_{\mathcal{B}}\, (m^2-1)\big]\Big\} C^{2m}_{\mathcal{B},\mathrm{in}}. \tag{4.35}$$

4.3.4 Degree of absorption

Now we need to compute a suitable quantity that measures the degree of absorption. If there were no spin, there would be no mixing of different l modes, and we could simply define the degree of absorption (or emission) for each l, m mode as $1 - |C^{lm}_{\mathcal{E}/\mathcal{B},\mathrm{out}}/C^{lm}_{\mathcal{E}/\mathcal{B},\mathrm{in}}|$. We can still do the same if we instead use a different basis, formed by a linear combination of the mode coefficients in the spherical basis. To guess the appropriate combination (basis) in which the modes should scatter independently, we now turn to hints from BHPT. In BHPT, the Teukolsky equation [212] governs the behaviour of curvature perturbations in an exact Kerr background. Specifically, it governs the behaviour of the spin weight (-2) Teukolsky scalar ${}_{-2}\psi(t, r, \theta\phi)$ related to the standard Newman-Penrose curvature scalar ψ_4 by ${}_{-2}\psi = (r - ia\cos(\theta))^4\psi_4$, where $a = GM\chi$. A crucial property of the Teukolsky equation for ${}_{-2}\psi$ is that it is separable in spheroidal harmonic basis with spin weight -2 with fixed frequency eigen solutions with the form ${}_{-2}\psi \propto \exp(-i\omega t) S^{lm}_{-2}(\theta, \phi, a\omega)\,{}_{-2}R_{lm\omega}(r)$ where we are using $S^{lm}_{s=-2}$ to denote normalized (to 1) spheroidal harmonics with spin weight -2 and ${}_{-2}R_{lm\omega}(r)$ is an eigen solution to the radial Teukolsky equation (see Sec. 4.3.5). Asymptotically far away from the BH, i.e., as $r \to \infty$, the standard Newman-Penrose curvature scalar ψ_4 takes the form (see Eq. (2.6) in Ref. [355])

$$\psi_4 \to \omega^2 \sum_{l,m,P=\pm 1} \Bigg\{ K^{\mathrm{out}}_{lmP} \frac{\exp[-i\omega(t - r^*)]}{\omega r}$$

$$
+\frac{1}{16}\left[\mathrm{Re}(C)+12i\epsilon P\right]\frac{1}{\omega^4 r^4}K^{\mathrm{in}}_{lmP}\frac{\exp[-i\omega(t+r^*)]}{\omega r}\Bigg\}S^{l}_{-2,m}(\theta,\phi)
$$

$$
+\,O\left(\frac{1}{r^6}\right), \tag{4.36}
$$

where r^* is the tortoise coordinate and $P = \pm 1$ is the index denoting the transformation under parity for each mode with $P = 1$ ($P = -1$) for modes that are symmetric (anti-symmetric) under reflection. The expression for $\mathrm{Re}(C)$ can be found in Eq. (31) of Ref. [166]. The outgoing and incoming mode coefficients for each spheroidal mode l, m and parity $P = \pm 1$ are related simply as

$$
K^{\mathrm{out}}_{lmP} = -(-1)^{l+m}\eta^{P}_{lm}\exp(2i\delta^{lm}_{P})K^{\mathrm{in}}_{lmP}, \tag{4.37}
$$

where $\delta^{lm}_{P} \in \mathcal{R}$ is the conservative scattering phase for each mode and η_{lm} is the degree of absorption/emission (i.e., the mode coefficients do not mix under scattering). Although these scattering phases and degree of absorption are defined for these abstract mode coefficients $K^{\mathrm{out/in}}_{lmP}$, they are directly related to the scattering of a GW off a Kerr BH and often employed for that purpose (see for e.g., Refs. [165, 166]). In particular, η^{P}_{lm} characterizes the dissipation due to energy flux into the horizon with the transmission factor for each mode defined as

$$
T_{lm} = 1 - |\eta^{\pm}_{lm}|^2. \tag{4.38}
$$

Absorption or emission of energy at the horizon is only nonzero when $|\eta^{P}_{lm}|$ differs from 1, and thus this is a suitable quantity to be labelled as ”degree of absorption” in the real theory.

In the effective worldline theory, we can continue to use the same quantity as the degree of absorption provided we relate the outgoing (incoming) mode coefficients $C^{lm}_{\mathcal{E}/\mathcal{B},\mathrm{out(in)}}$ of the wave-like metric perturbation to the outgoing (incoming) mode coefficients of ψ_4 i.e., $K^{\mathrm{out(in)}}_{lmP}$. In other words, relating $C^{lm}_{\mathcal{E}/\mathcal{B},\text{out(in)}}$ to $K^{\text{out(in)}}_{lmP}$ will reveal the basis in which the modes of the wave will scatter without mixing. We accomplish this by writing down the asymptotic behaviour of ψ_4 in the effective theory using its definition $\psi_4 = -R_{\mu\nu\gamma\delta}\bar{m}^\mu\bar{m}^\gamma n^\nu n^\delta$, where m^μ, $\bar{m}$, n^μ, l^μ form a null tetrad field satisfying $l^2 = m^2 = n^2 = 0 = l \cdot m = n \cdot m$, $l \cdot n = -1, m \cdot \bar{m} = 1$, where l^μ and n^μ are real vectors whereas m^μ is a complex null vector with $\bar{m}^\mu$ as its complex conjugate. In flat space, or at leading order when the background curvature may be treated as a small perturbation such as far away from the particle, we can write them in term of spherical polar coordinates as $\hat{m} = (\hat{\theta} + i\hat{\phi})/\sqrt{2}$, $n^\mu = (t^\mu - r^\mu)/\sqrt{2}$, $l^\mu = (t^\mu + \hat{r}^\mu)/\sqrt{2}$. In the effective worldline picture, we can thus evaluate ψ_4 at large distances by using the flat space-time null tetrad, using the linearized curvature due to the wave-like metric perturbation in Eq. (4.22), yielding

$$\begin{aligned} \psi_4 = \omega^2 \frac{\exp[-i\omega(t-r)]}{\omega r} \\ \times \sum_{a=\mathcal{E},\mathcal{B}} \sum_{l=2}^{\infty} i^{l-2} C^{K_{l-2}ij}_{a,out} \hat{r}_{K_{l-2}} \hat{m}_i \hat{m}_j + O\Big(\frac{1}{r^2}\Big), \end{aligned} \tag{4.39}$$

which we can rewrite as an expansion in spherical harmonics of spin weight -2 using the conventions in Eq. (4.29) as

$$\begin{aligned} \psi_4 = \omega^2 \frac{\exp[-i\omega(t-r)]}{\omega r} \sum_{a=\mathcal{E},\mathcal{B}} [\sum_{m=-2}^{2} Y^{2m}_{-2}(\theta,\phi) C^{lm}_{a,\text{out}} \\ + i \sum_{m=-3}^{3} Y^{3m}_{-2}(\theta,\phi) C^{lm}_{a,\text{out}}] + O\Big(\frac{1}{r^2}\Big), \end{aligned} \tag{4.40}$$

where we have dropped modes above $l = 3$ (hexadecapolar and above) as they are not relevant to the order of interest here. Also note that that our effective theory does not couple $l \geq 4$ modes with any of the lower modes (up to the order of interest in this work) and thus we can safely set the associated STF tensors to zero.

We can then switch to spheroidal harmonics of spin weight -2 via the relations $Y^{2m}_{-2} = S^{2m}_{-2} -$

$\epsilon\chi(2\sqrt{9-m^2})/(9\sqrt{7})S^{3m}_{-2}$, $Y^{3m}_{-2} = S^{3m}_{-2} + \epsilon\chi(2\sqrt{9-m^2})/(9\sqrt{7})S^{2}_{-2,m}$, valid at leading order in spheroidicity $= \epsilon\chi$, which is sufficient for our purposes. Also note that we have dropped the contribution to Y^{3m}_{-2} from $S^{l=4,m}_{-2}$. This gives us

$$\psi_4 = \omega^2 \frac{\exp[-i\omega(t-r)]}{\omega r} \sum_{l,m,P}^{3} C^{lm}_{P,\mathrm{out}} S^{lm}_{-2}(\theta,\phi) + O\left(\frac{1}{r^2}\right), \tag{4.41}$$

where we have defined the coefficients characterizing spheroidal modes as

$$C^{2m}_{P=1,\mathrm{out}} = \left(C^{2m}_{\mathcal{E},\mathrm{out}} + i\frac{2\epsilon\chi\sqrt{9-m^2}}{9\sqrt{7}}C^{3m}_{\mathcal{B},\mathrm{out}}\right),\ C^{2m}_{P=-1,\mathrm{out}} = \left(C^{2m}_{\mathcal{B},\mathrm{out}} + i\frac{2\epsilon\chi\sqrt{9-m^2}}{9\sqrt{7}}C^{3m}_{\mathcal{E},\mathrm{out}}\right), \tag{4.42}$$

$$C^{3m}_{P=1,\mathrm{out}} = \left(iC^{3m}_{\mathcal{B},\mathrm{out}} - \frac{2\epsilon\chi\sqrt{9-m^2}}{9\sqrt{7}}C^{2m}_{\mathcal{E},\mathrm{out}}\right),\ C^{3m}_{P=-1,\mathrm{out}} = \left(iC^{3m}_{\mathcal{E},\mathrm{out}} - \frac{2\epsilon\chi\sqrt{9-m^2}}{9\sqrt{7}}C^{2m}_{\mathcal{B},\mathrm{out}}\right), \tag{4.43}$$

and P is used to split them according to parity, with $P = 1$ for parity symmetric modes and $P = -1$ for parity antisymmetric modes. We can now compare with the known asymptotic form of ψ_4 from Eq. (4.36) to leading order in $1/r$. This gives us the simple identification between the coefficients of the outgoing modes of ψ_4 and that of the GW in effective theory as

$$K^{\mathrm{out}}_{lmP} = C^{lm}_{P,\mathrm{out}}, \tag{4.44}$$

where we used the fact that the tortoise coordinate r^* asymptotes to r in the limit $r \to \infty$. Now, we know the appropriate combination of coefficients of outgoing modes in the effective theory to use. To get a similar relation between K^{in}_{lmP} and the coefficients of incoming modes in the effective theory, the simplest way is to just guess the form by considering the limit where there is no scattering. In the real theory, this is the limit where $\eta^{P}_{lm} = 1$ and $\delta^{lm}_{P} = 0$, and we have $K^{\mathrm{up}}_{lmP} =$

$-(-1)^{l+m} K^{\text{in}}_{lmP}$. In the effective theory, this is simply when the irregular part of the wave should vanish or $C^{lm}_{\mathcal{E}/\mathcal{B},\text{irr}} = 0 \implies C^{lm}_{\mathcal{E}/\mathcal{B},\text{in}} = -C^{lm}_{\mathcal{E}/\mathcal{B},\text{in}}$, which in turn implies $C^{2m}_{P=\pm1,\text{out}} = -C^{2m}_{P=\pm1,\text{in}}$, where $C^{2m}_{P=\pm1,\text{in}}$ is defined exactly as $C^{2,m}_{P=\pm1,\text{out}}$ in Eqs. (4.42),(4.43) except after transforming out $\to$ in. Thus, we can simply identify $K^{\text{in}}_{lmP} = (-1)^{l+m} C^{2,m}_{P=\pm1,\text{in}}$. Then, the scattering phase relation in Eq. (4.37) can now be written in the effective theory simply as

$$C^{lm}_{P,\text{out}} = -\eta^P_{lm} \exp(2i\delta^{lm}_P) C^{lm}_{P,\text{in}}, \tag{4.45}$$

and the degree of absorption can be defined in the effective worldline theory as

$$1 - \eta^P_{lm} = 1 - \left| \frac{C^{lm}_{P,\text{out}}}{C^{lm}_{P,\text{in}}} \right|. \tag{4.46}$$

Note that in this way, we have defined a common quantity as the degree of absorption valid for both real and effective setups. Thus, this quantity will also serve for matching between the real and effective theories to fix the unknown tidal coefficients in the next subsection.

Essentially, comparing the form of ψ_4 in the full and effective theories at large distances has revealed to us the combination of incoming and outgoing coefficients in the spherical basis that scatter without mixing. However, unsurprisingly, for general choices of tidal coefficients, the relation between the outgoing and incoming spheroidal coefficients is not going to nicely factorize as given in Eq. (4.45). In fact, the tidal coefficients that mix the spherical $l = 2$, and $l = 3$ modes $g^i_{\mathcal{E}/\mathcal{B}}$ and $h^i_{\mathcal{E}/\mathcal{B}}$ have to be chosen on the effective theory side such that the combinations given in Eqs. (4.42), (4.43) scatter without mixing. In this work, we impose this on the effective theory by plugging in the expressions for the spherical outgoing modes from Eq. (4.35) into the LHS of Eq. (4.45) and demanding that it be proportional to the RHS, i.e., $C^{lm}_{P,\text{in}}$. We refer to this as imposing spheroidal separability on the effective theory and doing so yields the constraints

$$
\begin{aligned}
g^i_{\mathcal{B},0} &= h^i_{\mathcal{E},0} = \frac{2}{3}\chi f_{\mathcal{E},0}, \\
g^i_{\mathcal{E},0} &= h^i_{\mathcal{B},0} = -\frac{2}{3}\chi f^i_{\mathcal{B},0},
\end{aligned} \tag{4.47}
$$

which greatly reduces our list of unknown variables entering the tidal response, and fixes the ratio of the coefficients connecting the octupole(quadrupole) fields to the quadrupole(octupole) moments, i.e., the coefficients $g^i_{\mathcal{E}/\mathcal{B},0}(h^i_{\mathcal{E}/\mathcal{B},0})$, to the coefficients connecting the quadrupole fields to quadrupole moments, i.e., the coefficients $f^i_{\mathcal{E}/\mathcal{B},0}$.

Provided these relations are true, The different spheroidal modes will be scattered without mixing by the tidal moments in the effective worldline theory and we can compute the degree of absorption for the various modes using Eq. (4.46) with constraints in Eq. (4.47) to be[8]

$$
\begin{aligned}
1 - \left|\frac{C^{2m}_{P=1,\text{out}}}{C^{2m}_{P=1,\text{in}}}\right| &= -\epsilon^5 m\left[\frac{2f^1_{\mathcal{E},0}}{5} - (m^2-4)\frac{2}{15}f^3_{\mathcal{E},0}\right] \\
&\quad + \epsilon^6\left\{\frac{4f^0_{\mathcal{E},1}}{5} - (m^2-4)\left[\frac{2f^2_{\mathcal{E},1}}{15} + \frac{2f^4_{\mathcal{E},1}}{15}(m^2-1)\right]\right\} \\
&\quad + \mathcal{O}(\epsilon^7), \\
1 - \left|\frac{C^{2m}_{P=-1,\text{out}}}{C^{2m}_{P=-1,\text{in}}}\right| &= -\epsilon^5 m\left[\frac{2f^1_{\mathcal{B},0}}{5} - (m^2-4)\frac{2}{15}f^3_{\mathcal{B},0}\right] \\
&\quad + \epsilon^6\left\{\frac{4f^0_{\mathcal{B},1}}{5} - (m^2-4)\left[\frac{2f^2_{\mathcal{B},1}}{15} + \frac{2f^4_{\mathcal{B},1}}{15}(m^2-1)\right]\right\} \\
&\quad + \mathcal{O}(\epsilon^7), \\
1 - \left|\frac{C^{3m}_{P=1,\text{out}}}{C^{3m}_{P=1,\text{in}}}\right| &= 1 - \left|\frac{C^{3m}_{P=-1,\text{out}}}{C^{3m}_{P=-1,\text{in}}}\right| = \mathcal{O}(\epsilon^7),
\end{aligned} \tag{4.48}
$$

[8] We only focus on the degree of absorption and not on the conservative phase as the conservative phase also gains contributions from effects other than tidally induced multipole moments in the effective theory, for e.g., spin-induced multipole moments. A matching of the conservative phase can only be performed when all such effects are included in the solution of the scattering problem in the effective theory, which we do not.

where we find that the degree of absorption for the spheroidal $l = 3$ modes vanishes up to $O(\epsilon^7)$ in the effective theory. Also note that the coefficients $f^0_{\mathcal{E}/\mathcal{B},0}$, $f^2_{\mathcal{E}/\mathcal{B},0}$, $f^4_{\mathcal{E}/\mathcal{B},0}$, $f^1_{\mathcal{E}/\mathcal{B},1}$, $f^3_{\mathcal{E}/\mathcal{B},3}$ do not appear anywhere in the degree of absorption. These coefficients thus only add to the conservative phase, and we will see later in Eqs. (4.63), (4.64) that they behave similarly with mass/spin evolution equations as well contributing only total time derivatives to dm/dt and dJ/dt. We can now compare Eq. (4.48) with the degree of absorption derived in the real theory by solving the Teukolsky equation for η^P_{lm} and fix the coefficients that contribute to dissipation. However, because we solved the scattering problem in effective theory in flat space-time thus ignoring the nonlinear interactions between the wave and the stationary gravitatonal field of the particle, there are some subtleties in this matching process which we will have to tackle. We will very briefly outline the computation of η^P_{lm} in the real theory by solving the Teukolsky equation and then match with the result from the effective theory while keeping the subtleties in mind.

4.3.5 Matching with Teukolsky solution

In the full theory, the degree of absorption defined from the $O(1/r^6)$ expansion of ψ_4 in Eq. (4.36) as $1 - |K^{out}_{lmP}/K^{in}_{lmP}|$ can be computed from analytical solutions [217] to the Teukolsky equation [212] as follows. Following the review [217], the Teukolsky equation for ${}_{-2}\psi$ [$= (r - ia\cos(\theta))^4\psi_4$ in Boyer-Lindquist coordinates] is separable with fixed-frequency solutions given by ${}_{-2}\psi \propto e^{-i\omega t}\, S^{lm}_s(\theta, \phi, a\omega)\, {}_{-2}R_{lm\omega}(r)$, where $S^{lm}_s(\theta, \phi, a\omega)$ are spin-weighted spheroidal harmonics, and ${}_sR_{lm\omega}(r)$ is a solution to the (homogeneous) radial Teukolsky equation, with $s = -2$,

$$\left[\Delta^{-s}\frac{d}{dr}\left(\Delta^{s+1}\frac{d}{dr}\right) + \frac{K^2 - 2is(r - GM)K}{\Delta}\right.$$

$$+ 4is\omega r - {}_s\lambda_{lm}\Bigg]\, {}_sR_{\ell m\omega}(r) = 0, \tag{4.49}$$

where $\Delta = r^2 + a^2 - 2GMr$, $K = (r^2 + a^2)\omega - am$, and ${}_s\lambda_{lm}$ is the spheroidal eigenvalue. The relevant physical solutions, labelled ${}_{-2}R^{\text{in}}_{\ell m\omega}(r)$, satisfy the boundary condition demanding that they consist of purely ingoing radiation at the event horizon $r = r_+ := GM + \sqrt{(GM)^2 - a^2}$,

$$_{-2}R^{\text{in}}_{\ell m\omega} = B^{\text{trans}}_{\ell m\omega}\Delta^2 e^{-i\tilde{\omega}r_*} \quad \text{as} \quad r \to r_+, \tag{4.50}$$

where r_* is the tortoise coordinate and $\tilde{\omega} = \omega - ma/(2GMr_+)$. This fixes the asymptotic behavior at radial infinity to be of the form

$$_{-2}R^{\text{in}}_{\ell m\omega} = B^{\text{inc}}_{\ell m\omega} r^{-1} e^{-i\omega r_*} + B^{\text{ref}}_{\ell m\omega} r^3 e^{i\omega r_*} \tag{4.51}$$

$$\text{as} \quad r \to \infty,$$

where $B^{\text{inc}}_{\ell m\omega}$ and $B^{\text{ref}}_{\ell m\omega}$ [9] are the coefficients of the incident and reflected waves. The ratio $B^{\text{ref}}_{\ell m\omega}/B^{\text{inc}}_{\ell m\omega}$ is completely determined by demanding that ${}_{-2}R^{\text{in}}_{\ell m\omega}(r)$ solve the radial Teukolsky equation (4.49) with the boundary condition (4.50). We refer the reader to Ref. [217] for details of a procedure to produce the expansion of this ratio in powers of $GM\omega$. Finally, the relevant scattering phase shifts and transmission factor $\eta^P_{lm} e^{2i\delta^P_{lm\omega}}$ (equivalent to $C^{lm}_{P,\text{out}}/C^{lm}_{P,\text{in}}$ from the effective theory above) for waves of parity $P = \pm 1$ are given, e.g. as in Eq. (30) of Ref. [166], by

$$\eta^P_{lm}\exp(2i\delta^P_{lm\omega}) = (-1)^{l+1}\left(\frac{\text{Re}(C) + 12iGM\omega P}{16\omega^4}\right) \times \frac{B^{\text{ref}}_{\ell m\omega}}{B^{\text{inc}}_{\ell m\omega}}, \tag{4.52}$$

with $[\text{Re}(C)]^2$ as given in Eq. (31) of Ref. [166].

[9] Note that the above form is identical to the one used earlier in Eq. (4.36) except that the parity dependent factors have been absorbed into $B^{\text{inc}}_{lm\omega}$. As a result, the expression for the scattering phase now contains a parity-dependent factor [see Eq. (4.52)]. This maybe a more convenient convention for BHPT but the former is more transparent for matching with the effective theory.

This yields the complete expression for the degree of absorption for $l = 2$ and $l = 3$ spheroidal modes up to $\mathcal{O}(\epsilon^7)$ to be

$$
\begin{aligned}
1 - |\eta_{2m}^{P=\pm}| =& - \epsilon^5 m\left[\frac{2\mathcal{A}_0^1}{5} - (m^2-4)\frac{2}{15}\mathcal{A}_0^3\right](1+2\epsilon\pi) \\
&+ \epsilon^6\left\{\frac{4\mathcal{A}_1^0}{5} - (m^2-4)\left[\frac{2\mathcal{A}_1^2}{15} + \frac{2\mathcal{A}_1^4}{15}(m^2-1)\right]\right\} + \mathcal{O}(\epsilon^7),
\end{aligned} \tag{4.53}
$$

$$
1 - |\eta_{3m}^{P=\pm}| = \mathcal{O}(\epsilon^7), \tag{4.54}
$$

where

$$
\begin{aligned}
&\mathcal{A}_0^1 = \frac{16\chi}{45}(1+3\chi^2),\ \mathcal{A}_0^3 = -\frac{4\chi^3}{3}, &(4.55)\\
&\mathcal{A}_1^0 = \frac{16}{405}(9+9\kappa+97\chi^2+117\kappa\chi^2-6\chi^4+54\sigma\chi^4+36\chi B_2+108\chi^3B_2),\\
&\mathcal{A}_1^2 = -\frac{8}{135}(115\chi^2+135\kappa\chi^2+5\chi^4+90\kappa\chi^4-24\chi B_1+18\chi^3B_1+48\chi B_2+144\chi^3B_2),\\
&\mathcal{A}_1^4 = \frac{8}{135}(20\chi^4+45\kappa\chi^4-24\chi B_1+18\chi^3B_1+12\chi B_2+36\chi^3B_2),
\end{aligned}
$$

and we are using the notation $B_m = \mathrm{Im}[\mathrm{PolyGamma}(0, 3+im\chi/\kappa)]$, which is odd in χ, and $\kappa = \sqrt{1-\chi^2}$. Note that the degree of absorption obtained from solving the Teukolsky equation in Eqs. (4.53), (4.54) has almost exactly the same form as that obtained from the effective theory given in Eq. (4.48), with the only difference being the factor of $(1 + 2\epsilon\pi)$ next to the leading-order ϵ^5 result for $l = 2$ mode. This factor is missing in the degree of absorption derived in the effective theory in Eq. (4.48) due to us neglecting the leading-order nonlinear interaction between the GW and the gravitational field of the particle. In principle, this can be also obtained from the effective worldline theory by including the nonlinearities and regulating any resulting divergences. However, including the leading-order nonlinearities in this classical setup which we are using is a complicated task, and not very illuminating. It is easier instead to just replace the factor with 1 on the Teukolsky side by tracing its origins to the nonlinearities neglected in the scattering problem in the effective picture. We establish this explicitly for the simpler case of a scalar field scattering of a Schwarzschild BH by including the leading-order nonlinearities on the effective theory side in Appendix. C.1. There are essentially two physical processes involved in the effective theory picture, both arising from the interaction of the external wave (gravitational or otherwise) with the stationary gravitational field sourced by the particle. The first is that the value of the tidal field of the wave at the origin (location of the particle) is modified, as shown for a scalar wave in Eq. (C.19) by a factor of $(1 + \pi\epsilon)$. This in turn modifies the strength of the tidally induced multipole moment subsequently affecting the irregular (output) part of the wave and the degree of absorption. Additionally, the wave is modified in its journey away (to) the particle to (from) infinity again due to scattering off the particle's gravitational field. This factor modifies the form of the wave asymptotically far away from the particle, as shown again for a scalar wave in Eq. (C.15) in such a way that the degree of absorption is further multiplied by a factor of $(1 + \pi\epsilon)$. This result has also been derived for the case of GW amplitudes sourced by arbitrary multipole moments in Refs. [47, 249] and is seen to modify the radiated power by the square of that factor. Together, these two effects modify the leading-order degree of absorption by a factor $(1 + \epsilon\pi)^2 \approx (1 + 2\epsilon\pi) + O(\epsilon^2)$ which is seen in Eq. (4.53). We have in fact verified the presence of this factor multiplying the leading-order degree of absorption for all different l modes (for which we had the solution) for scalar, and tensor (gravitational) fields, specifically $l = 0,\ 1,\ 2,\ 3$ modes for the scalar field and $l = 2,\ 3$ for gravitational field. Thus, to match the part of the true degree of absorption which corresponds to the flat space-time scattering in the effective picture, it is sufficient to simply replace the $(1 + 2\pi\epsilon)$ factor for 1 from Eq. (4.53).

Thus, dropping the $(1+2\epsilon\pi)$ factor from Eq. (4.53), and then comparing it with Eq. (4.48), we fix the unknown coefficients to be

ff

$$
\begin{aligned}
&f^1_{\mathcal{E}/\mathcal{B},0} = \frac{16\chi}{45}(1+3\chi^2),\ f^3_{\mathcal{E}/\mathcal{B},0} = -\frac{4\chi^3}{3}, && (4.56)\\
&f^0_{\mathcal{E}/\mathcal{B},1} = \frac{16}{405}(9+9\kappa+97\chi^2+117\kappa\chi^2-6\chi^4+54\kappa\chi^4+36\chi B_2+108\chi^3 B_2),\\
&f^2_{\mathcal{E}/\mathcal{B},1} = -\frac{8}{135}(115\chi^2+135\kappa\chi^2+5\chi^4+90\kappa\chi^4-24\chi B_1+18\chi^3 B_1+48\chi B_2+144\chi^3 B_2),\\
&f^4_{\mathcal{E}/\mathcal{B},1} = \frac{8}{135}(20\chi^4+45\kappa\chi^4-24\chi B_1+18\chi^3 B_1+12\chi B_2+36\chi^3 B_2),\\
&g^i_{\mathcal{B},0} = h^i_{\mathcal{E},0} = \frac{2}{3}\chi f_{\mathcal{E},0},\\
&g^i_{\mathcal{E},0} = h^i_{\mathcal{B},0} = -\frac{2}{3}\chi f_{\mathcal{B},0}, && (4.57)
\end{aligned}
$$

where we have also restated the constraints obtained by imposing spheroidal separability from Eq. (4.47). Having fixed the (dissipative) response coefficients, we can now compute the (dissipative part of the) induced multipole moments in any setup. In particular, we can now consider the effect of induced tides in a binary system with two spinning BHs in the inspiral phase. Our focus is on computing the change in mass and angular momentum due to tidal effects in the worldline effective theory (and horizon fluxes in the real setup). In the next section, we derive general formulae for evolution equations of mass and spin and then specialize to the case of parallel-spin–quasi-circular orbits, which can then be compared with earlier results available in literature.

4.4 General expressions for evolution equations of mass and spin

In this section, we derive general formulae for computing the evolution of of mass and spin from the equations of motion. Then, we proceed to compute them explicitly using the now fixed response coefficients for the special case of parallel-spin–quasi-circular inspiral to relative 1.5PN order. We conclude this section by comparing these results with those obtained earlier in Refs. [58–60].

We can derive the formula for mass and spin evolution from the equations of motion for momentum and spin angular momentum respectively. For mass, we start with the equation of motion for momentum, i.e.,

$$\begin{aligned}\frac{Dp^\mu}{D\tau} &= -\frac{1}{2}R_{\mu\nu\rho\sigma}u^\nu S^{\rho\sigma} - \frac{1}{6}J^{\lambda\nu\rho\sigma}\nabla_\mu R_{\lambda\nu\rho\sigma} \\ &\quad - J^{\tau\lambda\nu\rho\sigma}\frac{1}{12}\nabla_\mu\nabla_\tau R_{\lambda\nu\rho\sigma},\end{aligned} \tag{4.58}$$

where we substitute the expressions for $J^{\mu\nu\rho\sigma}$ and $J^{\lambda\mu\nu\rho\sigma}$ given in Eqs. (4.7), (4.8), yielding

$$\begin{aligned}\frac{Dp^\mu}{D\tau} &= -\frac{1}{2}R_{\mu\nu\rho\sigma}u^\nu S^{\rho\sigma} - \frac{1}{2}Q^{\rho\sigma}\nabla^\mu\mathcal{E}_{\rho\sigma} - \frac{1}{2}Q_{\mathcal{B}}^{\rho\sigma}\nabla^\mu\mathcal{B}_{\rho\sigma} \\ &\quad - \frac{1}{2}Q_{\mathcal{E}}^{\rho\sigma\lambda}\nabla^\mu\mathcal{E}_{\rho\sigma\lambda} - \frac{1}{2}Q_{\mathcal{B}}^{\rho\sigma\lambda}\nabla^\mu\mathcal{B}_{\rho\sigma\lambda}.\end{aligned} \tag{4.59}$$

Now, we define in the effective worldline theory the mass m simply as $\sqrt{-p^2}$. Then we have

$$\begin{aligned}&p_\mu\frac{Dp^\mu}{D\tau} = -m\frac{dm}{d\tau} \\ &\implies \frac{dm}{d\tau} = \frac{1}{2m}p^\mu u^\nu R_{\mu\nu\rho\sigma}S^{\rho\sigma} + \frac{1}{2m}Q_{\mathcal{E}}^{\rho\sigma}(p\cdot\nabla)\mathcal{E}_{\rho\sigma} \\ &+ \frac{1}{2m}Q_{\mathcal{B}}^{\rho\sigma}(p\cdot\nabla)\mathcal{B}_{\rho\sigma} + \frac{1}{2m}Q_{\mathcal{E}}^{\rho\sigma\lambda}(p\cdot\nabla)\mathcal{E}_{\rho\sigma\lambda} \\ &+ \frac{1}{2m}Q_{\mathcal{B}}^{\rho\sigma\lambda}(p\cdot\nabla)\mathcal{B}_{\rho\sigma\lambda},\end{aligned} \tag{4.60}$$

and the first term can be shown to vanish using the relation between p^μ and u^μ if we neglect terms cubic or higher powers in curvature. They are not relevant to the relative 1.5PN order (in horizon fluxes) we are interested in this work. Similarly, we can substitute $p^\mu = mu^\mu$ in the terms with multipole moments to the order of interest to get

$$\frac{dm}{d\tau} = \frac{1}{2}Q_{\mathcal{E}}^{\rho\sigma}\dot{\mathcal{E}}_{\rho\sigma} + \frac{1}{2}Q_{\mathcal{E}}^{\rho\sigma\lambda}\dot{\mathcal{E}}_{\rho\sigma\lambda} + (\mathcal{E}\leftrightarrow\mathcal{B}) \tag{4.61}$$

which gives us the general formula for mass evolution valid to relative 1.5PN order. We expect this to match with the horizon energy flux up to any total time derivatives of functions of tidal fields, which should vanish for scattering events or for quasi periodic processes (like parallel-spin–quasi-circular inspiral which we shall consider shortly). The quadrupolar contribution to mass-change matches with that given in Ref. [61] if we identify our quadrupole tensors as twice of theirs. This is because they choose a different normalization in the tidal coupling terms. [10]

We can similarly derive the equation for spin evolution from the equation of motion for spin angular momentum, i.e.,

$$
\begin{aligned}
\frac{DS^{\mu\nu}}{D\tau} &= 2p^{[\mu}u^{\nu]} + \frac{4}{3}R^{[\mu}{}_{\tau\rho\sigma}J^{\nu\tau\rho\sigma} + \frac{2}{3}\nabla^{\lambda}R^{[\mu}{}_{\tau\rho\sigma}J_{\lambda}{}^{\nu\tau\rho\sigma} + \frac{1}{6}\nabla^{[\mu}R_{\lambda\tau\rho\sigma}J^{\nu]\lambda\tau\rho\sigma} \\
J\frac{DJ}{d\tau} = \frac{1}{2}S_{\mu\nu}\frac{DS^{\mu\nu}}{D\tau} &= \frac{2}{3}R^{\mu}{}_{\tau\rho\sigma}J^{\nu\tau\rho\sigma}S_{\mu\nu} + \frac{1}{3}\nabla^{\lambda}R^{\mu}{}_{\tau\rho\sigma}J_{\lambda}{}^{\nu\tau\rho\sigma}S_{\mu\nu} + \frac{1}{12}\nabla^{\mu}R_{\lambda\tau\rho\sigma}J^{\nu\lambda\tau\rho\sigma}S_{\mu\nu} \\
\frac{DJ}{d\tau} &= \frac{1}{J}Q^{\mu\nu}_{\mathcal{E}}\mathcal{E}_{\mu}{}^{\rho}S_{\rho\nu} + \frac{3}{2J}O^{\mu\nu\lambda}_{\mathcal{E}}\mathcal{E}_{\mu\lambda}{}^{\rho}S_{\rho\nu} + (\mathcal{E}\leftrightarrow\mathcal{B}),
\end{aligned}
\tag{4.62}
$$

where we have defined $J^2 = (1/2)S^{\mu\nu}S_{\mu\nu}$ as the magnitude of spin angular momentum of the BH. Again, the quadrupolar contribution to evolution of spin(dJ/dt) is identical to that in Ref. [61] once the multipole moments are properly identified (see footnote. 10).

Now, substituting the ansätze for the multipole moments from Eqs. (4.27) into the expressions for the evolution of mass and spin in Eqs. (4.61), (4.62). We get

$$
\begin{aligned}
\frac{dm^*}{d\tau} = \frac{m}{2}(Gm)^4\{&f^1_{\mathcal{E},0}(\dot{\mathcal{E}}^{\mu\nu}\mathcal{E}_{\mu}{}^{\rho}\hat{S}_{\nu\rho}) + f^3_{\mathcal{E},0}(\dot{\mathcal{E}}_{\mu}{}^{\rho}\mathcal{E}_{\nu}{}^{\sigma}\hat{s}^{\mu}\hat{s}^{\nu}\hat{S}_{\rho\sigma}) \\
&+ (Gm)[f^0_{\mathcal{E},1}(\dot{\mathcal{E}}^{\mu\nu}\dot{\mathcal{E}}_{\mu\nu}) + f^2_{\mathcal{E},1}(\dot{\mathcal{E}}_{\mu}{}^{\rho}\dot{\mathcal{E}}_{\nu\rho}\hat{s}^{\mu}\hat{s}^{\nu}) + f^4_{\mathcal{E},1}(\dot{\mathcal{E}}_{\mu\nu}\dot{\mathcal{E}}_{\rho\sigma}\hat{s}^{\mu}\hat{s}^{\nu}\hat{s}^{\rho}\hat{s}^{\sigma})
\end{aligned}
$$

[10] In Ref. [61], the quadrupole tidal coupling terms in the action are $Q^{\mu\nu}_{\mathcal{E}}\mathcal{E}_{\mu\nu} + (\mathcal{E}\leftrightarrow\mathcal{B})$. Thus, before comparing the expressions in this work with that in Ref. [61]. One must first transform as $Q^{\mu\nu}_{\mathcal{E}(\mathcal{B})} \to 2Q^{\mu\nu}_{\mathcal{E}(\mathcal{B})}$

$$+\xi\frac{2}{3}\chi f^1_{\mathcal{E},0}(\mathcal{B}_{\mu\rho\sigma}\dot{\mathcal{E}}^{\nu\rho}-\dot{\mathcal{B}}_{\mu\rho\sigma}\mathcal{E}^{\nu\rho})\hat{s}^\mu\hat{S}_\nu{}^\sigma+\xi\frac{2}{3}\chi f^3_{\mathcal{E},0}(\mathcal{B}_{\nu\rho\lambda}\dot{\mathcal{E}}_\mu{}^\sigma-\dot{\mathcal{B}}_{\nu\rho\lambda}\mathcal{E}_\mu{}^\sigma)\hat{s}^\mu\hat{s}^\nu\hat{s}^\rho\hat{S}_\sigma{}^\lambda]\}$$

$$+(\mathcal{E}\leftrightarrow\mathcal{B},\ \xi\to-\xi), \tag{4.63}$$

$$\frac{dJ^*}{d\tau}=\frac{M}{2}(Gm)^4\{-2f^1_{\mathcal{E},0}(\mathcal{E}_{ij}\mathcal{E}^{ij})+(3f^1_{\mathcal{E},0}-f^3_{\mathcal{E},0})(\mathcal{E}_i{}^k\mathcal{E}_{jk}\hat{s}^i\hat{s}^j)+f^3_{\mathcal{E},0}(\mathcal{E}_{ij}\hat{s}^i\hat{s}^j)^2$$

$$-(Gm)[f^0_{\mathcal{E},1}(\dot{\mathcal{E}}^{\mu\nu}\mathcal{E}_\mu{}^\rho\hat{S}_{\nu\rho})+f^2_{\mathcal{E},1}(\dot{\mathcal{E}}_\mu{}^\rho\mathcal{E}_\nu{}^\sigma\hat{s}^\mu\hat{s}^\nu\hat{S}_{\rho\sigma})$$

$$+\xi\frac{2}{3}\chi f^1_{\mathcal{E},0}(\mathcal{B}_{\mu\sigma\lambda}\mathcal{E}^{\nu\rho}\hat{s}^\mu\hat{S}_\nu{}^\sigma\hat{S}_\rho{}^\lambda)+\xi\frac{2}{3}\chi f^1_{\mathcal{E},0}(\mathcal{B}_{\mu\rho\lambda}\mathcal{E}^{\nu\rho}\hat{s}^\mu\hat{S}_\nu{}^\sigma\hat{S}_\sigma{}^\lambda)$$

$$+\xi\frac{2}{3}\chi f^3_{\mathcal{E},0}(\mathcal{B}_{\nu\rho\tau}\mathcal{E}_\mu{}^\sigma\hat{s}^\mu\hat{s}^\nu\hat{s}^\rho\hat{S}_\sigma{}^\lambda\hat{S}_\lambda{}^\tau)]\}+(\mathcal{E}\leftrightarrow\mathcal{B},\ \xi\to-\xi), \tag{4.64}$$

where dots represent covariant derivatives w.r.t proper time, $\xi = 1$, and we have imposed the constraints obtained by demanding spheroidal separability from Eq. (4.47). Additionally, we have

$$m^*=m-\frac{m}{4}(Gm)^4\{f^0_{\mathcal{E},0}(\mathcal{E}^{\mu\nu}\mathcal{E}_{\mu\nu})+f^2_{\mathcal{E},0}(\mathcal{E}_\mu{}^\rho\mathcal{E}^\sigma_{\nu\rho}\hat{s}^\mu\hat{s}^\nu)+f^4_{\mathcal{E},0}(\mathcal{E}_{\mu\nu}\mathcal{E}_{\rho\sigma}\hat{s}^\mu\hat{s}^\nu\hat{s}^\rho\hat{s}^\sigma)$$

$$+(Gm)[\xi\frac{2}{3}\chi f^0_{\mathcal{E},0}(\mathcal{B}_{\mu\nu\rho}\mathcal{E}^{\nu\rho}\hat{s}^\mu)+\xi\frac{2}{3}\chi f^2_{\mathcal{E},0}(\mathcal{B}_{\nu\rho\sigma}\mathcal{E}_\mu{}^\sigma\hat{s}^\mu\hat{s}^\nu\hat{s}^\rho)+\xi\frac{2}{3}\chi f^4_{\mathcal{E},0}(\mathcal{B}_{\rho\sigma\lambda}\mathcal{E}_{\mu\nu}\hat{s}^\mu\hat{s}^\nu\hat{s}^\rho\hat{s}^\sigma\hat{s}^\lambda)]\}$$

$$+(\mathcal{E}\leftrightarrow\mathcal{B},\ \xi\to-\xi), \tag{4.65}$$

$$J^*=J-\frac{M}{4}(GM)^5\{f^1_{\mathcal{E},1}[(\mathcal{E}^{\mu\nu}\mathcal{E}^{\rho\sigma}\hat{S}_{\mu\rho}\hat{S}_{\nu\sigma})-(\mathcal{E}^{\mu\nu}\mathcal{E}_\mu{}^\rho\hat{S}_\nu{}^\sigma\hat{S}_{\rho\sigma})]-f^3_{\mathcal{E},1}(\mathcal{E}_\mu{}^\rho\mathcal{E}_\nu{}^\sigma\hat{s}^\mu\hat{s}^\nu\hat{S}_\rho{}^\lambda\hat{S}_{\sigma\lambda})\}, \tag{4.66}$$

and we see that all the tidal coefficients that do not enter the degree of absorption in the RHS of Eq. (4.48) only shift the definition of mass and angular-momentum by quadratic functions of fields (i.e., they only contribute terms that are total-time derivatives to dm/dt and dJ/dt). Whereas the ones that do show up in degree of absorption contribute terms that cannot be absorbed as such in total time-derivatives. Thus, for any quasi periodic setup (like for parallel-spin–quasi-circular orbits) or in a scattering set up where the two particles are infinitely far in the distant past or future, the average or total change in mass/spin respectively is determined entirely by the coefficients that contribute to dissipation, which we have already fixed through comparison with the degree of absorption obtained in the real theory by solving the Teukolsky equation in Sec. 4.3.5. This is since the total-time derivative terms either vanish (when the particles are far away) or cancel (in a periodic setup). In deriving the above result, we have also used the fact that the covariant time-derivative of spin tensor and vector (which enter the ansätze) vanishes up to the relative order to which we have expanded the expressions for dm/dt and dJ/dt (i.e., up to relative 1.5PN).

The expressions for mass and spin evolution in Eqs. (4.63), (4.64) can be compared with those in Refs. [60, 61] by substituting the response coefficients from Eq. (4.56), and we indeed find that our expressions are identical at leading order in GM (i.e., the $(GM)^4$ part), but differs from Ref. [60] at next order in GM. A crucial difference in our expressions when compared with those in Ref. [60] is that octupolar tidal fields do not enter their expressions at all. Another interesting difference is that there are π^2-containing coefficients in their next-to-leading order expression for dJ/dt (and subsequently in dm/dt), whereas π^2 does not enter any of our tidal-response coefficients. However, we will see later in Sec. 4.4.2 that our expression for mass and spin evolution is consistent with Ref. [58] for the special case of a test-body in a circular orbit around a Kerr BH to relative 1.5PN order, unlike Ref. [60].

In the next section, we specialize to the parallel-spin–quasi-circular setting to compute the expression mass and spin evolution during inspiral up to 1.5PN relative to the same at leading order (4PN w.r.t leading-order flux to infinity), and compare with earlier works that produced expressions for the same.

4.4.1 Results for the special case of binaries with parallel spins in and circular orbits

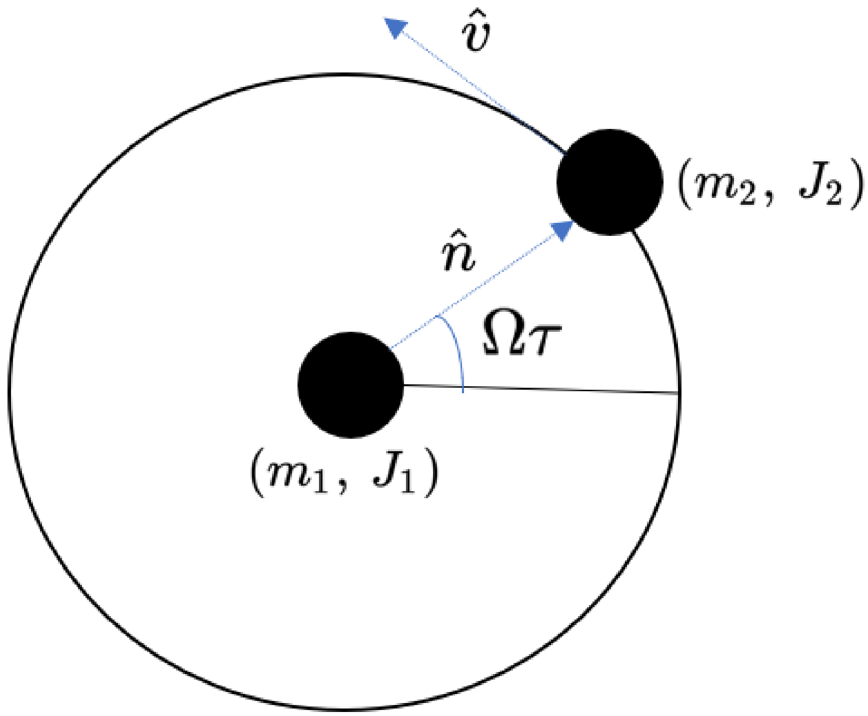

Figure 4.1: A graphic illustrating a parallel-spin–quasi-circular binary with two BHs with masses m_1 and m_2, and spins J_1 and J_2. The spin vectors are orthogonal to the orbital plane. The image is drawn in the comoving frame of BH with mass m_1, with $\hat{n}$ being the unit-vector pointing towards the other BH $(m_2,\ J_2)$ and $\hat{v}$ being the unit-vector along the other BH's velocity. Ω is the angular velocity of the other BH and hence of the tidal fields in this frame. τ is the proper time of mass m_1.

Now, we consider a system of two BHs with initial masses m_1 and m_2 and spin parameters χ_1 and χ_2. Their spins are parallel and orthogonal to the orbital plane and they are in a quasi-circular orbit. We can compute the rate of change of (initial) mass m_1 and spin $J_1 = Gm_1^2\chi_1$ averaged over one orbit using the equations Eqs. (4.61),(4.62). In this section, we will refer to the BH with initial mass m_1 and J_1 as the primary BH, and the other BH as secondary here onwards.

The tidal fields are sourced by the other BH of mass m_2 with spin parameter χ_2, although they are affected by nonlinear interaction with the fields due to the primary BH (m_1, J_1). This is most conveniently done when the tidal fields are computed in a locally flat rest frame of the primary BH (see Fig. 4.1), since then the covariant derivatives of the field w.r.t proper time can be treated simply as ordinary time derivatives . This has already been done for the quadrupolar fields $\mathcal{E}^{\mu\nu}$ and $\mathcal{B}^{\mu\nu}$ in Ref. [60], and we simply borrow the expressions from there. Rewriting the expressions here here, we have

$$\begin{aligned}
\frac{1}{2}(\mathcal{E}_{11}+\mathcal{E}_{22}) &= -\frac{m_2}{2r^3}\left[1+\frac{X_1}{2}V^2 - 6X_2\chi_2V^3 + O(V^4)\right],\\
\frac{1}{2}(\mathcal{E}_{11}-\mathcal{E}_{22}) &= -\frac{3m_2}{2r^3}\left[1+\frac{X_1-4}{2}V^2 - 2X_2\chi_2V^3 + O(V^4)\right]\cos(2\Omega\tau),\\
\mathcal{E}_{12} &= -\frac{3m_2}{2r^3}\left[1+\frac{X_1-4}{2}V^2 - 2X_2\chi_2V^3 + O(V^4)\right]\sin(2\Omega\tau),
\end{aligned} \tag{4.67}$$

$$\begin{aligned}
\mathcal{B}_{13} &= \frac{-3m_2}{r^3}V(1-X_2\chi_2V)\cos(\Omega\tau) + O(V^3),\\
\mathcal{B}_{23} &= \frac{-3m_2}{r^3}V(1-X_2\chi_2V)\sin(\Omega\tau) + O(V^3),
\end{aligned} \tag{4.68}$$

where Ω is the angular velocity of the tidal field in the primary BH frame (m_1) given by

$$\Omega = \sqrt{\frac{M}{r^3}}\left[1-\frac{1}{2}(3+\eta)V^2 - \frac{1}{2}\bar{\chi}V^3 + O(V^4)\right], \tag{4.69}$$

$$\bar{\chi} = X_1(1+X_1)\chi + 3\eta\chi_2, \tag{4.70}$$

and we are using the notation : $M = m_1 + m_2$ and $X_1 = m_1/M$, $X_2 = m_2/M$ are the mass-fractions. $\eta = X_1X_2$ is the symmetric mass ratio, r is the orbital separation in harmonic coordinates and $V = \sqrt{\frac{M}{r}}$. Here, we are working in units with $G = c = 1$, as was done in Ref. [60] so that we can easily compare our results although we have changed the notation quite a bit. Additionally, in Ref. [60], a sign factor $\epsilon = \pm 1$ was used in front of the expression for Ω, to denote whether the secondary BH was spin aligned or antialigned w.r.t the orbital angular momentum. However, we simply let the spin parameter(s) $\chi_{1,2}$ range over [-1,1] (instead of [0,1]) and always fix the orbital angular momentum to be aligned along the positive z-axis without loss of generality.

The octupolar fields were not derived in Ref. [60] since they were not relevant in their expression for the mass or spin evolution. For us, the octupolar fields do contribute to the expressions for mass and spin evolution as seen from Eqs. (4.63), (4.64). Fortunately, they (octupolar fields) are only relevant at leading order and thus can be easily computed from the test-body limit at leading post Newtonian order where the secondary BH (as test mass) is orbiting the primary BH in the limit $m_2 \ll m_1$. The formula for leading-order fields does not change from this for generic mass-ratio. We get the expressions

$$\mathcal{E}_{ijk} = -15\frac{m_2}{r^4}\hat{n}_{\langle i}\hat{n}_j\hat{n}_{k\rangle}, \tag{4.71}$$

$$\mathcal{B}_{ijk} = 30\frac{m_2}{r^4}V\epsilon_{\langle i}{}^{mn}\hat{n}_j\hat{n}_{k\rangle}\hat{n}_m\hat{v}_n, \tag{4.72}$$

$$\hat{n} = (\hat{n}_1, \hat{n}_2, \hat{n}_3) = (\cos(\Omega\tau), \sin(\Omega\tau), 0),$$

$$\hat{v} = (\hat{v}_1, \hat{v}_2, \hat{v}_3) = (-\sin(\Omega\tau), \cos(\Omega\tau), 0)$$

where n_i is the normal vector directed from the primary BH to the secondary BH in harmonic coordinates, and $\hat{v} = \dot{\hat{n}}$ is the relative velocity vector of the secondary BH w.r.t primary BH.

Now, substituting these tidal fields from Eqs. (4.67), (4.68), (4.71), and (4.72) into the formulas for mass and spin evolution in Eqs. (4.63), (4.64), with the fixed coefficients listed in Eqs. (4.56), (4.57), we get the orbit-averaged results

$$\left\langle\frac{dm_1}{d\tau}\right\rangle = \Omega(\Omega_{\rm H} - \Omega)C_V, \tag{4.73}$$

$$\left\langle \frac{dJ_1}{d\tau} \right\rangle = (\Omega_{\rm H} - \Omega) C_V, \tag{4.74}$$

$$\left\langle \frac{dA_1}{d\tau} \right\rangle = \frac{(dm_1 - \Omega_{\rm H} dJ_1)}{d\tau} \frac{8\pi}{\kappa} = \frac{-8\pi}{\kappa} (\Omega_H - \Omega)^2 C_V, \tag{4.75}$$

where $\Omega_{\rm H} = \chi_1/[2m_1(1+\kappa_1)]$, is the horizon angular velocity of the primary BH and $A_1 = 8\pi m_1^2(1+\kappa)$, is the horizon-surface area and

$$\begin{aligned} C_V = &- \frac{16}{5} m_1^2 X_1^2 \eta^2 (1+\kappa_1) V^{12} \Big\{ 1 + 3\chi_1^2 + V^2 \big(-3 + X_1 - \frac{51}{4}\chi_1^2 + 3X_1\chi_1^2 \big) \\ &+ V^3 \Big[\frac{-X_1\chi_1}{3} (64 + 60\kappa_1 + 33\chi_1^2 + 36\kappa_1\chi_1^2) - \frac{3}{2} X_2 (4 + 7\chi_1^2) \chi_2 - 8X_1 (1+\chi_1^2) B_2(\chi_1) \Big] \Big\}. \end{aligned} \tag{4.76}$$

The contributions to the definition of mass and angular momentum due to the conservative tidal coefficients as seen in Eqs. (4.65), (4.66) were removed upon averaging over an orbit. They will also not contribute in a scattering scenario provided we can set the tidal fields to zero along the worldlines of the particle asymptotically (in the distant past and future).

However, the results in Eqs. (4.73), (4.74), and (4.75) are written in terms of gauge-dependent quantities, namely r (which enters through V) and is the separation between the two bodies in harmonic coordinates. Further more, it is written in the frame of the primary BH as opposed to the more convenient PN barycentric frame (which coincides with the primary BH frame in the test-body limit for the secondary BH). Thus, before comparison, we convert the results to the PN barycentric frame using the relations

$$V = x\Big[1 + \frac{1}{6}(3-\eta)x^2 + \frac{1}{6}\tilde{\chi} x^3 + O(x^4) \Big], \tag{4.77}$$

$$t = \tau \Big[1 + \frac{1}{2}(2X_1 + 3X_2) X_2 x^2 + O(x^4) \Big], \tag{4.78}$$

where $x = (M\omega_{\rm orb})^{1/3}$ with $\omega_{\rm orb}$ is the orbital angular velocity, which is gauge invariant PN expansion parameter and $\tilde{\chi} = (2X_1^2 + 3\eta)\chi_1 + (3\eta + 2X_2^2)\chi_2$. t is the PN barycentric time and its relation to the proper time of the primary BH τ, is given in Eq. (4.78). These expressions have been taken from Eqs.(39) and (40) in Ref. [60]. Then, the expressions in Eqs. (4.73), (4.74), and (4.75) can be rewritten in the PN barycentric frame as an expansion in the gauge invariant parameter x as

$$\left\langle \frac{dm_1}{dt} \right\rangle = \Omega(\Omega_{\rm H} - \Omega) C_x, \tag{4.79}$$

$$\left\langle \frac{dJ_1}{dt} \right\rangle = (\Omega_{\rm H} - \Omega) C_x, \tag{4.80}$$

$$\left\langle \frac{dA}{dt} \right\rangle = \frac{(dm_1 - \Omega_{\rm H} dJ_1)}{dt} \frac{8\pi}{\kappa} = \frac{-8\pi}{\kappa} (\Omega_H - \Omega)^2 C_x, \tag{4.81}$$

where

$$\begin{aligned} C_x =& -\frac{16}{5} m_1^2 X_1^2 \eta^2 (1+\kappa_1) x^{12} \Bigg(1 + 3\chi_1^2 + \frac{1}{4} \big[3(2+\chi_1^2) + 2X_1(1+3\chi_1^2)(2+3X_1) \big] x^2 \\ & + x^3 \Bigg\{ \frac{1}{2}(-4+3\chi_1^2)\chi_2 - 2X_1(1+3\chi_1^2) \big[X_1(\chi_1+\chi_2) + 4B_2(\chi_1) \big] \\ & + X_1 \Bigg[-\frac{2}{3}(23+30\kappa_1)\chi_1 + (7-12\kappa_1)\chi_1^3 + 4\chi_2 + \frac{9\chi_1^2\chi_2}{2} \Bigg] \Bigg\} \Bigg). \end{aligned} \tag{4.82}$$

which can now be conveniently compared with the expressions for the same quantities given in Eq. (45) of Ref. [60]. We find that our expression for C_x for generic-mass ratios is consistent with the result [60] to NLO (to x^{14}) but not at NNLO (at x^{15}). An important visible difference is that we have no π^2-containing terms at NNLO. However, as we will see in the next subsection, it is consistent in the test body limit with earlier results computed by solving the Teukolsky equation for the curvature perturbation sourced by a test-body moving in a circular orbit around a spinning BH up to relative 1.5PN order (x^{15}).

4.4.2 The test body limit for circular orbits with parallel spins

In the special case where the other BH with mass m_2 becomes a test particle, we only evaluate the quantities to leading order in X_2, mass ratio of other particle. This is equivalent to simply setting $X_1 = 1$, $X_2 \to 0$ and thus $M = m_1 \to \infty$ such that $MX_2 = m_2$ remains constant. Then the result simplifies to

$$\begin{aligned}\frac{dm_1}{dt} =&\mathcal{F}_\infty\Bigg\{-\frac{x^5}{4}(\chi_1+3\chi_1^3)-x^7\left(\chi_1+\frac{33}{16}\chi_1^3\right)\\&+\frac{x^8}{12}\Big[6+70\chi_1^2-3\chi_1^4+6\kappa_1(1+13\chi_1^2+6\chi_1^4)+24(\chi_1+3\chi_1^3)B_2(\chi_1)\Big]\Bigg\},\\&\text{where } \mathcal{F}_\infty=\frac{32}{5}\left(\frac{m_2}{M}\right)^2x^{10} \text{ and } \Omega\frac{dJ_1}{dt}=\frac{dm_1}{dt}.\end{aligned} \tag{4.83}$$

which is consistent with the results obtained via BH perturbation theory for the case of a tiny test particle orbiting a spinning BH in Refs. [58]. This result has been produced by solving the Teukolsky equation for a perturbation sourced by a tiny nonspinning BH ($M_{\rm ext}$) around a large spinning BH M and computing the energy flux down the horizon. This result has also been reproduced in Ref. [356] and the method has been employed to push the results for flux to infinity and horizon fluxes to a very high PN order in the test-body limit (see Refs. [356–358]). It is thus reassuring that our expression for mass-loss matches with this in the appropriate limits, suggesting that our effective worldline picture is suitable for the purpose of modelling horizon-related dissipation in spinning BHs.

4.5 Effect of horizon fluxes on the waveform for circular orbits

A simple way to derive the contribution to the waveform phase from horizon fluxes for parallel-spin–quasi-circular inspiral in the adiabatic limit is via the stationary-phase approximation (SPA) [262, 263, 359]. This was used to incorporate the effect of leading-order rate of change of mass (at 2.5PN) in the waveform in the appendix of Ref. [350] and to 4 PN in Ref. [264], albeit the horizon fluxes used in Ref. [264] (which were taken from Ref. [59]) are only accurate to leading order and the contribution due to the changing mass in the expression for binding energy was not taken into account [see Eq. (4.87)]. Here, we use the same method (i.e., SPA) and extend the computation completely to 4PN order, while including all relevant effects due to the changing mass and spin and compute the phase contribution to the waveform due to horizon fluxes. We use x as the gauge-invariant–PN-counting parameter to relative 1.5PN (and absolute 4PN) order. We start from the relation

$$x = (M\omega_{\rm orb})^{\frac{1}{3}} = \left(M\frac{d\phi}{dt}\right)^{\frac{1}{3}}, \tag{4.84}$$

where ϕ is the orbital phase and $M = m_1 + m_2$ is the total mass of the system. The binding energy E of the system is given to 1.5PN order[11] (see, e.g., Ref. [350]) as

$$\begin{aligned} E = -\frac{M\eta x^2}{2}\Bigg\{1 + x^2\left(\frac{-3}{4} - \frac{\eta}{12}\right) \\ + x^3\left[\frac{8\delta\chi_a}{3} + \left(\frac{8}{3} - \frac{4\eta}{3}\right)\chi_s\right]\Bigg\}, \end{aligned} \tag{4.85}$$

[11] It is sufficient for us to include the expression for the binding energy to 1.5PN order as we are only interested in computing the waveform phase contribution due to horizon fluxes which were derived in this work to relative 1.5PN order.

where $\delta = (m_1 - m_2)/M$, $\eta = m_1 m_2/M^2$, $\chi_a = (\chi_1 - \chi_2)/2$, $\chi_s = (\chi_1 + \chi_2)/2$. Now, we use the energy balance law valid for circular orbits given by

$$\dot{E} = -\mathcal{F}_\infty - \dot{M}, \tag{4.86}$$

where $\mathcal{F}_\infty$ is the energy flux to infinity and over-dot represents derivative with respect to time. For noncircular orbits, one may have to include additional Schott terms [226]. Now, we see from Eq. (4.85) that E is a function of x, the masses m_1, m_2 and the spins χ_1, χ_2, and thus we can write

$$\begin{aligned}\dot{E} = &\frac{\partial E}{\partial x}\dot{x} + \frac{\partial E}{\partial m_1}\dot{m}_1 + \frac{\partial E}{\partial m_2}\dot{m}_2 \\ &+ \frac{\partial E}{\partial \chi_1}\dot{\chi}_1 + \frac{\partial E}{\partial \chi_2}\dot{\chi}_2,\end{aligned} \tag{4.87}$$

which, along with the balance relation, yields

$$\begin{aligned}\dot{x} = -&\left(\frac{\partial E}{\partial x}\right)^{-1} (\mathcal{F}_\infty + \dot{M} + \dot{m}_1 \partial_{m_1} E + \dot{m}_2 \partial_{m_2} E \\ &+ \dot{\chi}_1 \partial_{\chi_1} E + \dot{\chi}_2 \partial_{\chi_2 E}),\end{aligned} \tag{4.88}$$

where we can drop the terms arising from the spin-dependence as they do not contribute until relative 2.5PN order in horizon fluxes. Similarly, we can substitute the leading-order formula for E in partial derivatives with respect to m_1 and m_2 and only substitute the flux to infinity up to 1.5PN relative order to get

$$\dot{x} = -\left(\frac{\partial E}{\partial x}\right)^{-1} [\mathcal{F}_\infty^{1.5\mathrm{PN}} + \dot{M} - \frac{x^2}{2M^2}(m_2^2 \dot{m}_1 + m_1^2 \dot{m}_2)]. \tag{4.89}$$

The flux to infinity up to 1.5PN order can be found in Ref. [350]. We can then invert this expression and integrate to compute the time function $t(x)$ and orbital phase $\phi(x)$ as

$$\delta t(x) = \int \frac{1}{\dot{x}} dx, \quad \int \frac{d\phi}{dt} dt = \int \frac{x^3}{M} \frac{dt}{dx} dx = \phi(x). \tag{4.90}$$

Then, the orbital phase function $\phi(x)$ and the time function $t(x)$, can be related to the waveform phase ψ, in Fourier domain for any spherical mode m, via the relation [263]

$$\psi_{lm}(f) = 2\pi f t_f - m\phi(t_f) - \frac{\pi}{4}, \tag{4.91}$$

where f is the Fourier variable (frequency) and t_f corresponds to the time when the instantaneous GW frequency coincides with f, i.e.,

$$\frac{dm\phi}{dt}(t_f) = 2\pi f \implies x(t_f) = v = \left(\frac{2\pi M f}{m}\right)^{\frac{1}{3}}. \tag{4.92}$$

$\psi_{lm}(f)$ is a useful quantity directly relevant for detectors and we provide its correction due to the horizon fluxes explicitly as

$$\begin{aligned} \delta\psi_{lm}(f) = \frac{3}{128\eta v^5}\frac{m}{2}\Bigg[\sum_{n=5}^{8}\delta\psi_n^{(\mathrm{PN})}v^n \\ + \sum_{n=5}^{8}\delta\psi_{n(l)}^{(\mathrm{PN})}v^n log(v)\Bigg], \end{aligned} \tag{4.93}$$

$$v = \left(\frac{2\pi M f}{m}\right)^{\frac{1}{3}}, \tag{4.94}$$

where $\delta\psi_{lm}(f)$ is the correction to $\psi_{lm}(f)$ due to horizon fluxes with coefficients $\delta\psi_n^{(PN)}$ and $\delta\psi_{n(l)}^{(PN)}$ starting from 2.5PN ($n = 5$) and up to 4PN ($n = 8$) given by

$$\delta\psi_5^{(\mathrm{PN})} = -\frac{10}{9}\Big[(1-3\eta)\chi_s(1+9\chi_a^2+3\chi_s^2) + \delta(1-\eta)\chi_a(1+3\chi_a^2+9\chi_s^2)\Big], \tag{4.95}$$

$$\delta\psi_{5(l)}^{(\mathrm{PN})} = 3\delta\psi_5^{(\mathrm{PN})}, \tag{4.96}$$

$$\begin{aligned} \delta\psi_7^{(\mathrm{PN})} = \frac{5}{168}\Big\{\delta\chi_a\Big[-1667 - 4371\chi_a^2 - 13113\chi_s^2 + 616\eta^2(1+3\chi_a^2+9\chi_s^2) \\ + 5\eta(311 + 807\chi_a^2 + 2421\chi_s^2)\Big] + \chi_s\Big[840\eta^2(9\chi_a^2+3\chi_s^2+1) \\ + \eta(38331\chi_a^2 + 12777\chi_s^2 + 4889) - 13113\chi_a^2 - 4371\chi_s^2 - 1667\Big]\Big\}, \end{aligned} \tag{4.97}$$

$$\delta\psi_{7(l)}^{(\mathrm{PN})} = 0, \tag{4.98}$$

and

$$\delta\psi_{8}^{(\mathrm{PN})} = \delta\psi_{8}^{(\mathrm{PN}),a} + \delta\psi_{8}^{(\mathrm{PN}),b} + \delta\psi_{8}^{(\mathrm{PN}),c}, \tag{4.99}$$

$$\delta\psi_{8(l)}^{(\mathrm{PN})} = -3\delta\psi_{8}^{(\mathrm{PN})}, \tag{4.100}$$

with

$$\begin{aligned}
\delta\psi_{8}^{(\mathrm{PN}),a} = -\frac{5}{27}\Big\{ & 144\pi\delta(\eta-1)\chi_a^3 + 48\pi\delta(\eta-1)\chi_a + 3(278\eta^2-370\eta+75)\chi_a^4 \\
& + (-36\eta^2+213\eta-67)\chi_a^2 + \chi_s\Big[-12\delta(\eta^2+190\eta-75)\chi_a^3 \\
& + 2\delta(10\eta^2+124\eta-67)\chi_a + 432\pi(3\eta-1)\chi_a^2 + 48\pi(3\eta-1)\Big] \\
& + \chi_s^2\Big[432\pi\delta(\eta-1)\chi_a + 90(36\eta^2-62\eta+15)\chi_a^2 \\
& - 172\eta^2+303\eta-67\Big] + 3(82\eta^2-250\eta+75)\chi_s^4 \\
& + \chi_s^3\Big[12\delta(21\eta^2-130\eta+75)\chi_a + 144\pi(3\eta-1)\Big] \\
& - 12(2\eta^2-4\eta+1)\Big\},
\end{aligned} \tag{4.101}$$

$$\begin{aligned}
\delta\psi_{8}^{(\mathrm{PN}),b} = -\frac{20}{9}\Big\{ & \Big[\delta(2\eta-1)\kappa_a + (-1-2\eta^2+4\eta)\kappa_s\Big] \\
& \times\Big[1+6\chi_a^4+13\chi_s^2+6\chi_s^4+\chi_a^2(13+36\chi_s^2)\Big] \\
& - 2\Big[\kappa_a(1-4\eta+2\eta^2)+\delta(1-2\eta)\kappa_s\Big]\chi_a\chi_s\Big[13+12(\chi_a^2+\chi_s^2)\Big]\Big\},
\end{aligned} \tag{4.102}$$

$$\begin{aligned}
\delta\psi_{8}^{(\mathrm{PN}),c} = \frac{80}{9}\Big\{ & B_{2,s}\Big[\big(2\eta^2-4\eta+1\big)\chi_s\big(9\chi_a^2+3\chi_s^2+1\big) \\
& - \delta(2\eta-1)\chi_a\big(3\chi_a^2+9\chi_s^2+1\big)\Big] \\
& + B_{2,a}\Big[3\big(2\eta^2-4\eta+1\big)\chi_a^3 + 9\delta(1-2\eta)\chi_a^2\chi_s
\end{aligned}$$

$$+ \left(2\eta^2 - 4\eta + 1\right)\chi_a\left(9\chi_s^2 + 1\right) - \delta(2\eta - 1)\chi_s\left(3\chi_s^2 + 1\right)\Big]\Big\}. \tag{4.103}$$

where we have defined $\kappa_s = (\kappa_1 + \kappa_2)/2$, $\kappa_a = (\kappa_1 - \kappa_2)/2$, and $B_{2,s} = [B_2(\chi_1) + B_2(\chi_2)]/2$, $B_{2,a} = [B_2(\chi_1) - B_2(\chi_2)]/2$ for convenience. Note that the 2.5PN and 3.5PN corrections vanish for spinless case which is consistent with the fact that horizon fluxes only start at 4PN for nonspinning BHs (and 2.5PN for spinning case). We also find that the 4PN correction to the waveform phase contains functions that are nonpolynomial in the spin parameters through $\kappa = \sqrt{1 - \chi^2}$ and $B_2 = \mathrm{Im}[\mathrm{PolyGamma}(0, 3 + i2\chi/\kappa)]$, as expected from the expression for the horizon energy fluxes (or rate of change of masses) in Eq. (4.79) at relative 1.5PN order. The Fourier phase solely due to the flux to infinity (i.e., neglecting horizon fluxes) to 3.5PN can be found in Eq. (7) and Appendix A in Ref. [360]. The correction to the Fourier phase $\delta\psi_{lm}(f)$, can now be conveniently incorporated in waveform models to include the effect of horizon fluxes to next-to-next-to-leading order (up to 1.5PN relative, or 4PN absolute) during inspiral for quasi-circular aligned-spin binaries.

To get a qualitative idea of the relevance of horizon fluxes to the waveform, we can look at the correction to the orbital phase $\phi(x)$ and compute how many additional (or fewer) orbital cycles occur, as a result of the inclusion of those effects, for some specific choices of the initial masses of the BHs. We consider first the case of two initially equal-mass $m_1 = m_2 = 10M_\odot$ and equal-aligned-spin $\chi_1 = \chi_2 = \chi$ BHs, and second the case for a binary consisting of a non spinning 1.4 $M_\odot$ neutron star and a 10 $M_\odot$ BH with spin parameter χ. In the latter case, only the BH's horizon-flux contribution is considered and the neutron star is treated as a structureless particle. We then compute the additional (or fewer) number of cycles due to horizon flux(es) starting from

	$(10+10)M_\odot$, equal aligned spins $\chi_1 = \chi_2 = \chi$
0PN	603.6
1PN	59.4
1.5PN	$-51.4 + 32\chi$
2PN	$4.1 - 4.4\chi^2$
2.5PN	$-7.1 + 11.3\chi + \boxed{10^{-3}12.8(1+3\chi^2)\chi}$
3PN	$2.2 - 6.5\chi - 0.64\chi^2$
3.5PN	$-0.8 + 3.6\chi + 1.3\chi^2 - 0.4\chi^3 + \boxed{10^{-3}(8.4 + 22\chi^2)\chi}$
4PN	$\boxed{10^{-3}[-0.3(1+\kappa) - (6.7 + 1.1B_2)\chi(1+3\chi^2) - (0.4 + 3.5\kappa)\chi^2 + (9.5 - 1.6\kappa)\chi^4]}$

Table 4.1: Number of orbital cycles as the frequency (f) of the gravitational wave increases from $f = 10$Hz to the frequency at the innermost stable circular orbit (ISCO) $f_{\rm ISCO} = 1/(6^{3/2}M\pi)$Hz for equal masses (10 $M_\odot$) and equal aligned (to orbital angular momentum) spins. Recall that $\kappa = \sqrt{1-\chi^2}$. Here, B_2 = PolyGamma$(0, 3 + 2i\chi/\kappa)$ lies between 0 (at $\chi = 0$) and $\pi/2$ (at $\chi = 1$). The terms in boxes are contributions from horizon fluxes, and the remaining terms come from the flux to infinity, written here for comparison.

	$(10{+}1.4)\ M_\odot$, (BH-NS), $\chi_1 = \chi$, $\chi_2 = 0$
0PN	3587.6
1PN	213.5
1.5PN	$-181.5 + 126.2\chi$
2PN	$9.8 - 13.5\chi^2$
2.5PN	$-20.0 + 36.8\chi + \boxed{10^{-2} 9.4(1 + 3\chi^2)\chi}$
3PN	$2.3 - 18.6\chi - 0.5\chi^2$
3.5PN	$-1.8 + 10.5\chi + 3.1\chi^2 - \chi^3 + \boxed{10^{-2}(5.9 + 15.4\chi^2)\chi}$
4PN	$\boxed{10^{-2}[-0.3(1+\kappa) - (4.3 + 1.2B_2)\chi(1+3\chi^2) - (1.7 + 3.9\kappa)\chi^2 + (5.6 - 1.8\kappa)\chi^4]}$

Table 4.2: Number of orbital cycles as the frequency increases from $f = 10$Hz to the frequency at the innermost stable circular orbit (ISCO) $f_{\rm ISCO} = 1/(6^{3/2}M\pi)$Hz for a binary composed of a non-spinning 1.4 $M_\odot$ neutron star (NS) and a 10 $M_\odot$ BH with spin parameter χ. Any contributions due to the internal structure of the NS have not been included.

the minimum lower frequency of the bandwidth of LVK detectors, $\omega = \pi \times 10\text{Hz}$[12] to that of the innermost-stable circular orbit (ISCO) $\omega = \omega_{\rm ISCO} = 1/(6^{\frac{3}{2}}M)$Hz (in Schwarzschild), which generally is a good approximation of the binary's merger frequency. We use the formula

$$\mathcal{N}_{\rm GW} = \frac{\delta\phi[x = (M\omega_{\rm ISCO})^{\frac{1}{3}}] - \delta\phi[x = (M\pi \times 10\text{Hz})^{\frac{1}{3}}]}{\pi}, \tag{4.104}$$

where the correction to the orbital phase function due to horizon fluxes is obtained as shown in Eq. (4.90). We list the results obtained for the aforementioned special cases in Tables 4.1 and 4.2. In Table 4.1, we also list the contribution to the number of cycles due to the flux to infinity up to 3.5PN (but with only nonspinning contributions to flux to infinity at 3PN and 3.5PN) using the expressions for fluxes and binding energy from Ref. [350]. This is to facilitate comparison and get a qualitative understanding of the relevance of the horizon flux to the waveforms. Similar tables with flux-to-infinity contributions can be found for example in Refs. [50, 361]. There are slight numerical differences between Table 4.1 here and the tables in these works, because the final result is very sensitive to the precision used for the mass of the Sun and the gravitational constant. As clearly evident from the table, the contribution to the number of cycles from horizon fluxes (boxed terms in the table) is quite small when compared to the usual contributions from the flux to infinity even at the same PN order, although it is better for larger mass ratios. This is due to the (relatively) small numerical value of the coefficients in the horizon fluxes when compared with analogous terms in the fluxes to infinity when the masses are equal. This feature of small contribution due to the horizon fluxes has already been pointed out in Ref. [59] but it was obtained using an expression for the horizon fluxes that is only correct at leading order. This fact (relative

[12] Note that we are working in units where G=c=1.

smallness of horizon flux contributions) does not change much for other configurations of spins and masses either, at least for the frequency band of LVK detectors. Although the effect of the horizon flux on the waveform phase is small, they would need to be included when building highly accurate waveform models for next generation detectors on the ground and in space.

4.6 Conclusion

In this work, we set out to tackle the problem of including horizon-related dissipation effects in spinning BHs in an effective worldline theory, which is an important physical effect to include in precision GW predictions for future detectors. For that purpose, we wrote down an effective action with additional multipolar moment degrees of freedom which couple directly with tidal fields in the action, and are tidally induced by them in accordance with the symmetries of a Kerr BH, namely axissymmetry and parity invariance. We fixed the remaining freedom in the ansatz relating the tidal fields to the multipole moments by considering a scattering scenario wherein GWs were scattered off the effective particle and the degree of absorption was compared with that obtained from the full theory by solving the Teukolsky equation. A crucial ingredient in being able to fix the complete dissipative part of the ansatz through this method was to impose upon the effective theory the requirement that the scattering be independent for different spheroidal modes of the Weyl scalar ψ_4, which follows from the separability of the Teukolsky equation in the full theory in spheroidal harmonics with spin weight -2. Having fixed the relevant part (for horizon-related dissipation) of the ansatz in this way, we used the model to compute the orbit averaged variation in mass and spin due to horizon fluxes to relative 1.5PN order for a binary in circular orbit with parallel spins. The mass and spin rate of change derived using our effective model is consistent with the results obtained in the test-body limit in Ref. [58] to relative 1.5PN order, and with Ref. [60] for generic mass ratios up to relative 1PN order and at leading order with the generic mass ratio results in Refs. [59, 61–65]. Importantly, we have weighed in one side (specifically on the side of Ref. [58]) in the previous discrepancy in the expression for evolution of mass in a binary in the literature between Refs. [58] and [60]. While the source of the earlier discrepancy is still unclear and remains to be settled, our approach suggests that it may have something to do with including the effect of octupolar tidal fields in the evolution of mass and spin.

Having consistently modelled the horizon-related dissipation and the associated changes in mass, spin and area of the horizon in this manner, we then proceeded to compute the contribution to the phasing of the waveform due to the relative 1.5PN horizon fluxes, which is relevant to the waveform at 4PN with respect to that of the leading-order quadrupolar flux to infinity. This was done using the SPA valid in the adiabatic quasi-circular regime of interest during inspiral. We found that a qualitative measure of the contribution of the horizon fluxes, i.e., the number of cycles in the waveform as the frequency evolves from 10Hz to $f_{\rm ISCO}$ is very small (2 to 3 orders of magnitude) compared to other contributions arising from GW energy flux to infinity at the same PN orders for typical masses observed by LIGO-Virgo-KAGRA detectors.

An interesting future direction will be to use the model to derive the contribution to the waveform phasing without relying on the stationary-phase approximation to get a result valid outside of the adiabatic regime. This can be done for example by deriving the radiation-reaction forces due to the tidally-induced moments obtained from first-principles instead of relying on balance arguments. It is also of interest to consider how these results, namely the variation in mass and spin and the contribution to waveform phasing are affected in the presence of eccentricity or nonparallel spins. It may also be of interest to study possible resummations for the evolution equations of mass and spin and their contribution to the waveform phase along the lines of Refs. [347–349], now aided by an expression valid at higher (relative 1.5) PN orders for generic mass ratios. Finally, the approach used for modelling the particle in this work may be extended to generic compact bodies wherein the changes in mass and spin may occur due to tidal heating, e.g., in a viscous fluid. Parametrizing the changes in mass, spin and the subsequent contribution to waveform phasing for generic bodies could be very useful for testing the predictions of general relativity, and more specifically in the search for exotic compact bodies using next-generation GW detectors.

Acknowledgements

We thank Gustav Jakobsen, Chris Kavanagh, Gustav Mogull, Raj Patil and Khun Sang Phukon for useful discussions. We thank Chris Kavanagh in particular for sharing with us the knowledge for generating solutions to the Teukolsky equation.

Chapter 5: Dynamical tidal response of Kerr black holes from scattering amplitudes

Author[1]: *M. V. S. Saketh, Zihan Zhou, Mikhail Ivanov*

Abstract: We match scattering amplitudes in point particle effective field theory (EFT) and general relativity to extract low frequency dynamical tidal responses of rotating (Kerr) black holes to all orders in spin. In the conservative sector, we study local worldline couplings that correspond to the time-derivative expansion of the black hole tidal response function. These are dynamical (frequency-dependent) generalizations of the static Love numbers. We identify and extract couplings of three types of subleading local worldline operators: the curvature time derivative terms, the spin - curvature time derivative couplings, and quadrupole - octupole mixing operators that arise due to the violation of spherical symmetry. The first two subleading couplings are non-zero and exhibit a classical renormalization group running; we explicitly present their scheme-independent beta functions. The conservative mixing terms, however, vanish as a consequence of vanishing static Love numbers. In the non-conservative sector, we match the dissipation numbers at next-to-leading and next-to-next-to leading orders in frequency. In passing, we identify terms in the general relativity absorption probabilities that originate from tails and short-scale logarithmic corrections to the lowest order dissipation contributions.

[1]Originally published as Phys. Rev. D **109**, no.06, 064058 (2024)

5.1 Introduction

The growing list of gravitational wave (GW) events observed by the LIGO-Virgo-KAGRA collaboration has sparked a new era in the study of strongly gravitating compact objects [15, 19, 21, 23–25, 39, 335]. Parameter inference from this data requires accurate waveform templates, which must include, in particular, tidal effects [362, 363]. These effects are most prominent for neutron stars, whose static tidal deformations allow one to test their equation of state [362, 364, 365]. These practical applications motivated further theoretical studies of tidal deformations of compact bodies, especially black holes (BHs). In Newtonian theory, leading order tidal deformations of celestial bodies are captured by static Love numbers [366, 367], which depend only on the internal structure of the body. The post-Newtonian generalization of Love numbers in the case of static metric was done in [56, 57, 368]. Further generalizations to the case of spin and dynamical perturbations were made in [243, 244, 369–375] where certain conceptual issues were encountered, such as difficulties in the source-response split of the tidal moments, the presence of frame dragging, concerns about the coordinate dependence of the results, and the presence of logarithmic non-localities.

A conceptually clean definition of static Love numbers and more general tidal deformations can be given within the point particle worldline effective field theory (EFT), also known as non-relativistic perturbative general relativity (GR) [47, 48, 51, 61, 182, 197, 249, 376, 377]. In this approach, in the first approximation, a compact object is described as a point particle on a worldline. The true finite-size effects related to the internal structure are captured by local worldline couplings that start at quadratic order in curvature, e.g. for a spherically-symmetric background we have

$$S_{\text{finite-size}} = c_E M R^4 \int d\tau \, E_{\mu\nu} E^{\mu\nu} + c_B M R^4 \int d\tau \, B_{\mu\nu} B^{\mu\nu} \,, \tag{5.1}$$

where R and M are the radius and the mass of a compact body, τ is proper time, while $E_{\mu\nu}$ and $B_{\mu\nu}$ are electric and magnetic parts of the Weyl tensor. Performing linear static response calculations [378–380] one can see that the Wilson coefficients $c_{E,B}$ in (5.1) reproduce the classic definition of static Love numbers in the Newtonian limit, whereby defining the Love numbers in full GR. This definition of conservative tidal responses as worldline couplings is free of difficulties related to the non-linear structure of GR, the presence of spin[2], and gauge invariance issues. In particular, in order to include spin, one has to promote the Love numbers to spin-dependent tensors in order to account for the breaking of the spherical symmetry by the underlying gravitational background [61, 244, 374, 380]. Importantly, the non-analytic (logarithmic) corrections to the static Love numbers can readily be interpreted within the definition (5.1) as a familiar renormalization group running of Wilson coefficients. [3]Within the EFT framework, it has been shown that the static Love numbers of Scwarzschild and Kerr black holes vanish identically in four dimensional general relativity [243, 245, 246, 378–380][4], which implies a fine-tuning from the EFT perspective [400][5].

The time-dependent tides can also be consistently defined in the EFT. One can also introduce time-dependent (dynamical) Love numbers as EFT couplings in front of operators like [47, 182]

$$c_{\dot{E}} M R^6 \int d\tau \, u^\sigma \nabla_\sigma E_{\mu\nu} u^\rho \nabla_\rho E^{\mu\nu} = c_{\dot{E}} M R^6 \int d\tau \, \dot{E}^{ij} \, \dot{E}_{ij} \,, \tag{5.2}$$

[2]Note that the spin effects were included in the EFT in [2, 54, 137, 183, 184, 190, 302, 309, 311, 314, 315, 328, 330, 331, 381–399].

[3]The Love numbers of BHs in four dimensional GR do not run as a result of the fine-tuning hidden symmetry [246, 378, 400, 401]. They run, however, in higher dimensions [378].

[4]Love numbers have also been studied in the context of BHs in higher dimensions [245, 378, 402–405], supergravity solutions [406], and black string systems [405]. Non-linear static tidal Love numbers were studied in [407].

[5]Proposals for a hidden symmetry resolution of this paradox have been made in [401, 402, 408, 409].

where in the last equality we have switched to the local comoving frame. In analogy to static Love numbers, the Wilson coefficient $c_{\dot{E}}$ captures the leading order frequency-dependent conservative response to external perturbations. If the compact body carries spin, $c_{\dot{E}}$ should be promoted to a tensor. In addition, the breaking of spherical symmetry generates new local worldline couplings, e.g. [61, 175, 365, 380]

$$MR^5 \int d\tau \, \lambda_{ij,kl} E^{ij} \dot{E}_{kl} \, , \quad MR^5 \int d\tau \, (\nu)_{ij,kl,m} B^{ij} \nabla^{\langle k} E^{lm\rangle} \tag{5.3}$$

where $\lambda_{ij,kl}$ and $\nu_{ij,kl,m}$ are spin-dependent tensors. [6]The first term in Eq. (5.3) describes the leading order interaction between the spin and the curvature time derivative, while the last one captures the spin-induced quadrupole-octupole mixing.

As far as the non-conservative effects are concerned, the worldline EFT elegantly takes them into account by means of introducing internal worldline degrees of freedom that couple to ‘‘bulk’’ gravitational fields. The leading order effects of these couplings, such as the horizon absorption, superradiance, tidal torquing, heating, etc. have been extensively studied in the literature [3, 61, 197, 243, 244, 374, 380, 410–412]. In terms of the BH tidal response function, these effects may be parametrized by the so-called dissipation numbers, introduced by analogy with the Love numbers, but capturing the non-conservative part of the response. In this chapter, we will focus on their generalizations beyond the leading order.

The conservative effects associated with operators (5.2) and (5.3) are formally suppressed in the PN regime compared to the leading order (LO) static deformations, and therefore have not yet been extensively studied in the literature. [7]The non-conservative tidal effects also remain largely

[6]The symbol $\langle \ldots \rangle$ in Eq. (5.3) denotes symmetrization over relevant indices and consequent subtraction of traces.

[7]It is worth mentioning that Ref. [175] was the first one to show that the operators (5.2) are not zero for Schwarzschild black holes. Ref. [380] showed, for the first time, that the first operator in (5.3) (the dynamical Love number) is not zero for Kerr black holes. See also [200, 354, 371, 373, 413–415].

unexplored beyond the LO. There are strong reasons to consider these next-to-leading order (NLO) and next-to-next-to leading order (NNLO) tidal effects both in the conservative and dissipative sectors. In general, calculations of subleading effects put the LO results on firm ground. This is especially relevant for BHs, for which LO conservative tidal effects are absent for all multipoles, and hence the genuine finite-size tidal effects appear for the first time at NLO (for Kerr) and NNLO (for Schwarzschild) in the low frequency expansion. Since the vanishing of static (LO) Love numbers has recently attracted some attention in the context of hidden symmetries, it is worth noticing that the non-vanishing of NLO tidal couplings may provide important information about breaking mechanisms for these hidden symmetries. The higher order dynamical tidal effects could also shed light on the dispersive representation of BH tidal response function and its relation with the vanishing static Love numbers for 4D BHs [47, 182, 376, 416]. [8]

With these motivations in mind, in this work, we systematically study the frequency-dependent corrections to the tidal response function of rotating (Kerr) black holes perturbatively in $GM\omega$ (with ω being the frequency of the external source[9], and G is the Newton's constant), analogous to the post-Minkowskian (PM) expansion, up to next-to-next-to leading order (NNLO). We accomplish this by matching various EFT observables produced by tidal operators to known analytic GR results. Specifically, we match the phase shifts due to scattering of gravitational waves off Kerr black holes in the EFT and full general relativity. This on-shell matching method allows us to avoid gauge and coordinate dependence issues as the amplitudes are manifestly gauge invariant objects. For analytical expressions of the scattering phase shifts in GR, we use the black hole per-

[8] In addition to this, there is significant motivation to study dynamical responses even in the context of Newtonian fluid bodies. For example, it can provide us with a microscopic understanding of Love numbers in terms of the fluid's fundamental f-mode [367, 417]. In astrophysics, dynamical tides govern the evolution of an oscillating star which then backreact to the orbital motion [175, 418], even with resonances [419–421].

[9] In a particular case of an inspiraling binary, this would be the orbital frequency of the satellite body.

turbation theory (BHPT) methods of Mano, Suzuki, and Takasugi (MST) for the analytic solution of the Teukolsky master equation [58, 216–218, 422][10]. One important result of our calculations is that the NLO and NNLO tidal worldline couplings of Kerr BHs do not vanish and also exhibit a renormalization group running behavior, which is expected on the basis of Wilsonian naturalness and power counting [246, 378, 401]. Thus, the fine tuning of the worldline EFT for Kerr BHs takes place for static couplings only. As far as the quadrupole-octupole mixing local couplings are concerned, we will show that they vanish identically as a consequence of the vanishing of static Love numbers.

There are important technical and conceptual challenges what we have resolved in our study. First of all, we take into account the BH spin formally to all orders in its value. To that end, we use the most general expansion of the BH response function that is consistent with axial symmetry and parity, and decompose the unknown response tensors over a finite basis of master tensors. We then separate the conservative and dissipative parts by studying the behavior of the response under time reversal symmetry that includes spin flip [3, 61, 380]. The second important problem is the isolation of tidal contribution in the BHPT scattering expressions. This difficulty is overcome with the application of the near-far factorization arguments presented in [245], which we extend here to NLO and NNLO. The third important aspect is the tail effect [235, 249, 423] due to the wave scattering off the Newtonian potential before or after scattering off the tidal moments. If unaccounted for, the tail effect would obscure the matching of the dissipative numbers beyond LO. Using the EFT, we explicitly calculate tail corrections to BH absorption and identify them in the BHPT result. Finally, we systematically study the mentioned above quadrupole-octupole

[10]Note that similar in spirit matching calculations were recently performed by [3] in worldline theory and [135, 171, 174] in an on-shell-amplitudes approach.

mixing effect on the conservative and dissipative parts of the tidal response.

This chapter is structured as follows. In Sec. 5.2, we first explicitly construct the most general building blocks for the investigation of the tidal response of compact rotating objects. We then define all tidal response coefficients and discuss the wave scattering framework that will be used in this work. In Sec. 5.3, we provide a brief overview of the MST method. We also briefly present the near-far factorization arguments that allow for the extraction of the phase shift from dynamical tidal effects in BHPT. In Sec. 5.4, we match the EFT amplitude calculations with the BHPT phase shifts. This includes explicit matching of the static tidal Love numbers and the LO+NLO dissipation numbers in Sec. 5.4.1 and Sec. 5.4.2, respectively. In Sec. 5.4.3 we focus on the tail effects on the tidal response. Sec. 5.4.4 and Sec. 5.4.5 focus on the RG running of dynamical Love numbers and dissipation numbers. We present the explicit scheme-independent beta functions for relevant local couplings there. In Sec. 5.5, we match the quadrupole-octupole mixing terms in the tidal response for rotating black holes. Sec. 5.6 presents a discussion of the finite, scheme-dependent parts of the conservative couplings. Finally, in Sec. 5.7, we summarize the main results and discuss the future directions. Supplementary material is collected in two appendices. App. D.1 contains details of our tetrad choice and its relationship to that of Ref. [61]. In Appendix D.2 we set up conventions for the plane waves, spherical states, and the transformations between them.

5.2 Tidal effects in worldline effective field theory

When the relevant length scales are much larger than the size of a BH (more generally, any compact body), its dynamics can be described by a worldline EFT, which can be thought of as an expansion around the point particle approximation. In this approach, one typically writes down a universal point particle action and then perturbatively adds non-minimal coupling terms, consisting of higher powers or higher derivatives of the relevant fields to include finite size effects, e.g. spin-induced multipole moments and tidal effects. In this work, we will restrict ourselves to the tidal effects induced by linear external perturbations, which may subsequently be compared with results obtained via BHPT. These correspond to the quadratic curvature terms in the effective worldline action. In the worldline EFT finite size effects are taken into account by approximating the matter distribution inside the compact object via multipolar expansion. In the following, we will briefly go over this approach, starting with the simple case of a Schwarzschild BHs.

5.2.1 Spherically symmetric compact objects

In the case of spherical compact objects, the starting point for the action is simply that of a structure-less point particle, moving along a path that maximizes proper time given by [47, 48, 51, 61, 182, 197, 249, 376, 377]

$$S_{\rm p.p} = -M \int d\tau = -M \int d\sigma \sqrt{-\frac{dz^\mu}{d\sigma}\frac{dz^\nu}{d\sigma} g_{\mu\nu}}, \tag{5.4}$$

where M is the mass of the body, and τ is proper time. $z^\mu(\sigma)$ is the worldline with σ as a suitable parameter. p.p stands for point particle. Going forward, we will not explicitly write the dependence of the worldline coordinates z^μ on σ, and use an overdot to denote derivatives w.r.t proper-time, so that the 4-velocity $u^\mu = \dot{z}^\mu$.

As mentioned earlier, finite size effects may be included perturbatively via effective operators that consist of appropriate derivatives and powers of of the metric tensor $g_{\mu\nu}$. Due to general covariance, we cannot add terms with arbitrary dependence on derivatives of the metric, but only those consisting of the curvature tensors and their covariant derivatives. Furthermore, there is no need to add terms made up of Ricci tensors as they can be eliminated via a field redefinition. Thus, at leading order in finite size effects, we can write [307, 332]

$$S = S_{\text{p.p}} + \int d\tau\, J_Q^{\mu\nu\rho\sigma} C_{\mu\nu\rho\sigma}, \tag{5.5}$$

where $C_{\mu\nu\rho\sigma}$ is the Weyl tensor and $J_Q^{\mu\nu\rho\sigma}$ is an arbitrary tensor representing a generic quadrupole moment. The intuition for this effective action comes from studying finite size effects in Newtonian gravity, where the leading order term arises from the quadrupolar deformation of a body [367]. Extending the intuition further, we may write $J_Q^{\mu\nu\rho\sigma}$ in different forms, built of different tensors to include various finite size effects. For example, in the spinning case, we can build the tensor $J_Q^{\mu\nu\rho\sigma}$ out of the spin tensor $S_{\mu\nu}$, and the 4-velocity u^μ, to include the effect of spin-induced quadrupolar deformation. More generally, tidal deformation due to external gravitational fields can also be included by writing $J_Q^{\mu\nu\rho\sigma}$ in terms of the curvature tensors in the equations of motion. To make the parity transformation property manifest, it is convenient to first split up the finite size effective action into electric and magnetic parts as [184, 424]

$$S = S_{\text{p.p}} + \int d\tau \Big(Q_E^{\mu\nu} E_{\mu\nu} + Q_B^{\mu\nu} B_{\mu\nu} \Big), \tag{5.6}$$

where $E^{\mu\nu} = C^{\mu\rho\nu\sigma} u_\rho u_\sigma$ and $B^{\mu\nu} = (1/2)\epsilon_{\gamma\langle\mu}{}^{\alpha\beta} C_{\alpha\beta|\nu\rangle\delta} u^\gamma u^\delta$ are the electric and magnetic parts of the Weyl tensor, also referred to as the quadrupolar electric and magnetic tidal fields. By taking spatial derivatives on the quadrupolar electric and magnetic tidal fields, one can straightforwardly generalize the definition to higher order multipole moments [184].

The influence of finite size effects on the dynamics can then be easily obtained by varying the above action and substituting suitable ansatz for the quadrupole moments. In this work, we will focus on the case where the ansatz for the multipole moments is linear in the tidal fields, thus neglecting spin induced multipole moments or any non-linear effects. We can more generally extend the above action to include other multipole moments as

$$S = S_{\text{p.p}} + \sum_{\ell=2}^{\infty} \int d\tau (Q_E^{\mu_L} E_{\mu_L} + Q_B^{\mu_L} B_{\mu_L}), \tag{5.7}$$

where we are using the notation $\mu_L = \mu_1 \mu_2 ... \mu_\ell$ with multipole index ℓ. Noting that under parity transformation

$$E_{\mu_L} \to (-1)^\ell E_{\mu_L}\ , \quad B_{\mu_L} \to (-1)^{\ell+1} B_{\mu_L}\ , \tag{5.8}$$

thus the linear perturbations of different parities will not mix in this context. According to the linear response theory, we can write a general ansatz as

$$Q_E^{\mu_L} = -M(GM)^4 \sum_{n=0}^{\infty} (-1)^n (GM)^n \lambda_{\omega^n}^E \frac{d^n E^{\mu_L}}{d\tau^n},\ (E \leftrightarrow B) \tag{5.9}$$

which is an expansion about the adiabatic limit of static tides. By explicitly looking at the time-reversal symmetry, one immediately see that time-reversal even terms capture the conservative effects, e.g. tidal Love numbers, while time-reversal odd terms contribute to dissipation, e.g. horizon absorption. Transforming into the frequency domain, the above parametrization makes manifest that $GM\omega \ll 1$ is dimensionless power counting parameter. Since the multipole moments and the tidal fields are orthogonal to the 4-velocity, It is convenient to express them in an orthogonal tetrad $e^\mu_{I=0,1,2,3}$, and identify $e^\mu_0 = u^\mu$. In this way, we can replace the covariant indices μ_L with purely spatial indices i_L.

From response function to Love numbers and dissipation numbers

The time-reversal even part of the response function Eq. (5.9) can also be written as the higher dimensional operator in the worldline EFT. For example, in the case of static tides, one can get the effective action

$$S = S_{\rm p.p} - \frac{1}{2}\int d\tau M(GM)^4 \lambda^E E_{i_L} E^{i_L} + (E \leftrightarrow B)\,, \tag{5.10}$$

so the conservative tidal response is fully captured by local contact terms on the worldline EFT. $\lambda^{E/B}$ can then be identified with the Schwarzschild static tidal Love numbers that are known to be zero [56, 57, 368, 370, 378, 379]. Furthermore, the next-to-next-to-leading order (NNLO) term in Eq. (5.9), i.e. $(GM\omega)^2$ order term, is also invariant under time reversal symmetry, and therefore can be absorbed into the action via the local contact terms of the form

$$S = S_{\rm p.p} + \frac{1}{2}\int d\tau M(GM)^6 \lambda^E_{\omega^2} \dot{E}_{i_L} \dot{E}^{i_L} + (E \leftrightarrow B). \tag{5.11}$$

$\lambda^{E/B}_{\omega^2}$ will be referred to as dynamical tidal Love numbers for Schwarzschild BH.

The time-reversal odd terms, e.g. the next-to-leading order (NLO) term in Eq. (5.9)

$$Q_E^{i_L}\Big|_{\rm NLO} = M(GM)^5 \lambda^E_\omega \dot{E}^{i_L}.\ (E \leftrightarrow B). \tag{5.12}$$

cannot be absorbed into the local contact term on the worldline. We can re-write it in a non-local way as (see Ref. [246] for details)

$$S = S_{\rm p.p} - i\frac{1}{2} M(GM)^5 \lambda^E_\omega \int \frac{d\omega}{2\pi} |\omega| E_{i_L}(\omega) E^{*i_L}(\omega), \tag{5.13}$$

which reflects that the imaginary part of the effective action gives rise to non-conservative effects such as absorption. The coefficient λ^E_ω will be called a LO tidal dissipation number for Schwarzschild BH in what follows.

5.2.2 Rotating compact objects

The worldline EFT construction is conceptually similar in the spinning case, except for two critical distinctions. First, the EFT cannot be built solely upon a structure-less point particle.

Instead, it is necessary to incorporate spin-dependent interactions, which lead to the pole-dipole Mathisson-Papapetrou-Dixon (MPD) equations of motion [186–188, 425, 426]. These equations form the universal segment of the action for a body with spin. Second, the presence of spin not only modifies tidal effects but also introduces another kind of finite size effects: spin-induced multipole moments. As noted in previous studies [54, 330, 394], these two effects can be explicitly distinguished, as spin-induced multipole moments are linear in curvature, while tidal finite-size effects are quadratic in curvature. In this chapter, our focus will be strictly on the tidal effects.

Building blocks and SO(3) representation

In the spinning case, instead of simple proportionality relations as $Q_E^{ij} \sim \lambda_\omega^E E^{ij}$, we expect tensor relations of the form $Q_E^{ij} \sim (\lambda_\omega^E)^{ij}{}_{kl} E^{kl}$, where the unknown tensors in the tidal response (say λ_ω^E) can only have a non-trivial structure owing to the spin of the particle.

To parametrize the kind of tensors entering the tidal response in the spinning case, let us briefly revisit the algebraic structure of spins. In the rest frame of the central compact object, we find it beneficial to use the spin tensor S_{ij}, the Pauli-Lubanski spin vector $s^i = (1/2)\epsilon^{ijk} S_{jk}$, and the identity tensor δ_{ij} as our building blocks. The spin magnitude is defined as $J \equiv \chi G M^2 \equiv \sqrt{(1/2) S^{ij} S_{ij}}$, where χ is the dimensionless spin parameter. For sub-extremal Kerr BHs, we must require $\chi \leq 1$. In principle, one can now build up the effective action by combining these tensorial building blocks into scalar quantities. For convenience, we further introduce the unit spin tensor $\hat{S}_{ij} \equiv S_{ij}/J$, $\hat{S}^{ij}\hat{S}_{ij} = 2$ and the unit spin vector $\hat{s}^i \equiv s^i/J$, $\hat{s}^i \hat{s}_i = 1$.

Naively, one could make infinitely many combinations of building blocks $\{\hat{S}_{ij}, \hat{s}_i, \delta_{ij}\}$, to get tensors of the form $(\lambda_\omega^E)^{ij}{}_{kl}$. However, it turns out that only a finite number of them are linearly independent because of the identities

$$\begin{aligned}
&\hat{S}^{ij}\hat{s}_j = 0\,, \\
&\hat{S}^i{}_k\hat{S}^j{}_l = -\delta^i{}_l\delta^j{}_k + \delta^{ij}\delta_{kl} - \delta_{kl}\hat{s}^i\hat{s}^j + \delta^i{}_l\hat{s}^j\hat{s}_k + \delta^j{}_k\hat{s}^i\hat{s}_l - \delta^{ij}\hat{s}_k\hat{s}_l\,.
\end{aligned} \tag{5.14}$$

Since the spin breaks the SO(3) symmetry into a smaller SO(2) subgroup consisting of rotations about the spin-axis, it is convenient to organize our basis set of tensors based on the number of spin vectors and tensors used to construct them. We start from the Kronecker delta tensors with no spins and therefore respecting SO(3) invariance. Then we gradually break the SO(3) symmetry by adding additional spin vectors and tensors such that they still have axial invariance. Finally, we symmetrize and remove the traces as required for the response tensors. Specifically, in the quadrupolar case with $\ell = 2$, we are able to define the following five linearly independent basis tensors:

$$\left\{\delta^{\langle i}_{\langle k}\delta^{j\rangle}_{l\rangle},\ \hat{S}^{\langle i}{}_{\langle k}\delta^{j\rangle}_{l\rangle},\ \hat{s}^{\langle i}\hat{s}_{\langle k}\delta^{j\rangle}_{l\rangle},\hat{S}^{\langle i}{}_{\langle k}\hat{s}^{j\rangle}\hat{s}_{l\rangle},\ \hat{s}^{\langle i}\hat{s}_{\langle k}\hat{s}^{j\rangle}\hat{s}_{l\rangle}\right\}, \tag{5.15}$$

where $\langle i, j\rangle$ denotes the symmetrization and trace-removal of contained indices. Intuitively, the above base tensors can be distinguished by how many spin tensors (vectors) they have. Furthermore, according to the SO(3) representation theory, we explicitly show in App. D.2 that the above tensors can be re-rewritten into the operator form

$$\begin{aligned}
&\delta^{\langle i}_{\langle k}\delta^{j\rangle}_{l\rangle} \equiv \mathbf{I},\ \hat{S}^{\langle i}{}_{\langle k}\delta^{j\rangle}_{l\rangle} \equiv \frac{i}{2}\mathbf{J}_z,\ \hat{s}^{\langle i}\hat{s}_{\langle k}\delta^{j\rangle}_{l\rangle} \equiv -\frac{1}{6}(\mathbf{J}_z^2 - 4\,\mathbf{I}), \\
&\hat{S}^{\langle i}{}_{\langle k}\hat{s}^{j\rangle}\hat{s}_{l\rangle} \equiv -\frac{i}{6}(\mathbf{J}_z^3 - 4\mathbf{J}_z),\ \hat{s}^{\langle i}\hat{s}_{\langle k}\hat{s}^{j\rangle}\hat{s}_{l\rangle} \equiv \frac{1}{6}(\mathbf{J}_z^2 - 4\,\mathbf{I})(\mathbf{J}_z^2 - \mathbf{I}).
\end{aligned} \tag{5.16}$$

where $\mathbf{J}_z$ and $\mathbf{I}$ are respectively the (z-component) angular momentum operator and identity operator in rank-2 STF tensor space. The above equation not only makes the spin structure manifest, but also makes it easy to transform between tensor basis and spherical basis. This also makes it convenient later to switch scattering amplitudes from plane-wave basis to spherical basis.

Tensorial response function

In this chapter, our focus is on the dynamical tidal response of Kerr BHs. As a first step, we write down the following leading interactions in the quadrupolar and octupolar sectors,

$$S = S_{(0)} + \int d\tau \left[Q^E_{ij} E^{ij} + Q^B_{ij} B^{ij} + Q^E_{ijk} E^{ijk} + Q^B_{ijk} B^{ijk} \right] , \tag{5.17}$$

where we use $S_{(0)}$ for the spinning point particle effective action. Note again that we write the above action for a choice of tetrads that corresponds to a locally-flat comoving inertial frame. This basis is different from the one used in Ref. [61], and we discuss the technical differences w.r.t. this references in App. D.1. As a next step, we parametrize the electric and magnetic tidally induced multipole moments in the most general way as [3]

$$\begin{aligned}
Q^E_{ij} &= -M \Bigg[(GM)^4 (\lambda^E)_{ijkl} E^{kl} - (GM)^5 (\lambda^E_\omega)_{ijkl} \frac{D}{D\tau} E^{kl} + (GM)^6 (\lambda^E_{\omega^2})_{ijkl} \frac{D^2}{D\tau^2} E^{kl} \\
&\quad + (GM)^5 (\nu^E)_{ij\langle kl \hat{s}_m \rangle} B^{klm} + \cdots \Bigg] , \\
Q^B_{ij} &= -M \Bigg[(GM)^4 (\lambda^B)_{ijkl} B^{kl} - (GM)^5 (\lambda^B_\omega)_{ijkl} \frac{D}{D\tau} B^{kl} + (GM)^6 (\lambda^E_{\omega^2})_{ijkl} \frac{D^2}{D\tau^2} B^{kl} \\
&\quad + (GM)^5 (\nu^B)_{ij\langle kl \hat{s}_m \rangle} E^{klm} + \cdots \Bigg] , \\
Q^B_{ijk} &= -M \left[(GM)^5 \hat{s}_{\langle k} (\xi^B)_{ij\rangle lm} E^{lm} + \cdots \right] , \\
Q^E_{ijk} &= -M \left[(GM)^5 \hat{s}_{\langle k} (\xi^E)_{ij\rangle lm} B^{lm} + \cdots \right] ,
\end{aligned} \tag{5.18}$$

where we have promoted all the coefficients in Eq. (5.9) into tensors. Expanding these tensors over the master tensors from Eq. (5.16), we get

$$(\lambda^{E/B})^{ij}{}_{kl} = \Lambda^{E/B}_{\hat{s}^0} \delta^{\langle i}_{\langle k} \delta^{j\rangle}_{l\rangle} + H^{E/B}_{\hat{s}^1} \hat{S}^{\langle i}{}_{\langle k} \delta^{j\rangle}_{l\rangle} + \Lambda^{E/B}_{\hat{s}^2} \hat{s}^{\langle i} \hat{s}_{\langle k} \delta^{j\rangle}_{l\rangle} + H^{E/B}_{\hat{s}^3} \hat{s}^{\langle i} \hat{s}_{\langle k} \hat{S}^{j\rangle}{}_{l\rangle} + \Lambda^{E/B}_{\hat{s}^4} \hat{s}^{\langle i} \hat{s}_{\langle k} \hat{s}^{j\rangle} \hat{s}_{l\rangle} , \tag{5.19}$$

$$(\lambda_{\omega}^{E/B})^{ij}{}_{kl} = H^{E/B}_{\hat{s}^0,\omega}\delta^{\langle i}_{\langle k}\delta^{j\rangle}_{l\rangle} + \Lambda^{E/B}_{\hat{s}^1,\omega}\hat{S}^{\langle i}{}_{\langle k}\delta^{j\rangle}_{l\rangle} + H^{E/B}_{\hat{s}^2,\omega}\hat{s}^{\langle i}\hat{s}_{\langle k}\delta^{j\rangle}_{l\rangle} + \Lambda^{E/B}_{\hat{s}^3,\omega}\hat{s}^{\langle i}\hat{s}_{\langle k}\hat{S}^{j\rangle}{}_{l\rangle} + H^{E/B}_{\hat{s}^4,\omega}\hat{s}^{\langle i}\hat{s}_{\langle k}\hat{s}^{j\rangle}\hat{s}_{l\rangle}\,, \tag{5.20}$$

$$(\lambda_{\omega^2}^{E/B})^{ij}{}_{kl} = \Lambda^{E/B}_{\hat{s}^0,\omega^2}\delta^{\langle i}_{\langle k}\delta^{j\rangle}_{l\rangle} + H^{E/B}_{\hat{s}^1,\omega^2}\hat{S}^{\langle i}{}_{\langle k}\delta^{j\rangle}_{l\rangle} + \Lambda^{E/B}_{\hat{s}^2,\omega^2}\hat{s}^{\langle i}\hat{s}_{\langle k}\delta^{j\rangle}_{l\rangle} + H^{E/B}_{\hat{s}^3,\omega^2}\hat{s}^{\langle i}\hat{s}_{\langle k}\hat{S}^{j\rangle}{}_{l\rangle} + \Lambda^{E/B}_{\hat{s}^4,\omega^2}\hat{s}^{\langle i}\hat{s}_{\langle k}\hat{s}^{j\rangle}\hat{s}_{l\rangle}\,. \tag{5.21}$$

In this expression, all the $\Lambda^{E/B}$ terms correspond to the conservative tidal deformations, whereas all the $H^{E/B}$ terms account for the tidal dissipation. This follows from their behavior under time reversal transformations. Additionally, the above ansatz for the tidal response obeys parity invariance, which explains the absence of some other possible combinations one can add to the response :

- **Time-reversal transformation property**: In our parametrization of the response function, operators $D/D\tau$, $\hat{S}_{ij}$ and $\hat{s}^i$ are odd under time-reversal transformations. Thus, all terms with pre-coefficients $H^{E/B}$ break the time-reversal symmetry and thus correspond to tidal dissipation [11]. Similar to the discussion in the Schwarzschild case, these coefficients cannot be absorbed into local contact terms on the worldline. However, terms proportional to $\Lambda^{E/B}$ are time-reversal even and hence contribute to the conservative tidal deformations. Furthermore, for the external perturbations, the electric tidal field E_{i_L} is even under time-reversal transformation while the magnetic tidal field B_{i_L} is odd. Note that it is the behavior under time-reversal of the combination $Q^E_{i_L}E^{i_L}$ ($Q^B_{i_L}B^{i_L}$) that dictates whether a given term in the response is conservative or dissipative.

- **Parity transformation property**: The linear tidal response of Kerr BHs is parity invariant [12]. Therefore, to maintain parity invariance, the induced electric quadrupole moment

[11] In astrophysical context, this is sometimes known as tidal heating.
[12] In the case of Kerr BHs, both the background metric and the boundary conditions at the event horizon, which we

Q^E_{ij} should contain contributions from B^{klm}, but not from B^{ij}, and vice versa. As a result, we incorporate the free tensors $(\nu^{E/B})_{ijkl}$ and $(\xi^{E/B})_{ijkl}$ to encapsulate these mixing effects. We can further decompose these tensors into our spin building blocks, enabling us to consistently track time-reversal properties

$$\begin{aligned}(\nu^{E/B})^{ij}{}_{kl} = {} & \tilde{\Lambda}^{E/B}_{\hat{s}^0}\delta^{\langle i}_{\langle k}\delta^{j\rangle}_{l\rangle} + \tilde{H}^{E/B}_{\hat{s}^1}\hat{S}^{\langle i}{}_{\langle k}\delta^{j\rangle}_{l\rangle} + \tilde{\Lambda}^{E/B}_{\hat{s}^2}\hat{s}^{\langle i}\hat{s}_{\langle k}\delta^{j\rangle}_{l\rangle} \\ & + \tilde{H}^{E/B}_{\hat{s}^3}\hat{S}^{\langle i}{}_{\langle k}\hat{s}^{j\rangle}\hat{s}_{l\rangle} + \tilde{\Lambda}^{E}_{s^4}\hat{s}^{\langle i}\hat{s}_{\langle k}\hat{s}^{j\rangle}\hat{s}_{l\rangle} \ ,\end{aligned} \tag{5.22}$$

$$\begin{aligned}(\xi^{E/B})^{ij}{}_{kl} = {} & \Lambda'^{E/B}_{\hat{s}^0}\delta^{\langle i}_{\langle k}\delta^{j\rangle}_{l\rangle} + H'^{E/B}_{\hat{s}^1}\hat{S}^{\langle i}{}_{\langle k}\delta^{j\rangle}_{l\rangle} + \Lambda'^{E/B}_{\hat{s}^2}\hat{s}^{\langle i}\hat{s}_{\langle k}\delta^{j\rangle}_{l\rangle} \\ & + H'^{E/B}_{\hat{s}^3}\hat{S}^{\langle i}{}_{\langle k}\hat{s}^{j\rangle}\hat{s}_{l\rangle} + \Lambda'^{E}_{s^4}\hat{s}^{\langle i}\hat{s}_{\langle k}\hat{s}^{j\rangle}\hat{s}_{l\rangle} \ .\end{aligned} \tag{5.23}$$

Similar to the previous analysis, $\tilde{\Lambda}^{E/B}$, $\Lambda'^{E/B}$s capture the conservative tidal response while all $\tilde{H}^{E/B}$, $H'^{E/B}$s describe the dissipative tidal response.

5.2.3 Dynamical tidal Love numbers, dissipation numbers and Mixing Coefficients

Having established the symmetry properties of the tensorial tidal response function, let us now clarify some of the terminologies used.

Static tidal Love numbers and dynamical tidal Love numbers

Following previous literature, e.g. [380], we refer to the following coefficients as *static tidal Love numbers* (TLNs)

will consider during our scattering studies, respect parity invariance. Therefore, we anticipate that tidal response will also respect parity invariance. However, from the perspective of EFT, there is no fundamental principle mandating parity invariance, see discussions in [427] about the finite size effects from parity violating constituents.

$$\textbf{Static tidal Love numbers}: \quad \Lambda^{E/B}_{\hat{s}^0}, \quad \Lambda^{E/B}_{\hat{s}^2}, \quad \Lambda^{E/B}_{\hat{s}^4}. \tag{5.24}$$

As shown in [243, 245, 380], all static Love numbers of Kerr BHs vanish to all orders in the value of the BH spin. In this chapter, we generalize the conservative tidal response to the dynamical region where we have introduced 5 more parameters. We will refer to them as the *dynamical tidal Love numbers* (DTLNs),

$$\textbf{Dynamical tidal Love numbers}: \quad \Lambda^{E/B}_{\hat{s}^1,\omega}, \quad \Lambda^{E/B}_{\hat{s}^3,\omega}, \quad \Lambda^{E/B}_{\hat{s}^0,\omega^2}, \quad \Lambda^{E/B}_{\hat{s}^2,\omega^2}, \quad \Lambda^{E/B}_{\hat{s}^4,\omega^2}. \tag{5.25}$$

We show in Sec. 5.4 that all the dynamical tidal Love numbers exhibit the RG running behavior, similar to Love numbers in higher dimensions, e.g. [378, 379]. Furthermore, similar to the Schwarzschild case, all the static tidal Love numbers and DTLNs can be absorbed into the worldline effective action via local contact terms as

$$\begin{aligned} S = S_{(0)} &- \frac{1}{2}\int d\tau M(GM)^4\Big[\Lambda^E_{\hat{s}^0}E^{ij}E_{ij} + \Lambda^E_{\hat{s}^2}E^{ij}E_{kj}\hat{s}_i\hat{s}^k + \Lambda^E_{s^4}E^{ij}E_{kl}\hat{s}_i\hat{s}_j\hat{s}^k\hat{s}^l\Big] \\ &+ \frac{1}{2}\int d\tau M(GM)^5\Big[\Lambda^E_{\hat{s}^1,\omega}\hat{S}_{ik}\dot{E}^k{}_jE^{ij} + \Lambda^E_{\hat{s}^3,\omega}\hat{S}_{ik}\hat{s}_j\hat{s}_l\dot{E}^{kl}E^{ij}\Big] \\ &+ \frac{1}{2}\int d\tau M(GM)^6\Big[\Lambda^E_{\hat{s}^0,\omega^2}\dot{E}^{ij}\dot{E}_{ij} + \Lambda^E_{\hat{s}^2,\omega^2}\dot{E}^{ij}\dot{E}_{kj}\hat{s}_i\hat{s}^k + \Lambda^E_{s^4,\omega^2}\dot{E}^{ij}\dot{E}_{kl}s_is_js^ks^l\Big] \\ &+ (E \leftrightarrow B) . \end{aligned} \tag{5.26}$$

Note that this expression is missing the quadrupole-octupole mixing terms. They will be discussed shortly.

Tidal dissipation numbers

Similar to the Schwarzschild case, we call the following coefficients as leading order Kerr *tidal dissipation numbers* (TDNs)

$$\textbf{LO tidal dissipation numbers}: \quad H^{E/B}_{\hat{s}^1}, \quad H^{E/B}_{\hat{s}^3}. \tag{5.27}$$

These two numbers have been computed before with various methods [3, 61, 242, 243, 410, 411, 428–430]. In this work, we have extended the tidal response to $(GM\omega)^2$ order, so we need to introduce 5 more parameters to capture the tidal dissipations. Here, we call the following three *next-to-leading order (NLO) tidal dissipation numbers*

$$\textbf{NLO tidal dissipation numbers}: \quad H^{E/B}_{\hat{s}^0,\omega}, \quad H^{E/B}_{\hat{s}^2,\omega}, \quad H^{E/B}_{\hat{s}^4,\omega}. \tag{5.28}$$

These numbers were first matched in [3] that helped resolve the mismatch of horizon flux between Refs. [60] and [58] in the extremal-mass-ratio limit. In Sec. 5.4, we will show that these three NLO tidal dissipation numbers exhibit divergent behavior near the extremal limit, which gives large spin corrections that modify the superradiance condition. Furthermore, we also need the following *next-to-next-to-leading order (NNLO) tidal dissipation numbers*

$$\textbf{NNLO tidal dissipation numbers}: \quad H^{E/B}_{\hat{s}^1,\omega^2}, \quad H^{E/B}_{\hat{s}^3,\omega^2}. \tag{5.29}$$

In Sec. 5.4, we will show that all the NNLO tidal dissipation numbers also exhibit the RG running behavior that comes from the ultraviolet (UV) divergence in the EFT 2-loop corrections with two mass insertions. Note that the origin of the RG running here is different from that of the dynamical Love numbers.

Mixing coefficients

Consistent with the parity transformation property discussed previously, we introduced the free tensors $(\nu^{E/B})_{ijkl}$ and $(\xi^{E/B})_{ijkl}$ to capture the mixing effects. Here, we denote that the following 6 coefficients as *conservative tidal mixing numbers* (CTMNs)

$$\textbf{conservative tidal mixing numbers}: \tilde{\Lambda}^{E/B}_{\hat{s}^0}, \quad \tilde{\Lambda}^{E/B}_{\hat{s}^2}, \quad \tilde{\Lambda}^{E/B}_{\hat{s}^4}, \quad \Lambda'^{E/B}_{\hat{s}^0}, \quad \Lambda'^{E/B}_{\hat{s}^2}, \quad \Lambda'^{E/B}_{\hat{s}^4}. \tag{5.30}$$

These effect of the corresponding operators can be reproduced with the following effective action,

$$S_{\text{mixing}} = -\frac{1}{2}\left[M(GM)^5 \int d\tau E_{ij}\hat{s}^m B_{klm}(N^B)^{ij,kl} - M(GM)^5 \int d\tau B_{ij}\hat{s}^m E_{klm}(N^B)^{ij,kl}\right], \tag{5.31}$$

with

$$\begin{aligned} (N^E)^{ij,kl} &= (\nu^E)^{(ij,kl)} + (\xi^B)^{(kl,ij)}, \\ (N^B)^{(ij,kl)} &= (\nu^B)^{(ij,kl)} + (\xi^E)^{(kl,ij)}, \end{aligned} \tag{5.32}$$

where time-reversal invariance dictates that only the symmetric (under $ij \leftrightarrow kl$) parts of the tensors $(\nu^E)^{ij,kl}$, $(\xi^E)^{ij,kl}$ should contribute.

The other 4 coefficients will be referred to as *dissipative tidal mixing numbers* (DTMNs)

$$\textbf{dissipative tidal mixing numbers}: \tilde{H}^{E/B}_{\hat{s}^1}, \quad \tilde{H}^{E/B}_{\hat{s}^3}, \quad H'^{E/B}_{\hat{s}^1}, \quad H'^{E/B}_{\hat{s}^3}. \tag{5.33}$$

The first matching of these dissipative tidal mixing numbers was performed in [3]. They originate from the perturbative expansion of spheroidal harmonics in terms of spherical harmonics. Here in Sec. 5.5, we present a more straightforward way to match these coefficients in both conservative and dissipative sectors in terms of amplitudes.

5.2.4 Wave scattering off compact objects

We have completed the discussion of the various free coefficients in the dynamical tidal response for rotating (axi-symmetric, parity-preserving) compact objects. In the remaining part of the chapter, we explicitly fix these coefficients by matching the scattering amplitudes obtained in the EFT with the scattering phases obtained from BHPT. Before we go into the detailed discussion of the matching procedure, let us first set up the formalism to study the wave scatterings off compact objects. In the worldline EFT language, this corresponds to the following scattering process

$$\text{worldline} + \text{particle A} \longrightarrow \text{worldline} + \text{particle A}, \tag{5.34}$$

where we use the double solid line to denote the worldline and the yellow wavy lines for gravitons

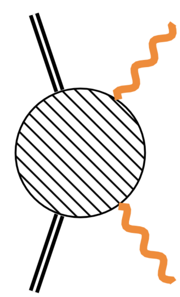

(5.35)

We choose the worldline to be static, which is motivated by the assumption that the BH mass M is much larger than the energy of the incoming massless particle ω. This also naturally leads to the power counter parameter $GM\omega \ll 1$ which we have been using in the parametrization of dynamical tidal response and will be later used as an expansion parameter in the BHPT solution. The scattering matrix now is defined as

$$_{\text{out}}\langle \boldsymbol{k}', h' | \boldsymbol{k}, h \rangle_{\text{in}} \equiv \langle \boldsymbol{k}', h' | S | \boldsymbol{k}, h \rangle \,, \tag{5.36}$$

where h is the helicity of the particle, and the normalization of the bulk particle state is $\langle \boldsymbol{k}, h | \boldsymbol{k}', h' \rangle = 2|\boldsymbol{k}| \times (2\pi)^3 \delta^3(\boldsymbol{k} - \boldsymbol{k}')\delta_{hh'}$ in four dimensional spacetime. The on-shell constraint for massless fields is $\omega^2 = \boldsymbol{k}^2$. In what follows we will formally decompose S-matrix as $S = 1 + iT$. In the worldline theory, the time translation invariance dictates that scattering processes are constrained by energy conservation. Therefore, it is convenient to define the dimensionful scattering amplitude $\mathcal{M}$ as

$$\langle \boldsymbol{k}', h' | iT | \boldsymbol{k}, h \rangle \equiv (2\pi)\delta(\omega' - \omega) \times i\mathcal{M}(\omega, \boldsymbol{k} \to \boldsymbol{k}', h \to h') \ . \tag{5.37}$$

The dimensionality of $\mathcal{M}(\omega, \boldsymbol{k} \to \boldsymbol{k}', h \to h')$ is $[\text{energy}]^{-1}$. In this chapter, we find it more convenient to calculate the scattering amplitude directly in the spherical basis. We define the spherical wave state $|\omega, \ell, m, h\rangle$ which describes the spherical wave with frequency ω, angular quantum number ℓ, magnetic quantum number m and helicity h. The normalization of such state is $\langle \omega, \ell, m, h | \omega', \ell', m', h' \rangle = (2\pi)\delta(\omega - \omega')\delta_{\ell\ell'}\delta_{mm'}\delta_{hh'}$. Now, we can compute the scattering amplitude in this basis

$$\langle \omega', \ell', m', h' | iT | \omega, \ell, m, h \rangle = (2\pi)\delta(\omega' - \omega) \times i\mathcal{A}(\omega, \ell, m, h \to \omega, \ell', m', h') \ , \tag{5.38}$$

where the scattering matrix $\mathcal{A}$ is dimensionless. The relation between $\mathcal{A}$ and $\mathcal{M}$ is given by

$$\begin{aligned} &\mathcal{A}(\omega, \ell, m, h \to \omega, \ell', m', h') \\ &= \int \frac{d^3\boldsymbol{k}_1 d^3\boldsymbol{k}_2}{(2\pi)^6 \times 4|\boldsymbol{k}_1||\boldsymbol{k}_2|} \sum_{h_1, h_2} \langle \omega, \ell', m', h' | \boldsymbol{k}_2, h_2 \rangle \mathcal{M}(\omega, \boldsymbol{k}_1 \to \boldsymbol{k}_2, h_1 \to h_2) \langle \boldsymbol{k}_1, h_1 | \omega, \ell, m, h \rangle \ , \end{aligned} \tag{5.39}$$

where the transformation matrix [61] is given by

$$\langle \omega, \ell, m, h | \boldsymbol{k}, h \rangle = (2\pi)^2 \sqrt{\frac{2\ell + 1}{2\pi\omega}} \delta(\omega - |\boldsymbol{k}|)\delta_{hh'} D^{\ell}_{mh}(\phi, \theta, 0) \ , \tag{5.40}$$

with $D^{\ell}_{mh}(\phi, \theta, 0)$ the Wigner-D matrix. Here (θ, ϕ) denotes the orientation of $\boldsymbol{k}$. In a diagonal basis, one can easily relate the amplitude with the scattering phase shift as

$$i\mathcal{A} = 1 - \eta_{\ell m} \exp(2i\delta_{\ell m}) \ , \tag{5.41}$$

where $\delta_{\ell m}$ is the elastic scattering phase shift and $1 - \eta_{\ell m}^2$ is the absorption probability. For gravitational perturbations, one can further write the polarization tensor into the spherical basis as

$$\epsilon_{ij}^{h=\pm 2}(\boldsymbol{k}) = \sum_{m=-2}^{2} \langle i, j | \ell = 2, m \rangle D^{\ell=2}_{mh=\pm 2}(\phi, \theta, 0) \ . \tag{5.42}$$

More detailed discussions are included in App. D.2.1.

Now, we are equipped with all the tools for studying the dynamical response on Kerr BHs. In the following three sections, we shall first present the wave scattering phase shifts of Kerr BHs from the analytic solution to the Teukolsky equation in Sec 5.3. Then, we will explicitly match the various tidal response coefficients mentioned before in Sec. 5.4 and Sec. 5.5.

5.3 Kerr perturbations and near-far factorization

As discussed in Sec. 5.2, various Love numbers and dissipation numbers are the unknown parameters in the ansatz for the tidal response, relating tidal fields to induced multipole moments. Love numbers may be further viewed as the Wilson coefficients in front of the quadratic-in-curvature terms in the worldline EFT. Determining these coefficients requires the computation of physical observables such as scattering amplitudes, which we then match with the corresponding results from the ultraviolet (UV) theory. In this context, as far as linear tidal effects are concerned, the UV theory is essentially linear BHPT. An important observation in this context is the so-called near-far factorization in black hole scattering amplitudes [245] that can be used to extract Love numbers, dissipation numbers, and their RG running without the interference from the post-Minkowskian correction from non-linearities of GR. In Sec. 5.3.1, we briefly review the Mano, Suzuki, and Takasugi (MST) method and discuss its factorization properties. This approach is particularly useful since it yields an explicit Taylor expansion in $GM\omega$, just as the perturbative EFT calculation. Subsequently, in Sec. 5.3.2, we present results for Kerr BHs for the quadrupolar sector $\ell = 2$.

5.3.1 Scattering of test fields by black holes and the near-far factorization

The study of wave scattering off Kerr Black Holes (BHs) is a longstanding field of research with foundational works by R. A.Matzner and others [164, 431–434]. Recently, this area of research has been revived thanks to novel insights from the S-Matrix theory, see e.g. [135, 174]. In this section, we will outline some key components of this theory relevant for the matching of dynamical Love numbers and dissipation numbers. A comprehensive discussion will be presented elsewhere [403].

We begin our analysis by considering a test field of a positive integer spin s propagating on a Kerr BH background, and choose the $\hat{z}$ direction to align with the BH spin. If the incoming wave of the test spin-s field has an incident angle of (γ, ϕ_0) with respect to the $\hat{z}$ direction, we can express the scattering differential cross section as follows

$$\frac{d\sigma}{d\Omega} = |f_s(\theta,\phi)|^2 + |g_s(\theta,\phi)|^2 \,, \tag{5.43}$$

with the helicity conserving amplitude [166, 174, 403, 435, 436]

$$f_s(\theta,\phi) = \frac{\pi}{i\omega}\sum_{\ell=s}^{\infty}\sum_{m=-\ell}^{\ell} {}_{-s}S_\ell^m(\cos\gamma, a\omega)\,{}_{-s}S_\ell^m(\cos\theta, a\omega)e^{im(\phi-\phi_0)}({}_s\eta_{\ell m}e^{2i_s\delta_{\ell m}} - 1)\times 2\,. \tag{5.44}$$

Here, ${}_{-s}S_\ell^m(\cos\theta, a\omega)$ is the spin-weighted spheroidal harmonics with orbital quantum number ℓ and magnetic quantum number m. The tortoise coordinate of Kerr BH is defined as

$$\frac{dr_*}{dr} \equiv \frac{(r^2+a^2)}{\Delta}\,, \quad \Delta \equiv (r-r_+)(r-r_-) \tag{5.45}$$

where r_+ and r_- are outer and inner horizon respectively. By analyzing the Teukolsky master variable [217, 422, 437]

$$\psi^{[-s]} = e^{-i\omega t} \sum_{\ell m} e^{im\phi} {}_{-s}S_\ell^m(\theta; a\omega)\, {}_{-s}R_{\ell m}(r) \ , \tag{5.46}$$

with the following asymptotic behavior in the tortoise coordinate

$${}_{-s}R_{\ell m}(r) \to B^{(\mathrm{inc})}_{-s\ell m} r^{-1} e^{-i\omega r_*} + B^{(\mathrm{refl})}_{-s\ell m} r^{-1+2s} e^{i\omega r_*} \ , \quad r_* \to +\infty \ , \tag{5.47}$$

we can get the scattering phase shift

$${}_s\eta_{\ell m} e^{2i_s\delta_{\ell m}} = (-1)^{\ell+1} \frac{\mathrm{Re}({}_sC_\ell^m(a\omega))}{(2\omega)^{2s}} \times \frac{B^{(\mathrm{refl})}_{-s\ell m}}{B^{(\mathrm{inc})}_{-s\ell m}} \ , \tag{5.48}$$

where ${}_sC_\ell^m(a\omega)$ is the Teukolsky-Starobinsky constant, ${}_s\delta_{\ell m}$ the elastic scattering phase shift and $1 - ({}_s\eta_{\ell m})^2$ the absorption probability. The helicity-reversing amplitude $g_s(\theta, \phi)$ vanishes for spin-0, 1 field [135, 403], but it is non-vanishing for spin-2 field due to the imaginary part of spin-2 Teukolsky-Starobinsky constant [166, 174, 403, 435, 436]

$$g_2(\theta) = \frac{\pi}{i\omega} \sum_{\ell=2}^{\infty} (-1)^\ell {}_{-2}S_\ell^m(\cos\gamma, a\omega) {}_{-2}S_\ell^m(-\cos\theta, a\omega) \times \left((-1)^{\ell+1+m} \frac{12iM\omega}{16\omega^4} \frac{B^{(\mathrm{refl})}_{-2\ell m}}{B^{(\mathrm{inc})}_{-2\ell m}} \right) \times 2 \ . \tag{5.49}$$

As the EFT is a low-frequency and long-wavelength expansion, its results have to be matched to the relevant low-frequency observables in BHPT. A solution to the Teukolsky equation in this context has been systematically developed through the matching of asymptotic expansions using the MST method [216–218, 422]. The key idea in this method is that one can construct the near zone solution based on the double-sided infinite series of hypergeometric function which converges within $r_+ \le r < \infty$ and the far zone solution based on the double-sided infinite series of Coulomb wave function which converges within $r_+ < r \le \infty$. The two solutions can be matched in the overlapping region. In order to ensure the convergence of solutions and the successful execution of the matching procedure, an auxiliary non-integer parameter, ν, is introduced. This parameter, often referred to as the ‘‘renormalized angular momentum,” is a fundamental necessity in the matched asymptotic expansion method, as mentioned in previous mathematical studies [438]. Ultimately, this process yields the wave amplitude ratio as follows

$$\frac{B^{(\mathrm{refl})}_{-s\ell m}}{B^{(\mathrm{inc})}_{-s\ell m}} = \omega^{2s} \underbrace{\frac{1 + ie^{i\pi\nu}\frac{K_{-\nu-1;-s}}{K_{\nu;-s}}}{1 - ie^{-i\pi\nu}\frac{\sin(\pi(\nu+s+i\epsilon))}{\sin(\pi(\nu-s-i\epsilon))}\frac{K_{-\nu-1;-s}}{K_{\nu;-s}}}}_{\text{Near zone}} \times \underbrace{\frac{A^{\nu}_{-;-s}}{A^{\nu}_{+;-s}} e^{i\epsilon(2\log\epsilon-(1-\kappa))}}_{\text{Far zone}}, \tag{5.50}$$

which manifestly factorizes into two parts, which is a property introduced in [245] as the near-far factorization. Here, $\epsilon = 2GM\omega$, $\kappa = \sqrt{1-\chi^2}$. The explicit expression for the functions entering this ratio can be found in [217]. By closely examining the low-frequency behavior, we find that the near zone part scales as, schematically,

$$\text{Near Zone} \sim (GM\omega)^{2\nu+1}(1 + GM\omega + (GM\omega)^2 + \cdots)\,, \tag{5.51}$$

which features a non-integer power of G for general ν, which we will shortly relate to the analytically continued angular momentum ℓ, while the far zone parts always feature only the integer power of G except for the tail effect that appears as the logarithmic function $\epsilon\log\epsilon$ in the phase shift [235, 423],

$$\text{Far Zone} \sim (GM\omega)\log(GM\omega) + (GM\omega) + (GM\omega)^2 + (GM\omega)^3 + \cdots \tag{5.52}$$

With this formula, one can naturally separate the relativistic post-Minkowskian corrections, i.e. loop diagrams in the EFT and the BH finite size effects simply by the power counting G without ambiguity. Furthermore, we find it useful to parametrize the scattering phase shift as

$${}_s\eta_{\ell m} e^{2i_s\delta_{\ell m}} = {}_s\eta_{\ell m} e^{2i_s\delta^{\mathrm{NZ}}_{\ell m}} \times e^{2i_s\delta^{\mathrm{FZ}}_{\ell m}}\,. \tag{5.53}$$

where NZ stands for near zone and FZ stands for far zone. Based on the near-far factorization, the near zone elastic phase shift can be written as

$$
{}_s\delta^{\rm NZ}_{\ell m} = \frac{1}{2}\mathrm{Arg}\left[\frac{1+ie^{i\pi\nu}\frac{K_{-\nu-1;-s}}{K_{\nu;-s}}}{1-ie^{-i\pi\nu}\frac{\sin(\pi(\nu+s+i\epsilon))}{\sin(\pi(\nu-s-i\epsilon))}\frac{K_{-\nu-1;-s}}{K_{\nu;-s}}}\right] , \tag{5.54}
$$

with far zone phase elastic shift

$$
{}_s\delta^{\rm FZ}_{\ell m} = \frac{1}{2}\mathrm{Arg}\left[\frac{A^{\nu}_{-;-s}}{A^{\nu}_{+;-s}}e^{i\epsilon(2\ln\epsilon-(1-\tilde{\kappa}))}\right] + \frac{\ell+1}{2}\pi , \tag{5.55}
$$

and the absorption probability

$$
1-{}_s\eta^2_{\ell m} = 1-\left|\frac{1+ie^{i\pi\nu}\frac{K_{-\nu-1;-s}}{K_{\nu;-s}}}{1-ie^{-i\pi\nu}\frac{\sin(\pi(\nu+s+i\epsilon))}{\sin(\pi(\nu-s-i\epsilon))}\frac{K_{-\nu-1;-s}}{K_{\nu;-s}}}\right|^2 , \tag{5.56}
$$

where we have used the non-trivial identity [216]

$$
\frac{|A^{\nu}_{-;-s}/A^{\nu}_{+;-s}|}{2^{2s}|{}_sC^m_{\ell}(a\omega)|^{-1}} = 1 \quad \text{when} \quad \nu\in\mathbb{R} \tag{5.57}
$$

This identity has been numerically tested in the Schwarzschild gravitational scatterings in [403]. For the Kerr BH, this identity has been perturbatively tested order by order in $(GM\omega)$ in [3]. Using the low-frequency expansion of the ‘‘renormalized angular momentum’’ $\nu = \ell + O((GM\omega)^2)$ around a generic angular momentum ℓ, Ref. [245], presented an on-shell proof of the vanishing of tidal Love numbers of Kerr BHs. Furthermore, that work also pointed out that the near zone elastic and inelastic absorption probabilities receive logarithmic corrections due to the low-frequency expansion of ν, i.e., schematically we have

$$
(GM\omega)^{2\nu+1}\Big|_{\nu=\ell+O((GM\omega)^2)+\dots} = (GM\omega)^{2\ell+1}(1+(GM\omega)^2\log(GM\omega)+\cdots) . \tag{5.58}
$$

Power counting in G, we notice that the near-far factorization presented in Eq. (5.50) holds for the analytically continued $\ell\in\mathbb{C}$. As discussed in [403] and [245], the near-far factorization will break down if one starts from the physical $\ell \in \mathbb{N}$ because the near zone and far zone terms now both scale as integer powers of G in the low frequency expansion. But this will not affect the study the logarithmic pieces because they always come from the near zone piece. The apparent factorization breakdown will affect the constant, scheme-dependent parts of the local worldline couplings, which we discuss separately in Sec. 5.6. Note that the factorization breakdown does not affect the matching of dissipation numbers. From Eq. (5.56), we see that the low-frequency absorption terms originate entirely from the near zone piece.

5.3.2 BHPT phase shifts

With the factorization mentioned above, we can successfully get the phase shift from tidal effects (near zone) for gravitational perturbations $\ell = 2, m = 2$ as ($r_s = 2GM$)

$$
\begin{aligned}
{}_2\eta_{22} = 1 &+ \frac{2}{225}(\chi + 3\chi^3)(r_s\omega)^5 \\
&+ \frac{1}{2025}\Bigg\{ 18\pi\left(3\chi^3 + \chi\right) - 36\left(3\chi^3 + \chi\right)\Im\left(H\left(\frac{2i\chi}{\sqrt{1-\chi^2}} - 3\right)\right) \\
&+ \left[6\left(9\sqrt{1-\chi^2} + 1\right)\chi^2 + 117\sqrt{1-\chi^2} - 97\right]\chi^2 + 9\left(\sqrt{1-\chi^2} - 1\right)\Bigg\}(r_s\omega)^6 \\
&+ \Bigg\{ -\frac{214}{23625}(\chi + 3\chi^3)\log\left(2\sqrt{1-\chi^2}\, r_s\omega\right) \\
&\quad + \frac{\pi}{2025}\Bigg[-36\left(3\chi^3 + \chi\right)\Im\left(H\left(\frac{2i\chi}{\sqrt{1-\chi^2}} - 3\right)\right) \\
&\quad + \left(6\left(9\sqrt{1-\chi^2} + 1\right)\chi^2 + 117\sqrt{1-\chi^2} - 97\right)\chi^2 + 9\left(\sqrt{1-\chi^2} - 1\right)\Bigg] \\
&\quad + \mathcal{A}_{22}(\chi)\Bigg\}(r_s\omega)^7 \,.
\end{aligned} \tag{5.59}
$$

and

$$
{}_2\delta_{22} = \left[\frac{2\chi\,(3\chi^2+1)}{225}\log\left(2\sqrt{1-\chi^2}r_s\omega\right) + \mathcal{B}_{22}(\chi)\right](r_s\omega)^6
$$
$$
+ \left\{\frac{1}{2025}\left[\left(-9-97\chi^2+6\chi^4\right)\log(2\sqrt{1-\chi^2}r_s\omega) + 18\pi(\chi+3\chi^3)\log(2\sqrt{1-\chi^2}r_s\omega)\right]\right.
$$
$$
\left. + \mathcal{B}_{22}(\chi)\pi + C_{22}(\chi)\right\}(r_s\omega)^7 . \tag{5.60}
$$

In the two expressions provided, $1-({}_2\eta_{22})^2$ calculates the absorption probability for the $\ell = 2, m = 2$ mode, while ${}_2\delta_{22}$ represents the elastic phase shift. We illustrate in Sec. 5.4 that the orange terms in Eq. (5.59) are related to the tail effect brought about by the gravitational wave scattering off the long-range Newtonian potential. Translating this into field theory terms, this effect is equivalent to a 1-loop IR divergence of the leading order tidal scattering. The purple logarithmic terms originate from the 2-loop UV divergences in the EFT loop diagrams during the computation of BH absorption, leading to the RG running of dissipation numbers. As for the green segment, the logarithmic pieces also correspond to UV divergences in the EFT loop diagrams, but they contribute to the elastic scattering pieces. For the Schwarzschild case, simple power counting in G reveals that the first logarithm will appear at G^7, i.e., at the 6-loop order. Kerr cases will be much more complicated and will be discussed in the next section.

Finally, there are also constant pieces $\mathcal{A}_{22}(\chi)$, $\mathcal{B}_{22}(\chi)$, and $C_{22}(\chi)$ alongside the logarithmic terms in the above equations. These constant pieces can be extracted analytically, but their expressions are quite cumbersome and does not provide any insights into the structure of BH scattering amplitudes. Therefore, we only present in this work their numerical estimates, given in Sec. 5.6, along with fitting formulas that may be used for all practical applications.

We also provide here the phase shift for the gravitational perturbations $\ell = 2, m = 1$ case

$$
\begin{aligned}
{}_2\eta_{21} = 1 &+ \frac{1}{900}(4\chi - 3\chi^3)(r_s\omega)^5 \\
&+ \frac{1}{8100}\Bigg\{9\pi\left(4-3\chi^2\right)\chi + 18\left(3\chi^2-4\right)\chi\Im\left(H\left(\frac{i\chi}{\sqrt{1-\chi^2}}-3\right)\right) \\
&+ \left[\left(39-54\sqrt{1-\chi^2}\right)\chi^2 + 63\sqrt{1-\chi^2} - 43\right]\chi^2 + 36\left(\sqrt{1-\chi^2}-1\right)\Bigg\}(r_s\omega)^6 \\
&+ \Bigg\{\frac{107(-4\chi+3\chi^3)}{94500}\log\left(2\sqrt{1-\chi^2}r_s\omega\right) \\
&\quad + \frac{\pi}{8100}\Bigg[18\left(3\chi^2-4\right)\chi\Im\left(H\left(\frac{i\chi}{\sqrt{1-\chi^2}}-3\right)\right) \\
&\quad + \left(\left(39-54\sqrt{1-\chi^2}\right)\chi^2 + 63\sqrt{1-\chi^2} - 43\right)\chi^2 + 36\left(\sqrt{1-\chi^2}-1\right)\Bigg] \\
&\quad + \mathcal{A}_{21}(\chi)\Bigg\}(r_s\omega)^7 \,.
\end{aligned}
\tag{5.61}
$$

and

$$
\begin{aligned}
{}_2\delta_{21} = &\left[\frac{\chi\left(4-3\chi^2\right)\log\left(2\sqrt{1-\chi^2}r_s\omega\right)}{900} + \mathcal{B}_{21}(\chi)\right](r_s\omega)^6 \\
&+ \Bigg[\frac{39\chi^4-43\chi^2-36}{8100}\log(2\sqrt{1-\chi^2}r_s\omega) + \frac{\pi}{900}\left(4-3\chi^2\right)\chi\log(2\sqrt{1-\chi^2}r_s\omega) \\
&+ \mathcal{B}_{21}(\chi)\pi + \mathcal{C}_{21}(\chi)\Bigg](r_s\omega)^7 \,.
\end{aligned}
\tag{5.62}
$$

For $\ell = 2, m = 0$ case, we have

$$
{}_2\eta_{20} = 1 - \frac{1}{225}\left(1-\chi^2\right)^2\left(\sqrt{1-\chi^2}+1\right)(r_s\omega)^6 - \frac{1}{225}\pi(1-\chi^2)^2(\sqrt{1-\chi^2}+1)(r_s\omega)^7 \,, \tag{5.63}
$$

and

$$
{}_2\delta_{20} = \left[-\frac{(1-\chi^2)^2\log(2\sqrt{1-\chi^2}r_s\omega)}{225} + \mathcal{C}_{20}(\chi)\right](r_s\omega)^7 \,. \tag{5.64}
$$

Now, with the above BHPT result, we are prepared for the matching to the EFT amplitude calculations to get the tidal response coefficients that we introduced in Sec. 5.2.3. One important aspect to remember is that BHPT phase shift values are not in the spherical harmonic basis, but rather in the spheroidal harmonic basis. This distinction becomes important when we consider non-zero spin and frequencies. In Sec. 5.5, we shall explore the impact of the mixing of spherical and spheroidal harmonics on conservative and dissipative tidal mixing numbers, crucial to accurately determinate the horizon flux at the 4PN order [3]. We also show in Sec. 5.5 that our findings in Sec. 5.4 are not affected by these mixing effects, therefore we can rely on spherical harmonics for these calculations.

5.4 Matching EFT with BHPT

The advantage of the near-far factorization is that separates scattering contributions from the near zone (tidal effect) and the far zone (background metric). We now use the worldline EFT outlined previously in Sec. 5.2 to better understand each term in the near zone scattering amplitudes of the full theory. In Sec. 5.4.1, we briefly outline the procedure of calculating scattering amplitudes in the worldline EFT and use it to match the static tidal Love numbers and LO dissipation numbers, which appear in the ansatz in Eq. (5.18) and further explicitly defined in Eqs. (5.24) and (5.27). In Sec. 5.4.2, we explicitly match the NLO dissipation numbers mentioned in Eq. (5.28) and discuss their contribution in the case of near-extremal BHs and their effect on superradiance. Then, in Sec. 5.4.3, we compute the one-loop correction to the leading order tidal scattering in the worldline EFT, corresponding to the tail effect arising from the scattering of gravitational waves off the background metric before or after scattering off the quadrupole moment. This yields an un-physical IR divergence in the EFT which, obviously, does not appear in the full theory or in any observables. This IR singularity, however, also generates a finite observable contribution associated with Sommerfield enhancement which modifies the scattering amplitude at the next order in $GM\omega$ [197]. We also find that these contributions correspond to the orange terms in BHPT, which disentangles them from genuine NLO dissipation numbers. In Sec. 5.4.4, we push similar calculation in the EFT to 2-loops for dissipation which has a physical UV divergence and leads to the RG running of the NNLO dissipation numbers corresponding to the logarithm in the purple terms in BHPT. Finally in Sec. 5.4.5, we give an interpretation to the logarithms of the green terms in BHPT. We argue that these logarithms arise from the RG flow of dynamical Love numbers introduced in Eq. (5.25). A power counting analysis shows that the EFT diagram which yields the corresponding UV divergence arises from non-linearities in GR via higher order loop corrections (6-loop order in the Scwarzschild case) to the scattering off the background metric.

5.4.1 Static Love and LO dissipation numbers

As explained in Sec. 5.2, the leading order tidal effects are included in the tidal tensor $(\lambda^{E/B})^{ij}{}_{kl}$, in which the conservative effects are encoded in static tidal Love numbers $\Lambda_{\hat{s}^0}, \Lambda_{\hat{s}^2}$ and $\Lambda_{\hat{s}^4}$ while dissipative effects are included in the LO dissipation numbers $H_{\hat{s}^1}$ and $H_{\hat{s}^3}$. Equipped with the BHPT scattering phase shift given in Sec. 5.3.2, we can get the explicit expressions for these two sets of coefficients through comparison of the scattering phases between the EFT and BHPT. Such a matching has been previously done in [380] in the off-shell way, and in [3, 61, 245] using on-shell observables. Some of these known results will be reproduced below for completeness.

We consider now the scattering of gravitational waves off a Kerr black hole in the worldline EFT and focus on the scattering phase due to the induced quadrupole moment $Q^{ij}_{E/B}(\tau)$. It couples to the graviton through in the interaction term $\int d\tau Q_E^{ij} E_{ij}$, $(E \leftrightarrow B)$ in the action. Classically, this process needs to be understood in a causal way: 1) external incoming waves with four momenta $(\omega, \boldsymbol{k}_{\rm in})$ generate the induced quadrupole in accordance with the ansatz in Eq. (5.18); 2) the quadrupole moment will radiate waves with four momenta $(\omega, \boldsymbol{k}_{\rm out})$. In the field theory language, this process can be nicely described by using the retarded Green function

$Q_{E/B}$  $Q_{E/B}$

$$\equiv i\langle [Q_{ij}^{E/B}(\tau) Q_{kl}^{E/B}(0)]\rangle \theta(\tau) \, , \tag{5.65}$$

which makes causality manifest. In the frequency domain, the retarded Green function is given by the Fourier transform of Eq. (5.18). Then, from the effective action in Eq. (5.17), the LO scattering amplitude reads

$i\mathcal{M}(\boldsymbol{k}_{\rm in} \to \boldsymbol{k}_{\rm out}, h \to h) =$ $\lambda^{E/B}$ 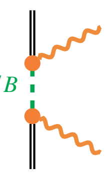

$$= -i\frac{\omega^4}{4M_{\rm pl}^2}(\lambda^E)_{ij,kl}\epsilon_h^{kl}(\boldsymbol{k}_{\rm in})\epsilon_h^{*ij}(\boldsymbol{k}_{\rm out})M(GM)^4 + \text{magnetic}, \tag{5.66}$$

where the yellow wavy lines represent gravitons. With the formulas in App. D.2, we can transform the amplitude in the plane wave basis into the spherical wave basis with definite helicities as

$$\begin{aligned} i\mathcal{A}(\omega, \ell = 2, m, h \to \ell = 2, m, h) &= -i\frac{\omega^5}{40M_{\rm pl}^2\pi}M(GM)^4 \\ &\times \left[\Lambda_{\hat{s}0}^E + \frac{1}{2}imH_{\hat{s}1}^E + \frac{1}{6}(m^2-4)\Big(-\Lambda_{\hat{s}2}^E - imH_{\hat{s}3}^E + \Lambda_{\hat{s}4}^E(m^2-1)\Big)\right] \\ &+ \text{magnetic} \, . \end{aligned} \tag{5.67}$$

where we have used the operator form of the tidal response tensor $\lambda_{kl}^{ij} = \langle i, j|\boldsymbol{\Lambda}|k, l\rangle$ with

$$\boldsymbol{\Lambda} = \Lambda_{\hat{s}^0} + i\frac{1}{2}H_{\hat{s}^1}\mathbf{J}_z + \frac{1}{6}(\mathbf{J}_z^2 - 4)[-\Lambda_{\hat{s}^2} - i\mathbf{J}_z H_{\hat{s}^3} + \Lambda_{\hat{s}^4}(\mathbf{J}_z^2 - 1)] \, , \tag{5.68}$$

given in App. D.2. By matching this expression to the BHPT phase shift in Sec. 5.3.2

$$i\mathcal{A}(\omega, \ell = 2, m, h \to \ell = 2, m, h) = 1 - {}_2\eta_{2m}\exp(2i{}_2\delta_{2m}) \tag{5.69}$$

we can get thex vanishing of Kerr Love numbers

$$\Lambda^{E/B}_{\hat{s}^0} = \Lambda^{E/B}_{\hat{s}^2} = \Lambda^{E/B}_{\hat{s}^4} = 0\,, \tag{5.70}$$

while the dissipation numbers are given by

$$H^{E/B}_{\hat{s}^1} = -\frac{8}{45}(\chi + 3\chi^3)\,, \quad H^{E/B}_{\hat{s}^3} = \frac{2}{3}\chi^3\,. \tag{5.71}$$

It is important here also to mention that one can also get the above results from the near zone approximation established by A.A.Starobinksy and D.N.Page in [242, 410, 411, 428].

5.4.2 NLO dissipation numbers: Large spin contribution and shrinking superradiance parameter space

In this section, we go beyond leading order Love and dissipation numbers and compute the NLO dissipation numbers that appear in the scattering phase at $\mathcal{O}\Big((r_s\omega)^6\Big)$. We first reproduce the results of [3]. Then we discuss its relationship to the so-called superradiance factor recently discussed in [243, 380] in the context of tidal responses. Very similar to the calculation in the previous section, we immediately get the scattering amplitude from Eq. (5.17) and (5.18)

$$i\mathcal{M}(\boldsymbol{k}_{\rm in} \to \boldsymbol{k}_{\rm out}, h \to h) = \lambda^{E/B}_{\omega}$$

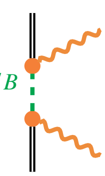

$$= \frac{\omega^5}{4M_{\rm pl}^2}(\lambda^E_\omega)^{ij,kl}\epsilon^{kl}_h(\boldsymbol{k}_{\rm in})\epsilon^{*ij}_h(\boldsymbol{k}_{\rm out})M(GM)^5 + \text{magnetic}\,. \tag{5.72}$$

Transforming this expression into the spherical basis states with definite helicity and using the tidal response tensor $(\lambda_\omega)^{ij}_{kl} = \langle i, j|\boldsymbol{\Lambda}_\omega|k, l\rangle$ with

$$\boldsymbol{\Lambda}_\omega = H_{\hat{s}^0,\omega} + i\frac{1}{2}\Lambda_{\hat{s}^1,\omega}\mathbf{J}_z + \frac{1}{6}(\mathbf{J}_z^2 - 4)\left[-H_{\hat{s}^2,\omega} - i\mathbf{J}_z\Lambda_{\hat{s}^3,\omega} + H_{\hat{s}^4,\omega}(\mathbf{J}_z^2 - 1)\right]\,, \tag{5.73}$$

we get

$$
\begin{aligned}
i\mathcal{A}(\omega, \ell=2, m, h \to \ell=2, m, h) &= \frac{\omega^6}{40M_{\rm pl}^2\pi} M(GM)^5 \\
&\times \left[H^E_{\hat{s}^0} + \frac{1}{2} i m \Lambda^E_{\hat{s}^1} + \frac{1}{6}(m^2-4)\left(-H^E_{\hat{s}^2} - i m \Lambda^E_{\hat{s}^3} + H^E_{\hat{s}^4}(m^2-1)\right)\right] \\
&+ \text{magnetic}\,.
\end{aligned}
\tag{5.74}
$$

As we expected, the conservative response coefficient and the dissipation coefficient switches their spin dependence due to the additional time derivatives which produces an additional factor of ω. We will discuss the conservative part in detail in in Sec. 5.4.5. Now let us focus on the dissipative part. After matching the EFT expression above to the BHPT phase shift, we get

$$
\begin{aligned}
H^{E/B}_{\hat{s}^0,\omega} &= \frac{8}{405}\left(9 + 9\kappa + 97\chi^2 + 117\kappa\chi^2 - 6\chi^4 + 54\kappa\chi^4 + 36\chi B_2 + 108\chi^3 B_2\right)\,, \\
H^{E/B}_{\hat{s}^2,\omega} &= -\frac{4}{135}\left(115\chi^2 + 135\kappa\chi^2 + 5\chi^4 + 90\kappa\chi^4 - 24\chi B_1 + 18\chi^3 B_1 + 48\chi B_2 + 144\chi^3 B_2\right)\,, \\
H^{E/B}_{\hat{s}^4,\omega} &= \frac{4}{135}\left(20\chi^4 + 45\kappa\chi^4 - 24\chi B_1 + 18\chi^3 B_1 + 12\chi B_2 + 36\chi^3 B_2\right)\,,
\end{aligned}
\tag{5.75}
$$

where $\kappa = \sqrt{1-\chi^2}$ and $B_m = \mathrm{Im}[\psi^{(0)}(3+im\chi/\kappa)]$ (for $m = 1, 2$), $\psi^{(0)}$ is the polygamma function. This expression agrees with [2]. In the Schwarzschild case, we have

$$
H^{E/B}_{\hat{s}^0,\omega}(\chi=0) = \frac{16}{45}\,. \tag{5.76}
$$

Interestingly, the polygamma function $\psi^{(0)}(3+im\chi/\kappa)$ goes to infinity as spin χ goes to extremality ($\chi \to 1$), indicating a large spin contribution to the dissipation.

The superradiance effect [439] dictates the functional form of dissipation for Kerr BH in the static limit. Specifically, the non-vanishing of $H^{E/B}_{\hat{s}^1}, H^{E/B}_{\hat{s}^3}$ directly follows from frame-dragging [61, 243, 380]. As shown in [61, 216, 242, 243, 380, 410, 411, 428, 429] using the near zone calculations, the low-frequency absorption probability can be written as

$$ {}_s\Gamma_{\ell m} = 2(-P_+)\left(\frac{(\ell+s)!(\ell-s)!}{(2\ell)!(2\ell+1)!}\right)^2 \left(2\omega(r_+-r_-)\right)^{2\ell+1}\prod_{j=1}^{\ell}(j^2+4P_+^2)\,, \tag{5.77} $$

with the superradiance factor P_+

$$ P_+ = \frac{am-2Mr_+\omega}{r_+-r_-} = \frac{m\Omega_{\rm H}-\omega}{4\pi T_{\rm H}}\,. \tag{5.78} $$

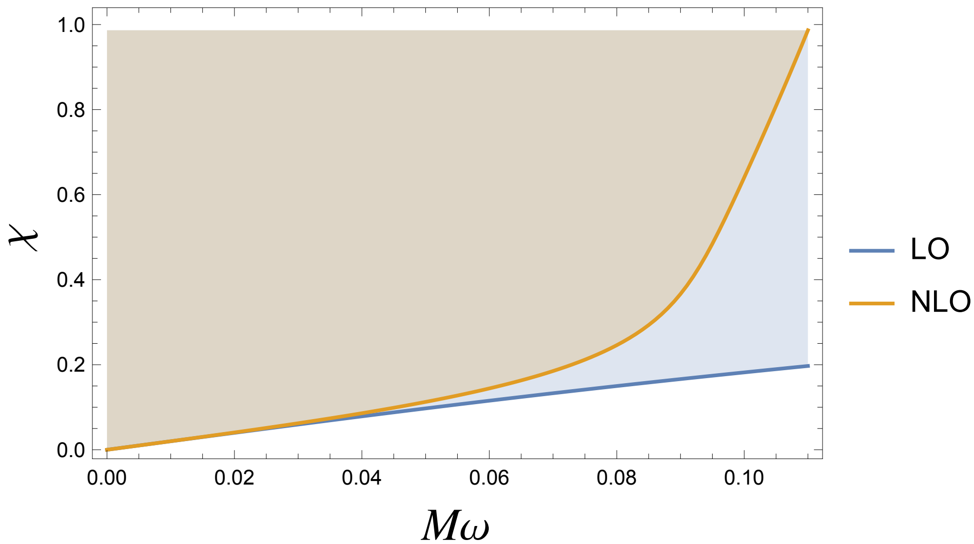

Figure 5.1: Comparison of LO and NLO supperadiance conditions, see Eq. (5.75). In this figure, we show the example with $\ell = 2, m = 2$. The colored region corresponds to the superradiance parameter space, with solid lines showing the critical values, i.e. $m\Omega_H = \omega$ at LO.

The appearance of the overall factor $m\Omega_H - \omega$ dictates a constraint on tidal response at leading and next-to-leading order in the small spin limit. This is seen by relating the above expression for absorption probability with the tidal response in the EFT to NLO as

$$ \begin{aligned} {}_2\Gamma_{22} = 1 - {}_2\eta_{22}^2 &= 2\mathrm{Re}[i\mathcal{A}(\omega, \ell = m = 2, h \to \ell = m = 2, h)], && (5.79)\\ &= M(GM)^4\frac{\omega^5}{20M_{pl}^2\pi}\left[H^E_{\hat{s}1} + (GM\omega)H^E_{\hat{s}0}\right] + \text{magnetic} + O(\omega^7), && (5.80) \end{aligned} $$

where we have used Eqs. (5.67), (5.69) and (5.74). Now, taking the limit $\chi \to 0$ in Eq. (5.77), where we have $\Omega_H \to \chi/(4GM)$, and expand until $\mathcal{O}(\omega^6)$ order we have

$$-\frac{128}{225}(GM\omega)^5\Big(\chi - 2(GM\omega)\Big) + \mathcal{O}(\omega^7) = M(GM)^4\frac{\omega^5}{20M_{\rm pl}^2\pi}\Big[H^E_{\hat{s}^1} + (GM\omega)H^E_{\hat{s}^0}\Big]$$
$$+ \text{magnetic} + \mathcal{O}(\omega^7)\ . \tag{5.81}$$

After using E/B duality, we arrive at the constraint

$$H^{E/B}_{\hat{s}^0,\omega} = -2\chi H^{E/B}_{\hat{s}^1}\ ,\ \text{for} \quad \chi \to 0\ , \tag{5.82}$$

as desired. This is consistent with the small spin limit of expressions we obtained in Eqs. (5.71), (5.76). When $m\Omega_{\rm H} > \omega$, BHs lose energy to external perturbations, i.e. superradiance takes place. The parameter space in the $\chi - (M\omega)$ plane that corresponds to this regime of superradiance is presented by the blue shaded region in Fig. 5.1. This superradiance condition is based on the near zone calculations. Consequently, it requires modification if one includes corrections from the far zone iteratively [60, 198]. The NLO Kerr dissipation number $H_{\hat{s}^0,\omega}$ in Eq. (5.75) includes these corrections and captures the modified superradiance condition by accounting for the large spin correction. The modified superradiance parameter space is plotted as the orange region in Fig. 5.1. We see that the parameter space for superradiance shrinks due to the large spin corrections coming from the polygamma functions $\psi^{(0)}(3 + im\chi/\kappa)$ in Eq. (5.75). This is a particularly intriguing observation as the polygamma function indicates a non-analytic behavior in the spin magnitude χ and even exhibits a singular point for the extremal spin value ($\chi = 1$). A similar pattern has been noted in [174]. As discussed in Sec. 5.3, these non-analytic functions are derived from what we refer to as the near zone part. Its derivation was formally carried out only for the sub-extremal cases ($0 \leq \chi < 1$). In contrast, the far zone pieces that are comprised of power laws in χ and $\kappa = \sqrt{1-\chi^2}$, exhibit only a branch point at $\chi = 1$, except for the logarithmic tail effect. This structure is suitable for an analytic continuation in χ to the super-extremal region $\chi \gg 1$. To summarize, the near zone terms only make sense in the physical sub-extremal region while the far zone terms can be formally extended into the extremal and super extremal region.

5.4.3 Tail effects

In this section, we focus on the orange terms in Sec. 5.3.2. We show that these terms correspond to the leading tail effect due to the scattering off the long-range Newtonian potential. Let's consider the following diagram (the 1-loop integration can be found in [249] and [390])

$i\mathcal{M} =$ 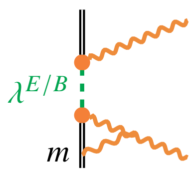

$+$ 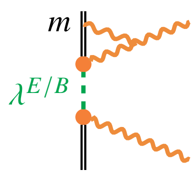

$=$ 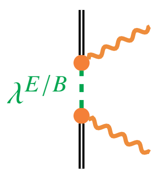

$$\times 2(16\pi G m\omega^2)\int \frac{d^{d-1}\boldsymbol{q}}{(2\pi)^{d-1}}\frac{1}{\boldsymbol{q}^2}\frac{1}{(\omega+i0)^2-(\boldsymbol{q}+\boldsymbol{k})^2}$$

$=$ 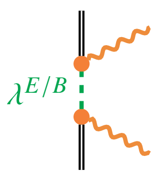

$$\times 2(iG_N m\omega)\left[-\frac{(\omega+i0)^2}{\pi\mu^2}e^{\gamma_E}\right]^{(d-4)/2}\times\left[\frac{2}{(d-4)_{\rm IR}}-\frac{11}{6}+\cdots\right] \tag{5.83}$$

$=$ 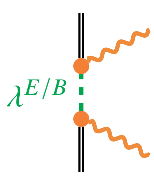

$$\times 2GM\omega\left[\operatorname{sign}(\omega)\pi + i\left(\frac{2}{(d-4)_{\rm IR}}+\log\frac{\omega^2}{\pi\mu^2}+\gamma_E-\frac{11}{6}\right)\right],$$

where $\boldsymbol{k}^2 = \omega^2$ and in the last expression we have performed an expansion around[13] $d = 4$. We now clearly see the IR divergences. As pointed out in [249, 390], the imaginary part of the above 1-loop integral will exponentiate into a universal pure phase out and can be dropped out in the

[13] In this expression, we have used the retarded propagator to make causality manifest. The $i0$-prescription here tells the relative position between the physical sheet and the branch cut. When $\omega > 0$, we choose the prescription $(-1)^{(d-4)/2} = e^{-i\pi(d-4)/2}$. When $\omega < 0$, we choose another prescription $(-1)^{(d-4)/2} = e^{i\pi(d-4)/2}$. To compare with BHPT, we only need $\omega > 0$ as the BHPT results we presented in Section 5.3.2 always assumes $\omega > 0$.

physical observable such as the cross sections $\sigma \sim |\mathcal{M}|^2$. Indeed, we do not find the associated logarithms in the BHPT phase shift [14]since they are unphysical, but we do find the finite terms obtained by multiplying the lower order amplitudes by the factor $2GM\omega\pi$, as the orange terms in the BHPT phase shift. The leading tail effect thus nicely explains all the orange terms appear in the BHPT reuslts in Sec. 5.3.2. Most importantly, this effect explains the presence of certain odd-looking spin dependencies in the BHPT phase shift. For instance, the orange piece appearing at NLO at $(r_s\omega)^6$ is odd in spin, as opposed to all the other terms which are even in spin. Thus, naively, it seems to transform differently from other terms at the same order under time-reversal $(\chi \to -\chi, \omega \to -\omega)$. But recognizing the orange term as due to the leading order tail effect, we realize that that the actual dependence on frequency is $(r_s\omega)^5 \times r_s|\omega|$ which makes the overall result even under time-reversal.

5.4.4 RG running of dissipation numbers at NNLO

In the next two sections, we explain all the logarithmic dependencies observed in the BHPT results from Sec. 5.3.2. First, we will examine the logarithmic terms that appear in the absorption probability $1 - ({}_2\eta_{\ell m})^2$, highlighted in purple. Subsequently, in Sec. 5.4.5, we will discuss the logarithmic terms in the elastic phase shift ${}_2\delta_{\ell m}$, marked in green.

We will start with the RG running of dissipation numbers. For simplicity, we will be using the optical theorem and the fluctuation-dissipation theorem [197, 238, 246] to calculate absorption probabilities. We have

[14]It is important to not confuse the logarithms in the green terms with the tail effect logarithm discussed here. Although they seem to coincide at leading order in for spinning BHs, the logarithms in the green part do not exponentiate.

With this method, we can now compute the 2-loop corrections to the absorption as [15]

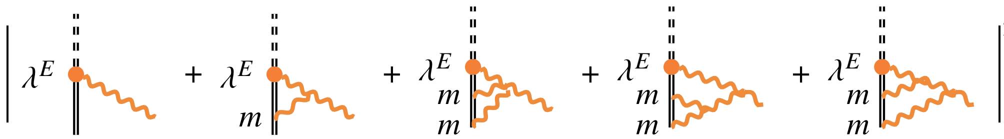

$$+\,|\text{magnetic}|^2 \tag{5.84}$$

As mentioned previously in [249], we notice that the third and fourth diagram in the above equation

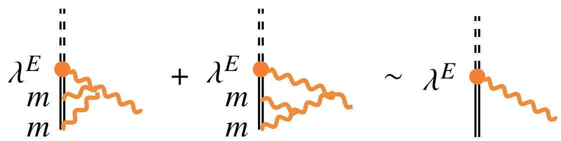

$$\times \int \frac{d^{d-1}\boldsymbol{q}}{(2\pi)^{d-1}} \frac{1}{(\omega+i0)^2-(\boldsymbol{k}+\boldsymbol{q})^2} \times \int \frac{d^{d-1}\boldsymbol{p}}{(2\pi)^{d-1}} \frac{1}{\boldsymbol{p}^2} \frac{1}{(\boldsymbol{p}+\boldsymbol{q})^2} \tag{5.85}$$

only has a UV divergence, while the last diagram contains both UV and IR divergences,

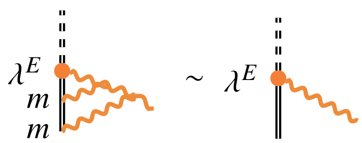

$$\times \int \frac{d^{d-1}\boldsymbol{q}}{(2\pi)^{d-1}} \frac{1}{\boldsymbol{q}^2} \frac{1}{(\omega+i0)^2-(\boldsymbol{k}+\boldsymbol{q})^2} \times \int \frac{d^{d-1}\boldsymbol{p}}{(2\pi)^{d-1}} \frac{1}{\boldsymbol{p}^2} \frac{1}{(\omega+i0)^2-(\boldsymbol{k}+\boldsymbol{p}+\boldsymbol{q})^2}\,. \tag{5.86}$$

Adding all these terms together, we get the final expression (the detailed calculation can be found in [249])

Eq. (5.84) =

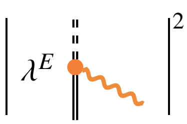

$$\times \left(1 + 2\pi GM\omega\,\mathrm{sign}(\omega) - \frac{428(GM\omega)^2}{210}\left[\frac{1}{(d-4)_{\mathrm{UV}}} + \gamma_E + \log\left(\frac{\omega^2}{\pi\mu^2}\right)\right] + (GM\omega)^2\left[\frac{4\pi^2}{3} + \frac{634913}{44100}\right]\right) + |\text{magnetic}|^2\,. \tag{5.87}$$

Interestingly, we observe that the IR divergences cancel in the above equation. However, we do encounter UV divergences, indicating that a renormalization is necessary. By the power counting in $(r_s\omega)$, we can estimate that the UV divergence appears $(r_s\omega)^2$ (2-loop) orders higher than the leading dissipation effect. This suggests that the divergence can be absorbed into $(\lambda^{E/B}_{\omega^2})_{ijkl}$, a term we introduced in Eq. (5.18). As discussed in Sec. 5.2, $(\lambda^{E/B})_{ijkl}$ and $(\lambda^{E/B}_{\omega^2})_{ijkl}$ share the

[15] Here, λ_E is a short notation for the dissipation degrees of freedom $H^E_{\hat{s}1}, H^E_{\hat{s}3}$ in Eq. (5.27).

same symmetry properties, i.e. the spin-even part corresponds to conservative effects while the spin-odd part corresponds to dissipation. Thus, if we further consider the following process

$$\left| \lambda^E_{\omega^2}\right.$$ 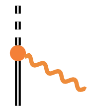 $$\left.\right|^2 + \left| \lambda^B_{\omega^2}\right.$$ 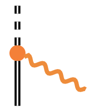 $$\left.\right|^2 = -M(GM)^6 \frac{\omega^7}{20\pi M_{\rm pl}^2}\left[\frac{1}{2} m H^E_{\hat{s}^1,\omega^2} - \frac{1}{6} m(m^2-4) H^E_{\hat{s}^3,\omega^2}\right] + |\text{magnetic}|^2 \,, \tag{5.88}$$

after renormalizing the diverging piece, we can extract the RG running of NNLO dissipation numbers $H_{\hat{s}^1,\omega^2}$ and $H_{\hat{s}^3,\omega^2}$ introduced in Eq. (5.29)

$$\frac{\partial H^{E/B}_{\hat{s}^1,\omega^2}}{\partial \log\mu} = \frac{428}{105} H_{\hat{s}^1} = -\frac{3424}{4725}(\chi + 3\chi^3)\,, \qquad \frac{\partial H^{E/B}_{\hat{s}^3,\omega^2}}{\partial \log\mu} = \frac{428}{105} H^{E/B}_{\hat{s}^3,\omega^2} = \frac{856}{315}\chi^3\,. \tag{5.89}$$

Such RG running effects can also be extracted from BHPT (purple term at $(r_s\omega)^7$) from Eq. (5.59) and (5.61)

$$\begin{aligned} & p(1+\text{BH} \to 0 + \text{BH}')|_{(r_s\omega)^7 \log(r_s\omega)} \\ &= M(GM)^6 \frac{\omega^7}{20\pi M_{\rm pl}^2}\left[\frac{1}{2} m \left(\frac{3424}{4725}(\chi+3\chi^3)\right) + \frac{1}{6}\left(\frac{856}{315}\chi^3\right) m(m^2-4)\right] \log(2\sqrt{1-\chi^2} r_s\omega) \times 2\,. \end{aligned} \tag{5.90}$$

Introducing the renormalization scale μ, we can split the logarithm into two pieces,

$$\log(2\sqrt{1-\chi^2}r_s\omega) = \underbrace{\log\left(2\sqrt{1-\chi^2}r_s\mu\right)}_{\text{NNLO dissipation counter term}} + \underbrace{\log\left(\frac{\omega}{\mu}\right)}_{\text{loop divergence}}\,. \tag{5.91}$$

The first term is the counter term that produces the RG running of the dissipation numbers at NNLO. The second term can be interpreted as a genuine logarithmic divergence from the loops. Including the constant piece from BHPT Eqs. (5.59) and (5.61), we get

$$\begin{aligned} H_{\hat{s}^1,\omega^2}(\mu) &= -\frac{3424}{4725}(\chi+3\chi^3)\log\left(4GM\sqrt{1-\chi^2}\mu\right) + 80\mathcal{A}_{22}(\chi)\,, \\ H_{\hat{s}^3,\omega^2}(\mu) &= \frac{856}{315}\chi^3 \log\left(4GM\sqrt{1-\chi^2}\mu\right) + 80(2\mathcal{A}_{21}(\chi) - \mathcal{A}_{22}(\chi))\,, \end{aligned} \tag{5.92}$$

The constant terms $\mathcal{A}_{22}(\chi)$ and $\mathcal{A}_{21}(\chi)$ are discussed Sec. 5.6. We show that their interpretation is somewhat intricate due to the spherical-spheroidal mixing discussed in Sec. 5.5.2.

The RG equation is useful because it can sum large logarithms. In the worldline EFT context, similar ideas were discussed in the gravitational radiation context in [249]. Here, we apply them to the horizon absorption. Let us first choose a specific matching scale μ_0. Intuitively, at the 2-loop level, all the logarithmic divergences will come from the following diagrams (we only estimate the diverging piece)

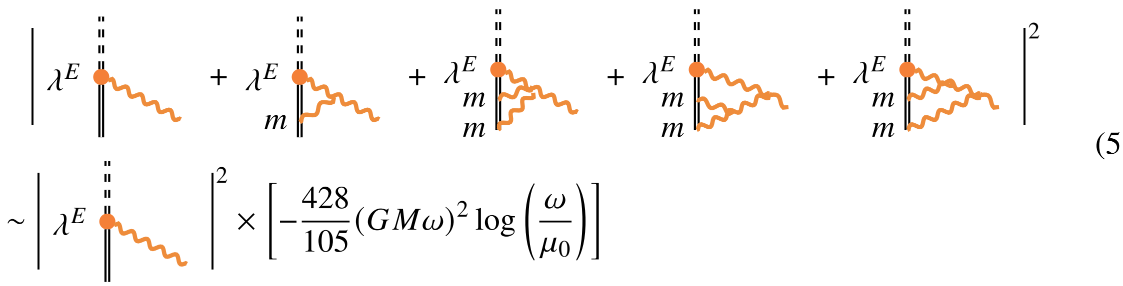

(5.93)

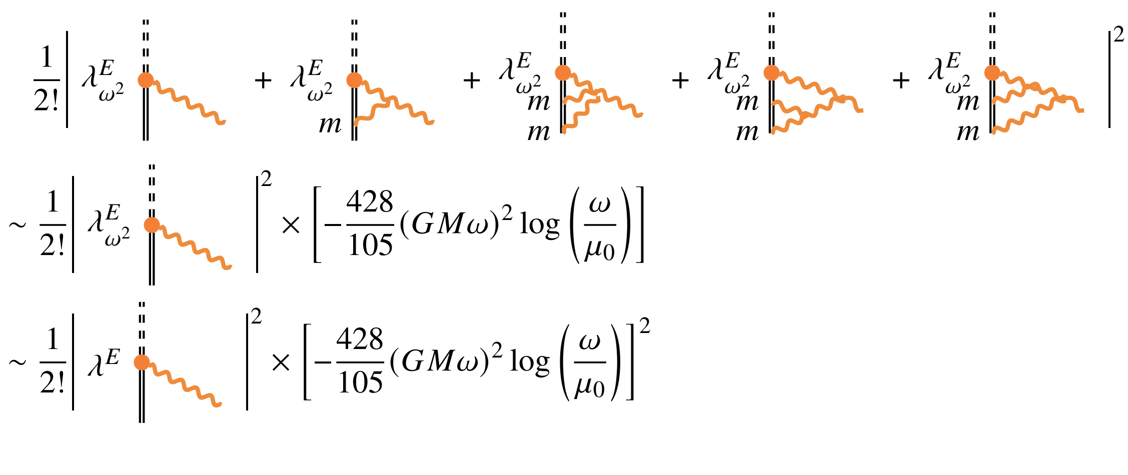

(5.94)

In the above equation, $1/(2!)$ is the symmetry factor. One can iterate the above corrections further to get

$\frac{1}{n!}\Big|\ \lambda^E_{\omega^{2n}}$ 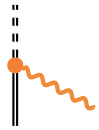 $+\ \lambda^E_{\omega^{2n}}\ m$ 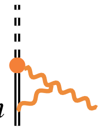 $+\ \lambda^E_{\omega^{2n}}\ m\ m$ 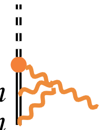 $+\ \lambda^E_{\omega^{2n}}\ m\ m$ 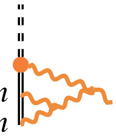 $+\ \lambda^E_{\omega^{2n}}\ m\ m$ 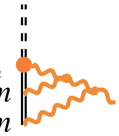 $\Big|^2$

$\sim \frac{1}{n!}\Big|\ \lambda^E$ 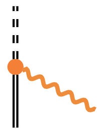 $\Big|^2 \times \left[-\frac{428}{105}(GM\omega)^2 \log\left(\frac{\omega}{\mu_0}\right)\right]^{2n}$

(5.95)

Summing all these diagrams together, we get the leading logarithmic RG running behavior (log from 2-loops) in the absorption probability

$\sim \Big|\ \lambda^E$ 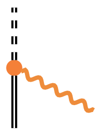 $\Big|^2 \times \left(\frac{\omega}{\mu_0}\right)^{-\frac{428}{105}(GM\omega)^2}\ .$ (5.96)

The above explicit resummation can also be written in a more general form of renormalized non-local (NL) retarded Green's function [249, 440] that accounts for the dissipations. We parametrize the bare retarded Green function in terms of the renormalized (physical) Green function as

$$\langle Q_{ij}Q_{kl}\rangle^{\rm NL}_{\rm ret,Bare}(\omega) = Z(\omega,\mu)^2\langle Q_{ij}Q_{kl}\rangle^{\rm NL}_{\rm ret}(\omega,\mu)\ . \tag{5.97}$$

where we have introduced the matching scale μ. By calculating the same diagram in Eq. (5.84) with λ^E replaced by Q^E, we can get the renormalization constant in $\overline{\rm MS}$ scheme as

$$Z^{\overline{\rm MS}} = 1 + \frac{107}{105}(GM\omega)^2 \times \left[\frac{1}{(d-4)_{\rm UV}} + \gamma_E - \log(4\pi)\right]\ , \tag{5.98}$$

which absorbs the UV divergence in dimensional regularization. By requiring the physical absorption probability to be independent on the sliding scale μ, we get the β function

$$\frac{d_2\Gamma_{\ell m}}{d\log\mu} = 0 \quad \Rightarrow \frac{d}{d\log\mu}\langle Q_{ij}Q_{kl}\rangle^{\rm NL}_{\rm ret}(\omega,\mu) = -\frac{428}{105}(GM\omega)^2\langle Q_{ij}Q_{kl}\rangle^{\rm NL}_{\rm ret}(\omega,\mu)\ . \tag{5.99}$$

The solution to this RG equation perfectly agrees the leading log (2-loop) resummation we see in Eq. (5.96). For general compact objects, the same set of diagrams should generate RG running in the conservative sector, which will be proportional to the tree-level Love number Wilson coefficients, see Ref. [251] for an explicit calculation. However, for black holes they vanish due to the vanishing of static Love numbers, and hence the RG running of their Love numbers will appear only at the 6-loop order.

To summarize, the purple logarithmic terms in the BHPT phase shifts Eq. (5.59) and Eq. (5.61) correspond to the RG running of the non-local retarded Green function at the 2-loop order.

5.4.5 RG running of dynamical Love numbers

The BHPT results in Sec. 5.3.2 contain another type of logarithmic dependence in the elastic phase shifts given in Eqs. (5.60), (5.62) and (5.64). In what follows, we will first match the RG running of the appropriate beta function coefficients by comparing the logarithms and then discuss the origin of the associated divergences.

As we have discussed in Sec. 5.3.1, the near-far factorization guarantees that the logarithmic terms will only appear in the near zone part, except for those arising from the loop corrections to the scattering off long-range Newtonian potential (tails). Thus, the matching of the logarithmic piece for the conservative effect is similar to what we have done for the static tidal Love numbers in Sec. 5.4.1. Consider now the same diagram as in Eq. (5.72), but focus on the conservative sector. Matching to the BHPT elastic phase shift in Eq. (5.60), (5.62) and Eq. (5.64). We get the following β functions

$$\frac{\partial \Lambda^{E/B}_{\hat{s}^1,\omega}}{\partial \log(\mu)} = -\frac{32}{45}(\chi + 3\chi^3), \qquad \frac{\partial \Lambda^{E/B}_{\hat{s}^3,\omega}}{\partial \log(\mu)} = \frac{8}{3}\chi^3 \,. \tag{5.100}$$

Similarly, we can also consider the scattering phase shift contribution at $(r_s\omega)^7$ order from the diagram

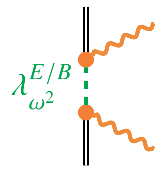

$$. \tag{5.101}$$

With similar methods we developed in Sec. 5.4.1 and 5.4.2, we can get the RG running for $\Lambda_{\hat{s}^0,\omega^2}$, $\Lambda_{\hat{s}^2,\omega^2}$ and $\Lambda_{\hat{s}^4,\omega^2}$

$$\begin{aligned}
\frac{\partial \Lambda^{E/B}_{\hat{s}^0,\omega^2}}{\partial \log \mu} &= \frac{32}{405}\left(9 + 97\chi^2 - 6\chi^4\right) \,, \\
\frac{\partial \Lambda^{E/B}_{\hat{s}^2,\omega^2}}{\partial \log \mu} &= -\frac{16}{27}\left(\chi^2 + 23\right)\chi^2 \,, \\
\frac{\Lambda^{E/B}_{\hat{s}^4}}{\partial \log \mu} &= \frac{64}{27}\chi^4 \,.
\end{aligned} \tag{5.102}$$

As an important check of our results, we can now take the Schwarzschild limit $\chi = 0$, and get

$$\frac{\partial \Lambda^{E/B}_{\hat{s}^0,\omega^2}}{\partial \log \mu} = \frac{32}{45} \,, \tag{5.103}$$

which perfectly agrees with the off-shell graviton one-point function calculations of [175] upon taking into account the difference in our conventions.

It is worth noting that the numerical value of the Wilson coefficient of the $\int d\tau \dot{E}^2$ operator in Eq. (5.102) depends on the black hole spin. It is important to distinguish such implicit dependencies of magnitudes of Wilson coefficients on spin from spin-dependent expressions generated directly by relevant tensors, c.f. (5.15). One should keep this subtlety in mind when interpreting the MST solution as a function of spin in the context of effective field theory.

The logarithmic running of dynamical Love numbers is generated by UV divergences of the GR loops. For the sake of simplicity, let us focus on the Schwarzschild case. As explained in Sec. 5.2, Eq. (5.26), the conservative effect can be represented as a local contact term on the worldline. When expressed in the language of diagrams, this suggests that the RG running of $\Lambda^{E/B}_{\omega^2}$ can be interpreted as the logarithmic dependence of the following diagram

$\Lambda^{E/B}_{\omega^2}$ 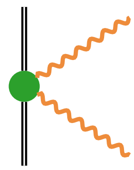 . (5.104)

Unlike the logarithms discussed in the RG flow of the dissipation numbers, this logarithms cannot be understood as loop corrections to the lower order tidal scatterings, since they vanish identically. In the context of BHPT, we have rigorously verified that varying the boundary conditions at the event horizon does not alter the RG running described by Eq. (5.100). Therefore, this logarithms is insensitive to the lower order tidal coefficients. But we find that this can act as a counter term for UV divergences in the scattering amplitude due to the gravitational non-linearities, e.g.

$i\mathcal{M}(\boldsymbol{k}_{\rm in} \to \boldsymbol{k}_{\rm out}, h \to h) =$ 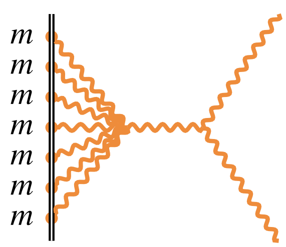

+ other diagrams at 6-loop order , (5.105)

According to the RG running computed in Eq. (5.103), the coefficient in from the log from the combination of all of such diagrams should be

$$i\mathcal{M}^{\rm EFT}_{\rm 6-loop}|_{\log}(\boldsymbol{k}_{\rm in} \to \boldsymbol{k}_{\rm out}, h \to h) = i\pi \frac{512}{45}(GM)^7\omega^6 \log\left(\frac{\omega}{\mu}\right)\cos^4\left(\frac{\theta}{2}\right) , \tag{5.106}$$

where μ is the matching scale. We leave the explicit calculation of these 6-loop diagrams for future work.

We would like to finish with an interesting observation that the RG running observed here is universal in the sense that it comes from the non-linearity of GR. Thus, it should produce the same RG running of dynamical Love numbers for all spherically symmetric compact object at the G^7 order. In [175], the authors also tried to calculate the dynamical response of a non-rotating Neutron star, see their Eq. (15), but miss this universal relation. It would be interesting to explore this generality further.

5.5 Quadrupole-octupole mixing

In this section, we shall study the quadrupole-octupole mixing effects in the tidal reponse function that originate from the breaking of the spherical symmetry by Kerr BHs. This is a particular examples of the general phenomena of the spherical-spheroidal mixing.

5.5.1 Imposing spheroidal separability and matching

As mentioned at the end of Sec. 5.3.2, the scattering phase shifts in BHPT are given in spheroidal harmonic basis because the presence of spin breaks spherical symmetry. Thus, there will be mixing terms in the scattering amplitude that transform the $\ell = 2$ states to $\ell = 3$ states and vice-versa as we have discussed in Sec. 5.2.3. However, since the Teukolsky equation is separable in the spheroidal basis, we need to impose the same spheroidal separability in the EFT. To do that, we can construct a new basis using the relation between the spherical and spheroidal harmonics at order $a\omega = GM\omega\chi = r_s\omega\chi/2$ given by

$$
{}_{-2}S_\ell^m(\cos\theta, a\omega) = {}_{-2}Y_\ell^m(\cos\theta) + (a\omega)\left[\frac{2\sqrt{(\ell+1)^2-4}\sqrt{(\ell+1)^2-m^2}}{(\ell+1)^2\sqrt{2(\ell+1)-1}\sqrt{2(\ell+1)+1}}\,{}_{-2}Y_{\ell+1}^m(\cos\theta)\right.
$$

$$
- \frac{2\sqrt{\ell^2-4}\sqrt{\ell^2-m^2}}{\ell^2\sqrt{2\ell-1}\sqrt{2\ell+1}}\,{}_{-2}Y^m_{\ell-1}(\cos\theta)\Bigg] + O\Big((a\omega)^2\Big)\,. \tag{5.107}
$$

Recall that the state $|\omega, \ell, m, h\rangle$ has the angular wavefunction $\sim {}_{-h}Y^m_\ell(\cos\theta)$, therefore we can define a new orthogonal spheroidal basis as

$$
\begin{aligned}
|\omega, \ell, m, h\rangle_{\text{sp}} = |\omega, \ell, m, h\rangle + \frac{h}{2}(a\omega)\Bigg[&\frac{2\sqrt{(\ell+1)^2-4}\sqrt{(\ell+1)^2-m^2}}{(\ell+1)^2\sqrt{2(\ell+1)-1}\sqrt{2(\ell+1)+1}}|\omega, \ell+1, m, h\rangle \\
&- \frac{2\sqrt{\ell^2-4}\sqrt{\ell^2-m^2}}{\ell^2\sqrt{2\ell-1}\sqrt{2\ell+1}}|\omega, \ell-1, m, h\rangle\Bigg] + O\Big((a\omega)^2\Big),
\end{aligned} \tag{5.108}
$$

where we are using the subscript 'sp' to denote the new spheroidal basis states with definite helicity. It turns out more convenient to work in the basis with definite parities. We can transform the above equation into the parity basis using Eq. (D.32) in App. D.2.1 and get

$$
\begin{aligned}
|\omega, \ell, m, P\rangle_{\text{sp}} = |\omega, \ell, m, P\rangle + (a\omega)\Bigg[&\frac{2\sqrt{(\ell+1)^2-4}\sqrt{(\ell+1)^2-m^2}}{(\ell+1)^2\sqrt{2(\ell+1)-1}\sqrt{2(\ell+1)+1}}|\omega, \ell+1, m, P\rangle \\
&- \frac{2\sqrt{\ell^2-4}\sqrt{\ell^2-m^2}}{\ell^2\sqrt{2\ell-1}\sqrt{2\ell+1}}|\omega, \ell-1, m, P\rangle\Bigg] + O\Big((a\omega)^2\Big).
\end{aligned} \tag{5.109}
$$

In the worldline EFT, spheroidal separability can be imposed simply be demanding that the S-matrix be diagonal in the spheroidal basis. Restricting to leading order mixing between quadrupolar ($\ell = 2$) and octupolar ($\ell = 3$) sectors, this means that

$$
{}_{\text{sp}}\langle\omega, 2, m, P|T|\omega, 3, m', P'\rangle_{\text{sp}} = {}_{\text{sp}}\langle\omega, 3, m, P|T|\omega, 2, m', P'\rangle_{\text{sp}} = 0, \tag{5.110}
$$

which implies

$$
\langle\omega, 2, m, P|T|\omega, 3, m', P'\rangle = \langle\omega, 3, m, P|T|\omega, 2, m', P'\rangle = (a\omega)\frac{2\sqrt{9-m^2}}{9\sqrt{7}}\langle\omega, 2, m, P|T|\omega, 2, m', P'\rangle\,. \tag{5.111}
$$

In the following, we will show that these relations can be used to fix the tidal mixing coefficients in $\nu^{E/B}$ and $\xi^{E/B}$ we introduced in Sec. 5.2.3. The tidal tensor $(\nu^E)^{ij}{}_{kl}$ relates the scattering process from octupolar sector ($\ell = 3$) to the quadrupolar sector ($\ell = 2$). and thus responsible for $\mathcal{A}(\omega, \ell = 3, m, P \to \ell = 2, m', P')$. Similar to the discussions in Sec. 5.4.1, we introduce the retarded Green function

Q^E_{ij}  Q^B_{klm}

$$\equiv i\langle[Q^E_{ij}(\tau)Q^B_{klm}(0)]\rangle\theta(\tau)\ . \tag{5.112}$$

According to Eq. (5.18), in the frequency domain, the above retarded Green function is just $-M(GM)^5(\nu^E)_{ij\langle kl}\hat{s}_{m\rangle}$. Then we can evaluate the following Feynman diagram

$i\mathcal{M}(\boldsymbol{k}_{\rm in} \to \boldsymbol{k}_{\rm out}, h \to h') =$ Q^E_{ij} Q^B_{klm} 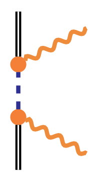

$$= -iM(GM)^5\frac{\omega^4}{4M_{\rm pl}^2}\left[\frac{h}{2}(\nu^E)^{ijkl}\hat{s}^m\epsilon^h_{(kl}(\boldsymbol{k}_{\rm in})k_{m)}\epsilon^{*h'}_{ij}(\boldsymbol{k}_{\rm out})\right]. \tag{5.113}$$

We now switch to spherical basis states with definite parities

$$\mathcal{A}(\omega, \ell = 3, m, P = +1 \to \ell = 2, m, P = +1) = -\frac{\sqrt{9-m^2}(GM\omega)^6}{4G\sqrt{7}\pi M_{\rm pl}^2}\Bigg\{\tilde{\Lambda}^E_{\hat{s}^0} + i\frac{1}{2}\tilde{H}^E_{\hat{s}^1}m \tag{5.114}$$

$$+\frac{1}{6}(m^2-4)\Big[-\tilde{\Lambda}^E_{\hat{s}^2} - i\tilde{H}^E_{\hat{s}^3} + \tilde{\Lambda}^E_{\hat{s}^4}(m^2-1)\Big]\Bigg\}\ . \tag{5.115}$$

Imposing the constraints in Eq. (5.111) and comparing with $\mathcal{A}(\omega, \ell = 2, m, P = + \to \ell = 2, m, P)$ derived from Eq. (5.67)

$$\mathcal{A}(\omega, \ell = 2, m, P = +1 \to \ell = 2, m, P = +1) = -\frac{\omega^5}{40M_{\rm pl}^2\pi}M(GM)^4 \times \Bigg[\Lambda^E_{\hat{s}^0} + \frac{1}{2}imH^E_{\hat{s}^1}$$

$$+\frac{1}{6}(m^2-4)\left(-\Lambda^E_{\hat{s}^2} - imH^E_{\hat{s}^3} + \Lambda^E_{\hat{s}^4}(m^2-1)\right)\Bigg], \tag{5.116}$$

we immediately get the following relation

$$\tilde{H}^E_{s^{1/3}} = \frac{2}{3}\chi H^E_{s^{1/3}},\ \tilde{\Lambda}^E_{s^{0/2/4}} = \frac{2}{3}\chi\Lambda^E_{s^{0/2/4}} \implies (\nu^E)^{ij}{}_{kl} = \frac{2}{3}\chi(\lambda^E)^{ij}{}_{kl}. \tag{5.117}$$

By comparing the above with the $P = -1$ scatterings, we can straightforwardly get

$$\tilde{H}^B_{s^{1/3}} = -\frac{2}{3}\chi H^B_{s^{1/3}},\ \tilde{\Lambda}^B_{s^{0/2/4}} = -\frac{2}{3}\chi\Lambda^B_{s^{0/2/4}} \implies (\nu^B)^{ij}{}_{kl} = -\frac{2}{3}\chi(\lambda^B)^{ij}{}_{kl}. \tag{5.118}$$

Similarly, we can also get the relation for $(\xi^{E/B})_{ijkl}$ tensors

$$\Lambda'^{B/E}_{s^i} = \tilde{\Lambda}^{E/B}_{s^i},\ H'^{B/E}_{s^i} = \tilde{H}^{E/B}_{s^i} \implies (\xi^{B/E})^{ij}{}_{kl} = (\nu^{E/B})^{ij}{}_{kl}. \tag{5.119}$$

The same results have been previously obtained in a more classical manner in [3].

A comment is in order. We have found that the LO quadrupole-octupole mixing terms are proportional to the static Love numbers. This can be thought of as a consistency condition in the EFT. Since the static Love numbers of Kerr BHs vanish, the leading order conservative quadrupole-octupole coupling vanishes as well.

5.5.2 Comments on higher order mixings

At the end of Sec. 5.3, we have briefly mentioned that all the results in Sec. 5.4 can be derived within spherical harmonics. This is because

$$\begin{aligned} {}_{\text{sp}}\langle\omega, 2, m, P|T|\omega, 2, m', P'\rangle_{\text{sp}} &= \langle\omega, 2, m, P|T|\omega, 2, m', P'\rangle\left[1 + \frac{4(9-m^2)}{567}\left(\frac{\chi}{2}r_s\omega\right)^2\right] \\ &\quad + O[(r_s\omega)^8], \end{aligned} \tag{5.120}$$

where we have used the expansion for ${}_{-2}S_2^m(\cos\theta, a\omega)$ to $(a\omega)^2$ along with the relations in Eq. (5.111). Thus, we see that the $\ell = 2 \to 2$ amplitude remains unchanged to NLO at $(r_s\omega)^6$ regardless of whether we use the spherical or spheroidal basis. However, at $(r_s\omega)^7$ order, the constant pieces will be affected by the above corrections from spheroidal harmonics, but not the logarithms. Thus, all the RG running discussions in Sec. 5.4 will not be affected.

5.6 Constant parts of RG running couplings

In this section, we discuss the constant pieces $\mathcal{A}_{\ell m}(\chi), \mathcal{B}_{\ell m}(\chi)$ and $C_{\ell m}(\chi)$ for $\ell = 2, m = 0, 1, 2$ mentioned in Sec. 5.3 Eqs. (5.59)-(5.64). Unlike the logarithmic terms which can be nicely interpreted as the RG runnings of dissipation numbers and dynamical Love numbers in Sec. 5.4.4 and Sec. 5.4.5, the physical meaning of these constant, scheme-dependent pieces is more uncertain. To match these terms, we need to carry out the appropriate EFT multi-loop calculations and match to the BHPT results in a given scheme. This goes beyond the scope of this chapter. An alternative would be to absorb the entire constant scattering contributions at a given order into the constant part of wordline couplings. This would simply be a particular scheme choice. In this section we try to follow this path, but find certain obstacles, mainly due to the mixing effects. With these caveats in mind, we proceed to the discussion of our results. We stress that main goal of this section is to estimate the constant, scheme-dependent parts of dynamical Love numbers and NNLO dissipation numbers, and outline challenges that one should encounter in a rigorous matching of these quantities.

We first list the analytic expression for $\mathcal{B}_{\ell m}(x)$ extracted from the analytic BHPT results,

$$\mathcal{B}_{22}(\chi) = \frac{2}{225}\left(3\chi^2+1\right)\chi\Re\left(\psi^{(0)}\left(\frac{2i\chi}{\sqrt{1-\chi^2}}-2\right)\right)+\left(\frac{4\gamma_E}{75}-\frac{313543499}{2939328000}\right)\chi^3 + \left(\frac{4\gamma_E}{225}-\frac{70741499}{653184000}\right)\chi-\frac{107\chi\zeta(3)}{630}\,, \tag{5.121}$$

$$\mathcal{B}_{21}(\chi) = \frac{7\chi\left(4-3\chi^2\right)\Re\left(\psi^{(0)}\left(\frac{i\chi}{\sqrt{1-\chi^2}}-2\right)\right)}{6300}+\left(\frac{28979207}{734832000}-\frac{\gamma_E}{150}\right)\chi^3 + \left(\frac{2\gamma_E}{225}-\frac{70741499}{1306368000}\right)\chi-\frac{107}{1260}\chi\zeta(3)\,, \tag{5.122}$$

where the tail contribution has been removed by considering the time-reversal symmetry properties and the Sommerfeld enhancement factor [249]. We are yet to interpret the $\zeta(3)$ factor in the above expressions. Moreover, we stress that the RG running of dynamical Love numbers implies the breakdown of the near-far factorization for the constant pieces, which means the near zone and far zone pieces for $\ell=2$ shall mix, and therefore the far zone pieces at high PM order should be carefully taken into account. Thus, in general one needs to consider the full expansion of the spheroidal harmonics in $(a\omega)$ to $(a\omega)^6$ order in the far zone part. We defer this task to future work.

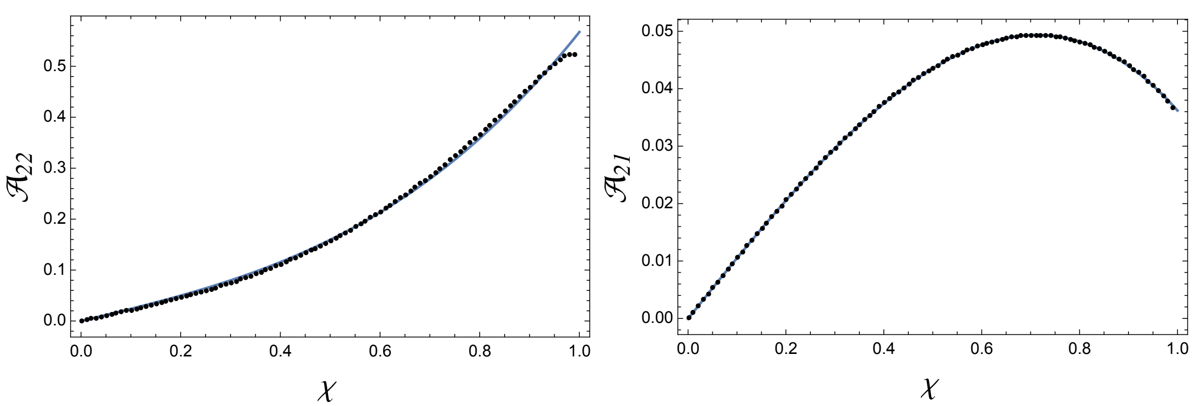

Figure 5.2: Numerical estimation of $\mathcal{A}_{22}$ and $\mathcal{A}_{21}$ as functions of χ. Dotted lines are the numerical value with blue curves showing the fitting result.

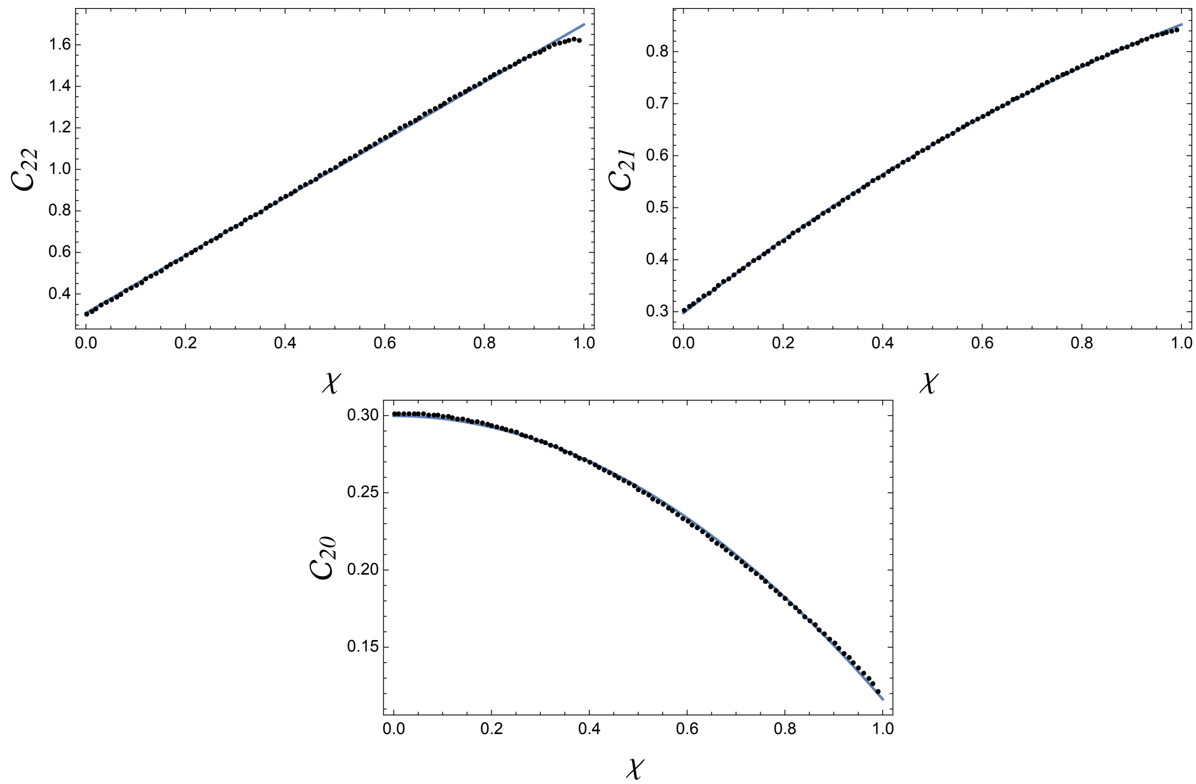

Figure 5.3: Numerical estimation of C_{22}, C_{21} and C_{20} as functions of χ. Dotted lines are the numerical value with blue curves showing the fitting result.

For the constant piece of $\mathcal{A}_{\ell m}(\chi)$ the analytic expression can be easily obtained [441], but it appears cumbersome and will not be presented here. Instead, we will present a numerical estimation in Fig. 5.2, which can be fit with a simple function

$$\mathcal{A}_{22}(\chi) = 0.236\chi + 0.331\chi^3 \,, \quad \mathcal{A}_{21}(\chi) = 0.104\chi - 0.068\chi^3 \,. \tag{5.123}$$

This expression involves linear and cubic in spin terms which are consistent with the time-reversal symmetry discussed in Sec. 5.2. Indeed, at $(r_s\omega)^7$ order, the linear and cubic in spin terms correspond to dissipation. Finally, we also obtain the numerical results for $C_{\ell m}(\chi)$ in Fig. 5.3, which can be fit as

$$C_{22}(\chi) = 1.389\chi + 0.309\,, \quad C_{21}(\chi) = 0.739\chi + 0.184(1-\chi^2) + 0.114\,,$$
$$C_{20}(\chi) = 0.183(1-\chi^2) + 0.116\,. \tag{5.124}$$

Interestingly, we observe that for in the Schwarzschild limit $\chi = 0$, C_{22}, C_{21} and C_{20} basically give the same number around 0.30, which is consistent with the emergence of the spherical symmetry so that results for different m modes become degenerate. However, we find it particular confusing to have the linear in spin term appear in $C_{22}(\chi)$ and $C_{21}(\chi)$. This term does not satisfy the time-reversal symmetry expected from the conservative tidal effects at $(r_s\omega)^7$ as we discussed in Sec. 5.2. One possible origin of such term will be the higher order tail effects contaminating the constant terms at this order. We leave a detailed study of this behavior for future work.

5.7 Conclusions and outlook

In this study, for the first time, we have taken a deep look at how Kerr BHs respond to changes in their gravitational environment at NLO and NNLO in frequency. We examined the dynamical tidal response in the framework of the worldline EFT. By comparing the scattering amplitudes in the EFT with phase shifts in BHPT, we have determined some key features of the black holes tidal response at higher orders in frequency, and to all order in the value of the BH spin. First of all, we reproduced the known results for the static tidal Love numbers, as well as LO and NLO tidal dissipation numbers. We also identified the leading order tail effects in the tidal response, using the explicit 1-loop calculation in the EFT. More interestingly, we scrutinized the RG running pattern of NNLO tidal dissipation numbers and dynamical tidal Love numbers. For dissipation numbers, we showed that the RG running can be understood as the UV divergence in the 2-loop corrections to the leading order absorptive tidal scattering diagrams in the EFT. For dynamical tidal Love numbers, we argue that the running should come from the UV divergence of higher order loop diagrams in the EFT due to non-linearities of GR. We explicitly identified the scheme-invariant beta functions of the NLO and NNLO local EFT couplings. Finally, we discussed the quadrupole-octupole mixing effects in the context of the Kerr tidal response.

The worldline EFT is generic, and the tidal response coefficients, once fixed, may be used for computing the dynamics of arbitrary compact objects. From a practical perspective, the most relevant system is an inspiraling binary, whose dynamics are typically studied in the post-Newtonian (PN) expansion. In the following, we summarize all the relevant coefficients for Kerr BHs and show the related PN order relevant for GW waveform modeling. Then we discuss possible future directions.

5.7.1 Summary of all tidal coefficients

In table **??**, we show all the coefficients that are responsible for conservative tidal interactions and the related PN order in the equation of motion (EoM). The RG running in the conservative sectors start from the 6.5PN order.

In table 5.1, we list all the coefficients that contribute to the dissipative tidal interactions and the related PN order in the energy flux as well as in the EoM through radiation reaction. The RG running in the dissipative sectors starts to contribute at 5.5 PN order in the energy flux.

Names	**Notation**	**Explicit expression**	**PN order in Flux (EoM)**
LO TDNs	$H^E_{\hat{s}^1}, H^E_{\hat{s}^3}$	Eq. (5.71)	2.5 (5)
	$H^B_{\hat{s}^1}, H^B_{\hat{s}^3}$		3.5 (6)
NLO TDNs	$H^E_{\hat{s}^0,\omega}, H^E_{\hat{s}^2,\omega}, H^E_{\hat{s}^4,\omega}$	Eq. (5.75)	4 (6.5)
	$H^B_{\hat{s}^0,\omega}, H^B_{\hat{s}^2,\omega}, H^B_{\hat{s}^4,\omega}$		5 (7.5)
NNLO TDNs	$H^E_{\hat{s}^1,\omega^2}, H^E_{\hat{s}^3,\omega^2}$	Eq. (5.89)	5.5 (8)
	$H^B_{\hat{s}^1,\omega^2}, H^B_{\hat{s}^3,\omega^2}$		6.5 (9)
DTMNs	$\tilde{H}^{E/B}_{\hat{s}^0}, \tilde{H}^{E/B}_{\hat{s}^2}, \tilde{H}^{E/B}_{\hat{s}^4}$	Eq. (5.117), Eq. (5.118)	4 (6.5)
	${H'}^{E/B}_{\hat{s}^0}, {H'}^{E/B}_{\hat{s}^2}, {H'}^{E/B}_{\hat{s}^4}$	Eq. (5.119)	

Table 5.1: Summary of all dissipative tidal response coefficients including LO/NLO/NNLO tidal dissipation numbers (TDNs) and dissipative tidal mixing numbers (DTMNs). We estimated the relative PN order where these coefficients will first appear in the energy flux with general spin orientation. We also show the PN order in which they enter the EoM through radiation-reaction in brackets.

5.7.2 Future directions

The dynamical tidal response is of particular importance in studying the structure of scatterings on Kerr BHs and the GW astrophysics. Our work can be extended in the following directions:

- **Constraining tidal dissipation numbers from data**: To better understand the nature of compact objects, one needs to consistently include all finite size effects such as spin-induced multipole moments, conservative tidal deformations and tidal dissipations [335]. Even though the literature studying the extraction of spin-induced multipoles and the tidal Love numbers from the current Gravitational-wave Transient Catalog (GWTC) catalog [23–25, 335] is vast, studies for constraining dissipation numbers are missing. Moreover, recently pointed out in Refs. [442–444], within the scenario of large bulk viscosity of the Neutron stars, the tidal dissipations could give non-negligible contributions.

- **Loop calculations and the analytic structure of scattering amplitudes in GR**: In Sec. 5.4.5, we pointed out that the RG running of dynamical Love numbers for Schwarzschild black holes should originate from the 6-loop UV divergences in the bulk diagrams. It would be interesting to carry out an explicit calculation of these diagrams. These calculations can also help us better understand the near-far factorization and its apparent breakdown discussed in Sec. 5.3, as well as the analytic structure of scattering amplitudes from the MST solution to the Teukolsky equation.

- **Extensions to the non-linear perturbations**: With the recently growing interest of the non-linearities in the Kerr BH perturbations [407, 445–447], it would be interesting to explore the non-linear tidal response function of Kerr BHs.

- **Extensions to arbitrary compact objects** : While the worldline EFT framework presented here applies to most of compact objects of interest, the analytic GR results are currently available only for black holes. Motivated by the current interest in searches for exotic compact objects, it would be very interesting to extend the methods in the chapter to generic compact objects, along the lines in [90].

Acknowledgements

We thank Rafael Aoude, Clifford Cheung, Horng Sheng Chia, Andreas Helset, Lam Hui, Austin Joyce, Jung-Wook Kim, Yue-Zhou Li, Julio-Parra Martinez, Raj Patil, Eric Poisson, Rafael Porto, Alexander Ochirov, Canxin Shi, Jan Steinoff, Justin Vines, Huan Yang, Heng-Rui Zhu for useful discussions. We thank Chris Kavanagh in particular for sharing with us the code for generating solutions to the Teukolsky equation. We also thank Huan Yang for organizing the Strong Gravity Seminar in Perimeter Institute where some of the results were presented.

Chapter 6: Investigating tidal heating in neutron stars via gravitational Raman scattering

Authors[1]: *M. V. S. Saketh, Zihan Zhou, Suprovo Ghosh, Jan Steinhoff, Debarati Chatterjee*

Abstract: We present a scattering amplitude formalism to study the tidal heating effects of nonspinning neutron stars incorporating both worldline effective field theory and relativistic stellar perturbation theory. In neutron stars, tidal heating arises from fluid viscosity due to various scattering processes in the interior. It also serves as a channel for the exchange of energy and angular momentum between the neutron star and its environment. In the interior of the neutron star, we first derive two master perturbation equations that capture fluid perturbations accurate to linear order in frequency. Remarkably, these equations receive no contribution from bulk viscosity due to a peculiar adiabatic incompressibility which arises in stellar fluid for non-barotropic perturbations. In the exterior, the metric perturbations reduce to the Regge-Wheeler (RW) equation which we solve using the analytical Mano-Suzuki-Takasugi (MST) method. We compute the amplitude for gravitational waves scattering off a neutron star, also known as gravitational Raman scattering. From the amplitude, we obtain expressions for the electric quadrupolar static Love number and the leading dissipation number to all orders in compactness. We then compute the leading dissipation number for various realistic equation-of-state(s) and estimate the change in the number of

[1]Originally published as Phys. Rev. D **110**, no.10, 103001 (2024).

gravitational wave cycles due to tidal heating during inspiral in the LIGO-Virgo-KAGRA (LVK) band.

6.1 Introduction

With the increasing number of events observed by the LIGO-Virgo-KAGRA (LVK) collaboration [23–25, 335], gravitational-wave (GW) astrophysics has entered an era of precision physics. As a result, the need for highly accurate waveforms has become increasingly apparent in order to accurately model the nature of self-gravitating compact objects, in particular their tidal effects [362, 363]. When the components of the binary are far apart, it is sufficient to model them as orbiting point particles, with their intrinsic parameters characterized by the component masses and spins. However, as they inspiral toward each other, finite-size effects such as tidal effects become important. For neutron stars, the detection of tidal effects would be very useful to distinguish between different equations of state (EoS) [178, 362, 363, 448–450], and thus to probe dense matter physics under extreme conditions [451–456].

Tidal effects describe the deformation of a body under external gravitational perturbations. In Newtonian gravity, they have been greatly explored in the literature (see [26, 195, 258, 259, 366] and their references). In general relativity (GR), tidal effects are much more complicated due to gravitational nonlinearities. However, when the external tidal field is weak, we can study tidal deformation from linear perturbation upon the compact objects. Moreover, with the modern quantum field theory (QFT)-inspired techniques, tidal effects can also be studied in the context of worldline effective field theory (EFT) by incorporating multipole moments within the worldline action as additional dynamical degrees of freedom [3, 4, 47, 48, 51, 61, 197, 249]. For e.g., the leading post-Newtonian (PN) tidal effects for a spherically symmetric object can be included by a worldline action of the form

$$S = \int d\tau \left[-m + \mathcal{L}_{\text{int}}(Q_{ij}, \dot{Q}_{ij}) - \frac{1}{2} Q_{ij} E^{kl} \right] \tag{6.1}$$

where dynamical quadrupolar degrees of freedom Q_{ij} have been included in addition to the point mass m in the action. The quadrupole is coupled to the external tidal field $E_{ij} = R_{\rho\mu\sigma\nu} u^\rho u^\sigma e_i{}^\mu e_j{}^\nu$, in the frame of the particle. The dynamics of the quadrupole moment is also encoded in the action, via the ''internal'' Lagrangian $\mathcal{L}_{\text{int}}$, although in practice it is easier to make an ansatz for it. That is, the dynamics of the quadrupole moment can be expressed according to linear response theory as [4, 61]

$$\langle Q_{ij}(\tau) \rangle = -\frac{1}{2} \int_{-\infty}^{\tau} d\tau' G^{\text{ret}}_{ij,kl}(\tau - \tau') E^{kl}(\tau') \tag{6.2}$$

where $G^{\text{ret}}_{ij,kl}(\tau - \tau')$ is the retarded tidal response function. For slowly varying external tidal fields, Eq. (6.2) can be systematically expanded in terms of time derivatives (corresponding to an expansion in orbital frequency of a binary ω, in Fourier domain)

$$Q_{ij} = -M(GM)^4 \left[\Lambda^E - (GM) H^E_\omega \frac{d}{d\tau} + \cdots \right] E_{ij} \ . \tag{6.3}$$

Here the coefficients Λ^E, H^E_ω, ... characterize the low-frequency tidal response of the particle. Specifically, Λ^E is the famous quadrupolar Love number [366], which characterizes the leading conservative tidal response, and H^E_ω is often referred to as the dissipation number [3, 4, 51], characterizing the leading dissipative part of the tidal response.

Love numbers are known to vanish for black holes [56, 57, 243, 245, 378–380]. For neutron stars, however, they are nonzero and have been studied extensively in the literature [55–57]. At the level of GW observables, Love numbers first formally appear at the 5PN order in the phase of the GW strain.

The dissipation number, on the other hand, is responsible for the phenomenon of tidal heating. It is nonzero if there exists non-conservative effects, such as viscosity for stars or the event horizon for black holes [3, 4, 61, 176]. Physically, dissipative tidal effects irreversibly transfer energy and angular momentum from the surrounding tidal environment into the body [2]. In the gravitational waveform, the tidal dissipation number first appears at 4PN order for a binary of spherically symmetric compact objects [3, 58, 60–62, 457].

Viscous sources in the interior of neutron stars are known to play an important role in the different evolutionary stages of neutron stars. They have been extensively studied in the context of damping the unstable oscillations of r-modes and f-modes of rapidly rotating newborn neutron stars [458–462]. More recently, several studies have suggested that viscous dissipation may affect the post-merger oscillations of binary neutron star merger remnants and their stability [463–467]. In the context of binary neutron star inspirals, previous studies had suggested that tidal heating could potentially cause mass ejection in a pre-merger radiation-driven outflow [468] or spin the stars up to corotation before the merger [469, 470], but these scenarios are not feasible for canonical neutron star viscosities (shear viscosity from $n-n$ or $e-e$ scattering and bulk viscosity from modified Urca reactions). Previous studies by Lai [196] and more recently by Arras et al. [471] estimated that neutron stars can be heated to a maximum of $\sim 10^8$K during the inspiral due to tidal heating. However, recent studies by Ghosh et al. [456] suggest that the viscosity from nonleptonic weak processes involving hyperons is much higher and could heat the star to $10^9 - 10^{10}$K, leaving

[2] Famously illustrated by the Earth-Moon system, the tidal lag time caused by the viscosity of the Moon ultimately results in tidal locking, whereby the Moon's rotational frequency synchronizes with its orbital frequency around Earth, which is why we always see the same side of the Moon.

a detectable imprint on the inspiral waveforms. In Ref. [442], it was shown that internal dissipative processes entering at 4PN can be constrained to the same extend as the static Love numbers. Later, in Ref. [472], the authors constrained the dissipation numbers for the event GW170817, and predictions were made regarding the improvement of constraints with upcoming next-generation detectors. The analysis was extended to include relative 1PN effects in tidal dissipation recently in Ref. [473].

However, most of the literature on the tidal response of neutron stars beyond the static limit has been Newtonian or treated in the mode-sum approximation. A relativistic analysis in the low-frequency regime, without a priori assuming the validity of the mode-sum approximation, was presented in Ref. [474] for polytropic stellar models without viscosity. Recently, Ref. [260] tackled the daunting problem of the relativistic dynamical tidal response by obtaining a resummed all-orders-in-frequency tidal response at linear order in viscosity. This was used to study both conservative and dissipative effects, including resonances for polytropic stellar models and perturbations. The relativistic dynamical tidal response of nonrotating objects has also been studied in Ref. [175] (and applied to conservative neutron-star and dissipative black-hole tides), based on a gauge-dependent matching of the worldine EFT. But starting from quadratic order in a low-frequency expansion, an ambiguity parameter enters the result; while in the scalar-field case it has been shown how the ambiguity could be removed [176], an implementation in the gravitational case is still missing, and a manifestly gauge-independent matching procedure [247] would be desirable.

In this chapter, we perform a comprehensive first-principle study of the behavior of realistic neutron stars with bulk and shear viscosity under tidal perturbations in the small frequency regime. We accomplish this by combining relativistic stellar perturbation theory (SPT), and worldline EFT, for realistic neutron star EoS(s). We compute the amplitude of GWs scattering off the neutron star (gravitational Raman scattering) in SPT and EFT. In SPT, the amplitude depends on the EoS, the compactness, and other internal physics of the neutron star. In the EFT it depends on the tidal response, parametrized by Love and dissipation numbers. By matching the amplitudes obtained in SPT and EFT, we can relate the properties of the neutron star to the tidal response. This method of fixing the world-line action by matching the Raman amplitudes in real and effective theories has already been used for black holes in several previous works [2–4, 135, 172, 174, 245, 247, 247, 475]. Here, we apply it to neutron stars. We give an overview of this work and briefly summarize the main results in the following subsection.

6.1.1 Summary of methodology and results

6.1.1.1 Master equations for SPT & adiabatic imcompressibility

To study the relativistic fluid dynamics, we start from the following energy-momentum tensor for viscous fluids

$$T_{\mu\nu} = \rho u_\mu u_\nu + (p - \zeta \nabla_\alpha u^\alpha) P_{\mu\nu} - 2\eta P^\alpha_\mu P^\beta_\nu \sigma_{\alpha\beta} \tag{6.4}$$

where u^μ is the 4-velocity, $P_{\mu\nu}$ is the spatial projector

$$P_{\mu\nu} \equiv g_{\mu\nu} + u_\mu u_\nu \ , \tag{6.5}$$

and $\sigma_{\mu\nu}$ is the shear tensor

$$\sigma_{\mu\nu} \equiv \frac{1}{2}\left(\nabla_\mu u_\nu + \nabla_\nu u_\mu - \frac{2}{3} g_{\mu\nu} \nabla_\alpha u^\alpha\right) . \tag{6.6}$$

The bulk ζ and shear η viscosity capture the damping associated with volume and layer frictions respectively. After simplifying the Einstein field equation, we get two master equations in Eqs. (6.55, 6.56) which govern the metric perturbations inside the star at linear order in frequency. A crucial feature of these equations is that, at linear order in frequency, they only receive contributions from shear viscosity η without any bulk viscosity contributions. We explicitly demonstrate that this is due to a peculiar fluid incompressibility in the static limit a.k.a adiabatic incompressibility, for non-barotropic perturbations, seen earlier in the Newtonian limit in Ref. [258, 259]. Physically, it indicates that the perturbed fluid packets preserve volume. This result is valid when the 'low'-frequency expansion as done in this work is well-defined. Specifically, we argue in Sec. 6.4.3 that the low-frequency expansion in this chapter is well-defined when the orbital frequency [3] ω, is sufficiently smaller than the characteristic Brunt-Väisälä frequency $N_{\rm ch}$, (the frequency of convective oscillations and characteristic frequency of the gravity (g-)modes) but much larger than the equilibrium-rate of m-Urca processes. The latter requirement is almost always true, but the former is valid only during early-mid inspiral as $N_{\rm ch} \sim (150-700)$Hz depending on the mass and equation of state [196, 476–478]. The results in Subsec. V.C in Ref. [260] probe the complementary regime where the frequency ω is much larger than the Brunt-Väisälä frequency as they work with barotropic perturbations where it is identically zero throughout the star. A more detailed study is required to understand the transition between the regimes during inspiral.

6.1.1.2 Love number and dissipation number for arbitrary compactness

To get the Love number and dissipation numbers for neutron stars, we also need to solve the stellar exterior, where the metric perturbations may be reduced to the Regge-Wheeler (RW) equation. With the master equations for the interior of the star, we first numerically obtain the RW variable ϕ and its radial derivative at the stellar surface. The information of the stellar interior is

[3] More generally, the frequency of the tidal field. In a binary, it is roughly the orbital frequency.

fully captured by the quantity

$$T \equiv \frac{r}{\phi}\frac{d\phi}{dr_*}\bigg|_{r=R} = T_0 - iR\omega T_1 + O(\omega^2). \tag{6.7}$$

T_0 and T_1 encode the conservative and dissipative tidal response respectively. r_* here is the tortoise coordinate. The on-shell information, i.e. the scattering phase shift can be extracted from the ratio of asymptotic expansion at infinity

$$\phi(r)|_{r\to\infty} = A^{\text{in}}_{\ell,\omega}e^{-i\omega r_*} + A^{\text{out}}_{\ell,\omega}e^{+i\omega r_*}. \tag{6.8}$$

with fixed T boundary condition. We compute the ratio $A^{\text{out}}_{\ell,\omega}/A^{\text{in}}_{\ell,\omega}$ analytically to the desired order using the Mano-Suzuki-Takasugi (MST) method following Ref. [219]. Subsequently, matching the SPT amplitude to EFT yields their relation to the static Love number and dissipation number. As a result, we provide in Eq. (6.84), expressions for the rescaled Love number k_2^E, and rescaled dissipation number ν_2^E, in terms of RW variable T in Eq. (6.7) for arbitrarily compact objects in GR. Our expression for k_2^E is consistent with the expression in Ref. [55] while the expression for ν_2^E has been obtained for the first time.

As a more quantitative study, we use Eq. (6.7) to compute the Love and dissipation number for various EoS(s) and compactness(s) in Table 6.1. The rescaled (w.r.t compactness) Love number k_2^E and dissipation number ν_2^E are defined in Eq. (6.18).

As bulk viscosity does not contribute to dissipation number at 4PN, the dissipation numbers here are entirely due to shear-viscosity, the dominant source of which is $e-e$ scattering [196, 261]. The viscosity scales inversely with the square of the temperature, see Eq. (6.33) and subsequently also the (rescaled) dissipation number(s) in the table. We thus multiply them with the factor $(T_K/10^5)^2$ to cancel this dependence leaving behind the (rescaled) dissipation number at T =

$10^5 K$. Here T_K simply means temperature in Kelvin. Note that the dissipation number H^E_ω falls sharply with compactness (roughly as $\sim C^{-6}$), and temperature $\sim T^{-2}$.

6.1.1.3 Effect on waveform due to tidal heating

We then proceed to roughly quantify the effect on the waveform during inspiral due to tidal heating at leading 4PN order in the stationary phase approximation [3, 262–264]. Specifically, we compute the change in the number of GW cycles, assuming the GW frequency to be twice the orbital frequency for a system of two neutron stars as

$$\begin{aligned}\delta\mathcal{N}_{\rm GW} &= \frac{\delta\phi[(GM\pi\omega_f)^{1/3}] - \delta\phi[(GM\omega_i\pi)^{1/3}]}{\pi},\\ &= \sum_{a=1,2}\frac{25R_a^6\nu_2^{E,a}}{512m_a^3(M-m_a)M^2}\times GM(\omega_i-\omega_f).\end{aligned} \tag{6.9}$$

Here $m_{a=1,2}$ are the masses of the neutron stars, and $M = m_1 + m_2$. $R_{a=1,2}$ are the radii, and $\nu_2^{a=1,2}$ are the rescaled dissipation numbers defined in Eq. (6.18).

As mentioned earlier, the bulk viscosity does not contribute at this order. The dominant contribution to the shear viscosity is from electron-electron scattering, which scales inversely with the square of the temperature of the neutron star. We thus evaluate Eq. (6.9) considering shear viscosity for identical neutron star binaries with various EoS(s) and compactness within the LIGO band. We also compare this with the contributions to the same quantity from other conservative 4PN contributions recently obtained in Ref. [265]. This is given in Table 6.2 for various EoS(s) and compactness. We thus find that cold viscous neutron stars with relatively low compactness have the strongest imprint. We find that the contribution of viscous dissipation can exceed other conservative contributions at 4PN for sufficiently cold and less-compact neutron stars.

EoS	M (in $M_\odot$)	R (in km)	M/R	k_2	$H^E_\omega \times (T_\mathrm{K}/10^5)^2$	$(H^E_\omega)_\mathrm{NS}/(H^E_\omega)_\mathrm{BH} \times (T_\mathrm{K}/10^5)^2$	$\nu^E_2 \times (T_\mathrm{K}/10^5)^2$
FSU2 [266]	1.01	14.00	0.107	0.133	22037.9	30990.9	0.0486
	1.34	13.95	0.141	0.121	3456.3	4860.4	0.0412
	1.71	13.95	0.180	0.099	617.0	867.7	0.0318
	2.34	13.8	0.25	0.056	47.8	67.3	0.0175
GM1 [267]	1.01	12.85	0.115	0.140	17966.3	25265.2	0.0640
	1.34	12.85	0.154	0.118	2462.4	3462.8	0.0502
	1.71	12.7	0.199	0.089	395.1	555.6	0.0367
	2.3	11.55	0.294	0.027	13.9	19.6	0.0135
HZTCS [268]	1.01	12.45	0.120	0.140	15916.7	22382.6	0.0701
	1.34	12.65	0.156	0.122	2511.6	3531.9	0.0547
	1.71	12.66	0.200	0.100	440.3	619.2	0.0417
	2.34	12.60	0.274	0.044	28.4	39.9	0.0180

Table 6.1: Tidal response characteristics for various EoS(s) and compactness for non-spinning neutron stars at $T = 10^5 K$. Dissipation numbers are computed using shear-viscosity due to electron-electron scattering, which scales inversely with square of temperature. T_K is the temperature of neutron star in Kelvin. Note that the rescaled dissipation number ν_E sharply falls with increasing compactness for each EoS. The rescaled dissipation number ν_2 does not change as much. The Love numbers obtained are consistent with known results.

EoS	M (in $M_\odot$)	R (in km)	M/R	$H^E_\omega \times (T_\mathrm{K}/10^5)^2$	$\nu^E_2 \times (T_\mathrm{K}/10^5)^2$	$\delta\mathcal{N}_\mathrm{GW} \times (T_\mathrm{K}/10^5)^2$	$\mathcal{N}^\mathrm{0PN}_\mathrm{GW}$	$\mathcal{N}^\mathrm{4PN}_\mathrm{GW}$
FSU2	1.01	14.00	0.107	22037.9	0.0486	-7.775	4428.93	-0.099
	1.34	13.95	0.141	3456.3	0.0412	-1.618	2764.77	-0.106
	1.71	13.95	0.180	617.0	0.0318	-0.369	1841.51	-0.108
	2.34	13.8	0.25	47.8	0.0175	-0.037	1091.46	-0.101
GM1	1.01	12.86	0.115	17966.3	0.0640	-6.339	4428.93	-0.099
	1.34	12.85	0.154	2462.4	0.0502	-1.153	2764.77	-0.106
	1.72	12.70	0.199	395.1	0.0367	-0.237	1823.70	-0.108
	2.30	11.55	0.294	13.9	0.0135	-0.011	1123.38	-0.102
HZTCS	1.01	12.45	0.120	15916.7	0.0701	-5.620	4428.93	-0.099
	1.34	12.65	0.156	2511.6	0.0547	-1.176	2764.77	-0.106
	1.71	12.65	0.200	440.3	0.0417	-0.265	1841.51	-0.108
	2.34	12.60	0.274	28.4	0.0180	-0.022	1091.46	-0.101

Table 6.2: Table showing correction to number of GW cycles due to tidal heating ($\delta\mathcal{N}_\mathrm{GW}$) in a symmetric spinless NS-NS binary at fixed temperature $T = 10^5 K$. $\mathcal{N}^\mathrm{0PN}_\mathrm{GW}$ is the number of gravitational cycles due to leading order quadrupolar flux, at 0PN. $\mathcal{N}^{4PN}_\mathrm{GW}$ is the contribution at 4PN due to other conservative post-Newtonian contributions [479]. The orbital frequency evolves from 30hz to min(ω_ISCO,1000hz), consistent with the LVK band.

6.1.2 Outline

The rest of this chapter is organized as follows. In Section 6.2, we provide a short review discussing the wave scattering formalism in EFT and SPT and the challenges involved isolating the tidal contribution to the amplitude in the latter. In Section 6.3, we review the neutron star background Tolman–Oppenheimer–Volkoff (TOV) equations and the realistic EoS(s) and viscosity profile(s) we use. In Section 6.4, we derive the linear perturbation equations for fluid and metric, and reduce them to two master equations for the metric perturbations to linear-order in frequency. We show the absence of bulk viscosity in the resultant equations, and its link to the fluid being incompressible in the static limit. In Section 6.5, we discuss the matching procedure between the neutron star interior and exterior along with the numerical techniques we use. We switch to the RW equation in the exterior of the star, and show how the interior perturbation equations can be integrated to obtain the boundary condition for the RW function at stellar surface. In Section 6.6, we compute the Raman scattering amplitude in terms of MST solutions to the RW equation outside the neutron star, and match with the EFT amplitude to provide expressions for the rescaled quadrupole tidal Love number and dissipation number to all order in compactness. In Section. 6.7.1 We use this to compute the electric quadrupolar Love number and dissipation numbers for various EoS(s) and compactness. In Section. 6.7.2, we compute the change in number of GW cycles within the LIGO band due to tidal heating by shear viscosity, for various EoS(s) and compactness. We compare this with other conservative post-Newtonian contributions at various orders up to 4PN. We finally conclude in Section. 6.8 with a discussion of the caveats in the current work, and potential future extensions and refinements.

6.2 Wave Scattering Formalism for tides : short review

In this section, we review the tidal dissipation in the worldline EFT formalism. Most of the material here is well-known in the literature and we refer the reader to [3, 4, 47, 51, 61, 182, 197, 238, 377, 457] for comprehensive reviews and detailed discussions.

A convenient starting point modeling a compact object including tidal effects in worldline EFT is by writing down a worldline action. The world-line is characterized by the position $z^\mu(\tau)$, τ being the proper-time. We also attach an orthonormal tetrad comprising of the 4-velocity $u^\mu = dz^\mu/d\tau$, and three space-like vectors e^μ_i. In addition, tidal effects are incorporated by including multipolar moment degrees of freedom $Q_{ij}(\tau), \ldots$. We can write

$$
\begin{aligned}
S = \int d\tau \Big[& - M + \mathcal{L}_{\text{int}}(Q^{E/B}_{ij}, \ldots) \\
& - \frac{1}{2} Q^E_{ij} E^{ij} - \frac{1}{2} Q^B_{ij} B^{ij} + \cdots \Big] ,
\end{aligned}
\tag{6.10}
$$

where the electric and magnetic tidal fields are defined as

$$
E_{ij} = u^\mu e^\nu_i u^\rho e^\sigma_j C_{\mu\nu\rho\sigma} \;\; B_{ij} = u^\mu e^\nu_i u^\rho e^{\sigma}_j {}^* C_{\mu\nu\rho\sigma} , \tag{6.11}
$$

and where $C_{\mu\nu\rho\sigma}$ is the Weyl tensor and ${}^*C_{\mu\nu\rho\sigma}$ stands for its dual. The generalization to higher order multipoles can be done by acting more derivatives on the tidal fields

$$
E_L = \partial_{\langle i_{L-2}} E_{ij\rangle} , \quad B_L = \partial_{\langle i_{L-2}} B_{ij\rangle} , \tag{6.12}
$$

with $i_L = i_1 \cdots i_\ell$ the multipolar index. $\langle \cdots \rangle$ here represents that the contained indices should be symmetrized and any traces removed. In this chapter, we will just focus on the quadrupolar electric part of the dynamics which corresponds to the $\ell = 2$, polar perturbations upon the star. The complete treatment including magnetic field for black holes can be found in [3, 4, 457]. However, tidal response to polar perturbations is typically much more important for stellar bodies. For the purpose of getting the evolution of the quadupole moments Q^E_{ij} of the compact objects, one can use the linear response theory

$$\langle Q^E_{ij}(\tau)\rangle = -\frac{1}{2}\int d\tau' G^{\rm ret}_{ij,kl}(\tau-\tau')E^{kl}(\tau')\,, \tag{6.13}$$

where the retarded Green's function is given by

$$G^{\rm ret}_{ij,kl}(\tau-\tau') = i\left\langle\left[Q_{ij}(\tau), Q_{kl}\left(\tau'\right)\right]\right\rangle\Theta\left(\tau-\tau'\right)\ . \tag{6.14}$$

In frequency domain, the retarded Green's function admits a well-defined low-frequency expansion

$$G^{\rm ret}_{ij,kl}(\omega) = F_2(\omega)\delta_{\langle ij\rangle,\langle kl\rangle}\ , \tag{6.15}$$

where

$$F_2(\omega) = 2(GM)^4\Big(\Lambda^E + (iGM\omega)H^E_\omega + \cdots\Big)\,. \tag{6.16}$$

Λ^E is known as the static Love number because it is time-reversal even and therefore corresponds to the conservative tidal deformations. Conversely, H^E_ω is time-reversal odd and therefore corresponds to nonconservative tidal effects. The tensorial structure of the response function is governed by the delta function

$$\delta_{\langle ij\rangle,\langle kl\rangle} = \frac{1}{2}\Big(\delta_{ik}\delta_{jl} + \delta_{il}\delta_{jk} - \frac{2}{3}\delta_{ij}\delta_{kl}\Big)\,. \tag{6.17}$$

From dimensional analysis, we can figure out that $\Lambda^E \sim (R/GM)^5$ while $H^E_\omega \sim (R/GM)^6$. Therefore, we find it convenient to parametrize the Love number and the dissipation number as

$$\Lambda^E = \frac{2}{3}k^E_2\Big(\frac{R}{GM}\Big)^5\,,\quad H^E_\omega = \frac{2}{3}\nu^E_2\Big(\frac{R}{GM}\Big)^6\,, \tag{6.18}$$

where k_2^E is the well-known rescaled dimensionless Love number in the literature [55, 367]. Similarly, ν_2^E is the rescaled dimensionless dissipation number. We refer to k_2^E (ν_2^E) as the 'rescaled' Love (dissipation) number when distinguishing them from Λ^E (H_ω^E). At the microscopic level, the tidal dissipation is related to the tidal lag time τ_d caused by the fluid kinematic viscosity $\nu_{\rm vis}$

$$H_\omega^E \sim \Lambda^E \times \frac{\tau_d}{Gm}\,, \quad \tau_d \sim \frac{\nu_{\rm vis}}{\nu_{\rm vis}^{\rm BH}} R\,, \tag{6.19}$$

where for black holes with the same mass $\nu_{\rm vis}^{\rm BH} = 2GM$.

In the framework of EFT, from the response function provided in Eq. (6.15), we can further calculate the change in mass-energy of the body due to tidal-heating (horizon energy flux for black holes) as

$$\frac{dE_{\rm body}}{dt} = \frac{1}{2} M (GM)^5 H_\omega^E \dot{E}^{ij} \dot{E}_{ij}\,. \tag{6.20}$$

In the stationary phase approximation, we can use the above formulae to compute the effect on the phase of the gravitational waveform. In the nonspinning case, H_ω^E affects the waveform-phase starting from 4PN [3, 457, 473].

The above EFT description can be universally applied to study any compact objects. However, the specfic value of Λ^E and H_ω^E will depend on the internal structure of the objects. In this chapter, we are going to fix these coefficients for nonspinning neutron stars by matching the GW scattering amplitude obtained in the EFT, known as gravitational Raman scattering or gravitational Compton amplitude with the one obtained from stellar perturbation theory [3, 4]. In the worldline theory or EFT, the gravitational Compton amplitude due to induced quadrupolar tides is given by the diagram

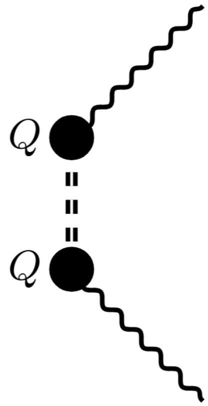

$$= i\frac{\omega^4}{16M_{\rm pl}^2}G^{\rm ret}_{ij,kl}(\omega)\epsilon_h^{ij}\,(\boldsymbol{k}_{\rm in})\,\epsilon_{h'}^{*kl}\,(\boldsymbol{k}_{\rm out}) \tag{6.21}$$

Here, $\epsilon^{ij}, \epsilon^{kl}$ are graviton polarization tensors. The scattering amplitude in Eq. (6.21) can be related to the scattering phase shift and the degree of absorption after transforming to partial wave basis [4] with $\ell = 2$ and even parity $P = +1$, corresponding to polar modes

$$\begin{aligned} 1 - \eta^{\rm EFT}_{2,+}e^{2i\delta^{\rm EFT}_{2,+}} =& i\mathcal{A}_{\rm EFT}(\ell = 2, \omega, + \to 2, \omega, +) \\ =& -i\frac{\omega^5}{80M_{\rm pl}^2\pi}F_2(\omega)(1 + GM\omega\pi) \\ & + \mathcal{O}(\omega^7) \end{aligned} \tag{6.22}$$

In the stellar perturbation theory, the scattering phase and degree of absorption may be computed as follows: in the non-spinning case, the metric perturbation equations in the vacuum outside the star may be reduced to a single source-free Schrodinger-like equation, the RW equation, for both axial and polar perturbations[4]. The RW equation is given by

$$\begin{aligned} &\frac{d^2\phi(r)}{dr_*^2} + \left[\omega^2 - f(r)V(r)\right]\phi(r) = 0, \\ &V(r) = \left(\frac{\ell(\ell+1)}{r^2} - \frac{6M}{r^3}\right),\ r_* = r + 2M\log(r - 2M). \end{aligned} \tag{6.23}$$

[4]We restrict to studying polar perturbations in this work. Axial perturbations couple weakly to neutron stars [56].

We can solve the RW equation in the vacuum outside a star if the boundary conditions at the surface of the star are provided. The boundary conditions can be obtained by numerical integration of the perturbation equations inside the star, as we show in Sec. 6.5. Once the RW equation is solved corresponding to the boundary conditions, we take the limit $r \to \infty$, where it becomes a simple wave equation and is solved by a linear combination of incoming and outgoing waves. Restricting to monochromatic perturbations, we can write

$$\phi(r)|_{r\to\infty} = A^{\text{in}}_{\ell,\omega} e^{-i\omega r_*} + A^{\text{out}}_{\ell,\omega} e^{i\omega r_*}. \tag{6.24}$$

The scattering phase, and the degree of absorption are then given by

$$\eta_\ell e^{2i\delta_\ell} = (-1)^{\ell+1} \frac{A^{\text{out}}_{\ell,\omega}}{A^{\text{in}}_{\ell,\omega}}. \tag{6.25}$$

The scattering amplitude in SPT can then be obtained using Eq. (6.22), as

$$1 - (-1)^{\ell+1} \frac{A^{\text{out}}_{\ell,\omega}}{A^{\text{in}}_{\ell,\omega}} = i\mathcal{A}_{\text{SPT}}(\ell, \omega, + \to 2, \omega, +) \tag{6.26}$$

At this stage, one might be tempted to directly compare the amplitude obtained above with that in Eq. (6.21). However, this is complicated by the fact that the scattering amplitude in the stellar perturbation theory does not just involve the contribution of tidal effects. The GWs also scatter off static background metric (Schwarzschild metric) due to the star. This is not an issue when it comes to extracting the dissipative tidal response, as shown in Ref. [3], because non-tidal effects do not contribute to dissipation. However, it complicates computing the conservative tidal response[5]. This is shown diagrammatically in Eq. (6.27). In this, the nontidal (tidal) contributions to the amplitude, are colored in blue (red) and referred to as far (near) zone-contributions following the notation in Ref. [245].

[5]Although the focus of this work is dissipative effects, It is a useful test of principle to see whether the conservative tidal response can be extracted, such as Love number using the approach.

In this work, to also extract the leading conservative tidal response, we isolate the tidal effects from the amplitude computed in stellar perturbation theory in two ways: **1)** By subtracting the full amplitude obtained using Eq. (6.26) for a neutron star, with that of a Schwarzschild black hole of the same mass, thus effectively removing all the common contributions (due to GWs scattering off the background gravitational field) leaving behind only[6] the difference in their tidal contributions. **2)** By making use of the near-far factorization valid for general ℓ, as shown in Ref. [245], to isolate the tidal contribution to scattering amplitudes in the stellar perturbation theory.

Once the tidal contribution to the scattering amplitude is isolated, we can compare it with the EFT amplitude in Eq. (6.22) and derive the Love number and dissipation number. Both approaches yield the same formulae for the Love number and the leading dissipation number as presented in Sec. 6.6.

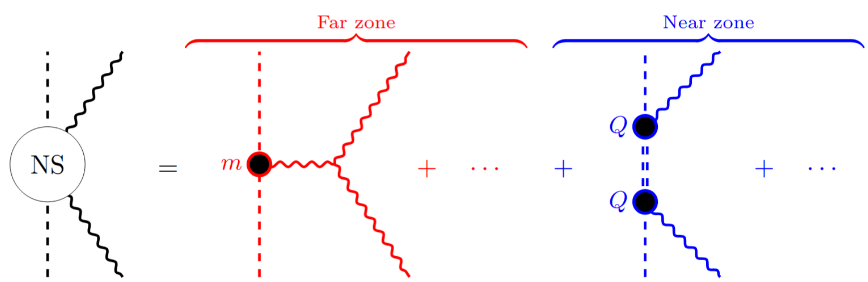

(6.27)

6.3 Stellar interior and viscosity

In this work, we consider a nonspinning spherically-symmetric neutron star, characterized by a particular density and pressure profile inside. The bounding surface of the star is where the pressure/density drops to zero. Being spherically symmetric, we can set up a polar-like coordinate system (t, r, θ, ϕ) where the bounding surface is at a fixed radial coordinate 'r' and density and

[6]The vanishing Love number of the Schwarzschild black hole aids us here.

pressure are independent of angular coordinates (θ, ϕ). We can then write down the most general spherically symmetric metric in these coordinates as [272]

$$g^{(0)}_{\mu\nu} = \begin{pmatrix} -e^{\nu(r)} & 0 & 0 & 0 \\ 0 & e^{\lambda(r)} & 0 & 0 \\ 0 & 0 & r^2 & 0 \\ 0 & 0 & 0 & r^2 \sin^2(\theta) \end{pmatrix}, \tag{6.28}$$

in the $(-, +, +, +)$ metric signature. Outside, Birkhoff's theorem ensures that the metric becomes Schwarzschild, and we have $\lambda(r) = -\nu(r)$ and $e^{-\lambda(r)} = (1 - 2M/r)$ for $r > R$, where R is the radial coordinate of the stellar surface. M is the Schwarzschild mass of the neutron star.

The unknown functions $\nu(r)$ and $\lambda(r)$ may be related to the stellar density and pressure profiles through the Einstein equation if the energy-momentum tensor of the stellar matter is known. When the star is static and unperturbed, the stellar matter may be treated as an ideal fluid and we can write

$$T^{(0)}_{\mu\nu} = \rho u_\mu u_\nu + p P_{\mu\nu}, \tag{6.29}$$

where $P_{\mu\nu} = g_{\mu\nu} + u_\mu u_\nu$. Here u^μ is the four velocity of the fluid elements comprising the star. When the (unperturbed and nonspinning) star is static, the four velocity is only along the time-like killing vector, and we can write $u^\mu = (1/\sqrt{-g_{tt}}, 0, 0, 0) = (e^{-\nu/2}, 0, 0, 0)$. The four velocity satisfies $u^2 = -1$. Now, we can compute the Einstein tensor $G_{\mu\nu}$ using the metric in Eq (6.28) and plug it into the Einstein equation $G_{\mu\nu} = \kappa T_{\mu\nu}$, where $\kappa = 8\pi$.

This yields the well known Tolman–Oppenheimer–Volkoff (TOV) equations, governing the equilibrium configurations of nonrotating relativistic neutron stars in hydrostatic equilibrium [9, 257],

$$
\begin{aligned}
\frac{dM(r)}{dr} &= 4\pi\rho(r)r^2 \,, \\
\frac{dp(r)}{dr} &= -\frac{[p(r)+\rho(r)][M(r)+4\pi r^3 p(r)]}{r(r-2m(r))} \,,
\end{aligned}
\tag{6.30}
$$

in units of $c = G = 1$. Here, we have defined $M(r) = (1 - e^{-\lambda(r)})(r/2)$, which may be regarded as the mass (energy) bounded by radius r in the non-relativistic limit. It can be regarded as a parameter which reduces to the Schwarzschild mass (i.e., mass inferred from the Schwarzschild metric outside) at the surface of the star. As it is, Eq. (6.30) is not enough to solve for the density and pressure profile. One more relation relating the density and pressure is required, also known as the equation of state (EoS). This crucial quantity depends on the constituents of the neutron star interior and their interactions. Given an EoS, one can integrate the TOV equations from the center of the star to the surface with the boundary conditions of vanishing mass, $m|_{r=0} = 0$, at the center of the star, and a vanishing pressure, $p|_{r=R} = 0$, at the surface. By changing the value of the central pressure, one obtains the mass-radius relation of neutron stars.

As we go from surface towards the core of neutron stars, the density increases rapidly, and the constituents of the neutron star matter as well as the strong interaction between them are unknown at such high density. So, one must resort to theoretical models to describe the behavior of dense matter at such high density and compare the predictions of neutron star observable properties with multi-messenger astrophysical data to put constraints on the models and their parameter space. Different theoretical schemes, ab-initio and phenomenological, have been applied to describe dense neutron star matter, including both non-relativistic and relativistic approaches [480].

While ab-initio models, such as Chiral Effective Field Theory (Chiral EFT) [481], provide a reliable microscopic description at sub-saturation densities, the calculations cannot be extended to supra-saturation densities, given our lack of understanding of baryonic three-body forces as well as the possible degrees of freedom (e.g. appearance of strange baryons or ‘‘hyperons”, condensates of mesons or deconfined quarks). Phenomenological models, on the other hand, describe baryon-baryon interactions via meson exchange, whose couplings can be fitted to reproduce nuclear saturation properties. In this work, we consider the broad class of the phenomenological Relativistic Mean Field (RMF) model for our core EoS. The uncertainty in the behavior of nuclear empirical quantities at higher densities is reflected in the uncertainty in the determination of the RMF model parameters. Recent studies [455, 482, 483] have used a Bayesian scheme within the RMF model to constrain the parameter space by imposing information from Chiral EFT at low densities and recent multi-messenger astrophysical observations of neutron stars at high densities, still leaving room for a large uncertainty in determining the behaviour of dense matter at high densities. To see the dependence and variance of our results with EoS and neutron star compactness, we have considered a few standard parameterizations within the RMF model; namely - ‘FSU2’ [266], ‘GM1’ [267] and ‘HZTCS’ [268]. For the crust of the neutron star which is mainly composed of aggregates of nuclei, we use density-dependent relativistic mean-field model parametrization ‘DD2’ [484] in beta equilibrium as taken from the Compose online database [485]. These EoS satisfy the current multi-messenger observation data of the neutron stars and also, spans the uncertainty range in the EoS. The astrophysical properties (mass and radius) corresponding to these EoSs are given in first three columns of Tables 6.1, 6.2.

The various EoSs used to solve the TOV equations in Eq. (6.30), for obtaining the background stellar profile assume that the various constituents of stellar matter are in chemical equilibrium. However, when the star is perturbed by (say) an external tidal field, the equilibrium condition may be violated depending on the rates of various reactions and the timescale of external perturbations. This can cause the stress energy tensor to deviate slightly from the form of the ideal fluid-stress-energy tensor in Eq. (6.29). In particular, we need to include shear-viscous and bulk-viscous terms in the stress energy tensor, and write

$$T_{\mu\nu} = \rho u_\mu u_\nu + (p - \zeta \nabla_\alpha u^\alpha) P_{\mu\nu} - 2\eta P^\alpha_\mu P^\beta_\nu \sigma_{\alpha\beta} \tag{6.31}$$

where $\sigma_{\mu\nu}$ is the shear tensor

$$\sigma_{\mu\nu} \equiv \frac{1}{2}\left(\nabla_\mu u_\nu + \nabla_\nu u_\mu - \frac{2}{3} g_{\mu\nu} \nabla_\alpha u^\alpha \right). \tag{6.32}$$

Here, ζ and η are the bulk and shear viscosity respectively. Note that ζ appears next to the fluid divergence $\nabla_\alpha u^\alpha$. The fluid-divergence may be related to the rate of volumetric change of the fluid packets comprising the neutron stars, and thus the bulk viscosity may be seen as a friction-force resisting such volumetric changes. Shear-viscosity η on the other hand enters alongside the shear tensor, which quantifies the shear-deformation of the fluid in the neutron star, and thus is the friction-force resisting shear deformation. There are several out-of-equilibrium viscous processes inside neutron stars that can lead to bulk and shear viscous contributions in the stress energy tensor. The main source of shear viscosity inside the neutron is the momentum transport due to the scattering of the constituents particles like electron, proton, muons and neutron. The shear viscosity generated by these microscopic processes in neutron stars depends on the local density (ρ) and the temperature (T) profile. Although neutron stars are born very hot $\sim 10^{11}$K, they cool down rapidly due to neutrino emission [486]. For neutron stars in a binary about to merge, that are very old, we expect the core temperature to be $10^5 - 10^6$K [196, 487]. In these temperature regions, the dominant source of shear viscosity comes from the $e-e$ scattering and an approximate fitting formula for the strength is given as [261, 488]

$$\eta_{ee} = 6 \times 10^6 \rho^2 T^{-2} \quad \text{gm cm}^{-1}\text{s}^{-1} \tag{6.33}$$

where ρ is the density and T is the temperature. There might be other sources of shear viscosity such as neutron-neutron scattering, neutron-muon scattering but they are very sub-dominant at these low temperatures [489]. Bulk viscosity may also originate from leptonic weak interactions such as direct-Urca and modified-Urca (m-Urca) reactions at the neutron star interior. The bulk viscosity originating from m-Urca reactions is given by [490]

$$\zeta_{\text{m-Urca}} = 6 \times 10^{-61} \rho^2 T^6/\omega^2 \quad \text{gm cm}^{-1}\text{s}^{-1}, \tag{6.34}$$

where ω is the perturbation frequency[7]. From the relative strength, we can see that the m-Urca bulk viscosity for $\omega = 1$ khz only dominate over the shear viscosity at very high temperature $10^9 - 10^{10}$K. As also mentioned earlier, nonleptonic weak interactions involving hyperons may also produce stronger bulk viscosity than other sources at low temperatures [456]. Given the EoS, the bulk viscosity coefficient (ζ) can be calculated in terms of the relaxation time (τ) of the nonleptonic weak process [459]

$$\zeta_{hyp} = n_B \frac{\partial P}{\partial n_n} \frac{dn_n}{dn_B} \frac{\tau}{1 + (\omega\tau)^2}, \tag{6.35}$$

where P is the pressure, n_B the total baryon number density, n_n the neutron density. For this particular reaction, τ is proportional to T^{-2} and for frequency ~ 100 Hz, ζ_{hyp} reaches its maximum value around 10^8K [456, 491]. Although we expect the binary neutron star core temperature to

[7]The factor $1/\omega^2$ seems to make the low-frequency expansion ill-defined. However, the expression in Eq. (6.34) is obtained in the limit where the equilibrium time scale for Urca processes is taken to be much larger than the orbital time-period $\sim \omega$. Thus, one cannot naively take the limit $\omega \to 0$.

be low ($\sim 10^5$K) at the early stages of inspiral, the viscous dissipation will cause heating and increase in the temperature. Lai (1994) [196] has shown that due to the shear viscous dissipation of the dominant f-mode energy during binary inspiral, the temperature can reach up to $\sim 10^7$K. All viscous sources considered in this work are confined to the core of the neutron stars. For the crust, the composition and the state of matter are different requiring separate physics for viscosity sources [492–494]. In this work, we fix the viscosity at the crust to be identically zero.

6.4 Stellar perturbation theory including viscosity

We now subject the stellar fluid to polar metric perturbations, and derive the relevant perturbation equations to linear order in frequency. In this work, we restrict to weak external perturbations and thus restrict to linear order in them.

6.4.1 Metric and matter perturbations

The metric given earlier in Eq. (6.28) is now linearly perturbed in a manner that depends on all coordinates. The time-dependence may be simplified by considering monochromatic perturbations, i.e., we thus consider all perturbations to have a separable time-dependence as $\exp(-i\omega t)$. This is equivalent to Fourier transforming a generic linear perturbation with respect to time, and then restricting to a single frequency in the Fourier domain. Similarly, dependence on the angular coordinates (θ, ϕ) may be simplified using a spherical harmonic decomposition, and then restricting to a given ℓ, m mode. The metric perturbations may be further decomposed into polar and axial modes. However, in this work, we restrict our attention to polar modes at $\ell = 2$, which have even parity, and induce the electric quadrupolar tidal response.

Then, the total metric is given by $g_{\mu\nu} = g^{(0)}_{\mu\nu} + \delta g_{\mu\nu}$, where $g^{(0)}_{\mu\nu}$ is the unperturbed metric given in Eq. (6.28), and $\delta g_{\mu\nu}$, the perturbation at a given frequency and ℓ, m mode. It is given by [254][8]

$$\delta g_{\mu\nu} dx^\mu dx^\nu = -e^{-i\omega t} \bar{r}^\ell Y_{\ell m} [H_0(r) e^\nu dt^2 \tag{6.36}$$
$$- 2i\omega H_1(r) dt dr + e^\lambda H_2(r) dr^2 + K(r) r^2 d\Omega^2],$$

where $\bar{r} = r/R$ inside the star ($r < R$), R being the radial coordinate of the unperturbed stellar surface and $\bar{r} = 1$ outside, and $d\Omega^2 = d\theta^2 + \sin^2(\theta) d\phi^2$.

In addition to metric perturbations, we have matter perturbations within the star. This involves density and pressure perturbations, as well as the shift in fluid elements leading to its deformation. We first parametrize the latter as follows. We can describe the fluid displacements with a vector field ξ^μ, so that the perturbed worldline of the fluid element at x^μ is described by $x^\mu + \xi^\mu$ in the perturbed configuration. We set $\xi_\mu u^\mu = 0$. The spatial components may then be parametrized as follows for polar perturbations. [254]

$$\xi^t = 0,\ \xi^r = e^{-i\omega t} \frac{\bar{r}^\ell}{r} e^{-\frac{\lambda}{2}} W\, Y_{\ell m}, \tag{6.37}$$
$$\{\xi^\theta, \xi^\phi\} = -e^{-i\omega t} \frac{\bar{r}^\ell}{r^2} V \{\partial_\theta Y_{\ell m}, \sin^{-2}\theta \partial_\phi Y_{\ell m}\}\ .$$

The fluid displacement is related to the perturbation of the four-velocity of the fluid through the relation

$$\delta u^\mu = \frac{D\xi^\mu}{D\tau} = (\delta u^0, -i\omega\xi^r, -i\omega\xi^\theta, -i\omega\xi^\phi), \tag{6.38}$$

with the gravitational redshift factor

$$\delta u^0 = -e^{-i\omega t} \frac{e^{-\nu/2} \bar{r}^\ell}{2} H_0 Y_{\ell m}. \tag{6.39}$$

[8] There are some conventional differences here w.r.t. Ref. [254].

We mentioned in Sec. 6.3 that the form of the stress energy tensor is deformed due to perturbations, leading to shear and bulk viscous terms. Similarly, the perturbations also shift the values of pressure and density. They can be obtained from the laws of thermodynamics, and the equation of state. Notice that for relativistic neutron stars, for each fluid element with a fixed number of baryons ($N_B = N_n + N_p$) obeying local charge neutrality ($N_p + N_e$)[9], we have the first law of thermodynamics

$$\Delta e = T\Delta s - p\Delta v + \sum_i \mu_i \Delta x_i, \tag{6.40}$$

where e, s, v is the average energy, entropy, and volume per baryon. $T\Delta s = \Delta q$ is the heat absorbed/lost by the fluid packet. $x_i = n_i/n_B$ here is the fractional number of each particle species. As we assume that the unperturbed star is in chemical equilibrium, the last term vanishes under the constraints. Furthermore, the predominant contribution to Δq, is due to neutrino cooling and black body radiation, both of which have timescales much longer than the inspiral timescale [456, 468]. Thus, we can just focus on the isentropic perturbations, i.e. $\Delta s = 0$ and write, $\Delta e = -p\Delta v$. Now, the Lagrangian variation of energy density for a given fluid element can be obtained as

$$\begin{aligned} \Delta\rho &= \Delta(e/v) = \Delta e/v - \rho(\Delta v/v) \\ &= -(p+\rho)(\Delta v/v), \end{aligned} \tag{6.41}$$

Since we are tracking a fluid packet with fixed baryon number, we can relate the fractional change of volume to the fractional change of baryon number density, and subsequently to the fluid-

[9]More generally, we can have processes that change Baryon number and introduce additional charged species in the mix (for e.g., Hyperons [495]). In that case, if the additional particles are also in chemical equilibrium we can simply define new quantities that are conserved to replace n_B. The charge neutrality condition can be simply redefined to include all charged particle species.

displacement vector ξ^μ via

$$\frac{\Delta v}{v} = -\frac{\Delta n_B}{n_B} = D_\mu \xi^\mu + \frac{1}{2}\delta\left[{}^{(3)}g\right]\Big/{}^{(3)}g \ , \tag{6.42}$$
$$= -Y_{\ell m}\frac{\bar{r}^\ell e^{-i\omega t}}{2}\left(H_2 + 2K - \frac{2\ell(\ell+1)V}{r^2} - \frac{2e^{-\frac{\lambda}{2}}\left[(\ell+1)W + rW'\right]}{r^2}\right)$$

where D_μ is the spatial covariant derivative and ${}^{(3)}g$ is the determinant of the spatial metric. Alternatively, one can also write $\Delta v/v = e^{\nu/2}(-i\omega)^{-1}\nabla_\mu u^\mu$.

6.4.1.1 Pressure perturbation

Computing the change in pressure is more subtle, and depends on equilibrium equation of state as well as the rates of various chemical reactions in the star, and how they compare with the orbital-time scale[10]. Generally, pressure can be viewed as a function of temperature, density and particle fraction $p(T, \rho, x_i)$. Simply by changing of variables, we can also write the above function as $p(T, \rho, \mu_i)$. This relation between pressure and other intrinsic thermodynamic quantities is referred to as the equation of state relation. In neutron stars, the effect of temperature in this relation is only relevant when they are very hot $T \geq 10^{10}K$ [496, 497]. Thus, the pressure is generally assumed to be a two parameter function as $p \equiv p(\rho, x_p)$ or $p(\rho, \mu)$ [498, 499]. The Lagrangian variation in a fluid packet with fixed baryon number n_B may then be written as

$$\Delta p(\rho, x_i) = \left(\frac{\partial p}{\partial \rho}\right)\bigg|_{x_i}\Delta\rho + \sum_i\left(\frac{\partial p}{\partial x_i}\right)\bigg|_{\rho}\Delta x_i \ ,$$
$$\Delta p(\rho, \mu_i) = \left(\frac{\partial p}{\partial \rho}\right)\bigg|_{\mu_i}\Delta\rho + \sum_i\left(\frac{\partial p}{\partial \mu_i}\right)\bigg|_{\rho}\Delta\mu_i. \tag{6.43}$$

[10]The orbital time scale is the inverse of the orbital frequency in a binary. Here, it is $1/\omega$, where ω is the frequency of the tidal perturbation.

In the general case, one needs to consider the various chemical reactions in the star and their rates to solve for the change in particle fraction or chemical potential [498]. However, the problem is simplified in the following two extreme regimes. The first extreme is the fast reaction regime where the reaction-time scale for the relevant nuclear reactions are much smaller than the inspiral timescale, in which case the reactions are able to maintain equilibrium even in the perturbed fluid packets. The fractions of various particle species continuously shift to maintain equilibrium. In this case, we can simply set $\Delta\mu_i = 0$, and therefore the change in pressure w.r.t change in density has the same relation as in the background profile because the unperturbed star was also in chemical equilibrium as well . Thus, we have

$$\textbf{fast reactions}: \ \Delta p = \left(\frac{\partial p}{\partial \rho}\right)\bigg|_{\mu_i} \Delta\rho. \tag{6.44}$$

The other regime is the slow reaction regime where the reaction timescales are too large compared to the orbital time-period, and the chemical composition is essentially frozen in the perturbed fluid packet. We can then neglect the change in particle number fraction, i.e. $\Delta x_i = 0$ and write

$$\textbf{slow reactions}: \ \Delta p = \left(\frac{\partial p}{\partial \rho}\right)\bigg|_{x_i} \Delta\rho. \tag{6.45}$$

We can generally define an index γ to be

$$\gamma \equiv \frac{\Delta p/p}{\Delta\rho/(p+\rho)} = -\frac{\Delta p/p}{\Delta v/v} \ . \tag{6.46}$$

In the fast reaction regime, this index is fully determined by the background since it is also at chemical equilibrium. i.e., $(dp/dr)/(d\rho/dr) = (\partial p/\partial\rho)|_{\mu_i}$, and so

$$\gamma_{\rm eq} = \frac{\rho+p}{p}\frac{p'}{\rho'} = c_{\rm eq}^2 \frac{p+\rho}{p} \ , \tag{6.47}$$

where $'$ corresponds to the radial derivative. For slow reactions instead, γ is given by

$$\gamma_{\rm ins} = \frac{\rho+p}{p}\left(\frac{\partial p}{\partial\rho}\right)\bigg|_{x_i} = c_{\rm ins}^2 \frac{p+\rho}{p} \ . \tag{6.48}$$

We have defined the two sound speeds $c_{\rm ins}$ and $c_{\rm eq}$ for later use. We will see further below in Sec. 6.4.3, that the value of γ plays a crucial role in determining the validity of the low-frequency expansion in this work. It also affects the frequency of the g-modes as shown in the Newtonian limit in Appendix. E.1, also see Refs. [498]. This is due to its relation with convective stability as discussed in Ref. [260].

We show in Sec. 6.4.3 that when Eq. (6.47) holds, the low-frequency expansion of the perturbation equations in the manner performed in this work is ill defined. This is also the limit in which all the g-mode frequencies collapse to $\omega = 0$ [500]. The star is marginally unstable under convective perturbations in this case [260]. This turns out to be crucial in the following discussions regarding the contribution of bulk viscosity to tidal heating in Sec. 6.4.3.

Realistically, the various nuclear reactions have vastly different timescales, and γ lies in between the two extremes. A detailed discussion of the rate of nuclear reactions and its effect on the Lagrangian change in pressure, and on the g-mode frequencies may be found in Ref. [498]. However in our work, we find that the linear-in-frequency perturbation equations are actually insensitive to the value of γ provided the low-frequency expansion is valid, which is true when Eq. (6.47) does not hold. This is true during the inspiral within the LIGO band, as the equilibrium-timescale for the dominant m-Urca processes is very large compared to the inspiral time scale(s) [490]. Instead, Eq. (6.48) corresponding to the frozen-composition is a good approximation in this case [254]. Thus, it is important to keep in mind going forward that the 'static limit' $\omega \to 0$ in this work corresponds to neglecting ω in the perturbation equations but keeping it much higher than the rate of the dominant m-Urca reaction-rates so that Eq. (6.48) holds.

6.4.1.2 Eulerian perturbation to pressure and density

Finally, once we obtain the Lagrangian changes in pressure and density, we need the corresponding Eulerian quantities to get the perturbation in pressure and density at a given coordinate point. Thus we have,

$$\delta\rho = \Delta\rho - \xi^{\mu}\nabla_{\mu}p,$$
$$\delta p = \Delta p - \xi^{\mu}\nabla_{\mu}p. \tag{6.49}$$

For spherically symmetric configurations, this reduces to

$$\delta\rho = \Delta\rho - \xi^{r}\rho',$$
$$\delta p = \Delta p - \xi^{r}p'. \tag{6.50}$$

These may be directly plugged into the Einstein equation as perturbations to the pressure and density.

Once we have all the above quantities, we are able to derive the linearized Einstein field equation $\delta G_{\mu\nu} = \kappa\delta T_{\mu\nu}$ along with the associated conservation laws $\delta(\nabla_{\mu}T^{\mu}{}_{\nu}) = 0$ with the stress energy tensor including the contributions from fluid viscosity given in Eq. (6.4).

6.4.2 Equations governing the perturbations to linear order in frequency

We will restrict ourselves to the $\ell = 2$ mode. Before proceeding further, we introduce another function $X(r)$ defined as [254]

$$X(r)Y_{\ell m}e^{-i\omega t} \equiv -\frac{\Delta n_B}{n_B}\bar{r}^{-\ell}(e^{\nu/2}p\gamma - i\omega\zeta)\ , \tag{6.51}$$

which captures the variation of baryon number density, along with some convenient factors.

We first consider the combination $G_{\theta\phi} = \kappa T_{\theta\phi}$, which yields the relation to eliminate $H_2(r)$,

$$H_2 = H_0 - 4i\omega\kappa e^{-\nu/2} V\eta. \tag{6.52}$$

We then consider $G_{12} = \kappa T_{12} = 0$, yielding

$$\begin{aligned} H_1 = \frac{r}{6}\Big[& -2H_2 + 2rK' - K(-7 + e^{\lambda} + e^{\lambda} r^2 \kappa p) \\ & + 2\kappa e^{\frac{\lambda}{2}} W(p+\rho)\Big], \end{aligned} \tag{6.53}$$

Eqs. (6.52) and (6.53) are useful for eliminating $H_2(r)$ and $H_1(r)$ in all other equations.

We then consider the conservation law $\nabla_\mu T^{\mu}{}_{\theta} = 0$, to get the relation

$$\begin{aligned} \omega^2 V(r) = & -\frac{1}{2} e^{\nu} H_0 - \frac{e^{\nu-\frac{\lambda}{2}}(-1 + e^{\lambda} + e^{\lambda} r^2 \kappa p)}{2r^2} W + \frac{e^{\frac{\nu}{2}}}{p+\rho} X - i\omega\Bigg[\frac{e^{-\lambda+\frac{\nu}{2}}(e^{\frac{\lambda}{2}}W - rV')\eta'}{r(p+\rho)} \\ & + \frac{\eta e^{-\lambda+\frac{\nu}{2}}(e^{\lambda} r^2 H_0 + 8e^{\lambda} V + 4e^{\frac{\lambda}{2}} W - 7rV' - e^{\lambda} rV' + e^{\lambda} r^3 \kappa\rho V' - 2r^2 V'')}{2r^2(p+\rho)} \\ & + \frac{e^{\frac{\nu}{2}} X\eta}{3(e^{\frac{\nu}{2}} p\gamma + i\omega\zeta)(p+\rho)}\Bigg]. \end{aligned} \tag{6.54}$$

The above relation will be used to simplify other equations containing $V(r)$. We can now proceed to derive the equations governing the metric perturbations H_0 and K to linear order-in-frequency. To that end, we start with $G_{23} - \kappa T_{23} = 0$, and eliminate $H_1(r)$ and $H_2(r)$ using Eqs. (6.52, 6.53) and truncate to $O(\omega^2)$ to get

$$\begin{aligned} & -\frac{2K}{r} + H_0' + \frac{H_0\left(\kappa r^2 p e^{\lambda} + e^{\lambda} + 1\right)}{r} - K' - \frac{2i\kappa\omega\eta e^{-\frac{\nu}{2}}\left(\kappa r^2 p e^{\lambda} V + rV' + e^{\lambda} V + V - e^{\frac{\lambda}{2}} W\right)}{r} \\ & = O(\omega^2) \end{aligned} \tag{6.55}$$

Then, we consider the combination $r(G_{22} - \kappa T_{22}) - 2(G_{23} - \kappa T_{23}) = 0$, and use Eqs. (6.52, 6.53, 6.54) to eliminate H_2, H_1 and V, and then truncate to $O(\omega^2)$ get

$$\begin{aligned}
&H_0' + \frac{H_0 e^{\lambda}\left(\kappa r^2(p-\rho)+8\right)}{2r} + \frac{1}{2}K'\left(e^{\lambda(r)}\left(\kappa r^2 p+1\right)-3\right) + \frac{K\left(e^{\lambda}\left(\kappa r^2 p-1\right)-3\right)}{r} \\
&-\frac{i\kappa\omega\eta e^{-\frac{\nu}{2}}}{2r}[8\left(4e^{\lambda}+1\right)V + V'\left(\kappa r^3 e^{\lambda}\rho - re^{\lambda}+r\right) - 2r^2V'' + 4e^{\frac{\lambda}{2}}W + r^2e^{\lambda}(H_0-4K)] \\
&-\frac{i\kappa r\omega\eta e^{\lambda-\nu}}{3p\gamma}X - ie^{-\frac{\nu}{2}}\kappa\omega\eta'(r)\left(e^{\frac{\lambda}{2}}W - rV'\right) = O(\omega^2)\ .
\end{aligned} \tag{6.56}$$

Eqs. (6.55) and (6.56) are still coupled to the fluid perturbations W and V, but those coupling terms only arise in terms relevant when there is viscosity which are all at linear order in frequency (colored in orange). Thus, when solving perturbatively in frequency, one can replace the fluid perturbations in the terms containing viscosity with the static solutions (when $\omega = 0$). We derive the expressions for fluid perturbations in the static limit below in Sec. 6.4.3.

However, another curious observation from Eqs. (6.55), (6.56) is the absence of the bulk viscosity ζ. The source terms (in orange) contain only shear viscosity and its derivative ($\eta,\ \eta'$). We show in the next Sec. 6.6 that the linear-in-frequency corrections to the perturbation equations contribute to the leading dissipation number which is relevant at 4PN in the flux (subsequently waveform). Thus, the absence of bulk viscosity tells us that it plays no role in dissipation at leading order. This is due to the vanishing of the fluid divergence $\propto X$ in the static-limit as we also show below in Sec. 6.4.3.

6.4.3 Static limit, incompressibility and validity of the small frequency expansion

We can solve for the fluid perturbations W and V in terms of the metric perturbations H and K in the static limit as follows. We first again consider the conservation laws $\nabla_\mu T^\mu{}_\nu = 0$, but without plugging in the explicit formula for pressure and density perturbations from Eq. (6.50).

We also set $\omega = 0$ and work strictly in the static limit. The conservation law $\nabla_\mu T^\mu_\theta = 0$ yields the formula

$$\delta p = -\frac{\nu^\ell H_0^{\omega^0}}{2}(p+\rho)Y_{\ell m}e^{-i\omega t}, \tag{6.57}$$

where we are using the superscript ω^0 to denote that the quantity has been evaluated in the static limit, i.e., $\omega = 0$. Inserting this into $\nabla_\mu T^\mu_r = 0$, we can get an expression for the density perturbation in the static limit as

$$\delta\rho = -\frac{\nu^\ell H_0^{\omega^0}}{2}(\rho+p)\frac{\rho'}{p'}Y_{\ell m}e^{-i\omega t}\ . \tag{6.58}$$

Note that the often assumed statement in the literature, that $\delta p = \delta\rho \times c^2_{\rm eq}$, where c_{eq} is the equilibrium sound speed in Eq. (6.47), arises automatically in the static limit, without requiring additional assumptions. Now, we demand consistency between the expressions for density and pressure perturbations obtained in Eqs. (6.57), (6.58), with those obtained earlier in terms of the fluid perturbations in Eq. (6.50). To that end, we rewrite Eq. (6.50) by substituting in Eqs. (6.57), (6.58) as

$$\begin{aligned} \frac{H_0^{\omega^0}}{2}(p+\rho) &= e^{-\frac{\nu}{2}}X^{\omega^0} + e^{-\frac{\lambda}{2}}W^{\omega^0}\frac{p'}{r}, \\ \frac{H_0^{\omega^0}\rho'}{2p'}(\rho+p) &= e^{-\frac{\nu}{2}}X^{\omega^0}\frac{p+\rho}{p\gamma} + e^{-\frac{\lambda}{2}}W^{\omega^0}\frac{\rho'}{r}\ . \end{aligned} \tag{6.59}$$

The above equation can only be satisfied either for

$$X^{\omega^0} = 0,\ W^{\omega^0} = \frac{H_0^{\omega^0}(\rho+p)e^{\frac{\lambda}{2}}r}{p'}\ , \tag{6.60}$$

or

$$\gamma = \frac{p'}{\rho'}\frac{p+\rho}{p}. \tag{6.61}$$

For the first case, the definition of $X(r)$ in Eq. (6.51) reveals that the fractional volume change $dv/v = -dn/n$ vanishes in the static limit. In other words, the fluid becomes incompressible when $\omega \to 0$. As the bulk viscosity only contributes when the fluid is compressible, this explains the curious disappearance of bulk viscosity at leading order in frequency in Eqs. (6.55), (6.56). Additionally, we now also have an expression for $W^{\omega^0}(r)$. This was shown analogously in the Newtonian limit in Ref. [258].

For the second case, Eq. (6.61) along with the discussion in Sec. 6.4.1.1 implies that the fluid perturbation is strictly barotropic, meaning the pressure is effectively the same function $p(\rho)$ of the density in both unperturbed and perturbed configurations [501, 502]. Additionally, we are unable to obtain unique solutions for W^{ω^0}, X^{ω^0} implying a degeneracy in the static limit. This is explained by noting that, from the eigen-mode analysis, this is the limit in which all g-mode frequencies condense to 0. This leads to infinite dimensional null space of the linear fluid perturbations. As a result, the static fluid configuration can be any linear combination of the g-mode eigen-functions. As famously argued by Cowling in [500], the star is in neutral equilibrium under indefinitely slow perturbations. In other words, we are unable to find a unique-static limit configuration to perform a Taylor expansion about it. It may be possible to use a different expansion scheme to obtain an analytical approximation to the perturbation equations in this case as well, but we do not tackle that here.

However, as discussed in Sec. 6.4.1.1, the perturbations are barotropic only when all chemical reactions are fast enough to always maintain equilibrium. The dominant m-Urca processes however are not rapid enough to do so [490]. Thus, for realistic neutron stars, γ is instead given by Eq. (6.48) and we can accept the solution in Eq. (6.60). Nevertheless, it is reasonable to assume that the difference between this γ and its value in the barotropic case in Eq. (6.61) likely sets the limits on the validity of the low frequency expansion in this work. More concretly, the perturbing frequency ω, should be smaller than a characteristic frequency scale associated with the difference between γ in Eq. (6.48) from its barotropic value in Eqs. (6.61, 6.47).

Such a characteristic frequency scale may be obtained from is the Brunt-Väisälä frequency N, which in the Newtonian limit is given by [503]

$$N = g\left(\frac{1}{c_{\rm eq}^2} - \frac{1}{c_{\rm ins}^2}\right)^{1/2}, \tag{6.62}$$

where $g = GM(r)/r^2$ is the local acceleration due to gravity inside the star. $c_{\rm eq}$ and $c_{\rm ins}$ were defined in Eqs. (6.48, 6.47). N is the oscillation frequency for local convective oscillations inside the star[11], and proportional to the difference between γ (from Eq. (6.48) from its barotropic value. N varies with stellar radius, but a characteristic value, $N_{\rm ch}$ may be computed inside the neutron star. This can be done by substituting typical values of the parameters entering Eq. (6.62), yielding $N_{\rm ch} \sim 500$Hz [503]. Alternatively, the g-mode with the largest resonant frequency may be used as an estimate for $N_{\rm ch}$, typically yielding $N_{\rm ch} \sim 300$Hz [196, 476]. Strictly speaking, the linear-in-frequency expansion in this work may be taken as valid when $\omega \ll N_{\rm ch}$. [12]). Tidal dissipation in the complementary regime where $\omega \gg N_{\rm ch}$ was probed numerically in Ref. [260], where the barotropic case $N = 0$ everywhere inside the star, was considered. Realistically, a binary would start in the former regime $\omega \ll N_{\rm ch}$, and its orbital frequency would eventually cross and exceed the characteristic Brunt-Väisälä frequency in the middle and late inspiral respectively. A more refined study is needed to understand the transition and its implications. In this work, we accept the solution in Eq. (6.60) as the static limit and work to linear order in frequency about this, and use the Brunt-Väisälä frequency to estimate its limits of validity.

[11] Assuming the star is stable under convective oscillations, otherwise N is imaginary. We do not consider that case in this work.

[12] This is more clearly seen in the Newtonian limit, (see Appendix. E.1 or Ref. [259]

Yet another subtlety to consider when taking the static limit is that the presence of viscosity adds another frequency scale to the system, as shown in Ref. [260], given by

$$\Omega_{\rm vis} = \frac{pR}{\eta|\boldsymbol{\xi}|}, \text{ or } \frac{pR}{\zeta|\boldsymbol{\xi}|} \tag{6.63}$$

where $|\boldsymbol{\xi}| \leq R$ is the magnitude of typical displacement vector of the fluid due to perturbations. The results obtained via the small-frequency expansion in the presence of viscosity should then be a suitable approximation when

$$\frac{\omega}{\Omega_{\rm vis}} = \frac{\omega\eta|\boldsymbol{\xi}|}{pR} \text{ or } \frac{\omega\zeta|\xi|}{pR} \ll 1 \tag{6.64}$$

We have checked that this condition is comfortably valid for inspiral frequencies (10-1000Hz) for all (most) sources of shear (bulk) viscosity throughout the star[13]. The important exception to this is the bulk viscosity due to non-leptonic weak interactions involving hyperons which were shown in Refs. [456, 459, 491] to exhibit a 'resonance' at certain temperatures and frequencies, at which point $\zeta(r)$ can get so large inside the star that this approximation no longer holds for select ranges of temperatures during inspiral. The static limit itself is likely to be significantly modified due to viscosity in this case. However, in this case, the whole scheme of incorporating viscosity by just adding terms linear in the gradient of 4-velocity may be insufficient [504]. Thus, in this work, we do not consider this regime and work with the assumption that the viscosity is small enough to only perturbatively affect the small-frequency tidal response of the neutron star.

Thus, having concluded that the fluid in realistic neutron stars for any EoS is incompressible in the static limit, we can use the vanishing of $X^{\omega^0}(r)$ to get the expression for $V^{\omega^0}(r)$ from

[13]In the crust, this condition can be more difficult to satisfy as $p \to 0$. In this work, we set viscosity to be identically 0 in the crust.

Eqs. (6.51, 6.42) to get

$$V^{\omega^0}(r) = \frac{e^{-\frac{\lambda}{2}}}{12}[e^{\frac{\lambda}{2}}r^2 H_0^{\omega^0} + 2e^{\frac{\lambda}{2}}r^2 K^{\omega^0} - 2(3W^{\omega^0} + rW^{\omega^0\prime})] \tag{6.65}$$

This completes the discussion of the static limit of the perturbations inside a neutron star. We can now substitute the expressions for V, W and X in the viscous terms at linear order in frequency (coloured in orange) in Eqs. (6.55), (6.56), in terms of H_0 and K in the static limit, and numerically integrate the two first order differential equations to solve for H_0 and K in the stellar interior.

6.5 Numerical integration and matching

In the master equations in Eqs. (6.55), (6.56), we first substitute the linear-in-frequency expansions as

$$\begin{aligned}
H_0(r) &= H_0^{\omega^0} - i\omega H_0^{\omega^1} + \mathcal{O}(\omega^2), \\
K(r) &= K^{\omega^0} - i\omega K^{\omega^1} + \mathcal{O}(\omega^2), \\
W(r) &= W^{\omega^0} + \mathcal{O}(\omega),\ V(r) = V^{\omega^0} + \mathcal{O}(\omega).
\end{aligned} \tag{6.66}$$

Then, collecting terms at the same order in ω, the master equations split into sub-equations for the static part and the linear-in-frequency part respectively. The static equations need to be first solved, to obtain the source terms (in orange) in the master Eqs. (6.55), (6.56). Then, the linear-in-frequency pieces may be obtained subsequently. We discuss them separately below.

6.5.1 Static part

The metric perturbations in the static limit obey the equations

$$H_0^{\omega^0}\left(\frac{1+e^\lambda}{r}+e^\lambda r\kappa p\right)-\frac{2}{r}K^{\omega^0}+H^{\omega^0\prime}-K^{\omega^0\prime}=0, \tag{6.67}$$

$$\begin{aligned}&-\frac{3+e^\lambda(1-r^2\kappa p)}{r}K^{\omega^0}-\frac{3}{2}K^{\omega^0\prime}+H_0^{\omega^0\prime}\\&+\frac{e^\lambda[8+r^2\kappa(p+\rho)]}{2r}H_0^{\omega^0}+\frac{e^\lambda}{2}(1+r^2\kappa p)K^{\omega^0\prime}\\&=0.\end{aligned} \tag{6.68}$$

The above equations may be further reduced to a single second-order differential equation for $H_0^{\omega^0}$. We have verified that doing so yields the same equation (up to difference in conventions) as in Ref. [55].

6.5.1.1 Initial conditions

Eqs. (6.67), (6.68) comprise two first order differential equations for the functions $H_0^{\omega^0}(r)$ and $K^{\omega^0}(r)$. To integrate them in the stellar interior, we also need to know the initial value(s), i.e., two parameters characterizing the boundary condition. We can obtain this near $r = 0$, by solving the perturbation equations around the origin. We can choose without loss of generality that $H_0^{\omega^0}(0) = 1$. Then, plugging in the Taylor expansions for $H_0^{\omega^0}(r)$ and $K^{\omega^0}(r)$ around $r = 0$, we obtain the expressions

$$\begin{aligned}H_0^{\omega^0}(r)&\approx 1+\frac{r^2}{84}\left[-\kappa(33p_c+\rho_c)+\frac{18\rho_c''}{3p_c+\rho_c}\right],\\K^{\omega^0}(r)&\approx 1+\frac{r^2}{14}\left[-\kappa(2p_c-\rho_c)+\frac{3\rho_c''}{3p_c+\rho_c}\right],\end{aligned} \tag{6.69}$$

valid to $O(r^3)$. Here $\rho_c = \rho(0)$ ($p_c = p(0)$) are the unperturbed central density (pressure). Similarly $\rho_c'' = \rho''(0)$ is its second radial derivative at $r = 0$. Note that $\rho'(0) = p'(0) = 0$. Equipped with the initial conditions in Eq. (6.69), we can integrate from a point close to $r = 0$ to the surface. Thus, solving for H^{ω^0}, K^{ω^0} throughout the interior of the star.

6.5.2 Linear-in-frequency part

The linear-in-frequency part of the metric variables obeys the same master equations as in Eqs. (6.55), (6.56), but with the source terms computed using the static quantities. We just outlined the process of solving for the $H_0^{\omega^0}$ and K^{ω^0} in Sec. 6.5.1. The fluid perturbations in the static case, i.e., W^{ω^0} and V^{ω^0}, can be obtained using Eqs. (6.60), (6.65). We have already shown that $X(r)$ vanishes in the static limit. Thus, the source terms, colored in orange, in the master equations are fully specified.

6.5.2.1 Initial conditions

To perform the integration from a point near $r = 0$, we once again need the near-origin solutions for $H_0^{\omega^1}$ and K^{ω^1}. Similar to the static case, this can be done substituting the Taylor expansions near $r = 0$ for the metric and fluid perturbations. Alongside, we also make use of the relations in Eqs. (6.60), (6.65). This yields the Taylor series expansions to $O(r^3)$. We provide the expressions in Eq. (6.70).

$$H_0^{\omega^1}(r) = \frac{e^{-\frac{\nu_c}{2}} r^2}{350\kappa(3p_c+\rho_c)^4}\Big\{2\eta_c[50\kappa^2(3p_c+\rho_c)^4 + 15\kappa(18p_c^2+9p_c\rho_c+\rho_c^2)\rho_c'' - 351(\rho_c'')^2$$

$$+ 75(3p_c+\rho_c)\rho_c^{(4)}] - 75(3p_c+\rho_c)[\kappa(21p_c^2+22p_c\rho_c+5p_c^2)+6\rho_c'']\eta_c''$$

$$+ 150(3p_c + \rho_c)^2 \eta_c^{(4)} \Bigg\},$$

$$K^{\omega^1}(r) \approx \frac{6e^{-\frac{\nu_c}{2}}\eta_c}{3p_c + \rho_c} + \frac{e^{-\frac{\nu_c}{2}} r^2}{350\kappa(3p_c + \rho_c)^4} \Bigg\{ 150(3p_c + \rho_c)^2 \eta_c^{(4)} + 150(3p_c + \rho_c)\eta_c'' [\kappa(21p_c^2 + 10p_c\rho_c$$
$$+ \rho_c^2) - 3\rho_c''] - \eta_c [50\kappa^2(2p_c - 3\rho_c)(3p_c + \rho_c)^3 + 45\kappa(51p_c^2 + 32p_c\rho_c + 5p_c^2)\rho_c''$$
$$- 702(\rho_c'')^2 + 150(3p_c + \rho_c)\rho_c^{(4)}] \Bigg\}, \tag{6.70}$$

where we have set $H_0^{\omega^1}(0) = 0$, without loss of generality. Here $\eta_c = \eta(0)$ is the shear viscosity at the origin. Note that $\eta'(0) = 0$, due to Eq. (6.33).

Note that, due to the expansions in Eq. (6.66), the linear-in-frequency parts are responsible for making the initial conditions for the metric perturbation functions complex. The equations governing the static fields in Eqs. (6.67), (6.68) also do not have any complex terms in them. Thus, in the absence of shear viscosity, it is possible to choose the overall normalization such that H_0 and K are purely real. The presence of shear viscosity necessarily renders them complex.

6.5.3 Matching at surface with the RW function

Equipped with the initial conditions for the metric perturbations to linear order in frequency given in Eqs. (6.69), (6.70), we can integrate the master equations perturbatively to solve for the functions H_0 and K to linear order in frequency up to the stellar surface. It is trivial to establish their continuity at the stellar surface, and thus we obtain their values just outside the star.

Outside the star, as mentioned before, the vacuum perturbation equations governing H_0 and K may be reduced to a single Schrödinger-like equation, the RW equation, Eq. (6.23). This is accomplished using the relations in Eqs. (59), (60) in Ref. [272], rewritten here to $O(\omega^2)$:

$$\phi = \frac{-1}{(n+1)M}[\{-n(n+1)r(r-3M)\}K$$

$$+ (n+1)r(nr+3M)e^{-\lambda}H_0] \ , \tag{6.71}$$

$$\phi' = \frac{1}{-(n+1)M}[\{n(n+1)\}\{(n+1)r - 3M\}K.$$

$$. + \{-n(n+1)^2 r - 3(n+1)Me^{-\lambda}\}H_0] \ ,$$

where $n = (\ell - 1)(\ell + 2)/2$. The above two equations can be combined into a dimensionless one via logarithmic derivative of the RW variable w.r.t the radial coordinate

$$T \equiv \frac{r}{\phi}\frac{d\phi}{dr_*}\bigg|_{r=R} = \frac{r}{r_*}\frac{d\log\phi}{d\log r_*}\bigg|_{r=R} . \tag{6.72}$$

This quantity will serve as the boundary condition for solving the RW equation outside the star. To determine the leading-order dissipative response, it is sufficient for us to restrict our discussion to linear order in frequency

$$T \equiv T_0 - iR\omega T_1 + O(\omega^2) \ . \tag{6.73}$$

In Sec. 6.6, we will see that the leading Love number and dissipation number are fully determined by T_0 and T_1 respectively.

6.6 RW scattering problem using MST

In this section, we relate this boundary condition of the RW scalar in Eq. (6.72) to the static Love number and the leading dissipation number of the star. As outlined in Sec. 6.2, we accomplish this by considering the problem of monochromatic GWs scattering off the neutron star. In this case, sufficiently far from the star, i.e, in the limit $r \to \infty$, the RW equation takes the form

$$\frac{d^2\phi(r)}{dr_*^2} + \omega^2\phi(r) = 0, \tag{6.74}$$

which is solved by a linear combination of incoming and outgoing free-wave solutions, i.e, $\phi(r) = A^{\rm in}_{\ell,\omega}\exp(-i\omega r_*) + A^{\rm out}_{\ell,\omega}\exp(i\omega r_*)$. The quantity $A^{\rm out}_{\ell,\omega}/A^{\rm in}_{\ell,\omega}$ can be related to the static Love and leading dissipation numbers, as outlined in Sec. 6.2.

To accomplish this, we employ the analytical MST scheme for the RW equation, which was first presented in Ref. [218]. In this work, we follow the conventions and notations employed in Ref. [219]. In the MST scheme, we can write down analytical solutions for the RW equation as a sum of infinite hypergeometric functions, convergent in different domains.

In the near-zone, we can write a general solution to the RW equation as

$$\phi(r) = B_{\bar\nu} X_0^{\bar\nu}(r) + B_{-\bar\nu-1} X_0^{-\bar\nu-1}(r), \tag{6.75}$$

where $X_0^{\bar\nu}$ and $X_0^{-\bar\nu-1}$ are near-zone Coulomb-type solutions with convergence radius $r_s = 2GM \leq r < \infty$. $\bar\nu$ stands for the renormalized angular momentum. Moreover, these functions have asymptotic behavior $X_0^{\bar\nu} \sim r^{\bar\nu}, X_0^{-\bar\nu-1} \sim r^{-\bar\nu-1}$ when $r \to \infty$. Their explicit expansions is given in Ref. [219]. We can fix the ratio of $B_{\bar\nu}$ and $B_{-\bar\nu-1}$ at the surface of the neutron star using Eq. (6.72).

Solving the scattering problem requires connecting the near-zone solution to the far-zone, i.e., $\infty \geq r > r_s$. Here, the solution may be written as a combination of incoming and outgoing waves. To connect this to the far-zone, we first switch to the far zone Coulomb-type solutions denoted by $X_C^{\bar\nu}, X_C^{-\bar\nu-1}$ in [219] with convergence radius $r_s < r \leq \infty$. In the overlap region, where $r_s < r < \infty$, we can match these two solutions and get

$$X_0^{\bar\nu} = K_{\bar\nu} X_C^{\bar\nu}\,,\, X_0^{-\bar\nu-1} = K_{-\bar\nu-1} X_C^{-\bar\nu-1}\,, \tag{6.76}$$

where the coefficient $K_{\bar\nu}$ is given by Eq.(3.32) in Ref. [219]. Now, we switch to the basis of incoming and outgoing waves using Eqs.(3.29, 3.34, 3.35) in Ref. [219]. Then, in the limit $r \to \infty$, Eq. (6.75) takes the form

$$\phi(r)|_{r\to\infty} = A^{\rm out}_{\ell,\omega} e^{i\omega r_*} + A^{\rm in}_{\ell,\omega} e^{-i\omega r_*}, \tag{6.77}$$

where

$$\frac{A^{\rm out}_{\ell,\omega}}{A^{\rm in}_{\ell,\omega}} = \frac{(1+ie^{i\pi\bar{\nu}}\mathcal{K}_{\rm NS})}{(1-ie^{-i\pi\bar{\nu}}\frac{\sin[\pi(\bar{\nu}+i\epsilon)]}{\sin[\pi(\bar{\nu}-i\epsilon)]}\mathcal{K}_{\rm NS}}\frac{A^{\bar{\nu}}_{-}}{A^{\bar{\nu}}_{+}}e^{2i\epsilon\log(\epsilon)} \tag{6.78}$$

where $\epsilon = 2GM\omega$, $\mathcal{K}_{\rm NS} = (B_{-\bar{\nu}-1}K_{-\bar{\nu}-1}/B_{\bar{\nu}}K_{\bar{\nu}})$ and expressions for $A^{\bar{\nu}}_{-(+)}$ given in Eqs. (3.19, 3.38) in Ref. [219].

As mentioned in Sec. 6.2, we cannot immediately relate the ratio in Eq. (6.78) to the amplitude computed in EFT in Eq. (6.21). This is because we have not yet isolated the contributions of tidal effects to the scattering process. As it is, the ratio in Eq. (6.78) contains the combined effect of both tidal effects, and non-tidal effects (such as scattering of GWs off the gravitational background). Dissipative tidal effects may be easily extracted from the phase following Ref. [3], since non-tidal effects do not contribute to dissipation.

The leading conservative tidal response as well may be distilled in two ways. One way is to subtract the total-scattering amplitude of a neutron star with that of a Schwarzschild black hole with same mass, both computed in the perturbation theory framework. This cancels out all common contributions[14], leaving behind only the difference in their tidal contributions. Then, using the known amplitude due to the black hole's tidal response, we can compute the corresponding result for neutron star[15]. This has been schematically shown in Eq. (6.81). Alternatively, we can make use of the near-far factorization first presented in Ref. [245]. This was used to show the

[14]Due to scattering of GWs off the background metric

[15]In fact, as far as the dissipation number computation is concerned, since only tidal effects contribute to dissipation, and thus no such subtraction is required and we can just take the absolute values on both sides of Eq. (6.26), and write the expression for η_2, as was done in Ref. [3].

vanishing of black hole Love numbers, as well as computation of the renormalization-group flows of the dynamical tidal response in Refs. [3, 245]. However, this is justified only for the generic-ℓ solution to the Teukolsky equation [475]. The essential idea is that the far-zone scattering phase shift corresponds to the wave scattering against the background metric, while the near-zone phase shift is the scattering against the star surface which contains the tidal response:

$$\frac{A^{\text{out}}_{\ell,\omega}}{A^{\text{in}}_{\ell,\omega}} = \underbrace{\frac{A^{\bar{\nu}}_{-}}{A^{\bar{\nu}}_{+}} e^{2i\epsilon\log(\epsilon)}}_{\text{far zone}} \times \underbrace{\frac{1 + ie^{i\pi\bar{\nu}}\mathcal{K}_{\text{NS}}}{1 - ie^{-i\pi\bar{\nu}}\frac{\sin(\pi(\bar{\nu}+i\epsilon))}{\sin(\pi(\bar{\nu}-i\epsilon))}\mathcal{K}_{\text{NS}}}}_{\text{near zone}} \,. \tag{6.79}$$

From Eq. (6.79), we can straightforwardly get the near-zone phase shift as

$$\eta^{\text{NZ}}_{\ell} e^{2i\delta^{\text{NZ}}_{\ell}} = \frac{1 + ie^{i\pi\bar{\nu}}\mathcal{K}_{\text{NS}}}{1 - ie^{-i\pi\bar{\nu}}\frac{\sin(\pi(\bar{\nu}+i\epsilon))}{\sin(\pi(\bar{\nu}-i\epsilon))}\mathcal{K}_{\text{NS}}} \,. \tag{6.80}$$

Regardless of method used, we can write down the tidal contribution to the phase shift and absorption as shown in Eqs. (6.82), (6.83):

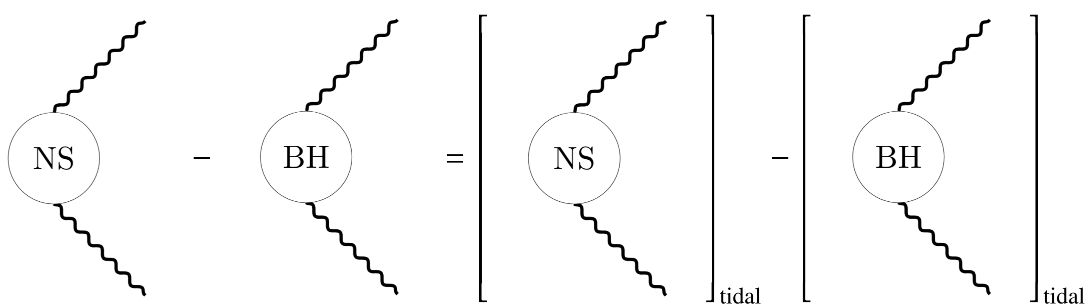

(6.81)

$$
\begin{aligned}
\delta_\ell^{\mathrm{NZ}} &= (2R\omega)^{2\ell+1} \times (-1)^{\ell+1} \frac{\Gamma(-2\ell)\Gamma(\ell+2)}{\Gamma(1-\ell)\Gamma(2\ell+2)} \\
&\times \Bigg[\ell\Big(-\frac{T_0}{1-2C} + \ell + 1 \Big) \, {}_2F_1(-\ell-2, 2-\ell, -2\ell, 2C) \\
&+ C\left(\ell^2 - 4\right) \, {}_2F_1(-\ell-1, 3-\ell, 1-2\ell, 2C) \Bigg] \\
&\times \Bigg[(\ell+1)\Big(\frac{T_0}{1-2C} + \ell \Big) \, {}_2F_1(\ell-1, \ell+3, 2(\ell+1), 2C) \\
&+ C(\ell-1)(\ell+3) \, {}_2F_1(\ell, \ell+4, 2\ell+3, 2C) \Bigg]^{-1},
\end{aligned}
\tag{6.82}
$$

$$
\begin{aligned}
\eta_\ell^{\mathrm{NZ}} &= 1 + (2R\omega)^{2\ell+2} \times (-1)^{\ell} \frac{T_1}{1-2C} \frac{\Gamma(-2\ell)\Gamma(\ell+2)}{\Gamma(1-\ell)\Gamma(2\ell+2)} \\
&\times \Bigg[C(\ell-2)(\ell+1)(\ell+2) \\
&\quad \times \, {}_2F_1(-\ell-1, 3-\ell; 1-2\ell; 2C) \, {}_2F_1(\ell-1, \ell+3, 2(\ell+1), 2C) \\
&+ \ell(\ell+1)(2\ell+1) \, {}_2F_1(-\ell-2, 2-\ell, -2\ell, 2C) \\
&\quad \times \, {}_2F_1(\ell-1, \ell+3, 2(\ell+1), 2C) \\
&+ C\ell(\ell-1)(\ell+3) \, {}_2F_1(-\ell-2, 2-\ell, -2\ell, 2C) \\
&\quad \times \, {}_2F_1(\ell, \ell+4, 2\ell+3, 2C) \Bigg] \\
&\times \Bigg[(\ell+1)\Big(\frac{T_0}{1-2C} + \ell \Big) \\
&\quad \times \, {}_2F_1(\ell-1, \ell+3, 2(\ell+1), 2C) \\
&+ C(\ell-1)(\ell+3) \, {}_2F_1(\ell, \ell+4, 2\ell+3, 2C) \Bigg]^{-2}.
\end{aligned}
\tag{6.83}
$$

6.6.1 Matching with EFT

Finally, we can get the Love number and dissipation number by matching the EFT phase shifts in Eq. (6.22) with the ones from stellar perturbation theory given in Eqs. (6.82), (6.83). The expressions for the rescaled Love and dissipation number are as follows:

$$
\begin{aligned}
k_2^E &= -\frac{8C^5\,(6C-3+T_0)}{\mathcal{D}}\,, \quad \nu_2^E = \frac{3840C^{10}T_1}{\mathcal{D}^2}\,, \\
\mathcal{D} &= 5(-2C\left(C\left(6C^2+4C+3\right)+3\right)T_0 + 6(C-1)C\left(4C^3+2C^2-3\right) \\
&\quad -3\,(6C-3+T_0)\log(1-2C)
\end{aligned}
\tag{6.84}
$$

From the above two expressions, we see that the dissipation number vanishes when the boundary condition at the star surface has no linear-in-frequency dependence, i.e. $T_1 = 0$. This is consistent with the time-reversal property of the retarded Green's function in Eq. (6.16). Secondly, there is a relation between the rescaled Love number and dissipation number

$$
\nu_2^E = \frac{60T_1}{(6C-3+T_0)^2}(k_2^E)^2\,. \tag{6.85}
$$

Eq. (6.84) is also consistent with the BH limit, where we have

$$
C \to \frac{1}{2}\,, \quad T \to -i\omega r_s\,, \tag{6.86}
$$

corresponding to purely ingoing boundary at the horizon. Thus, $T_0 \to 0,\ T_1 \to 1$ and Eq. (6.84) correctly reduces to

$$
k_2^E = 0,\ \nu_2^E = \frac{1}{60} \tag{6.87}
$$

Finally, we have also verified that our formula for the rescaled Love number k_2^E is consistent with the one given by T. Hinderer in Ref. [55] apart from convention-related differences after rewriting the boundary condition T_0 of the RW variable in terms of the logarithmic derivative of the metric perturbation function $H_0(r)$, i.e., $y \equiv RH_0'(R)/H_0(R)$, as

$$\begin{aligned} T_0 = &\Big(-3(1+2(-2+C)C) + 3(-1+C)(-1+2C)y \Big) \\ &\Big((3-8C+6C^2) + (-1+(5-6C)C)y \Big)^{-1} (1-2C). \end{aligned} \tag{6.88}$$

6.7 Observables

In the previous sections, we have developed the formalism for computing Love and dissipation numbers of viscous neutron stars in the small-frequency limit for nonbarotropic perturbations. We now use it to numerically compute some of the relevant quantities and relate the dissipation number to the waveform contribution at 4PN.

6.7.1 Love and dissipation numbers for various EoS(s) and compactness

To compute the Love and dissipation number(s), we first integrate the master Eqs. (6.55), (6.56) and then switch to the RW function using Eq. (6.71), and compute the quantities T_0 and T_1 in Eq. (6.73). We can then use Eqs. (6.84) to compute the Love and dissipation number(s). The compactness $C = M/R$ is obtained from the stellar profiles generated for various EoS(s).

We present the Love and dissipation numbers thus obtained for various EoS(s) and compactness in Table. 6.1. Here, the first column labeled EoS lists the equation(s) of state for which the relevant quantities in each row have been computed. The details regarding the various EoS(s) have been discussed before in Sec. 6.3. The remaining columns sequentially show the rescaled Love number k_2, the dissipation number H_ω^E, and the rescaled dissipation number ν_2^E, and finally the ratio of the dissipation number H_ω^E with that for a black hole with the same mass, where

$(H_\omega^E)_{\rm BH} = 32/45$. This is to get a relative measure of the 'absorptivity' of a neutron star compared to a black hole.

As we showed in Sec. 6.4.2, the bulk viscosity does not affect the (leading) dissipation number. Thus, the dissipation numbers obtained in the table are entirely due to shear viscosity. Here, we consider the most dominant contribution to the shear viscosity which is due to $e-e$ scattering in the temperature range relevant during inspiral [196, 456]. The shear-viscosity due to this process scales inversely with the square of temperature (i.e., $\sim 1/T^2$) as seen from Eq. (6.33). Thus, colder neutron stars have a greater contribution to shear viscosity. Since the viscosity linearly affects T_1, and subsequently the (rescaled) dissipation number ν_E, i.e., they too scale as $1/T^2$. Although neutron stars are born very hot ($\sim 10^{11}$K), they cool rapidly to lower temperatures ($\sim 10^9 K$) due to neutrino emission within $\sim 10^5$ years [486]. The temperature of cold neutron stars about to merge during inspiral is expected to be within $10^5 - 10^{10} K$, with the likely range being within $10^7 - 10^9 K$ [196, 456, 471]. We show the results at the coldest possible temperature $T = 10^5 K$ when the shear viscosity due to $e-e$ scattering is strongest. The temperature dependence is captured in the first row of the table through the factor $(T_K/10^5 K)^2$ next to the relevant quantities, where T is the actual temperature of the neutron star in Kelvin. Since H_ω^E and ν_2^E scale as $\sim T^{-2}$, multiplying the factor $(T_K/10^5 K)^2$ renders them constant and gives their value at $T = 10^5 K$.

Within each EoS, we have considered stars with different compactness in increasing order. It is clear from the table that within any EoS, the dissipation number decreases with increasing compactness. For instance, for the case of 'FSU2', as we go from $1 \mathrm{M}_\odot$ to $2.34 \mathrm{M}_\odot$, where the radius barely changes (14.0 km to 13.8 km), the dissipation number H_ω^E falls sharply with compactness by almost 3 orders of magnitude. This is actually expected from Eq. (6.84) if we assume that the T_0 and T_1 do not change a lot with changing compactness. Then, the rest of the expression explains the sharp decrease with increasing compactness. This is seen easily in the Newtonian limit $C \ll 1$, where we have

$$H_\omega^E = \frac{10T_1}{36(2+T_0)^2 C^6}, \tag{6.89}$$

which shows that the dissipation number falls sharply with the inverse of the compactness at the sixth power.

In reality, $T_{0,1}$ do not actually stay constant with changing compactness as they depend on the density and pressure profile(s) which in turn also affects the shear viscosity. However, we find that the change in them is quite small (relatively) and not adequate to compensate for the sharp-dependence on compactness. This can be seen clearly from the last column in Table. 6.1, where the rescaled dissipation number is seen to be in the same order of magnitude regardless of compactness (and even EoS(s)).

The importance of compactness in tuning the dissipation number is also seen in the variation of EoS(s). For example, consider the three stars in the table with a mass $M \approx 1.01 M_\odot$. They all correspond to different equations of state. Despite having the same mass, the 'HZTCS' star is more compact than 'GM1' which in turn is more compact than 'FSU2'. Despite the differences in their EoS(s), and consequently the shear-viscosity profile, we find that the dissipation numbers fall with increasing compactness as expected. The compactness does not however capture the complete variation in the dissipation numbers. For the three stars with $M = 1.34 M_\odot$ ($M = 1.71 M_\odot$), the compactness still increases as one goes from 'FSU2' to 'GM1' to 'HZTCS'. However, while the H_ω^E for 'GM1' and 'HZTCS' is smaller than that of 'FSU2' as expected, the relative ordering of H_ω^E between 'GM1' and 'HZTCS' is not consistent with the ordering of the compactness. However this is not surprising as the compactness for both of them are very similar (with in $\sim 1\%$).

6.7.2 Correction to number of GW cycles due to dissipation

Dissipation in a binary leads to transfer of orbital energy into the mass (thermal energy) of the compact objects, here the neutron stars. This modifies the energy conservation law for quasi-circular inspiral as

$$\dot{E} = -\mathcal{F}_\infty - \dot{m}_1 - \dot{m}_2. \tag{6.90}$$

Here $\dot{E}$ is the rate of change of orbital energy, $\mathcal{F}_\infty$ is the gravitational energy flux leaving the system and $\dot{m}_{1,2}$ is the rate of heating (due to tidal dissipation). We can use this modified energy conservation law to compute the leading (4PN) correction to the phase of the inspiral waveform due to tidal heating in the stationary-phase approximation [3, 262–264]. We do that below as a way to roughly quantify the relevance of shear viscosity.

Since we are only interested in the leading order correction, it is sufficient to compute the correction to the orbital phase due to one star and then linearly sum their contributions. So we first compute the correction to the orbital phase when only one star gets tidally heated.

The rate of heating (or equally rate of increase in mass) for a neutron star of mass m_1 in a quasi-circular binary (with another mass m_2) is given by [3]

$$\begin{aligned}\dot{m}_1 &= \frac{1}{2} m_1 (G m_1)^5 H_\omega^{E,1} \dot{E}_{\rho\sigma} \dot{E}^{\rho\sigma} \\ &= H_\omega^{E,1} \frac{9 m_1^6 m_2^2}{G M^8} \left(\frac{G M}{r}\right)^9 \\ &= H_\omega^{E,1} \frac{9 m_1^6 m_2^2}{G M^8} x^{18},\end{aligned} \tag{6.91}$$

where $M = m_1 + m_2$, r the radius of the orbit, $\Omega = (GM/r)^{1/3}$ is the orbital velocity, $V = x =$

$(GM\Omega)^{1/3} = (GM/r)^{1/2}$. The leading quadrupolar flux of the binary to infinity is given by

$$\mathcal{F}_\infty = \frac{32 m_1^2 m_2^2}{5GM^4} x^{10}. \tag{6.92}$$

The relative contribution of the tidal heating to the waveform may then be characterized by the ratio

$$\begin{aligned} \dot{m}_1/\mathcal{F}_\infty &= (45 H^E_\omega/32)(m_1/M)^4 x^8 \\ &= (15 \nu_2^{E,1}/16)(R/m_1)^2 (R/r)^4. \end{aligned} \tag{6.93}$$

Note that the net effect is enhanced by lower compactness (m_1/r), and closeness (R/r) of the binary.

Now, the energy conservation law for the system reads

$$\dot{E} = -\mathcal{F}_\infty - \dot{m}_1 - \dot{m}_2, \tag{6.94}$$

$$\implies \dot{x} = \frac{1}{M\eta x}(\mathcal{F}_\infty + \dot{m}_1 + \dot{m}_2) \tag{6.95}$$

where $E = M\eta v^2/2$, with $\eta = (m_1 m_2)/M^2$ being the orbital binding energy, sapped away to infinity and into the heat of the bodies. We can now determine the orbital phase of the binary during inspiral as

$$\begin{aligned} \phi(x) &= \int \frac{x^3}{M}\frac{dt}{dx} dx \\ &\approx \int \frac{5M^2}{32 m_1 m_2 x^6}\left[1 - \frac{15\nu_2^{E,1}}{16}\frac{R^6}{m_1^2 M^4} x^8 - (1 \leftrightarrow 2)\right] dx \\ &= -\frac{M^2}{32 m_1 m_2 x^5} - \frac{25M^2}{m_1 m_2}\frac{\nu_2^{E,1}}{512}\frac{R^6}{m_1^2 M^4} x^3 - (1 \leftrightarrow 2) \\ &= \phi_{\mathrm{0PN}} + \delta\phi(x). \end{aligned} \tag{6.96}$$

Eq. (6.96) contains $\delta\phi$, which is the correction to the orbital phase due to one neutron stars getting tidally heated. Then, using the fact that the GW frequency in the most dominant mode is twice the orbital frequency, we can compute the change in number of GW cycles due to tidal dissipation within a frequency range as

$$\begin{aligned}
\delta\mathcal{N}_{\rm GW} &= \frac{\delta\phi[(GM\pi\omega_f)^{1/3}] - \delta\phi[(GM\omega_i\pi)^{1/3}]}{\pi}, \\
&= \sum_{a=1,2} \frac{25R_a^6\nu_2^{E,a}}{512m_a^3(M-m_a)M^2} \times GM(\omega_i - \omega_f).
\end{aligned} \tag{6.97}$$

Here $m_{a=1,2}$ are the masses of the neutron stars, and $M = m_1 + m_2$. $R_{a=1,2}$ are the radii, and $\nu_2^{E,a=1,2}$ are the rescaled dissipation numbers defined in Eq. (6.18). The inspiral enters the detector frequency band at orbital frequency ω_i to ω_f. Eq. (6.97) could be evaluated using the dissipation numbers in Table. 6.1, for inspiral within the LVK band for which $\omega_i \approx 30$Hz and $\omega_f \approx \min(1000\text{Hz}, \omega_{\rm ISCO})$. However, it is important to remember here the discussion in Sec. 6.4.3, where we noted that the small-frequency expansion of the perturbation equations as done in this work is valid when the inspiral frequency is small compared to the characteristic Brunt-Väisälä frequency $N_{\rm ch}$. The latter may be estimated by some averaging scheme [503] or by the highest frequency among the g-modes [196, 476] yielding $N_{\rm ch} \in (150, 700)$Hz depending on the mass and EoS of the star, and so the dissipation numbers provided in Table. 6.1 may not suffice throughout the inspiral. Nevertheless, at least for conservative effects, the contribution of the oscillation modes associated with convection, i.e., g-modes is often negligible due to their weak coupling with external tidal fields [476]. We proceed with the expectation that the same may be true for shear-viscous dissipation as well. Bulk-viscosity on the other hand was shown to be vanishing in the regime $\omega \ll N_{\rm ch}$ in this work. Thus, the correction to it could be a lot more significant and non-negligible in middle and late inspiral. However, such effects are likely to only enhance the contribution to tidal heating and thus the results in this work may be used to obtain a lower limit for the contribution of tidal heating during inspiral.

We compute Eq. (6.97) and present the results for various EoS(s) and compactness in Table 6.2. Once again the first column lists out the various EoS(s) similar to Table 6.1. The subsequent four columns show neutron star mass, radius, H_ω^E and ν_2^E.

Then, the fifth column shows $\delta\mathcal{N}_{\rm GW}$, change in the number of cycles. The sixth column shows the Newtonian (leading) contribution to the total number of cycles within the detector band, which we take to be from 30Hz to min($\omega_{\rm ISCO}$,1000Hz). Finally, the seventh column shows the correction to the number of cycles at 4PN due to other conservative contributions in the spin-less case [265, 479, 505].

As mentioned previously, the dissipation considered here is entirely due to $e-e$ scattering, with a known dependence on temperature given in Eq. (6.33). This temperature dependence is canceled by the factor $(T_K/10^5)^2$ next to H_ω^E, ν_2^E and $\delta\mathcal{N}_{\rm GW}$, so that the results in the table correspond to neutron stars $T = 10^5 K$. Here T_K is the temperature in Kelvin of the neutron star at the start of the inspiral which we have kept fixed while evaluating $\delta\mathcal{N}_{\rm GW}$.

In the symmetric NS case, Eq. (6.97) reduces to

$$\delta\mathcal{N}_{\rm GW} = \frac{75 H_\omega^E}{2048} G M(\omega_i - \omega_f). \tag{6.98}$$

Thus, for a given initial and final frequency, the product of the dissipation number and the mass decides the magnitude of $\delta\mathcal{N}_{\rm GW}$. We can see from the table that within an EoS, the compactness generally increases with mass (except for the EoS 'HZTCS'). Thus, there is a competition between the falling dissipation number (with compactness) and the increasing mass. However, we know that the dissipation number decreases sharply with compactness, ($\sim C^{-6}$ in the Newtonian limit), and thus $\delta\mathcal{N}_{\rm GW}$ decreases in any EoS, as visible in Table. 6.2.

Also note that barring the most compact configuration in each EoS ($M \sim 2.3 M_\odot$), the correction to the number of cycles due to tidal heating at $T = 10^5 K$ exceeds that due to conservative contributions at 4PN in the eighth column. Additionally, recent studies [506] suggest that a mismodeling at 4PN order could lead to significant systematic errors in the data analysis even of current GW detector networks (and future detectors may even require improvements in the accuracy of the gravitational waveforms of at least three orders of magnitude [340, 507]). Thus, shear-viscosity could be relevant during inspiral for sufficiently cold and not-too-compact neutron stars. However, note that this will fall sharply with the square of temperature. Thus, for larger temperatures such as at $10^7 - 10^9 K$, the effect of shear-viscosity on the waveform could be all but negligible. Thus, colder and less compact stars have a stronger tidal imprint when considering the shear viscosity due to $e - e$ scattering.

6.8 Conclusion and future Work

In this work, we have studied in detail the tidal response of nonspinning neutron stars in the low-frequency limit, with the goal of determining the leading dissipation numbers due to shear and bulk viscosity, which correspond to the next-to-leading order (in frequency) tidal effects. We found that the bulk viscosity has no contribution to the dissipation number, and demonstrated that this is physically due to the vanishing divergence of the fluid velocity at linear order in frequency, and this is related to a peculiar incompressibility in the static limit. We showed that this conclusion holds only for non-barotropic perturbations, when the perturbing frequency (inspiral frequency in a binary) ω, is small compared to characteristic Brunt-Väisälä frequency $N_{\rm ch}$ in the star, but much larger than the rate of m-Urca processes.

On the other hand, the leading shear viscous contribution to the dissipation number was seen to be nonzero in this regime. We derived two master equations governing metric perturbations to linear order in the frequency inside the neutron star, including viscous contributions.

We then considered the problem of scattering GWs off a neutron star i.e., gravitational Raman scattering, and related the scattering phase and degrees of absorption to the static Love and leading dissipation numbers.

To achieve this, we first integrated the master equations for the metric perturbations from the center to the surface of the star. Outside the star, the metric perturbation equations could be reduced to the RW equation, and the boundary conditions for the RW function at the stellar surface were obtained earlier by integrating the master equations. We then used the analytical MST approach to compute the scattering amplitude as a function of the RW boundary conditions at the stellar surface. We isolated the tidal contribution to this amplitude and extracted expressions for the rescaled static Love and dissipation numbers. The formula for the rescaled Love number was shown to be consistent with previous formulas by Hinderer [55].

We then used the formulae to calculate the Love and dissipation numbers for various EoS(s) and compactness. We found that compactness was the most important parameter tuning the strength of the tidal dissipation number for a given EoS.

Finally, we computed the correction to the number of GW cycles due to shear viscosity from $e-e$ scattering at 4PN in the waveform for a binary system of two identical neutron stars within the LIGO band. We found that this effect can be comparable to or even exceed the usual nontidal contributions at 4PN if the neutron stars are sufficiently cold, $T \sim 10^5 - 10^6 K$, and not too compact. Thus, we show that cold and less compact neutron stars are likely to have the strongest tidal heating at the leading 4PN order during inspiral, neglecting any resonant or spin-related effects.

The work can be extended in several directions in the future. An obvious next step would be to extend the validity of this work to arbitrary frequencies. The low-frequency expansion of the perturbation equations inside the star is sufficient in a binary system when the inspiral frequency is smaller than any resonant frequencies. While the often considered f-mode frequency is much higher than the orbital frequency during inspiral, but the class of g-modes have much lower resonant frequencies and can be excited during inspiral. This is also related to the discussions surrounding the Brunt-Väisälä frequency as it is the characteristic frequency of the g-modes. The effect of resonances during inspiral on the conservative tidal response in polytropic systems was recently been studied in Ref. [260]. It may be interesting to extend this to realistic EoS(s) and dissipation. This is particularly important in light of the vanishing contribution of bulk viscosity at 4PN order that we have shown in this chapter, as resonant dissipation due to g-modes may be its leading nonzero contribution to tidal heating.

Second, in this work we restricted ourselves to spherically symmetric systems for simplicity. In addition, we have neglected axial modes [354, 372, 419, 420], since the polar modes dominantly couple to neutron stars. The presence of spin would lead to a violation of spherical symmetry, and thus also couple axial and polar sectors, leading to a more complicated system of equations, and a potentially interesting and perhaps stronger tidal response. It has recently been shown in the Newtonian limit in Ref. [199] that moderately spinning neutron stars in binaries can reach f-mode resonances during the inspiral (see also Ref. [508] for earlier work and Ref. [413] for a relativistic treatment). They also showed that such a resonance could make the orbit eccentric. Thus, a general-relativistic study of the tidal response of spinning compact objects could lead to the discovery of interesting potentially observable effects.

Other interesting directions could be the extension to other (possibly exotic) compact objects or to alternative theories of gravity, or simply add more details relevant for a realistic neutron star, such as an in-depth consideration of the various microscopic processes, their rates, and their impact on the observed macro-physics.

For now, we leave such considerations to future works. With the advent of future detectors [340, 507]), and with improved sensitivities, the rich internal physics of neutron stars may be better understood and constrained. Along with the EoS of the neutron star which relates the equilibrium pressure with the density, a knowledge of the out-of-equilibrium transport properties such as viscosity inferred through tidal heating in binary inspiral will be influential in understanding the dense matter behavior as well as the neutron star interior composition. It is thus important that theoretical investigations now rigorously take into account the various possible micro-physics relevant to the neutron star and their observational imprints.

ACKNOWLEDGEMENTS

We thank Alessandra Buonanno, Abhishek Hegade, Misha Ivanov, Ben Leather, Julio Parra-Martinez, Justin Ripley, Hector Silva, Teja Venumadhav, Pratik Waghle, Nicolás Yunes, and Matias Zaldarriaga for useful comments and discussions. We thank Swarnim Shirke for providing a comprehensive review of the dissipation sources inside neutron stars.

Chapter 7: Quasinormal modes of slowly-spinning horizonless compact objects

Authors[1]: *M. V. S. Saketh, Elisa Maggio*

Abstract: One of the main predictions of general relativity is the existence of black holes featuring a horizon beyond which nothing can escape. Gravitational waves from the remnants of compact binary coalescences have the potential to probe new physics close to the black hole horizons. This prospect is of particular interest given several quantum-gravity models that predict the presence of horizonless and singularity-free compact objects. The membrane paradigm is a generic framework that allows one to parametrise the interior of compact objects in terms of the properties of a fictitious fluid located at the object's radius. It has been used to derive the quasi-normal mode spectrum of static horizonless compact objects. Extending the membrane paradigm to rotating objects is crucial to constrain the properties of the spinning merger remnants. In this work, we extend the membrane paradigm to linear order in spin and use it to analyse the relationships between the quasi-normal modes, the object's reflectivity, and the membrane parameters. We find a breaking of isospectrality between axial and polar modes when the object is partially reflecting or the compactness differs from the black hole case. We also find that in reflective ultracompact objects some of the modes tend towards instability as the spin increases. Finally, we show that the spin enhances the deviations from the black-hole quasinormal mode spectrum as

[1]Originally published as Phys. Rev. D **110**, no.8, 084038 (2024).

the compactness decreases. This implies that spinning horizonless compact objects may be more easily differentiated than nonspinning ones in the prompt ringdown.

7.1 Introduction

Gravitational waves (GWs) provide a unique opportunity to test gravity and investigate the nature of compact objects. The ground-based detectors LIGO and Virgo have detected ninety GW candidates from the coalescence of compact binaries up to the end of their third observing run [23–25, 335]. Some important discoveries include the first observation of a black-hole (BH) coalescence [15], the multi-messenger observation of a binary-neutron-star merger [178], and an intermediate-mass BH [509]. Parametrised tests of general relativity (GR) can constrain the degree to which the data agree with GR by introducing fractional deviations to the inspiral and postmerger stages of the gravitational waveform [360, 495, 510–518]. No evidence in support of physics beyond GR has been found by the LIGO-Virgo-KAGRA collaboration, and increasingly stringent limits have been set on GW data [44, 276, 519, 520].

GWs offer the promising prospect of testing one of the main predictions of GR, namely the presence of horizons in BHs. On the theoretical side, BHs feature horizons beyond which nothing – not even light – can escape. Moreover, BHs contain a curvature singularity with infinite tidal forces where Einstein equations break down. In the semiclassical approximation, when a massless field is quantized in the Schwarzschild background, BHs are thermodynamically unstable and radiate a thermal spectrum at the Hawking temperature [521]. They are characterised by the information-loss paradox [522] and their entropy is far over the one of a typical stellar progenitor [523, 524].

Several models of horizonless and singularity-free compact objects have been proposed to address the BH paradoxes [89, 525–527]. New physics can prevent the formation of horizons in quantum-gravity extensions of GR (e.g., fuzzballs [91, 528, 529], gravastars [530], nonlocal stars [531, 532]) and in GR with the presence of dark matter and exotic fields (e.g., boson stars [533–537], wormholes [538–540]). Horizonless compact objects can mimic the observational features of BHs – since they can be as compact as BHs – and quantify the existence of horizons in astrophysical sources. Horizonless compact objects can deviate from BHs for their compactness, i.e., the inverse of the effective radius in units of the total mass, and reflectivity, which is generically complex and frequency-dependent and differs from the totally absorbing BH case.

The absence of horizons in compact objects affects the gravitational waveform in the inspiral and postinspiral stages. In the inspiral, the energy flux at the radius of horizonless compact objects differs from the energy flux at the horizon of BHs [3, 344, 346]. Furthermore, resonances are excited when the orbital frequency matches the characteristic oscillation frequencies of the inspiralling compact objects [541–543]. Also, the tidal Love numbers, which measure the deformability of a compact object when immersed in an external tidal field, are nonzero for horizonless compact objects [544–550]. During the ringdown, the quasinormal mode (QNM) frequencies of the perturbed remnant deviate from the BH QNM spectrum in the absence of horizons. If the remnant is an ultracompact horizonless object, the prompt ringdown signal would be nearly the same as the one emitted by a BH since it is excited at the light ring [92, 180]. Additional signal would be emitted in the form of GW echoes at late times due to the absence of horizons in the remnant [551–559]. The QNM spectrum would also deviate from the BH one as a function of the compactness of the object [90]. Future observatories, such as the Einstein Telescope, Cosmic

Explorer and LISA, will allow us to detect or rule out the imprints of horizonless compact objects in the gravitational waveform with unprecedented accuracy [343, 546, 560–563].

Here, we study the behaviour of generic horizonless compact objects to external gravitational perturbations to distinguish them from BHs. It is useful and convenient to incorporate the study of various compact objects into a single framework. This can also lead to an understanding of the relations between the parameters describing compact objects – such as compactness and reflectivity – and their GW observables – such as QNMs and tidal Love numbers. One way to effectively parametrise a generic compact object is by using the membrane paradigm [95, 96, 564]. The membrane paradigm is a theoretical framework originally developed to describe BHs, according to which the BH interior can be replaced by a three-dimensional membrane located at the event horizon. The membrane is made of a viscous fluid whose density, pressure and viscosity are fixed by the Israel-Darmois junction conditions [269, 565, 566].

The membrane paradigm was recently applied to compact objects other than BHs by locating the membrane at the object's radius [90, 550, 567]. The fluid parameters may be freely varied to parametrise different models of compact objects, and only a specific choice of these parameters describes BHs.

The membrane paradigm was first used to derive the QNM spectrum of generic nonspinning compact objects in Ref. [90], along with a comparison with the measurement accuracy of the fundamental QNM of GW150914 [276]. However, due to the initial orbital angular momentum of the binary, the final merged remnant is expected to be spinning [23–25, 335]. This necessitates the importance of incorporating the spin into the membrane paradigm for generic compact objects.

In this work, we present an extension of the membrane paradigm for generic compact objects to the linear order in spin. In Sec. 7.2, we present the theoretical details involved in constructing the membrane paradigm to linear order in spin. Particularly, we discuss the background metric, the linear perturbations, and outline the derivation of the boundary conditions that the metric perturbations must obey at the membrane surface from the Israel-Damour junction conditions. In Sec. 7.3, we analyse the reflectivity of compact objects as a function of the fluid viscous parameters. We also show the resolution to an apparent paradox that arises in the linear-in-spin approximation associated with the superradiant scattering. Furthermore, we derive the QNM frequencies in the BH limit, and compare them with known Kerr QNM spectrum to quantify the upper limit (in spin) to which the linear-in-spin approximation may be trusted. Finally, we compute the QNM frequencies of generic horizonless compact objects as a function of the compactness and the fluid viscous parameters. We discuss the breaking of isospectrality between axial and polar modes, and potential constraints that can be put on the object's compactness based on the current measurement accuracies of the fundamental QNM. In Sec. 7.4, we summarise the results and conclude with a brief discussion of the related future extensions. We assume $G = c = 1$ units throughout.

7.2 The membrane paradigm

The membrane paradigm allows one to derive the QNM spectrum of compact objects with a given exterior geometry and different interior solutions. In its standard formulation, a static observer can replace the interior of a compact object with a fictitious membrane located at the boundary of the object. The Israel-Darmois junction conditions set the properties of the membrane as [269, 565]

$$[[K_{ab} - K h_{ab}]] = -8\pi T_{ab}\,, \qquad [[h_{ab}]] = 0\,, \tag{7.1}$$

where h_{ab} is the induced metric on the membrane, K_{ab} is the extrinsic curvature, $K = K_{ab}h^{ab}$, and T_{ab} is the stress-energy tensor of the fluid on the membrane. The notation $[[...]] = (...)^+ - (...)^-$ denotes the jump of a quantity across the membrane, where $\mathcal{M}^+$ and $\mathcal{M}^-$ are the exterior and interior spacetimes to the membrane, and a, b are the indices of a 3-D coordinate system laid on the membrane.

The fictitious membrane is such that the extrinsic curvature of the interior spacetime vanishes, i.e., $K^-_{ab} = 0$. This constraint allows one to map different geometries for the interior spacetime into the properties of the fictitious membrane. The Israel-Darmois junction conditions impose that the membrane is a viscous fluid with stress-energy tensor [95]

$$T_{ab} = \rho u_a u_b + (p - \zeta\Theta)\gamma_{ab} - 2\eta\sigma_{ab} \,, \tag{7.2}$$

where ρ is the surface energy density, p is the surface pressure, ζ and η are the bulk and shear viscosities, u_a is the 3-velocity of the fluid, $\Theta = u^a_{;a}$ is the expansion, $\gamma_{ab} = h_{ab} + u_a u_b$ is the projector tensor, $\sigma_{ab} = \frac{1}{2}\left(u_{a;c}\gamma^c_b + u_{b;c}\gamma^c_a - \Theta\gamma_{ab}\right)$ is the shear tensor, and the semicolon is a covariant derivative with the induced metric.

The membrane paradigm was originally developed to describe perturbed BHs [95, 96, 564, 567] in terms of the shear and bulk viscosities of a fictitious viscous fluid located at the horizon, where

$$\eta_{\rm BH} = \frac{1}{16\pi} \,, \quad \zeta_{\rm BH} = -\frac{1}{16\pi} \,. \tag{7.3}$$

The membrane paradigm was then extended to perturbed horizonless compact objects with a Schwarzschild exterior [90], where the fictitious fluid is located at the object's radius, and the shear and bulk viscosity are generically complex and frequency-dependent. For each model of horizonless compact object, the shear and bulk viscosity are uniquely determined and are related to the reflective properties of the object.

7.2.1 Background metric

Motivated by the fact that the remnants of compact binary coalescences have large values of the spin [23–25, 335], here we extend the membrane paradigm to spinning horizonless compact objects which are generally described by the Kerr metric at the first order in the spin. Our approach should be considered as a first step towards the inclusion of spin effects into compact bodies, as performed in literature for compact objects beyond Kerr and in modified theories of gravity [568–572]. The linear-in-spin approximation is also useful for understanding the new features and conceptual challenges that arise with the inclusion of spin. The extension to higher orders in the spin is left for future work following Refs. [573–575] It is worth mentioning that the Kerr geometry does not necessarily describe the vacuum region outside a spinning object due to the absence of Birkhoff's theorem beyond spherical symmetry. Here, we assume that GR works sufficiently well on the exterior of the compact object, and no specific model is considered for the object's interior. This assumption is valid in modified theories of gravity where the corrections to the metric are suppressed by powers of $\ell_P/r_0 \ll 1$, being r_0 the object's radius and ℓ_P the Planck length or the scale of new physics [576].

The background is the Kerr metric at the linear order in spin, which in Boyer-Lindquist coordinates is given by [272]

$$ds^2 - f(r)dt^2 + \frac{1}{f(r)}dr^2 + r^2 d\Sigma^2 - 4\frac{J}{r}\sin^2\theta dt d\phi\,, \tag{7.4}$$

where $f(r) = 1 - 2M/r$, $d\Sigma^2 = d\theta^2 + \sin^2\theta d\phi^2$, $J = aM$ is the angular momentum, and M is the total mass of the compact object. For future convenience, we also define $\chi = a/M$ as the dimensionless spin. Note that for BHs, the magnitude of the spin parameter is $|\chi| \leq 1$ to prevent naked singularities, but no such constraint exists for generic compact objects. A generic spinning body is also characterized by the spin-induced multipole moments, which are relevant from the second order in spin [2, 328]. For the Kerr metric, all the multipole moments are known as unique functions of M and J. In this work, we truncate to linear order in spin and thus remove contribution of spin-induced multipole moments to the metric. Moreover, the exterior spacetime has no ergoregion, i.e., the region outside the horizon where a static observer cannot exist and is forced to corotate with the compact object.

From the linear-in-spin metric given above, the BH horizon is located at $r_+ = 2M$. We analyse horizonless compact objects whose radius is located at

$$r_0 = r_+(1+\epsilon)\,, \tag{7.5}$$

where $\epsilon > 0$, particularly $\epsilon = O(10^{-40})$ for compact objects with Planckian corrections at the horizon scale, and $\epsilon = O(1)$ for objects whose compactness is comparable to that of a neutron star.

In the unperturbed case, the fictitious membrane is located at the object's radius, and the normal vector to the membrane has components

$$n_t = 0,\ n_r = 1/\sqrt{f(r)},\ n_\theta = 0,\ n_\phi = 0\,. \tag{7.6}$$

The Israel-Darmois junction conditions in Eq. (7.1) determine the density, pressure, and 3-velocity of the viscous fluid as

$$\begin{aligned}&\rho_0 = -\frac{\sqrt{f(r_0)}}{4\pi r_0},\ p_0 = \frac{1+f(r_0)}{16\pi r_0\sqrt{f(r_0)}},\\ &u_0^a = \left(\frac{1}{\sqrt{f(r_0)}}, 0, \frac{2J}{r_0^3\,(1-3f(r_0))\,\sqrt{f(r_0)}}\right).\end{aligned} \tag{7.7}$$

The detailed derivation of the membrane parameters is given in Appendix E.1. As expected, the presence of the angular momentum induces a non-zero azimuthal velocity to the fluid.

7.2.2 Linear perturbations

Let us now perturb the background metric as

$$g_{\mu\nu} = g^0_{\mu\nu} + \epsilon_p \delta g_{\mu\nu}\,, \tag{7.8}$$

where $g^0_{\mu\nu}$ is the metric in Eq. (7.4) and ϵ_p is a small parameter controlling the strength of perturbation. The metric perturbation $\delta g_{\mu\nu}$ can be split into two parity sectors as [209, 210]

$$\delta g_{\mu\nu} = \delta g^{\rm axial}_{\mu\nu} + \delta g^{\rm polar}_{\mu\nu}\,. \tag{7.9}$$

In the absence of spin, the two sectors evolve independently without mixing. However, in the presence of spin, they mix in the field equations and the boundary conditions. In the slow-rotation limit, it can be shown that the coupling terms between the axial and polar sectors can be dropped for the computation of th QNM frequencies to linear order in spin [273]. After decomposing the perturbation into spherical harmonic basis, the axial and polar perturbations in the Regge-Wheeler gauge to linear order in spin are given by [272, 273]

$$\begin{aligned}\delta g^{\rm axial}_{\mu\nu} dx^\mu dx^\nu = \textstyle\sum_{\ell m} 2\Big\{ h_0^{\ell m}(r,t)\Big[S_\theta^{\ell m}(\theta,\phi) d\theta + S_\phi^{\ell m}(\theta,\phi) \\ d\phi\Big] dt + h_1^{\ell m}(r,t)\Big[S_\theta^{\ell m}(\theta,\phi) d\theta + S_\phi^{\ell m}(\theta,\phi) d\phi\Big] dr\Big\}\,,\end{aligned} \tag{7.10}$$

$$\begin{aligned}\delta g^{\rm polar}_{\mu\nu} dx^\mu dx^\nu = \textstyle\sum_{\ell m} \Big[H_0^{\ell m}(r,t) dt^2 + H_2^{\ell m}(r,t) dr^2 \\ + r^2 K^{\ell m}(r,t) d\Sigma^2 + 2 H_1^{\ell m}(r,t) dt dr\Big] Y^{\ell m}(\theta,\phi)\,,\end{aligned} \tag{7.11}$$

where $S_\theta^{\ell m}(\theta,\phi) = -\partial_\phi Y_{\ell m}(\theta,\phi)/\sin\theta$, $S_\phi^{\ell m}(\theta,\phi) = \sin\theta \partial_\theta Y_{\ell m}(\theta,\phi)$, $Y_{\ell m}(\theta,\phi)$ are the tensor spherical harmonics, and ℓ and m are the angular and azimuthal numbers of the perturbation. In the following, we will omit the dependence of the radial and angular functions on the angular and azimuthal numbers for brevity of notation. The time dependence can be factorised out as

$$h_0(r,t) = h_0(r)e^{-i\omega t}\,, \tag{7.12}$$

where the same holds for $h_1(r,t)$, $H_0(r,t)$, $H_1(r,t)$, $H_2(r,t)$, $K(r,t)$.

In response to the metric perturbation, the density, pressure and 3-velocity of the membrane stress-energy tensor are perturbed as

$$\begin{aligned}
\rho &= \rho_0 + \epsilon_p \delta\rho(\theta,\phi)e^{-i\omega t}\,, \\
p &= p_0 + \epsilon_p \delta p(\theta,\phi)e^{-i\omega t}\,, \\
u^a &= u_0^a + \epsilon_p \delta u^a(\theta,\phi)e^{-i\omega t}\,,
\end{aligned} \tag{7.13}$$

where ρ_0, p_0 and u_0^a are given in Eq. (7.7), and their perturbations can be decomposed in the spherical harmonic basis. In the spinless case ($J = 0$) the axial perturbations couple with the azimuthal component of the velocity perturbation of the fluid, whereas the polar perturbations couple with the density perturbation, the pressure perturbation, and the radial and polar deformations of the membrane location defined in Eq. (E.29). At the first order in spin, the perturbations with a given parity and angular number ℓ are coupled to those with opposite parity and angular number $\ell \pm 1$. However, it can be shown that the couplings to the $\ell \pm 1$ terms do not contribute to the QNM spectrum to the linear order in spin [273]. Thus, we neglect these terms in the following, and work with axial and polar modes separately. See Appendix E.3 for the derivation of the equations relating the metric perturbations to the fluid perturbations of the membrane.

Outside the membrane, the Einstein equations governing the metric perturbations can be reduced to two Schrödinger-like equations, namely the Regge-Wheeler and Zerilli equations describing axial and polar perturbations, respectively [209, 210]. They are of the form:

$$\frac{d^2\psi(r)}{dr_*^2} + \left[\omega^2 - \frac{4mJ\omega}{r^3} - V(r)\right]\psi(r) = 0\,, \tag{7.14}$$

where the Regge-Wheeler effective potential at linear order in the spin is [272, 273]

$$V_{\rm RW} = f(r)\left[\frac{\ell(\ell+1)}{r^2} - \frac{6M}{r^3} + \frac{24Jm(3r-7M)}{\ell(\ell+1)\omega r^6}\right]\,, \tag{7.15}$$

and the Zerilli effective potential is given in Eq. (E.19), where the tortoise coordinate is defined as $dr_*/dr = 1/f(r)$. The Regge-Wheeler function $\psi_{\rm RW}(r)$ is related to the metric perturbation function $h_1(r)$ as

$$\psi_{\rm RW}(r) = \left(1 - \frac{2mJ}{r^3\omega}\right)^{-1}\frac{f(r)}{r}h_1(r)\,, \tag{7.16}$$

and $h_0(r)$ is related to $h_1(r)$ via Eq. (E.16). Similarly, the Zerilli function $\psi_{\rm Z}(r)$ can be written as a linear combination of $H_0(r)$, $H_1(r)$, $H_2(r)$ and $K(r)$ as in Eqs. (E.20)-(E.24) at linear order in spin.

7.2.3 Boundary conditions

By imposing boundary conditions at infinity and the radius of the compact object, Eq. (7.14) defines an eigenvalue problem. From the junction condition in Eq. (7.1), one finds a constraint on the metric perturbation at the membrane surface, i.e., a boundary condition at the radius of the compact object. Different models of horizonless compact objects are described by different boundary conditions, which depend on the membrane parameters such as the shear and bulk viscosities of the fluid. The boundary condition at membrane surface for axial perturbations turns out to be

$$\frac{1}{\psi_{\rm RW}(r)}\frac{d\psi_{\rm RW}(r)}{dr_*}\Big|_{r=r_0} = -\frac{i\omega}{\nu} + \frac{My^2V_{\rm RW}(r_0)}{2w(3w-y)} +$$

$$
\frac{m\chi}{2\ell(\ell+1)My^5(y-3w)^2\nu}\Big\{w^3\Big[36w^2y\Big(i\left(\ell^2+\ell+9\right)y+
16\nu+\nu y^2\Big)+6wy^2\Big(\left(\ell^2+\ell-7\right)\nu y^2-2iy\left(2\ell^2+2\ell+13\right)
-42\nu\Big)+y^3\Big(-3\left(\ell^2+\ell-4\right)\nu y^2+4i\left(\ell^2+\ell+6\right)y+
36\nu\Big)-216iw^3\left(y-2i\nu\right)\Big]-3w^3(2w-y)\left(6w-\ell(\ell+1)y\right)
\Big[\left(4w-2y+y^3\right)\nu-2iy(3w-y)\Big]\Big\}, \tag{7.17}
$$

where $\nu = 16\pi\eta$, $y = \omega r_0$, and $w = M\omega$. The polar boundary condition turns out to be

$$
\frac{1}{\psi_{\mathrm{Z}}(r)}\frac{d\psi_{\mathrm{Z}}(r)}{dr_*}\Big|_{r=r_0} = -16\pi\eta i\omega + G(r_0,\omega,\eta,\zeta)
+ m\chi H(r_0,\omega,\eta,\zeta)\,, \tag{7.18}
$$

where $G(r_0,\omega,\eta,\zeta)$ is given in Ref. [90], and the supplemental Mathematica notebook in [274] contains the complete expression for the polar boundary condition including $H(r_0,\omega,\eta,\zeta)$. The detailed derivation of the above boundary conditions starting from the junction conditions in Eq. (7.1) is provided in Appendix E.3.

Note that the above boundary conditions are invariant under the transformation ($m \to -m$, $\chi \to -\chi$). It is also worth noting that the axial boundary condition does not depend on the bulk viscosity ζ of the fluid membrane.

The BH boundary condition is recovered in the $\epsilon \to 0$ limit, for which $V(r_0) = 0$ and $y = 2w$, and by setting the membrane shear and bulk viscosities to BH values as in Eq. (7.3). In this limit, the axial and polar boundary conditions in Eqs. (7.17) and (7.18) reduce to

$$
\frac{d\psi_{\mathrm{RW}}(r)/dr_*}{\psi_{\mathrm{RW}}(r)}\Big|_{r=r_+} = \frac{d\psi_{\mathrm{Z}}(r)/dr_*}{\psi_{\mathrm{Z}}(r)}\Big|_{r=r_+} = -i\tilde{\omega}\,, \tag{7.19}
$$

where $\tilde{\omega} = \omega - m\Omega_H$ and $\Omega_H = J/(4M^3)$ is the horizon angular velocity. This is consistent with

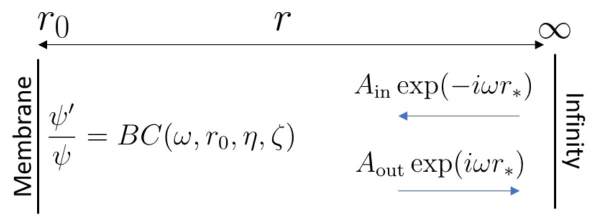

Figure 7.1: Time-independent scattering of gravitational perturbations off a compact object, which is described by a membrane located at the object's radius. At infinity, the Regge-Wheeler and Zerilli wave functions asymptote towards free-wave solutions. At the membrane surface, the boundary conditions in Eqs. (7.17) and (7.18) are obeyed. The reflectivity of the compact object at infinity is defined as $\mathcal{R} = A_{\text{out}}/A_{\text{in}}$.

the expected BH boundary condition of a purely ingoing perturbation near the horizon, i.e.,

$$\psi_{\text{RW}}(r) \sim \psi_{\text{Z}}(r) \sim e^{-i\tilde{\omega}r_*}\,, \quad \text{as } r_* \to -\infty\,. \tag{7.20}$$

Finally, we check that in the spinless limit, $\chi \to 0$, the boundary conditions in Eqs. (7.17) and (7.18) reduce to those obtained in Ref. [90] for a horizonless compact object with a Schwarzschild exterior.

7.3 Reflectivity and quasinormal mode spectrum

7.3.1 Reflectivity of compact objects

One way to differentiate between compact objects is based on their reflectivity as measured from infinity. Given an ingoing wave packet sent from infinity in the distant past, the reflectivity is defined as the resultant scattered waveform at infinity in the distant future. It is convenient to study a time-independent scattering, where both ingoing and outgoing spherical waves are simultaneously present. This is schematically represented in Fig. 7.1, where the ratio of the amplitudes of the outgoing and ingoing waves at infinity defines the reflectivity as

$$\psi(r) \sim e^{-i\omega r_*} + \mathcal{R} e^{i\omega r_*}\,, \quad \text{as } r_* \to \infty\,, \tag{7.21}$$

after the wave interacts with the compact object and is subjected to the boundary conditions in Eqs. (7.17) and (7.18) for axial and polar perturbations, respectively.

For non-spinning BHs, with a horizon but no ergoregion, the absolute value of reflectivity, $|\mathcal{R}|$, is bounded from above by 1. For small frequencies, or equivalently large wavelengths, the wave packets larger than the BH size are only negligibly absorbed, yielding $|\mathcal{R}| \approx 1$. As the wavelength becomes comparable with the BH size, absorption is more relevant and $|\mathcal{R}| < 1$.

For Kerr BHs possessing an ergoregion, the reflectivity can exceed 1 when the frequency of the perturbation is smaller than the BH horizon angular velocity, i.e., $\omega < m\Omega_H$. This is due to the phenomenon of superradiance, in which the energy associated with the object's rotation may be transmitted to the waves/particles scattered by it. In this case, the BH loses its rotational energy, leading to an amplification of the outgoing radiation. The analytical expression for the reflectivity of Kerr BHs at low frequencies to the next-to-leading order in $M\omega$ was derived in Refs. [3, 4, 166, 410, 577, 578].

For generic compact objects, the reflectivity $|\mathcal{R}|$ is related to the membrane parameters (i.e., shear and bulk viscosity of the fluid) through the boundary conditions in Eqs. (7.17) and (7.18) for axial and polar perturbations, respectively. The computation of the reflectivity for arbitrary frequencies is done via numerical integration of the perturbation equations in Eq. (7.14) and discussed in Sec. 7.3.1.2. Some features of the reflectivity may be extracted analytically and are discussed in the next few paragraphs. We will also discuss the limitations of the linear-in-spin approximation in the form of spurious effects, specifically superradiance, leading to $|\mathcal{R}| > 1$ when the spin parameter χ becomes large enough. This is physically not allowed as superradiance requires the presence of an ergoregion, which is absent at the linear order in spin. Nevertheless, this spuriousness is understood in terms of the limits of validity of the linear-in-spin approximation.

For an ultracompact object ($\epsilon \ll 1$), in the limits $r \to 2M$ and $r \to \infty$, the Regge-Wheeler and Zerilli equations at the linear order in spin reduce to free-wave equations

$$\frac{d^2\psi(r)}{dr_*^2} + \left[\omega^2 - \frac{m\chi\omega}{2M}\right]\psi(r) = 0, \quad r \to 2M\,, \tag{7.22}$$

$$\frac{d^2\psi(r)}{dr_*^2} + \omega^2\psi(r) = 0, \quad r \to \infty, \tag{7.23}$$

In both these limits, the asymptotic solutions can be written as

$$\psi(r) \sim C_{\rm trans}\, e^{-i\omega' r_*} + C_{\rm ref}\, e^{i\omega' r_*}, \quad r \to 2M\,, \tag{7.24}$$

$$\psi(r) \sim A_{\rm in}\, e^{-i\omega r_*} + A_{\rm out}\, e^{i\omega r_*}, \quad r \to \infty\,, \tag{7.25}$$

where $\omega' = \omega\sqrt{1 - m\chi/(2M\omega)}$ and $\omega \in$ Reals. For BHs, the purely ingoing boundary condition at the horizon fixes $C_{\rm ref} = 0$. In order to provide an analytical description of the reflectivity, we use the following conservation law valid for the solution of a Schrödinger-like equation $\psi'' + (\omega^2 - V)\,\psi = 0$ with real potential and frequency:

$$\begin{aligned} &\frac{d}{dr_*}\left(\psi'\bar\psi - \bar\psi'\psi\right) = \psi''\bar\psi - \bar\psi''\psi = -\tilde V\psi\bar\psi + \tilde V\bar\psi\psi = 0 \\ \Longrightarrow\;\; &\left(\psi'\bar\psi - \bar\psi'\psi\right)\Big|_{r=2M} = \left(\psi'\bar\psi - \bar\psi'\psi\right)\Big|_{r\to\infty}, \end{aligned} \tag{7.26}$$

where the prime denotes a derivative with respect to the tortoise coordinate, $\bar\psi$ is the complex conjugate of ψ, and $\tilde V = -\omega^2 + 4mJ\omega/r^3 + V(r)$. Eq. (7.26) together with Eqs. (7.22),(7.23) implies in turn the relation

$$\frac{\mathrm{Re}(\omega')}{\omega}|C_{\rm trans}|^2 e^{2\mathrm{Im}(\omega')r_*} = |A_{\rm in}|^2 - |A_{\rm out}|^2\,, \tag{7.27}$$

where we note that $\omega' \in$ Reals, provided $\omega > m\chi/2M$, and furthermore $\omega' > 0$. Thus, for sufficiently large frequencies, i.e., $\omega > m\chi/2M$, we have $|A_{\rm in}|^2 > |A_{\rm out}|^2$ or $|\mathcal{R}|^2 < 1$ as expected from BHs. When the frequency is small, i.e., $\omega < m\chi/2M$, ω' becomes purely imaginary and the right hand side of Eq. (7.27) vanishes, yielding $|\mathcal{R}|^2 = 1$. This is different from the behaviour of Kerr BHs where one observes a superradiant amplification, i.e., $|\mathcal{R}|^2 > 1$, when $\omega < m\Omega_H$ [236, 579–581]. This can be explained by the fact that we are using a linear-in-spin approximation of the Kerr metric, which does not possess an ergoregion and cannot reproduce a superradiant scattering.

Something interesting happens, however, when we expand ω' to linear order in spin, i.e., $\omega' = \omega - m\chi/(4M) + \mathcal{O}(\chi^2)$, which modifies Eq. (7.27) to

$$\frac{\tilde{\omega}}{\omega}|C_{\rm trans}|^2 = |A_{\rm in}|^2 - |A_{\rm out}|^2, \tag{7.28}$$

where $\tilde{\omega}$ is defined below Eq. (7.19) and $\tilde{\omega} \in$ Reals. Now, we find a superradiant behaviour when $\omega < m\Omega_H$, which is analogous to the Kerr BH case. Nevertheless, since we do not expect superradiance at linear order in spin due to the absence of an ergoregion, we interpret this as a spurious result. Indeed, a consistent study of the slow rotation approximation requires going to at least second order in spin [273, 568]. This argument requires extra care when dealing with membranes as their boundary condition is valid up to leading order in spin (unlike the expression in Eqs. (7.24)). We thus interpret any observation of effects related to the presence of an ergoregion as a spurious result. This will become relevant for the analysis of the stability of QNMs as shown in Sec. 7.3.2.

For the compact objects analysed here, the asymptotic behaviour of the perturbations at infinity in Eq. (7.25) is still valid, however the asymptotic solution near the object's radius does not have a simple analytical form. The following conservation law holds

$$\left(\psi'\bar{\psi} - \bar{\psi}'\psi\right)\Big|_{r=r_0} = \left(\psi'\bar{\psi} - \bar{\psi}'\psi\right)\Big|_{r=\infty}, \tag{7.29}$$

where r_0 is the location of the membrane. We now use the boundary conditions in Eqs. (7.17) and (7.18) for axial and polar perturbations to rewrite the conservation law as

$$-|\psi|^2 \frac{\mathrm{Im}[\mathrm{BC}(\omega, r_0, \eta, \zeta)]}{i\omega} = |A_{\rm in}|^2 - |A_{\rm out}|^2 \tag{7.30}$$

where $\mathrm{BC}(\omega, r_0, \eta, \zeta) = \psi'/\psi|_{r=r_0}$ is the boundary condition to be satisfied by the relevant perturbation functions (Regge-Wheeler or Zerilli). In the BH limit, i.e., $\epsilon \to 0$, $\eta \to \eta_{\rm BH}$ and $\zeta \to \zeta_{\rm BH}$, Eq. (7.30) reduces to Eq. (7.28) as expected. Since the exterior spacetime is the Kerr metric at the linear order in spin, which does not have an ergoregion, we cannot trust the regime in which $|\mathcal{R}|^2 > 1$. It is also worth noting that a vanishing of the imaginary part of the boundary condition on the membrane leads to a perfect reflection where $|A_{\rm out}|^2 = |A_{\rm in}|^2$. This can also be achieved by setting $\psi = 0$ on the membrane, corresponding to a Dirichlet boundary condition.

7.3.1.1 Numerical computation of the reflectivity : Methods

The reflectivity can be computed numerically by integrating the perturbation equations in Eq. (7.14) with the boundary conditions represented in Fig. 7.1. The second-order Regge-Wheeler and Zerilli equations are integrated outwards starting from the membrane radius r_0, where the wave function and its first derivative need to be specified at the membrane surface. Among the two unknown functions, one is simply a scale, therefore we can set $\psi(r_0) = 1$. Then, $\psi'(r_0)$ is specified by the boundary conditions in Eqs. (7.17) and (7.18) for axial and polar perturbations, respectively.

The equations are numerically integrated outwards up to a point sufficiently far away (say $r_\infty = 50M$), which may be regarded as ''infinity''. We check that the result of the integration is numerically stable by changing the numerical value for the infinity. The asymptotic solutions at infinity are given in Eq. (7.25). Then, given the (numerically obtained) wavefunction and its first derivative, we compute the reflectivity as

$$|\mathcal{R}| = \left|\frac{A_{\rm out}}{A_{\rm in}}\right| = \left|\frac{i\omega\psi(r_\infty) + \psi'(r_\infty)}{i\omega\psi(r_\infty) - \psi'(r_\infty)}\right|. \tag{7.31}$$

The accuracy of the integration can be improved by making use of series solutions at infinity or close to the horizon in the BH case. This modifies the relation in Eq. (7.31) between the wavefunction and the reflectivity at infinity accordingly. However, concerning the computation of the reflectivity, series solutions at infinity do not affect significantly the result. For instance, for a compact object with $\epsilon = 10^{-10}$ and $\eta = \eta_{\rm BH}$, the absolute value of the reflectivity obtained without asymptotic series solutions at infinity and using a nineteenth-order asymptotic series solution in powers of $1/r$ differ by less than 0.1% at the frequency $M\omega = 0.37$. For this reason, we use Eq. (7.31) for the computation of the reflectivity, where $\psi(r_\infty)$ and $\psi'(r_\infty)$ are obtained from a direct integration.

7.3.1.2 Numerical computation of the reflectivity : Results

Let us discuss the variation of reflectivity of the compact object with respect to the fluid parameters. The shear viscosity η, appearing in both the axial and polar boundary conditions, controls the reflectivity of the object in the ultracompact limit. This can be seen from the $\epsilon \to 0$ limit of Eqs. (7.17) and (7.18), which is

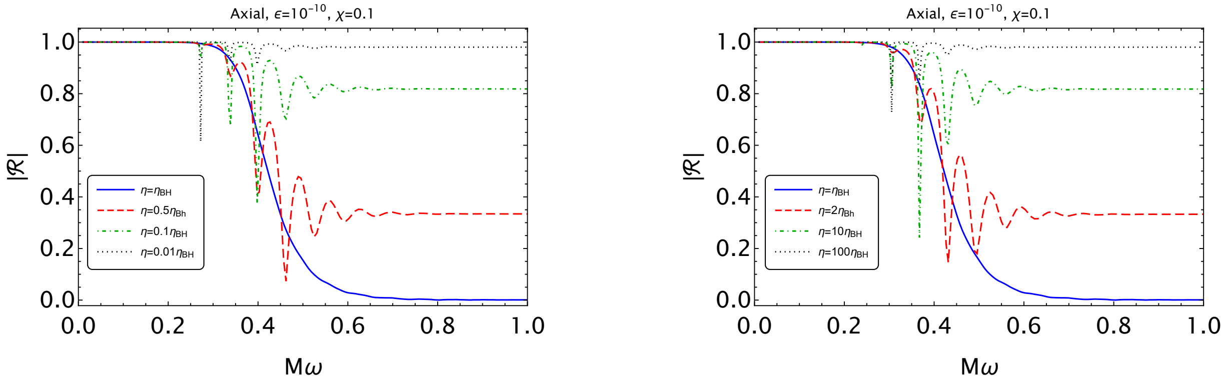

Figure 7.2: Reflectivity of a compact object for axial perturbations in terms of the shear viscosity, η, of a fictitious fluid located at the object's radius, $r_0 = 2M(1+\epsilon)$, with $\epsilon = 10^{-10}$, $\chi = 0.1$ and $\ell = m = 2$. The shear viscosity varies as $\eta \in (0, \eta_{\rm BH})$ in the top panel and $\eta \in (\eta_{\rm BH}, \infty)$ in the bottom panel. Note that the limits $\eta \to 0$ and $\eta \to \infty$ lead to a perfectly reflecting compact object, described by Dirichlet and Neumann boundary conditions, respectively. When $\eta \neq \eta_{\rm BH}$, the reflectivity has an oscillatory structure, which is related to the QNMs of the object.

$$\frac{1}{\psi_{\rm RW}(r)} \frac{d\psi_{\rm RW}(r)}{dr_*}\Big|_{r=r_0} = -\frac{i}{16\pi\eta}\left(\omega - m\frac{\chi}{4M}\right), \tag{7.32}$$

$$\frac{1}{\psi_{\rm Z}(r)} \frac{d\psi_{\rm Z}(r)}{dr_*}\Big|_{r=r_0} = -16\pi i\eta\left(\omega - m\frac{\chi}{4M}\right) + \frac{\left(\ell^2+\ell-1\right) m \left[(16\pi\eta)^2 - 1\right] \chi\omega}{2l\,(\ell+1)\left(\ell^2+\ell+1\right)}. \tag{7.33}$$

In the BH limit, $\eta \to \eta_{\rm BH}$, the above equations reduces to the purely ingoing boundary condition as expected from BHs. In the spinless limit ($\chi = 0$), the limit $\eta \to 0$ corresponds to a Dirichlet ($\psi_{\rm RW} = 0$) and a Neumann ($\psi'_{\rm Z} = 0$) boundary condition on axial and polar perturbations, respectively. Whereas the limit $\eta \to \infty$ corresponds to a Dirichlet ($\psi_{\rm Z} = 0$) and a Neumann ($\psi'_{\rm RW} = 0$) boundary condition on polar and axial perturbations, respectively. In both of these limits, the compact object is purely reflecting at any frequency, i.e., $|\mathcal{R}| = 1$. Note that when the spin is turned on ($\chi \neq 0$), the limit $\eta \to 0$ no longer corresponds to a Neumann boundary condition for polar perturbations. However, this limit still describes a purely reflective compact object with $|\mathcal{R}| = 1$. This can be seen from Eq. (7.30), where the imaginary part of the boundary condition (i.e., the right hand side of Eq. (7.33)) vanishes in the limit $\eta \to 0$ while $\psi_Z(r_0)$ remains finite.

Fig. 7.2 shows the absolute value of the reflectivity of a compact object with $\epsilon \ll 1$ and different values of the shear viscosity, particularly $\eta \in (0, \eta_{\rm BH})$ in the top panel and $\eta \in (\eta_{\rm BH}, +\infty)$ in the bottom panel. We have set $\chi = 0.1$ for simplicity. The plots are for axial perturbations, but they look qualitatively similar in the polar case, yielding to the same results. The reflectivity profile coincides with the BH one when $\eta = \eta_{\rm BH}$, and describes a perfectly reflecting object in the $\eta \to 0$ and $\eta \to +\infty$ limits. The approximate symmetry in the two panels of Fig. 7.2 can be understood analytically in the large-frequency limit, where the absolute value of the reflectivity is invariant under the transformation $\eta/\eta_{\rm BH} \to \eta_{\rm BH}/\eta$, as shown in Eq. (16) of Ref. [90]. An example of this apparent symmetry is provided by the wormhole, which is a purely reflecting object that can be described by either Dirichlet or Neumann boundary conditions, corresponding to $\eta \to 0$ and $\eta \to \infty$ [92, 275, 582]. While the absolute value of the reflectivity may be similar in the large-frequency limit, the quasinormal mode spectrum is generally different as seen in the differing oscillatory pattern at smaller values of frequency. Note that the oscillatory structure in reflectivity becomes sharply peaked when $\eta \to 0$ and $\eta \to +\infty$. This behaviour is due to the QNMs of the compact object, where the frequencies at which the dips (or resonances) occur coincide with the real part of the QNMs of the object. Using the analytical formulae for the QNMs of ultracompact objects in the small-frequency regime [275, 543], we check that the distance between subsequent dips (or resonances) is given by

$$\Delta\omega = \frac{\pi}{|r_*^0|} \sim \frac{\pi}{2M|\log\epsilon|}\,. \tag{7.34}$$

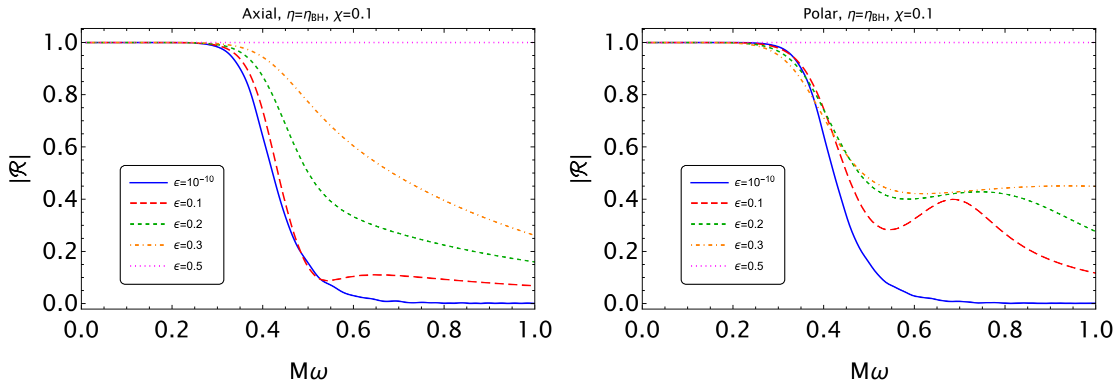

Figure 7.3: Reflectivity of a compact object for axial (top panel) and polar (bottom panel) perturbations in terms of the shear ($\eta = \eta_{\rm BH}$) viscosity of a fictitious fluid located at the object's radius, $r_0 = 2M(1+\epsilon)$, for $\chi = 0.1$ and $\ell = m = 2$. The object's compactness varies as $\epsilon \in (10^{-10}, 0.5)$. Note that the reflectivity approaches 1 as $\epsilon \to 0.5$, which corresponds to the object's radius approaching the light ring.

The resonance width is proportional to the imaginary part of the QNMs [275, 543], which becomes smaller in the perfectly reflecting cases compared to the partially absorbing ones. This explains the sharpness of the resonances in the $\eta \to 0$ and $\eta \to \infty$ limits.

Let us now analyse the variation of the reflectivity with the object's compactness for a fixed viscosity. For this purpose, we fix the viscosity in the axial boundary condition in Eq. (7.17) to the BH value. The purely ingoing boundary condition is recovered for $\epsilon \to 0$, as seen from Eq. (7.32). However, in the limit $\epsilon \to 1/2$, corresponding to the membrane radius located at the light ring, $r_0 \to 3M$, the reflectivity becomes unity as the axial boundary condition tends to the Dirichlet boundary condition, i.e., $\psi_{\rm RW}(r_0) = 0$. This happens regardless of the spin as the second and third terms in the right hand side of Eq. (7.32) are divergent. The top panel of Fig. 7.3 shows the variation of the reflectivity with the object's compactness for axial modes in the slowly spinning case where $\chi = 0.1$. The reflectivity coincides with the BH one when $\eta = \eta_{\rm BH}$ and ϵ is small enough, and describes a perfectly reflecting object in the $\epsilon \to 1/2$ limit.

In the polar case, interestingly, the boundary condition in the spinless case ($\chi = 0$) does not reach the perfectly reflecting limit as $\epsilon \to 1/2$. Moreover, the reflectivity depends on the choice of the bulk viscosity of the membrane fluid. However, the linear-in-spin term $H(r_0, \omega, \eta, \zeta)$ in Eq. (7.18) is divergent in the limit $\epsilon \to 1/2$, thus changing the behaviour even for a small value of spin. The bottom panel of Fig. 7.3 shows the variation of the reflectivity with the object's compactness for polar modes in the slowly spinning case where $\chi = 0.1$. Note that the small-spin approximation breaks down for axial and polar modes in the limit $\epsilon \to 1/2$. This is because the linear-in-spin term of the boundary condition scales as $(\epsilon - 1/2)^{-2}$, whereas the spinless term of the boundary condition scales as $(\epsilon - 1/2)^{-1}$, as shown in Eq. (7.17). Nevertheless, due to the boundary condition diverging in the limit $\epsilon \to 1/2$ both in the nonspinning and spinning cases, for $\epsilon = 1/2$ the compact object is purely reflecting. It is important to mention that for a given model of compact object, the viscosities (η, ζ) are uniquely determined and will depend on the compactness parameter ϵ. For simplicity, here we keep the viscosities fixed while varying the compactness (and vice versa). Model-specific studies are left for future work.

7.3.2 Quasinormal mode spectrum

Another important observable, which is useful for differentiating between compact objects, is the QNM spectrum. By imposing boundary conditions at infinity and the radius of the compact object, the complex eigenvalues of Eq. (7.14) are the QNM frequencies of the system, $\omega = \omega_R + i\omega_I$. In our convention, a stable mode has $\omega_I < 0$ and corresponds to an exponentially damped sinusoidal signal with frequency $f = \omega_R/(2\pi)$ and damping time $\tau_{\text{damp}} = -1/\omega_I$. Conversely, an unstable mode has $\omega_I > 0$ with instability timescale $\tau_{\text{inst}} = 1/\omega_I$. At infinity, we impose that the perturbation is a purely outgoing wave, i.e.,

$$\psi(r) \sim e^{i\omega r_*}\,, \quad \text{as } r_* \to \infty\,. \tag{7.35}$$

At the object's radius, we impose the boundary conditions in Eqs. (7.17) and (7.18) for axial and polar perturbations, respectively. In the following, we discuss the differences from the BH QNM spectrum for different values of the membrane parameters and the object's compactness.

7.3.2.1 Numerical methods for the QNMs

In this work, we employ the direct integration and continued fractions methods for the numerical computation of the QNMs [273, 583, 584]. In the direct integration method, the perturbation equations are integrated numerically starting from the membrane location, where the boundary conditions in Eqs. (7.17) and (7.18) are imposed, to a sufficiently large value of r. Then at infinity, the purely outgoing boundary condition in Eq. (7.35) is imposed. The latter condition is satisfied for certain values of the frequency, which are the QNM frequencies. The equations are solved numerically using root-finding algorithms, along with an initial guess for the frequency. This approach needs to use high-order asymptotic solutions sufficiently far from the compact object (at $r \to \infty$) and at the horizon of BHs ($r \to 2M$) to guarantee numerical accuracy. A limitation of the direct integration method is that is does not give accurate results for overtones, and is mainly useful for computing fundamental mode frequencies.

The continued fractions method was originally developed in Ref. [583] to compute the QNMs as roots of implicit equations. The eigenfunction is written as a series expansion whose coefficients satisfy a finite-term recurrence relation. This method was generalized to work with boundary conditions at the radius of compact objects in Refs. [90, 584].

7.3.2.2 Validity of the linear-in-spin approximation

Let us compute the fundamental QNM of a Kerr BH at linear order in spin, and compare it with the fundamental QNM of a Kerr BH as a function of the spin. This comparison allows one to set the maximum spin to which the linear-in-spin approximatiom can be trusted. Since axial and polar modes are isospectral in BHs regardless of the spin, we restrict our analysis to the axial QNMs.

To compute the QNM frequencies for a BH to linear order in spin, we impose either a purely ingoing boundary condition at the horizon as in Eq. (7.19) or the membrane boundary condition in Eq. (7.17) in the BH limit, i.e., $\epsilon \to 0$, $\eta \to \eta_{\rm BH}$ and $\zeta \to \zeta_{\rm BH}$. From the numerical integration, $\epsilon = 0$ leads to a coordinate singularity, however it is sufficient to choose a sufficiently small value of ϵ, for example $\epsilon = 10^{-10}$, for which the integration is well defined. We checked that the BH QNM does not depend on the choice of the numerical value for ϵ.

Since our analysis is valid in the slow-spin approximation, we expand the numerically computed QNM frequencies as [273, 574]

$$\omega(\chi) = \omega^{(0)} + m\chi\omega^{(1)} + O(\chi^2), \tag{7.36}$$

and we discard the second-order-in-spin terms. The numerically solved QNMs even using the linearised boundary conditions have a general dependence on χ. Thus, we Taylor-expand the numerically computed QNMs and truncate them to linear order in spin. The quantity $\omega^{(0)}$ is computed when $\chi = 0$, and the quantity $\omega^{(1)}$ is computed as the slope of the linear-in-spin expansion by simply using the finite difference formula

$$\omega^{(1)} = \frac{\omega(\chi_2) - \omega(\chi_1)}{m(\chi_2 - \chi_1)}, \tag{7.37}$$

where $\chi_1 = 0$ and we choose $\chi_2 = 10^{-4}$. Alternatively, we can construct a polynomial fit for $\omega(\chi)$ and truncate the fitted polynomial to the linear order in spin. Both methods yield the same result for $\omega^{(1)}$ within $10^{-3}\%$.

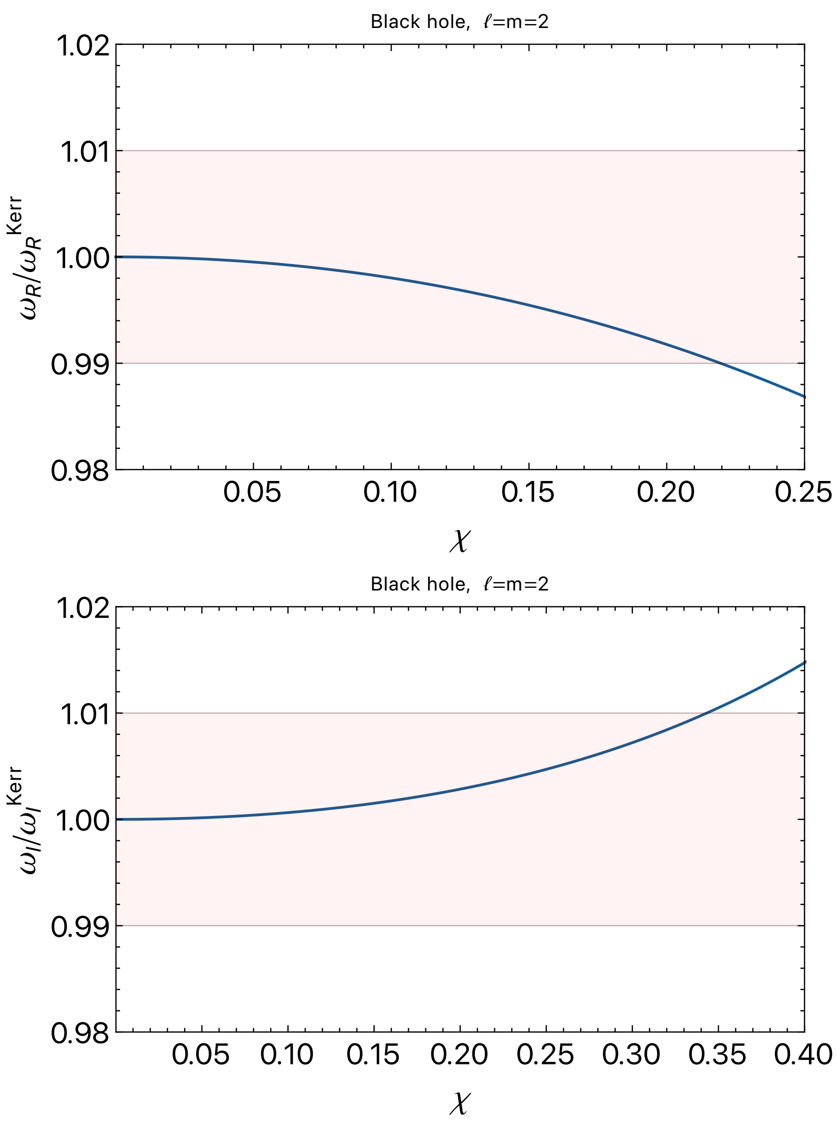

Figure 7.4: Real (top panel) and imaginary (bottom panel) part of the fundamental $\ell = m = 2$ QNM of a slowly-spinning BH with respect to a Kerr BH as a function of the spin. The shaded band shows the 1% range beyond which the linear-in-spin approximation is not valid.

To estimate the maximum value of the spin for which the linear-in-spin approximation is valid, we plot the ratio $\omega/\omega^{\mathrm{Kerr}}$ as a function of the spin in Fig. 7.4. The plot shows that the linear-in-spin BH QNMs are consistent with the Kerr QNMs within 1% (shaded region) up to $\chi \sim 0.2$ for the real part of the frequency and $\chi \sim 0.35$ for the imaginary part of the frequency. Based on this argument, we restrict to $\chi \leq 0.2$ as the region in which the linear-in-spin approximation is valid in the rest of this work.

An additional constraint applies if clear unphysical features appear in the results. For instance, as discussed in Sec. 7.3.1, the linear-in-spin approximation can lead to spurious superradiant effects for sufficiently small frequencies, i.e., $m\chi/(4M\omega) > 1$. In the next section, we show that certain modes become unstable in purely reflecting ultracompact objects with large values of the spin. This is explained as an ergoregion instability, which is a spurious effect at linear order in spin [273, 275].

7.3.2.3 QNMs with the membrane paradigm

Let us now investigate the QNM frequencies of slowly spinning horizonless compact objects, and their variation with the membrane parameters.

First, we analyse a horizonless compact object with $\epsilon \ll 1$, whose reflectivity is related to the shear viscosity of the membrane as in Fig. 7.2. In this limit, the axial boundary condition approaches the expression in Eq. (7.32). We derive numerically the variation of the QNM frequencies with the shear viscosity η. This corresponds to the study of how the fundamental mode evolves by varying the reflectivity of the compact object away from the BH case. Fig. 7.5 shows the real (top panel) and imaginary (bottom panel) part of the axial QNMs of an ultracompact object as a function of the shear viscosity for different values of the spin. The nonspinning case was

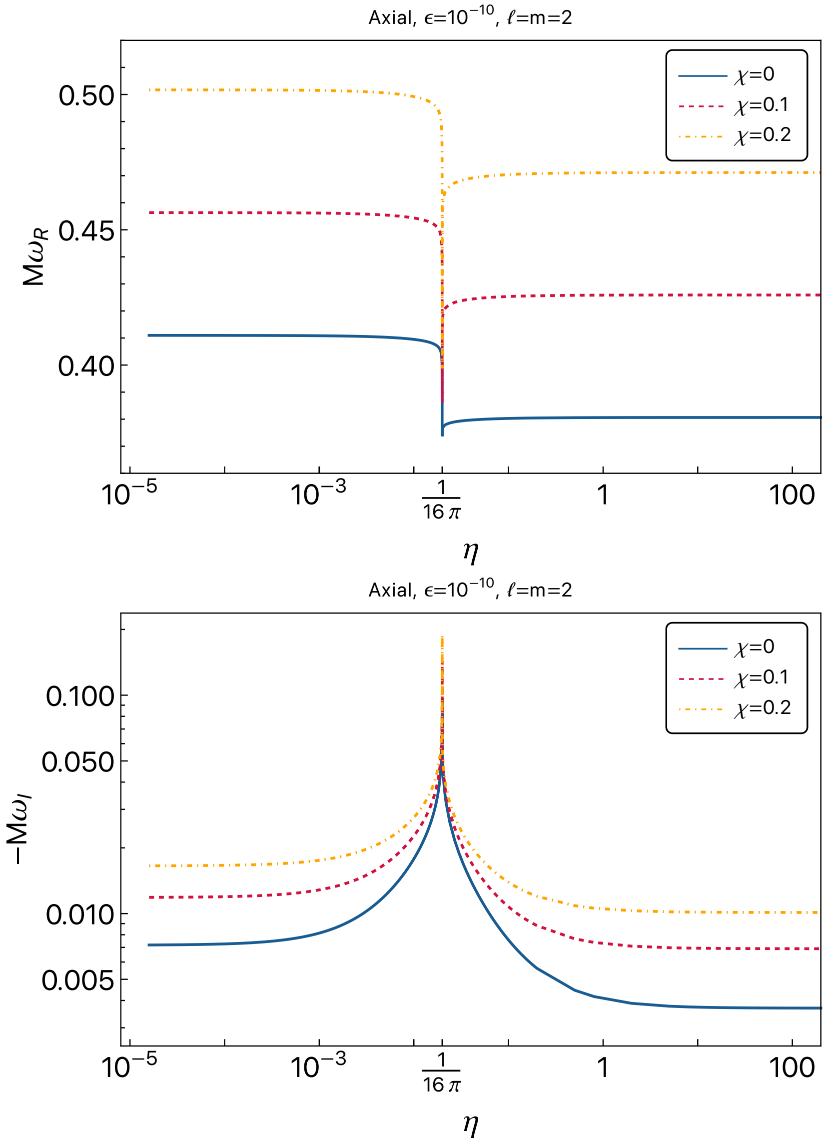

Figure 7.5: Real (top panel) and imaginary (bottom panel) part of the fundamental $\ell = m = 2$ QNM of an ultracompact object as a function of the viscosity parameter η for different values of the spin. For $\eta = 1/(16\pi)$, the compact object is totally absorbing; whereas for $\eta \to 0$ and $\eta \to \infty$, the compact object is perfectly reflecting.

derived earlier in Ref. [90].

When $\eta = 1/(16\pi)$, the compact object is totally absorbing and we recover the BH fundamental QNM. Then, the variation of the viscosity affects drastically the mode, with a sharp behaviour around the the BH limit. For $\eta \to 0$ and $\eta \to \infty$, the compact object is perfectly reflecting, as shown in Fig. 7.2.

It is interesting to note the increase in the imaginary part of the QNMs when the spin increases in the limits $\eta \to 0,\ \infty$. This shows that the $\ell = m = 2$ mode decays faster with the spin. Moreover, according to Eq. (7.36), the $m = -2$ modes should become longer lived. In particular, the imaginary part of these modes can cross 0 indicating an instability (this phenomenon was already observed in Refs. [275, 585] for totally reflecting boundary conditions). Fig. 7.6 shows the imaginary part of the fundamental $(\ell, m) = (2, \pm 2)$ QNMs as a function of the spin for the limits of $\eta \to 0$ and $\eta \to \infty$, corresponding to total reflection.

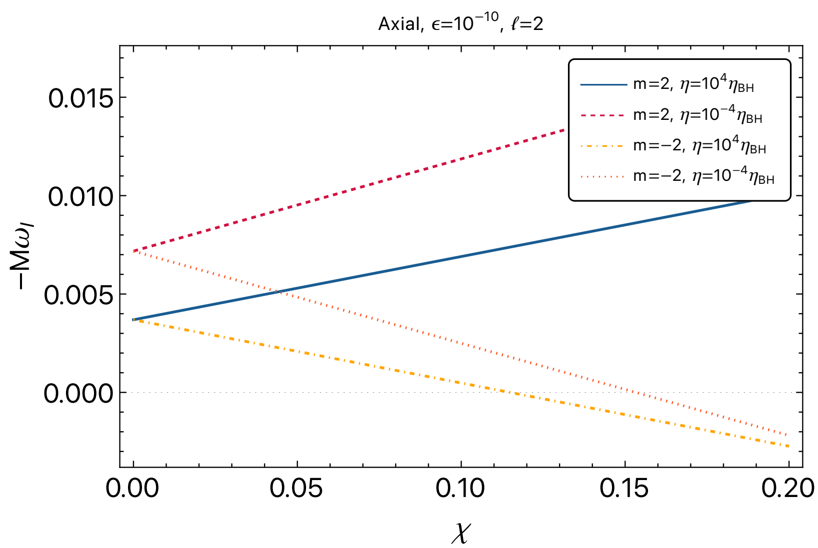

Figure 7.6: Imaginary part of the $\ell = 2$, $m = \pm 2$ QNMs of an ultracompact object as a function of the spin for a perfectly reflecting compact object with viscosity $\eta \gg \eta_{\rm BH}$ and $\eta \ll \eta_{\rm BH}$. Note that the imaginary part for $m = -2$ changes sign above a critical value of the spin rendering the mode unstable.

We note that the imaginary part of the $m = -2$ QNMs indeed changes sign, signalling an instability in the totally reflecting limits. The critical value of the spin where this happens

($\chi \sim 0.11, 0.15$ for $\eta \to 0, \infty$, respectively) is compatible to Ref. [275], where the instability is associated with the ergoregion instability for spinning and totally reflective ultracompact objects. However, from the earlier discussion in Sec. 7.3.1, we know that the presence of ergoregion-related behaviour is an artefact of the expansion at the linear order in spin. Thus, it is merely a coincidence that the linear-in-spin expansion makes the result more consistent with the behaviour for arbitrary values of the spin. Nevertheless, it is clear from Fig. 7.6 that the modes become longer lived as the spin increases in the purely reflecting limit.

The variation of the polar fundamental QNM mode as a function of the shear viscosity is qualitatively similar to the axial case. Thus, we do not show it here. However, due to the differing boundary conditions in the $\epsilon \to 0$ limit in Eqs. (7.32) and (7.33), the isospectrality between axial and polar QNMs is broken when η differs from the BH value in both spinning and nonspinning cases. We also note that, for $\epsilon \to 0$, the polar boundary condition does not depend on the bulk viscosity of the membrane. Fig. 7.7 shows the breaking of isospectrality between axial and polar modes for $\chi = 0, 0.1$ as a function of the shear viscosity of the fluid. Let us now analyse the variation of the QNMs with the compactness of the object for a fixed shear viscosity. Fig. 7.8 shows the real (top panel) and imaginary (bottom panel) part of the axial and polar QNMs of a spinning horizonless compact object as a function of ϵ, where $\chi = 0.2$ and $\eta = \eta_{\rm BH}$. For $\epsilon \to 0$ we recover fundamental $\ell = m = 2$ QNM of a Kerr BH at the first order in spin. For larger values of ϵ, the compactness of the object decreases and the QNMs depart from the BH picture. The axial and polar QNMs are not isospectral; moreover, the polar QNMs depend on the bulk viscosity of the membrane fluid.

The variation of the fundamental QNM in the spinless case for axial and polar modes was derived in Ref. [90]. It was estimated that horizonless compact objects with $\epsilon \lesssim 0.1$ are com-

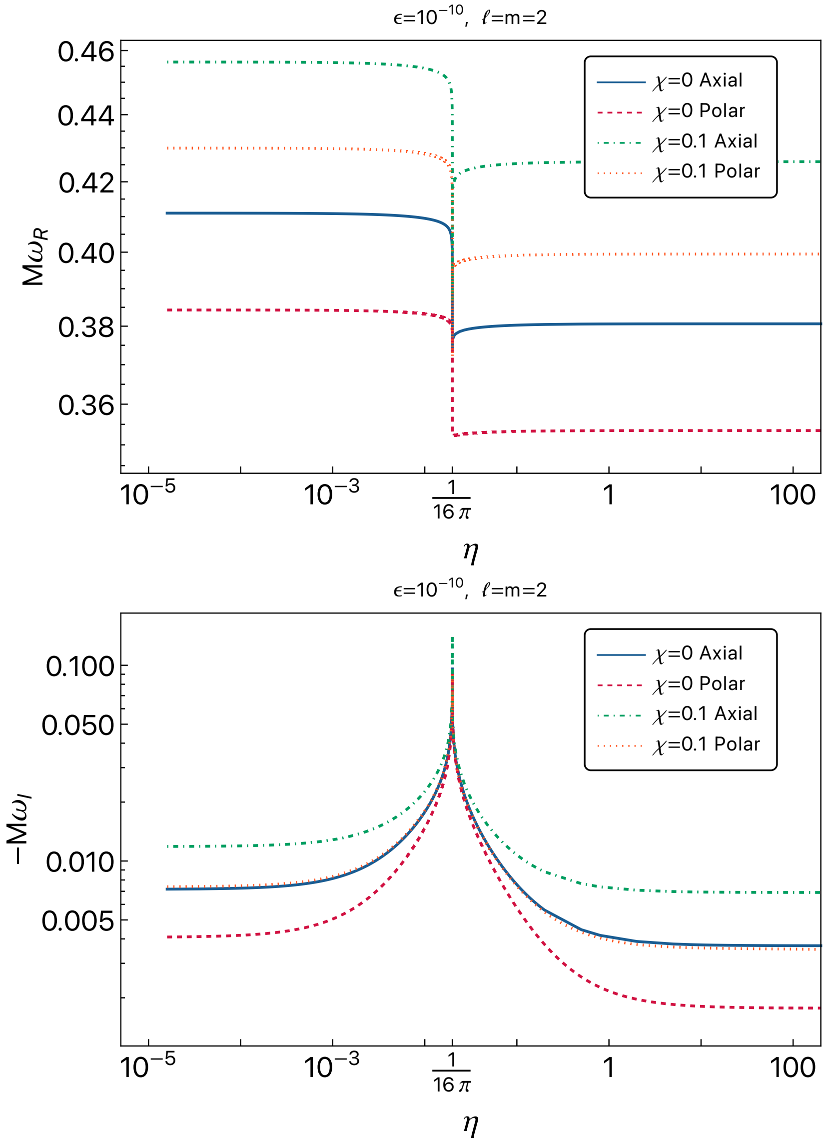

Figure 7.7: Real (top panel) and imaginary (bottom panel) part of the $\ell = m = 2$ QNM of an ultracompact object as a function of the viscosity parameter η for axial and polar perturbations, and different values of the spin. Note that the isospectrality between axial and polar modes is broken in both the spinless and spinning cases.

patible with the measurement accuracy of the fundamental QNM in GW150914 [276], which is approximately 10% and 15% for the real and imaginary part of the frequency, respectively (corresponding to the shaded area in Fig. 7.8). Here, we reconsider this argument by including the spin at the linear order. By comparing Fig. 7.8 with Ref. [90], we find that the variation of the

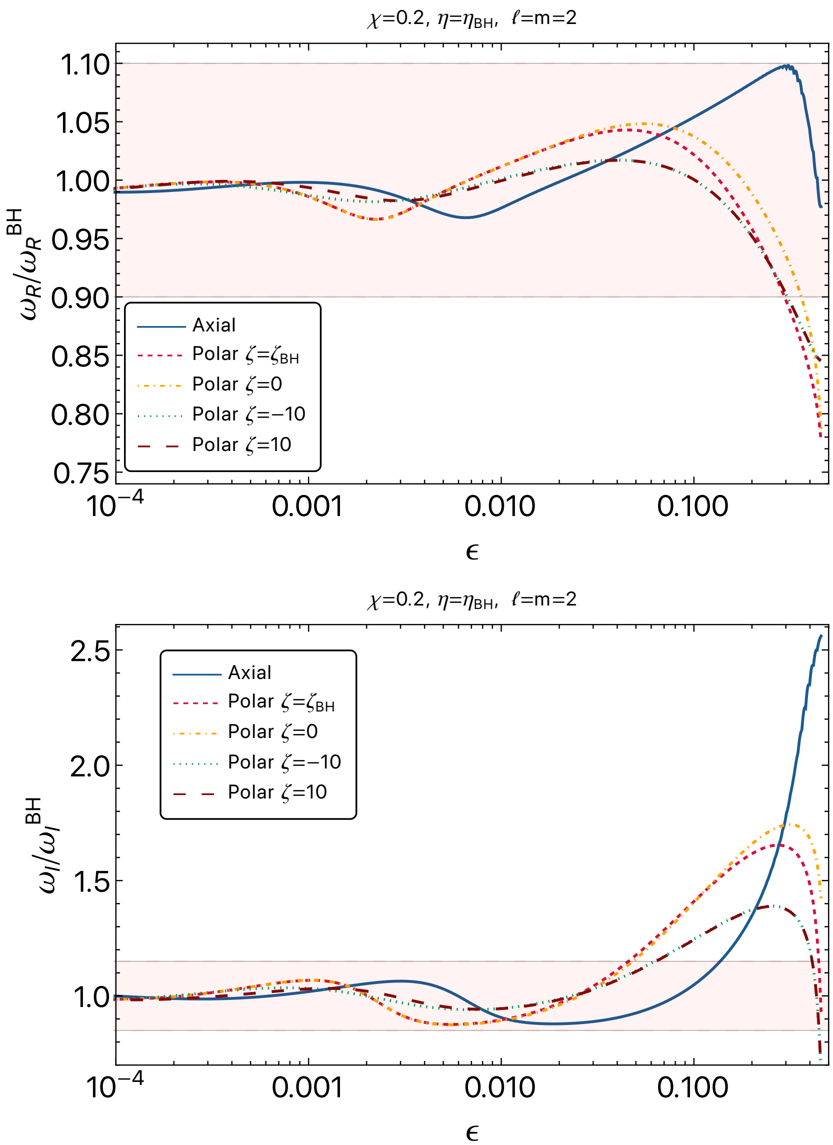

Figure 7.8: Real (top panel) and imaginary (bottom panel) part of the fundamental $\ell = m = 2$ QNM of a compact object with effective shear viscosity $\eta = \eta_{\rm BH}$, with respect to their corresponding value for the BH case. The QNMs are functions of the parameter ϵ, which is related to the compactness of the object. For $\epsilon \to 0$, we recover the fundamental BH QNM and axial and polar modes are isospectral. The shaded band correspond to the error bars (10% and 15%, respectively) for the real and the imaginary part of the fundamental QNM for the merger event GW150914 [276].

real part of the fundamental mode as a function of ϵ is suppressed by the spin. However, the variation of the imaginary part of the fundamental mode is enhanced by the spin and it crosses the shaded band for smaller values of ϵ than in the nonspinning case. Fig. 7.8 shows that spinning ($\chi = 0.2$) horizonless compact objects with $\epsilon \lesssim 0.05$ are compatible with measurement accuracy of the fundamental QNM in GW150914. This suggests that spinning horizonless compact objects may be more easily differentiated than nonspinning ones in the prompt ringdown. Moreover, the breaking of isospectrality between axial and polar modes may be more readily seen for increasing the values of the compactness.

7.4 Summary and conclusions

In this work, we have extended the membrane paradigm to linear order in spin, to investigate slowly spinning horizonless compact objects. We have derived the boundary conditions describing axial and polar perturbations of generic compact objects to linear order in spin, and presented their expressions in the Appendix and the supplemental Mathematica document [274]. We have discussed the effect of spin in observables such as the object's reflectivity at infinity and the fundamental QNM frequencies in the ringdown. In particular, we numerically computed the reflectivity as a function of the shear η and bulk ζ viscosities of the membrane and the object's compactness. We discussed the relation between the viscosity and the reflectivity in the limit of the BH compactness ($\epsilon \to 0$), where the limits $\eta \to 0,\ \infty$ lead to the cases of purely reflecting compact objects. In the spinning case, the reflectivity changes discontinuously when the object's radius approaches the light ring ($\epsilon \to 1/2$) even for small values of the spin, both for axial and polar perturbations.

We analysed the variation of the fundamental QNM frequency with the membrane parameters in the presence of spin. We computed the fundamental $\ell = m = 2$ mode for the membrane parameters of a Kerr BH at linear order in spin ($\epsilon \to 0$, $\eta = 1/16\pi$, $\zeta = -1/16\pi$) as a function of the spin, and compared it with the fundamental QNM of a Kerr BH. We found that the linear-in-spin QNM frequency is within 1% of the Kerr value up to $\chi \sim 0.2$. We thus restricted the upper limit on the spin in this work at $\chi = 0.2$. However, considering the presence of spurious superradiance at linear order in spin, we cautioned that one must keep a look out for such unphysical effects, and setting $\chi < 0.2$ as the regime of validity for generic compact objects can lead to incorrect conclusions.

We analysed the shift in the fundamental QNM frequency starting from the BH case ($\eta = 1/16\pi$) and going towards the purely reflecting cases ($\eta \to 0,\ \infty$). We noticed that for $m = -2$, the fundamental mode frequencies become longer lived (i.e., the imaginary part tends to 0) as the spin increases in the purely reflecting limits ($\eta \to 0,\ \infty$). In particular, for $\chi \sim 0.1 - 0.15$, the imaginary part of the fundamental mode switches sign signalling an instability. While this is consistent with previous literature on QNMs of purely reflecting spinning objects, we argued that the linear-in-spin approximation cannot exhibit such effects lacking an ergosphere. Thus, we cannot claim the presence of an instability from the linear-in-spin approach, but the trend of longer lived fundamental mode as the spin is increased for purely reflecting bodies can be taken as a result. We then considered the variation of the fundamental mode frequency as the compactness approaches the BH value, for both axial and polar modes. The polar modes have an additional dependence on the bulk viscosity ζ when $\epsilon \neq 0$. Similarly to the nonspinning case analysed earlier, we found that the axial and polar modes are not isospectral when $\epsilon \neq 0$. Moreover, the spin enhances the variation of the imaginary part of the fundamental mode with respect to the BH value. Therefore, spinning horizonless compact objects may be more easily differentiated than nonspinning ones in the prompt ringdown.

Overall, the inclusion of spin causes the QNM spectrum of a horizonless compact object to deviate more strongly from the one of a BH with the same spin parameter, even at linear order when the spin-induced multipole moments are neglected. However, the remnants of compact binary coalescences have large values of the spins, $\chi \gtrsim 0.6$. Therefore, it is important to extend this framework to higher orders in spin as a future work. Finally, the development of a Bayesian framework to map current constraints from parametrised tests of GR into constraints on the properties of compact objects is left for future work.

Acknowledgements

We thank Hector O. Silva and Sebastian Völkel for useful discussions. E.M. acknowledges funding from the Deutsche Forschungsgemeinschaft (DFG) - project number: 386119226. E.M. is supported by the European Union's Horizon Europe research and innovation programme under the Marie Skłodowska-Curie grant agreement No. 101107586.

Chapter 8: Conclusions and future work

The primary focus of the dissertation was to advance our understanding of the gravitational dynamics of compact objects (such as black holes (BHs) and neutron stars (NSs)) and their applications in gravitational-wave (GW) astronomy. A key aspect of this work involved the study of gravitational Raman and Compton scattering of GWs off compact objects. This problem was chosen for its tractability within both worldline effective field theory (WEFT) frameworks and BH/stellar perturbation theory (BHPT/SPT), making it particularly well-suited for analyzing finite-size effects, such as tidal interactions, and for probing how the internal structure of compact objects influences their interaction with the surrounding gravitational field. Additionally, the dissertation explored the two-body scattering problem and the translation of scattering observables to bound binary systems—a crucial step for applying scattering results to GW astrophysics. Lastly, the work investigated the shift in the fundamental QNM frequencies for spinning, reflective compact objects.

8.1 Gravitational Raman scattering and tidal effects

The scattering of gravitational waves off a compact object provides a clean and insightful playground to study its coupling to external gravitational fields. The resulting amplitude can also be employed to constrain the two-body dynamics. Moreover, this setup is particularly well-suited for matching computations to fix parameters in WEFTs, especially the Wilson coefficients associated with tidal interactions, as it remains analytically and numerically tractable both in the full theory and within relativistic perturbation theory (BHPT/SPT). More broadly, it offers an ideal framework to understand how compact objects respond to external perturbations—a question of universal relevance across gravitating systems. Additionally, the gravitational Compton amplitude connects naturally to quantum field theory (QFT)-inspired approaches that aim to bootstrap scattering amplitudes based on general principles.

In Chapter 3, we computed the gravitational Compton amplitude for a spinning-parity invariant body with spin-induced quadrupole and octupole moments to third order in spin at linear order in the mass of the scattering body. We showed that the resultant amplitude was consistent with some previous conjectures based on a best-behaved high-energy limit considerations when the spin-induced multipole moments were that of a Kerr BH. Additionally, we obtained expressions for the deviation from the BH case as a function of the strength of induced multipole moments.

In Chapters 4, 5, and 6, we investigated the problem of gravitational Raman scattering within both BHPT and WEFT frameworks, using the comparison to constrain the tidal responses of Kerr BHs and non-spinning NSs. In Chapter 4, we constrained the dissipative response of Kerr BHs and computed the associated changes in mass and angular momentum for quasi-circular, aligned-spin binaries during inspiral, evaluating their contribution to the waveform at NNLO. Chapter 5 extended this analysis to conservative coefficients, recovering the vanishing of static Love numbers and establishing the classical renormalization group flow in the dynamical Love and dissipation numbers. We also analyzed tail effects in the scattering process and their role in shaping the tidal response. In Chapter 6, we applied these methods to neutron stars, accounting for the coupling between matter and gravitational perturbations in the fluid interior. We computed the static Love number and leading dissipation number for various equations of state (EOS), and studied the influence of tidal dissipation, within a fully relativistic framework, during the inspiral phase.

These works collectively illustrate how gravitational Raman scattering serves as a powerful probe of compact-object binary dynamics, particularly in modeling tidal effects during the inspiral. It is timely and important to refine these results further and explore their potential applications in the broader context of gravitational scattering.

Some related future directions that are currently actively being pursued with collaborators are

- A direct practical application of Raman scattering lies in the context of GW lensing. GW lensing is typically analyzed in the geometric optics limit, where BHPT is not well suited. However, this approximation breaks down when the GW wavelength becomes comparable to the characteristic scale of the lens, which can occur in certain events. In such cases, the wave-like nature of GWs must be accounted for, requiring a full scattering analysis via BHPT. This has recently been carried out for non-spinning lenses in Ref. [586]. Building on our previous work, we possess the tools to extend this analysis to Kerr BHs and are currently pursuing this direction.

- It is also worthwhile to investigate how tidal interactions are modified in spinning NSs without relying on the Newtonian approximation, extending the analysis presented in Chapter 6 [5]. Such a study will refine our understanding of relativistic tidal effects in spinning NSs and provide an independent verification of recent results concerning tides in binaries with spinning components [199].

- A related avenue involves extending our framework beyond the adiabatic tide regime, which assumes static or slowly-varying external fields. This extension is particularly relevant for NSs, where dynamical tides and tidal resonances can play a crucial role during the inspiral. Addressing this requires semi-analytical or numerical generalizations of our formalism. For NS binaries, it will lead to improved waveform modeling, while for BHs, it will enhance our understanding of the link between tidal responses and QNM spectra.

8.2 Two-body scattering and its relationship to the bound dynamics

For highly eccentric binaries or during the late stages of inspiral, the PN expansion becomes inadequate due to its reliance on small velocities and weak-field assumptions. A significant approach to circumvent these limitations involves analyzing two-body scattering encounters within the post-Minkowskian (PM) framework. The PM scheme, being an expansion in powers of the gravitational constant rather than velocity, does not assume non-relativistic motion. This allows for the resummation of results to all orders in v/c, where v denotes the typical velocities in the system. Crucially, scattering observables computed in this framework can also be repurposed to extract information about bound binaries [131, 153, 227].

In Chapter 2, we investigated the scattering of two charged particles in electromagnetism up to third order in the coupling (third post-Lorentzian order, corresponding to sixth order in the charges), incorporating radiation reaction effects. We computed key observables such as the scattering angle, impulse, radiated energy, and angular momentum. Furthermore, we derived new analytical continuation maps connecting the radiated energy and angular momentum in scattering encounters to their counterparts per radial period in bound orbits. We demonstrated the validity of these mappings in both the electromagnetic case and in the gravitational case at 1PN. The chapter concluded with a critical discussion on the applicability and limitations of such mappings.

- A promising direction for future research is the incorporation of dynamical tides into scattering encounters. In particular, it would be interesting to investigate how oscillation modes—such as QNMs in BHs—can be excited in these scenarios. Numerical simulations have already demonstrated that QNMs can be triggered in highly eccentric systems, especially in extreme-mass-ratio binaries. In contrast, during quasi-circular inspirals, the typical orbital frequencies remain too low to efficiently excite QNMs. However, in scattering events, the absence of a single characteristic time scale opens up the possibility of mode excitation under different conditions. Understanding the mechanisms behind such excitations, and assessing their observational significance, could yield novel insights for gravitational-wave astronomy.

8.3 Modeling ringdown for generic compact objects

The characteristic frequencies emitted by compact objects during the ringdown phase—when the object relaxes to a stationary state—serve as crucial probes of their nature. They depend sensitively on intrinsic properties such as reflectivity, spin, and compactness.

In Chapter 7, we analyzed how the fundamental QNM frequency varies for spinning compact objects with differing reflectivity and radius. To this end, we employed the membrane paradigm as a phenomenological tool to parametrize generic compact objects. Specifically, we incorporated linearized spin into the framework and derived boundary conditions for the metric perturbations in terms of membrane parameters. We then examined how varying these parameters affects reflectivity characteristics and the fundamental mode, providing physical interpretations of the results.

Potential directions for future research include:

- A key avenue is to explore how spin-induced deformations influence QNM frequencies. This is of both conceptual and observational relevance, particularly for constraining deviations from Kerr based on ringdown signals. From a practical standpoint, this requires parameterizing boundary conditions at the surface of spinning, deformed compact objects. Extending the membrane paradigm to higher orders in spin offers a viable approach to achieve this.

- Another important objective is to elucidate the relationship between QNM frequencies and the tidal response. In the Newtonian limit, QNMs correspond to the poles of the tidal-response function, interpreted as oscillation modes. However, in the relativistic regime, this connection is obscured by the inherent nonlinearities of GR. A detailed investigation into this link is warranted. In earlier chapters, we demonstrated how the tidal response is encoded in the boundary conditions at the stellar surface. Comparing these findings with semi-analytical or numerical studies that relate QNMs to boundary conditions could help relate QNMs to the tidal response in a relativistic context.

Appendix A: Conservative and radiative dynamics in classical relativistic scattering and bound systems

A.1 The 2nd order worldline corrections

A.1.1 Evaluating the force

Here, we show the steps leading to the explicit computation of the 2nd order worldline corrections. We first need to find the partial derivatives of the field tensor ($F^{\mu\nu}$) w.r.t. the coordinates of the particles' worldlines, velocities and accelerations. We list them below and then use them to compute the 2nd order force in terms of 1st order worldline corrections $z^{(1)}$. We have

$$F^{\mu\nu}(z_1(\tau_1))[z_2(\tau_{2,\text{ret}}) = z_{2,\text{ret}}] = \frac{2q_2\rho_2^{[\mu}[r_2\ddot{z}_{2,\text{ret}}^{\nu]} - \dot{z}_{2,\text{ret}}^{\nu]}(\ddot{z}_{2,\text{ret}}\cdot\rho_2 - 1)]}{r_2^3},$$

$$\rho_2^\mu = z_1^\mu - z_{2,\text{ret}}^\mu, \quad r_2 = \dot{z}_{2,\text{ret}}\cdot\rho_2. \tag{A.1}$$

This is the field sourced by particle 2 at particle 1's position ($x = z(\tau_1)$). It depends on the worldlines directly via the expression shown above and indirectly through the retarded time $\tau_{2,\text{ret}}$. It is convenient to separately deal with the dependence on retarded time. The required partial derivaties are

$$\frac{\partial F_{\mu\nu}(z_1)[z_{2,\text{ret}}]}{\partial z_{1,\alpha}} = \frac{2q_2}{r_2^4}\Big[\big(r_2\delta^\alpha_{[\mu} - 3\dot{z}^\alpha_{2,\text{ret}}\rho_{2,[\mu}\big)\big(r_2\ddot{z}_{2,\text{ret},\nu]} - \dot{z}_{2,\text{ret},\nu]}(\ddot{z}_{2,\text{ret}}\cdot\rho_2 - 1)\big)$$

$$+ r_2\rho_{2,[\mu}\left(\dot{z}^{\alpha}_{2,\text{ret}}\ddot{z}_{2,\text{ret},\nu]} - \dot{z}_{2,\text{ret},\nu]}\ddot{z}^{\alpha}_{2,\text{ret}}\right)\Bigg], \tag{A.2}$$

$$\frac{\partial F_{\mu\nu}(z_1)[z_{2,\text{ret}}]}{\partial z_{2,\text{ret},\alpha}} = -\frac{\partial F_{\mu\nu}(z_1)[z_{2,\text{ret}}]}{\partial z_{1,\alpha}}, \tag{A.3}$$

$$\frac{\partial F_{\mu\nu}(z_1)[z_{2,\text{ret}}]}{\partial \dot{z}_{2,\text{ret},\alpha}} = \frac{-2q_2\rho_{2,[\mu}}{r_2^4}\left[2\rho_2^{\alpha}\ddot{z}_{2,\text{ret},\nu]} - \left(3\rho_2^{\alpha}\dot{z}_{2,\text{ret},\nu]} - \delta^{\alpha}_{\nu]}\right)(\ddot{z}_{2,\text{ret}}\cdot\rho_2 - 1)\right], \tag{A.4}$$

$$\frac{\partial F_{\mu\nu}(z_1)[z_{2,\text{ret}}]}{\partial \ddot{z}_{2,\text{ret},\alpha}} = \frac{2q_2\rho_{2,[\mu}}{r_2^3}\left(r_2\delta^{\alpha}_{\nu]} - \dot{z}_{2,\text{ret},\nu]}\rho_2^{\alpha}\right), \tag{A.5}$$

where we have kept the retarded time fixed while varying the coordinates. We now quantify the dependence on retarded time by the total derivative:

$$\begin{aligned}\frac{dF_{\mu\nu}(z_1)[z_2(\tau_{2,\text{ret}})]}{d\tau_{2,\text{ret}}} &= \frac{\partial F_{\mu\nu}(z_1)[z_2(\tau_{2,\text{ret}})]}{\partial z_{2,\text{ret},\alpha}}\dot{z}_{2,\text{ret},\alpha} + \frac{\partial F_{\mu\nu}(z_1)[z_2(\tau_{2,\text{ret}})]}{\partial \dot{z}_{2,\text{ret},\alpha}}\ddot{z}_{2,\text{ret},\alpha} \\ &\quad + \frac{\partial F_{\mu\nu}(z_1)[z_2(\tau_{2,\text{ret}})]}{\partial \ddot{z}_{2,\text{ret},\alpha}}\dddot{z}_{2,\text{ret},\alpha}.\end{aligned} \tag{A.6}$$

We can now compute the 2$^{\text{nd}}$ order corrections to the force. The 2$^{\text{nd}}$ order correction to the force is obtained by substituting 1$^{\text{st}}$ order worldlines (and retarded time) in the force and taking the coefficient of e^4, i.e.,

$$m_1\ddot{z}_1^{(2)\mu} = \left[e^4\right]\left[e^2 q_1 F^{\mu\nu}\dot{z}_{1,\nu} + e^2\frac{2q^2}{3}\left(\dddot{z}_1^{\mu} + \ddot{z}_1^2\dot{z}_1^{\mu}\right)\right] = f^{(2)\mu}$$

where $[x^2]f(x)$ = Coefficient of x^2 in $f(x)$, and in RHS, we have

$$z_1^{\mu} \to z_1^{(0)\mu} + e^2 z_1^{(1)\mu},\ z_2^{\mu} \to z_2^{(0)\mu} + e^2 z_2^{(1)\mu},\ \tau_{2,\text{ret}} = \tau^{(0)}_{2,\text{ret}} + e^2\tau^{(1)}_{2,\text{ret}}, \tag{A.7}$$

where $f^{(2)\mu}$ is the total force correction at 2$^{\text{nd}}$ order. We expand the RHS of Eq. (2.27) into four parts using Taylor series, as was shown in the diagrams in figure 2.29 in main text. Here, we write those contributions explicitly in terms of 1$^{\text{st}}$ order worldline corrections using the partial derivatives of the field tensor derived above.

I

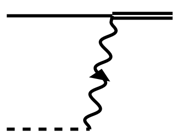

a) Correction to $e^2 q_1 F^{\mu\nu}\dot{z}_{1,\nu}$ due to $e^2 z_1^{(1)}$.

Diagram I is the force correction due to the 1st order worldline corrections to particle 1 in the zeroth order field of particle 2, via the explicit dependence of $z_1(\tau_1)$, $\dot{z}_1(\tau_1)$ in the Lorentz force (first term in RHS of Eq. (A.7)). It thus scales as $1/m_1$. It is given by

$$e^4 f_{\mathrm{I}}^{(2)\mu} = e^4 \frac{\partial(q_1 F^{\mu\nu}\dot{z}_{1,\nu})}{\partial z_1^{\alpha}}|_{(0)} z_1^{(1),\alpha} + e^4 \frac{\partial(q_1 F^{\mu\nu}\dot{z}_{1,\nu})}{\partial \dot{z}_1^{\alpha}}|_{(0)} \dot{z}_1^{(1),\alpha}. \tag{A.8}$$

At zeroth order, we have $\ddot{z}^{(0)} = 0$, $\dot{z}_i = u_i$, $\rho_2^{(0),\mu} = b^\mu + u_1^\mu \tau_1 - u_2^\mu \tau_{2,\mathrm{ret}}^{(0)}$, $r_2 = -\tau_{2,\mathrm{ret}}^{(0)} + \gamma\tau_1$. We define $r_2(\tau_1, \tau_{2,\mathrm{ret}}^{(0)}) = r_{21} = \sqrt{|b|^2 + (\gamma v)^2 \tau_1^2}$ and $s_1 = \gamma v \tau_1 + r_{21}$. Thus, the contribution to force is given by

$$\begin{aligned} f_{\mathrm{I}}^{(2)\mu} =& \frac{q_1 q_2[\gamma(r_{21} z_1^{(1),\mu} - 3\rho_2^{(0),\mu} u_2 \cdot z_1^{(1)}) - u_2^\mu (r_{21} u_1 \cdot z_1^{(1)} - 3 u_1 \cdot \rho_2^{(0)} u_2 \cdot z_1^{(1)})]}{r_{21}^4} \\ &+ \frac{q_1 q_2[\rho_2^{(0),\mu}(u_2 \cdot \dot{z}_1^{(1)}) - u_2^\mu(\rho_2^{(0)} \cdot \dot{z}_1^{(1)})]}{r_{21}^3}, \end{aligned} \tag{A.9}$$

where the $1/m_1$ dependence comes from 1st order worldline corrections $z_1^{(1)}$. Using this expression and the 1st order corrections (Eq. (2.23)), it is easy to see that this is composed of a linear combination of terms such as

$$\frac{1}{m_1}\left\{ \frac{(r_{21} \text{ or } s_1 \text{ or } \tau_1) \times \log(s_1)}{r_{21}^4}, \frac{(r_{21} \text{ or } s_1 \text{ or } \tau_1) \times s_1}{r_{21}^4}, \frac{(\tau_1 \text{ or } s_1)}{r_{21}^4} \right\} \tag{A.10}$$

b) Correction to $e^2 q_1 F^{\mu\nu}\dot{z}_{1,\nu}$ due to $e^2 z_2^{(1)}$.

II

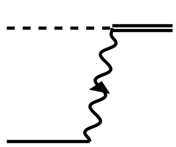

Diagram II is the force correction due to 1st order worldline correction of particle 2 via explicit dependence of the Lorentz force term on $[z_2]$. It thus scales as $1/m_2$.

It is given by,

$$
\begin{aligned}
e^4 f_{\mathrm{II}}^{(2)\mu} =& e^4 \frac{\partial(q_1 F^{\mu\nu} u_{1,\nu})}{\partial z_2^\alpha}|_{(0)} z_2^{(1),\alpha} + e^4 \frac{\partial(q_1 F^{\mu\nu} u_{1,\nu})}{\partial \dot{z}_2^\alpha}|_{(0)} \dot{z}_2^{(1),\alpha} \\
&+ e^4 \frac{\partial(q_1 F^{\mu\nu} u_{1,\nu})}{\partial \ddot{z}_2^\alpha}|_{(0)} \ddot{z}_2^{(1),\alpha}
\end{aligned}
\tag{A.11}
$$

Evaluating the partial derivatives with zeroth order worldlines gives us

$$
\begin{aligned}
f_{\mathrm{II}}^{(2)\mu} =& \frac{-q_1 q_2 [\gamma(r_{21} z_2^{(1).\mu} - 3\rho_2^{(0),\mu} u_2 \cdot z_2^{(1)}) - u_2^\mu (r_{21} u_1 \cdot z_2^{(1)} - 3 u_1 \cdot \rho_2^{(0)} u_2 \cdot z_2^{(1)})]}{r_{21}^4} \\
&- \frac{q_1 q_2 [\rho_2^{(0),\mu} (3\rho_2^{(0)} \cdot \dot{z}_2^{(1)} \gamma - u_1 \cdot \dot{z}_2^{(1)}) - (\rho_2^{(0)} \cdot u_1)(3 u_2^\mu \rho_2^{(0)} \cdot \dot{z}_2^{(1)} - \dot{z}_2^{(1),\mu})]}{r_{21}^4} \\
&+ \frac{q_1 q_2 [\rho_2^{(0),\mu} (r_{21}(u_1 \cdot \ddot{z}_2^{(1)}) - \gamma \rho_2^{(0)} \cdot \ddot{z}_2^{(1)}) - (u_1 \cdot \rho_2^{(0)})(\ddot{z}_2^{(1),\mu} - u_2^\mu (\rho_2^{(0)} \cdot \ddot{z}_2^{(1)}))]}{r_{21}^3},
\end{aligned}
\tag{A.12}
$$

where the $1/m_2$ dependence comes from the first order worldline corrections $z_2^{(1)}$, and we can use this expression and the 1st order corrections (Eq. (2.26)) to see that it is a linear combination of terms like

$$
\begin{aligned}
&\frac{1}{m_2} \left\{ \frac{(r_{21} \text{ or } \tau_1 \text{ or } s_1) \times s_2}{r_{21}^4}, \frac{(r_{21} \text{ or } \tau_1 \text{ or } s_1) \times \log(s_2)}{r_{21}^4}, \frac{(s_1 \tau_1 \text{ or } \tau_1^2 \text{ or } s_1^2 \text{ or } s_1 \text{ or } \tau_1) \times (1 \text{ or } s_2)}{r_{21}^4 r_{12}}, \right. \\
&\quad \left. \frac{r_{21} \text{ or } s_1 \text{ or } \tau_1 \text{ or } s_1^2 \text{ or } \tau_1 s_1 \text{ or } \tau_1^2 \text{ or } s_1^3 \text{ or } s_1^2 \tau_1 \text{ or } \tau_1^3}{r_{21}^3 r_{12}^3} \right\}, \\
&r_{12} = \sqrt{|b|^2 + (\gamma v)^2 \tau_2^2}, \quad s_2 = \gamma v \tau_2 + r_{12}.
\end{aligned}
\tag{A.13}
$$

In the above expressions, all functions of τ_2 should be evaluated at $\tau_{2,\mathrm{ret}}^{(0)}$.

c) Correction to $e^2 q_1 F^{\mu\nu} \dot{z}_{1,\nu}$ due to $e^2 \tau_{2,\mathrm{ret}}^{(1)}$.

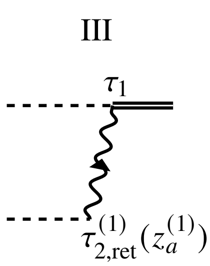

Diagram III is the force correction due to first order corrections to retarded time which in turn comes from 1st order correction to both particles' worldlines. It gains contributions linear in both $z_1^{(1)}$ and $z_2^{(1)}$ (and their derivatives) and thus has terms with both kinds of scaling $(1/m_1, 1/m_2)$. It is given by,

$$e^2 q_1 \frac{dF^{\mu\nu} u_{1,\nu}}{d\tau_{2,\text{ret}}} \tau^{(1)}_{2,\text{ret}} = e^4 \frac{\partial (q_1 F_{\mu\nu}(z_1, z_{2,\text{ret}}) u_{1,\nu})}{\partial z^{\alpha}_{2,\text{ret}}} u^{\alpha}_2 \tau^{(1)}_{2,\text{ret}}. \tag{A.14}$$

The 1st order correction to retarded time is obtained by solving $|\rho|^2 = 0$ with first order corrected worldlines to order e^2. Thus, we have

$$|z_1 - z_2(\tau_{2,\text{ret}})|^2 \approx (b^2 + \tau_1^2 + \tau^2_{2,\text{ret}} - 2\tau_1 \tau_{2,\text{ret}} \gamma) + 2e^2 (b + u_1 \tau_1 - u_2 \tau_{2,\text{ret}}) \cdot (z^{(1)}_1 - z^{(1)}_2) = 0. \tag{A.15}$$

To solve iteratively, we substitute $\tau_{2,\text{ret}} = \tau^{(0)}_{2,\text{ret}} + e^2 \tau^{(1)}_{2,\text{ret}}$, $\tau^{(0)}_{2,\text{ret}} = \gamma\tau_1 - r_{21}$. We get

$$\begin{aligned} e^2 \tau^{(1)}_{2,\text{ret}} (\tau^{(0)}_{2,\text{ret}} - \gamma\tau_1) &= e^2 \tau^{(1)}_{2,\text{ret}} r_{21} = -e^2 (b + u_1\tau_1 - u_2 \tau^{(0)}_{2,\text{ret}}) \cdot (z^{(1)}_1 - z^{(2)}_2), \\ e^2 \tau^{(1)}_{2,\text{ret}} &= \frac{e^2 \rho^{(0)}_2 \cdot (z^{(1)}_1 - z^{(1)}_2)}{r_{21}}. \end{aligned} \tag{A.16}$$

As expected, the retarded time is linear in both $z^{(1)}_1$ and $z^{(1)}_2$ and thus has terms with both types of mass dependencies m_1^{-1}, m_2^{-1}. We can now evaluate its contribution to force to be

$$f^{(2)\mu}_{\text{III}} = \frac{-q_1 q_2 (\rho^{(0)}_2 \cdot (z^{(1)}_1 - z^{(1)}_2))[(r_{21} u^{\mu}_2 - 3\rho^{\mu}_2 \gamma)\gamma - (\gamma r_{21} - 3(\rho^{(0)}_2 \cdot u_1)) u^{\mu}_2]}{r^5_{21}}. \tag{A.17}$$

It contains new types of terms such as

$$\frac{(s_1 \text{ or } \tau_1 \text{ or } s_1^2 \text{ or } \tau_1 s_1 \text{ or } \tau_1^2) \times (s_1 \text{ or } \log(s_1) \text{ or } s_2 \text{ or } \log(s_2))}{r^5_{21}}. \tag{A.18}$$

We omit discussion of Diagram IV in the appendix since it is much simpler and was explicitly treated in the main text. The total force is the sum of all four contributions,

$$e^4 m_1 z^{(2)\mu}_1 = e^4 (f^{(2)\mu}_{\text{I}} + f^{(2)\mu}_{\text{II}} + f^{(2)\mu}_{\text{III}} + f^{(2)\mu}_{\text{IV}}). \tag{A.19}$$

A.1.2 Performing the integrals

All three sets of terms in Eq. (A.10), Eq. (A.13), and Eq. (A.18) contain many square roots coming from $r_{21} = \sqrt{|b|^2 + (\gamma v)^2 \tau_1^2}$, $r_{12}(\tau^{(0)}_{2,\text{ret}}) = \sqrt{|b|^2 + (\gamma v)^2 (\gamma\tau_1 - r_{21})^2}$. The latter even appears to contribute nested square roots. This however can be resolved by using the relation

$$r_2^{12}(\tau_{2,\mathrm{ret}}^{(0)}) = |b|^2 + (\gamma v)^2(\gamma\tau_1 - r_{21})^2 = |b|^2 + (\gamma^2-1)\gamma^2\tau_1^2 + (\gamma^2-1)r_{21}^2 - 2(\gamma^2-1)\gamma\tau_1 r_{21}$$
$$= \gamma^2(|b|^2 + (\gamma^2-1)\tau_1^2) + (\gamma^2-1)^2\tau_1^2 + 2(\gamma^2-1)\gamma\tau_1 r_{21}$$
$$= (\gamma r_{21} + (\gamma v)\tau_1)^2, \tag{A.20}$$

which removes the nested square roots but the square roots still complicate analytical integration. We can remove all the square roots by using the very convenient variable $s_1 = \gamma v\tau_1 + r_{21}$ along with the relations

$$\tau_1 = \frac{|b|(s_1^2-1)}{2s_1\sinh(\phi)}, \quad \tau_2\big|_{\tau_2=\tau_{2,\mathrm{ret}}^{(0)}} = \frac{|b|(s_1^2 - e^{2\phi})}{2s_1 e^{\phi}}, \quad r_{21} = \frac{|b|(1+s_1^2)}{2s_1},$$
$$r_{12}\big|_{\tau_2=\tau_{2,\mathrm{ret}}^{(0)}} = \frac{|b|(e^{2\phi}+s_1^2)}{2e^{\phi}s_1}, \quad s_2\big|_{\tau_2=\tau_{2,\mathrm{ret}}^{(0)}} = e^{-\phi}s_1, \tag{A.21}$$

where $\phi = \mathrm{arccosh}(\gamma)$. This reduces the many terms in the acceleration to these simpler classes of terms

$$\frac{s_1^3\mathrm{Poly}(s_1)\log(s_1)}{(m_1 \text{ or } m_2)(1+s_1^2)^5}, \quad \frac{s_1^3\mathrm{Poly}(s_1)}{(m_1 \text{ or } m_2)(1+s_1^2)^5}, \quad \frac{s_1^3\mathrm{Poly}(s_1)}{m_2(1+s_1^2)^4(e^{2\phi}+s_1^2)^3}. \tag{A.22}$$

We continue to use s_1 as our main variable during integration, we multiply the acceleration (force/m_1) with the Jacobian $(d\tau_1/ds_1) = r_{21}/(s_1\sinh(\phi))) = (1+s_1^2)/(2s_1^2\sinh(\phi))$. We can now integrate w.r.t. s_1 to get the correction to the velocity ($\dot{z}_1^{(2)}$) up to a constant. The integrals are of the type(s)

$$\int ds_1 \frac{s_1 \times \mathrm{Poly}(s_1)\log(s_1)}{(1+s_1^2)^4}, \quad \int ds_1 \frac{s_1 \times \mathrm{Poly}(s_1)}{(1+s_1^2)^4}, \quad \int ds_1 \frac{s_1\times\mathrm{Poly}(s_1)}{(1+s_1^2)^3(e^{2\phi}+s_1^2)^3}. \tag{A.23}$$

`Mathematica` has no trouble evaluating these integrals in this form, no futher simplification is required from a practical point of view. It may be tempting to divide them further into basis integrals (say of the form $\int ds_1 s_1^n \log(s_1)/(1+s_1^2)^3$) but this does not provide any insight or lead to further simplification. In fact, dividing in such a way can lead to non-elementary functions (PolyLogs) upon integration which cancel out in the overall expression. A better way to divide them further (if one wishes to) is to divide the terms in the force in the forms given in Eq. (A.10), Eq. (A.13), and Eq. (A.18) except expressed as functions of s_1. Then each individual integral is made only of elementary functions. Regardless, performing all the integrals and putting them together gives an expression for 2nd order velocity ($\dot{z}_1^{(2)}$) made of a linear combination of terms of the form

$$\begin{aligned}&\frac{\mathrm{Poly}(s_1)}{(m_1m_2 \text{ or } m_1^2)(1+s_1^2)^3}, \quad \frac{1}{(m_1m_2 \text{ or } m_1^2)}\arctan(s_1), \frac{\mathrm{Poly}(s_1)\log(|b|s_1\sinh(\phi))}{(m_1m_2 \text{ or } m_1^2)(1+s_1^2)^3},,\\ &\frac{1}{m_1m_2}\arctan(e^{-\phi}s_1), \; \frac{\mathrm{Poly}(s_1)}{m_1m_2(1+s_1^2)^3(e^{2\phi}+s_1^2)^2}.\end{aligned} \tag{A.24}$$

We get the worldline correction ($z_1^{(2)}$) by repeating the integration process one more time. Thus, we once again multiply the Jacobian $(d\tau_1/ds_1) = r_{21}/(s_1\sinh(\phi)) = (1+s_1^2)/(2s_1^2\sinh(\phi))$ integrate w.r.t. s_1. `Mathematica` can do these integrals with relative ease and we get the 2nd order corrections to the worldlines. Explicit calculation gives the following expression after imposing the boundary conditions $\lim_{\tau_1\to-\infty} z_1^{(2)}\cdot b = 0$ and $\lim_{\tau_1\to-\infty}\dot{z}_1^{(2)} = 0$:

$$\begin{aligned} z_1^{(2)\mu} = \frac{q_1^2q_2^2}{m_1^2}\Bigg\{ &\arctan\left(\frac{\tau_1\gamma v}{|b|}\right)\frac{-\cosh(2\phi)\tau_1\hat{b}^\mu + |b|(u_1^\mu - \gamma u_2^\mu)}{2|b|^2(\gamma v)^3}\\ &+\frac{\tau_1\arctan(s_1/|b|)\hat{b}^\mu}{|b|^2\gamma v^3} - \frac{\log(s_1\gamma v)(s_1\gamma^3 v\hat{b}^\mu + \gamma|b|(u_2^\mu - \gamma u_1^\mu))}{|b|r_{21}(\gamma v)^5}\\ &+\frac{-2(3|b|^2+s_1^2)\gamma u_1^\mu + [5|b|^2+s_1^2+(|b|^2+s_1^2)\cosh(2\phi)]u_2^\mu}{4|b|^2r_{21}\gamma^4v^5}\\ &+\frac{2|b|(|b|^2s_1+5s_1^3)+[\pi(|b|^4-s_1^4)-2s_1|b|^3+6s_1^3|b|]\cosh(2\phi)}{16|b|^3s_1^2r_{21}(\gamma v)^4}b^\mu\Bigg\}\\ &+\frac{q_1^2q_2^2}{m_1m_2}\Bigg\{\frac{\tau_1[2\arctan(s_1/|b|)-\arctan(\tau_1\gamma v/|b|)]\hat{b}^\mu}{2|b|^2\gamma^2v^3} \end{aligned}$$

$$
\begin{aligned}
&- \frac{\log(e^{-\phi} s_1 \gamma v)(s_1 \gamma^2 v \hat{b}^\mu - (\gamma u_1^\mu - u_2^\mu))}{r_{21}(\gamma v)^5} \\
&+ \frac{[\arctan(r_{21}/(|b|\gamma v)) + \arctan(v\tau_1/|b|)](-\tau_1 \gamma v^2 \hat{b}^\mu + |b|(\gamma u_1^\mu - u_2^\mu))}{2|b|^2\gamma^2 v^3} \\
&+ \frac{e^{-3\phi}(u_2^\mu - \gamma u_1^\mu)}{32 r_{12} r_{21} s_1 |b|^2 (\gamma v)^5} \big[|b|^4 + 11 s_1^2 |b|^2 + 2 s_1^4 \\
&+ e^{4\phi}(15|b|^4 + 9 s_1^2 |b|^2 + 2 s_1^4) + e^{2\phi}(7|b|^4 + 11 s_1^2 |b|^2 + 4 s_1^4) \\
&+ 2 e^{6\phi} r_{21} s_1 |b|^2 \big] + \frac{\hat{b}^\mu (1-v) s_1}{|b| r_{21} \gamma^3 v^4} - \frac{\pi \tau_1 \hat{b}^\mu}{4|b|^2 \gamma^2 v^3} \\
&+ \left.\frac{\hat{b}^\mu (s_1^2 - e^{2\phi}\gamma^2 v^2 \tau_1^2)}{2 e^{2\phi} \gamma^2 v^2 r_{21} r_{12} |b|} \right\} \\
&+ \frac{2 e^4 q_1^3 q_2 [\gamma^2 v s_1 b^\mu + |b|^2(-\gamma u_1^\mu + u_2^\mu)]}{3 \gamma v^2 m_1^2 |b|^2 r_{21}}.
\end{aligned}
\tag{A.25}
$$

A.2 Contributions to the 3rd order impulse

The force correction at 3rd order is obtained similarly by expanding the expression for force using 1st and 2nd order trajectories. We also need to find the retarded time corrections at next order, i.e., we need to compute,

$$
m_1 \ddot{z}_1^{(3)\mu} = \left[e^6\right] \left[e^2 q_1 F^{\mu\nu} \dot{z}_{1,\nu} + e^2 \frac{q^2}{6\pi} \left(\dddot{z}_1 + \ddot{z}_1^2 \dot{z}_1^\mu \right) \right] = f^{(3)\mu}, \tag{A.26}
$$

$$
(z_1 \to b + u_1 \tau_1 + e^2 z_1^{(1)} + e^4 z_1^{(2)},\ z_2 \to u_2 \tau_2 + e^2 z_2^{(1)} + e^4 z_2^{(2)},\ \tau_{2,\text{ret}} = \tau_{2,\text{ret}}^{(0)} + e^2 \tau_{2,\text{ret}}^{(1)} + e^4 \tau_{2,\text{ret}}^{(2)}).
$$

In the main text, the various contributions to force correction at 3rd order were given in diagrammatic form in figures (2.36) and (2.35). Here, we write them down in terms of the partial derivatives of the field tensor explicitly and lower order worldline corrections. We also provide the formulae for retarded time corrections, and elaborate on the kind of terms that appear at this order. As mentioned in the main text, contributions at this order come from quadratic in 1st order worldline corrections ($\sim e^4 (z^{(1)})^2$) and linear in 2nd order worldline corrections ($\sim e^4 z^{(2)}$). It is convenient to deal with them separately.

A.2.1 Quadratic Contributions

I) Correction to $e^2 q_1 F^{\mu\nu}\dot{z}_{1,\nu}$ from $e^4(z_1^{(1)})^2$.

I

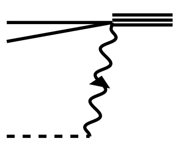

Diagram I comes from quadratic contribution of 1st order worldlines for particle 1 (i.e., $e^4(z_1^{(1)})^2$), thus it scales as m_1^{-2}. We can write this down either by using the rules for diagrams or Taylor series as

$$\begin{aligned} f_{\mathrm{I}}^{(3)\mu} =& \frac{e^6}{2}\frac{\partial^2(q_1 F^{\mu\nu}\dot{z}_{1,\nu})}{\partial z_1^\alpha \partial z_1^\beta} z_1^{(1),\alpha} z_1^{(1),\beta} + e^6 \frac{\partial^2(q_1 F^{\mu\nu}\dot{z}_{1,\nu})}{\partial \dot{z}_1^\alpha \partial z_1^\beta} \dot{z}_1^{(1),\mu} z_1^{(1),\beta} \\ &+ e^6 \frac{1}{2}\frac{\partial^2(q_1 F^{\mu\nu}\dot{z}_{1,\nu})}{\partial \dot{z}_1^\alpha \partial \dot{z}_1^\beta} \dot{z}_1^{(1),\alpha} \dot{z}_1^{(1),\beta}, \end{aligned} \tag{A.27}$$

and since the field tensor does not depend on particle 1's velocity, we can simplify this to

$$e^6 f_{\mathrm{I}}^{(3)\mu} = \frac{1}{2}\frac{\partial^2(q_1 F^{\mu\nu}\dot{z}_{1,\nu})}{\partial z_1^\alpha \partial z_1^\beta} z_1^{(1),\alpha} z_1^{(1),\beta} + \frac{\partial(q_1 F^{\mu\alpha})}{\partial z_1^\beta} \dot{z}_1^{(1),\alpha} z_1^{(1),\beta}. \tag{A.28}$$

II) Correction to $e^2 q_1 F^{\mu\nu}\dot{z}_{1,\nu}$ from $e^4(z_2^{(2)})^2$.

Diagram II comes from quadratic contribution of 1st order worldlines for particle 2 (i.e., $e^4(z_1^{(2)})^2$), thus it scales as m_1^{-2}. This is more complicated since the field tensor depends on position, velocity and acceleration of particle 2,

$$\begin{aligned} e^6 f_{\mathrm{II}}^{(3)\mu} =& \frac{e^6}{2}\frac{\partial^2(q_1 F^{\mu\nu}\dot{z}_{1,\nu})}{\partial z_1^\alpha \partial z_1^\beta} z_1^{(1),\alpha} z_1^{(1),\beta} + \frac{e^6}{2}\frac{\partial^2(q_1 F^{\mu\nu}\dot{z}_{1,\nu})}{\partial \dot{z}_1^\alpha \partial \dot{z}_1^\beta} \dot{z}_1^{(1),\alpha} \dot{z}_1^{(1),\beta} \\ &+ \frac{e^6}{2}\frac{\partial^2(q_1 F^{\mu\nu}\dot{z}_{1,\nu})}{\partial \ddot{z}_1^\alpha \partial \ddot{z}_1^\beta} \ddot{z}_1^{(1),\alpha} \ddot{z}_1^{(1),\beta} + e^6 \frac{\partial^2(q_1 F^{\mu\nu}\dot{z}_{1,\nu})}{\partial z_1^\alpha \partial z_1^\beta} \dot{z}_2^{(1),\mu} z_2^{(1),\beta} + e^6 \frac{\partial^2(q_1 F^{\mu\nu}\dot{z}_{1,\nu})}{\partial \dot{z}_1^\alpha \partial \ddot{z}_1^\beta} \dot{z}_2^{(1),\mu} \ddot{z}_2^{(1),\beta} \\ &+ e^6 \frac{\partial^2(q_1 F^{\mu\nu}\dot{z}_{1,\nu})}{\partial \ddot{z}_1^\alpha \partial z_1^\beta} \ddot{z}_2^{(1),\mu} z_2^{(1),\beta}. \end{aligned} \tag{A.29}$$

II

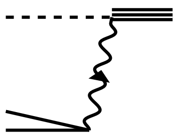

III) Correction to $e^2 q_1 F^{\mu\nu}\dot{z}_{1,\nu}$ from cross terms $e^4(z_1^{(1)} \times z_2^{(1)})$.

III

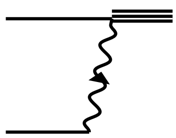

Diagram III ise due to quadratic contribution of cross terms from the 1st order worldline corrections of both particles, thus it scales as $(m_1 m_2)^{-1}$,

$$
\begin{aligned}
e^6 f_{\mathrm{III}}^{(3)\mu} &= e^6 \frac{\partial^2 (q_1 F^{\mu\nu}\dot{z}_{1,\nu})}{\partial z_1^\alpha \partial z_2^\beta} z_1^{(1),\alpha} z_2^{(1),\beta} + e^6 \frac{\partial^2 (q_1 F^{\mu\nu}\dot{z}_{1,\nu})}{\partial \dot{z}_1^\alpha \partial z_2^\beta} \dot{z}_2^{(1),\alpha} z_2^{(1),\beta} \\
&+ e^6 \frac{\partial^2 (q_1 F^{\mu\nu}\dot{z}_{1,\nu})}{\partial z_1^\alpha \partial \dot{z}_2^\beta} z_1^{(1),\alpha} \dot{z}_2^{(1),\beta} \\
&+ e^6 \frac{\partial^2 (q_1 F^{\mu\nu}\dot{z}_{1,\nu})}{\partial \dot{z}_1^\alpha \partial \dot{z}_2^\beta} \dot{z}_1^{(1),\alpha} \dot{z}_2^{(1),\beta} + e^6 \frac{\partial^2 (q_1 F^{\mu\nu}\dot{z}_{1,\nu})}{\partial z_1^\alpha \partial \ddot{z}_2^\beta} z_1^{(1),\alpha} \ddot{z}_2^{(1),\beta} + e^6 \frac{\partial^2 (q_1 F^{\mu\nu}\dot{z}_{1,\nu})}{\partial \dot{z}_1^\alpha \partial \ddot{z}_2^\beta} \dot{z}_1^{(1),\alpha} \ddot{z}_2^{(1),\beta}.
\end{aligned}
\tag{A.30}
$$

IV) Correction to $e^2 q_1 F^{\mu\nu}\dot{z}_{1,\nu}$ linear in $e^2 z_1^{(1)}$ and 1st order retarded time correction ($e^2\tau_{2,\mathrm{ret}}^{(1)}$).

Diagram IV is due to the combined contribution of first order worldline correction of particle 1 ($e^2 z_1^{(1)}$) and 1st order retarded time correction ($e^2\tau_{2,\mathrm{ret}}^{(1)}$). This has terms that scale as $(m_1 m_2)^{-1}$ or m_1^{-2} (see expression of $\tau_{2,\mathrm{ret}}^{(1)}$ in Eq. (A.16)),

$$
e^6 f_{\mathrm{IV}}^{(3)\mu} = e^6 \frac{d}{d\tau_{2,\mathrm{ret}}} \left[\frac{\partial (q_1 F^{\mu\nu}\dot{z}_{1,\nu})}{\partial z_1^\alpha}\Big|_{(0)} z_1^{(1),\alpha} + e^6 \frac{\partial (q_1 F^{\mu\nu}\dot{z}_{1,\nu})}{\partial \dot{z}_1^\alpha}\Big|_{(0)} \dot{z}_1^{(1),\alpha} \right] \tau_{2,\mathrm{ret}}^{(1)}. \tag{A.31}
$$

IV

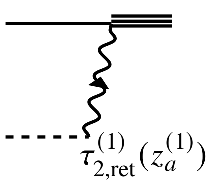

V

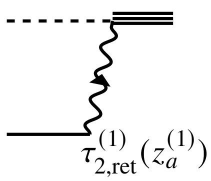

V) Correction to $e^2 q_1 F^{\mu\nu}\dot{z}_{1,\nu}$ linear in $z_2^{(1)}$ and 1^{st} order retarded time correction ($e^2\tau^{(1)}_{2,\mathrm{ret}}$).

This is the counterpart of IV. This has terms that scale as $(m_1 m_2)^{-1}$ or m_2^{-2},

$$e^6 f_{\mathrm{V}}^{(3)\mu} = e^6 \frac{d}{d\tau_{2,\mathrm{ret}}}\left[\frac{\partial(q_1 F^{\mu\nu}u_{1,\nu})}{\partial z_2^{\alpha}}|_{(0)} z_2^{(1),\alpha} + \frac{\partial(q_1 F^{\mu\nu}u_{1,\nu})}{\partial \dot{z}_2^{\alpha}}|_{(0)} \dot{z}_2^{(1),\alpha} + \frac{\partial(q_1 F^{\mu\nu}u_{1,\nu})}{\partial \ddot{z}_2^{\alpha}}|_{(0)} \ddot{z}_2^{(1),\alpha}\right]\tau^{(1)}_{2,\mathrm{ret}}. \tag{A.32}$$

VI) Correction to $e^2 q_1 F^{\mu\nu}\dot{z}_{1,\nu}$ quadratic in 1^{st} order retarded time correction ($e^4(\tau^{(1)}_{2,\mathrm{ret}})^2$).

Diagram VI should be self explanatory. This scales as $(m_1 m_2)^{-1}, m_1^{-2}$ or m_2^{-2},

$$e^6 f_{\mathrm{VI}}^{(3)\mu} = e^6 \frac{(\tau^{(1)}_{2,\mathrm{ret}})^2}{2}\frac{d^2}{d\tau^2_{2,\mathrm{ret}}}(e^2 q_1 F^{\mu\nu}\dot{z}_{1,\nu}). \tag{A.33}$$

VI

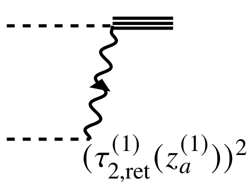

VII

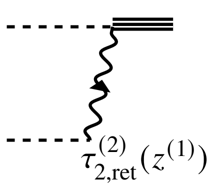

VII) Correction to $e^2 q_1 F^{\mu\nu}\dot{z}_{1,\nu}$ linear in 2^{nd} order retarded time correction ($e^4\tau^{(2)}_{2,\mathrm{ret}}$) (due to 1st order worldline corrections , $e^2 z_1^{(1)}$ and $e^2 z_2^{(1)}$).

1^{st} order worldline corrections also produce a 2^{nd} order correction to retarded time since the relation $|z_1 - z_2|^2 = 0$ is quadratic. To find the 2^{nd} order retarded time correction (due to 1^{st} order worldline corrections) $e^4\tau^{(2)}_{2,\mathrm{ret}}(z^{(1)})$, we need to solve the relation $|z_1 - z_2|^2 = 0$ to NNLO (e^4). Substituting worldlines with 1^{st} order corrections, we have

$$|z_1 - z_2|^2 = b^2 + \tau_1^2 + \tau^2_{2,\mathrm{ret}} - 2\tau_1\tau_{2,\mathrm{ret}}\gamma + 2e^2(b + u_1\tau_1 - u_2\tau_{2,\mathrm{ret}})\cdot(z_1^{(1)} - z_2^{(1)}) + e^4(z_1^{(1)} - z_2^{(1)})^2 = 0, \tag{A.34}$$

where we substitute $\tau_{2,\text{ret}} = \tau^{(0)}_{2,\text{ret}} + e^2\tau^{(1)}_{2,\text{ret}} + e^4\tau^{(2)}_{2,\text{ret}}$, and then solve for $\tau^{(2)}_{2,\text{ret}}$. We get

$$
\begin{aligned}
&(\tau^{(1)}_{2,\text{ret}})^2 + 2r_1\tau^{(2)}_{2,\text{ret}} - 2u_2\cdot(z^{(1)}_1 - z^{(1)}_2(\tau^{(0)}_{2,\text{ret}}))\tau^{(1)}_{2,\text{ret}} \\
&\quad - 2\rho^{(0)}\dot{z}^{(1)}_2(\tau^{(0)}_{2,\text{ret}})\tau^{(1)}_{2,\text{ret}} + (z^{(1)}_1 - z^{(1)}_2(\tau^{(0)}_{2,\text{ret}}))^2 = 0, \\
\tau^{(2)}_{2,\text{ret}} &= \frac{-(z^{(1)}_1 - z^{(1)}_2(\tau^{(0)}_{2,\text{ret}}))^2 + 2\rho^{(0)}\dot{z}^{(1)}_2(\tau^{(0)}_{2,\text{ret}})\tau^{(1)}_{2,\text{ret}}}{2r_1} \\
&\quad + \frac{2u_2\cdot(z^{(1)}_1 - z^{(1)}_2(\tau^{(0)}_{2,\text{ret}}))\tau^{(1)}_{2,\text{ret}} - (\tau^{(1)}_{2,\text{ret}})^2}{2r_1}.
\end{aligned}
\tag{A.35}
$$

Once we have $\tau^{(2)}_{2,\text{ret}}$, we can substitute it into subsequent equations.

$$
e^6 f^{(3)\mu}_{\text{VII}} = e^6 q_1 \frac{dF^{\mu\nu}u_{1,\nu}}{d\tau_{2,\text{ret}}}\tau^{(2)}_{2,\text{ret}} = e^6\frac{\partial(q_1F_{\mu\nu}(z_1, z_{2,\text{ret}})u_{1,\nu})}{\partial z^{\alpha}_{2,\text{ret}}}u^{\alpha}_2\tau^{(2)}_{2,\text{ret}}. \tag{A.36}
$$

These are all the quadratic corrections to Lorentz force at 3rd order (e^6).

IX) Self-force contribution - In addition, there is a quadratic contribution to the ALD force $(2e^2q_1^2/3)(\dddot{z}^{\mu}_1 + \ddot{z}^2_1\dot{z}^{\mu}_1)$. We only need to include the second term at this order since we are interested in the impulse, and the first term is a total derivative of acceleration (which vanishes at boundaries). Thus, it gains no relevant contribution from 2nd order worldline corrections at 3rd order. We omit the diagram here. Thus, the relevant contribution is

$$
e^6 f^{(3)\mu}_{\text{IX}} = (2e^6q_1^2/3)\times(\ddot{z}^{(1)}_1)^2u^{\mu}_1 = \frac{2e^6q_1^4q_2^2[\gamma^2b^2 + \tau_1^2(\gamma-1)^2]}{3m_1^2\pi^3r_1^6}u^{\mu}_1. \tag{A.37}
$$

A.2.2 Linear contributions

The next set of contributions are corrections to the Lorentz force term that are linear in 2nd order worldline corrections. These are similar in form to the diagrams at 2nd order. We thus have three diagrams again, IX

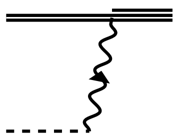

IX) Correction to $e^2 q_1 F^{\mu\nu}\dot{z}_{1,\nu}$ linear in $e^4 z_1^{(2)}$.

Diagram IX is due to the 2nd order world line correction to particle 1 to the Lorentz force, while fixing retarded time and particle 2's worldline at zeroth order. It is linear in $e^4 z_1^{(2)}$, thus scales as $1/m_1 m_2$ or $1/m_1^2$. It is given by

$$e^6 f_{\mathrm{IX}}^{(3)\mu} = e^6 \frac{\partial(q_1 F^{\mu\nu}\dot{z}_{1,\nu})}{\partial z_1^{\alpha}}|_{(0)} z_1^{(2),\alpha} + e^6 \frac{\partial(q_1 F^{\mu\nu}\dot{z}_{1,\nu})}{\partial \dot{z}_1^{\alpha}}|_{(0)} \dot{z}_1^{(2),\alpha}. \tag{A.38}$$

X) Correction to $e^2 q_1 F^{\mu\nu}\dot{z}_{1,\nu}$ linear in $e^4 z_2^{(2)}$.

Diagram X is due to 2nd order worldline correction to particle 2 while fixing retarded time and particle 1's worldline at zeroth order. It is linear in $e^4 z_2^{(2)}$, thus scales as $1/m_1 m_2$ or $1/m_2^2$. It is given by

$$\begin{aligned} e^6 f_{\mathrm{X}}^{(3)\mu} =& e^6 \frac{\partial(q_1 F^{\mu\nu}u_{1,\nu})}{\partial z_2^{\alpha}}|_{(0)} z_2^{(2),\alpha} + e^6 \frac{\partial(q_1 F^{\mu\nu}u_{1,\nu})}{\partial \dot{z}_2^{\alpha}}|_{(0)} \dot{z}_2^{(2),\alpha} \\ &+ e^6 \frac{\partial(q_1 F^{\mu\nu}u_{1,\nu})}{\partial \ddot{z}_2^{\alpha}}|_{(0)} \ddot{z}_2^{(2),\alpha}. \end{aligned} \tag{A.39}$$

X

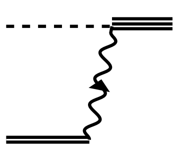

XI) Correction to $e^2 q_1 F^{\mu\nu}\dot{z}_{1,\nu}$ from 2nd order retarded time correction due to 2nd order worldline corrections ($e^4 \tau_{2,\mathrm{ret}}^{(2)}(z_a^{(2)})$).

XI

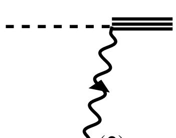

$\tau_{2,\mathrm{ret}}^{(2)}(z^{(2)})$

The second order correction to retarded time also gets contribution from $z^{(2)}$ as one would expect. We can find it in the same manner we found the first order retarded time correction (see derivation in Eq. A.16), to get $\tau_{2,\mathrm{ret}}^{(2)} = \frac{\rho^{(0)}\cdot(z_1^{(2)}-z_2^{(2)})}{r_1}$.

Thus, we have

$$e^6 f_{\mathrm{XI}}^{(3)\mu} = e^6 \frac{d(q_1 F^{\mu\nu}\dot{z}_{1,\nu})}{d\tau_{2,\mathrm{ret}}}|_{(0)} \tau_{2,\mathrm{ret}}^{(2)} = e^6 \frac{\partial(q_1 F_{\mu\nu}(z_1, z_{2,\mathrm{ret}})u_{1,\nu})}{\partial z_{2,\mathrm{ret}}^{\alpha}} u_2^{\alpha}\tau_{2,\mathrm{ret}}^{(2)}. \tag{A.40}$$

These are all the contributions to the acceleration and subsequently impulse at 3^{rd} order.

Appendix B: Scattering of gravitational waves off spinning compact objects with an effective worldline theory

B.1 Compton amplitudes for generic polarization vectors and generic C_2, C_3

In this appendix, we write down the Compton amplitudes for generic incoming and outgoing polarization vectors. However, as with the rest of the paper, we continue to work in the traceless-transverse gauge, where $h^{\mu\nu}k_\nu = 0$ and $h^\mu_{\ \mu} = 0$. Thus, our incoming polarization vector, denoted by ε^μ and the outgoing polarization vector, denoted by ζ^μ_b with $a,\ b = \pm 2$ satisfy $\varepsilon^2 = 0,\ \zeta^2 = 0$. For spinless bodies, the Compton amplitude to linear order in G prior to substitution of polarization vectors is given by

$$\mathcal{M}_{ab} = \frac{4GM\omega^3(\varepsilon_a \cdot \zeta_b)^2}{(l-k)^2}, \tag{B.1}$$

where k^μ and l^μ are the incoming and outgoing momenta/wave-vectors and ε^μ_a and ζ^μ_b are the polarization vectors for the incoming and outgoing waves, respectively. M is the mass of the compact body and ω is the frequency of the incident wave in the initial rest frame of the particle ($\omega = -k \cdot u^{(0)}$).

At linear order in spin and G, the addition to the Compton amplitude for generic polarization vectors is given by

$$\Delta\mathcal{M}_{ab}|_S = \frac{i4G\omega^2(q^\mu S_{\mu\nu}\varepsilon^\mu_a)(q\cdot\zeta_b)(\varepsilon_a\cdot\zeta_b)}{q^2} - \frac{i4G\omega^2(k^\mu q^\nu S_{\mu\nu})(\varepsilon_a\cdot\zeta_b)^2}{q^2} \tag{B.2}$$

$$-\frac{i4G\omega^2(q\cdot\varepsilon_a)(\varepsilon_a\cdot\zeta_b)(q^\mu S_{\mu\nu}\zeta_b^\nu)}{q^2}+2iG\omega^2(\varepsilon_a\cdot\zeta_b)(S_{\mu\nu}\varepsilon_a^\mu\zeta_b^\nu),$$

which is also independent of C_2, C_3. The amplitude is thus universal to linear order in spin.

At second order in spin, the coefficient controlling the strength of spin-induced quadrupole moment, C_2 enters the amplitude. The addition to the Compton amplitude for generic polarization vectors at S^2 is given by

$$\begin{aligned}\Delta\mathcal{M}_{ab}|_{S^2}=&-C_2\frac{2G\omega^3(q^\mu q^\nu S_\mu^{\ \rho}S_{\nu\rho})(\varepsilon_a\cdot\zeta_b)^2}{mq^2}-\frac{2G\omega(k^\mu S_{\mu\nu}\varepsilon_a^\nu)(\varepsilon_a\cdot\zeta_b)(l^\mu S_{\mu\nu}\zeta_b^\nu)}{m}\\&+C_2\frac{2G\omega^3(\varepsilon_a\cdot\zeta_b)(S_{\mu\gamma}S_\nu^{\ \gamma}\varepsilon_a^\mu\zeta_b^\nu)}{m}\end{aligned}\tag{B.3}$$

Finally, at third order in spin, the amplitude depends on both C_2 and C_3. The addition to the amplitude at S^3 has terms proportional to C_2, C_2^2 and C_3. Interestingly, there are no terms that are independent of C_2 and C_3 at this order in spin. It is useful to separate the various contributions, since the overall expression is very long. Thus, the addition to the Compton amplitude for generic polarization vectors that is linear in C_2 is given by

$$\begin{aligned}\Delta\mathcal{M}_{ab}|_{S^3,C_2}=C_2\frac{iG\omega^2}{m^2}&[(S_\mu^{\ \gamma}S_{\nu\gamma}\varepsilon_a^\mu\varepsilon_a^\nu)(k\cdot\zeta_b)(l^\mu S_{\mu\nu}\zeta_b^\nu)-2(k^\mu S_\mu^{\ \gamma}S_{\nu\gamma}\varepsilon_a^\nu)(\varepsilon_a\cdot\zeta_b)(l^\mu S_{\mu\nu}\zeta_b^\nu)\\&-(k^\mu\leftrightarrow l^\mu,\varepsilon_a^\mu\leftrightarrow\zeta_b^\mu)].\end{aligned}\tag{B.4}$$

Then, the addition to the Compton amplitude $\propto$ C_2^2 is given by

$$\Delta\mathcal{M}_{ab}|_{S^3,C_2^2}=-C_2^2\frac{2iG\omega^4}{m^2}[(S_{\mu\nu}\varepsilon_a^\mu\zeta_b^\nu)(S_\mu^{\ \gamma}S_{\nu\gamma}\varepsilon_a^\mu\zeta_b^\nu)-(\varepsilon_a\cdot\zeta_b)(S_\mu^{\ \gamma}S_\nu^{\ \delta}S_{\gamma\delta}\varepsilon_a^\mu\zeta_b^\nu)].\tag{B.5}$$

Finally, the addition to the Compton amplitude at third order in spin, $\propto$ C_3 is given by

$$\begin{aligned}\Delta\mathcal{M}_{ab}|_{S^3,C_3}=C_3\frac{iG\omega^2}{3m^2q^2}\Big[&-2(q^\mu q^\nu S_\mu^{\ \gamma}S_{\nu\gamma})(q^\mu S_{\mu\nu}\varepsilon^\nu)(q\cdot\zeta)(\varepsilon\cdot\zeta)\\&+(k^\mu q^\nu S_{\mu\nu})(q^\mu q^\nu S_\mu^{\ \gamma}S_{\nu\gamma})(\varepsilon\cdot\zeta)^2-q^2(S_\mu^{\ \alpha}S_{\nu\alpha}\varepsilon^\mu\varepsilon^\nu)(k\cdot\zeta)(l^\alpha S_{\alpha\beta}\zeta^\beta)\end{aligned}$$

$$
\begin{aligned}
&+2q^2(k^\mu S_\mu^{\ \gamma} S_{\nu\gamma}\varepsilon^\nu)(\varepsilon\cdot\zeta)(l^\alpha S_{\alpha\beta}\zeta^\beta) - 2q^2(l^\mu S_\mu^{\ \gamma} S_{\nu\gamma}\varepsilon^\nu)(\varepsilon\cdot\zeta)(l^\alpha S_{\alpha\beta}\zeta^\beta) \\
&- q^2(k^\mu k^\nu S_\mu^{\ \gamma} S_{\nu\gamma})(\varepsilon\cdot\zeta)(S_{\alpha\beta}\varepsilon^\alpha\zeta^\beta) + q^2(k^\mu l^\nu S_\mu^{\ \gamma} S_{\nu\gamma})(\varepsilon\cdot\zeta)(S_{\alpha\beta}\varepsilon^\alpha\zeta^\beta) \\
&- 2q^2(l^\mu S_{\mu\nu}\varepsilon^\nu)(k\cdot\zeta)(S_\mu^{\ \gamma} S_{\nu\gamma}\varepsilon^\mu\zeta^\nu) - q^2(k^\mu l^\nu S_{\mu\nu})(\varepsilon\cdot\zeta)(S_\mu^{\ \gamma} S_{\nu\gamma}\varepsilon^\mu\zeta^\nu) \\
&- q^2(k\cdot l)(S_{\mu\nu}\varepsilon^\mu\zeta^\nu)(S_\mu^{\ \gamma} S_{\nu\gamma}\varepsilon^\mu\zeta^\nu) - (k^\mu \leftrightarrow l^\mu, \varepsilon_a^\mu \leftrightarrow \zeta_b^\mu)\Big].
\end{aligned} \tag{B.6}
$$

where we have written simply $\varepsilon = \varepsilon_a$ and $\zeta = \zeta_b$ for brevity. With this, we have written down the complete expression for the Compton amplitude for generic polarization vectors for generic $C_2,\ C_3$ to third order in spin.

Appendix C: Modeling horizon absorption in spinning binary black holes using effective worldline theory

C.1 Scalar field scattering in effective worldline theory including leading-order tail effects

In the main text, we mentioned that the leading-order tail effect, due to the scattering of GWs off the particle's gravitational field leads to a factor of $(1 + 2\epsilon\pi)$ multiplying the leading-order degree of absorption. This is seen clearly in the Teukolsky solution given in Eq. (4.53), but not in the one derived using effective worldline theory in Eq. (4.48) since we only solved the scattering problem in flat space. We motivated that this can be reproduced in the effective theory as well by including the effect of leading-order nonlinearities due to the gravitational field of the particle while solving the wave equation but did not prove it. Here, we show this explicitly in the case of a scalar field scattering off a spinless BH. In particular, we consider the scattering of the monopole mode $l = m = 0$ to $O(\epsilon^4)$ and show that an identical factor of $(1 + 2\epsilon\pi)$ multiplies the leading-order degree of absorption for this mode when the leading-order tail effects are included.

In the effective theory, we model the spinless BH as a particle with mass m with an inducible monopole moment $m_\phi(\tau)$ in the presence of an external scalar field. We write an effective worldline action including a tidal scalar monopole moment as

$$S = -\int d\tau (m - K_{\mathrm{Q}} m_\phi(\tau)\phi) - \frac{K_\phi}{2}\int dt d^3\vec{x}\sqrt{-g}g^{\alpha\beta}\nabla_\alpha\phi\nabla_\beta\phi + \frac{1}{16\pi G}\int d^4x\sqrt{-g}R, \tag{C.1}$$

which is identical to the action used in Ref. [176] except we have restricted to just including a monopole moment for simplicity.

Spherical symmetry ensures that the scalar monopole moment can only be induced by a scalar monopole mode. Since we are only interested in dissipative effects, we can write a general ansatz for the moment simply as

$$m_\phi(\tau) = GMK_\phi\sum_{n=0}^{\infty}(GM)^n\nu_n\frac{d^{2n+1}\phi}{d\tau^{2n+1}}, \tag{C.2}$$

The particle sources a static gravitational field given at linear order in G in the rest frame as

$$h^{00} = -4\frac{GM}{r},\ h^{0i} = h^{ij} = 0, \tag{C.3}$$

$$h^{\mu\nu} = \sqrt{-g}g^{\mu\nu} - \eta^{\mu\nu}, \tag{C.4}$$

which will affect the behaviour of the scalar field through the Klein Gordon equation. The scalar field obeys the Klein Gordon equation in curved space-time, which to linear order in G with the above metric perturbation is given by

$$\Box\phi = -\ddot{\phi} + \nabla^2\phi = \frac{4GM}{r}\ddot{\phi} + \frac{K_Q}{K_\phi}m_\phi(\tau)\delta^{(3)}(\vec{r}), \tag{C.5}$$

$$\implies \omega^2\phi + \nabla^2\phi = -\frac{4\epsilon\omega}{r}\phi + \frac{K_Q}{K_\phi}m_\phi(\tau)\delta^{(3)}(\vec{r}), \tag{C.6}$$

in the rest frame of the particle. Here we have dropped divergent terms arising from the expansion of $(\sqrt{-g} - 1) \times \delta^{(3)}(\vec{x})$ in the Klein-Gordon equation. Such terms can also be shown to cancel amongst themselves perturbatively but it is not relevant to our purpose. We have also restricted our attention to a single frequency mode of the wave, i.e., we set $\phi \sim \exp(-i\omega t)\psi(\vec{r})$. Now, we can expand the scalar field as

$$\phi = \phi^{(0)} + \epsilon\phi^{(1)}, \tag{C.7}$$

$$\phi^{(0)} = C_{\text{out}}\frac{\exp[-i\omega(t-r)]}{\omega r} + C_{\text{in}}\frac{\exp[-i\omega(t+r)]}{\omega r} = C_{\text{reg}}\frac{\sin(\omega r)}{\omega r} + C_{\text{irr}}\frac{\cos(\omega r)}{\omega r}, \tag{C.8}$$

$$\Box\phi^{(0)} = m_\phi(\tau)\delta^{(3)}(\vec{r}) \tag{C.9}$$

where $\phi^{(0)}$ is the leading-order flat space-time solution and $\phi^{(1)}$ is the leading-order correction due to gravitational interaction. We have split $\phi^{(0)}$ into incoming (C_{in}) and outgoing modes (C_{out}), and into regular (C_{reg}) and irregular (C_{irr}) modes. The regular mode is the homogeneous part of the flat space-time wave equation and the irregular part is the particular solution obtained from the source with the time-symmetric propagator. We can perturbatively write down an equation for $\phi^{(1)}$ as

$$\Box\phi^{(1)} = -\frac{4\omega}{r}\phi^{(0)} + O(\epsilon^2). \tag{C.10}$$

Solving this in general is difficult, but we only need to understand the asymptotic behaviour far away of $\phi^{(1)}$ and its behaviour at origin (location of the particle). This is because the asymptotic behaviour dictates the form of the wave as measured by a distant observer who can then measure the degree of absorption from that, and the value at origin perturbs the strength of the induced monopole moment through the ansatz.

The general solution can be written as

$$\phi^{(1)} = \frac{\omega}{2\pi}\int d^3\vec{r}'\left[\frac{\phi^{(0)}(t-|\vec{r}'-\vec{r}|,\vec{r}')}{r'|\vec{r}-\vec{r}'|} + \frac{\phi^{(0)}(t+|\vec{r}'-\vec{r}|,\vec{r}')}{r'|\vec{r}-\vec{r}'|}\right], \tag{C.11}$$

where we are using the time-symmetric propagator for consistency (as the irregular part of the leading-order solution contains both incoming and outgoing modes) and convenience. We can now derive its asymptotic behaviour as

$$\lim_{r\to\infty}\epsilon\phi^{(1)} = \frac{\epsilon\omega}{2\pi r}\int d^3\vec{r}'\left[\frac{\phi^{(0)}(t-r+\hat{r}\cdot\vec{r}')}{r'}+\frac{\phi^{(0)}(t+r-\hat{r}\cdot\vec{r}')}{r'}\right], \tag{C.12}$$

$$= 4\epsilon\exp(-i\omega t)\frac{\cos(\omega r)}{\omega r}\left[C_{\rm irr}\int_0^\infty d\rho\frac{cos(\rho)\sin(\rho)}{\rho}+iC_{\rm reg}\int_0^\infty d\rho\frac{\sin^2(\rho)}{\rho}\right], \tag{C.13}$$

$$= \exp(-i\omega t)\frac{\cos(\omega r)}{\omega r}\big(\pi\epsilon C_{\rm irr}+4\epsilon i C_{\rm reg}\int_0^\infty d\rho\frac{sin^2(\rho)}{\rho}\big), \tag{C.14}$$

where the second integral next to $C_{\rm reg}$ which comes from the scattering of the homogenous solution off the static gravitational field of the particle is divergent but also does not contribute to absorption due to the i in front of it. Thus, we can ignore it. The remaining part has the familiar $\pi\epsilon$ factor in front of it. Thus dropping the irrelevant part, we can write the total field asymptotically as

$$\lim_{r\to\infty}\phi = \lim_{r\to\infty}[\phi^{(0)}+\epsilon\phi^{(1)}] = C_{\rm reg}\frac{\sin(\omega r)}{\omega r}+C_{\rm irr}(1+\epsilon\pi)\frac{\cos(\omega r)}{\omega r}. \tag{C.15}$$

Now, before deriving the degree of absorption, we need to find the relation between $C_{\rm reg}$ and $C_{\rm irr}$ through the induced monopole moment. The strength of induced monopole moment depends on the value of the field at origin, and thus we also need to understand how the value of the field at origin is affected due to gravitational interaction. We will only use the regular part of the wave for computing the value of the field at origin since it is the input which induces the moment. Also, we are only interested in linear tidal effects in this work.

At origin, we have

$$\lim_{r\to 0}\epsilon\phi^{(1)} = \frac{\epsilon\omega}{2\pi}\int d^3\vec{r}'\left[\frac{\phi^{(0)}_{\rm reg}(t-r',\vec{r}')}{(r')^2}+\frac{\phi^{(0)}_{\rm reg}(t+r',\vec{r}')}{(r')^2}\right] \tag{C.16}$$

$$= 4\epsilon\exp(-i\omega t)\left[C_{\rm reg}\int_0^\infty d\rho\frac{\cos(\rho)\sin(\rho)}{\rho}\right] \tag{C.17}$$

$$= \exp(-i\omega t)\pi\epsilon C_{\rm reg}. \tag{C.18}$$

Thus, we have for the total regular part of the field

$$\lim_{r\to 0}\phi^{(0)}_{\rm reg} = (1+\epsilon\pi)C_{\rm reg}\exp(-i\omega t), \tag{C.19}$$

which as claimed in the main text brings in another factor of $\epsilon\pi$. We can now compute the induced monopole moment as

$$m_\phi(t) = -K_\phi GM\exp(-i\omega t)(1+\epsilon\pi)iC_{\rm reg}\sum_{n=0}^{\infty}\nu_n(-1)^n\epsilon^{2n+1}. \tag{C.20}$$

Finally, we can now use the leading-order wave equation to solve for the relation between the regular and irregular coefficients as

$$\Box\phi^{(0)} = \frac{4\pi}{\omega}\delta^{(3)}(\vec{r})C_{\rm irr} = \frac{K_Q}{K_\phi}m_\phi(t)\delta^{(3)}(\vec{r}), \tag{C.21}$$

$$\Longrightarrow C_{\rm irr} = \frac{K_Q}{K_\phi}m_\phi(t)\frac{\omega}{4\pi} = -(1+\epsilon\pi)\frac{K_Q}{4\pi}iC_{\rm reg}\epsilon^2\sum_{n=0}^{\infty}\nu_n(-1)^n\epsilon^{2n}, \tag{C.22}$$

which we can now substitute in Eq. (C.15) to get

$$\lim_{r\to\infty}\phi = \frac{\sin(\omega r)}{\omega r}C_{\rm reg} - \frac{\cos(\omega r)}{\omega r}(1+\epsilon\pi)^2\frac{K_Q}{4\pi}iC_{\rm reg}\epsilon^2\sum_{n=0}^{\infty}\nu_n(-1)^n\epsilon^{2n}, \tag{C.23}$$

$$= \frac{\sin(\omega r)}{\omega r}C_{\rm reg} + \frac{\cos(\omega r)}{\omega r}C^{\rm eff}_{\rm irr}. \tag{C.24}$$

Note the factor of $(1+\epsilon\pi)^2 = [1+2\epsilon\pi+\mathcal{O}(\epsilon^2)]$ modifying the effective values of the irregular part ($C^{\rm eff}_{\rm irr}$) of the wave far away from the source. This in turn modifies the coefficients next to the incoming and outgoing parts of the wave as well, changing the degree of absorption and the scattering phase. The the degree of absorption can now be obtained as

$$1-\left|\frac{C^{\rm eff}_{\rm out}}{C^{\rm eff}_{\rm in}}\right| = 1-\left|\frac{C_{\rm reg}+iC^{\rm eff}_{\rm irr}}{C_{\rm reg}-iC^{\rm eff}_{\rm irr}}\right| = 1-\left|\frac{1+(1+2\epsilon\pi)\hat{K}_Q\epsilon^2\sum_{n=0}^{\infty}\nu_n(i\epsilon)^{2n}}{1-(1-2\epsilon\pi)\hat{K}_Q\epsilon^2\sum_{n=0}^{\infty}\nu_n(i\epsilon)^{2n}}\right|, \tag{C.25}$$

where $C^{\rm eff}_{\rm in/out}$ are the coefficients next to the incoming/outgoing parts of the complete solution at asymptotic infinity. We have also defined $\hat{K}_Q = K_Q/(4\pi)$. Note that in the absence of tail corrections, there are no odd powers of ϵ in the degree of absorption for a spinless BH. Now, expanding this in ϵ, we get

$$1 - \left|\frac{C^{\text{eff}}_{\text{out}}}{C^{\text{eff}}_{\text{in}}}\right| = -2\hat{K}_Q \epsilon^2 (1 + 2\epsilon\pi) + O(\epsilon^4), \tag{C.26}$$

where we have truncated our expression to next-to-leading order since we only included leading-order tail effects in this analysis. Here, we see explicitly that the leading-order tail effect, arising from the scattering of the wave off the static gravitational field of the particle modifies the leading-order degree of absorption by a factor of $(1 + 2\epsilon\pi)$. Crucially, this introduces odd powers of ϵ as well which the effective theory cannot otherwise reproduce. We have checked it against the same result obtained in the real theory by solving the Klein Gordon equation in the vicinity of a real BH with incoming boundary conditions at the horizon and obtained

$$8\epsilon^2(1 + 2\pi\epsilon) + O(\epsilon^4), \tag{C.27}$$

as the degree of absorption for the monopole mode of a scalar wave. Note that this has a form identical to that obtained from the effective theory when leading-order tail effects are included, thus proving our claim in the main text for the special case of monopolar scalar-field scattering.

Appendix D: Dynamical Tidal Response of Kerr Black Holes from Scattering Amplitudes

D.1 Worldline Action For Spinning Particles With Tidal Moments

In the main text, we briefly explained the inclusion of (tidally induced) multipole moments and their respective couplings with the tidal fields. Here, we provide some additional details regarding the worldline action for a spinning particle including tidal effects and our choice of tetrad for describing the tidal response. We follow the presentation given in [3] for the inclusion of tidally induced multipole moments.

A general worldline action for a spinning particle with tidally induced[1] quadrupole and octupole degrees of freedom in worldline theory may be written in the implicit form

$$
\begin{aligned}
S &= \int d\tau \mathcal{L}(u^\mu = \dot{z}^\mu, \Omega^{\mu\nu} = \epsilon_A{}^\mu \frac{D\epsilon^{A\nu}}{D\tau}, Q^{\mu_L}_{E,B}, \frac{DQ^{\mu_L}_{E,B}}{D\tau}, R_{\mu\nu\rho\sigma}, \nabla_\lambda R_{\mu\nu\rho\sigma}),\ (\ell = 2,3) \qquad \text{(D.1)}\\
&= \int d\tau L(u^\mu, \Omega^{\mu\nu}, Q^{\mu_L}_{E,B}, \frac{DQ^{\mu_L}_{E,B}}{D\tau}) + \int d\tau Q^{\mu\nu}_E E_{\mu\nu} + \int d\tau Q^{\mu\nu\rho}_B B_{\mu\nu\rho} + (E \leftrightarrow B),
\end{aligned}
$$

where $\epsilon_A{}^\mu$ is a co-rotating orthonormal tetrad satisfying $\epsilon_A{}^\mu \epsilon^{B\nu} = g^{\mu\nu},\ \epsilon_A{}^\mu \epsilon_{B\mu} = \eta_{AB}$, which move and spins along with the particle. Varying the action with respect to the tetrad $\epsilon_A{}^\mu(\tau)$, and the worldline $z^\mu(\tau)$, while respecting all constraints yields the well known pole-dipole MPD equations of motion for momentum and spin, along with the contribution of tidal forces and torques

[1] In principle, this action may also be used for including spin-induced multipole moments.

given by

$$\frac{DS^{\mu\nu}}{D\tau} = 2p^{[\mu}u^{\nu]} + \frac{4}{3}R^{[\mu}{}_{\lambda\rho\sigma}J_{\lambda}{}^{\nu]\tau\rho\sigma} + \frac{2}{3}\nabla^{\lambda}R^{[\mu}{}_{\tau\rho\sigma}J_{\lambda}{}^{\nu]\tau\rho\sigma} + \frac{1}{6}\nabla^{[\mu}R_{\lambda\tau\rho\sigma}J^{\nu]\lambda\tau\rho\sigma}. \tag{D.2}$$

$$\frac{Dp_{\mu}}{D\tau} = -\frac{1}{2}R_{\mu\nu\rho\sigma}u^{\nu}S^{\rho\sigma} - \frac{1}{6}J^{\lambda\nu\rho\sigma}\nabla_{\mu}R_{\lambda\nu\rho\sigma} - \frac{1}{12}J^{\tau\lambda\nu\rho\sigma}\nabla_{\mu}\nabla_{\tau}R_{\lambda\nu\rho\sigma}. \tag{D.3}$$

where $p_{\mu} = (\partial\mathcal{L}/\partial u^{\mu})|_{\Omega^{\mu\nu}}$, $S_{\mu\nu} = \frac{1}{2}(\partial\mathcal{L}/\partial\Omega^{\mu\nu}) - \sum_{\ell=2}^{3}\ell[P_{E}^{[\mu}{}_{\mu_{L-1}}Q_{E}^{\nu]\mu_{L-1}} + (E \leftrightarrow B)]$, with $P_{E/B}^{\mu_L} = (\partial\mathcal{L}/\partial\dot{Q}_{\mu_L}^{E/B})$, and[2]

$$J^{\mu\nu\rho\sigma} = -6\frac{\partial\mathcal{L}}{\partial R_{\mu\nu\rho\sigma}} = -3u^{[\mu}Q_{E}^{\nu][\rho}u^{\sigma]} + \frac{3}{2}Q_{B}^{\alpha\langle\rho}\epsilon_{\beta\alpha}{}^{\mu\nu}u^{|\beta|}u^{\sigma\rangle_R}, \tag{D.4}$$

$$J^{\lambda\mu\nu\rho\sigma} = -12\frac{\partial\mathcal{L}}{\partial\nabla_{\lambda}R_{\mu\nu\rho\sigma}} = -6u^{\langle\mu}Q_{E}^{\nu\rho\lambda}u^{\sigma\rangle_{\nabla R}} + 3Q_{B}^{\alpha\langle\rho\lambda}\epsilon_{\beta\alpha}{}^{\mu\nu}u^{|\beta|}u^{\sigma\rangle_{\nabla R}}. \tag{D.5}$$

To solve the equations of motion, we also need to impose a ‘‘spin supplementary condition’’ (SSC) to ensure that $S_{\mu\nu}$ it is a spatial tensor with the right number of degrees of freedom. Here, we impose the ‘‘covariant’’ or Tulczyjew-Dixon SSC at the level of the equations of motion upon the total physical spin angular momentum as $S^{\mu\nu}p_{\mu} = 0$. This enforces that the spin tensor is a spatial antisymmetric tensor in the frame defined by p_{μ}, with 3 degrees of freedom, as expected. Similarly, we also need to place constraints on the quadrupole (octupole) moments, to render them orthogonal to u^{μ} , symmetric and trace-free as expected from the tidal fields with which they couple. It is convenient to impose this by appropriately choosing the tidal response such that $Q_{E}^{\mu\nu}u_{\nu}$ or $Q_{E}^{\mu\nu}p_{\nu} = 0$[3].

[2]We are using $\langle abcd\rangle_R$ ($\langle abcd\rangle_{\nabla R}$) to represent the symmetrization of indices according to the symmetries of the Riemann tensor (covariant derivative of the Riemann tensor).

[3]Note that the difference between p_{μ} and u_{μ} becomes relevant only in the presence of external curvature. However, in this work, since we restrict ourselves to linearly induced tides and comparisons with linear perturbation theory, we can neglect the difference in the tidal response. For the same reason, we can treat the black hole as a stationary object with fixed spin following a geodesic in the tidal response.

For instance, consider a generic tidal response for the electric quadrupole moment $Q_E^{\mu\nu}$ to next-to-leading order ignoring quadrupole-octupole mixing. Consistent with parity, we can write

$$Q_E^{\mu\nu} = -M(GM)^5\left[(\lambda_E)^{\mu\nu,\rho\sigma}E_{\rho\sigma} - (GM)(\lambda_{E,\omega})^{\mu\nu,\rho\sigma}\frac{DE_{\rho\sigma}}{D\tau}\right]. \tag{D.6}$$

Here, we require $\lambda_E^{\mu\nu,\rho\sigma}$ to be symmetric and trace-free in $\mu\nu$ and $\rho\sigma$ respectively, and also orthogonal to u^μ, thus curtailing undesired degrees of freedom. Given the space-like nature of the multipole moments, it is convenient to rewrite the above response equation in a suitably chosen orthonormal tetrad $e_I{}^\mu$, with $e_{I=0}{}^\mu = u^\mu$. Then, we can express both the multipole moments and tidal fields as spatial STF tensors in the tetrad as $Q_E^{ij} = Q_E^{\mu\nu}e^i{}_\mu e^j{}_\mu$, $E_{ij} = E_{\mu\nu}e^i{}_\mu e^j{}_\mu$ where $i, j = 1, 2, 3$. We can then rewrite Eq. (D.6) by contracting with $e^i{}_\mu e^j{}_\nu$ as

$$\begin{aligned}
Q_E^{ij} &= -M(GM)^5\left[(\lambda_E)^{ij,kl}E_{kl} - (GM)(\lambda_{E,\omega})^{ij,mn}e_m{}^\rho e_n{}^\sigma\frac{D(E_{kl}e^k{}_\rho e^l{}_\sigma)}{D\tau}\right],\\
&= -M(GM)^5\left[(\lambda_E)^{ij,kl}E_{kl} - (GM)(\lambda_{E,\omega})^{ij,kl}\frac{d(E_{kl})}{d\tau} - \right.\\
&\quad\left. - (GM)(\lambda_{E,\omega})^{ij,ml}\hat{\Omega}_m{}^kE_{kl} - (GM)(\lambda_{E,\omega})^{ij,kn}\hat{\Omega}_n{}^lE_{kl}\right],
\end{aligned} \tag{D.7}$$

where $\hat{\Omega}^{ij} \equiv e^{i\mu}(De^j{}_\mu/D\tau)$ is the angular velocity of the space-like vectors in the tetrad, measuring their evolution along the worldline. The simplest choice is to let them be parallel transported along the worldline so that $\hat{\Omega}^{ij} = 0$, which is consistent with the orthonormality conditions on the tetrad provided the black hole follows a geodesic. We can regard this choice of tetrad as a comoving tetrad, corresponding to an inertial observer co-translating (but not corotating) along the worldline. Then, we simply have

$$Q_E^{ij} = -M(GM)^5\left[(\lambda_E)^{ij,kl}E_{kl} - (GM)(\lambda_{E,\omega})^{ij,kl}\frac{\partial(E_{kl})}{\partial t}\right], \tag{D.8}$$

where the ordinary proper-time derivative reduces to a simple partial time-derivative w.r.t coordinate time measured by the observer at infinity. In BHPT, this coordinate time corresponds to time measured at asymptotic infinity by an inertial stationary (w.r.t black hole) observer (e.g., the t coordinate in the Kerr metric in Boyer-Lindquist coordinates). In this work, we consistently describe the tidal response and associated couplings in this comoving tetrad. In [61], the spatial tetrad vectors are not parallel transported along the worldline, but instead identified with the corotating tetrad. Thus, the covariant-time derivative does not reduce to a simple partial derivative in the response. The two choices are related by a spatial rotation about the rotation axis $\epsilon_i{}^\mu = R_i{}^j(\tau)e_j^\mu$, $\epsilon_0{}^\mu \approx e_0{}^\mu = u^\mu$. This does not affect any physical results or conclusions.

D.2 Plane Wave, Sperical Wave and Operator Form of Response Tensors

D.2.1 Basis for single particle states

Plane wave basis - The physical graviton plane wave states $|\boldsymbol{k}, h\rangle$, with fixed momentum $k = (\omega, \boldsymbol{k})$ and helicity $h = \pm 2$ are chosen to have the normalization and wavefunction

$$\langle \boldsymbol{k}', h'|\boldsymbol{k}, h\rangle = 2|\boldsymbol{k}|(2\pi)^3\delta^{(3)}(\boldsymbol{k}' - \boldsymbol{k})\delta_{hh'}, \quad \langle 0|h_{ij}(\boldsymbol{x})|\boldsymbol{k}, h\rangle = \frac{1}{M_{\rm pl}}\exp(-ik\cdot x)\epsilon_{ij}^h(\boldsymbol{k}), \quad \text{(D.9)}$$

where $\epsilon_{ij}^h(\boldsymbol{k})$ is the purely spatial symmetric polarization tensor satisfying $\epsilon^i{}_i = 0$ and $\epsilon^{ij}k_j = 0$. Finally, the completeness relation is given by

$$\sum_h \int \frac{d^3\boldsymbol{k}}{(2\pi)^3}\frac{|\boldsymbol{k}, h\rangle\langle \boldsymbol{k}, h|}{2|\boldsymbol{k}|} = \mathbf{I} \quad \text{(D.10)}$$

Spherical basis - We also define a different basis for single particle states, with fixed energy ω, total angular momentum ℓ, and angular momentum along z-axis m, i.e., labeled as $|\omega, \ell, m, h\rangle$ with normalization

$$\langle \omega, \ell, m, h|\omega', \ell', m', h'\rangle = 2\pi\delta(\omega - \omega')\delta_{\ell\ell'}\delta_{mm'}\delta_{hh'}. \quad \text{(D.11)}$$

Note that although it is meaningless to define the helicity in the spherical basis, we still use the label $h = \pm 2$ to indicate that they are a superposition of plane waves with definite helicity. The completeness relation is then given by

$$\int \frac{d\omega}{2\pi} \sum_{\ell,m,h} |\omega, \ell, m, h\rangle\langle\omega, \ell, m, h| = \mathbf{I} \, . \tag{D.12}$$

Transformation between plane wave states and spherical states - For simplicity, we first consider a plane wave state with momentum along the $\hat{z}$-direction. i.e., $|\omega\hat{\boldsymbol{z}}, h\rangle$. Its wave function is given by $\exp(-i\omega t + kr\cos(\theta))\epsilon^h_{ij}(\boldsymbol{k})$. First of all, it is important to notice the plane wave state $|\omega\hat{\boldsymbol{z}}, h\rangle$ only has overlap with spherical state $|\omega, \ell, m, h\rangle$ when $m = h$. This is because they are both the eigenstate of $\hat{z}$-direction angular momentum $\mathbf{J}_z$. Thus, we can expand it in spherical basis simply as

$$|\omega\hat{\boldsymbol{z}}, h = \pm 2\rangle = \sum_{\ell=2}^{\infty} C^{\ell}_{h}(\omega)|\omega, \ell, m = h, h = \pm 2\rangle, \tag{D.13}$$

where the coefficients $C^{\ell}_{h}(\omega)$ will be fixed later by the normalization of the plane wave states. Now, to obtain the expansion for momentum along arbitrary direction, we can simply multiply with the following rotation operator with definition of Euler angle follow [587]

$$\mathbf{R}(\phi, \theta, \psi) = \exp(-i\phi\mathbf{J}_z)\exp(-i\theta\mathbf{J}_y)\exp(-i\psi\mathbf{J}_z) \, . \tag{D.14}$$

which rotates the vector $\hat{z}$ into the direction $\hat{\boldsymbol{k}} = (\theta, \phi)$ in spherical-polar coordinates. Note that the parameter ψ is of no consequence when acting on a vector that is already along $\hat{z}$-axis, or more generally an eigenvector of $\mathbf{J}_z$. Also, from now on, we use the short hand notation

$$\mathbf{R}(\hat{\boldsymbol{k}}, 0) \equiv \mathbf{R}(\phi, \theta, 0) \tag{D.15}$$

for rotational matrix. Acting this operator upon the expansion in Eq. (D.13), we get

$$|\boldsymbol{k}, h = \pm 2\rangle = \mathbf{R}(\hat{\boldsymbol{k}}, 0)|\omega\hat{\boldsymbol{z}}, h = \pm 2\rangle = \sum_{\ell=2}^{\infty} C^{\ell}_{h}(\omega)\mathbf{R}(\hat{\boldsymbol{k}}, 0)|\omega, \ell, m = h, h = \pm 2\rangle. \tag{D.16}$$

We find it useful to introduce the Wigner D-matrix as

$$\langle \ell, m' | \mathbf{R}(\hat{\boldsymbol{k}}, 0) | \ell, m \rangle \equiv D^{\ell}_{m'm}(\hat{\boldsymbol{k}}, 0) \ . \tag{D.17}$$

with

$$D^{\ell}_{mh}(\hat{\boldsymbol{k}}, 0) = (-1)^m \sqrt{\frac{4\pi}{2\ell+1}}\, {}_hY_{\ell,-m}(\hat{\boldsymbol{k}}), \tag{D.18}$$

where ${}_hY_{\ell m}$ are the spin-weighted spherical harmonics. After using the completeness relation for the spherical basis in Eq. (D.12), we can rewrite this as

$$|\boldsymbol{k}, h\rangle = \sum_{\ell=2}^{\infty} \sum_{m=-\ell}^{\ell} C^{\ell}_{h}(\omega) D^{\ell}_{mh}(\hat{\boldsymbol{k}}, 0) |\omega, \ell, m, h\rangle, \tag{D.19}$$

where we have used $\langle \omega', \ell', m', h' | \mathbf{R}(\hat{k}, 0) | \omega = |\vec{\boldsymbol{k}}|, \ell, m, h \rangle = 2\pi\delta(\omega - \omega')\delta_{hh'}\delta_{\ell\ell'} D^{\ell}_{m'm}(\hat{\boldsymbol{k}}, 0)$ which follows from the invariance of the helicity label h and energy (or frequency ω) under rotations.

We can now fix the coefficients $C^{\ell}_{h}(\omega)$ by considering the normalization of plane waves in Eq. (D.9) and get

$$C^{\ell}_{h}(|\boldsymbol{k}|) = 2\pi \sqrt{\frac{(2\ell+1)}{2\pi|\boldsymbol{k}|}}, \tag{D.20}$$

which is consistent with [61]. Now, we can write down the final expression that relates plane wave states and spherical wave states

$$|\boldsymbol{k}, h\rangle = \sum_{\ell=2}^{\infty} \sum_{m=-\ell}^{\ell} 2\pi \sqrt{\frac{(2\ell+1)}{2\pi|\boldsymbol{k}|}} D^{\ell}_{mh}(\hat{\boldsymbol{k}}, 0) ||\boldsymbol{k}|, l, m, h\rangle. \tag{D.21}$$

In principle, we are now set for writing amplitudes calculated for plane waves in spherical basis. However, to simplify them further, we want to write the polarization tensors $\epsilon^{h}_{ij}(\boldsymbol{k})$ in terms of the Wigner D-matrix as well. So, let us establish the conventions used for the polarization tensors, and their relation to Wigner D-matrix.

Relating polarization tensors to Wigner-D matrix - Let's now discussing the relation between polarization tensors and the Wigner-D matrix. Before going to details, let's first make clear the following concept:

- **Rank-ℓ STF tensors**: symmetric trace-free (STF) tensor with L indices. For example, the electric tidal field E_{ij} is a rank-2 STF tensor. Furthermore, all the rank-L STF tensors form a vector space with dimention $2\ell+1$, and thus can be used as a vector space for $SO(3)$ representation. The transformation law between the spherical harmonics and tensorial spherical harmoncis is given by

$$Y_{\ell m} = \mathcal{Y}^{\ell m}_{i_1 \cdots i_\ell} n^{i_1} \cdots n^{i_\ell} \ , \tag{D.22}$$

  in which $Y^{\ell m}_{i_1 \cdots i_\ell}$ can be viewed as the base vector in rank-ℓ STF space.

Going back to the graviton polarization tensor, since it encodes the spin of gravitons, we can define it as the eigenstate of $\hat{z}$-direction angular momentum operator as

$$J_z|_{\text{rank}-2} \epsilon_{h=\pm 2}(\hat{z}) = h\epsilon_h(\hat{z}) \ , \tag{D.23}$$

where

$$J_z|_{\text{rank}-2} = I \otimes J_z + J_z \otimes I \ . \tag{D.24}$$

The right hand needs to be evaluated in the fundamental representation. In component form, we can write it as

$$J_z|_{\text{rank}-2}{}^{ij}{}_{kl} = \delta^i_k J_z{}^j{}_l + J_z{}^i{}_k \delta^j_\ell \ . \tag{D.25}$$

We can get a nicer formula by further symmetrizing (i, j) and (k, l) to get

$$J_z|_{\text{rank}-2}{}^{ij}{}_{kl} = \frac{1}{2}(\delta^i_k J_z{}^j{}_l + \delta^i_l J_z{}^j{}_k + \delta^j_k J_z{}^i{}_l + \delta^j_l J_z{}^i{}_k) \ . \tag{D.26}$$

Since we know that in the spherical basis $\mathbf{J}_z|\ell = 2, m = h = \pm 2\rangle = \pm 2|\ell = 2, m = h = \pm 2\rangle$, then we naturally have

$$\epsilon^h_{ij}(z) = \langle i, j|\ell = 2, m = h = \pm 2\rangle, \tag{D.27}$$

where we have chosen the normalization such that

$$\epsilon^{+2}_{ij}(z) = \begin{pmatrix} \frac{1}{2} & \frac{i}{2} & 0 \\ \frac{i}{2} & -\frac{1}{2} & 0 \\ 0 & 0 & 0 \end{pmatrix} \propto \mathcal{Y}^{22}_{ij}\,, \quad \epsilon^{-2}_{ij}(z) = \begin{pmatrix} \frac{1}{2} & -\frac{i}{2} & 0 \\ -\frac{i}{2} & -\frac{1}{2} & 0 \\ 0 & 0 & 0 \end{pmatrix} \propto \mathcal{Y}^{2-2}_{ij} \tag{D.28}$$

and $\epsilon^{*ij}(\hat{\boldsymbol{k}})\epsilon_{ij}(\hat{\boldsymbol{k}}) = 1$.

Now, given the polarization tensor for when the momentum is along $\hat{z}$, we can derive the polarization tensor for arbitrary direction $\hat{\boldsymbol{k}}$

$$\begin{aligned} \epsilon^h_{ij}(\boldsymbol{k}) &= \langle i, j|\mathbf{R}(\phi, \theta, 0)|\ell = 2, m = h = \pm 2\rangle \\ &= \sum_{m=-2}^{2} D^{\ell=2}_{mh}(\hat{\boldsymbol{k}}, 0)\langle i, j|\ell = 2, m\rangle. \end{aligned} \tag{D.29}$$

States with definite Parity - Sometimes, it is convenient instead to switch to spherical basis states with definite parity. To that end, we define a parity operator $\mathbf{P}$, which flips momentum and helicity. It acts on plane wave states as

$$\mathbf{P}|\vec{k}, h\rangle = |-\vec{k}, -h\rangle,\ \mathbf{P}^2 = \mathbf{I}. \tag{D.30}$$

We can use Eq. (D.19) to identify its action on spherical basis states, which is

$$\mathbf{P}|\omega, \ell, m, h\rangle = (-1)^\ell|\omega, \ell, m, -h\rangle. \tag{D.31}$$

Using this, we can easily define the parity even and odd states in the spherical basis as

$$|\omega, \ell, m, P = \pm\rangle = \frac{1}{\sqrt{2}}\Big(|\omega, \ell, m, h = +2\rangle \pm (-1)^\ell|\omega, \ell, m, -h = -2\rangle\Big). \tag{D.32}$$

D.2.2 Operator Form of Tidal Response Tensors

In Section 5.2, we have shown that the tidal response tensor can be nicely written as the operator form. In this appendix, we are going to show part of the derivation.

- **zero spin**: The simplest case would be the zeroth order in spin where

$$\langle i,j|\mathbf{\Lambda}_{\hat{s}^0}|k,l\rangle = \Lambda_{\hat{s}^0}\delta^{\langle i}_{\langle k}\delta^{j\rangle}_{l\rangle}\ . \tag{D.33}$$

  In the abstract notation, this means that

$$\mathbf{\Lambda}_{\hat{s}^0} = \Lambda_{\hat{s}^0}\mathbf{I}\ . \tag{D.34}$$

- **linear in spin**: Now, we are moving to the linear in spin case

$$\langle i,j|\mathbf{\Lambda}_{\hat{s}^1}|k,l\rangle = H_{\hat{s}^1}\hat{S}^{\langle i}{}_{\langle k}\delta^{j\rangle}_{l\rangle}. \tag{D.35}$$

  Recall that $\hat{S}_{ij} \equiv \epsilon^{ijk}\hat{s}_k$, where $\hat{s}$ is normal vector pointing along the spin of the particle in the rest frame. Since we have oriented the spin to be along the $\hat{z}$-axis, we have $\hat{s}^i = \delta^{i3}$. By noting the following relation

$$J_z{}^i{}_j = -i\epsilon^i{}_{jk}\hat{s}^k = -i\hat{S}^i{}_j\ , \tag{D.36}$$

  we immediately see that

$$\langle i,j|\mathbf{\Lambda}_{\hat{s}^1}|k,l\rangle = \frac{1}{2}iH_{\hat{s}^1}J_z|_{\text{rank}-2} \tag{D.37}$$

  In the abstract notation, we can write this as

$$\mathbf{\Lambda}_{\hat{s}^1} = \frac{1}{2}iH_{\hat{s}^1}\mathbf{J}_z \tag{D.38}$$

- **quadratic in spin**: The quadratic in spin part of the response tensor is given as

$$\langle i, j|\mathbf{\Lambda}_{\hat{s}^2}|k, l\rangle = \Lambda_{\hat{s}^2}\hat{s}^{\langle i}\hat{s}_{\langle k}\delta^{j\rangle}_{l\rangle} = \frac{\Lambda_{\hat{s}^2}}{2}\left((\hat{s}^2)^{\langle i}{}_{\langle k} \otimes I^{j\rangle}{}_{l\rangle} + I^{\langle i}{}_{\langle k} \otimes (\hat{s}^2)^{j\rangle}{}_{l\rangle}\right), \tag{D.39}$$

where we have defining $\hat{s}^2 \equiv \hat{s} \otimes \hat{s}$. First of all, we notice the following relation

$$\hat{s}_i\hat{s}_k = \delta_{ik} - J_{z ij}J_{z}{}^{j}_{k} , \tag{D.40}$$

which implies

$$J_z^2|_{\text{rank}-2} = 2(I \otimes I + J_z \otimes J_z) - \hat{s}^2 \otimes I - I \otimes \hat{s}^2. \tag{D.41}$$

To proceed further, we symmetrize and remove the traces over i, j and k, l to get

$$\langle i, j|J_z^2|_{\text{rank}-2}|k, l\rangle = 2\langle i, j|I|_{\text{rank}-2}|k, l\rangle + 2J_{z\langle k}^{\langle i}J_{zl\rangle}^{j\rangle} - 2\hat{s}^{\langle i}\hat{s}_{\langle k}\delta^{j\rangle}_{l\rangle}, \tag{D.42}$$

and use the following relation

$$2J_{z\langle k}^{\langle i}J_{zl\rangle}^{j\rangle} = 2\langle i, j|I|_{\text{rank}-2}|k, l\rangle - 4\hat{s}^{\langle i}\hat{s}_{\langle k}\delta^{j\rangle}_{l\rangle}, \tag{D.43}$$

which can be derived using the Eq. (D.36). Eventually, we arrive at

$$\mathbf{\Lambda}_{\hat{s}^2} = -\frac{1}{6}\Lambda_{\hat{s}^2}(\mathbf{J}_z^2 - 4\,\mathbf{I}). \tag{D.44}$$

- **cubic in spin**: Consider now the cubic in spin interactions

$$\langle i, j|\mathbf{\Lambda}_{\hat{s}^3}|k, l\rangle = H_{\hat{s}^3}\hat{S}^{\langle i}{}_{\langle k}\hat{s}^{j\rangle}\hat{s}_{l\rangle} . \tag{D.45}$$

To simplify this expression, we first notice that

$$\begin{aligned} &\hat{S} \otimes \hat{s} \otimes \hat{s} + \hat{s} \otimes \hat{s} \otimes \hat{S} \\ &= iJ_z|_{\text{rank}-2} - i(J_z \otimes (J_z)^2 + (J_z)^2 \otimes J_z) \end{aligned} \tag{D.46}$$

The last term can be simplified using the following relation:

$$J_z^3|_{\text{rank}-2} = (J_z \otimes I + I \otimes J_z)^3 = J_z^3 \otimes I + 3J_z^2 \otimes J_z + 3J_z \otimes J_z^2 + I \otimes J_z^3. \tag{D.47}$$

We further notice that $J_z^3 = J_z$ following from $J \cdot (\hat{s} \otimes \hat{s}) = 0$, we get

$$\hat{S} \otimes \hat{s} \otimes \hat{s} + \hat{s} \otimes \hat{s} \otimes \hat{S} = -\frac{i}{3}(J_z|^3_{\text{rank}-2} - 4J_z|_{\text{rank}-2}). \tag{D.48}$$

Since $\Lambda_{\hat{s}^3}$ is STF in i, j and k, l, and thus we can simply symmetrize the indices and remove the trace to get

$$\mathbf{\Lambda}_{\hat{s}^3} = -\frac{i}{6}H_{\hat{s}^3}(\mathbf{J}_z^3 - 4\mathbf{J}_z). \tag{D.49}$$

- **quartic in spin** : Finally, the quartic-in-spin part of the response tensor is given by

$$\langle i, j|\mathbf{\Lambda}_{\hat{s}^4}|k, l\rangle = \Lambda_{\hat{s}^4}\hat{s}^{\langle i}\hat{s}_{\langle k}\hat{s}^{j\rangle}\hat{s}_{l\rangle}. \tag{D.50}$$

To rewrite this, we once again start with the expression for the appropriate power of $\mathbf{J}_z|_{\text{rank}-2}$, as

$$J_z^4|_{\text{rank}-2} = 8I \otimes I - 7\ (\hat{s}^2 \otimes I + I \otimes \hat{s}^2) + 6\ \hat{s}^2 \otimes \hat{s}^2 + 8J_z \otimes J_z. \tag{D.51}$$

where we have used $J_z^3 = J_z$ and $\mathbf{J}_z^2 = \mathbf{I} - \hat{\mathbf{s}}^2$. Now, using Eq. (D.43) and Eq. (D.44), we finally arrive at

$$\mathbf{\Lambda}_{s^4} = \frac{1}{6}\Lambda_{\hat{s}^4}(\mathbf{J}_z^2 - 4\mathbf{I})(\mathbf{J}_z^2 - \mathbf{I})\ . \tag{D.52}$$

Appendix E: Investigating tidal heating in neutron stars via gravitational Raman scattering

E.1 Newtonian stellar fluid

In this appendix, we briefly review the non-viscous linear stellar perturbation theory for neutron stars in Newtonian gravity following [588, 589]. The Newtonian limit makes it easier to understand the approach towards static limit $\omega \to 0$ and the low-frequency expansion presented in the main text starting from complete all-orders-in-ω perturbation equations.

With the fluid displacement vector $\boldsymbol{\xi}$, we can write the continuity equation to solve for the density perturbation as

$$\delta\rho = -\nabla \cdot (\rho\boldsymbol{\xi}) \,, \quad \Delta\rho = -\rho\nabla \cdot \boldsymbol{\xi} \,. \tag{E.1}$$

The perturbed Euler equation (Newton's second law) is given by

$$\rho\ddot{\boldsymbol{\xi}} = -\nabla\delta p + \delta\rho\nabla U + \rho\nabla\delta U \,, \tag{E.2}$$

where U is the background Newtonian potential and δU is its perturbation. We also have the perturbed Poisson equation

$$\nabla^2\delta U = -4\pi G\delta\rho \,. \tag{E.3}$$

The above equations are not complete, and one needs to solve for the perturbation to pressure as well. As mentioned in the main-text in Sec. 6.4.1.1, we can generally define the adiabatic index

γ and sound speed c_s as

$$\frac{\Delta p}{\Delta \rho} = \gamma \frac{p}{\rho} = c_s^2.$$

Then, in the two extremes of very fast reactions and very slow reactions, we have

$$\textbf{fast reactions}: \ \frac{\Delta p}{\Delta \rho} = \left(\frac{\partial p}{\partial \rho}\right)\bigg|_{\mu_i} = c_{\rm eq}^2 \ . \tag{E.4}$$

$$\textbf{slow reactions}: \ \frac{\Delta p}{\Delta \rho} = \left(\frac{\partial p}{\partial \rho}\right)\bigg|_{x_i} = c_{\rm ins}^2 \ . \tag{E.5}$$

On the other hand, the unperturbed background profile is in chemical equilibrium and thus

$$\frac{dp/dr}{d\rho/dr} = \left(\frac{\partial p}{\partial \rho}\right)_{\mu_i} = c_{\rm eq}^2, \tag{E.6}$$

Generally for neutron stars, the dominant m-Urca reactions have a very large characteristic time-scale for equilibrium compared to the orbital time period in binaries during inspiral, and thus $c_{\rm eq} \neq c_s \approx c_{\rm inst}$.

Now, decomposing the fluid displacement as

$$\boldsymbol{\xi} = \left[\xi_r(r)\hat{\boldsymbol{r}} + \frac{\xi_{\rm H}(r)}{r}\left(\hat{\boldsymbol{\theta}}\frac{\partial}{\partial\theta} + \frac{\hat{\boldsymbol{\phi}}}{\sin\theta}\frac{\partial}{\partial\phi}\right)\right] Y_{\ell m} \ , \tag{E.7}$$

and defining the following variables for convenience

$$w_1 = r\xi_r \ , w_2 = \xi_{\rm H} \ , w_3 = \delta U \ , w_4 = \frac{d\delta U}{d\log r} \ . \tag{E.8}$$

The perturbation equation can be rewritten as [589]

$$\begin{aligned}
\frac{dw_1}{dr} &= \left(\frac{g}{c_s^2} - \frac{1}{r}\right) w_1 + \left[\frac{\ell(\ell+1)}{r^2} - \frac{\omega^2}{c_s^2}\right] r w_2 \\
&\quad + \frac{r}{c_s^2} w_3, \\
\frac{dw_2}{dr} &= \left(1 - \frac{N^2}{\omega^2}\right)\frac{1}{r} w_1 + \frac{N^2}{g} w_2 - \frac{1}{\omega^2}\frac{N^2}{g} w_3,
\end{aligned}$$

$$
\begin{aligned}
\frac{dw_3}{dr} =& \frac{1}{r} w_4, \\
\frac{dw_4}{dr} =& 4\pi G\rho \frac{N^2}{g} w_1 + \omega^2 \frac{4\pi G\rho}{c_s^2} r w_2 \\
& + \left[\frac{\ell(\ell+1)}{r^2} - \frac{4\pi G\rho}{c_s^2} \right] r w_3 - \frac{1}{r} w_4 ,
\end{aligned} \tag{E.9}
$$

where the function $g(r)$ here is the local acceleration due to gravity inside the star

$$
g \equiv U'(r) = \frac{Gm(r)}{r^2} \tag{E.10}
$$

and N is the Brunt-Väisälä frequency

$$
\begin{aligned}
N^2 &= -\frac{g}{r} \left(\frac{1}{\gamma} \frac{d \log p}{d \log r} - \frac{d \log \rho}{d \log r} \right) . \\
&= g^2 \left(\frac{1}{c_{\mathrm{eq}}^2} - \frac{1}{c_s^2} \right) \approx g^2 \left(\frac{1}{c_{\mathrm{eq}}^2} - \frac{1}{c_{\mathrm{ins}}^2} \right) ,
\end{aligned} \tag{E.11}
$$

which is non-zero. Physically, the Brunt-Väisälä frequency captures the derivation of the perturbations from chemical equilibrium. [1] We will see shortly that this yields the characteristic frequencies of gravity (g-)modes in the stellar oscillations.

Starting from the pioneer work by Cowling [500] and Chandrasekhar [590], it has been shown that the fluid displacement vector $\boldsymbol{\xi}$ governed by the system of Eqs. (E.9) admits a decomposition into an Eigenbasis $\boldsymbol{\xi}_i$, which have real eigenvalues ω_i^2, and form a complete basis of the system. The index i is discrete when ρ has compact support. A great effort has then been devoted into the analysis of these fluid oscillation modes (see [500] for a review). Basically, one can classify the stellar oscillations via their dispersion relations and the corresponding restoring force. For acoustic waves, pressure serves as the restoring force and leads to the dispersion relation

$$
\omega^2 \sim c_s^2 |\boldsymbol{k}|^2 \tag{E.12}
$$

[1] Note that for main sequence stars, perturbations beyond thermal equilibrium can also lead to non-zero N [589].

where we denote the wavenumber as $\boldsymbol{k} \equiv k_r \hat{r} + \boldsymbol{k}_{\rm H}$. These modes are also known as $p-$modes. The second type of waves are the gravity waves known as $g-$modes where buoyancy force serves as the restoring force. The corresponding dispersion relation can be written as

$$\omega^2 \sim N^2 \frac{|\boldsymbol{k}_{\rm H}|^2}{|\boldsymbol{k}|^2} \, . \tag{E.13}$$

The detailed analysis in Ref. [500] also shows that all the $p-$ and $g-$modes have infinite number of overtones $n = 1, 2, \cdots$. With the increasing of n, the eigen-frequency of $p-$modes will increase while it will decrease for $g-$modes. Moreover, depending on the sign of the Brunt-Väisälä frequency N, the eigen-frequency of $g-$modes can be either positive or negative. In this work, we restrict to the case $N^2 > 0$. Note that the frequency of the g-modes is bounded from above by N[2].

Now, let us consider the approach towards the small frequency limit in the system of Eqs. (E.9). Examining the second equation in them, we find that there exists a formal mathematical ambiguity in the small frequency limit depending on the relative ordering of the Brunt-Väisälä frequency N and perturbation ω. When $\omega \ll N_{\rm ch}$, assuming that all variables have a well-defined static limit ($\omega = 0$), the second equation shrinks to a constraint equation between the fluid radial displacement and the perturbations of Newtonian potential

$$w_1 = -\frac{r}{g} w_3 \, . \tag{E.14}$$

Combined with the first equation, this yields in the static limit

$$(r w_1)' - \ell(\ell+1) w_2 = 0 \, , \tag{E.15}$$

which is equivalent to the condition $\nabla \cdot \boldsymbol{\xi} = 0$. Thus, in the static limit, the fluid is incompressible as shown in the relativistic case in Sec. 6.4.3.

[2] Since N varies throughout the star, its value in Eq. (E.13) should be taken as its characteristic/typical value $N_{\rm ch}$ inside the star.

However, if the regime of interest has $\omega \geq N$, which is true for instance in the fast reaction case, where the Brunt-Väisälä frequency $N \approx 0$ and thus $\omega \gg N_{\rm ch}$. In this regime, the orbital-frequency also exceeds all the g-mode resonant frequencies. We cannot then take $\omega \to 0$ disregarding all other parameters in Eq. (E.9) as before. In this case, the arguments leading to Eq. (E.14), (E.15) and thus adiabatic-incompressibility is no longer true. While the specific details may differ in the relativistic case, the general feature that the scheme presented in this work is valid for $\omega \ll N_{\rm ch}$ is not likely to change. Thus, the low-frequency expansion presented in the main-text is likely valid in the regime $\omega \ll N_{\rm ch}$, where $N_{\rm ch}$ is the characteristic value of N in the stellar interior.

The results for tidal heating in the barotropic regime ($N = 0 \equiv N_{\rm ch} \ll \omega$) were shown for relativistic polytropic neutron stars in Ref. [260], where a small but non-zero contribution to the dissipation number due to bulk-viscosity (which is relevant only when $\nabla \cdot \xi \neq 0$) was obtained. In an actual inspiral, the binary usually transitions from $\omega \ll N$ to $\omega \geq N$. A more refined study including the transition could help better understand the tidal characteristics and their influence on the waveform, especially the contribution due to bulk-viscosity.

Appendix E: Quasinormal modes of slowly-spinning horizonless compact objects

E.1 Membrane paradigm at the linear order in spin: unperturbed background

The unperturbed metric outside the membrane to linear order in spin is given by :

$$ds^2\Big|_{(0)} = g^{(0)}_{\mu\nu} dx^\mu dx^\nu = -f(r)dt^2 + \frac{1}{f(r)}dr^2 + r^2 d\Sigma^2 - 4\frac{J}{r}\sin^2\theta dt d\phi, \tag{E.1}$$

where $f(r) = 1 - 2M/r$, $d\Sigma^2 = d\theta^2 + \sin^2\theta d\phi^2$, and $J = Ma = M^2\chi$ is the angular momentum of the compact object (being modelled by the membrane). The unperturbed membrane is located at the radius $r = r_0$. We will use $x^\mu = \{t, r, \theta, \phi\}$ to refer to the global coordinates and $y^a = \{T = t, \Theta = \theta, \Phi = \phi\}$ for the membrane coordinates. The basis vectors for the membrane coordinates are defined as $e^\mu_a = \partial x^\mu / \partial y^a$, where

$$e^\mu_T = \{1, 0, 0, 0\},\ e^\mu_\Theta = \{0, 0, 1, 0\},\ e^\mu_\Phi = \{0, 0, 0, 1\}. \tag{E.2}$$

The normal vector to the membrane, n^μ, is fixed by the requirements $n_\mu e^\mu_a = 0$ and $g^{\mu\nu} n_\mu n_\nu = 1$ to be $n_\mu = \{0, 1/\sqrt{f(r)}, 0, 0\}$. The induced metric on the membrane h_{ab} is then given by

$$\begin{aligned} ds^2\Big|_{\text{membrane}} &= h_{ab} dy^a dy^b = g_{\mu\nu} e^\mu_a e^\nu_b dy^a dy^b = -f(r_0)dT^2 + r_0^2 d\Theta^2 + r_0^2 \sin^2\Theta d\Phi^2 \\ &\quad - 4\frac{J}{r_0}\sin^2\Theta dT d\Phi\,. \end{aligned} \tag{E.3}$$

The extrinsic curvature is defined as $K_{ab} = e^{\mu}_{a} e^{\nu}_{b} \nabla_{(\mu} n_{\nu)}$ and is given by

$$K_{ab} = \sqrt{f(r_0)} \begin{bmatrix} -\frac{M}{r_0^2} & 0 & \frac{J\sin^2\Theta}{r_0^2} \\ 0 & r_0 & 0 \\ \frac{J\sin^2\Theta}{r_0^2} & 0 & r_0 \sin^2\Theta \end{bmatrix}, \tag{E.4}$$

where the trace is $K = K_{ab}h^{ab} = \frac{2r_0 - 3M}{\sqrt{f(r_0)} r_0^2}$. Thus the left hand side of the junction condition in Eq. (7.1) is given by

$$K_{ab} - Kh_{ab} = \begin{bmatrix} \frac{2f(r_0)^{3/2}}{r_0} & 0 & \frac{J(5r_0-8M)\sin^2\Theta}{\sqrt{f(r_0)}r_0^3} \\ 0 & \frac{M-r_0}{\sqrt{f(r_0)}} & 0 \\ \frac{J(5r_0-8M)\sin^2\Theta}{\sqrt{f(r_0)}r_0^3} & 0 & \frac{M-r_0}{\sqrt{f(r_0)}}\sin^2\Theta \end{bmatrix}. \tag{E.5}$$

To relate the extrinsic curvature to the membrane fluid parameters, we also need to compute the energy-momentum tensor in Eq. (7.2). This depends on the fluid velocity u^a in membrane coordinates. Intuitively, we expect the fluid to be rotating in the global coordinates, while remaining static on the membrane surface. Thus, we expect the radial and polar components to vanish $u^{\mu} = \{u^t, 0, 0, Jv^{\phi}\}$, where we factor out J from the azimuthal component of the fluid velocity. Using the metric in Eq. (E.1), we can see this is also true for the contravariant components $u_{\mu} = \{u_t, 0, 0, Jv_{\phi}\}$. We also expect the components to be independent of t and ϕ due to stationarity and axial symmetry. In the membrane coordinates, we can write

$$u_a = u_{\mu} e^{\mu}_{a} = \{u_T = u_t(\Theta), 0, u_{\Phi} = Jv_{\phi}(\Theta)\}\,. \tag{E.6}$$

Now, demanding normalization $u^{\mu}u_{\mu} = -1$, we obtain $u^t = 1/\sqrt{f(r)}$ and for the contravariant components,

$$u_T \;=\; g_{t\mu}u^{\mu} = g_{tt}u^t + O(J^2) \approx -\sqrt{f(r_0)}\,, \tag{E.7}$$

$$u_\Phi \;=\; g_{\phi\mu}u^\mu = -2J\sin^2\theta/(r_0\sqrt{f(r_0)}) + r_0^2 v^\phi) + O(J^2)\,. \tag{E.8}$$

Plugging this into Eq. (7.2), we obtain the stress energy tensor to be

$$-8\pi T_{ab} = -8\pi \begin{bmatrix} \rho f(r_0) & 0 & \frac{J\sin^2\Theta}{r_0}\left[2\rho - f(r_0)r_0^3(\rho+p)v^\phi\right] \\ 0 & p r_0^2 & -r_0^2 J\sin^2\Theta\eta\partial_\Theta v^\phi \\ \frac{J\sin^2\Theta}{r_0}\left[2\rho - f(r_0)r_0^3(\rho+p)v^\phi\right] & -r_0^2 J\sin^2\Theta\eta\partial_\Theta v^\phi & p r_0^2\sin^2\Theta \end{bmatrix}. \tag{E.9}$$

Now, comparing Eq. (E.9) with Eq (E.5), and imposing the junction condition in Eq. (7.1), we get

$$\rho = -\frac{\sqrt{f(r_0)}}{4\pi r_0},\; p = \frac{1+f(r_0)}{16\pi r_0\sqrt{f(r_0)}},\; J v^\Phi = \frac{2J}{r_0^3\,(1-3f(r_0))\,\sqrt{f(r_0)}}\,. \tag{E.10}$$

The membrane fluid parameters with $J \to 0$ are consistent with the ones obtained in the spinless case in Ref. [90] .

E.2 Perturbation equations

The perturbations can be expanded in the spherical harmonic basis as

$$g_{\mu\nu} = g^0_{\mu\nu} + \epsilon_p \delta g_{\mu\nu}, \tag{E.11}$$

$$\begin{aligned}\delta g_{\mu\nu} = \sum_{\ell,m}\Big\{ &\left[H_0^{\ell m}(r,t)dt^2 + H_2^{\ell m}(r,t)dr^2 + r^2K^{\ell m}(r,t)d\Sigma^2 + 2H_1^{\ell m}(r,t)drdt\right]Y_{\ell m}(\theta,\phi) + \\ &2h_0^{\ell m}(r,t)\left[S_\theta^{\ell m}(\theta,\phi)d\theta + S_\phi^{\ell m}(\theta,\phi)d\phi\right]dt + 2h_1^{\ell m}(r,t)\left[S_\theta^{\ell m}(\theta,\phi)d\theta + S_\phi^{\ell m}(\theta,\phi)d\phi\right]dr\Big\},\end{aligned} \tag{E.12}$$

where $S_\theta^{\ell m}(\theta,\phi) = -\partial_\phi Y_{\ell m}(\theta,\phi)/\sin\theta$, $S_\phi^{\ell m}(\theta,\phi) = \sin\theta\partial_\theta Y_{\ell m}(\theta,\phi)$, ϵ_p is a small parameter controlling the strength of perturbation, and we restrict to linear order in ϵ_p. The metric perturbation can be split into the axial and polar sectors considering their transformation under parity. In the absence of spin, perturbations with different parity do not mix, and satisfy the Regge-Wheeler and

Zerilli equations for axial and polar perturbations, respectively. To the linear order in spin, the coupling between axial and polar modes can be neglected as far as the computation of the QNM frequencies is concerned.

E.2.1 Axial sector

The axial sector is the part of the metric perturbation that transforms as $(-1)^{\ell+1}$ under parity transformation, i.e., $(\theta \to \pi - \theta, \phi \to \phi + \pi)$. This is given by

$$\delta g_{\mu\nu}^{\text{axial}} = 2 \sum_{\ell,m} \{ h_0^{\ell m}(r,t) \left[S_\theta^{\ell m}(\theta,\phi) d\theta + S_\phi^{\ell m}(\theta,\phi) d\phi \right] dt + h_1(r,t) [S_\theta^{\ell m}(\theta,\phi) d\theta + S_\phi^{\ell m}(\theta,\phi) d\phi] dr \}. \tag{E.13}$$

The Einstein equations in vacuum, $G_{\mu\nu} = 0$, for axial perturbations to the linear order in spin and in the perturbation, can be reduced to a modified Regge-Wheeler equation to first order in spin given by [273]

$$\frac{d^2 \psi_{\text{RW}}(r)}{dr_*^2} + \left[\omega^2 - \frac{4mJ\omega}{r^3} - f(r) \left(\frac{\ell(\ell+1)}{r^2} - \frac{6M}{r^3} + \frac{24Jm(-7M+3r)}{\ell(\ell+1) r^6 \omega} \right) \right] \psi_{\text{RW}}(r) = 0, \tag{E.14}$$

where

$$\psi_{\text{RW}}(r) = h_1(r) \frac{f(r)}{r} \left(1 + \frac{2mJ}{r^3 \omega} \right), \tag{E.15}$$

and we have suppressed the ℓ, m indices for simplicity of notation. The other function in the axial sector, $h_0(r)$, is related to $h_1(r)$ through the relation

$$h_0(r) = \frac{i f(r) \left[\ell(\ell+1) r^4 \omega h_1(r) f'(r) + f(r)(-12Jqm h_1(r) + \tilde{q} r^4 \omega h_1'(r) \right]}{\tilde{q} \omega r(-2Jm + r^3 \omega)}, \tag{E.16}$$

where $q = (\ell-1)(\ell+2)/2$, $\tilde{q} = \ell(\ell+1)$, and the prime stands for radial derivative (d/dr). Note that in the above equations, we have factorized the time-dependence as $h_1(r,t) = h_1(r) e^{-i\omega t}$ and similarly for $h_0(r,t)$.

E.2.2 Polar sector

The polar sector transforms as $(-1)^\ell$ under parity transformations, and is given by

$$\delta g_{\mu\nu}^{\rm polar} = \sum_{\ell,m} \left[H_0^{\ell m}(r,t)dt^2 + H_2^{\ell m}(r,t)dr^2 + r^2 K(r,t)d\Sigma^2 + 2H_1^{\ell m}(r,t)dr dt\right] Y_{\ell m}(\theta,\phi). \quad \text{(E.17)}$$

The Einstein equations for the polar perturbations can be reduced to a modified Zerilli equation to the first order in spin given by [273]

$$\frac{d^2\psi_{\rm Z}(r)}{dr_*^2} + \left[\omega^2 - \frac{4mJ\omega}{r^3} - f(r)V_{\rm Z}(r)\right]\psi_{\rm Z}(r) = 0, \quad \text{(E.18)}$$

where

$$\begin{aligned}
V_{\rm Z}(r) = {} & \frac{2M}{r^3} + \frac{(\ell-1)(\ell+2)}{3}\left[\frac{2(\ell-1)(\ell+2)(\ell^2+\ell+1)}{(6M+r(\ell^2+\ell-2))^2} + \frac{1}{r^2}\right] \\
& + \frac{4mJ}{r^7\omega\ell(\ell+1)(6M+r(\ell^2+\ell-2))^4}\Big\{27648M^6 + 2592M^5 r(6\ell(\ell+1)-19) \\
& + 144M^4r^2\left[6r^2\omega^2 + \ell(\ell+1)(21\ell(\ell+1)-148)+230\right] \\
& + 12M^3r^3(\ell^2+\ell-2)\left[72r^2\omega^2 + \ell(\ell+1)(29\ell(\ell+1)-200)+374\right] \\
& + 12M^2r^4(\ell^2+\ell-2)^2\left[28r^2\omega^2 + \ell(\ell+1)(5\ell(\ell+1)-12)-4\right] \\
& + Mr^5(\ell^2+\ell-2)^2\Big[24r^2\omega^2(2\ell(\ell+1)-5) \\
& + (\ell-1)(\ell+2)(\ell^2+\ell+2)(7\ell(\ell+1)-38)\Big] \\
& + r^6(\ell^2+\ell-2)^3\left[2r^2\omega^2(\ell^2+\ell-4) - 3(\ell^2+\ell-2)(\ell^2+\ell+2)\right]\Big\}. \quad \text{(E.19)}
\end{aligned}$$

The Zerilli function $\psi_{\rm Z}(r)$ is related to the radial functions in the polar sector via the relations

$$\begin{bmatrix} K(r) \\ H_1(r) \end{bmatrix} = \begin{bmatrix} A_{11} & A_{12} \\ A_{21} & A_{22} \end{bmatrix} \cdot \begin{bmatrix} \tilde\psi_{\rm Z}(r) \\ \tilde\psi'_{\rm Z}(r) \end{bmatrix}, \quad \text{(E.20)}$$

where

$$\mathbf{A} = \begin{bmatrix} \frac{12M^2+6Mqr+\ell(\ell+1)qr^2}{2r^2(3M+qr)} & 1 \\ -i\omega\left[1+M\left(\frac{1}{2M-r}-\frac{6}{2M+2qr}\right)\right] & \frac{i\omega r^2}{2M-r} \end{bmatrix}, \tag{E.21}$$

and

$$\tilde{\psi}_{\rm Z}(r) = \psi_{\rm Z}(r)\left[1+\frac{2mJ(12M^3-6M^2r+qr^3(q+r^2\omega^2)+M(-2q^2r^2+3r^4\omega^2)}{\ell(\ell+1)r^4(3M+qr)^2\omega}\right]. \tag{E.22}$$

The other functions describing polar metric perturbrations, H_0 and H_2, can be written in terms of H_1 and K via the relations

$$H_2(r) = \frac{r^2}{(r-2M)^2}H_0(r)+4mJ\omega r\frac{K(r)}{\ell(\ell+1)(r-2M)^2}, \tag{E.23}$$

$$\begin{aligned} H_0(r) = {} & \frac{i(2M-r)(\tilde{q}M-2r^3\omega^2)}{2r^2(3M+qr)\omega}H_1(r)-\frac{3M^2+M(-1+2q)r-qr^2+r^4\omega^2}{r(3M+qr)}K(r) \\ & +\frac{mJ}{2\tilde{q}r^5(3M+qr)^2\omega^2}\Big\{i(2M-r)\big[\tilde{q}^2M(3M+qr)-2(\tilde{q}M-2r^3\omega^2)(\tilde{q}M+r^3\omega^2)\big]H_1(r) \\ & +r\omega\big[4(\tilde{q}M+r^3\omega^2)(3M^2+M(-1+2q)r-qr^2+r^4\omega^2) \\ & +(6M+2qr)(2(3M-2r)r^3\omega^2+\tilde{q}(-3M^2+Mr+2r^4\omega^2))\big]K(r)\Big\}. \end{aligned} \tag{E.24}$$

Although the Zerilli equation appears different than the Regge-Wheeler equation, they both yield the same spectrum of QNMs when the boundary condition is that of BHs. This can be shown in the non-spinning case via the Chandrashekar transformation, and at the linear order in spin with a more general transformation. For a generic compact object described by the membrane paradigm, the boundary condition at the membrane surface can break the isospectrality.

E.3 Membrane paradigm at the linear order in spin: gravitational perturbations

In accordance with the junction conditions, the extrinsic curvature and the induced metric from either side of the membrane surface must satisfy

$$(K^{+}_{ab} - h^{+}_{ab}K^{+}) - (K^{-}_{ab} - h^{-}_{ab}K^{-}) = -8\pi T_{ab}, \qquad h^{+}_{ab} = h^{-}_{ab}, \tag{E.25}$$

where T_{ab} is the surface stress-energy tensor of the membrane. Normally, to proceed further, one needs to fix the spacetime in the interior region to the membrane. However, in this work, the membrane is intended to be an effective way to parametrise an arbitrary compact object. This choice does not break any symmetries and lets the stress-energy tensor do all the heavy lifting. A simple way to implement this choice is to demand $K^{-}_{ab} = 0$, which is also the standard choice when the membrane is used to describe BHs. Then, the junction condition reduces to

$$K_{ab} - h_{ab}K = -8\pi T_{ab}, \tag{E.26}$$

where we have removed the + signs denoting that quantities are evaluated outside the membrane for convenience. The surface stress energy tensor is given by [90]

$$T_{ab} = \rho u_a u_b + (p - \zeta\Theta)\gamma_{ab} - 2\eta\sigma_{ab}, \tag{E.27}$$

where $\Theta = h^{ab}\nabla_b u_a$, is the expansion rate, $\sigma_{ab} = \nabla_{(a}u_{b)} - \frac{1}{2}\Theta\gamma_{ab}$ is the shear tensor, and $\gamma_{ab} = h_{ab} + u_a u_b$ is the projection tensor orthogonal to the fluid velocity. The derivation of the density, pressure and fluid velocity when the membrane is unperturbed is given in Appendix E.1. Here, we derive the boundary conditions for the metric perturbations at the surface of the membrane to the linear order in spin.

When the perturbation is added to the background, its contribution appears both on the membrane parameters and the metric perturbations in Eq. (E.26). Thus, the outside metric is given by Eq. (E.11), and the membrane surface is parametrised as

$$x^\mu(y^a) = \Big(t = T, r = r_0 + \epsilon_p \delta r(\Theta, \Phi) e^{-i\omega T}, \theta = \Theta, \phi = \Phi\Big), \tag{E.28}$$

$$\delta r(\Theta, \Phi) = \sum_{\ell, m} \xi_r^{\ell m} Y_{\ell m}(\Theta, \Phi), \tag{E.29}$$

where (T, Θ, Φ) are intrinsic coordinates to parametrise the (perturbed) membrane, and $\delta r(\Theta, \Phi)$ is the radial deformation of the membrane surface. We can derive the perturbed tangent vectors as $e_a^\mu = dx^\mu / dy^a = (e_a^\mu)^0 + \epsilon_p \delta e_a^\mu$ where

$$\delta e_a^\mu \equiv \begin{bmatrix} \delta e_t^\mu \\ \delta e_\Theta^\mu \\ \delta e_\phi^\mu \end{bmatrix} = \sum_{\ell m} \begin{bmatrix} 0 & -i\omega \xi_r^{\ell m} Y_{\ell m}(\Theta, \Phi) & 0 & 0 \\ 0 & \xi_r^{\ell m} \partial_\Theta Y_{\ell m}(\Theta, \Phi) & 0 & 0 \\ 0 & \xi_r^{\ell m} \partial_\Phi Y_{\ell m}(\Theta, \Phi) & 0 & 0 \end{bmatrix} e^{-i\omega T}, \tag{E.30}$$

and the basis vectors in the unperturbed case, $(e_a^\mu)^0$, is given in Eq. (E.2). We can now derive the perturbations in the induced metric $h_{ab} = g_{\mu\nu} e_a^\mu e_b^\nu = h_{ab}^0 + \epsilon_p \delta h_{ab} e^{-i\omega T}$, with h_{ab}^0 given in Eq. (E.3) and

$$\delta h_{ab} = \sum_{\ell m} \begin{bmatrix} \frac{r_0^2 H_0^{\ell m}(r_0) - 2M\xi_r^{\ell m}}{r_0^2} & -\csc\Theta h_0^{\ell m}(r_0)\partial_\Phi & h_0^{\ell m}(r_0)\sin\Theta\partial_\Theta + \frac{2J\sin^2\Theta}{r_0^2}\xi_r^{\ell m} \\ -\csc\Theta h_0^{\ell m}(r_0)\partial_\Phi & r_0\left(r_0 K^{\ell m}(r_0) + 2\xi_r^{\ell m}\right) & 0 \\ h_0^{\ell m}(r_0)\sin\Theta\partial_\Theta + \frac{2J\sin^2\Theta}{r_0^2}\xi_r^{\ell m} & 0 & r_0\left(r_0 K^{\ell m}(r_0) + 2\xi_r^{\ell m}\right)\sin^2\Theta \end{bmatrix}$$
$$\times Y_{\ell m}(\Theta, \Phi). \tag{E.31}$$

The normal vector $n_\mu = n_\mu^0 + \epsilon_p \delta n_\mu e^{-i\omega T}$, defined through the relations $n_\mu e_a^\mu = 0$, and

$n_\mu n_\nu g^{\mu\nu} = 1$, is perturbed as

$$\delta n_\mu = \sum_{\ell m} \begin{bmatrix} i\omega \frac{\xi_r^{\ell m}}{\sqrt{f(r_0)}} \\ \frac{H_2^{\ell m}(r_0)}{2}\sqrt{f(r_0)} \\ -\frac{\xi_r^{\ell m}}{\sqrt{f(r_0)}}\partial_\Theta \\ -\frac{\xi_r^{\ell m}}{\sqrt{f(r_0)}}\partial_\Phi \end{bmatrix} Y_{\ell m}(\Theta,\Phi).\,, \tag{E.32}$$

where $n^0_\mu = \{0, 1/\sqrt{f(r_0)}, 0, 0\}$. Subsequently, we can compute the perturbation to the extrinsic curvature $K_{ab} = K^0_{ab} + \epsilon_p \delta K_{ab} e^{-i\omega T}$, using $K_{ab} = e^\mu_a e^\nu_b \nabla_{(\mu} n_{\nu)}$. K^0_{ab} is defined in Eq. (E.4), and

$$\begin{aligned}
\delta K_{TT} = \sum_{\ell m} & \frac{\left(-5f^2 + 6f + 4r_0^2\omega^2 - 1\right)\xi_r^{\ell m}}{4r_0^2\sqrt{f}} + \frac{r_0 f\left(-f^2 H_2^{\ell m} + f H_2^{\ell m} + 4i\omega r_0 H_1^{\ell m} + 2r_0 (H_0^{\ell m})'\right)}{4r_0^2\sqrt{f}} \\
& \times Y_{\ell m}(\Theta,\Phi)\,, \\
\delta K_{\Theta\Theta} = \sum_{\ell m} & \frac{f\left(2\partial_\Phi h_1^{\ell m}\csc\Theta\,(\cot\Theta - \partial_\Theta) + r_0^2 (K^{\ell m})' + 2r_0 K^{\ell m} + \xi_r^{\ell m}\right)}{2\sqrt{f}} \\
& - \frac{r_0 f^2 H_2^{\ell m} - \left(1 - 2\partial_\Theta^2\right)\xi_r^{\ell m}}{2\sqrt{f}} Y_{\ell m}(\Theta,\Phi)\,, \\
\delta K_{T\Theta} = \sum_{\ell m} & \Bigg[\frac{f\left[\partial_\Theta H_1^{\ell m} + i\partial_\Phi \csc\Theta\left(\omega h_1^{\ell m} + i(h_0^{\ell m})'\right)\right]}{2\sqrt{f}} \\
& + \frac{2i\omega\partial_\Theta \xi_r^{\ell m}}{2\sqrt{f}} + \frac{2J\cot\Theta\left(f h_1^{\ell m}\sin\Theta\partial_\Theta - \partial_\Phi \xi_r^{\ell m}\right)}{r_0^3\sqrt{f}}\Bigg] \\
& \times Y_{\ell m}(\Theta,\Phi)\,,
\end{aligned} \tag{E.33}$$

$$\begin{aligned}
\delta K_{T\Phi} = \sum_{\ell m} & \Bigg\{\frac{f\left(i\omega h_1^{\ell m}\sin\Theta\partial_\Theta + \sin\Theta\partial_\Theta (h_0^{\ell m})' - \partial_\Phi H_1^{\ell m}\right)}{2\sqrt{f}} \\
& + \frac{2i\omega\partial_\Phi \xi_r^{\ell m}}{2\sqrt{f}} + \frac{J\Big[-f\left(4\partial_\Phi h_1^{\ell m}\cos\Theta + 5\sin^2\Theta\xi_r^{\ell m}\right)}{2r_0^3\sqrt{f}} \\
& + \frac{r_0 f^2 H_2^{\ell m}\sin^2\Theta + \sin\Theta\xi_r^{\ell m}\left(4\cos\Theta\partial_\Theta + \sin\Theta\right)\Big]}{2r_0^3\sqrt{f}}\Bigg\} \\
& \times Y_{\ell m}(\Theta,\Phi)\,,
\end{aligned} \tag{E.34}$$

$$\delta K_{\Theta\Phi} = \sum_{\ell m} \frac{2\partial_\Phi \left(\cot\Theta - \partial_\Theta\right) \xi_r^{\ell m} - f h_1^{\ell m} \sin\Theta \left(\partial_\Phi^2 \csc^2\Theta - \partial_\Theta^2 + \cot\Theta\partial_\Theta\right)}{2\sqrt{f}}$$

$$\times Y_{\ell m}(\Theta, \Phi)\,,$$

$$\delta K_{\Phi\Phi} = \delta K_{\Theta\Theta} \sin^2\Theta + \sum_{\ell m} \frac{2\partial_\Phi f h_1^{\ell m} \left(\sin\Theta\partial_\Theta - \cos\Theta\right)}{\sqrt{f}}$$

$$- \frac{\xi_r^{\ell m} \left(-\sin^2\Theta\partial_\Theta^2 + \sin\Theta\cos\Theta\partial_\Theta + \partial_\Phi^2\right)}{\sqrt{f}} Y_{\ell m}(\Theta, \Phi)\,. \tag{E.35}$$

where we have suppressed the radial argument in the perturbation variables for simplicity of notation. All the radial functions and their derivatives are to be evaluated at $r = r_0$. Also note that ∂_Θ (∂_Φ) denote a differentiation with respect to Θ (Φ), acting on the spherical harmonic $Y_{\ell m}(\Theta, \Phi)$, and the prime denotes a radial derivative.

The fluid membrane parameters are also perturbed so that Eq. (E.26) continues to hold. We parametrise the fluid perturbations as

$$\rho = \rho^0 + \epsilon_p \delta\rho(\Theta, \Phi) e^{-i\omega T}, \tag{E.36}$$

$$p = p^0 + \epsilon_p \delta p(\Theta, \Phi) e^{-i\omega T}, \tag{E.37}$$

$$u^a = (u^a)^0 + \epsilon_p \delta u^a(\Theta, \Phi) e^{-i\omega T}. \tag{E.38}$$

Furthermore, we expand the membrane perturbations in spherical harmonics (analogous to stellar perturbation theory in Ref. [272]) as

$$\delta u^\Theta = \sum_{\ell m} \left[V^{\ell m} \frac{S_\phi^{\ell m}(\Theta, \Phi)}{\sin\Theta} + U^{\ell m} S_\theta^{\ell m}(\Theta, \Phi)\right], \tag{E.39}$$

$$\delta u^\Phi = \sum_{\ell m} \left[-V^{\ell m} \frac{S_\theta^{\ell m}(\Theta, \Phi)}{\sin\Theta} + U^{\ell m} S_\phi^{\ell m}(\Theta, \Phi)\right], \tag{E.40}$$

$$\delta\rho(\Theta, \Phi) = \sum_{\ell m} \delta\rho^{\ell m} Y_{\ell m}(\Theta, \Phi), \tag{E.41}$$

$$\delta p(\Theta, \Phi) = \sum_{\ell m} \delta p^{\ell m} Y_{\ell m}(\Theta, \Phi). \tag{E.42}$$

This makes the process of deriving the boundary conditions more convenient, and splits the perturbations based on their transformation under parity. The perturbed stress energy tensor is then given by

$$\begin{aligned}
\delta T_{TT} &= \sum_{\ell m}\left[\frac{\sqrt{f}\left((f-1)\xi_r^{\ell m}+r_0 H_0^{\ell m}\right)}{4\pi r_0^2}+f\delta\rho^{\ell m}-\frac{J(\sin\Theta U^{\ell m}\partial_\Theta+\partial_\Phi U^{\ell m})}{4\pi r_0^2}\right]Y_{\ell m}(\Theta,\Phi)\,,\\
\delta T_{\Theta\Theta} &= \sum_{\ell m}\Big\{r_0^2\Big[\delta p^{\ell m}-2\eta\partial_\Phi\cot\Theta\csc\Theta U^{\ell m}+\left(2\eta\partial_\Phi\csc\Theta U^{\ell m}-(\zeta-\eta)\cot\Theta V^{\ell m}\right)\partial_\Theta\\
&\quad -V^{\ell m}\left(\partial_\Phi^2(\zeta-\eta)\csc^2\Theta+\partial_\Theta^2(\zeta+\eta)\right)\Big]\\
&\quad +\frac{\left(r_0K^{\ell m}+2\xi_r^{\ell m}\right)\left(-M+8i\pi\zeta r_0^2\omega+r_0\right)}{8\pi r_0\sqrt{f}}\\
&\quad +\frac{J\left[-\partial_\Phi\left(2\zeta r_0K^{\ell m}+(3\zeta+\eta)\xi_r^{\ell m}\right)-6ir_0\omega(\zeta-\eta)h_0^{\ell m}\sin\Theta\partial_\Theta\right]}{2r_0\sqrt{f}\,(r_0-3M)}\\
&\quad +\frac{J(\zeta-\eta)}{f^{3/2}(3f-1)r_0^2}\Big[4ir_0\omega h_0^{\ell m}\sin\Theta\partial_\Theta-\partial_\Phi\left(\xi_r^{\ell m}-r_0H_0^{\ell m}\right)\\
&\quad -6ir_0^3\omega f^{3/2}\left(\sin\Theta U^{\ell m}\partial_\Theta+\partial_\Phi V^{\ell m}\right)+4ir_0^3\omega\sqrt{f}\left(\sin\Theta U^{\ell m}\partial_\Theta+\partial_\Phi V^{\ell m}\right)\Big]\Big\}Y_{\ell m}(\Theta,\Phi)\,,\\
\delta T_{T\Theta} &= \sum_{\ell m}\Big\{\frac{r_0^2\partial_\Theta\left(3f-1\right)V^{\ell m}-\partial_\Phi\csc\Theta\left(4\sqrt{f}h_0^{\ell m}+3r_0^2fU^{\ell m}-r_0^2U^{\ell m}\right)}{16\pi r_0}\\
&\quad -\frac{2\eta J\sin\Theta\left[-U^{\ell m}\partial_\Theta^2+\partial_\Phi\csc^2\Theta\left(\partial_\Phi U^{\ell m}+2\cos\Theta V^{\ell m}\right)\right]}{r_0(3f-1)}\,,\\
&\quad -\frac{2\eta J\sin\Theta\left[\csc\Theta\left(\cos\Theta U^{\ell m}\partial_\Theta-2\partial_\Phi V^{\ell m}\right)\right]}{r_0(3f-1)}\Big\}Y_{\ell m}(\Theta,\Phi)\,,\\
\delta T_{T\Phi} &= \sum_{\ell m}\Big\{\frac{r_0^2\partial_\Phi\left(3f-1\right)V^{\ell m}-\sin\Theta\partial_\Theta\left(4\sqrt{f}h_0^{\ell m}+3r_0^2fU^{\ell m}-r_0^2U^{\ell m}\right)}{16\pi r_0}\\
&\quad -\frac{J}{r_0\left(r_0-3M\right)}\Big[6M\sin^2\Theta\delta\rho^{\ell m}+r_0\Big(\sin^2\Theta\left(\delta p^{\ell m}-\delta\rho^{\ell m}\right)+2\eta\partial_\Phi\cos\Theta U^{\ell m}\\
&\quad +\sin\Theta\left(2\eta\partial_\Phi U^{\ell m}+(\zeta+\eta)\cos\Theta V^{\ell m}\right)\partial_\Theta-(\zeta-\eta)\sin^2\Theta V^{\ell m}\partial_\Theta^2-\partial_\Phi^2(\zeta+\eta)V^{\ell m}\Big)\Big]\\
&\quad +\frac{J\sin^2\Theta}{16\pi r_0^3 f^{3/2}\left(3f-1\right)}\Big[-ir_0f\left(-3iH_0^{\ell m}+32\pi\zeta r_0\omega K^{\ell m}-2iK^{\ell m}+64\pi\zeta\omega\xi_r^{\ell m}\right)\\
&\quad +f^2\left(6r_0K^{\ell m}+\xi_r^{\ell m}\right)+24f^3\xi_r^{\ell m}+r_0H_0^{\ell m}-\xi_r^{\ell m}\Big]\Big\}Y_{\ell m}(\Theta,\Phi)\,,\\
\delta T_{\Theta\Phi} &= \sum_{\ell m}\Big\{\eta r_0^2\csc\Theta\Big[-U^{\ell m}\sin^2\Theta\partial_\Theta^2+\partial_\Phi\left(\partial_\Phi U^{\ell m}+2\cos\Theta V^{\ell m}\right)
\end{aligned}$$

$$+\sin\Theta\left(\cos\Theta U^{\ell m}-2\partial_\Phi V^{\ell m}\right)\partial_\Theta\Big]$$

$$+\frac{J\sin\Theta}{8\pi r_0^2 f^{3/2}(3f-1)}\Big[f\Big(8\pi\eta\sin\Theta\partial_\Theta\xi_r^{\ell m}+3\partial_\Phi h_0^{\ell m}(3+16i\pi\eta r_0\omega)\Big)$$

$$-9\partial_\Phi f^2 h_0^{\ell m}-3ir_0^2 f^{3/2}(16\pi\eta r_0\omega-3i)\left(\sin\Theta V^{\ell m}\partial_\Theta-\partial_\Phi U^{\ell m}\right)$$

$$+2r_0^2\sqrt{f}(1+16i\pi\eta r_0\omega)\left(\sin\Theta V^{\ell m}\partial_\Theta-\partial_\Phi U^{\ell m}\right)$$

$$+9r_0^2 f^{5/2}\left(\sin\Theta V^{\ell m}\partial_\Theta-\partial_\Phi U^{\ell m}\right)-2\partial_\Phi h_0^{\ell m}(1+16i\pi\eta r_0\omega)$$

$$+8\pi\eta r_0 H_0^{\ell m}\sin\Theta\partial_\Theta-8\pi\eta\sin\Theta\xi_r^{\ell m}\partial_\Theta\Big]\Big\}Y_{\ell m}(\Theta,\Phi)\,, \tag{E.43}$$

$$\begin{aligned}\delta T_{\Phi\Phi} \;=\;& \delta T_{\Theta\Theta}\sin^2\Theta-\sum_{\ell m}\Big\{2\eta r_0^2\Big[\partial_\Phi\left(\partial_\Phi V^{\ell m}-2\cos\Theta U^{\ell m}\right)\\
&+\sin\Theta\left(2\partial_\Phi U^{\ell m}+\cos\Theta V^{\ell m}\right)\partial_\Theta-\sin^2\Theta V^{\ell m}\partial_\Theta^2\Big]\\
&+\frac{J\sin^2\Theta}{4\pi r_0^2 f^{3/2}(3f-1)}\Big[f\Big(8\pi\eta\partial_\Phi\xi_r^{\ell m}-3ih_0^{\ell m}\sin\Theta\partial_\Theta(16\pi\eta r_0\omega-3i)\Big)\\
&+9f^2h_0^{\ell m}\sin\Theta\partial_\Theta-3ir_0^2f^{3/2}(16\pi\eta r_0\omega-3i)\left(\sin\Theta U^{\ell m}\partial_\Theta+\partial_\Phi V^{\ell m}\right)\\
&+2r_0^2\sqrt{f}(1+16i\pi\eta r_0\omega)\left(\sin\Theta U^{\ell m}\partial_\Theta+\partial_\Phi V^{\ell m}\right)\\
&+9r_0^2f^{5/2}\left(\sin\Theta U^{\ell m}\partial_\Theta+\partial_\Phi V^{\ell m}\right)\\
&+2h_0^{\ell m}\sin\Theta\partial_\Theta(1+16i\pi\eta r_0\omega)-8\pi\eta\partial_\Phi\left(\xi_r^{\ell m}-r_0H_0^{\ell m}\right)\Big]\Big\}Y_{\ell m}(\Theta,\Phi)\,.\end{aligned} \tag{E.44}$$

Now, using Eq. (E.26), we can write the constraints on the perturbations to these quantities as

$$\delta K_{ab}-h_{ab}\delta K-K\delta h_{ab}=-8\pi\delta T_{ab}, \tag{E.45}$$

which is a total of six equations that fix the perturbations to the membrane as well as the boundary condition. We project the equations onto the spherical harmonics $Y_{\ell m}(\Theta,\Phi)$ and extract the relations for a given (ℓ, m) mode (and its interaction with the neighbouring modes) [272, 273] yielding to

$$(ab)=(T\Phi)\to \ell(\ell+1)\beta_0^{\ell m}+imJ\big[(\ell-1)(\ell+2)\chi_0^{\ell m}+\tilde{\alpha}_0^{\ell m}+\eta_0^{\ell m}\big]$$
$$-JQ^{\ell m}(\ell+1)\big[(\ell-2)(\ell-1)\xi_0^{\ell-1,m}-(\ell-1)\tilde{\beta}_0^{\ell-1,m}+\zeta_0^{\ell-1,m}\big]$$
$$+JQ^{\ell+1,m}\ell\big[(\ell+2)(\ell+3)\xi_0^{\ell+1,m}+(\ell+2)\tilde{\beta}_0^{\ell+1,m}+\zeta_0^{\ell+1,m}\big]=0, \tag{E.46}$$

$$(\Theta\Theta)-(\Phi\Phi)\to \ell(\ell+1)K_{00}^{\ell m}+imJK_{gg}^{\ell m}-JQ^{\ell m}(\ell+1)K_{ff}^{\ell-1,m}+JQ^{\ell+1,m}\ell K_{ff}^{\ell+1,m}=0. \tag{E.47}$$

for the predominantly axial sector, and similarly

$$(ab)=(TT)\to A_{00}^{\ell m}+imJC_0^{\ell m}+JQ^{\ell m}B_0^{\ell-1,m}-JQ^{\ell+1,m}B_0^{\ell+1,m}=0, \tag{E.48}$$

$$(\Theta\Theta)+(\Phi\Phi)\to A_{33}^{\ell m}+imJC_3^{\ell m}+JQ^{\ell m}B_3^{\ell-1,m}-JQ^{\ell+1,m}B_3^{\ell+1,m}=0, \tag{E.49}$$

$$(T\Theta)\to \ell(\ell+1)\alpha_0^{\ell m}+imJ\big[(\ell-1)(\ell+2)\xi_0^{\ell m}-\tilde{\beta}_0^{\ell m}-\zeta_0^{\ell m}\big]$$
$$-JQ^{\ell m}(\ell+1)\big[(\ell-2)(\ell-1)\chi_0^{\ell-1,m}+(\ell-1)\tilde{\alpha}_0^{\ell-1,m}-\eta_0^{\ell-1,m}\big]$$
$$-JQ^{\ell+1,m}\ell\big[(\ell+2)(\ell+3)\chi_0^{\ell+1,m}-(\ell+2)\tilde{\alpha}_0^{\ell+1,m}-\eta_0^{\ell+1,m}\big]=0, \tag{E.50}$$

$$(\Theta\Phi)\to \ell(\ell+1)K_s^{\ell m}+imJK_f^{\ell m}-JQ^{\ell m}(\ell+1)K_g^{\ell-1,m}+JQ^{\ell+1,m}\ell K_g^{\ell+1,m}=0. \tag{E.51}$$

for predominantly polar sector. Here, $Q^{\ell m}=\sqrt{(\ell^2-m^2)/(4l^2-1)}$ and the other variables are functions of the individual modes of axial and polar perturbations which help us to organize the equations in a similar manner as in Ref. [272, 273]. Note that among the terms proportional to J, each equation contains functions that are proportional to ℓ and the neighbouring modes $\ell-1$, $\ell+1$. Among these, the latter ones lead to a mixing of axial and polar modes, as parity conservation prevents any coupling between axial and polar modes with the same angular number. For example in Eq. (E.46), $\beta_0^{\ell m}$, $\chi_0^{\ell m}$, $\tilde{\alpha}_0^{\ell m}$ and $\eta_0^{\ell m}$ depend only on the axial perturbation functions, i.e., $h_{0/1/2}^{\ell m}(r_0)$ and $U^{\ell m}$; whereas $\xi_0^{\ell m}$, $\tilde{\beta}_0^{\ell m}$ and $\zeta_0^{\ell m}$, which contribute as neighbouring modes, depend only on the polar perturbation functions, i.e., $\xi_r^{\ell m}$, $V_0^{\ell m}$, $\delta p^{\ell m}$, $\delta\rho^{\ell m}$, $H_{0/1/2}^{\ell m}(r_0)$ and $K^{\ell m}(r_0)$.

To leading order in spin, we can drop the mixing between axial and polar modes without affecting the derived QNM frequencies. This is true both in the equations of motions and in the junction conditions. To see this, we first note that the equations are invariant under

$$a^{\ell m} \to (-1)^{\ell+1} a^{\ell,-m}, \quad p^{\ell m} \to (-1)^{\ell} p^{\ell,-m}, \quad J \to -J, \quad m \to -m, \tag{E.52}$$

where $a^{\ell m}$ collectively refers to all the linear functions of axial perturbations in the above equations (e.g., $\beta_0^{\ell m}$) and $p^{\ell m}$ collectively refers to all the linear functions of polar perturbations in the above equations (e.g., $A_{00}^{\ell m}$). At the first order in spin, the QNM frequencies can be expanded as $\omega = \omega_0 + m\chi\omega_1 + O(\chi^2)$, where $J = M^2\chi$. This implies that the linear-in-spin terms in the equations of motion that do not have an extra factor of m cannot affect ω_1, and may be dropped for their computation. This is also true for the perturbation equations, as shown in Ref. [273]. Thus, we can decouple the axial and polar sectors and simplify the junction conditions to

$$(ab) = (T\Phi) \to \ell(\ell+1)\beta_0^{\ell m} + imJ[(\ell-1)(\ell+2)\chi_0^{\ell m} + \tilde{\alpha}_0^{\ell m} + \eta_0^{\ell m}] = 0, \tag{E.53}$$

$$(\Theta\Theta) - (\Phi\Phi) \to \ell(\ell+1)K_{00}^{\ell m} + imJK_{gg}^{\ell m} = 0, \tag{E.54}$$

for axial modes and

$$(ab) = (TT) \to A_{00}^{\ell m} + imJC_0^{\ell m} = 0, \tag{E.55}$$

$$(\Theta\Theta) + (\Phi\Phi) \to A_{33}^{\ell m} + imJC_3^{\ell m} = 0, \tag{E.56}$$

$$(T\Theta) \to \ell(\ell+1)\alpha_0^{\ell m} + imJ[(\ell-1)(\ell+2)\xi_0^{\ell m} - \tilde{\beta}_0^{\ell m} - \zeta_0^{\ell m}] = 0, \tag{E.57}$$

$$(\Theta\Phi) \to \ell(\ell+1)K_s^{\ell m} + imJK_f^{\ell m} = 0, \tag{E.58}$$

for polar modes to the first order in spin.

E.3.1 Axial boundary condition

Using Eqs. (E.53) and (E.54), we can eliminate the axial matter perturbation ($V^{\ell m}$) between these two equations to get the boundary condition for the Regge-Wheeler function $\psi_{\rm RW}(r)$ to linear order in spin to be

$$\begin{aligned}\frac{1}{\psi_{\rm RW}(r)}\frac{d\psi_{\rm RW}(r)}{dr_*}\bigg|_{r=r_0} = &\frac{3M^2y^2\nu V_{\rm RW}(r_0)-6iw^3+2iw^2y}{6Mw\nu(3w-y)}\\ &+\frac{m\chi}{6\ell(\ell+1)My^5(y-3w)^2\nu}\Big[w^3\big(36w^2y\big(i(\ell^2+\ell+9)y+16\nu+\nu y^2\big)\\ &\quad+6wy^2\big((\ell^2+\ell-7)\nu y^2-2i(2\ell^2+2\ell+13)y-42\nu\big)\\ &\quad+y^3\big(-3(\ell^2+\ell-4)\nu y^2+4i(\ell^2+\ell+6)y+36\nu\big)\\ &\quad-216iw^3(y-2i\nu)\big)\\ &-3M^2wy^4V_{\rm RW}(r_0)\big(4\nu w-6iwy+\nu y^3+2iy^2-2\nu y\big)\Big],\end{aligned} \tag{E.59}$$

where $w=M\omega$, $y=\omega r_0$, $\nu=16\pi\eta$ and

$$V_{\rm RW}(r_0)=f(r)\Big(\frac{\ell(\ell+1)}{r^2}-\frac{6M}{r^3}+\frac{24mJ(-7M+3r_0)}{\ell(\ell+1)r_0^6\omega}\Big). \tag{E.60}$$

The above boundary condition is consistent with the earlier results in Ref. [90] in the non spinning case for $\chi=0$. In the BH limit, i.e., $\eta\to(16\pi)^{-1}$ and $r_0\to 2M$, we have

$$\frac{1}{\psi_{\rm RW}(r)}\frac{d\psi_{\rm RW}(r)}{dr_*}\bigg|_{r=r_0}=-i\Big(\omega-\frac{m\chi}{4M}\Big)=-i(\omega-m\Omega_H), \tag{E.61}$$

as expected.

E.3.2 Polar boundary condition

The polar boundary condition requires an extra ingredient, which is the equation of state of the membrane fluid. Since there are four equations in the polar sector and four matter perturbations, i.e., $\delta\rho^{\ell m}$, $\delta p^{\ell m}$, $V^{\ell m}$ and $\xi_r^{\ell m}$, we do not have any remaining constraint upon eliminating the matter variables to serve as the boundary condition. Thus, we additionally impose that the perturbations to the pressure and the density are related via the equilibrium sound-speed [90, 272]

$$c_s^2 = \frac{\delta p^{\ell m}}{\delta\rho^{\ell m}} = \frac{dp_0/dr}{d\rho^0/dr} = -\frac{3M^2 - 3Mr_0 + r_0^2}{2(6M^2 - 5Mr_0 + r_0^2)}. \tag{E.62}$$

With this extra constraint, we obtain the boundary condition to the linear order in spin for the Zerilli function $\psi_{\rm Z}(r)$, using the relations in Appendix. E.2. We write it implicitly here as

$$\frac{1}{\psi_{\rm Z}(r)}\frac{d\psi_{\rm Z}(r)}{dr_*}\Big|_{r=r_0} = -16\pi\eta i\omega + G(r_0,\omega,\eta,\zeta) + m\chi H(r_0,\omega,\eta,\zeta).\,, \tag{E.63}$$

where $G(r_0,\omega,\eta,\zeta)$ is given explicitly in Ref. [90]. We provide the polar boundary condition in the supplemental Mathematica document in [274]. Note that unlike the axial sector, there is dependence on the bulk viscosity both in spinless case and at the linear order in spin for the polar sector. In the BH limit, i.e., $\eta \to (16\pi)^{-1}$, $\zeta \to -(16\pi)^{-1}$ and $r_0 \to 2M$, we have

$$\frac{1}{\psi_{\rm Z}(r)}\frac{d\psi_{\rm Z}(r)}{dr_*}\Big|_{r=r_0} = -i\Big(\omega - \frac{m\chi}{4M}\Big) = -i(\omega - m\Omega_H), \tag{E.64}$$

as expected.

Bibliography

[1] M. V. S. Saketh, J. Vines, J. Steinhoff, and A. Buonanno, Conservative and radiative dynamics in classical relativistic scattering and bound systems, Phys. Rev. Res. **4**, 013127 (2022), arXiv:2109.05994 [gr-qc] .

[2] M. V. S. Saketh and J. Vines, Scattering of gravitational waves off spinning compact objects with an effective worldline theory, Phys. Rev. D **106**, 124026 (2022), arXiv:2208.03170 [gr-qc] .

[3] M. V. S. Saketh, J. Steinhoff, J. Vines, and A. Buonanno, Modeling horizon absorption in spinning binary black holes using effective worldline theory, Phys. Rev. D **107**, 084006 (2023), arXiv:2212.13095 [gr-qc] .

[4] M. V. S. Saketh, Z. Zhou, and M. M. Ivanov, Dynamical tidal response of Kerr black holes from scattering amplitudes, Phys. Rev. D **109**, 064058 (2024), arXiv:2307.10391 [hep-th] .

[5] M. V. S. Saketh, Z. Zhou, S. Ghosh, J. Steinhoff, and D. Chatterjee, Investigating tidal heating in neutron stars via gravitational Raman scattering, Phys. Rev. D **110**, 103001 (2024), arXiv:2407.08327 [gr-qc] .

[6] M. V. S. Saketh and E. Maggio, Quasinormal modes of slowly-spinning horizonless compact objects, Phys. Rev. D **110**, 084038 (2024), arXiv:2406.10070 [gr-qc] .

[7] K. Schwarzschild, On the gravitational field of a mass point according to Einstein's theory, Sitzungsber. Preuss. Akad. Wiss. Berlin (Math. Phys.) **1916**, 189 (1916), arXiv:physics/9905030 [physics] .

[8] R. P. Kerr, Gravitational field of a spinning mass as an example of algebraically special metrics, Physical review letters **11**, 237 (1963).

[9] J. R. Oppenheimer and G. M. Volkoff, On Massive neutron cores, Phys. Rev. **55**, 374 (1939).

[10] J. Bekenstein, Bekenstein-Hawking entropy, Scholarpedia **3**, 7375 (2008).

[11] S. W. Hawking, Particle Creation by Black Holes, Commun. Math. Phys. **43**, 199 (1975), [Erratum: Commun.Math.Phys. 46, 206 (1976)].

[12] A. Hewish, S. J. Bell, J. D. H. Pilkington, P. F. Scott, and R. A. Collins, Observation of a rapidly pulsating radio source, Nature **217**, 709 (1968).

[13] N. I. Shakura and R. A. Sunyaev, Black holes in binary systems. Observational appearance, Astron. Astrophys. **24**, 337 (1973).

[14] J. Kormendy and D. Richstone, Inward bound: The Search for supermassive black holes in galactic nuclei, Ann. Rev. Astron. Astrophys. **33**, 581 (1995).

[15] B. P. Abbott *et al.* (LIGO Scientific, Virgo), Observation of Gravitational Waves from a Binary Black Hole Merger, Phys. Rev. Lett. **116**, 061102 (2016), arXiv:1602.03837 [gr-qc] .

[16] A. Einstein, The Foundation of the General Theory of Relativity, Annalen Phys. **49**, 769 (1916).

[17] A. Einstein, Über Gravitationswellen, Sitzungsber. Preuss. Akad. Wiss. Berlin (Math. Phys.) **1918**, 154 (1918).

[18] C. W. Misner, K. S. Thorne, and J. A. Wheeler, *Gravitation* (W. H. Freeman, San Francisco, 1973).

[19] J. Aasi *et al.* (LIGO Scientific), Advanced LIGO, Class. Quant. Grav. **32**, 074001 (2015), arXiv:1411.4547 [gr-qc] .

[20] K. Somiya (KAGRA), Detector configuration of KAGRA: The Japanese cryogenic gravitational-wave detector, Class. Quant. Grav. **29**, 124007 (2012), arXiv:1111.7185 [gr-qc] .

[21] T. Akutsu *et al.* (KAGRA), Overview of KAGRA: Calibration, detector characterization, physical environmental monitors, and the geophysics interferometer, PTEP **2021**, 05A102 (2021), arXiv:2009.09305 [gr-qc] .

[22] F. Acernese *et al.* (Virgo), Advanced Virgo: a second-generation interferometric gravitational wave detector, Class. Quant. Grav. **32**, 024001 (2015), arXiv:1408.3978 [gr-qc] .

[23] B. Abbott *et al.* (LIGO Scientific, Virgo), GWTC-1: A Gravitational-Wave Transient Catalog of Compact Binary Mergers Observed by LIGO and Virgo during the First and Second Observing Runs, Phys. Rev. X **9**, 031040 (2019), arXiv:1811.12907 [astro-ph.HE] .

[24] R. Abbott *et al.* (LIGO Scientific, Virgo), GWTC-2: Compact Binary Coalescences Observed by LIGO and Virgo During the First Half of the Third Observing Run, Phys. Rev. X **11**, 021053 (2021), arXiv:2010.14527 [gr-qc] .

[25] R. Abbott *et al.* (LIGO Scientific, VIRGO), GWTC-2.1: Deep extended catalog of compact binary coalescences observed by LIGO and Virgo during the first half of the third observing run, Phys. Rev. D **109**, 022001 (2024), arXiv:2108.01045 [gr-qc] .

[26] C. M. Will, The Confrontation between General Relativity and Experiment, Living Rev. Rel. **17**, 4 (2014), arXiv:1403.7377 [gr-qc] .

[27] M. Maggiore, *Gravitational Waves. Vol. 1: Theory and Experiments* (Oxford University Press, 2007).

[28] A. Einstein and N. Rosen, On Gravitational waves, J. Franklin Inst. **223**, 43 (1937).

[29] D. Kennefick, *Traveling at the Speed of Thought: Einstein and the Quest for Gravitational Waves* (Princeton University Press, 2007).

[30] F. Pirani, On the Physical significance of the Riemann tensor, Acta Phys.Polon. **15**, 389 (1956).

[31] F. A. E. Pirani, Invariant formulation of gravitational radiation theory, Phys. Rev. **105**, 1089 (1957).

[32] M. Di Mauro, S. Esposito, and A. Naddeo, Towards detecting gravitational waves: A contribution by Richard Feynman, in *16th Marcel Grossmann Meeting on Recent Developments in Theoretical and Experimental General Relativity, Astrophysics and Relativistic Field Theories* (2021) arXiv:2111.00330 [physics.hist-ph] .

[33] R. A. Hulse and J. H. Taylor, Discovery of a pulsar in a binary system, Astrophys. J. Lett. **195**, L51 (1975).

[34] J. H. Taylor and J. M. Weisberg, A new test of general relativity: Gravitational radiation and the binary pulsar PS R 1913+16, Astrophys. J. **253**, 908 (1982).

[35] J. M. Weisberg and J. H. Taylor, Relativistic binary pulsar B1913+16: Thirty years of observations and analysis, ASP Conf. Ser. **328**, 25 (2005), arXiv:astro-ph/0407149 .

[36] B. P. Abbott *et al.*, Sensitivity of the Advanced LIGO detectors at the beginning of gravitational wave astronomy, Phys. Rev. D **93**, 112004 (2016), [Addendum: Phys.Rev.D 97, 059901 (2018)], arXiv:1604.00439 [astro-ph.IM] .

[37] P. R. Saulson, *Fundamentals of Interferometric Gravitational Wave Detectors*, 2nd ed. (World Scientific, 2017).

[38] B. P. Abbott *et al.* (LIGO Scientific), Search for gravitational wave ringdowns from perturbed black holes in LIGO S4 data, Phys. Rev. **D80**, 062001 (2009), arXiv:0905.1654 [gr-qc] .

[39] F. Acernese *et al.* (VIRGO), Advanced Virgo: a second-generation interferometric gravitational wave detector, Class. Quant. Grav. **32**, 024001 (2015), arXiv:1408.3978 [gr-qc] .

[40] K. Somiya (KAGRA), Detector configuration of KAGRA: The Japanese cryogenic gravitational-wave detector, Class. Quant. Grav. **29**, 124007 (2012), arXiv:1111.7185 [gr-qc] .

[41] T. Akutsu *et al.* (KAGRA), KAGRA: 2.5 Generation Interferometric Gravitational Wave Detector, Nature Astron. **3**, 35 (2019), arXiv:1811.08079 [gr-qc] .

[42] B. P. Abbott *et al.* (LIGO Scientific, Virgo), A guide to LIGO–Virgo detector noise and extraction of transient gravitational-wave signals, Class. Quant. Grav. **37**, 055002 (2020), arXiv:1908.11170 [gr-qc] .

[43] B. J. Owen, Search templates for gravitational waves from inspiraling binaries: Choice of template spacing, Phys. Rev. D **53**, 6749 (1996), arXiv:gr-qc/9511032 .

[44] R. Abbott *et al.* (LIGO Scientific, VIRGO, KAGRA), Tests of General Relativity with GWTC-3, (2021), arXiv:2112.06861 [gr-qc] .

[45] C. M. Will, Gravity: Newtonian, Post-Newtonian, and General Relativistic, in *Gravity: Where Do We Stand?*, edited by R. Peron, M. Colpi, V. Gorini, and U. Moschella (2016) pp. 9–72.

[46] L. Blanchet, Gravitational Radiation from Post-Newtonian Sources and Inspiralling Compact Binaries, Living Rev. Rel. **17**, 2 (2014), arXiv:1310.1528 [gr-qc] .

[47] R. A. Porto, The effective field theorist's approach to gravitational dynamics, Phys. Rept. **633**, 1 (2016), arXiv:1601.04914 [hep-th] .

[48] M. Levi, Effective Field Theories of Post-Newtonian Gravity: A comprehensive review, Rept. Prog. Phys. **83**, 075901 (2020), arXiv:1807.01699 [hep-th] .

[49] G. Schäfer and P. Jaranowski, Hamiltonian formulation of general relativity and post-Newtonian dynamics of compact binaries, Living Rev. Rel. **21**, 7 (2018), arXiv:1805.07240 [gr-qc] .

[50] L. Blanchet, A. Buonanno, and G. Faye, Higher-order spin effects in the dynamics of compact binaries. II. Radiation field, Phys. Rev. D **74**, 104034 (2006), [Erratum: Phys.Rev.D 75, 049903 (2007), Erratum: Phys.Rev.D 81, 089901 (2010)], arXiv:gr-qc/0605140 .

[51] W. D. Goldberger and I. Z. Rothstein, An Effective field theory of gravity for extended objects, Phys. Rev. D **73**, 104029 (2006), arXiv:hep-th/0409156 .

[52] B. M. Barker and R. F. O'Connell, Gravitational Two-Body Problem with Arbitrary Masses, Spins, and Quadrupole Moments, Phys. Rev. **D12**, 329 (1975).

[53] L. E. Kidder, C. M. Will, and A. G. Wiseman, Spin effects in the inspiral of coalescing compact binaries, Phys. Rev. D **47**, R4183 (1993).

[54] M. Levi and J. Steinhoff, Spinning gravitating objects in the effective field theory in the post-Newtonian scheme, JHEP **09**, 219, arXiv:1501.04956 [gr-qc] .

[55] T. Hinderer, Tidal Love numbers of neutron stars, Astrophys. J. **677**, 1216 (2008), Erratum: *ibid.* **697**, 964 (2009), arXiv:0711.2420 [astro-ph] .

[56] T. Binnington and E. Poisson, Relativistic theory of tidal Love numbers, Phys. Rev. **D80**, 084018 (2009), arXiv:0906.1366 [gr-qc] .

[57] T. Damour and A. Nagar, Relativistic tidal properties of neutron stars, Phys. Rev. **D80**, 084035 (2009), arXiv:0906.0096 [gr-qc] .

[58] H. Tagoshi, S. Mano, and E. Takasugi, PostNewtonian expansion of gravitational waves from a particle in circular orbits around a rotating black hole: Effects of black hole absorption, Prog. Theor. Phys. **98**, 829 (1997), arXiv:gr-qc/9711072 .

[59] K. Alvi, Energy and angular momentum flow into a black hole in a binary, Phys. Rev. **D64**, 104020 (2001), arXiv:gr-qc/0107080 [gr-qc] .

[60] K. Chatziioannou, E. Poisson, and N. Yunes, Improved next-to-leading order tidal heating and torquing of a Kerr black hole, Phys. Rev. D **94**, 084043 (2016), arXiv:1608.02899 [gr-qc] .

[61] W. D. Goldberger, J. Li, and I. Z. Rothstein, Non-conservative effects on spinning black holes from world-line effective field theory, JHEP **06**, 053, arXiv:2012.14869 [hep-th] .

[62] E. Poisson, Metric of a tidally distorted, nonrotating black hole, Phys. Rev. Lett. **94**, 161103 (2005), arXiv:gr-qc/0501032 .

[63] S. Comeau and E. Poisson, Tidal interaction of a small black hole in the field of a large Kerr black hole, Phys. Rev. D **80**, 087501 (2009), arXiv:0908.4518 [gr-qc] .

[64] E. Poisson, Absorption of mass and angular momentum by a black hole: Time-domain formalisms for gravitational perturbations, and the small-hole / slow-motion approximation, Phys. Rev. **D70**, 084044 (2004), arXiv:gr-qc/0407050 [gr-qc] .

[65] N. Yunes and J. Gonzalez, Metric of a tidally perturbed spinning black hole, Phys. Rev. D **73**, 024010 (2006), [Erratum: Phys.Rev.D 89, 089902 (2014)], arXiv:gr-qc/0510076 .

[66] A. Einstein, Explanation of the Perihelion Motion of Mercury from the General Theory of Relativity, Sitzungsber. Preuss. Akad. Wiss. Berlin (Math. Phys.) **1915**, 831 (1915).

[67] Y. Mino, M. Sasaki, and T. Tanaka, Gravitational radiation reaction to a particle motion, Phys. Rev. **D55**, 3457 (1997), arXiv:gr-qc/9606018 [gr-qc] .

[68] T. C. Quinn and R. M. Wald, An Axiomatic approach to electromagnetic and gravitational radiation reaction of particles in curved space-time, Phys. Rev. **D56**, 3381 (1997), arXiv:gr-qc/9610053 [gr-qc] .

[69] C. R. Galley and B. L. Hu, Self-force on extreme mass ratio inspirals via curved spacetime effective field theory, Phys. Rev. D **79**, 064002 (2009), arXiv:0801.0900 [gr-qc] .

[70] E. Poisson, A. Pound, and I. Vega, The Motion of point particles in curved spacetime, Living Rev. Rel. **14**, 7 (2011), arXiv:1102.0529 [gr-qc] .

[71] S. L. Detweiler, A Consequence of the gravitational self-force for circular orbits of the Schwarzschild geometry, Phys. Rev. **D77**, 124026 (2008), arXiv:0804.3529 [gr-qc] .

[72] L. Barack, Gravitational self force in extreme mass-ratio inspirals, Class. Quant. Grav. **26**, 213001 (2009), arXiv:0908.1664 [gr-qc] .

[73] L. Barack and A. Pound, Self-force and radiation reaction in general relativity, Rept. Prog. Phys. **82**, 016904 (2019), arXiv:1805.10385 [gr-qc] .

[74] P. Amaro-Seoane, H. Audley, S. Babak, J. Baker, E. Barausse, P. Bender, E. Berti, P. Binetruy, M. Born, D. Bortoluzzi, J. Camp, C. Caprini, V. Cardoso, M. Colpi, J. Conklin, N. Cornish, C. Cutler, K. Danzmann, R. Dolesi, L. Ferraioli, V. Ferroni, E. Fitzsimons, J. Gair, L. Gesa Bote, D. Giardini, F. Gibert, C. Grimani, H. Halloin, G. Heinzel, T. Hertog, M. Hewitson, K. Holley-Bockelmann, D. Hollington, M. Hueller, H. Inchauspe, P. Jetzer, N. Karnesis, C. Killow, A. Klein, B. Klipstein, N. Korsakova, S. L. Larson, J. Livas, I. Lloro, N. Man, D. Mance, J. Martino, I. Mateos, K. McKenzie, S. T. McWilliams, C. Miller, G. Mueller, G. Nardini, G. Nelemans, M. Nofrarias, A. Petiteau, P. Pivato, E. Plagnol, E. Porter, J. Reiche, D. Robertson, N. Robertson, E. Rossi, G. Russano, B. Schutz, A. Sesana, D. Shoemaker, J. Slutsky, C. F. Sopuerta, T. Sumner, N. Tamanini, I. Thorpe, M. Troebs, M. Vallisneri, A. Vecchio, D. Vetrugno, S. Vitale, M. Volonteri, G. Wanner, H. Ward, P. Wass, W. Weber, J. Ziemer, and P. Zweifel, Laser Interferometer Space Antenna, arXiv e-prints , arXiv:1702.00786 (2017), arXiv:1702.00786 [astro-ph.IM] .

[75] F. Pretorius, Evolution of binary black hole spacetimes, Phys. Rev. Lett. **95**, 121101 (2005), arXiv:gr-qc/0507014 [gr-qc] .

[76] A. Ori and K. S. Thorne, The Transition from inspiral to plunge for a compact body in a circular equatorial orbit around a massive, spinning black hole, Phys. Rev. D **62**, 124022 (2000), arXiv:gr-qc/0003032 .

[77] A. Buonanno and T. Damour, Effective one-body approach to general relativistic two-body dynamics, Phys. Rev. D **59**, 084006 (1999), arXiv:gr-qc/9811091 .

[78] A. Buonanno and T. Damour, Transition from inspiral to plunge in binary black hole coalescences, Phys. Rev. D **62**, 064015 (2000), arXiv:gr-qc/0001013 .

[79] R. Arnowitt, S. Deser, and C. W. Misner, Dynamical structure and definition of energy in general relativity, Phys. Rev. **116**, 1322 (1959).

[80] T. W. Baumgarte and S. L. Shapiro, On the numerical integration of Einstein's field equations, Phys. Rev. D **59**, 024007 (1998), arXiv:gr-qc/9810065 .

[81] M. Shibata and T. Nakamura, Evolution of three-dimensional gravitational waves: Harmonic slicing case, Phys. Rev. D **52**, 5428 (1995).

[82] F. Pretorius, Evolution of binary black-hole spacetimes, Phys. Rev. Lett. **95**, 121101 (2005).

[83] M. A. Scheel, M. Boyle, T. Chu, L. E. Kidder, K. D. Matthews, and H. P. Pfeiffer, High-accuracy waveforms for binary black hole inspiral, merger, and ringdown, Phys. Rev. D **79**, 024003 (2009), arXiv:0810.1767 [gr-qc] .

[84] A. Buonanno, Y. Pan, H. P. Pfeiffer, M. A. Scheel, L. T. Buchman, and L. E. Kidder, Effective-one-body waveforms calibrated to numerical relativity simulations: Coalescence

of non-spinning, equal-mass black holes, Phys. Rev. **D79**, 124028 (2009), arXiv:0902.0790 [gr-qc] .

[85] Y. Pan, A. Buonanno, L. T. Buchman, T. Chu, L. E. Kidder, H. P. Pfeiffer, and M. A. Scheel, Effective-one-body waveforms calibrated to numerical relativity simulations: coalescence of non-precessing, spinning, equal-mass black holes, Phys. Rev. D **81**, 084041 (2010), arXiv:0912.3466 [gr-qc] .

[86] R. H. Price, Nonspherical perturbations of relativistic gravitational collapse. 1. Scalar and gravitational perturbations, Phys. Rev. **D5**, 2419 (1972).

[87] E. Berti, V. Cardoso, and C. M. Will, On gravitational-wave spectroscopy of massive black holes with the space interferometer LISA, Phys. Rev. **D73**, 064030 (2006), arXiv:gr-qc/0512160 [gr-qc] .

[88] E. Berti, V. Cardoso, and A. O. Starinets, Quasinormal modes of black holes and black branes, Class. Quantum Grav. **26**, 163001 (2009), arXiv:0905.2975 [gr-qc] .

[89] V. Cardoso and P. Pani, Testing the nature of dark compact objects: a status report, Living Rev. Rel. **22**, 4 (2019), arXiv:1904.05363 [gr-qc] .

[90] E. Maggio, L. Buoninfante, A. Mazumdar, and P. Pani, How does a dark compact object ringdown?, Phys. Rev. D **102**, 064053 (2020), arXiv:2006.14628 [gr-qc] .

[91] S. D. Mathur, The Fuzzball proposal for black holes: An Elementary review, *The quantum structure of space-time and the geometric nature of fundamental interactions. Proceedings, 4th Meeting, RTN2004, Kolymbari, Crete, Greece, September 5-10, 2004*, Fortsch. Phys. **53**, 793 (2005), arXiv:hep-th/0502050 [hep-th] .

[92] V. Cardoso, E. Franzin, and P. Pani, Is the gravitational-wave ringdown a probe of the event horizon?, Phys. Rev. Lett. **116**, 171101 (2016), arXiv:1602.07309 [gr-qc] .

[93] B. Holdom and J. Ren, Not quite a black hole, Phys. Rev. **D95**, 084034 (2017), arXiv:1612.04889 [gr-qc] .

[94] O. Dreyer, B. J. Kelly, B. Krishnan, L. S. Finn, D. Garrison, and R. Lopez-Aleman, Black hole spectroscopy: Testing general relativity through gravitational wave observations, Class. Quant. Grav. **21**, 787 (2004), arXiv:gr-qc/0309007 [gr-qc] .

[95] K. S. Thorne, R. Price, and D. Macdonald, eds., *BLACK HOLES: THE MEMBRANE PARADIGM* (1986).

[96] R. Price and K. Thorne, Membrane Viewpoint on Black Holes: Properties and Evolution of the Stretched Horizon, Phys. Rev. D **33**, 915 (1986).

[97] T. Jacobson, A. Mohd, and S. Sarkar, Membrane paradigm for Einstein-Gauss-Bonnet gravity, Phys. Rev. D **95**, 064036 (2017), arXiv:1107.1260 [gr-qc] .

[98] B. Bertotti, On gravitational motion, Nuovo Cim. **4**, 898 (1956).

[99] B. Bertotti and J. Plebanski, Theory of gravitational perturbations in the fast motion approximation, Annals Phys. **11**, 169 (1960).

[100] K. Westpfahl and M. Goller, GRAVITATIONAL SCATTERING OF TWO RELATIVISTIC PARTICLES IN POSTLINEAR APPROXIMATION, Lett. Nuovo Cim. **26**, 573 (1979).

[101] K. Westpfahl and H. Hoyler, Gravitational bremsstrahlung in post-linear fast-motion approximation, Lett. Nuovo Cim. **27**, 581 (1980).

[102] M. Portilla, SCATTERING OF TWO GRAVITATING PARTICLES: CLASSICAL APPROACH, J. Phys. A **13**, 3677 (1980).

[103] A. Rosenblum, Gravitational Radiation Energy Loss in Scattering Problems and the Einstein Quadrupole Formula, Phys. Lett. A **81**, 1 (1981).

[104] K. Westpfahl, High-Speed Scattering of Charged and Uncharged Particles in General Relativity, Fortsch. Phys. **33**, 417 (1985).

[105] K. Westpfahl, R. Mohles, and H. Simonis, Energy-momentum conservation for gravitational two-body scattering in the post-linear approximation, Class. Quant. Grav. **4**, L185 (1987).

[106] L. Bel, T. Damour, N. Deruelle, J. Ibanez, and J. Martin, Poincaré-invariant gravitational field and equations of motion of two pointlike objects: The postlinear approximation of general relativity, Gen. Rel. Grav. **13**, 963 (1981).

[107] T. Damour and N. Deruelle, Radiation Reaction and Angular Momentum Loss in Small Angle Gravitational Scattering, Phys. Lett. A **87**, 81 (1981).

[108] G. Schäfer, The adm hamiltonian at the postlinear approximation, General relativity and gravitation **18**, 255 (1986).

[109] T. Damour, Gravitational scattering, post-Minkowskian approximation and Effective One-Body theory, Phys. Rev. D **94**, 104015 (2016), arXiv:1609.00354 [gr-qc] .

[110] T. Damour, High-energy gravitational scattering and the general relativistic two-body problem, Phys. Rev. D **97**, 044038 (2018), arXiv:1710.10599 [gr-qc] .

[111] N. Arkani-Hamed, T.-C. Huang, and Y.-t. Huang, Scattering amplitudes for all masses and spins, JHEP **11**, 070, arXiv:1709.04891 [hep-th] .

[112] N. E. J. Bjerrum-Bohr, P. H. Damgaard, G. Festuccia, L. Planté, and P. Vanhove, General Relativity from Scattering Amplitudes, Phys. Rev. Lett. **121**, 171601 (2018), arXiv:1806.04920 [hep-th] .

[113] D. A. Kosower, B. Maybee, and D. O'Connell, Amplitudes, Observables, and Classical Scattering, JHEP **02**, 137, arXiv:1811.10950 [hep-th] .

[114] C. Cheung, I. Z. Rothstein, and M. P. Solon, From Scattering Amplitudes to Classical Potentials in the Post-Minkowskian Expansion, Phys. Rev. Lett. **121**, 251101 (2018), arXiv:1808.02489 [hep-th] .

[115] Y. F. Bautista and A. Guevara, From Scattering Amplitudes to Classical Physics: Universality, Double Copy and Soft Theorems, (2019), arXiv:1903.12419 [hep-th] .

[116] Z. Bern, C. Cheung, R. Roiban, C.-H. Shen, M. P. Solon, and M. Zeng, Scattering Amplitudes and the Conservative Hamiltonian for Binary Systems at Third Post-Minkowskian Order, Phys. Rev. Lett. **122**, 201603 (2019), arXiv:1901.04424 [hep-th] .

[117] N. E. J. Bjerrum-Bohr, A. Cristofoli, and P. H. Damgaard, Post-Minkowskian Scattering Angle in Einstein Gravity, JHEP **08**, 038, arXiv:1910.09366 [hep-th] .

[118] A. Cristofoli, P. H. Damgaard, P. Di Vecchia, and C. Heissenberg, Second-order Post-Minkowskian scattering in arbitrary dimensions, JHEP **07**, 122, arXiv:2003.10274 [hep-th] .

[119] Z. Bern, J. Parra-Martinez, R. Roiban, M. S. Ruf, C.-H. Shen, M. P. Solon, and M. Zeng, Scattering Amplitudes and Conservative Binary Dynamics at $O(G^4)$, Phys. Rev. Lett. **126**, 171601 (2021), arXiv:2101.07254 [hep-th] .

[120] Z. Bern, J. Parra-Martinez, R. Roiban, M. S. Ruf, C.-H. Shen, M. P. Solon, and M. Zeng, Scattering Amplitudes, the Tail Effect, and Conservative Binary Dynamics at $O(G^4)$, (2021), arXiv:2112.10750 [hep-th] .

[121] G. Travaglini *et al.*, The SAGEX Review on Scattering Amplitudes, (2022), arXiv:2203.13011 [hep-th] .

[122] N. E. J. Bjerrum-Bohr, P. H. Damgaard, L. Plante, and P. Vanhove, The SAGEX Review on Scattering Amplitudes, Chapter 13: Post-Minkowskian expansion from Scattering Amplitudes, (2022), arXiv:2203.13024 [hep-th] .

[123] D. A. Kosower, R. Monteiro, and D. O'Connell, The SAGEX Review on Scattering Amplitudes, Chapter 14: Classical Gravity from Scattering Amplitudes, (2022), arXiv:2203.13025 [hep-th] .

[124] G. Mogull, J. Plefka, and J. Steinhoff, Classical black hole scattering from a worldline quantum field theory, JHEP **02**, 048, arXiv:2010.02865 [hep-th] .

[125] G. U. Jakobsen, G. Mogull, J. Plefka, and J. Steinhoff, Classical Gravitational Bremsstrahlung from a Worldline Quantum Field Theory, Phys. Rev. Lett. **126**, 201103 (2021), arXiv:2101.12688 [gr-qc] .

[126] D. Bini and T. Damour, Gravitational spin-orbit coupling in binary systems, post-Minkowskian approximation and effective one-body theory, Phys. Rev. **D96**, 104038 (2017), arXiv:1709.00590 [gr-qc] .

[127] D. Bini and T. Damour, Gravitational spin-orbit coupling in binary systems at the second post-Minkowskian approximation, Phys. Rev. **D98**, 044036 (2018), arXiv:1805.10809 [gr-qc] .

[128] J. Vines, Scattering of two spinning black holes in post-Minkowskian gravity, to all orders in spin, and effective-one-body mappings, Class. Quant. Grav. **35**, 084002 (2018), arXiv:1709.06016 [gr-qc] .

[129] J. Vines, J. Steinhoff, and A. Buonanno, Spinning-black-hole scattering and the test-black-hole limit at second post-Minkowskian order, Phys. Rev. D **99**, 064054 (2019), arXiv:1812.00956 [gr-qc] .

[130] A. Guevara, A. Ochirov, and J. Vines, Black-hole scattering with general spin directions from minimal-coupling amplitudes, Phys. Rev. D **100**, 104024 (2019), arXiv:1906.10071 [hep-th] .

[131] G. Kälin and R. A. Porto, From boundary data to bound states. Part II. Scattering angle to dynamical invariants (with twist), JHEP **02**, 120, arXiv:1911.09130 [hep-th] .

[132] Z. Bern, A. Luna, R. Roiban, C.-H. Shen, and M. Zeng, Spinning black hole binary dynamics, scattering amplitudes, and effective field theory, Phys. Rev. D **104**, 065014 (2021), arXiv:2005.03071 [hep-th] .

[133] M.-Z. Chung, Y.-t. Huang, J.-W. Kim, and S. Lee, Complete Hamiltonian for spinning binary systems at first post-Minkowskian order, JHEP **05**, 105, arXiv:2003.06600 [hep-th] .

[134] B. Maybee, D. O'Connell, and J. Vines, Observables and amplitudes for spinning particles and black holes, JHEP **12**, 156, arXiv:1906.09260 [hep-th] .

[135] Y. F. Bautista, A. Guevara, C. Kavanagh, and J. Vines, Scattering in black hole backgrounds and higher-spin amplitudes. Part I, JHEP **03**, 136, arXiv:2107.10179 [hep-th] .

[136] D. Kosmopoulos and A. Luna, Quadratic-in-spin Hamiltonian at $\mathcal{O}(\mathrm{G}^2)$ from scattering amplitudes, JHEP **07**, 037, arXiv:2102.10137 [hep-th] .

[137] Z. Liu, R. A. Porto, and Z. Yang, Spin Effects in the Effective Field Theory Approach to Post-Minkowskian Conservative Dynamics, JHEP **06**, 012, arXiv:2102.10059 [hep-th] .

[138] G. U. Jakobsen, G. Mogull, J. Plefka, and J. Steinhoff, Gravitational Bremsstrahlung and Hidden Supersymmetry of Spinning Bodies, Phys. Rev. Lett. **128**, 011101 (2022), arXiv:2106.10256 [hep-th] .

[139] G. U. Jakobsen, G. Mogull, J. Plefka, and J. Steinhoff, SUSY in the sky with gravitons, JHEP **01**, 027, arXiv:2109.04465 [hep-th] .

[140] R. Aoude, K. Haddad, and A. Helset, Classical gravitational spinning-spinless scattering at $O(G^2S^\infty)$, (2022), arXiv:2205.02809 [hep-th] .

[141] G. U. Jakobsen, G. Mogull, J. Plefka, B. Sauer, and Y. Xu, Conservative Scattering of Spinning Black Holes at Fourth Post-Minkowskian Order, Phys. Rev. Lett. **131**, 151401 (2023), arXiv:2306.01714 [hep-th] .

[142] T. Damour, Radiative contribution to classical gravitational scattering at the third order in G, Phys. Rev. D **102**, 124008 (2020), arXiv:2010.01641 [gr-qc] .

[143] D. Bini, T. Damour, and A. Geralico, Radiative contributions to gravitational scattering, (2021), arXiv:2107.08896 [gr-qc] .

[144] D. Bini and A. Geralico, Higher-order tail contributions to the energy and angular momentum fluxes in a two-body scattering process, Phys. Rev. D **104**, 104020 (2021), arXiv:2108.05445 [gr-qc] .

[145] P. Di Vecchia, C. Heissenberg, R. Russo, and G. Veneziano, The Eikonal Approach to Gravitational Scattering and Radiation at $O(G^3)$, (2021), arXiv:2104.03256 [hep-th] .

[146] N. E. J. Bjerrum-Bohr, P. H. Damgaard, L. Planté, and P. Vanhove, The Amplitude for Classical Gravitational Scattering at Third Post-Minkowskian Order, (2021), arXiv:2105.05218 [hep-th] .

[147] A. Brandhuber, G. Chen, G. Travaglini, and C. Wen, Classical gravitational scattering from a gauge-invariant double copy, (2021), arXiv:2108.04216 [hep-th] .

[148] P. H. Damgaard, L. Plante, and P. Vanhove, On an exponential representation of the gravitational S-matrix, JHEP **11**, 213, arXiv:2107.12891 [hep-th] .

[149] E. Herrmann, J. Parra-Martinez, M. S. Ruf, and M. Zeng, Gravitational Bremsstrahlung from Reverse Unitarity, (2021), arXiv:2101.07255 [hep-th] .

[150] E. Herrmann, J. Parra-Martinez, M. S. Ruf, and M. Zeng, Radiative classical gravitational observables at $O(\mathrm{G}^3)$ from scattering amplitudes, JHEP **10**, 148, arXiv:2104.03957 [hep-th] .

[151] P. Di Vecchia, C. Heissenberg, R. Russo, and G. Veneziano, Radiation Reaction from Soft Theorems, Phys. Lett. B **818**, 136379 (2021), arXiv:2101.05772 [hep-th] .

[152] M. M. Riva and F. Vernizzi, Radiated momentum in the post-Minkowskian worldline approach via reverse unitarity, JHEP **11**, 228, arXiv:2110.10140 [hep-th] .

[153] G. Cho, G. Kälin, and R. A. Porto, From Boundary Data to Bound States III: Radiative Effects, (2021), arXiv:2112.03976 [hep-th] .

[154] A. V. Manohar, A. K. Ridgway, and C.-H. Shen, Radiated Angular Momentum and Dissipative Effects in Classical Scattering, (2022), arXiv:2203.04283 [hep-th] .

[155] G. U. Jakobsen, G. Mogull, J. Plefka, and B. Sauer, Dissipative Scattering of Spinning Black Holes at Fourth Post-Minkowskian Order, Phys. Rev. Lett. **131**, 241402 (2023), arXiv:2308.11514 [hep-th] .

[156] G. U. Jakobsen, G. Mogull, J. Plefka, and B. Sauer, Tidal effects and renormalization at fourth post-Minkowskian order, Phys. Rev. D **109**, L041504 (2024), arXiv:2312.00719 [hep-th] .

[157] M. Driesse, G. U. Jakobsen, G. Mogull, J. Plefka, B. Sauer, and J. Usovitsch, Conservative Black Hole Scattering at Fifth Post-Minkowskian and First Self-Force Order, Phys. Rev. Lett. **132**, 241402 (2024), arXiv:2403.07781 [hep-th] .

[158] A. Buonanno, G. U. Jakobsen, and G. Mogull, Post-Minkowskian theory meets the spinning effective-one-body approach for two-body scattering, Phys. Rev. D **110**, 044038 (2024), arXiv:2402.12342 [gr-qc] .

[159] A. Buonanno, G. Mogull, R. Patil, and L. Pompili, Post-Minkowskian Theory Meets the Spinning Effective-One-Body Approach for Bound-Orbit Waveforms, Phys. Rev. Lett. **133**, 211402 (2024), arXiv:2405.19181 [gr-qc] .

[160] C. V. Raman and K. S. Krishnan, A New Type of Secondary Radiation, **121**, 501 (1928).

[161] A. H. Compton, A quantum theory of the scattering of x-rays by light elements, Phys. Rev. **21**, 483 (1923).

[162] C. V. Vishveshwara, Scattering of Gravitational Radiation by a Schwarzschild Black-hole, Nature **227**, 936 (1970).

[163] P. C. Peters, Differential cross sections for weak-field gravitational scattering, Phys. Rev. D **13**, 775 (1976).

[164] R. A. Matzner and M. P. Ryan, Low Frequency Limit of Gravitational Scattering, Phys. Rev. D **16**, 1636 (1977).

[165] S. R. Dolan, Scattering of long-wavelength gravitational waves, Phys. Rev. D **77**, 044004 (2008), arXiv:0710.4252 [gr-qc] .

[166] S. R. Dolan, Scattering and Absorption of Gravitational Plane Waves by Rotating Black Holes, Class. Quant. Grav. **25**, 235002 (2008), arXiv:0801.3805 [gr-qc] .

[167] A. Guevara, Holomorphic Classical Limit for Spin Effects in Gravitational and Electromagnetic Scattering, JHEP **04**, 033, arXiv:1706.02314 [hep-th] .

[168] A. Guevara, A. Ochirov, and J. Vines, Scattering of Spinning Black Holes from Exponentiated Soft Factors, JHEP **09**, 056, arXiv:1812.06895 [hep-th] .

[169] M.-Z. Chung, Y.-T. Huang, J.-W. Kim, and S. Lee, The simplest massive S-matrix: from minimal coupling to Black Holes, JHEP **04**, 156, arXiv:1812.08752 [hep-th] .

[170] W.-M. Chen, M.-Z. Chung, Y.-t. Huang, and J.-W. Kim, The 2PM Hamiltonian for binary Kerr to quartic in spin, (2021), arXiv:2111.13639 [hep-th] .

[171] R. Aoude and A. Ochirov, Gravitational partial-wave absorption from scattering amplitudes, (2023), arXiv:2307.07504 [hep-th] .

[172] T. Scheopner and J. Vines, Dynamical Implications of the Kerr Multipole Moments for Spinning Black Holes, (2023), arXiv:2311.18421 [gr-qc] .

[173] Y. F. Bautista, A. Guevara, C. Kavanagh, and J. Vines, From Scattering in Black Hole Backgrounds to Higher-Spin Amplitudes: Part II (yet to be submitted), .

[174] Y. F. Bautista, A. Guevara, C. Kavanagh, and J. Vines, Scattering in black hole backgrounds and higher-spin amplitudes. Part II, JHEP **05**, 211, arXiv:2212.07965 [hep-th] .

[175] S. Chakrabarti, T. Delsate, and J. Steinhoff, New perspectives on neutron star and black hole spectroscopy and dynamic tides, (2013), arXiv:1304.2228 [gr-qc] .

[176] G. Creci, T. Hinderer, and J. Steinhoff, Tidal response from scattering and the role of analytic continuation, Phys. Rev. D **104**, 124061 (2021), [Erratum: Phys.Rev.D 105, 109902 (2022)], arXiv:2108.03385 [gr-qc] .

[177] B. P. Abbott *et al.* (The LIGO/Virgo Scientific Collaboration), Observation of Gravitational Waves from a Binary Black Hole Merger, Phys. Rev. Lett. **116**, 061102 (2016), arXiv:1602.03837 [gr-qc] .

[178] B. P. Abbott *et al.* (LIGO Scientific, Virgo), GW170817: Observation of Gravitational Waves from a Binary Neutron Star Inspiral, Phys. Rev. Lett. **119**, 161101 (2017), arXiv:1710.05832 [gr-qc] .

[179] A. Goldstein *et al.*, An Ordinary Short Gamma-Ray Burst with Extraordinary Implications: Fermi-GBM Detection of GRB 170817A, Astrophys. J. Lett. **848**, L14 (2017), arXiv:1710.05446 [astro-ph.HE] .

[180] V. Cardoso, S. Hopper, C. F. B. Macedo, C. Palenzuela, and P. Pani, Gravitational-wave signatures of exotic compact objects and of quantum corrections at the horizon scale, Phys. Rev. **D94**, 084031 (2016), arXiv:1608.08637 [gr-qc] .

[181] J. M. Lattimer and M. Prakash, Neutron Star Observations: Prognosis for Equation of State Constraints, Phys. Rept. **442**, 109 (2007), arXiv:astro-ph/0612440 [astro-ph] .

[182] W. D. Goldberger, Effective Field Theory for Compact Binary Dynamics, (2022), arXiv:2212.06677 [hep-th] .

[183] R. A. Porto, Post-Newtonian corrections to the motion of spinning bodies in NRGR, Phys. Rev. D **73**, 104031 (2006), arXiv:gr-qc/0511061 .

[184] S. Marsat, Cubic order spin effects in the dynamics and gravitational wave energy flux of compact object binaries, Class. Quant. Grav. **32**, 085008 (2015), arXiv:1411.4118 [gr-qc] .

[185] M. Mathisson, Neue mechanik materieller systemes, Acta Phys. Polon. **6**, 163 (1937).

[186] A. Papapetrou, Spinning test particles in general relativity. 1., Proc. Roy. Soc. Lond. A **209**, 248 (1951).

[187] W. G. Dixon, Dynamics of extended bodies in general relativity. I. Momentum and angular momentum, Proc. Roy. Soc. Lond. A **314**, 499 (1970).

[188] W. G. Dixon, Dynamics of extended bodies in general relativity. II. Moments of the charge-current vector, Proc. Roy. Soc. Lond. A **319**, 509 (1970).

[189] W. Tulczyjew, Equations of motion of rotating bodies in general relativity theory, Acta Phys. Polon. **18**, 37 (1959), [Erratum: Acta Phys. Polon. **18**, 534 (1959)].

[190] J. Steinhoff, Spin gauge symmetry in the action principle for classical relativistic particles, (2015), arXiv:1501.04951 [gr-qc] .

[191] W. Beiglböck, The center-of-mass in einstein's theory of gravitation, Communications in Mathematical Physics **5**, 106 (1967).

[192] W. G. Dixon, Dynamics of extended bodies in general relativity III. Equations of motion, Phil. Trans. Roy. Soc. Lond. A **277**, 59 (1974).

[193] A. E. H. Love, The Yielding of the Earth to Disturbing Forces, Proceedings of the Royal Society of London Series A **82**, 73 (1909).

[194] W. Munk and G. J. F. MacDonald, *The Rotation of the Earth: A Geophysical Discussion* (Cambridge University Press, 1960).

[195] E. Poisson and C. Will, *Gravity: Newtonian, Post-Newtonian, Relativistic* (Cambridge University Press, Cambridge, UK, 1953).

[196] D. Lai, Resonant oscillations and tidal heating in coalescing binary neutron stars, Mon. Not. Roy. Astron. Soc. **270**, 611 (1994), arXiv:astro-ph/9404062 .

[197] W. D. Goldberger and I. Z. Rothstein, Dissipative effects in the worldline approach to black hole dynamics, Phys. Rev. D **73**, 104030 (2006), arXiv:hep-th/0511133 .

[198] K. Chatziioannou, E. Poisson, and N. Yunes, Tidal heating and torquing of a Kerr black hole to next-to-leading order in the tidal coupling, Phys. Rev. D **87**, 044022 (2013), arXiv:1211.1686 [gr-qc] .

[199] H. Yu, P. Arras, and N. N. Weinberg, Dynamical tides during the inspiral of rapidly spinning neutron stars: Solutions beyond mode resonance, (2024), arXiv:2404.00147 [gr-qc] .

[200] J. Steinhoff, T. Hinderer, A. Buonanno, and A. Taracchini, Dynamical Tides in General Relativity: Effective Action and Effective-One-Body Hamiltonian, Phys. Rev. D **94**, 104028 (2016), arXiv:1608.01907 [gr-qc] .

[201] C. R. Galley, Classical mechanics of nonconservative systems, Phys. Rev. Lett. **110**, 174301 (2013).

[202] C. R. Galley and M. Tiglio, Radiation reaction and gravitational waves in the effective field theory approach, Phys. Rev. D **79**, 124027 (2009), arXiv:0903.1122 [gr-qc] .

[203] C. R. Galley and B.-L. Hu, New analytical methods for gravitational radiation and reaction in binaries with arbitrary mass ratio and relative velocity, in *6th Biennial Conference on Classical and Quantum Relativistic Dynamics of Particles and Fields* (2009) arXiv:0906.0968 [gr-qc] .

[204] O. Combaluzier-Szteinsznaider, L. Hui, L. Santoni, A. R. Solomon, and S. S. C. Wong, Symmetries of vanishing nonlinear Love numbers of Schwarzschild black holes, JHEP **03**, 124, arXiv:2410.10952 [gr-qc] .

[205] W. Israel, Event horizons in static vacuum space-times, Phys. Rev. **164**, 1776 (1967).

[206] B. Carter, Axisymmetric Black Hole Has Only Two Degrees of Freedom, Phys. Rev. Lett. **26**, 331 (1971).

[207] R. P. Kerr, Gravitational field of a spinning mass as an example of algebraically special metrics, Phys. Rev. Lett. **11**, 237 (1963).

[208] R. P. Geroch, Multipole moments. II. Curved space, J.Math.Phys. **11**, 2580 (1970).

[209] T. Regge and J. A. Wheeler, Stability of a Schwarzschild singularity, Phys. Rev. **108**, 1063 (1957).

[210] F. J. Zerilli, Effective potential for even parity Regge-Wheeler gravitational perturbation equations, Phys. Rev. Lett. **24**, 737 (1970).

[211] E. Newman and R. Penrose, An approach to gravitational radiation by a method of spin coefficients, Journal of Mathematical Physics **3**, 566 (1962).

[212] S. A. Teukolsky, Rotating black holes - separable wave equations for gravitational and electromagnetic perturbations, Phys. Rev. Lett. **29**, 1114 (1972).

[213] S. A. Teukolsky, Perturbations of a rotating black hole. 1. Fundamental equations for gravitational electromagnetic and neutrino field perturbations, Astrophys. J. **185**, 635 (1973).

[214] S. A. Teukolsky, Rotating black holes: Separable wave equations for gravitational and electromagnetic perturbations, Physical Review Letters **29**, 1114 (1972).

[215] W. H. Press and S. A. Teukolsky, Perturbations of a Rotating Black Hole. II. Dynamical Stability of the Kerr Metric, Astrophys. J. **185**, 649 (1973).

[216] S. Mano and E. Takasugi, Analytic solutions of the Teukolsky equation and their properties, Prog. Theor. Phys. **97**, 213 (1997), arXiv:gr-qc/9611014 .

[217] M. Sasaki and H. Tagoshi, Analytic black hole perturbation approach to gravitational radiation, Living Rev. Rel. **6**, 6 (2003), arXiv:gr-qc/0306120 .

[218] S. Mano, H. Suzuki, and E. Takasugi, Analytic solutions of the Regge-Wheeler equation and the postMinkowskian expansion, Prog. Theor. Phys. **96**, 549 (1996), arXiv:gr-qc/9605057 .

[219] M. Casals and A. C. Ottewill, High-order tail in Schwarzschild spacetime, Phys. Rev. D **92**, 124055 (2015), arXiv:1509.04702 [gr-qc] .

[220] J. M. Bardeen and W. H. Press, Radiation fields in the schwarzschild background, J. Math. Phys. **14**, 7 (1973).

[221] S. Chandrasekhar, ON THE EQUATIONS GOVERNING THE PERTURBATIONS OF THE REISSNER-NORDSTROM BLACK HOLE, Proc. Roy. Soc. Lond. A **365**, 453 (1979).

[222] M. M. Ivanov, Y.-Z. Li, J. Parra-Martinez, and Z. Zhou, Resummation of Universal Tails in Gravitational Waveforms, (2025), arXiv:2504.07862 [hep-th] .

[223] A. Pound and B. Wardell, Black hole perturbation theory and gravitational self-force 10.1007/978-981-15-4702-7_38-1 (2021), arXiv:2101.04592 [gr-qc] .

[224] G. W. Gibbons and K.-i. Maeda, Black Holes and Membranes in Higher Dimensional Theories with Dilaton Fields, Nucl. Phys. **B298**, 741 (1988).

[225] Z. Bern, A. Luna, and J. P. Gatica, Private communication, (2020).

[226] D. Bini and T. Damour, Gravitational radiation reaction along general orbits in the effective one-body formalism, Phys. Rev. D **86**, 124012 (2012), arXiv:1210.2834 [gr-qc] .

[227] G. Kälin and R. A. Porto, From Boundary Data to Bound States, JHEP **01**, 072, arXiv:1910.03008 [hep-th] .

[228] D. Bini, T. Damour, and A. Geralico, Sixth post-Newtonian nonlocal-in-time dynamics of binary systems, Phys. Rev. D **102**, 084047 (2020), arXiv:2007.11239 [gr-qc] .

[229] W. Junker and G. Schäfer, Binary systems: higher order gravitational radiation damping and wave emission, Mon. Not. Roy. Astron. Soc. **254**, 146 (1992).

[230] G. Schott, Electromagnetic radiation and the mechanical reactions arising from it, Nature **90**, 301 (1912).

[231] N. Arkani-Hamed, S. Dimopoulos, and G. R. Dvali, The Hierarchy problem and new dimensions at a millimeter, Phys. Lett. **B429**, 263 (1998), arXiv:hep-ph/9803315 [hep-ph] .

[232] P. C. Peters, Differential Cross-Sections for Weak Field Gravitational Scattering, Phys. Rev. D **13**, 775 (1976).

[233] R. Aoude, K. Haddad, and A. Helset, On-shell heavy particle effective theories, JHEP **05**, 051, arXiv:2001.09164 [hep-th] .

[234] J. M. Bardeen, B. Carter, and S. W. Hawking, The Four laws of black hole mechanics, Commun. Math. Phys. **31**, 161 (1973).

[235] E. Poisson and M. Sasaki, Gravitational radiation from a particle in circular orbit around a black hole. 5: Black hole absorption and tail corrections, Phys. Rev. D **51**, 5753 (1995), arXiv:gr-qc/9412027 .

[236] R. Penrose and R. M. Floyd, Extraction of rotational energy from a black hole, Nature **229**, 177 (1971).

[237] J. M. Bardeen, W. H. Press, and S. A. Teukolsky, Rotating black holes: Locally nonrotating frames, energy extraction, and scalar synchrotron radiation, Astrophys. J. **178**, 347 (1972).

[238] R. A. Porto, Absorption effects due to spin in the worldline approach to black hole dynamics, Phys. Rev. D **77**, 064026 (2008), arXiv:0710.5150 [hep-th] .

[239] S. Endlich and R. Penco, Effective field theory approach to tidal dynamics of spinning astrophysical systems, Phys. Rev. D **93**, 064021 (2016), arXiv:1510.08889 [gr-qc] .

[240] S. Endlich and R. Penco, A Modern Approach to Superradiance, JHEP **05**, 052, arXiv:1609.06723 [hep-th] .

[241] W. D. Goldberger and I. Z. Rothstein, Horizon radiation reaction forces, JHEP **10**, 026, arXiv:2007.00731 [hep-th] .

[242] D. N. Page, Particle Emission Rates from a Black Hole: Massless Particles from an Uncharged, Nonrotating Hole, Phys. Rev. D **13**, 198 (1976).

[243] H. S. Chia, Tidal deformation and dissipation of rotating black holes, Phys. Rev. D **104**, 024013 (2021), arXiv:2010.07300 [gr-qc] .

[244] A. Le Tiec, M. Casals, and E. Franzin, Tidal Love Numbers of Kerr Black Holes, Phys. Rev. D **103**, 084021 (2021), arXiv:2010.15795 [gr-qc] .

[245] M. M. Ivanov and Z. Zhou, Vanishing of Black Hole Tidal Love Numbers from Scattering Amplitudes, Phys. Rev. Lett. **130**, 091403 (2023), arXiv:2209.14324 [hep-th] .

[246] M. M. Ivanov and Z. Zhou, Black Hole Tidal Love Numbers and Dissipation Numbers in Worldline Effective Field Theory, (2022), arXiv:2208.08459 [hep-th] .

[247] M. M. Ivanov, Y.-Z. Li, J. Parra-Martinez, and Z. Zhou, Gravitational Raman Scattering in Effective Field Theory: A Scalar Tidal Matching at O(G3), Phys. Rev. Lett. **132**, 131401 (2024), arXiv:2401.08752 [hep-th] .

[248] S. Caron-Huot, M. Correia, G. Isabella, and M. Solon, Gravitational Wave Scattering via the Born Series: Scalar Tidal Matching to $O(G^7)$ and Beyond, (2025), arXiv:2503.13593 [hep-th] .

[249] W. D. Goldberger and A. Ross, Gravitational radiative corrections from effective field theory, Phys. Rev. D **81**, 124015 (2010), arXiv:0912.4254 [gr-qc] .

[250] S. Weinberg, Infrared photons and gravitons, Phys. Rev. **140**, B516 (1965).

[251] M. K. Mandal, P. Mastrolia, H. O. Silva, R. Patil, and J. Steinhoff, Renormalizing Love: tidal effects at the third post-Newtonian order, (2023), arXiv:2308.01865 [hep-th] .

[252] T. Hinderer, B. D. Lackey, R. N. Lang, and J. S. Read, Tidal deformability of neutron stars with realistic equations of state and their gravitational wave signatures in binary inspiral, Phys. Rev. **D81**, 123016 (2010), arXiv:0911.3535 [astro-ph.HE] .

[253] W. C. Ho and D. Lai, Resonant tidal excitations of rotating neutron stars in coalescing binaries, Mon. Not. Roy. Astron. Soc. **308**, 153 (1999), arXiv:astro-ph/9812116 [astro-ph] .

[254] L. Lindblom and S. L. Detweiler, The quadrupole oscillations of neutron stars, Astrophys. J. Suppl. **53**, 73 (1983).

[255] S. Chandrasekhar and V. Ferrari, On the non-radial oscillations of a star, Proceedings of the Royal Society of London Series A **432**, 247 (1991).

[256] K. D. Kokkotas and B. G. Schmidt, Quasinormal modes of stars and black holes, Living Rev. Rel. **2**, 2 (1999), arXiv:gr-qc/9909058 [gr-qc] .

[257] R. C. Tolman, Static solutions of Einstein's field equations for spheres of fluid, Phys. Rev. **55**, 364 (1939).

[258] G. I. Ogilvie, Tidal Dissipation in Stars and Giant Planets, ARA&A **52**, 171 (2014), arXiv:1406.2207 [astro-ph.SR] .

[259] C. Terquem, J. C. B. Papaloizou, R. P. Nelson, and D. N. C. Lin, On the tidal interaction of a solar-type star with an orbiting companion: excitation of g mode oscillation and orbital evolution, Astrophys. J. **502**, 788 (1998), arXiv:astro-ph/9801280 .

[260] A. Hegade K. R., J. L. Ripley, and N. Yunes, Dynamical tidal response of non-rotating relativistic stars, (2024), arXiv:2403.03254 [gr-qc] .

[261] C. Cutler and L. Lindblom, The Effect of Viscosity on Neutron Star Oscillations, The Astrophysical Journal **314**, 234 (1987).

[262] A. Buonanno, B. Iyer, E. Ochsner, Y. Pan, and B. S. Sathyaprakash, Comparison of post-Newtonian templates for compact binary inspiral signals in gravitational-wave detectors, Phys. Rev. D **80**, 084043 (2009), arXiv:0907.0700 [gr-qc] .

[263] K. G. Arun, A. Buonanno, G. Faye, and E. Ochsner, Higher-order spin effects in the amplitude and phase of gravitational waveforms emitted by inspiraling compact binaries: Ready-to-use gravitational waveforms, Phys. Rev. D **79**, 104023 (2009), [Erratum: Phys.Rev.D 84, 049901 (2011)], arXiv:0810.5336 [gr-qc] .

[264] S. Datta, K. S. Phukon, and S. Bose, Recognizing black holes in gravitational-wave observations: Challenges in telling apart impostors in mass-gap binaries, Phys. Rev. D **104**, 084006 (2021), arXiv:2004.05974 [gr-qc] .

[265] L. Blanchet, G. Faye, Q. Henry, F. Larrouturou, and D. Trestini, Gravitational waves from compact binaries to the fourth post-Newtonian order, in *57th Rencontres de Moriond on Gravitation* (2023) arXiv:2304.13647 [gr-qc] .

[266] W.-C. Chen and J. Piekarewicz, Building relativistic mean field models for finite nuclei and neutron stars, Phys. Rev. C **90**, 044305 (2014).

[267] N. K. Glendenning and S. A. Moszkowski, Reconciliation of neutron-star masses and binding of the λ in hypernuclei, Phys. Rev. Lett. **67**, 2414 (1991).

[268] N. Hornick, L. Tolos, A. Zacchi, J.-E. Christian, and J. Schaffner-Bielich, Relativistic parameterizations of neutron matter and implications for neutron stars, Phys. Rev. C **98**, 065804 (2018).

[269] W. Israel, Singular hypersurfaces and thin shells in general relativity, Nuovo Cim. **B44S10**, 1 (1966), [Nuovo Cim.B44,1(1966)].

[270] T. Damour, Black-hole eddy currents, Phys. Rev. D **18**, 3598 (1978).

[271] Y. Kojima, Equations governing the nonradial oscillations of a slowly rotating relativistic star, Phys. Rev. D **46**, 4289 (1992).

[272] Y. Kojima, Equations governing the nonradial oscillations of a slowly rotating relativistic star, Phys. Rev. D **46**, 4289 (1992).

[273] P. Pani, Advanced Methods in Black-Hole Perturbation Theory, Int. J. Mod. Phys. A **28**, 1340018 (2013), arXiv:1305.6759 [gr-qc] .

[274] `https://github.com/elisamaggio/ThorGW`.

[275] E. Maggio, V. Cardoso, S. R. Dolan, and P. Pani, Ergoregion instability of exotic compact objects: electromagnetic and gravitational perturbations and the role of absorption, Phys. Rev. **D99**, 064007 (2019), arXiv:1807.08840 [gr-qc] .

[276] B. P. Abbott *et al.* (LIGO Scientific, Virgo), Tests of general relativity with GW150914, Phys. Rev. Lett. **116**, 221101 (2016), [Erratum: Phys.Rev.Lett. 121, 129902 (2018)], arXiv:1602.03841 [gr-qc] .

[277] B. P. Abbott *et al.* (LIGO Scientific, Virgo), Binary Black Hole Mergers in the first Advanced LIGO Observing Run, Phys. Rev. X **6**, 041015 (2016), [Erratum: Phys.Rev.X 8, 039903 (2018)], arXiv:1606.04856 [gr-qc] .

[278] B. P. Abbott *et al.* (LIGO Scientific, Virgo), GW170817: Observation of Gravitational Waves from a Binary Neutron Star Inspiral, Phys. Rev. Lett. **119**, 161101 (2017), arXiv:1710.05832 [gr-qc] .

[279] R. Abbott *et al.* (LIGO Scientific, Virgo), GWTC-2: Compact Binary Coalescences Observed by LIGO and Virgo During the First Half of the Third Observing Run, (2020), arXiv:2010.14527 [gr-qc] .

[280] M. Punturo *et al.*, The Einstein Telescope: A third-generation gravitational wave observatory, *Proceedings, 14th Workshop on Gravitational wave data analysis (GWDAW-14): Rome, Italy, January 26-29, 2010*, Class. Quant. Grav. **27**, 194002 (2010).

[281] H. Audley, S. Babak, J. Baker, E. Barausse, P. Bender, E. Berti, P. Binetruy, M. Born, D. Bortoluzzi, J. Camp, C. Caprini, V. Cardoso, M. Colpi, J. Conklin, N. Cornish, C. Cutler, *et al.*, Laser Interferometer Space Antenna, ArXiv e-prints (2017), arXiv:1702.00786 [astro-ph.IM] .

[282] D. Reitze *et al.*, Cosmic Explorer: The U.S. Contribution to Gravitational-Wave Astronomy beyond LIGO, Bull. Am. Astron. Soc. **51**, 035 (2019), arXiv:1907.04833 [astro-ph.IM] .

[283] H. Kawai, D. C. Lewellen, and S. H. H. Tye, A Relation Between Tree Amplitudes of Closed and Open Strings, Nucl. Phys. **B269**, 1 (1986).

[284] Z. Bern, J. J. M. Carrasco, and H. Johansson, New Relations for Gauge-Theory Amplitudes, Phys. Rev. D **78**, 085011 (2008), arXiv:0805.3993 [hep-ph] .

[285] Z. Bern, J. J. M. Carrasco, and H. Johansson, Perturbative Quantum Gravity as a Double Copy of Gauge Theory, Phys. Rev. Lett. **105**, 061602 (2010), arXiv:1004.0476 [hep-th] .

[286] Z. Bern, J. J. Carrasco, M. Chiodaroli, H. Johansson, and R. Roiban, The Duality Between Color and Kinematics and its Applications, (2019), arXiv:1909.01358 [hep-th] .

[287] Z. Bern, C. Cheung, R. Roiban, C.-H. Shen, M. P. Solon, and M. Zeng, Black Hole Binary Dynamics from the Double Copy and Effective Theory, JHEP **10**, 206, arXiv:1908.01493 [hep-th] .

[288] Z. Bern, L. J. Dixon, D. C. Dunbar, and D. A. Kosower, One loop n point gauge theory amplitudes, unitarity and collinear limits, Nucl. Phys. B **425**, 217 (1994), arXiv:hep-ph/9403226 .

[289] Z. Bern, L. J. Dixon, D. C. Dunbar, and D. A. Kosower, Fusing gauge theory tree amplitudes into loop amplitudes, Nucl. Phys. B **435**, 59 (1995), arXiv:hep-ph/9409265 .

[290] R. Britto, F. Cachazo, and B. Feng, Generalized unitarity and one-loop amplitudes in N=4 super-Yang-Mills, Nucl. Phys. B **725**, 275 (2005), arXiv:hep-th/0412103 .

[291] C. Cheung and M. P. Solon, Classical gravitational scattering at $\mathcal{O}(G^3)$ from Feynman diagrams, JHEP **06**, 144, arXiv:2003.08351 [hep-th] .

[292] G. Kälin, Z. Liu, and R. A. Porto, Conservative Dynamics of Binary Systems to Third Post-Minkowskian Order from the Effective Field Theory Approach, Phys. Rev. Lett. **125**, 261103 (2020), arXiv:2007.04977 [hep-th] .

[293] T. Damour, Classical and quantum scattering in post-Minkowskian gravity, Phys. Rev. D **102**, 024060 (2020), arXiv:1912.02139 [gr-qc] .

[294] D. Amati, M. Ciafaloni, and G. Veneziano, Higher Order Gravitational Deflection and Soft Bremsstrahlung in Planckian Energy Superstring Collisions, Nucl. Phys. B **347**, 550 (1990).

[295] P. Di Vecchia, S. G. Naculich, R. Russo, G. Veneziano, and C. D. White, A tale of two exponentiations in $\mathcal{N} = 8$ supergravity at subleading level, JHEP **03**, 173, arXiv:1911.11716 [hep-th] .

[296] Z. Bern, H. Ita, J. Parra-Martinez, and M. S. Ruf, Universality in the classical limit of massless gravitational scattering, Phys. Rev. Lett. **125**, 031601 (2020), arXiv:2002.02459 [hep-th] .

[297] P. Di Vecchia, C. Heissenberg, R. Russo, and G. Veneziano, Universality of ultra-relativistic gravitational scattering, Phys. Lett. B **811**, 135924 (2020), arXiv:2008.12743 [hep-th] .

[298] C. Dlapa, G. Kälin, Z. Liu, and R. A. Porto, Dynamics of Binary Systems to Fourth Post-Minkowskian Order from the Effective Field Theory Approach, (2021), arXiv:2106.08276 [hep-th] .

[299] E. Poisson, An Introduction to the Lorentz-Dirac equation, (1999), arXiv:gr-qc/9912045 .

[300] L. Blanchet and G. Schaefer, Higher order gravitational radiation losses in binary systems, Monthly notices of the royal astronomical society **239**, 845 (1989).

[301] A. Einstein, The Field Equations of Gravitation, Sitzungsber. Preuss. Akad. Wiss. Berlin (Math. Phys.) **1915**, 844 (1915).

[302] J. Steinhoff and D. Puetzfeld, Multipolar equations of motion for extended test bodies in General Relativity, Phys. Rev. D **81**, 044019 (2010), arXiv:0909.3756 [gr-qc] .

[303] W. G. Dixon, A covariant multipole formalism for extended test bodies in general relativity, Il Nuovo Cimento (1955-1965) https://doi.org/10.1007/BF027345793 (1964).

[304] W. G. Dixon, The definition of multipole moments for extended bodies, General Relativity and Gravitation **4**, https://doi.org/10.1007/BF02412488 ().

[305] W. G. Dixon, Dynamics of extended bodies in general relativity III. Equations of motion, Philosophical Transactions of the Royal Society of London. Series A, Mathematical and Physical Sciences **277**, https://doi.org/10.1098/rsta.1974.0046 ().

[306] A. J. Hanson and T. Regge, The Relativistic Spherical Top, Annals Phys. **87**, 498 (1974).

[307] I. Bailey and W. Israel, Lagrangian Dynamics of Spinning Particles and Polarized Media in General Relativity, Commun. Math. Phys. **42**, 65 (1975).

[308] E. Poisson, Gravitational waves from inspiraling compact binaries: The Quadrupole moment term, Phys. Rev. D **57**, 5287 (1998), arXiv:gr-qc/9709032 .

[309] M. Levi, A. J. Mcleod, and M. Von Hippel, $\mathrm{N^3LO}$ gravitational spin-orbit coupling at order G^4, JHEP **07**, 115, arXiv:2003.02827 [hep-th] .

[310] A. Antonelli, C. Kavanagh, M. Khalil, J. Steinhoff, and J. Vines, Gravitational spin-orbit coupling through third-subleading post-Newtonian order: from first-order self-force to arbitrary mass ratios, Phys. Rev. Lett. **125**, 011103 (2020), arXiv:2003.11391 [gr-qc] .

[311] M. Levi, A. J. Mcleod, and M. Von Hippel, N^{3}LO gravitational quadratic-in-spin interactions at G^4, JHEP **07**, 116, arXiv:2003.07890 [hep-th] .

[312] A. Antonelli, C. Kavanagh, M. Khalil, J. Steinhoff, and J. Vines, Gravitational spin-orbit and aligned spin_1-spin_2 couplings through third-subleading post-Newtonian orders, Phys. Rev. D **102**, 124024 (2020), arXiv:2010.02018 [gr-qc] .

[313] J.-W. Kim, M. Levi, and Z. Yin, Quadratic-in-spin interactions at fifth post-Newtonian order probe new physics, (2021), arXiv:2112.01509 [hep-th] .

[314] M. Levi, S. Mougiakakos, and M. Vieira, Gravitational cubic-in-spin interaction at the next-to-leading post-Newtonian order, JHEP **01**, 036, arXiv:1912.06276 [hep-th] .

[315] M. Levi and F. Teng, NLO gravitational quartic-in-spin interaction, JHEP **01**, 066, arXiv:2008.12280 [hep-th] .

[316] G. Kälin and R. A. Porto, Post-Minkowskian Effective Field Theory for Conservative Binary Dynamics, JHEP **11**, 106, arXiv:2006.01184 [hep-th] .

[317] C. Dlapa, G. Kälin, Z. Liu, and R. A. Porto, Conservative Dynamics of Binary Systems at Fourth Post-Minkowskian Order in the Large-Eccentricity Expansion, Phys. Rev. Lett. **128**, 161104 (2022), arXiv:2112.11296 [hep-th] .

[318] G. U. Jakobsen and G. Mogull, Conservative and Radiative Dynamics of Spinning Bodies at Third Post-Minkowskian Order Using Worldline Quantum Field Theory, Phys. Rev. Lett. **128**, 141102 (2022), arXiv:2201.07778 [hep-th] .

[319] G. Kälin, J. Neef, and R. A. Porto, Radiation-reaction in the Effective Field Theory approach to Post-Minkowskian dynamics, JHEP **01**, 140, arXiv:2207.00580 [hep-th] .

[320] G. U. Jakobsen, G. Mogull, J. Plefka, and B. Sauer, All Things Retarded: Radiation-Reaction in Worldline Quantum Field Theory, (2022), arXiv:2207.00569 [hep-th] .

[321] V. Vaidya, Gravitational spin Hamiltonians from the S matrix, Phys. Rev. D **91**, 024017 (2015), arXiv:1410.5348 [hep-th] .

[322] Z. Bern, D. Kosmopoulos, A. Luna, R. Roiban, and F. Teng, Binary Dynamics Through the Fifth Power of Spin at $O(G^2)$, (2022), arXiv:2203.06202 [hep-th] .

[323] Y. F. Bautista and A. Guevara, On the double copy for spinning matter, JHEP **11**, 184, arXiv:1908.11349 [hep-th] .

[324] H. Johansson and A. Ochirov, Double copy for massive quantum particles with spin, JHEP **09**, 040, arXiv:1906.12292 [hep-th] .

[325] R. Aoude, K. Haddad, and A. Helset, Searching for Kerr in the 2PM amplitude, JHEP **07**, 072, arXiv:2203.06197 [hep-th] .

[326] M. Chiodaroli, H. Johansson, and P. Pichini, Compton black-hole scattering for s $\leq$ 5/2, JHEP **02**, 156, arXiv:2107.14779 [hep-th] .

[327] W.-M. Chen, M.-Z. Chung, Y.-t. Huang, and J.-W. Kim, Lense-Thirring effects from on-shell amplitudes, (2022), arXiv:2205.07305 [hep-th] .

[328] J. Vines and J. Steinhoff, Spin-multipole effects in binary black holes and the test-body limit, Phys. Rev. D **97**, 064010 (2018), arXiv:1606.08832 [gr-qc] .

[329] A. I. Harte and J. Vines, Generating exact solutions to Einstein's equation using linearized approximations, Phys. Rev. D **94**, 084009 (2016), arXiv:1608.04359 [gr-qc] .

[330] N. Siemonsen and J. Vines, Test black holes, scattering amplitudes and perturbations of Kerr spacetime, Phys. Rev. D **101**, 064066 (2020), arXiv:1909.07361 [gr-qc] .

[331] J. Vines, D. Kunst, J. Steinhoff, and T. Hinderer, Canonical Hamiltonian for an extended test body in curved spacetime: To quadratic order in spin, Phys. Rev. D **93**, 103008 (2016), [Erratum: Phys.Rev.D 104, 029902 (2021)], arXiv:1601.07529 [gr-qc] .

[332] T. Damour and G. Esposito-Farese, Gravitational wave versus binary - pulsar tests of strong field gravity, Phys. Rev. D **58**, 042001 (1998), arXiv:gr-qc/9803031 .

[333] E. Guadagnini, Gravitational deflection of light and helicity asymmetry, Phys. Lett. B **548**, 19 (2002), arXiv:gr-qc/0207036 .

[334] E. Guadagnini, Gravitons scattering from classical matter, Class. Quant. Grav. **25**, 095012 (2008), arXiv:0803.2855 [gr-qc] .

[335] R. Abbott *et al.* (LIGO Scientific, VIRGO, KAGRA), GWTC-3: Compact Binary Coalescences Observed by LIGO and Virgo During the Second Part of the Third Observing Run, (2021), arXiv:2111.03606 [gr-qc] .

[336] M. Saleem *et al.*, The science case for LIGO-India, Class. Quant. Grav. **39**, 025004 (2022), arXiv:2105.01716 [gr-qc] .

[337] B. P. Abbott *et al.* (LIGO Scientific), Exploring the Sensitivity of Next Generation Gravitational Wave Detectors, Class. Quant. Grav. **34**, 044001 (2017), arXiv:1607.08697 [astro-ph.IM] .

[338] M. Punturo *et al.*, The third generation of gravitational wave observatories and their science reach, Class. Quant. Grav. **27**, 084007 (2010).

[339] P. Amaro-Seoane *et al.* (LISA), Laser Interferometer Space Antenna, (2017), arXiv:1702.00786 [astro-ph.IM] .

[340] M. Pürrer and C.-J. Haster, Gravitational waveform accuracy requirements for future ground-based detectors, Phys. Rev. Res. **2**, 023151 (2020), arXiv:1912.10055 [gr-qc] .

[341] S. W. Hawking, Black holes in general relativity, Commun. Math. Phys. **25**, 152 (1972).

[342] P. Meszaros and M. J. Rees, Tidal heating and mass loss in neutron star binaries - Implications for gamma-ray burst models, Astrophys. J. **397**, 570 (1992).

[343] A. Maselli, P. Pani, V. Cardoso, T. Abdelsalhin, L. Gualtieri, and V. Ferrari, Probing Planckian corrections at the horizon scale with LISA binaries, Phys. Rev. Lett. **120**, 081101 (2018), arXiv:1703.10612 [gr-qc] .

[344] S. Datta, R. Brito, S. Bose, P. Pani, and S. A. Hughes, Tidal heating as a discriminator for horizons in extreme mass ratio inspirals, Phys. Rev. D **101**, 044004 (2020), arXiv:1910.07841 [gr-qc] .

[345] S. Datta and S. Bose, Probing the nature of central objects in extreme-mass-ratio inspirals with gravitational waves, (2019), arXiv:1902.01723 [gr-qc] .

[346] S. Mukherjee, S. Datta, S. Tiwari, K. S. Phukon, and S. Bose, Toward establishing the presence or absence of horizons in coalescing binaries of compact objects by using their gravitational wave signals, Phys. Rev. D **106**, 104032 (2022), arXiv:2202.08661 [gr-qc] .

[347] A. Nagar and S. Akcay, Horizon-absorbed energy flux in circularized, nonspinning black-hole binaries and its effective-one-body representation, Phys. Rev. **D85**, 044025 (2012), arXiv:1112.2840 [gr-qc] .

[348] S. Bernuzzi, A. Nagar, and A. Zenginoglu, Horizon-absorption effects in coalescing black-hole binaries: An effective-one-body study of the non-spinning case, Phys. Rev. D **86**, 104038 (2012), arXiv:1207.0769 [gr-qc] .

[349] A. Taracchini, A. Buonanno, S. A. Hughes, and G. Khanna, Modeling the horizon-absorbed gravitational flux for equatorial-circular orbits in Kerr spacetime, Phys. Rev. D **88**, 044001 (2013), [Erratum: Phys.Rev.D 88, 109903 (2013)], arXiv:1305.2184 [gr-qc] .

[350] D. Brown, S. Fairhurst, B. Krishnan, R. A. Mercer, R. K. Kopparapu, L. Santamaria, and J. T. Whelan, Data formats for numerical relativity waves, (2007), arXiv:0709.0093 [gr-qc] .

[351] S. Isoyama and H. Nakano, Post-Newtonian templates for binary black-hole inspirals: the effect of the horizon fluxes and the secular change in the black-hole masses and spins, Class. Quant. Grav. **35**, 024001 (2018), arXiv:1705.03869 [gr-qc] .

[352] W. D. Goldberger, A. Ross, and I. Z. Rothstein, Black hole mass dynamics and renormalization group evolution, Phys. Rev. D **89**, 124033 (2014), arXiv:1211.6095 [hep-th] .

[353] L. V. Delacrétaz, S. Endlich, A. Monin, R. Penco, and F. Riva, (Re-)Inventing the Relativistic Wheel: Gravity, Cosets, and Spinning Objects, JHEP **11**, 008, arXiv:1405.7384 [hep-th] .

[354] P. K. Gupta, J. Steinhoff, and T. Hinderer, Relativistic effective action of dynamical gravitomagnetic tides for slowly rotating neutron stars, Phys. Rev. Res. **3**, 013147 (2021), arXiv:2011.03508 [gr-qc] .

[355] R. A. Matzner and J. Ryan, M. P., Scattering of gravitational radiation from vacuum black holes., APJS **36**, 451 (1978).

[356] A. G. Shah, Gravitational-wave flux for a particle orbiting a Kerr black hole to 20th post-Newtonian order: a numerical approach, Phys. Rev. D **90**, 044025 (2014), arXiv:1403.2697 [gr-qc] .

[357] R. Fujita, Gravitational radiation for extreme mass ratio inspirals to the 14th post-Newtonian order, Prog. Theor. Phys. **127**, 583 (2012), arXiv:1104.5615 [gr-qc] .

[358] R. Fujita, Gravitational Waves from a Particle in Circular Orbits around a Rotating Black Hole to the 11th Post-Newtonian Order, PTEP **2015**, 033E01 (2015), arXiv:1412.5689 [gr-qc] .

[359] B. S. Sathyaprakash and S. V. Dhurandhar, Choice of filters for the detection of gravitational waves from coalescing binaries, Phys. Rev. D **44**, 3819 (1991).

[360] A. K. Mehta, A. Buonanno, R. Cotesta, A. Ghosh, N. Sennett, and J. Steinhoff, Tests of general relativity with gravitational-wave observations using a flexible theory-independent method, Phys. Rev. D **107**, 044020 (2023), arXiv:2203.13937 [gr-qc] .

[361] L. Blanchet, G. Faye, B. R. Iyer, and B. Joguet, Gravitational wave inspiral of compact binary systems to 7/2 postNewtonian order, Phys. Rev. D **65**, 061501 (2002), [Erratum: Phys.Rev.D 71, 129902 (2005)], arXiv:gr-qc/0105099 .

[362] E. E. Flanagan and T. Hinderer, Constraining neutron star tidal Love numbers with gravitational wave detectors, Phys. Rev. **D77**, 021502 (2008), arXiv:0709.1915 [astro-ph] .

[363] A. Buonanno, M. Khalil, D. O'Connell, R. Roiban, M. P. Solon, and M. Zeng, Snowmass White Paper: Gravitational Waves and Scattering Amplitudes, in *Snowmass 2021* (2022) arXiv:2204.05194 [hep-th] .

[364] J. Vines, E. E. Flanagan, and T. Hinderer, Post-1-Newtonian tidal effects in the gravitational waveform from binary inspirals, Phys. Rev. **D83**, 084051 (2011), arXiv:1101.1673 [gr-qc] .

[365] D. Bini, T. Damour, and G. Faye, Effective action approach to higher-order relativistic tidal interactions in binary systems and their effective one body description, Phys. Rev. D **85**, 124034 (2012), arXiv:1202.3565 [gr-qc] .

[366] A. E. H. Love, The yielding of the earth to disturbing forces, Proceedings of the Royal Society of London. Series A, Containing Papers of a Mathematical and Physical Character **82**, 73 (1909).

[367] E. Poisson and C. M. Will, Gravity, Gravity (2014).

[368] H. Fang and G. Lovelace, Tidal coupling of a Schwarzschild black hole and circularly orbiting moon, Phys. Rev. **D72**, 124016 (2005), arXiv:gr-qc/0505156 [gr-qc] .

[369] E. Poisson, Tidal deformation of a slowly rotating black hole, Phys. Rev. **D91**, 044004 (2015), arXiv:1411.4711 [gr-qc] .

[370] P. Landry and E. Poisson, Tidal deformation of a slowly rotating material body. External metric, Phys. Rev. **D91**, 104018 (2015), arXiv:1503.07366 [gr-qc] .

[371] P. Landry and E. Poisson, Dynamical response to a stationary tidal field, Phys. Rev. D **92**, 124041 (2015), arXiv:1510.09170 [gr-qc] .

[372] E. Poisson, Gravitomagnetic Love tensor of a slowly rotating body: post-Newtonian theory, Phys. Rev. D **102**, 064059 (2020), arXiv:2007.01678 [gr-qc] .

[373] E. Poisson, Compact body in a tidal environment: New types of relativistic Love numbers, and a post-Newtonian operational definition for tidally induced multipole moments, Phys. Rev. D **103**, 064023 (2021), arXiv:2012.10184 [gr-qc] .

[374] A. Le Tiec and M. Casals, Spinning Black Holes Fall in Love, Phys. Rev. Lett. **126**, 131102 (2021), arXiv:2007.00214 [gr-qc] .

[375] E. Poisson, Tidally induced multipole moments of a nonrotating black hole vanish to all post-Newtonian orders, Phys. Rev. D **104**, 104062 (2021), arXiv:2108.07328 [gr-qc] .

[376] I. Z. Rothstein, Progress in effective field theory approach to the binary inspiral problem, Gen. Rel. Grav. **46**, 1726 (2014).

[377] W. D. Goldberger, Effective field theories of gravity and compact binary dynamics: A Snowmass 2021 whitepaper, in *Snowmass 2021* (2022) arXiv:2206.14249 [hep-th] .

[378] B. Kol and M. Smolkin, Black hole stereotyping: Induced gravito-static polarization, JHEP **02**, 010, arXiv:1110.3764 [hep-th] .

[379] L. Hui, A. Joyce, R. Penco, L. Santoni, and A. R. Solomon, Static response and Love numbers of Schwarzschild black holes, JCAP **04**, 052, arXiv:2010.00593 [hep-th] .

[380] P. Charalambous, S. Dubovsky, and M. M. Ivanov, On the Vanishing of Love Numbers for Kerr Black Holes, JHEP **05**, 038, arXiv:2102.08917 [hep-th] .

[381] R. A. Porto, New results at 3PN via an effective field theory of gravity, in *11th Marcel Grossmann Meeting on General Relativity* (2007) pp. 2493–2496, arXiv:gr-qc/0701106 .

[382] J. Steinhoff, S. Hergt, and G. Schaefer, On the next-to-leading order gravitational spin(1)-spin(2) dynamics, Phys. Rev. D **77**, 081501 (2008), arXiv:0712.1716 [gr-qc] .

[383] R. A. Porto and I. Z. Rothstein, Next to Leading Order Spin(1)Spin(1) Effects in the Motion of Inspiralling Compact Binaries, Phys. Rev. D **78**, 044013 (2008), [Erratum: Phys.Rev.D 81, 029905 (2010)], arXiv:0804.0260 [gr-qc] .

[384] R. A. Porto and I. Z. Rothstein, Spin(1)Spin(2) Effects in the Motion of Inspiralling Compact Binaries at Third Order in the Post-Newtonian Expansion, Phys. Rev. D **78**, 044012 (2008), [Erratum: Phys.Rev.D 81, 029904 (2010)], arXiv:0802.0720 [gr-qc] .

[385] R. A. Porto, Next to leading order spin-orbit effects in the motion of inspiralling compact binaries, Class. Quant. Grav. **27**, 205001 (2010), arXiv:1005.5730 [gr-qc] .

[386] R. A. Porto, A. Ross, and I. Z. Rothstein, Spin induced multipole moments for the gravitational wave flux from binary inspirals to third Post-Newtonian order, JCAP **03**, 009, arXiv:1007.1312 [gr-qc] .

[387] H. Wang, J. Steinhoff, J. Zeng, and G. Schafer, Leading-order spin-orbit and spin(1)-spin(2) radiation-reaction Hamiltonians, Phys. Rev. D **84**, 124005 (2011), arXiv:1109.1182 [gr-qc] .

[388] J. Hartung and J. Steinhoff, Next-to-next-to-leading order post-Newtonian spin(1)-spin(2) Hamiltonian for self-gravitating binaries, Annalen Phys. **523**, 919 (2011), arXiv:1107.4294 [gr-qc] .

[389] J. Hartung and J. Steinhoff, Next-to-next-to-leading order post-Newtonian spin-orbit Hamiltonian for self-gravitating binaries, Annalen Phys. **523**, 783 (2011), arXiv:1104.3079 [gr-qc] .

[390] R. A. Porto, A. Ross, and I. Z. Rothstein, Spin induced multipole moments for the gravitational wave amplitude from binary inspirals to 2.5 Post-Newtonian order, JCAP **09**, 028, arXiv:1203.2962 [gr-qc] .

[391] J. Steinhoff, Spin and quadrupole contributions to the motion of astrophysical binaries, Fund. Theor. Phys. **179**, 615 (2015), arXiv:1412.3251 [gr-qc] .

[392] M. Levi and J. Steinhoff, Leading order finite size effects with spins for inspiralling compact binaries, JHEP **06**, 059, arXiv:1410.2601 [gr-qc] .

[393] M. Levi and J. Steinhoff, Complete conservative dynamics for inspiralling compact binaries with spins at the fourth post-Newtonian order, JCAP **09**, 029, arXiv:1607.04252 [gr-qc] .

[394] N. Siemonsen, J. Steinhoff, and J. Vines, Gravitational waves from spinning binary black holes at the leading post-Newtonian orders at all orders in spin, Phys. Rev. D **97**, 124046 (2018), arXiv:1712.08603 [gr-qc] .

[395] G. Cho, R. A. Porto, and Z. Yang, Gravitational radiation from inspiralling compact objects: Spin effects to the fourth post-Newtonian order, Phys. Rev. D **106**, L101501 (2022), arXiv:2201.05138 [gr-qc] .

[396] J.-W. Kim, M. Levi, and Z. Yin, N^3LO spin-orbit interaction via the EFT of spinning gravitating objects, JHEP **05**, 184, arXiv:2208.14949 [hep-th] .

[397] M. Levi, R. Morales, and Z. Yin, From the EFT of Spinning Gravitating Objects to Poincaré and Gauge Invariance at the 4.5PN Precision Frontier, (2022), arXiv:2210.17538 [hep-th] .

[398] J.-W. Kim, M. Levi, and Z. Yin, N^3LO quadratic-in-spin interactions for generic compact binaries, JHEP **03**, 098, arXiv:2209.09235 [hep-th] .

[399] M. Levi and Z. Yin, Completing the fifth PN precision frontier via the EFT of spinning gravitating objects, JHEP **04**, 079, arXiv:2211.14018 [hep-th] .

[400] R. A. Porto, The Tune of Love and the Nature(ness) of Spacetime, Fortsch. Phys. **64**, 723 (2016), arXiv:1606.08895 [gr-qc] .

[401] P. Charalambous, S. Dubovsky, and M. M. Ivanov, Love symmetry, JHEP **10**, 175, arXiv:2209.02091 [hep-th] .

[402] L. Hui, A. Joyce, R. Penco, L. Santoni, and A. R. Solomon, Ladder symmetries of black holes. Implications for love numbers and no-hair theorems, JCAP **01** (01), 032, arXiv:2105.01069 [hep-th] .

[403] M. M. Ivanov and Z. Zhou, Near-Far Factorization in Black Hole Scattering Amplitudes, *in preparation* .

[404] P. Charalambous and M. M. Ivanov, Scalar Love numbers and Love symmetries of 5-dimensional Myers-Perry black hole, (2023), arXiv:2303.16036 [hep-th] .

[405] M. J. Rodriguez, L. Santoni, A. R. Solomon, and L. F. Temoche, Love Numbers for Rotating Black Holes in Higher Dimensions, (2023), arXiv:2304.03743 [hep-th] .

[406] M. Cvetic, G. W. Gibbons, C. N. Pope, and B. F. Whiting, Supergravity black holes, Love numbers, and harmonic coordinates, Phys. Rev. D **105**, 084035 (2022), arXiv:2109.03254 [gr-qc] .

[407] V. De Luca, J. Khoury, and S. S. C. Wong, Non-linearities in the tidal Love numbers of black holes, (2023), arXiv:2305.14444 [gr-qc] .

[408] P. Charalambous, S. Dubovsky, and M. M. Ivanov, Hidden Symmetry of Vanishing Love Numbers, Phys. Rev. Lett. **127**, 101101 (2021), arXiv:2103.01234 [hep-th] .

[409] L. Hui, A. Joyce, R. Penco, L. Santoni, and A. R. Solomon, Near-Zone Symmetries of Kerr Black Holes, (2022), arXiv:2203.08832 [hep-th] .

[410] A. A. Starobinsky, Amplification of waves reflected from a rotating ''black hole''., Sov. Phys. JETP **37**, 28 (1973).

[411] A. A. Starobinskil and S. M. Churilov, Amplification of electromagnetic and gravitational waves scattered by a rotating ''black hole'', Sov. Phys. JETP **65**, 1 (1974).

[412] J. M. Maldacena and A. Strominger, Black hole grey body factors and d-brane spectroscopy, Phys. Rev. D **55**, 861 (1997), arXiv:hep-th/9609026 .

[413] J. Steinhoff, T. Hinderer, T. Dietrich, and F. Foucart, Spin effects on neutron star fundamental-mode dynamical tides: Phenomenology and comparison to numerical simulations, Phys. Rev. Res. **3**, 033129 (2021), arXiv:2103.06100 [gr-qc] .

[414] P. K. Gupta, J. Steinhoff, and T. Hinderer, Effect of dynamical gravitomagnetic tides on measurability of tidal parameters for binary neutron stars using gravitational waves, Phys. Rev. D **108**, 124040 (2023), arXiv:2302.11274 [gr-qc] .

[415] M. K. Mandal, P. Mastrolia, H. O. Silva, R. Patil, and J. Steinhoff, Gravitoelectric dynamical tides at second post-Newtonian order, (2023), arXiv:2304.02030 [hep-th] .

[416] J.-W. Kim and M. Shim, Quantum corrections to tidal Love number for Schwarzschild black holes, Phys. Rev. D **104**, 046022 (2021), arXiv:2011.03337 [hep-th] .

[417] N. Andersson, *Gravitational-Wave Astronomy*, Oxford Graduate Texts (Oxford University Press, 2019).

[418] Y. Rathore, A. E. Broderick, and R. Blandford, A variational formalism for tidal excitation: non-rotating, homentropic stars, Monthly Notices of the Royal Astronomical Society **339**, 25 (2003).

[419] E. E. Flanagan and E. Racine, Gravitomagnetic resonant excitation of Rossby modes in coalescing neutron star binaries, Phys. Rev. D **75**, 044001 (2007), arXiv:gr-qc/0601029 .

[420] S. Ma, H. Yu, and Y. Chen, Detecting resonant tidal excitations of Rossby modes in coalescing neutron-star binaries with third-generation gravitational-wave detectors, Phys. Rev. D **103**, 063020 (2021), arXiv:2010.03066 [gr-qc] .

[421] E. Poisson, Gravitomagnetic tidal resonance in neutron-star binary inspirals, Phys. Rev. D **101**, 104028 (2020), arXiv:2003.10427 [gr-qc] .

[422] S. Mano, H. Suzuki, and E. Takasugi, Analytic solutions of the Teukolsky equation and their low frequency expansions, Prog. Theor. Phys. **95**, 1079 (1996), arXiv:gr-qc/9603020 .

[423] L. Blanchet and G. Schaefer, Gravitational wave tails and binary star systems, Class. Quant. Grav. **10**, 2699 (1993).

[424] L. Bel, Definition dune densite denergie et dun etat de radiation totale generalisee, COMPTES RENDUS HEBDOMADAIRES DES SEANCES DE L ACADEMIE DES SCIENCES **246**, 3015 (1958).

[425] M. Mathisson, *Neue mechanik materieller systeme* (1937).

[426] E. Corinaldesi and A. Papapetrou, Spinning test particles in general relativity. 2., Proc. Roy. Soc. Lond. A **209**, 259 (1951).

[427] B. Modrekiladze, Gravitational wave signals from finite size effects in spinning binary inspirals including parity violating constituents, JHEP **03**, 019, arXiv:2204.00028 [hep-th] .

[428] D. N. Page, Particle Emission Rates from a Black Hole. 2. Massless Particles from a Rotating Hole, Phys. Rev. D **14**, 3260 (1976).

[429] J. M. Maldacena and A. Strominger, Universal low-energy dynamics for rotating black holes, Phys. Rev. D **56**, 4975 (1997), arXiv:hep-th/9702015 .

[430] I. Bredberg, T. Hartman, W. Song, and A. Strominger, Black Hole Superradiance From Kerr/CFT, JHEP **04**, 019, arXiv:0907.3477 [hep-th] .

[431] R. A. Matzner, Scattering of massless scalar waves by a schwarzschild‘‘singularity’’, Journal of Mathematical Physics **9**, 163 (1968).

[432] P. L. Chrzanowski, R. A. Matzner, V. D. Sandberg, and M. P. Ryan, Zero Mass Plane Waves in Nonzero Gravitational Backgrounds, Phys. Rev. D **14**, 317 (1976).

[433] F. A. Handler and R. A. Matzner, GRAVITATIONAL WAVE SCATTERING, Phys. Rev. D **22**, 2331 (1980).

[434] J. A. H. Futterman, F. A. Handler, and R. A. Matzner, *SCATTERING FROM BLACK HOLES*, Cambridge Monographs on Mathematical Physics (Cambridge University Press, 2012).

[435] K. Glampedakis and N. Andersson, Scattering of scalar waves by rotating black holes, Class. Quant. Grav. **18**, 1939 (2001), arXiv:gr-qc/0102100 .

[436] T. Stratton, L. C. S. Leite, S. R. Dolan, and L. C. B. Crispino, Series reduction method for scattering of planar waves by Kerr black holes, Phys. Rev. D **102**, 044025 (2020), arXiv:2004.10773 [gr-qc] .

[437] S. A. Teukolsky and W. Press, Perturbations of a rotating black hole. iii-interaction of the hole with gravitational and electromagnetic radiation, The Astrophysical Journal **193**, 443 (1974).

[438] L. J. El-Jaick and B. D. Figueiredo, Solutions for confluent and double-confluent heun equations, Journal of Mathematical Physics **49**, 083508 (2008).

[439] Y. B. Zel’Dovich, Generation of waves by a rotating body, Soviet Journal of Experimental and Theoretical Physics Letters **14**, 180 (1971).

[440] W. D. Goldberger and I. Z. Rothstein, Virtual Hawking Radiation, Phys. Rev. Lett. **125**, 211301 (2020), arXiv:2007.00726 [hep-th] .

[441] `https://github.com/ZihanZhou26/Constant-Piece-of-RG-for-Dynamical-Tidal-Response`.

[442] J. L. Ripley, A. Hegade K. R., and N. Yunes, Probing internal dissipative processes of neutron stars with gravitational waves during the inspiral of neutron star binaries, Phys. Rev. D **108**, 103037 (2023), arXiv:2306.15633 [gr-qc] .

[443] E. R. Most, S. P. Harris, C. Plumberg, M. G. Alford, J. Noronha, J. Noronha-Hostler, F. Pretorius, H. Witek, and N. Yunes, Projecting the likely importance of weak-interaction-driven bulk viscosity in neutron star mergers, Mon. Not. Roy. Astron. Soc. **509**, 1096 (2021), arXiv:2107.05094 [astro-ph.HE] .

[444] E. R. Most, A. Haber, S. P. Harris, Z. Zhang, M. G. Alford, and J. Noronha, Emergence of microphysical viscosity in binary neutron star post-merger dynamics, (2022), arXiv:2207.00442 [astro-ph.HE] .

[445] M. Lagos and L. Hui, Generation and propagation of nonlinear quasinormal modes of a Schwarzschild black hole, Phys. Rev. D **107**, 044040 (2023), arXiv:2208.07379 [gr-qc] .

[446] K. Mitman *et al.*, Nonlinearities in Black Hole Ringdowns, Phys. Rev. Lett. **130**, 081402 (2023), arXiv:2208.07380 [gr-qc] .

[447] M. H.-Y. Cheung *et al.*, Nonlinear Effects in Black Hole Ringdown, Phys. Rev. Lett. **130**, 081401 (2023), arXiv:2208.07374 [gr-qc] .

[448] J. S. Read, B. D. Lackey, B. J. Owen, and J. L. Friedman, Constraints on a phenomenologically parametrized neutron-star equation of state, Physical Review D **79**, 10.1103/physrevd.79.124032 (2009).

[449] B. P. Abbott *et al.* (LIGO Scientific, Virgo), Properties of the binary neutron star merger GW170817, Phys. Rev. X **9**, 011001 (2019), arXiv:1805.11579 [gr-qc] .

[450] B. P. Abbott *et al.* (LIGO Scientific, Virgo), GW170817: Measurements of neutron star radii and equation of state, Phys. Rev. Lett. **121**, 161101 (2018), arXiv:1805.11581 [gr-qc] .

[451] M. W. Coughlin, T. Dietrich, B. Margalit, and B. D. Metzger, Multimessenger bayesian parameter inference of a binary neutron star merger, Monthly Notices of the Royal Astronomical Society: Letters **489**, L91–L96 (2019).

[452] B. Biswas, P. Char, R. Nandi, and S. Bose, Towards mitigation of apparent tension between nuclear physics and astrophysical observations by improved modeling of neutron star matter, Physical Review D **103**, 10.1103/physrevd.103.103015 (2021).

[453] T. Dietrich, M. W. Coughlin, P. T. H. Pang, M. Bulla, J. Heinzel, L. Issa, I. Tews, and S. Antier, Multimessenger constraints on the neutron-star equation of state and the hubble constant, Science **370**, 1450–1453 (2020).

[454] M. F. O'Boyle, C. Markakis, N. Stergioulas, and J. S. Read, Parametrized equation of state for neutron star matter with continuous sound speed, Physical Review D **102**, 10.1103/physrevd.102.083027 (2020).

[455] S. Ghosh, D. Chatterjee, and J. Schaffner-Bielich, Imposing multi-physics constraints at different densities on the neutron star equation of state, The European Physical Journal A **58**, 10.1140/epja/s10050-022-00679-w (2022).

[456] S. Ghosh, B. K. Pradhan, and D. Chatterjee, Tidal heating as a direct probe of strangeness inside neutron stars, Phys. Rev. D **109**, 103036 (2024), arXiv:2306.14737 [gr-qc] .

[457] H. S. Chia, Z. Zhou, and M. M. Ivanov, Bring the Heat: Tidal Heating Constraints for Black Holes and Exotic Compact Objects from the LIGO-Virgo-KAGRA Data, (2024), arXiv:2404.14641 [gr-qc] .

[458] P. B. Jones, Bulk viscosity of neutron-star matter, Phys. Rev. D **64**, 084003 (2001).

[459] L. Lindblom and B. J. Owen, Effect of hyperon bulk viscosity on neutron-star r-modes, Phys. Rev. D **65**, 063006 (2002).

[460] A. Passamonti and K. Glampedakis, Non-linear viscous damping and gravitational wave detectability of the f-mode instability in neutron stars: The f-mode instability in neutron stars, Monthly Notices of the Royal Astronomical Society **422**, 3327–3338 (2012).

[461] M. Alford, S. Mahmoodifar, and K. Schwenzer, Non-linear viscous saturation of r-modes, in *AIP Conference Proceedings* (AIP, 2011).

[462] J. L. Hernandez, C. Manuel, and L. Tolos, Damping of density oscillations from bulk viscosity in quark matter (2024), arXiv:2402.06595 [hep-ph] .

[463] M. G. Alford, L. Bovard, M. Hanauske, L. Rezzolla, and K. Schwenzer, Viscous dissipation and heat conduction in binary neutron-star mergers, Phys. Rev. Lett. **120**, 041101 (2018).

[464] E. R. Most, S. P. Harris, C. Plumberg, M. G. Alford, J. Noronha, J. Noronha-Hostler, F. Pretorius, H. Witek, and N. Yunes, Projecting the likely importance of weak-interaction-driven bulk viscosity in neutron star mergers, Monthly Notices of the Royal Astronomical Society **509**, 1096–1108 (2021).

[465] T. Celora, I. Hawke, P. C. Hammond, N. Andersson, and G. L. Comer, Formulating bulk viscosity for neutron star simulations, Physical Review D **105**, 10.1103/physrevd.105.103016 (2022).

[466] E. R. Most, A. Haber, S. P. Harris, Z. Zhang, M. G. Alford, and J. Noronha, Emergence of microphysical bulk viscosity in binary neutron star postmerger dynamics, The Astrophysical Journal Letters **967**, L14 (2024).

[467] M. Chabanov and L. Rezzolla, Impact of bulk viscosity on the post-merger gravitational-wave signal from merging neutron stars (2023), arXiv:2307.10464 [gr-qc] .

[468] P. Meszaros and M. J. Rees, Tidal Heating and Mass Loss in Neutron Star Binaries: Implications for Gamma-Ray Burst Models, The Astrophysical Journal **397**, 570 (1992).

[469] C. S. Kochanek, Coalescing Binary Neutron Stars, The Astrophysical Journal **398**, 234 (1992).

[470] L. Bildsten and C. Cutler, Tidal Interactions of Inspiraling Compact Binaries, The Astrophysical Journal **400**, 175 (1992).

[471] P. Arras and N. N. Weinberg, Urca reactions during neutron star inspiral, Mon. Not. Roy. Astron. Soc. **486**, 1424 (2019), arXiv:1806.04163 [astro-ph.HE] .

[472] J. L. Ripley, A. Hegade K. R., R. S. Chandramouli, and N. Yunes, First constraint on the dissipative tidal deformability of neutron stars, (2023), arXiv:2312.11659 [gr-qc] .

[473] A. Hegade K. R., J. L. Ripley, and N. Yunes, Dissipative tidal effects to next-to-leading order and constraints on the dissipative tidal deformability using gravitational wave data, (2024), arXiv:2407.02584 [gr-qc] .

[474] T. Pitre and E. Poisson, General relativistic dynamical tides in binary inspirals without modes, Phys. Rev. D **109**, 064004 (2024), arXiv:2311.04075 [gr-qc] .

[475] Y. F. Bautista, G. Bonelli, C. Iossa, A. Tanzini, and Z. Zhou, Black hole perturbation theory meets CFT2: Kerr-Compton amplitudes from Nekrasov-Shatashvili functions, Phys. Rev. D **109**, 084071 (2024), arXiv:2312.05965 [hep-th] .

[476] N. Andersson and P. Pnigouras, Exploring the effective tidal deformability of neutron stars, Phys. Rev. D **101**, 083001 (2020), arXiv:1906.08982 [astro-ph.HE] .

[477] I. F. Ranea-Sandoval, O. M. Guilera, M. Mariani, and M. G. Orsaria, Oscillation modes of hybrid stars within the relativistic cowling approximation, Journal of Cosmology and Astroparticle Physics **2018** (12), 031–031.

[478] V. Tran, S. Ghosh, N. Lozano, D. Chatterjee, and P. Jaikumar, g-mode oscillations in neutron stars with hyperons, Physical Review C **108**, 10.1103/physrevc.108.015803 (2023).

[479] L. Blanchet, G. Faye, Q. Henry, F. Larrouturou, and D. Trestini, Gravitational-Wave Phasing of Quasicircular Compact Binary Systems to the Fourth-and-a-Half Post-Newtonian Order, Phys. Rev. Lett. **131**, 121402 (2023), arXiv:2304.11185 [gr-qc] .

[480] G. Fiorella Burgio and A. F. Fantina, Nuclear equation of state for compact stars and supernovae, Astrophysics and Space Science Library , 255–335 (2018).

[481] C. Drischler, R. J. Furnstahl, J. A. Melendez, and D. R. Phillips, How well do we know the neutron-matter equation of state at the densities inside neutron stars? a bayesian approach with correlated uncertainties, Phys. Rev. Lett. **125**, 202702 (2020).

[482] S. Ghosh, B. K. Pradhan, D. Chatterjee, and J. Schaffner-Bielich, Multi-physics constraints at different densities to probe nuclear symmetry energy in hyperonic neutron stars, Frontiers in Astronomy and Space Sciences **9**, 10.3389/fspas.2022.864294 (2022).

[483] S. Traversi, P. Char, and G. Pagliara, Bayesian inference of dense matter equation of state within relativistic mean field models using astrophysical measurements, The Astrophysical Journal **897**, 165 (2020).

[484] S. Typel, G. Röpke, T. Klähn, D. Blaschke, and H. H. Wolter, Composition and thermodynamics of nuclear matter with light clusters, Phys. Rev. C **81**, 015803 (2010).

[485] M. Oertel, M. Hempel, T. Klaehn, and S. Typel, (`https://compose.obspm.fr/`) (2017).

[486] D. Yakovlev, O. Gnedin, M. Gusakov, A. Kaminker, K. Levenfish, and A. Potekhin, Neutron star cooling, Nuclear Physics A **752**, 590–599 (2005).

[487] B. Haskell, N. Degenaar, and W. C. G. Ho, Constraining the physics of the r-mode instability in neutron stars with X-ray and UV observations, Mon. Not. Roy. Astron. Soc. **424**, 93 (2012), arXiv:1201.2101 [astro-ph.SR] .

[488] E. Flowers and N. Itoh, Transport properties of dense matter., The Astrophysical Journal **206**, 218 (1976).

[489] P. S. Shternin and D. G. Yakovlev, Shear viscosity in neutron star cores, Phys. Rev. D **78**, 063006 (2008).

[490] R. F. Sawyer, Bulk viscosity of hot neutron-star matter and the maximum rotation rates of neutron stars, Phys. Rev. D **39**, 3804 (1989).

[491] D. Chatterjee and D. Bandyopadhyay, Effect of hyperon-hyperon interaction on bulk viscosity and r-mode instability in neutron stars, Phys. Rev. D **74**, 023003 (2006).

[492] D. D. Ofengeim and D. G. Yakovlev, Shear viscosity in magnetized neutron star crust, EPL (Europhysics Letters) **112**, 59001 (2015).

[493] A. I. Chugunov and D. G. Yakovlev, Shear Viscosity and Oscillations of Neutron Star Crust, Astronomy Reports **49**, 724 (2005), arXiv:astro-ph/0511300 [astro-ph] .

[494] D. G. Yakovlev, M. E. Gusakov, and P. Haensel, Bulk viscosity in a neutron star mantle, Mon. Not. Roy. Astron. Soc. **481**, 4924 (2018), arXiv:1809.08609 [astro-ph.HE] .

[495] A. Ghosh *et al.*, Testing general relativity using golden black-hole binaries, Phys. Rev. D **94**, 021101 (2016), arXiv:1602.02453 [gr-qc] .

[496] C. A. Raithel, F. Özel, and D. Psaltis, Finite-temperature extension for cold neutron star equations of state, The Astrophysical Journal **875**, 12 (2019).

[497] A. R. Raduta, F. Nacu, and M. Oertel, Equations of state for hot neutron stars, Eur. Phys. J. A **57**, 329 (2021), arXiv:2109.00251 [nucl-th] .

[498] A. R. Counsell, F. Gittins, and N. Andersson, The impact of nuclear reactions on the neutron-star g-mode spectrum, Mon. Not. Roy. Astron. Soc. **531**, 1721 (2024), arXiv:2310.13586 [astro-ph.HE] .

[499] N. Andersson and P. Pnigouras, The g-mode spectrum of reactive neutron star cores, Mon. Not. Roy. Astron. Soc. **489**, 4043 (2019), arXiv:1905.00010 [gr-qc] .

[500] T. G. Cowling, The Non-radial Oscillations of Polytropic Stars, Mon. Not. Roy. Astron. Soc. **101**, 367 (1941).

[501] J. R. Ipser and R. H. Price, Nonradial pulsations of stellar models in general relativity, Phys. Rev. D **43**, 1768 (1991).

[502] J. R. Ipser and R. A. Managan, An eulerian variational principle and a criterion for the occurrence of nonaxisymmetric neutral modes along rotating axisymmetric sequences, Astrophysical Journal, Part 1 (ISSN 0004-637X), vol. 292, May 15, 1985, p. 517-521. **292**, 517 (1985).

[503] A. Reisenegger and P. Goldreich, A New Class of g-Modes in Neutron Stars, The Astrophysical Journal **395**, 240 (1992).

[504] G. Camelio, L. Gavassino, M. Antonelli, S. Bernuzzi, and B. Haskell, Simulating bulk viscosity in neutron stars. i. formalism, Phys. Rev. D **107**, 103031 (2023).

[505] L. Blanchet, G. Faye, Q. Henry, F. Larrouturou, and D. Trestini, Gravitational-wave flux and quadrupole modes from quasicircular nonspinning compact binaries to the fourth post-Newtonian order, Phys. Rev. D **108**, 064041 (2023), arXiv:2304.11186 [gr-qc] .

[506] C. B. Owen, C.-J. Haster, S. Perkins, N. J. Cornish, and N. Yunes, Waveform accuracy and systematic uncertainties in current gravitational wave observations, Phys. Rev. D **108**, 044018 (2023), arXiv:2301.11941 [gr-qc] .

[507] Q. Hu and J. Veitch, Assessing the model waveform accuracy of gravitational waves, Phys. Rev. D **106**, 044042 (2022), arXiv:2205.08448 [gr-qc] .

[508] S. Ma, H. Yu, and Y. Chen, Excitation of f-modes during mergers of spinning binary neutron star, Phys. Rev. D **101**, 123020 (2020), arXiv:2003.02373 [gr-qc] .

[509] R. Abbott *et al.* (LIGO Scientific, Virgo), GW190521: A Binary Black Hole Merger with a Total Mass of $150M\_\odot$, Phys. Rev. Lett. **125**, 101102 (2020), arXiv:2009.01075 [gr-qc] .

[510] T. G. F. Li, W. Del Pozzo, S. Vitale, C. Van Den Broeck, M. Agathos, J. Veitch, K. Grover, T. Sidery, R. Sturani, and A. Vecchio, Towards a generic test of the strong field dynamics of general relativity using compact binary coalescence, Phys. Rev. D **85**, 082003 (2012), arXiv:1110.0530 [gr-qc] .

[511] M. Agathos, W. Del Pozzo, T. G. F. Li, C. Van Den Broeck, J. Veitch, and S. Vitale, TIGER: A data analysis pipeline for testing the strong-field dynamics of general relativity with gravitational wave signals from coalescing compact binaries, Phys. Rev. D **89**, 082001 (2014), arXiv:1311.0420 [gr-qc] .

[512] A. Ghosh, N. K. Johnson-Mcdaniel, A. Ghosh, C. K. Mishra, P. Ajith, W. Del Pozzo, C. P. L. Berry, A. B. Nielsen, and L. London, Testing general relativity using gravitational wave signals from the inspiral, merger and ringdown of binary black holes, Class. Quant. Grav. **35**, 014002 (2018), arXiv:1704.06784 [gr-qc] .

[513] R. Brito, A. Buonanno, and V. Raymond, Black-hole Spectroscopy by Making Full Use of Gravitational-Wave Modeling, Phys. Rev. D **98**, 084038 (2018), arXiv:1805.00293 [gr-qc] .

[514] G. Carullo, W. Del Pozzo, and J. Veitch, Observational Black Hole Spectroscopy: A time-domain multimode analysis of GW150914, Phys. Rev. D **99**, 123029 (2019), [Erratum: Phys.Rev.D 100, 089903 (2019)], arXiv:1902.07527 [gr-qc] .

[515] A. Ghosh, R. Brito, and A. Buonanno, Constraints on quasinormal-mode frequencies with LIGO-Virgo binary–black-hole observations, Phys. Rev. D **103**, 124041 (2021), arXiv:2104.01906 [gr-qc] .

[516] M. Isi and W. M. Farr, Analyzing black-hole ringdowns, (2021), arXiv:2107.05609 [gr-qc] .

[517] E. Maggio, H. O. Silva, A. Buonanno, and A. Ghosh, Tests of general relativity in the nonlinear regime: A parametrized plunge-merger-ringdown gravitational waveform model, Phys. Rev. D **108**, 024043 (2023), arXiv:2212.09655 [gr-qc] .

[518] V. Gennari, G. Carullo, and W. Del Pozzo, Searching for ringdown higher modes with a numerical relativity-informed post-merger model, Eur. Phys. J. C **84**, 233 (2024), arXiv:2312.12515 [gr-qc] .

[519] B. Abbott *et al.* (LIGO Scientific, Virgo), Tests of General Relativity with the Binary Black Hole Signals from the LIGO-Virgo Catalog GWTC-1, Phys. Rev. D **100**, 104036 (2019), arXiv:1903.04467 [gr-qc] .

[520] R. Abbott *et al.* (LIGO Scientific, Virgo), Tests of general relativity with binary black holes from the second LIGO-Virgo gravitational-wave transient catalog, Phys. Rev. D **103**, 122002 (2021), arXiv:2010.14529 [gr-qc] .

[521] S. W. Hawking, Black hole explosions, Nature **248**, 30 (1974).

[522] S. D. Mathur, The Information paradox: A Pedagogical introduction, *Strings, Supergravity and Gauge Theories. Proceedings, CERN Winter School, CERN, Geneva, Switzerland, February 9-13 2009*, Class. Quant. Grav. **26**, 224001 (2009), arXiv:0909.1038 [hep-th] .

[523] J. D. Bekenstein, Black holes and entropy, Phys. Rev. D **7**, 2333 (1973).

[524] S. W. Hawking, Black Holes and Thermodynamics, Phys. Rev. D **13**, 191 (1976).

[525] G. F. Giudice, M. McCullough, and A. Urbano, Hunting for Dark Particles with Gravitational Waves, JCAP **1610** (10), 001, arXiv:1605.01209 [hep-ph] .

[526] V. Cardoso and P. Pani, Tests for the existence of black holes through gravitational wave echoes, Nat. Astron. **1**, 586 (2017), arXiv:1709.01525 [gr-qc] .

[527] E. Maggio, P. Pani, and G. Raposo, Testing the nature of dark compact objects with gravitational waves 10.1007/978-981-15-4702-7_29-1 (2021), arXiv:2105.06410 [gr-qc] .

[528] I. Bena and N. P. Warner, Black holes, black rings and their microstates, *Winter School on Attractor Mechanism (SAM 2006) Frascati, Italy, March 20-24, 2006*, Lect. Notes Phys. **755**, 1 (2008), arXiv:hep-th/0701216 [hep-th] .

[529] V. Balasubramanian, J. de Boer, S. El-Showk, and I. Messamah, Black Holes as Effective Geometries, *Strings, supergravity and gauge theories. Proceedings, European RTN Winter School, CERN, Geneva, Switzerland, January 21-25, 2008*, Class. Quant. Grav. **25**, 214004 (2008), arXiv:0811.0263 [hep-th] .

[530] P. O. Mazur and E. Mottola, Gravitational vacuum condensate stars, Proc. Nat. Acad. Sci. **101**, 9545 (2004), arXiv:gr-qc/0407075 [gr-qc] .

[531] L. Buoninfante, A. S. Cornell, G. Harmsen, A. S. Koshelev, G. Lambiase, J. Marto, and A. Mazumdar, Towards nonsingular rotating compact object in ghost-free infinite derivative gravity, Phys. Rev. D **98**, 084041 (2018), arXiv:1807.08896 [gr-qc] .

[532] L. Buoninfante and A. Mazumdar, Nonlocal star as a blackhole mimicker, Phys. Rev. D **100**, 024031 (2019), arXiv:1903.01542 [gr-qc] .

[533] D. J. Kaup, Klein-Gordon Geon, Phys. Rev. **172**, 1331 (1968).

[534] R. Ruffini and S. Bonazzola, Systems of selfgravitating particles in general relativity and the concept of an equation of state, Phys. Rev. **187**, 1767 (1969).

[535] E. Seidel and W. Suen, Oscillating soliton stars, Phys.Rev.Lett. **66**, 1659 (1991).

[536] S. L. Liebling and C. Palenzuela, Dynamical Boson Stars, Living Rev. Rel. **15**, 6 (2012), arXiv:1202.5809 [gr-qc] .

[537] R. Brito, V. Cardoso, C. A. R. Herdeiro, and E. Radu, Proca stars: Gravitating Bose-Einstein condensates of massive spin 1 particles, Phys. Lett. **B752**, 291 (2016), arXiv:1508.05395 [gr-qc] .

[538] M. S. Morris and K. S. Thorne, Wormholes in space-time and their use for interstellar travel: A tool for teaching general relativity, Am. J. Phys. **56**, 395 (1988).

[539] M. Visser, *Lorentzian wormholes: From Einstein to Hawking* (1995).

[540] T. Damour and S. N. Solodukhin, Wormholes as black hole foils, Phys. Rev. **D76**, 024016 (2007), arXiv:0704.2667 [gr-qc] .

[541] V. Cardoso, A. del Rio, and M. Kimura, Distinguishing black holes from horizonless objects through the excitation of resonances during inspiral, Phys. Rev. D **100**, 084046 (2019), [Erratum: Phys.Rev.D 101, 069902 (2020)], arXiv:1907.01561 [gr-qc] .

[542] Y. Asali, P. T. H. Pang, A. Samajdar, and C. Van Den Broeck, Probing resonant excitations in exotic compact objects via gravitational waves, Phys. Rev. D **102**, 024016 (2020), arXiv:2004.05128 [gr-qc] .

[543] E. Maggio, M. van de Meent, and P. Pani, Extreme mass-ratio inspirals around a spinning horizonless compact object, Phys. Rev. D **104**, 104026 (2021), arXiv:2106.07195 [gr-qc] .

[544] P. Pani, I-Love-Q relations for gravastars and the approach to the black-hole limit, Phys. Rev. **D92**, 124030 (2015), arXiv:1506.06050 [gr-qc] .

[545] N. Uchikata, S. Yoshida, and P. Pani, Tidal deformability and I-Love-Q relations for gravastars with polytropic thin shells, Phys. Rev. **D94**, 064015 (2016), arXiv:1607.03593 [gr-qc] .

[546] V. Cardoso, E. Franzin, A. Maselli, P. Pani, and G. Raposo, Testing strong-field gravity with tidal Love numbers, Phys. Rev. **D95**, 084014 (2017), arXiv:1701.01116 [gr-qc] .

[547] N. Sennett, T. Hinderer, J. Steinhoff, A. Buonanno, and S. Ossokine, Distinguishing Boson Stars from Black Holes and Neutron Stars from Tidal Interactions in Inspiraling Binary Systems, Phys. Rev. **D96**, 024002 (2017), arXiv:1704.08651 [gr-qc] .

[548] G. Raposo, P. Pani, M. Bezares, C. Palenzuela, and V. Cardoso, Anisotropic stars as ultracompact objects in General Relativity, Phys. Rev. **D99**, 104072 (2019), arXiv:1811.07917 [gr-qc] .

[549] S. Nair, S. Chakraborty, and S. Sarkar, Dynamical Love numbers for area quantized black holes, Phys. Rev. D **107**, 124041 (2023), arXiv:2208.06235 [gr-qc] .

[550] S. Chakraborty, E. Maggio, M. Silvestrini, and P. Pani, Dynamical tidal Love numbers of Kerr-like compact objects, (2023), arXiv:2310.06023 [gr-qc] .

[551] J. Abedi, H. Dykaar, and N. Afshordi, Echoes from the Abyss: Tentative evidence for Planck-scale structure at black hole horizons, Phys. Rev. **D96**, 082004 (2017), arXiv:1612.00266 [gr-qc] .

[552] Q. Wang, N. Oshita, and N. Afshordi, Echoes from Quantum Black Holes, Phys. Rev. D **101**, 024031 (2020), arXiv:1905.00446 [gr-qc] .

[553] Z. Mark, A. Zimmerman, S. M. Du, and Y. Chen, A recipe for echoes from exotic compact objects, Phys. Rev. **D96**, 084002 (2017), arXiv:1706.06155 [gr-qc] .

[554] A. Testa and P. Pani, Analytical template for gravitational-wave echoes: signal characterization and prospects of detection with current and future interferometers, Phys. Rev. **D98**, 044018 (2018), arXiv:1806.04253 [gr-qc] .

[555] E. Maggio, A. Testa, S. Bhagwat, and P. Pani, Analytical model for gravitational-wave echoes from spinning remnants, Phys. Rev. D **100**, 064056 (2019), arXiv:1907.03091 [gr-qc] .

[556] S. Xin, B. Chen, R. K. L. Lo, L. Sun, W.-B. Han, X. Zhong, M. Srivastava, S. Ma, Q. Wang, and Y. Chen, Gravitational-wave echoes from spinning exotic compact objects: Numerical waveforms from the Teukolsky equation, Phys. Rev. D **104**, 104005 (2021), arXiv:2105.12313 [gr-qc] .

[557] S. Ma, Q. Wang, N. Deppe, F. Hébert, L. E. Kidder, J. Moxon, W. Throwe, N. L. Vu, M. A. Scheel, and Y. Chen, Gravitational-wave echoes from numerical-relativity waveforms via spacetime construction near merging compact objects, Phys. Rev. D **105**, 104007 (2022), arXiv:2203.03174 [gr-qc] .

[558] V. Vellucci, E. Franzin, and S. Liberati, Echoes from backreacting exotic compact objects, Phys. Rev. D **107**, 044027 (2023), arXiv:2205.14170 [gr-qc] .

[559] N. Siemonsen, Nonlinear treatment of a black hole mimicker ringdown, (2024), arXiv:2404.14536 [gr-qc] .

[560] M. Branchesi *et al.*, Science with the Einstein Telescope: a comparison of different designs, JCAP **07**, 068, arXiv:2303.15923 [gr-qc] .

[561] K. G. Arun *et al.* (LISA), New horizons for fundamental physics with LISA, Living Rev. Rel. **25**, 4 (2022), arXiv:2205.01597 [gr-qc] .

[562] G. A. Piovano, A. Maselli, and P. Pani, Constraining the tidal deformability of supermassive objects with extreme mass ratio inspirals and semianalytical frequency-domain waveforms, Phys. Rev. D **107**, 024021 (2023), arXiv:2207.07452 [gr-qc] .

[563] S. Barsanti, A. Maselli, T. P. Sotiriou, and L. Gualtieri, Detecting Massive Scalar Fields with Extreme Mass-Ratio Inspirals, Phys. Rev. Lett. **131**, 051401 (2023), arXiv:2212.03888 [gr-qc] .

[564] T. Damour, Surface Effects in Black-Hole Physics, in *Marcel Grossmann Meeting: General Relativity* (1982) p. 587.

[565] G. Darmois, Les équations de la gravitation einsteinienne, Mémorial de Sciences Mathématiques **fascicule 25**, 1 (1927).

[566] M. Visser, *Lorentzian wormholes: From Einstein to Hawking* (AIP, Woodbury, USA, 1996) p. 412 p.

[567] J. Abedi, N. Afshordi, N. Oshita, and Q. Wang, Quantum Black Holes in the Sky, Universe **6**, 43 (2020), arXiv:2001.09553 [gr-qc] .

[568] P. Pani, V. Cardoso, L. Gualtieri, E. Berti, and A. Ishibashi, Perturbations of slowly rotating black holes: massive vector fields in the Kerr metric, Phys. Rev. D **86**, 104017 (2012), arXiv:1209.0773 [gr-qc] .

[569] P. Pani, E. Berti, and L. Gualtieri, Gravitoelectromagnetic Perturbations of Kerr-Newman Black Holes: Stability and Isospectrality in the Slow-Rotation Limit, Phys. Rev. Lett. **110**, 241103 (2013), arXiv:1304.1160 [gr-qc] .

[570] N. Uchikata and S. Yoshida, Slowly rotating thin shell gravastars, Class. Quant. Grav. **33**, 025005 (2016), arXiv:1506.06485 [gr-qc] .

[571] L. Pierini and L. Gualtieri, Quasi-normal modes of rotating black holes in Einstein-dilaton Gauss-Bonnet gravity: the first order in rotation, Phys. Rev. D **103**, 124017 (2021), arXiv:2103.09870 [gr-qc] .

[572] P. Wagle, N. Yunes, and H. O. Silva, Quasinormal modes of slowly-rotating black holes in dynamical Chern-Simons gravity, Phys. Rev. D **105**, 124003 (2022), arXiv:2103.09913 [gr-qc] .

[573] J. B. Hartle and K. S. Thorne, Slowly Rotating Relativistic Stars. II. Models for Neutron Stars and Supermassive Stars, Astrophys. J. **153**, 807 (1968).

[574] L. Pierini and L. Gualtieri, Quasinormal modes of rotating black holes in Einstein-dilaton Gauss-Bonnet gravity: The second order in rotation, Phys. Rev. D **106**, 104009 (2022), arXiv:2207.11267 [gr-qc] .

[575] P. Wagle, D. Li, Y. Chen, and N. Yunes, Perturbations of spinning black holes in dynamical Chern-Simons gravity: Slow rotation equations, Phys. Rev. D **109**, 104029 (2024), arXiv:2311.07706 [gr-qc] .

[576] E. Berti *et al.*, Testing General Relativity with Present and Future Astrophysical Observations, Class. Quant. Grav. **32**, 243001 (2015), arXiv:1501.07274 [gr-qc] .

[577] A. A. Starobinskij and S. M. Churilov, Amplification of electromagnetic and gravitational waves scattered by a rotating black hole., Zhurnal Eksperimentalnoi i Teoreticheskoi Fiziki **65**, 3 (1973).

[578] G. Creci, T. Hinderer, and J. Steinhoff, Tidal response from scattering and the role of analytic continuation, Phys. Rev. D **104**, 124061 (2021).

[579] Y. B. Zel'Dovich, Generation of Waves by a Rotating Body, Soviet Journal of Experimental and Theoretical Physics Letters **14**, 180 (1971).

[580] R. D. Blandford and R. L. Znajek, Electromagnetic extractions of energy from Kerr black holes, Mon. Not. Roy. Astron. Soc. **179**, 433 (1977).

[581] R. Brito, V. Cardoso, and P. Pani, Superradiance, Lect. Notes Phys. **906**, pp.1 (2015), arXiv:1501.06570 [gr-qc] .

[582] E. Maggio, P. Pani, and V. Ferrari, Exotic Compact Objects and How to Quench their Ergoregion Instability, Phys. Rev. **D96**, 104047 (2017), arXiv:1703.03696 [gr-qc] .

[583] E. Leaver, An Analytic representation for the quasi normal modes of Kerr black holes, Proc. Roy. Soc. Lond. A **A402**, 285 (1985).

[584] P. Pani, E. Berti, V. Cardoso, Y. Chen, and R. Norte, Gravitational wave signatures of the absence of an event horizon. I. Nonradial oscillations of a thin-shell gravastar, Phys. Rev. **D80**, 124047 (2009), arXiv:0909.0287 [gr-qc] .

[585] Z. Zhong, V. Cardoso, and E. Maggio, Instability of ultracompact horizonless spacetimes, Phys. Rev. D **107**, 044035 (2023), arXiv:2211.16526 [gr-qc] .

[586] J. C. L. Chan, C. Dyson, M. Garcia, J. Redondo-Yuste, and L. Vujeva, Lensing and wave optics in the strong field of a black hole, (2025), arXiv:2502.14073 [gr-qc] .

[587] Wikipedia contributors, Euler angles — Wikipedia, the free encyclopedia (2023), [Online; accessed 11-June-2023].

[588] K. S. Thorne, Nonradial Pulsation of General-Relativistic Stellar Models.IV. The Weakfield Limit, Astrophys. J. **158**, 997 (1969).

[589] P. Smeyers and T. Van Hoolst, *Linear Isentropic Oscillations of Stars: Theoretical Foundations*, Vol. 371 (Springer Science & Business Media, 2011).

[590] S. Chandrasekhar, A general variational principle governing the radial and the non-radial oscillations of gaseous masses, VI. Ellipsoidal Figures of Equilibrium **1** (1960).